UNIVERSITÉ DU LUXEMBOURG

PhD-FSTM-2025-107

Faculty of Life Sciences, Technology and Medicine

DISSERTATION

Defence held on 13 October 2025 in Luxembourg
to obtain the degree of

DOCTEUR DE L'UNIVERSITÉ DU LUXEMBOURG EN SCIENCES DE L'INGÉNIEUR

by

Rodrigo DA SILVA GESSER

Born on 20 August 1991 in Florianópolis, Santa Catarina (Brazil)

Pollution-Based and Multi-Layer Model Predictive Control of Urban Drainage Systems

Dissertation Defence Committee:

Prof. Dr. Holger Voos, Dissertation supervisor
Professor, University of Luxembourg

Dr. Alex Cornelissen, Dissertation supervisor
Business Development Director, RTC4Water

Prof. Dr. Inès Chihi, Chairman
Professor, University of Luxembourg

Prof. Dr. Job Van der Werf
Professor, Delft University of Technology

Prof. Dr. Mohamed Darouach
Professor, Université de Lorraine

1 Affidavit / Statement of originality

I declare that this thesis:

- is the result of my own work. Any contribution from any other party, and any use of generative artificial intelligence technologies have been duly cited and acknowledged;
- is not substantially the same as any other that I have submitted, and;
- is not being concurrently submitted for a degree, diploma or other qualification at the University of Luxembourg or any other University or similar institution except as specified in the text.

With my approval I furthermore confirm the following:

- Where I have quoted from the work of others, the source is always given. With the exception of such quotations, this thesis is entirely my own work.
- I have acknowledged all main sources of help.
- Where the thesis is based on work done by myself jointly with others, I have made clear exactly what was done by others and what I have contributed myself.

I acknowledge that if any issues are raised regarding good research practices based on the review of the thesis, the examination may be postponed pending the outcome of any investigation of such issues. If a degree was conferred, any such subsequently discovered issues may result in the cancellation of the degree.

Approved on 2025-08-11

2 Abstract

Urban Drainage Systems (UDS), particularly Combined Sewer Overflows (CSO), face challenges in managing overflows during heavy rainfall, often leading to a negative environmental impact. Traditional CSO mitigation methods are costly, prompting interest in software-based strategies such as Model Predictive Control (MPC). This research focuses on enhancing Volume-based MPC through two complementary frameworks: (1) a pollution-based framework, and (2) an optimisation-based RTC framework, integrating pollutant concentrations into the control process to prioritise treatment of highly contaminated flows. To address practical limitations, this work introduces a Pollution-weighted MPC (PWMPC) for fast linear optimisation, a Non-linear Pollution-based MPC (NPMPC) for best load reduction performance, and a multi-layer MPC framework to ensure feasible solutions under real-time constraints. Stochastic MPC variants are also explored to account for uncertainty in system dynamics.

The results show that the multi-layer MPC and its stochastic counterpart improve reliability, reducing infeasibility instances in NPMPC. Although NPMPC offers the best performance in low- to mid-uncertainty conditions, stochastic methods are more robust under high uncertainties. Furthermore, PWMPC is identified as the most computationally efficient, but depends heavily on accurate concentration data. Finally, Volume-based MPC remains useful when concentration data is unavailable and as an ultimate fallback. The study also presents a methodology for weight selection in all types of MPCs, which improves tuning and performance. Ultimately, NPMPC was found to deliver near-optimal pollutant reduction, making it an attractive strategy to reduce overflow load. Other MPC implementations, while approaching optimal solutions, do not exceed the performance of NPMPC in most scenarios, establishing it as the most effective strategy. However, for practical implementations, both PWMPC and SPWMPC are arguably the most cost-effective method due to their powerful performance on reducing load with a low computational cost. Finally, the Multi-layer MPC improved the performance by enabling a better use of NPMPC or SNPMPC methods in complex systems.

3 Acknowledgements

First of all, I would like to thank Prof. Dr. Holger Voos for the supervision, support and guidance through the course of the journey, always solicit to help. I would like to thank Dr. Alex Cornelissen for the tough love support, always available to hear my complaining and being key to the success of this research.

Furthermore, I would like to thank RTC4Water and Dr. Georges Schutz for his kindness, guidance and informative walks around Roeser. RTC4Water gave me an unique opportunity to learn and grow, to be a better professional and person. I deeply thank RTC4Water for giving me the chance to have a better quality of life.

My deep thanks to my great friends that followed my journey in some way. A special gratitude for Sabuj Biswas that was a constant friend and support. I would like to thank Adriano, Alice and Fabrício for always being there, even though far away.

Finally, I would like to send all my love to my family that, although far away, supported me, and helped being a better person and parent. The conclusion of this thesis was only possible with the love of the two most important people of my life, Thaís, the best person in the world, and Nina, the best thing I ever did, always by my side in the bad and good moments, always brightening my days.

Contents

1 Affidavit / Statement of originality iii

2 Abstract v

3 Acknowledgements vii

Contents viii

List of Figures xx

List of Tables xxv

Acronyms xxvii

4 Symbols xxxi

5 Introduction 1

5.1 Context of the Study . . . 1
5.2 Problem Statement and Motivation . . . 2
5.3 Objective and Scope . . . 4
5.4 Relevance of the Research . . . 5
5.4.1 Scientific Contribution . . . 6
5.5 Summary of the Thesis . . . 7

6 State of the Art 9

6.1 Urban Drainage Systems . . . 9
6.2 Software for Modelling Urban Drainage Systems . . . 11
6.2.1 EPA Storm Water Management Model . . . 12
6.2.2 Urban Drainage System Modelling with SWMM . . . 15
6.3 Water Quality Models for Prediction . . . 21
6.3.1 Modelling Taxonomy . . . 22
6.3.2 Simplified Models . . . 24

6.3.3 Data-driven Models . . . 28
6.3.4 Probability Models . . . 33
6.4 Pollution-based Control Strategies . . . 36
6.4.1 Rule-based RTC . . . 36
6.4.2 Optimisation-based RTC . . . 39
6.4.3 Reinforcement Learning-based RTC . . . 45
6.5 Literature Gaps and Contribution . . . 49
6.6 Conclusion . . . 49

7 Volume-based Model Predictive Control 51
7.1 Description of Model Predictive Control . . . 53
7.1.1 Linear State-Space Dynamic Models . . . 53
7.1.2 Optimisation Problem . . . 54
7.2 Model Predictive Control for Urban Drainage Systems . . . 56
7.3 Volume-based Model Predictive Control . . . 57
7.3.1 Description . . . 58
7.3.2 Optimisation Problem . . . 59
7.3.3 Methodology Validation - Single Storage Unit Configuration . . . 61
7.3.4 Methodology Validation - Parallel Storage Units Configuration . . . 64
7.3.5 Methodology Validation - Parallel + Series Storage Units Configuration . . . 70
7.3.6 Weight Sensitivity Analysis . . . 71
7.3.7 Genetic Algorithm for weight optimisation . . . 78
7.3.8 Computation Time Analysis . . . 82
7.3.9 Water Quality Analysis . . . 84

8 Pollution-based Model Predictive Control 87
8.1 Non-linear Pollution-based Model Predictive Control . . . 87
8.1.1 Estimation of $C_{\text{in}}(k)$ and $C(k)$ . . . 89
8.1.2 Uncertainty Estimation . . . 93
8.1.3 Optimisation Problem . . . 94
8.1.4 Methodology Validation - Parallel + Series Configuration . . . 98
8.1.5 Weight Sensitivity Analysis . . . 99
8.1.6 Global Sensitivity Analysis - Random Search . . . 102
8.1.7 Genetic Algorithm for weight optimisation . . . 103
8.1.8 Computation Time Analysis . . . 105
8.2 Pollution-weighted Model Predictive Control . . . 107
8.2.1 Description . . . 107

8.2.2 Optimisation Problem . . . 108
8.2.3 Methodology Validation - Parallel + Series Configuration . . . 110
8.2.4 Weight Sensitivity Analysis . . . 110
8.2.5 Genetic Algorithm for weight optimisation . . . 114
8.2.6 Computation Time Analysis . . . 116

9 Uncertainty Analysis and Stochastic Model Predictive Control 119
9.1 Uncertainty Analysis . . . 119
9.1.1 Uncertainty on $V(k)$ . . . 122
9.1.2 Uncertainty on $Q_{\text{out}}(k)$ . . . 126
9.1.3 Uncertainty on $Q_{\text{ov}}(k)$ . . . 130
9.2 Stochastic Model Predictive Control . . . 133
9.3 Stochastic Volume-based Model Predictive Control . . . 135
9.3.1 Description . . . 135
9.3.2 Optimisation Problem . . . 137
9.3.3 Methodology Validation . . . 141
9.3.4 Local Sensitivity Analysis - Morris screening . . . 151
9.3.5 Global Sensitivity Analysis - Grid and Random Search . . . 153
9.3.6 Genetic Algorithm for weight optimisation . . . 155
9.4 Stochastic Pollution-weighted Model Predictive Control . . . 167
9.4.1 Description . . . 167
9.4.2 Optimisation Problem . . . 168
9.4.3 Methodology Validation . . . 171
9.4.4 Local Sensitivity Analysis - Morris Screening . . . 175
9.4.5 Global Sensitivity Analysis - Grid and Random Search . . . 176
9.4.6 Genetic Algorithm for weight optimisation . . . 178
9.5 Stochastic Non-linear Pollution-based Model Predictive Control . . . 184
9.5.1 Description . . . 184
9.5.2 Optimisation Problem . . . 186
9.5.3 Methodology Validation . . . 190
9.5.4 Local Sensitivity Analysis - Morris Screening . . . 190
9.5.5 Global Sensitivity Analysis - Grid and Random Search . . . 192
9.5.6 Genetic Algorithm for weight optimisation . . . 195
9.6 Comparison between MPC methods . . . 201

10 High-Complexity Urban Drainage Simulations 205
10.1 Urban Drainage System 1 . . . 207
10.1.1 Sensitivity Analysis and Genetic Algorithm Optimisation . . . 212

10.1.2 Comparison of MPC Methods . . . 216
10.1.3 Global View of Urban Drainage System 1 . . . 223
10.2 Urban Drainage System 2 . . . 224
10.2.1 Comparison of MPC Methods . . . 231
10.3 Urban Drainage System 3 . . . 239
10.3.1 Qualitative Analysis . . . 243
10.3.2 Comparison of MPC Methods . . . 246

11 Multi-layer Model Predictive Control 249
11.1 Feasibility of Non-linear MPC Strategies . . . 249
11.2 Multi-layer Model Predictive Control . . . 253
11.2.1 Literature Review . . . 253
11.2.2 Fallback Strategy 1 - FBS1 . . . 254
11.2.3 Fallback Strategy 2 - FBS2 . . . 254
11.2.4 Fallback Strategy 3 - FBS3 . . . 255
11.3 Scenario 1 - Fallback Strategy 1 . . . 256
11.4 Scenario 2 - All Fallback Strategies . . . 262

12 Conclusion and Perspectives 269

A Appendix 271
A.1 Additional Results for VMPC . . . 271
A.2 Additional Results for NPMPC . . . 276
A.3 Additional Results for SPWMPC . . . 280
A.4 Additional Results for SNPMPC . . . 283
A.5 Additional Results for Urban Drainage System 1 . . . 286
A.6 Additional Results for Urban Drainage System 2 . . . 289
A.7 Additional Results for ML-MPC . . . 291

Bibliography 297

List of Figures

6.1 Total publications per year from 1980 to 2025, estimated by searching the key words "Real time control" and "Wastewater" in the data-set provided by [30]. . . . 10
6.2 Total publications per year from 1980 to 2025, estimated by searching the key words "Pollution-based" and "Real time control" and "Wastewater" in the data-set provided by [30]. . . . 11
6.3 Physical objects used to model a drainage system [40]. . . . 13
6.4 Single SU configuration: Conceptual and SWMM model. . . . 15
6.5 Single SU configuration - precipitation. . . . 16
6.6 Single SU configuration - dry weather flow. . . . 16
6.7 Single SU configuration - dry weather load. . . . 16
6.8 Single SU system - Volume (left y-axis, red) and Outflow (right y-axis, blue). 17
6.9 Single SU configuration - Volume (left y-axis, red) and Overflow (right y-axis, blue). . . . 17
6.10 Parallel SU configuration: Conceptual and SWMM model. . . . 18
6.11 Parallel SU configuration - precipitation. . . . 18
6.12 Parallel SU configuration - dry weather flow. . . . 19
6.13 Parallel SU configuration - Volume (left axis, red) and Outflow (right axis, blue). . . . 19
6.14 Parallel SU configuration - Volume (red) and Overflow (blue). . . . 20
6.15 Parallel+Series SU configuration: Conceptual and SWMM model. . . . 20
6.16 General characterisation of the sewage system [52]. . . . 21
6.17 Mathematical-based model Taxonomy by [57]. . . . 22
6.18 Sewage system model taxonomy proposed by [3]. . . . 23
6.19 Proposed sewage system control-oriented model taxonomy. . . . 24
6.20 SU model for wastewater quantity modelling [19]. . . . 25
6.21 SU model for wastewater quality modelling [19]. . . . 25
6.22 Water SU container [52]. . . . 27
6.23 Methodology for MLR and ANN methods [75]. . . . 30

6.24 Framework for water quality prediction [74]. 32
6.25 Representation of a catchment by [86]. 34

7.1 MPC scheme. 51
7.2 MPC strategy. 52
7.3 VMPC scheme for Urban Drainage Systems. 58
7.4 Single SU configuration - outflow comparison between static control and VMPC. 63
7.5 Single SU configuration - overflow comparison between static control and VMPC. 64
7.6 Parallel SU configuration - outflow comparison between static control and VMPC. 66
7.7 Parallel SU configuration - overflow comparison between static control and VMPC. 66
7.8 VMPC scheme for Urban Drainage Systems. 67
7.9 Parallel SU configuration - overflow comparison between static control and VMPC with $Q_{\text{out}_{\max}} \geq Q_{\text{design}}$. 68
7.10 Parallel SU configuration - outflow comparison between static control and VMPC - 12$^{\text{nd}}$ of May to 14$^{\text{th}}$ of May. 69
7.11 Parallel SU configuration - overflow comparison between static control and VMPC - 12$^{\text{nd}}$ of May to 14$^{\text{th}}$ of May. 69
7.12 Global Sensitivity Analysis [125]. 73
7.13 DWF + WWF data for sensitivity analysis from 1$^{\text{st}}$ of May to 1$^{\text{st}}$ of June. 74
7.14 DWF + WWF data for sensitivity analysis from 24$^{\text{th}}$ of March to 24$^{\text{th}}$ of April. 74
7.15 Morris Screening LSA for Parallel+Series SU configuration. 75
7.16 Grid Search SA for the total overflow in the system from 1$^{\text{st}}$ of May to 1$^{\text{st}}$ of June for $\epsilon = 153$. 76
7.17 Representation in the grid of the weights chosen in Section 7.3.5. 78
7.18 Pareto-front for all simulations. 80
7.19 Hypervolume for all simulations. 81
7.20 Comparison of Computation Times for VMPC - Line plot represents mean and shaded area the standard deviation. 83
7.21 Urban Drainage System with and without industrial activity in SU3. . . . 84
7.22 COD Load from two different sources. 85

8.1 NPMPC scheme for Urban Drainage Systems. 88
8.2 Storage Unit model for water quality [19]. 88

8.3 Two different normalized daily patterns sampled hourly. . . . 90
8.4 Flow daily pattern sampled hourly. . . . 91
8.5 Concentration daily pattern sampled hourly. . . . 91
8.6 Uniform uncertainty law. . . . 94
8.7 Morris screening for NPMPC. . . . 99
8.8 Grid Search SA for the total load overflow in the system. . . . 101
8.9 Random Search for NPMPC. . . . 102
8.10 Pareto-front for all simulations. . . . 104
8.11 Hypervolume for all simulations. . . . 104
8.12 Comparison of Computation Times for NPMPC - Line plot represents mean and shaded area the standard deviation. . . . 106
8.13 PWMPC scheme for Urban Drainage Systems. . . . 107
8.14 Morris screening for PWMPC. . . . 111
8.15 Grid Search Analysis for PWMPC. . . . 113
8.16 Random Search Analysis for PWMPC. . . . 114
8.17 Pareto-front for all simulations. . . . 115
8.18 Hypervolume for all simulations. . . . 115
8.19 Computation time for PWMPC and VMPC - Line plot represents mean and shaded area the standard deviation. . . . 116
8.20 Computation time for each MPC against the Prediction Horizon with fixed SUs $= 4$. . . . 117
8.21 Computation time for each MPC against the number of MPCs with fixed $N = 10$. . . . 118

9.1 Control diagram including uncertainty measurements. . . . 122
9.2 Volume for a range of u_p. . . . 123
9.3 Volume for a range of u_p zoomed in. . . . 123
9.4 Overestimation of u_{off}. . . . 124
9.5 Underestimation of u_{off}. . . . 125
9.6 Outflow for a range of u_p. . . . 127
9.7 Outflow for a range of u_p zoomed in. . . . 127
9.8 Overestimation of u_{off}. . . . 128
9.9 Underestimation of u_{off}. . . . 129
9.10 Overflow uncertainty for u_p in different ranges. . . . 130
9.11 Overestimation of u_{off}. . . . 131
9.12 Underestimation of u_{off}. . . . 132
9.13 CC-MPC scheme. . . . 134
9.14 SVMPC scheme for Urban Drainage Systems. . . . 136

9.15 Confidence level. . . . 141
9.16 Morris screening for SVMPC - $Q_{\text{ov}_{\text{total}}}$. . . . 152
9.17 Morris screening for SVMPC - ξ. . . . 152
9.18 Grid Search SA for SVMPC for Scenario 1. . . . 154
9.19 Random Search applied to Scenario 2. . . . 156
9.20 Pareto front SVMPC. . . . 157
9.21 SPWMPC scheme for Urban Drainage Systems. . . . 168
9.22 Morris screening for $m^{\text{NH}_4}_{\text{ov}_{\text{total}}}$. . . . 175
9.23 Morris screening for ξ. . . . 176
9.24 Grid Search SA for SPWMPC for Scenario 1. . . . 177
9.25 Random Search applied to Scenario 2. . . . 178
9.26 Pareto front SPWMPC. . . . 178
9.27 SNPMPC scheme for Urban Drainage Systems. . . . 185
9.28 Morris screening for $m^{\text{NH}_4}_{\text{ov}_{\text{total}}}$ and ξ. . . . 194
9.29 Grid Search SA for SNPMPC with base values. . . . 194
9.30 Random Search. . . . 195
9.31 Pareto front SPWMPC. . . . 196

10.1 Example of State Machine with $V_{\text{controlled}}$, $V_{\text{controllable}}$, $Q_{\text{in}_{\text{controlled}}}$ and $Q_{\text{in}_{\text{controllable}}}$. 206
10.2 Urban Drainage System 1 - red line indicates sections that are controlled by MPC - green line indicates sections that are measured, but not controlled by MPC - blue line indicate sections that are not controlled by MPC and not measured - gray line indicates sections unknown to MPC and not considered in the formulation. . . . 207
10.3 Schema for controlled section of Urban Drainage System 1. . . . 208
10.4 Normalized daily patterns sampled hourly. . . . 208
10.5 Dry weather flow for the Storage Units. . . . 209
10.6 Runoff for Storage Units for the year of 2019. . . . 210
10.7 Q_{ov} and $m^{\text{NH}_4}_{\text{ov}}$ for Urban Drainage System 1 with static control. . . . 211
10.8 Urban Drainage System 1 with static control for Period 1. . . . 212
10.9 Urban Drainage System 1 with static control for Period 2. . . . 213
10.10 Urban Drainage System 1 - Period 1 - Pareto front. . . . 214
10.11 Urban Drainage System 1 - Period 2 - Pareto front. . . . 215
10.12 R_{V} - Relative Overflow Volume % using weights identified in Period 1. . . . 217
10.13 R_{m} - Relative Overflow Load % using weights identified in Period 1. . . . 217
10.14 Urban Drainage System 1 - Comparison of MPC in terms of total overflow volume and load using weights identified in Period 1. . . . 218
10.15 R_{V} - Relative Overflow Volume % using weights identified in Period 2. . . . 218

10.16 R_m - Relative Overflow Load % using weights identified in Period 2. 219
10.17 Urban Drainage System 1 - Comparison of MPC in terms of total overflow volume and load using weights identified in Period 2. 219
10.18 Accumulated Runoff over 1 year period. 220
10.19 Accumulated Runoff and Overflow for the Static Control with Highlighted Regions. 221
10.20 Comparison of overflow load and volume improvement between VMPC and static control across four regions with varying hydrological characteristics. . 222
10.21 Comparison of overflow load and volume improvement between NPMPC and static control across four regions with varying hydrological characteristics. 222
10.22 Urban Drainage System 2 - red line indicates sections that are controlled by MPC - blue line indicate sections that are not controlled by MPC and not measured - yellow triangle is an industrial flow. 225
10.23 Schema for controlled section of Urban Drainage System 2. 225
10.24 Normalized daily patterns sampled hourly. 226
10.25 Dry weather flow for the Storage Units. 227
10.26 Runoff for Storage Units between June 1st 2023 until June 1st 2024. 227
10.27 Q_{ov} and m_{ov}^{COD} for Urban Drainage System 2 with static control. 229
10.28 Urban Drainage System 2 with static control from November 9th to November 16th. 230
10.29 R_V - Relative Overflow Volume % for NH_4^+. 232
10.30 R_m - Relative Overflow Load % for NH_4^+. 232
10.31 Urban Drainage System 2 - Comparison of MPC in terms of total overflow volume and load for NH_4^+. 233
10.32 R_V - Relative Overflow Volume % for COD. 233
10.33 R_m - Relative Overflow Load % for COD. 234
10.34 Urban Drainage System 2 - Comparison of MPC in terms of total overflow volume and load for COD. 234
10.35 R_V - Relative Overflow Volume % for COD. 235
10.36 R_m - Relative Overflow Load % for COD. 236
10.37 Urban Drainage System 2 - Comparison of MPC in terms of total overflow volume and load for COD with updated weights. 237
10.38 Accumulated Runoff over 1 year period. 237
10.39 Accumulated Runoff and Overflow for the Static Control with Highlighted Regions. 238

10.40Comparison of overflow load and volume improvement between VMPC and static control across four regions with varying hydrological characteristics. . 238
10.41Comparison of overflow load and volume improvement between NPMPC and static control across four regions with varying hydrological characteristics. 239
10.42Urban Drainage System 3 - red line indicates sections that are controlled by MPC - green line indicate sections that are not controlled by MPC but are measured. 240
10.43Schema for controlled section of Urban Drainage System 3. 241
10.44Dry weather flow for the Storage Units. 242
10.45Accumulated runoff at Urban Drainage System 3. 243
10.46Q_{ov} and m_{ov}^{NH4} for Urban Drainage System 3 with static control. 244
10.47Boxplot comparing the computation cost (in seconds) of each MPC strategy.245

11.1 Feasibility instances for NPMPC. 250
11.2 Feasibility instances for SNPMPC. 250
11.3 Feasibility instances for NPMPC with uncertainty $u_p = 50\%$ and $u_{off} = -50\%$. 250
11.4 Feasibility instances for SNPMPC with uncertainty $u_p = 50\%$ and $u_{off} = -50\%$. 251
11.5 Outflow comparison (left y-axis) of controllers with and without uncertainties, including feasible solutions for uncertain scenario (right y-axis). 251
11.6 Feasibility instances for NPMPC with NH_4^+ as controlled pollutant. 252
11.7 Feasibility instances for NPMPC with COD as controlled pollutant. 252
11.8 Feasibility instances for SNPMPC with NH_4^+ as controlled pollutant. 253
11.9 Feasibility instances for SNPMPC with COD as controlled pollutant. 253
11.10Diagram for Fallback strategy 1: Multi-layer and Stochastic Multi-layer. . . 254
11.11Diagram for Fallback strategy 2: Multi-layer and Stochastic Multi-layer. . . 255
11.12Diagram for Fallback strategy 3: Multi-layer and Stochastic Multi-layer. . . 256
11.13R_V - Relative Overflow Volume %. 256
11.14R_m - Relative Overflow Load %. 257
11.15ML-MPC and SML-MPC - Urban Drainage System 1 - Absolute overflow comparison of MPC without additional uncertainty. 257
11.16R_V - Relative Overflow Volume %. 258
11.17R_m - Relative Overflow Load %. 258
11.18ML-MPC and SML-MPC - Urban Drainage System 1 - Absolute overflow comparison of MPC with additional uncertainty. 259
11.19R_V - Relative Overflow Volume % with NH_4^+ as pollutant indicator. 259

11.20 R_m - Relative Overflow Load % with NH_4^+ as pollutant indicator. 260
11.21 Urban Drainage System 2 - Comparison of MPC in terms of total overflow volume and load with NH_4^+ as pollutant indicator. 260
11.22 R_V - Relative Overflow Volume % with COD as pollutant indicator. 261
11.23 R_m - Relative Overflow Load % with COD as pollutant indicator. 261
11.24 Urban Drainage System 2 - Comparison of MPC in terms of total overflow volume and load with COD as pollutant indicator. 262
11.25 Multi-layer for full period between 01/01/2025 and 31/12/2025. 264
11.26 Comparison of control action (left y-axis) from SNPMPC and SML-MPC FBS1, and which layer is used (right y-axis) in Period 2. 265
11.27 Comparison of control action (right y-axis) from SNPMPC and SML-MPC FBS2, and which layer is used (right y-axis) in Period 2. 266
11.28 Comparison of control action (left y-axis) from SNPMPC and SML-MPC FBS1, and which layer is used (right y-axis) in Period 5. 267
11.29 Comparison of control action (left y-axis) from SNPMPC and SML-MPC FBS2, and which layer is used (right y-axis) in Period 5. 267

A.1 Grid Search SA for $Q_{ov_{total}}$ from May 1 to June 1 for $\epsilon = 3, 21$ for VMPC. . 271
A.2 Grid Search SA for $Q_{ov_{total}}$ from May 1 to June 1 for $\epsilon = 52, 89$ for VMPC. 271
A.3 Grid Search SA for $Q_{ov_{total}}$ from May 1 to June 1 for $\epsilon = 102, 153$ for VMPC. 272
A.4 Grid Search SA for ξ from May 1 to June 1 for $\epsilon = 3, 21$ for VMPC. 272
A.5 Grid Search SA for ξ from May 1 to June 1 for $\epsilon = 52, 89$ for VMPC. . . . 272
A.6 Grid Search SA for ξ from May 1 to June 1 for $\epsilon = 102, 153$ for VMPC. . . 273
A.7 Grid Search SA for $Q_{ov_{total}}$ from March 24 to April 24 for $\epsilon = 3, 21$ for VMPC. 273
A.8 Grid Search SA for $Q_{ov_{total}}$ from March 24 to April 24 for $\epsilon = 52, 89$ for VMPC. 273
A.9 Grid Search SA for $Q_{ov_{total}}$ from March 24 to April 24 for $\epsilon = 102, 153$ for VMPC. 274
A.10 Grid Search SA for ξ from March 24 to April 24 for $\epsilon = 3, 21$ for VMPC. . 274
A.11 Grid Search SA for ξ from March 24 to April 24 for $\epsilon = 52, 89$ for VMPC. . 274
A.12 Grid Search SA for ξ from March 24 to April 24 for $\epsilon = 102, 153$ for VMPC. 275
A.13 Random Search Sensitivity Analysis from May 1 to July 1 for VMPC. . . . 275
A.14 Random Search Sensitivity Analysis from March 24 to April 24 for VMPC. 275
A.15 Grid Search SA for $m_{ov_{total}}^{NH_4}$ with $\beta = 1, 113$ and for NPMPC. 276
A.16 Grid Search SA for $m_{ov_{total}}^{NH_4}$ with $\beta = 226$, for ξ with $\beta = 1$ and for NPMPC. 276
A.17 Grid Search SA for ξ with $\beta = 113, 226$ and for NPMPC. 277
A.18 Grid Search SA for $m_{ov_{total}}^{NH_4}$ with $\gamma = 1, 33$ and for NPMPC. 277
A.19 Grid Search SA for $m_{ov_{total}}^{NH_4}$ with $\gamma = 66$, for ξ with $\gamma = 1$ and for NPMPC. 277

A.20 Grid Search SA for ξ with $\gamma = 33, 66$ and for NPMPC. 278
A.21 Grid Search SA for $m^{\mathrm{NH_4}}_{\mathrm{ov_{total}}}$ with $\epsilon = 98, 189$ and for NPMPC. 278
A.22 Grid Search SA for ξ with $\epsilon = 98, 189$ and for NPMPC. 278
A.23 Grid Search SA for $m^{\mathrm{NH_4}}_{\mathrm{ov_{total}}}$ with $\tau = 42, 84$ and for NPMPC. 279
A.24 Grid Search SA for ξ with $\tau = 42, 84$ and for NPMPC. 279
A.25 Morris Screening for Urban Drainage System 1. 287
A.26 Comparison of overflow load and volume improvement between PWMPC and static control across four regions with varying hydrological characteristics. 287
A.27 Comparison of overflow load and volume improvement between SVMPC and static control across four regions with varying hydrological characteristics. 287
A.28 Comparison of overflow load and volume improvement between SPWMPC and static control across four regions with varying hydrological characteristics. 288
A.29 Comparison of overflow load and volume improvement between SNPMPC and static control across four regions with varying hydrological characteristics. 288
A.30 Comparison of overflow load and volume improvement between PWMPC and static control across four regions with varying hydrological characteristics. 289
A.31 Comparison of overflow load and volume improvement between SVMPC and static control across four regions with varying hydrological characteristics. 289
A.32 Comparison of overflow load and volume improvement between SPWMPC and static control across four regions with varying hydrological characteristics. 290
A.33 Comparison of overflow load and volume improvement between SNPMPC and static control across four regions with varying hydrological characteristics. 290
A.34 Multi-layer for period between 01/01/2025 and 01/03/2025 with $u_{\mathrm{off}} = -10\%$. 291
A.35 Multi-layer for period between 01/03/2025 and 01/05/2025 with $u_{\mathrm{off}} = -10\%$. 292
A.36 Multi-layer for period between 01/05/2025 and 01/07/2025 with $u_{\mathrm{off}} = -10\%$. 293
A.37 Multi-layer for period between 01/07/2025 and 01/09/2025 with $u_{\mathrm{off}} = -10\%$. 294
A.38 Multi-layer for period between 01/09/2025 and 31/12/2025 with $u_{\mathrm{off}} = -10\%$. 295

List of Tables

6.1 Variables and their definitions [75]. 29
6.2 Control rules implemented in [90]. 37
6.3 Papers on rule-based RTC methods with pollution aspects. 40
6.4 Papers on optimisation-based RTC methods with pollution aspects. 46

7.1 Single SU configuration - Urban Drainage System Parameters. 63
7.2 Metric results for 1-month simulation with Single SU configuration. 64
7.3 Parallel SU configuration - Urban Drainage System parameters. 65
7.4 Metric results for 1-month simulation with Parallel SU configuration. . . . 65
7.5 Parallel SU configuration - Urban Drainage System parameters. 67
7.6 Metric results for 1-month simulation with Parallel SU configuration. . . . 68
7.7 Parallel + Series SU configuration - Urban Drainage System parameters. . 70
7.8 Overall results for first scenario. 71
7.9 GA Simulations. 80
7.10 Results for optimised weights α, β, γ, $\epsilon = (6.9, 56.5, 106.4, 153.0)$. 82
7.11 Comparison of Computation Times in seconds (Mean $\pm$ Std) for VMPC. . 83
7.12 Comparison of results for scenarios with and without industry. 85

8.1 Results for weights α, β, γ, ϵ, ψ, ω, τ, $\upsilon = (64.6, 148.6, 91.0, 189.0, 28.0, 76.2, 28.3, 0.8)$. 98
8.2 Results for weights α, β, γ, ϵ, ψ, ω, τ, υ = (11.2, 228.6, 90.7, 190.0, 10.0, 241.4, 19.4, 0.04). 105
8.3 Comparison of Computation Times in seconds (Mean $\pm$ Std) for NPMPC. 105
8.4 Results for weights α, β, γ, $\epsilon = (33, 126, 38, 150)$. 111
8.5 Results for weights α, β, γ, $\epsilon = (19.1, 149.1, 30.1, 190.0)$. 116
8.6 Comparison of Computation Times (Mean $\pm$ Std) for PWMPC. 117

9.1 Volume uncertainty: Analysis of ξ_{rain}, volume and load overflow for u_p. . . 124
9.2 Volume uncertainty: Analysis of ξ_{rain}, volume and load overflow for $u^{\text{vol+}}_{\text{offset}}$. . 125
9.3 Volume uncertainty: Analysis of ξ_{rain}, volume and load overflow for $u^{\text{vol-}}_{\text{offset}}$. . 126
9.4 Outflow uncertainty: Analysis of ξ_{rain}, volume and load overflow for u_p. . . 128
9.5 Outflow uncertainty: Analysis of ξ_{rain}, volume and load overflow for $u^{\text{out+}}_{\text{offset}}$. 129

9.6 Outflow uncertainty: Analysis of ξ_{rain}, volume and load overflow for $u_{\text{offset}}^{\text{out-}}$. 130
9.7 Overflow uncertainty: Analysis of volume and load overflow for u_p. 131
9.8 Overflow uncertainty: Analysis of volume and load overflow for $u_{\text{offset}}^{\text{ov+}}$. . . . 132
9.9 Overflow uncertainty: Analysis of volume and load overflow for $u_{\text{offset}}^{\text{ov-}}$. . . . 133
9.10 Volume uncertainty: Comparison between VMPC and SVMPC for u_p. . . . 142
9.11 Volume uncertainty: Comparison between VMPC and SVMPC for $u_{\text{offset}}^{\text{vol+}}$. . 143
9.12 Volume uncertainty: Comparison between VMPC and SVMPC for $u_{\text{offset}}^{\text{vol-}}$. . 144
9.13 Outflow uncertainty: Comparison between VMPC and SVMPC for u_p. . . 145
9.14 Outflow uncertainty: Comparison between VMPC and SVMPC for $u_{\text{offset}}^{\text{out+}}$. . 146
9.15 Outflow uncertainty: Comparison between VMPC and SVMPC for $u_{\text{offset}}^{\text{out-}}$. . 147
9.16 Overflow uncertainty: Comparison between VMPC and SVMPC for u_p. . . 148
9.17 Overflow uncertainty: Comparison between VMPC and SVMPC for $u_{\text{offset}}^{\text{ov+}}$. 149
9.18 Overflow uncertainty: Comparison between VMPC and SVMPC for $u_{\text{offset}}^{\text{ov-}}$. 150
9.19 Scenarios for Morris screening Sensitivity Analysis. 151
9.20 Grid Search applied for all scenarios. 155
9.21 Optimal (α, β, γ, ϵ) for each uncertainty scenario. 156
9.22 Volume uncertainty: Comparison between VMPC and optimal SVMPC with u_p. 158
9.23 Volume uncertainty: Comparison between VMPC and optimal SVMPC for $u_{\text{offset}}^{\text{vol+}}$. 159
9.24 Volume uncertainty: Comparison between VMPC and optimal SVMPC for $u_{\text{offset}}^{\text{vol-}}$. 160
9.25 Outflow uncertainty: Comparison between VMPC and optimal SVMPC for u_p. 161
9.26 Outflow uncertainty: Comparison between VMPC and optimal SVMPC for $u_{\text{offset}}^{\text{out+}}$. 162
9.27 Outflow uncertainty: Comparison between VMPC and optimal SVMPC for $u_{\text{offset}}^{\text{out-}}$. 163
9.28 Overflow uncertainty: Comparison between VMPC and optimal SVMPC for u_p. 164
9.29 Overflow uncertainty: Comparison between VMPC and optimal SVMPC for $u_{\text{offset}}^{\text{ov+}}$. 165
9.30 Overflow uncertainty: Comparison between VMPC and optimal SVMPC for $u_{\text{offset}}^{\text{ov-}}$. 166
9.31 Volume uncertainty: Comparison between PWMPC and SPWMPC for u_p. 172
9.32 Volume uncertainty: Comparison between PWMPC and SPWMPC for $u_{\text{offset}}^{\text{vol-}}$. 173

9.33 Outflow uncertainty: Comparison between PWMPC and SPWMPC for $u_{\text{offset}}^{\text{out-}}$. . . . 174
9.34 Grid Search applied for all scenarios. . . . 177
9.35 Optimal (α, β, γ, ϵ) for each uncertainty scenario. . . . 179
9.36 Volume uncertainty: Comparison between PWMPC and optimal SPWMPC for u_p. . . . 180
9.37 Volume uncertainty: Comparison between PWMPC and optimal SPWMPC for $u_{\text{offset}}^{\text{vol-}}$. . . . 182
9.38 Outflow uncertainty: Comparison between PWMPC and optimal SPWMPC for $u_{\text{offset}}^{\text{out-}}$. . . . 183
9.39 Volume uncertainty: Comparison between NPMPC and SNPMPC for u_p. . . . 191
9.40 Volume uncertainty: Comparison between NPMPC and SNPMPC for $u_{\text{offset}}^{\text{vol+}}$. . . . 192
9.41 Volume uncertainty: Comparison between NPMPC and SNPMPC for $u_{\text{offset}}^{\text{vol-}}$. . . . 193
9.42 Optimal (α, β, γ, ϵ, ψ, ω, υ) for each uncertainty scenario. . . . 196
9.43 Volume uncertainty: Comparison between NPMPC and optimal SNPMPC for u_p. . . . 198
9.44 Volume uncertainty: Comparison between NPMPC and optimal SNPMPC for $u_{\text{offset}}^{\text{vol+}}$. . . . 199
9.45 Volume uncertainty: Comparison between NPMPC and optimal SNPMPC for $u_{\text{offset}}^{\text{vol-}}$. . . . 200
9.46 Volume uncertainty: Analysis of $u_{\text{offset}}^{\text{vol-}}$ for all MPCs. . . . 201
9.47 Volume uncertainty: Analysis of $u_{\text{offset}}^{\text{vol+}}$ for all MPCs. . . . 202

10.1 Additional parameters in the model for Urban Drainage System 2. . . . 208
10.2 Total overflow volume and load for Urban Drainage System 1 with static control . . . 210
10.3 Weights Ranges for Urban Drainage System 1 for each MPC. . . . 214
10.4 Optimal Weights for Urban Drainage System 1 for each MPC and Period. . . 216
10.5 Comparison of results for Urban Drainage System 1 with uncertainties and $Q_{\text{ov}_{\text{sensitivity}}} = (5, 1, 3, 5)$. Rows in red indicate SUs with higher weight sensitivity. . . . 223
10.6 Comparison of results for Urban Drainage System 1 considering the complete network. . . . 224
10.7 Additional parameters in the model. . . . 227
10.8 Total overflow volume and load for Urban Drainage System 2 with static control. . . . 230
10.9 Optimal Weights for Urban Drainage System 2 for each MPC. . . . 231

10.10 New Optimal Weights for Urban Drainage System 2 for each MPC to control COD. . . . 235
10.11 Comparison between MPC methods with updated weights controlling COD. Methods followed by * are the ones with updated weights. Each cell corresponds to the pair (R_V, R_m) for a MPC at a specific SU. Columns with light red colouring represent the SUs with higher $Q_{ov_{sensitivity}}$. . . . 236
10.12 Model parameters. . . . 242
10.13 Descriptive statistics of computation time (in seconds) for each MPC method. 245
10.14 Comparison of results for Urban Drainage System 3. . . . 247

11.1 Settings for multi-layer simulation. . . . 262
11.2 Heatmap comparing R_m^i (%) and $m_{ov_{total}}^{NH_4}$ (kg) for each MPC strategy. . . . 263
11.3 Number of times each MPC was used by each ML-MPC strategy. . . . 265

12.1 Recommended MPC methods for Urban Drainage Systems based on system characteristics and uncertainty levels. . . . 270

A.1 Volume uncertainty: Comparison between PWMPC and SPWMPC for overestimating u_{off} . . . 280
A.2 Outflow uncertainty: Comparison between PWMPC and SPWMPC for u_p 280
A.3 Outflow uncertainty: Comparison between PWMPC and SPWMPC for overestimating u_{off} . . . 280
A.4 Overflow uncertainty: Comparison between PWMPC and SPWMPC for u_p 280
A.5 Overflow uncertainty: Comparison between PWMPC and SPWMPC for overestimating u_{off} . . . 280
A.6 Overflow uncertainty: Comparison between PWMPC and SPWMPC for underestimating u_{off} . . . 281
A.7 Volume uncertainty: Comparison between PWMPC and optimal SPWMPC for overestimating u_{off} . . . 281
A.8 Outflow uncertainty: Comparison between PWMPC and optimal SPWMPC for u_p . . . 281
A.9 Outflow uncertainty: Comparison between PWMPC and optimal SPWMPC for overestimating u_{off} . . . 281
A.10 Overflow uncertainty: Comparison between PWMPC and optimal SPWMPC for u_p . . . 281
A.11 Overflow uncertainty: Comparison between PWMPC and optimal SPWMPC for overestimating u_{off} . . . 282
A.12 Overflow uncertainty: Comparison between PWMPC and optimal SPWMPC for underestimating u_{off} . . . 282

A.13 Outflow uncertainty: Comparison between NPMPC and SNPMPC for u_p . 283
A.14 Outflow uncertainty: Comparison between NPMPC and SNPMPC for overestimating u_{off} . . . 283
A.15 Outflow uncertainty: Comparison between NPMPC and SNPMPC for underestimating u_{off} . . . 283
A.16 Overflow uncertainty: Comparison between NPMPC and SNPMPC for u_p 283
A.17 Overflow uncertainty: Comparison between NPMPC and SNPMPC for overestimating u_{off} . . . 283
A.18 Overflow uncertainty: Comparison between NPMPC and SNPMPC for underestimating u_{off} . . . 284
A.19 Outflow uncertainty: Comparison between NPMPC and optimal SNPMPC for u_p . . . 284
A.20 Outflow uncertainty: Comparison between NPMPC and optimal SNPMPC for overestimating u_{off} . . . 284
A.21 Outflow uncertainty: Comparison between NPMPC and optimal SNPMPC for underestimating u_{off} . . . 284
A.22 Overflow uncertainty: Comparison between NPMPC and optimal SNPMPC for u_p . . . 284
A.23 Overflow uncertainty: Comparison between NPMPC and optimal SNPMPC for overestimating u_{off} . . . 285
A.24 Overflow uncertainty: Comparison between NPMPC and optimal SNPMPC for underestimating u_{off} . . . 285

Acronyms

ANN Artificial Neural Network. xiii, 30–33

BOD Biochemical Oxygen Demand. 22, 27, 32–34

CC-MPC Chance-Constrained Model Predictive Control. xv, 133–135, 167, 181, 184

COD Chemical Oxygen Demand. xvii–xix, xxiv, xxxii, 5, 16, 17, 19, 21, 22, 26, 27, 32, 33, 38–40, 84, 85, 225–231, 233–237, 251–253, 259–262

CSO Combined Sewer Overflow. 1, 9, 14, 21, 39, 57, 58, 61, 82, 87, 120, 229

DO Dissolved Oxygen. 22, 33, 34

DODE Deterministic Ordinary Differential Equations Models. 22, 23

DWF Dry Weather Flow. xiv, 15, 21, 59, 60, 62, 64, 70, 74, 85, 89, 90, 208, 226, 227, 240, 241

FBS Fallback Strategy. xix, 253, 256, 260, 262–268

GA Genetic Algorithm. 6, 78–80, 82–85, 103, 110, 114, 122, 155, 158, 176, 178, 181, 214, 218, 220, 222, 223, 231, 234, 246, 247, 269

GRU Recurrent Gate Unit. 29, 33

GSA Global Sensitivity Analysis. 6, 71–73, 75, 99, 100, 110, 112, 151, 212

LSA Local Sensitivity Analysis. xiv, 6, 71, 73, 75, 99, 110, 151, 212

LSTM Long Short-term Memory. 29, 33

ML Machine Learning. 2

ML-MPC Multi-Layer Model Predictive Control. xviii, xxiv, 1, 3, 4, 6, 7, 249, 252–260, 262–265, 269, 270, 291

MLP Multilayer Perceptron. 29, 31–33

MLR Multi Linear Regression. xiii, 29–31, 33

MPC Model Predictive Control. xiv–xix, xxiii, xxiv, xxxi, xxxiii, 1–7, 9, 15, 36, 41, 42, 44, 46, 49, 51–57, 61, 75, 78, 82, 84, 85, 87, 89, 103, 107, 110, 114, 115, 117–120, 122–125, 127–129, 131–133, 135, 201, 203, 205–210, 212–214, 216–224, 226, 230, 231, 233–237, 239, 240, 243–247, 249, 253–255, 257, 259, 260, 262, 263, 265, 269, 270

NH_4^+ Ammonium Ion. xvii–xix, xxxii, 5, 16, 17, 19, 21, 22, 32, 33, 40, 98, 103, 122, 221, 224–226, 228, 229, 231–234, 236, 237, 251–253, 259, 260

NO_X Oxides of Nitrogen. 22, 27

NPMPC Nonlinear Pollution-based Model Predictive Control. xiv, xv, xvii–xxi, 3, 7, 56, 87–89, 92, 94, 97–99, 102–107, 110, 111, 115–117, 122–126, 128, 129, 132, 135, 167, 181, 184, 188–190, 196, 197, 201, 213–216, 218, 221–224, 231, 233–236, 238, 239, 245–247, 249–252, 254, 257, 259, 260, 262, 264, 265, 268–270, 276–279, 283, 286

PDE Partial Differential Equations. 22, 23

PE People Equivalent. 91, 207–209, 226, 239, 240

PID Proportional-Integral-Derivative. 57, 253

PLC Programmable Logic Controller. 57

PMPC Pollution-based Model Predictive Control. 49

PRTC Pollution-based Real-Time Control. 10, 36, 49

PWMPC Pollution-weighted Model Predictive Control. xv, xx, xxi, xxxi, 3, 7, 56, 107, 109–117, 122, 124–129, 132, 135, 167, 170–172, 179, 181, 201, 202, 213–219, 223, 224, 231, 235, 236, 247, 249, 254, 260, 263–265, 267, 269, 270, 280, 286, 287, 289

RL Reinforcement Learning. 36, 45, 47, 48

RNN Recurrent Neural Network. 29, 33

RTC Real-Time Control. 1, 2, 4–7, 9, 10, 12, 14, 17, 19, 20, 23, 26, 27, 29, 36–42, 44–49, 57, 58, 82, 87, 120, 243

SA Sensitivity Analysis. xvi, 71, 72, 79, 80, 82, 103, 114, 154, 155, 178, 214, 247, 269

SCADA Supervisory Control and Data Acquisition. 243

SI International System of Units - Système International d'unités. 2, 169, 170

SML-MPC Stochastic Multi-Layer Model Predictive Control. xviii, xix, 254, 257, 259–270

SMPC Stochastic Model Predictive Control. xxxi, 7, 133, 135

SNPMPC Stochastic Nonlinear Pollution-based Model Predictive Control. xvi, xviii–xx, xxxi, 56, 184, 185, 189–191, 194, 195, 197, 201, 202, 213–216, 218, 223, 224, 231–237, 245–247, 249–254, 257–259, 262–270, 283, 287, 288, 290

SODE Stochastic Ordinary Differential Equations. 22, 23

SPWMPC Stochastic Pollution-weighted Model Predictive Control. xvi, xx, 56, 167, 168, 171, 172, 177–179, 181, 201, 213–216, 218, 219, 223, 224, 231, 232, 235, 236, 247, 249, 254, 262, 264–266, 268–270, 280, 286, 288, 290

SU Storage Unit. xiii, xiv, xxi, xxiii, xxiv, 14–21, 23–27, 36–39, 43, 46, 56–61, 63–71, 75, 80, 82–85, 87–96, 98, 104–109, 111, 116, 117, 120–122, 124, 125, 127, 129, 140, 153, 167, 189, 205, 207–210, 212, 213, 216–220, 223–229, 231, 233, 235, 236, 239–242, 251, 257–264, 266

SVMPC Stochastic Volume-based Model Predictive Control. xv, xvi, xx, 56, 135, 136, 138–146, 148, 151–155, 157, 158, 162, 163, 165–168, 172, 175, 176, 179, 181, 184, 201, 213–216, 218, 219, 223, 224, 231–233, 247, 249, 264–266, 268–270, 286, 287, 289

SWMM Storm Water Management Model. xiii, 11–15, 18, 20, 21, 34, 49

TKN Total Kjedahl Nitrogen. 22, 27, 32, 33

TP Total Phosphorus. 22, 27, 32, 33

TSS Total Suspended Solids. xxxii, 22, 26, 27, 35, 37, 38, 40–42, 46–48

UDS Urban Drainage System. 1, 2, 4–7, 9, 10, 12, 14, 49, 58, 60, 61, 63, 65, 73, 80, 82, 84, 87, 97, 98, 107, 110, 120, 122, 136, 139, 168, 170, 184, 189, 202, 203, 224, 226, 231, 237, 244, 249, 253, 269

VMPC Volume-based Model Predictive Control. xiv, xv, xvii–xix, xxi, 3, 7, 56–72, 77, 79, 82–85, 94, 98, 100, 103, 105–108, 110–112, 115–117, 122–126, 128, 129, 132, 135, 136, 138, 141–146, 148, 151, 153, 157, 162–165, 167, 202, 213–219, 221–224, 231, 233, 237, 238, 246, 247, 249, 255, 263–265, 269–275, 286

WWF Wet Weather Flow. xiv, 15, 19–21, 59, 60, 62–65, 68, 70, 74, 77, 82, 85, 89–91

WWTP Wastewater Treatment Plant. 6, 9, 10, 15, 17–21, 40–42, 46, 59–71, 73, 82, 94–99, 102, 103, 105, 109, 111, 112, 116, 122, 123, 125, 129, 139, 163, 169, 181, 187, 188, 207, 215, 216, 224, 226, 229, 239–241, 243

4 Symbols

Greek letters

Symbol	Description	Unit
β_x	Weights for each pollutant x in the effluent quality index model	-
ρ	Regression coefficients for the independent variables in MLP Model	-
χ	Errors associated with MLP Model	-
$\Xi_{i,\text{perv}}$	Total constituent loads from the ith pervious region	kg/h
$\Xi_{i,\text{imp}}$	Total constituent loads from the ith impervious region	kg/h
Ξ_{DWF_i}	Total constituent loads from the ith dry weather flow region	kg/h
ϕ	Specific objective function	-
α	MPC weight for volume homogeneity minimisation	-
β	MPC weight for tracking inflow to the Wastewater Treatment Plant	-
γ	MPC weight for volume overflow minimisation	-
ψ	MPC weight for load homogeneity minimisation	-
ω	MPC weight for load overflow minimisation	-
τ	MPC weight for uncertainty minimisation	-
υ	MPC weight for load inflow to Wastewater Treatment Plant maximisation	-
θ	Slack variable for volume constraint used in MPC	-
θ_{min}	Lower bound slack variable for volume constraint used in SMPC	-
θ_{max}	Upper bound slack variable for volume constraint used in SMPC	-
θ^c_{max}	Upper bound slack variable for concentration constraint used in SNPMPC	-
ϵ	MPC weight for slack minimisation	-
ξ	Error between inflow and reference inflow to the Wastewater Treatment Plant	-
ξ_{rain}	Error between inflow and reference inflow to the Wastewater Treatment Plant during rain events	-
μ	Mean of a variable	-
σ	Standard deviation of a variable	-
φ	Weighting factor for concentration in PWMPC	-
ζ	Confidence level parameter for stochastic methods	-

Latin letters

Symbol	Description	Unit
C	Concentration within a Storage Unit	kg/m^3 or mg/L
C_{DW}	Concentration of dry-weather inflow	kg/m^3 or mg/L
C_{WW}	Concentration of wet-weather inflow	kg/m^3 or mg/L
$C_{\mathrm{in}_{\mathrm{cascade}}}$	Concentration of inflow at a Storage Unit from upstream units	kg/m^3 or mg/L
$C_{\mathrm{in}_{\mathrm{catchment}}}$	Concentration of inflow at a Storage Unit from catchment	kg/m^3 or mg/L
$C_{\mathrm{in}_{\mathrm{infiltration}}}$	Concentration of inflow at a Storage Unit from infiltration	kg/m^3 or mg/L
d	Time delay	s
EE	Elementary effect in Morris Screening	-
EQI	Effluent quality index	kg/h or g/s
h	Water level	m
I_{m}	Improvement metric for volume overflow	%
I_{m}	Improvement metric for load overflow	%
J	Cost function of an optimisation problem	-
k	Discrete time variable	s
m	Mass within a Storage Unit	kg/h or mg/s
m_{in}	Mass entering a Storage Unit	kg/h or mg/s
$m_{\mathrm{in}}^{\mathrm{COD}}$	Mass of COD entering a Storage Unit	kg/h or mg/s
$m_{\mathrm{in}}^{\mathrm{NH4}}$	Mass of NH_4^+ entering a Storage Unit	kg/h or mg/s
$m_{\mathrm{in}}^{\mathrm{TSS}}$	Mass of TSS entering a Storage Unit	kg/h or mg/s
$m_{\mathrm{in}_{\mathrm{catchment}}}$	Mass of inflow at a Storage Unit from catchment	kg/h or mg/s
$m_{\mathrm{in}_{\mathrm{cascade}}}$	Mass of inflow at a Storage Unit from upstream units	kg/h or mg/s
$m_{\mathrm{in}_{\mathrm{infiltration}}}$	Mass of inflow at a Storage Unit from infiltration	kg/h or mg/s
m_{out}	Mass leaving a Storage Unit	kg/h or mg/s
$m_{\mathrm{out}}^{\mathrm{COD}}$	Mass of COD leaving a Storage Unit	kg/h or mg/s
$m_{\mathrm{out}}^{\mathrm{NH4}}$	Mass of NH_4^+ leaving a Storage Unit	kg/h or mg/s
$m_{\mathrm{out}}^{\mathrm{TSS}}$	Mass of TSS leaving a Storage Unit	kg/h or mg/s
$m_{\mathrm{out}_{\mathrm{catchment}}}$	Mass of inflow at a Storage Unit from catchment	kg/h or mg/s
$m_{\mathrm{out}_{\mathrm{cascade}}}$	Mass of inflow at a Storage Unit from upstream units	kg/h or mg/s
$m_{\mathrm{out}_{\mathrm{infiltration}}}$	Mass of inflow at a Storage Unit from infiltration	kg/h or mg/s
$m_{\mathrm{ov_i}}$	Mass overflow of i-th Storage Unit	m^3/h or L/s
$m_{\mathrm{ov}_{\mathrm{total}}}$	Total load overflow of a Storage Unit	m^3/h or L/s
$m_{\mathrm{ov_i}}^{\mathrm{COD}}$	Mass of COD in overflow of i-th Storage Unit	kg/h or mg/s
$m_{\mathrm{ov}_{\mathrm{total}}}^{\mathrm{COD}}$	Sum of load of COD in overflow of all Storage Units	kg/h or mg/s
$m_{\mathrm{ov_i}}^{\mathrm{NH4}}$	Mass of NH_4^+ in overflow of i-th Storage Unit	kg/h or mg/s
$m_{\mathrm{ov}_{\mathrm{total}}}^{\mathrm{NH4}}$	Sum of load of NH_4^+ in overflow of all Storage Units	kg/h or mg/s

Symbol	Description	Unit
N	Prediction horizon of MPC	s
N_t	Number of Storage Units in Urban Drainage System	-
N^*_{wwtp}	Number of Storage Units upstream to the Wastewater Treatment Plant	
P	Probability indicator	%
Q_{DW}	Dry-weather inflow	m^3/h or L/s
Q_{in}	Inflow of a Storage Unit	m^3/h or L/s
$Q_{\text{in}_{\text{cascade}}}$	Inflow at a Storage Unit from upstream units	m^3/h or L/s
$Q_{\text{in}_{\text{catchment}}}$	Inflow at a Storage Unit from catchment	m^3/h or L/s
$Q_{\text{in}_{\text{infiltration}}}$	Inflow at a Storage Unit from infiltration	m^3/h or L/s
$Q_{\text{incontrolled}}$	Inflow limit to switch MPC state from controlled to controllable	m^3/h or L/s
$Q_{\text{in}_{\text{controllable}}}$	Volume limit to switch MPC state from controllable to controlled	m^3/h or L/s
$Q_{\text{in}_{\text{ref}}}$	Reference inflow to the Wastewater Treatment Plant	m^3/h or L/s
$Q_{\text{in}_{\text{wwtp}_{\text{max}}}}$	Maximum inflow to the Wastewater Treatment Plant	m^3/h or L/s
Q_{inref}	Reference inflow to the Wastewater Treatment Plant	m^3/h or L/s
Q_{out}	Outflow of a Storage Unit	m^3/h or L/s
$Q_{\text{out}_{\text{max}}}$	Maximum outflow from Storage Unit	m^3/h or L/s
$Q_{\text{ov}_{\text{i}}}$	Volume overflow of i-th Storage Unit	m^3/h or L/s
$Q_{\text{ov}_{\text{total}}}$	Total volume overflow of a Storage Unit	m^3/h or L/s
$Q_{\text{wwtp}_{\text{max}}}$	Maximum inflow to the Wastewater Treatment Plant	m^3/h or L/s
R_{V}	Relative volume overflow	%
R_{m}	Relative load overflow	%
T_s	Sampling time of control loop	s
u_{offset}	Offset added to expected value in uncertainty	%
u_{p}	Scaling factor added to standard deviation in uncertainty	%
u_{sc}	Scaling factor added to expected value in uncertainty	%
V	Volume within a Storage Unit	m^3 or L
$V_{\text{controlled}}$	Volume limit to switch MPC state from controlled to controllable	m^3 or L
$V_{\text{controllable}}$	Volume limit to switch MPC state from controllable to controlled	m^3 or L
V_{max}	Maximum volume within Storage Unit	m^3 or L
$\%\mathbf{F}_Q$	Error of $Q_{\text{ov}_{\text{total}}}$ between the baseline (without uncertainty) and the value with uncertainty	%
$\%\mathbf{F}^*_Q$	Error of $Q_{\text{ov}_{\text{total}}}$ between non-optimal MPC and optimal MPC	%
$\%\mathbf{F}_m$	Error of $m_{\text{ov}_{\text{total}}}$ between the baseline (without uncertainty) and the value with uncertainty	%
$\%\mathbf{F}^*_m$	Error of $m_{\text{ov}_{\text{total}}}$ between non-optimal MPC and optimal MPC	%
$\%\mathbf{F}^*_\xi$	Error of ξ_{rain} between non-optimal MPC and optimal MPC	%
x	State variables in state-space formulation	-
u	Output variables in state-space formulation	-
w	Disturbance variables in state-space formulation	-

5 Introduction

This thesis presents the design and implementation of several Model Predictive Control (MPC) methods applied to Urban Drainage Systems (UDS), focusing mainly on pollution-based frameworks and culminating in the development of a new framework called Multi-Layer Model Predictive Control (ML-MPC). The research also proposes a stochastic formulation of the MPC methods and analyses their impact on the management of the UDS, while discussing the advantages and disadvantages of each method in different scenarios under uncertainties.

This chapter is organised as follows; Section 1.1 provides an overview of the research context. Section 1.2 introduces the problem statement and highlights the motivation behind this study. The aim and scope are detailed in Section 1.3, followed by the scientific contributions of this thesis, which are discussed in Section 1.4. Finally, Section 1.5 presents the general structure of the thesis.

5.1 Context of the Study

An Urban Drainage System (UDS) is a complex network of structures designed to manage and control urban water flows. These systems are essential for managing rainwater, surface runoff and wastewater, reducing the possibility of flooding, pollution, or environmental impacts. One of the key components of urban drainage systems is the combined sewer system, which is a type of drainage infrastructure that conveys both stormwater (rainwater runoff) and domestic wastewater (from toilets, sinks, showers and industrial processes) in the same pipe network [1]. Today, conventional solutions for urban drainage systems in combined sewer systems mainly focus on minimising overflow incidents, also known as Combined Sewer Overflow (CSO) [2], caused by excessive rainwater entering the sewage system and overloading the network, resulting in discharge of untreated waste into receiving water bodies [3]. Although expanding physical sewer infrastructure can mitigate these issues, such an approach is costly and labour intensive. A more cost-effective and practical alternative is the adoption of software-based solutions [4]. Among these, Real-Time Control (RTC) [3] has emerged as a promising strategy, capable of optimising system performance and reducing overflow volumes by 10 to 50% [5].

For this thesis, the definition of RTC has a specific meaning: **it refers to the dynamic and automated adjustment of actuators, such as pumps, weirs and valves, based on current or forecasted system states, in order to optimise the performance of the network under varying hydrological and operational conditions** [6–9]. The control system automatically adjusts the actuators, diverting or storing water when potential overflows are foreseen [10]. These systems use advanced technologies, combining traditional/advanced control methods with innovative artificial intelligence approaches, improving environmental sustainability by reducing the impacts of wastewater overflow events. There are

many different algorithms that implement RTC and they can be separated in the following frameworks depending on the characteristics analysed [11]:

1. Based on the type of controlled and manipulated variables:
    - **Volume-based** RTC: in the controller's formulation, the volume, in L or m^3 International System of Units - Système International d'unités (SI), is utilized as the main variable of the implementation [5].
    - **Pollution-based** RTC: the concentration (mg/L or g/m^3 in (SI) or the load (mg/s or kg/s in (SI) of the pollutant in the wastewater is included in the controller's formulation [11] as a main variable to be controlled.
2. Based on the controller's algorithm, i.e., how the control action is calculated:
    - **Rule-based** RTC: the control algorithm is defined using heuristics. These heuristics are usually in the form of rules that are imposed on the problem and are expected to result in a specific desired behaviour for the system [12].
    - **Optimisation-based** RTC: in this approach, the overall goal is achieved by minimising (or maximising) a function using optimisation techniques, ensuring that the system operates at its optimal performance considering the available information [13].
    - **Machine learning based** RTC: the controller utilises Machine Learning (ML) techniques to manage the system, integrating machine learning algorithms to improve decision-making processes. Among them, Reinforcement Learning is the most commonly used, as it allows the system to learn optimal control policies through trial and error, continually adapting to changing conditions, and improving performance over time and repetition [14].

Among these, volume-based approaches combined with rule-based approaches are the most common, although still rare in real implementations [3,15,16]. This research is mainly concerned with the application of RTC systems in the management of sewage networks in the following frameworks: (1) pollution-based RTC and (2) optimisation-based RTC. More specifically, Model Predictive Control (MPC) is the main subject of the study [13, 17]. Despite the potential of state-of-the-art MPC approaches, current implementations often neglect to consider the concentration of pollutant within the sewage network [18]. By incorporating water quality information into the control process, MPC can prioritise the management of heavily polluted wastewater [19]. In cases where overflows are unavoidable, such an approach enables the system to direct highly contaminated flows to treatment plants, while discharging cleaner water into the environment, minimising ecological harm. Therefore, this thesis explores the development and application of advanced MPC frameworks, integrating pollution load considerations to improve the management and environmental impact of urban drainage systems.

5.2 Problem Statement and Motivation

This research investigates the integration of the pollutant load and concentration into MPC frameworks applied to UDS. **The primary hypothesis is that the incorporation of water quality in the control process can effectively reduce the discharge of untreated sewage into the environment**

while ensuring that heavily contaminated wastewater is directed to treatment facilities. Although the above hypothesis is conceptually intuitive, the practical implementation of this approach presents several challenges:

- **Measurement limitations**: Accurate and continuous real-time measurement of water quality in sewer systems remains difficult due to sensor limitations, including drift and instability.
- **Model complexity**: Modelling water quality inherently introduces non-linearities, requiring advanced non-linear optimisation methods.
- **Optimisation challenges**: Non-linear solvers may fail to find globally optimal solutions or, in some cases, any solution at all.
- **Computational burden**: Solving high-dimensional non-linear optimisation problems within the constrained real-time window (typically 5 minutes) is computationally demanding.
- **Uncertainties**: The urban drainage system is affected by various uncertainties, such as faulty sensors or inaccuracy in the hydraulic and runoff models.

To address these challenges, this study proposes the development of several MPC strategies, culminating in a Multi-Layer Model Predictive Control (ML-MPC) framework. Firstly, a comparison between a Nonlinear Pollution-based Model Predictive Control (NPMPC) and the Volume-based Model Predictive Control (VMPC) is realised to validate the first hypothesis. The NPMPC introduces non-linearities, which creates a challenge and additional computational burden.

To overcome the computational burden, **a second hypothesis is formulated, stating that it is possible to approximate the non-linear MPC by a linear counterpart in a pollution-based framework**. Therefore, a linear pollution-based method is developed, called Pollution-weighted Model Predictive Control (PWMPC), which has faster optimisation and is capable of properly handling water quality using it as a weight in the cost function.

Finally, this research addresses the algorithmic complexity of non-linear optimisation by proposing the combination of NPMPC with a newly developed PWMPC ensuring continuous control system operation, even in cases where NPMPC fails to produce an optimal output. The solution for this hypothesis was the development of a multi-layer approach, creating a layered control strategy, starting from a baseline volume-based MPC (representing the current state-of-the-art) to advanced pollution-based MPC strategies. The objective of this layered approach is to ensure that a feasible solution is always available within real-time constraints, even if the most advanced layer fails to compute an optimal solution. This redundancy is achieved by solving problems in parallel across layers, though a new set of challenges is introduced by the approach mainly around choosing which layer to use and avoid instabilities caused by transitioning between layers.

Another important motivation for this research is to address the challenge of modelling pollutant loads. Real-time direct measurement of pollutant concentrations is often infeasible; therefore, this study adopts an indirect approach using estimations of water quality. This is achieved using wastewater generation profiles, derived from existing research [20], which are used to estimate the pollutant loads entering the wastewater network. Uncertainties are always present in any system, especially in sewage applications, and the latest approaches do not intrinsically consider them in the formulation. Uncertainties can reduce controller performance if not properly considered [21]. In this research, the uncertainty is

analysed to understand the impact on MPC, while studying the potential of reformulating each MPC to a stochastic approach. By handling these technical and methodological challenges, this research aims to advance the state-of-the-art in RTC systems for UDS, improving both environmental outcomes and system efficiency.

5.3 Objective and Scope

The objective of this thesis is to evaluate the pollution-based framework in RTC, specifically utilising MPC methods, and to overcome the implementation challenges that are expected in each method, such that the final implementation, the ML-MPC, is capable of effectively addressing the limitations of each individual RTC method studied.

In order to reach the objectives of this study, the following research questions will be addressed:

1. What are the available RTC methods for managing UDS?
2. How can a pollution-based framework reduce the overflow load?
3. How should water quality be estimated when direct measurements are unavailable?
4. How can the parameters (e.g., weights of cost function, prediction horizon, etc.) of a MPC be selected specifically for each UDS?
5. How can the complexities and non-linearities introduced by the pollution-based frameworks be addressed?
6. How can the uncertainties inherent to the UDS be addressed? Which uncertainties have the most significant impact and what is the best way to model them?
7. How can these uncertainties be integrated into a MPC framework?
8. How should the challenges of infeasibility in non-linear methods be approached?
9. How does the computational effort of the MPC methods scale with the number of storage units and the length of the prediction horizon?
10. How do the proposed MPC methods perform when applied to systems of higher complexity?

To answer the first question, a literature review has been performed to evaluate RTC methods, their advantages and disadvantages. This review revealed a noticeable gap in the literature regarding pollution-based RTC approaches, which encouraged the need for a complete analysis to complement the state-of-the-art [11]. Additionally, the research pointed to the importance of studying different modelling techniques and model types, given their importance in the performance of RTC systems.

The second and third questions are addressed using established water quality models and techniques to estimate water quality parameters. For instance, the load of the sewage entering the network is approximated by patterns identified in previous research. The pollution-based method goes through a methodological evaluation where it is compared with a volume-based approach with known relevance in

the literature, in order to verify the effectiveness of the new method in reducing overflow load compared to current state of the art RTC strategies.

The fourth question is intrinsic to any MPC method, as selecting the appropriate weights and prediction horizon is often a challenging and time-consuming task. Therefore, a methodology has been developed to assist in the weight-selection process. This methodology involves performing a weight sensitivity analysis and integrating the results with an optimisation algorithm to identify a nearly optimal set of weights.

The development of a linear pollution-based MPC addresses the fifth question by simplifying the algorithm. This approach uses the estimated concentration as a weight in the current objective function, which enables the minimisation of overflows while reducing complexity.

Questions 6 and 7 are answered by performing a comprehensive analysis of uncertainties and research stochastic controllers. This process leads to the development of stochastic MPC methods that are specifically designed to manage and handle uncertainties.

The answer to the eighth question is the development of a multi-layer approach that integrates both non-linear and linear MPC methods. This approach uses both controllers simultaneously, guaranteeing that when the non-linear method fails to find a solution, the linear method acts as a backup, providing an alternative control action and ensuring continuous system operation.

Finally, questions 8 and 9 are addressed by evaluating and comparing each MPC method on performance and computational effort. Comparisons are made between several different wastewater network configurations and complexities to assess how each method performs under different conditions.

5.4 Relevance of the Research

Publications involving MPC applied to UDS that includes the concentration in the optimisation problem are gradually increasing in number overtime [18, 22], as reviewed in [11], but no actual systems implementing were found at the time, mainly due to perceived complexity, and research is needed to bring this approach to the first real application. To address the complexity issue, a multi-layer optimisation is proposed, where multiple optimum solutions are calculated in parallel. Current research on non-linear MPC applied to sewer networks only uses a single layer optimisation [23] and is susceptible to convergence problems in the case where the complexity is too high.

Therefore, the importance of the multi-layer approach is to guarantee a solution in case of convergence issues, including scenarios where the convergence time is above the control sampling time, resulting in a stable system and a robust controller. Although this approach could already be regarded as innovative, one of the novelties lies in the development of a decision-making algorithm capable of evaluating and selecting the most appropriate optimisation layer to be used. Consequently, a critical component of this research is a methodology for determining which layer to activate, ensuring robust and efficient operation under all conditions. A potential difficulty may be the switching between layers and a potential instability resulting from frequent switching. Moreover, current works [23, 24] specify sewage as a general concept without separating it into different types of analytes, such as Chemical Oxygen Demand (COD) or Ammonium Ion (NH_4^+). This can be achieved by defining a model that more specifically describes each

pollutant or analyte using a mathematical estimation, creating a more complete and more descriptive model of the wastewater network.

5.4.1 Scientific Contribution

The main contributions of this thesis to the field of RTC applied to UDS as well as the novel approach of sensitivity analysis to appropriately select parameters of controllers are outlined in the following tasks:

1. *Development of a novel pollution-based RTC in a linear formulation that is capable of reducing CSO events and mitigating load reaching receiving water bodies.*

   The non-linear pollution-based MPC is the best solution among the techniques proposed in this thesis to reduce untreated wastewater reaching the environment; however, it may have practical problems due to its high computational cost. Therefore, a simpler, yet effective solution was developed to reduce the necessary computations while still minimising environmental impact, compared to current state-of-the-art RTC systems used in sewers.

2. *Development of a sensitivity analysis framework that is capable of performing screenings as well as global sensitivity analyses applied to RTC parameters and the system they are controlling.*

   A suitable sensitivity framework is developed, consisting of a Local Sensitivity Analysis (LSA) via Morris screening and a Global Sensitivity Analysis (GSA) using Grid Search and/or Random Search. The analysis provides insights into the relationship between parameters (such as the weights of MPC) and outputs (e.g., overflow load), as well as suitable ranges for the weights.

3. *Using sensitivity analysis results as a foundation for selecting the weights of MPC by combining it with a Genetic Algorithm (GA) optimisation.*

   The genetic algorithm is developed to identify the weights of the MPCs by running consecutive simulations and comparing their outputs, such that the algorithm converges to the weights where the outputs are minimized. In the context of urban drainage systems, the outputs can vary from minimising the overflow (volume or load) to maximising the inflow to the Wastewater Treatment Plant (WWTP).

4. *Development of a stochastic pollution-based methods to deal with uncertainties in UDS.*

   An uncertainty analysis is performed to quantify the performance degradation of deterministic MPCs under various degrees of uncertainty. A reformulation of these methods is proposed to increase robustness and even outperform deterministic controllers when high uncertainties are present. Moreover, the reformulation of the method is flexible for most RTC controllers, as it only requires adding a stochastic constraint to the optimisation.

5. *Proposing a multi-layer algorithm to address non-linear solver issues and maintain operation of the control system under various conditions.*

   The ML-MPC is developed as an alternative, considering that in most scenarios, the non-linear MPC performs better. It tries to use it whenever possible and, when the controller fails, it falls back to the linear method to ensure continuous operation. The stability of the multi-layer system is evaluated with several configurations of the layers.

6. *Analysing the methods developed in three systems based on actual UDS with their own complexities.* The final evaluation of the methods is carried out in systems with their own challenges and specificities, demonstrating the versatility and adaptability of the proposed approaches in real-world applications.

5.5 Summary of the Thesis

The structure of the thesis is as follows:

Chapter 2 provides an overview of the state of the art in pollution-based RTC, highlighting the background knowledge on urban drainage systems, their modelling, and the application of real-time control systems to improve their operation.

Chapter 3 focuses on MPC, describing its fundamental principles and detailing the implementation of Volume-based Model Predictive Control (VMPC) on Urban Drainage Systems, evaluating it on three simple networks: a network with a single storage unit, a network with two storage units in parallel, and a network with three storage units, two in parallel and a third in series.

Chapter 4 details Nonlinear Pollution-based Model Predictive Control (NPMPC) and Pollution-weighted Model Predictive Control (PWMPC), the pollution-based methods proposed in this research. Their performance is compared to the VMPC in the network with three storage units.

Chapter 5 extends the discussion to Stochastic Model Predictive Control (SMPC), first starting with an uncertainty analysis of the UDS and, afterwards, presenting the formulation and application of MPC in a stochastic context to address uncertainties in the system. Their performance is compared with the deterministic methods in a network with three storage units.

Chapter 6 showcases the application of these control strategies in models based on actual urban drainage systems with higher complexities. The strengths and weaknesses of each MPC approach are evaluated.

In Chapter 7, the convergence of non-linear MPC methods is studied, and the ML-MPC algorithm is introduced, explaining the multi-layered decision-making process and its role in improving control strategies.

Finally, Chapter 8 concludes the thesis, summarising the most important findings, discussing their implications, and suggesting directions for future research.

6 State of the Art

Modernisation increased the use of many fundamental resources and thus required an evolution of the techniques responsible for handling, distributing, collecting, and disposing of these resources. The prime example is water, which is arguably the most important natural resource, and wastewater, both having critical environmental, social, and economical impacts [1]. In most countries, water is collected, treated, and distributed mainly for personal use in dwellings, while wastewater is the result of its consumption, which is transported by sewage or wastewater systems, treated in Wastewater Treatment Plants (WWTP), and discharged into receiving water bodies such as rivers or seas [24]. Wastewater, the focus of this research, needs to be treated to avoid negative impacts on the environment and, therefore, requires advanced techniques to guarantee that these resources are being collected efficiently and reliably [19].

6.1 Urban Drainage Systems

The main challenge in UDS is the occurrence of overflows in combined sewer networks, where rainwater and sewage are collected and transported through a shared system. Here, CSO events occur during rainfall events when stormwater inflow exceeds the storage capacity of the network, leading to untreated discharges into the environment [4]. The frequency and severity of CSO events are expected to increase due to factors such as climate change, growth of the urban population, and decreased natural infiltration caused by soil sealing [3]. For a comprehensive overview of current methodologies on the prediction of overflows, the works of [10] and [25] provide detailed information on the state of the art in this domain.

Minimising CSO events is therefore essential for every urban area [4]. Traditional engineering approaches to address this issue include increasing storage volume, upgrading pipes and pumps, or separating rainwater from the sewage system by transitioning to a separate sewer network. However, these infrastructure-based solutions are often costly and disruptive. A more cost-effective and flexible alternative lies in the implementation of software-based strategies. Several real-world applications have demonstrated the effectiveness of such approaches. For example, [7] implemented a MPC strategy in Barcelona, while [26] developed a global optimal control solution in Quebec. In Luxembourg, a multi-objective MPC framework was applied in studies by [27] and [5], and [28] designed a rule-based control algorithm for sewer network management in Copenhagen.

These software-driven solutions are collectively referred to as RTC, reflecting their ability to monitor and adjust the operation of urban drainage systems dynamically, based on current and forecast conditions. The underlying reason for applying a RTC is that wastewater networks are systems with highly dynamic behaviour, with constantly changing operational variables, requiring a controller capable of reacting in real time [29]. The overall literature of RTC applied to drainage systems is growing constantly, as can be

observed in Figure 6.1, and according to the online data-set available in [30], the estimation of cumulative published studies on the topic is approximately 9,398 articles by July 2025. There are several reviews detailing many different algorithms and implementations, for example: [3], [22] and [16] reviewed the modelling and real-time control of sewage systems, in [31] the performance of different RTC methods is evaluated and [32] illustrated the impact of RTC algorithms on stormwater control measures.

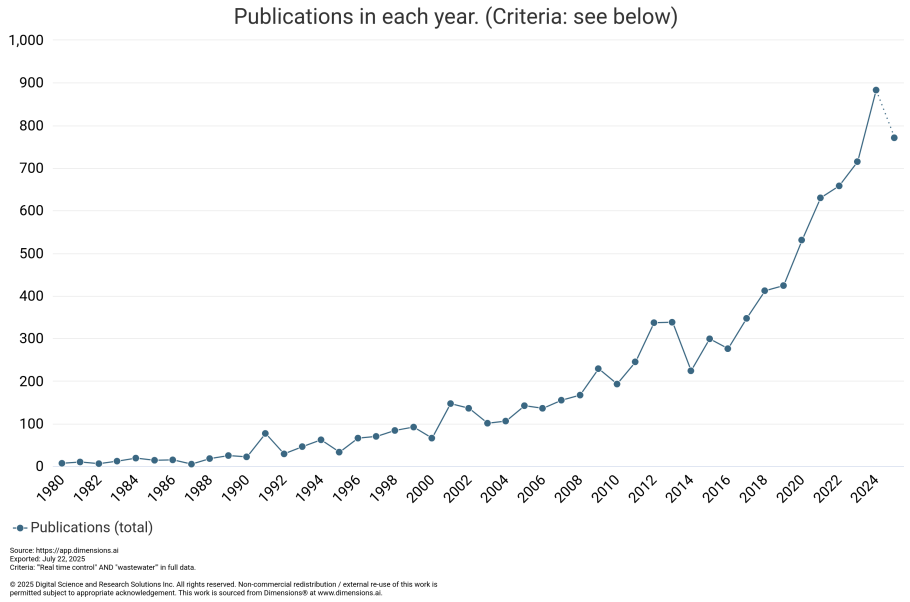

Figure 6.1: Total publications per year from 1980 to 2025, estimated by searching the key words "Real time control" and "Wastewater" in the data-set provided by [30].

However, the usual application of RTC does not implicitly consider the pollution load [18], which is only feasible by using more complex models or adding water quality information to the algorithm. Measurement of water quality in sewage systems are difficult due to the harsh environment and associated maintenance costs [33]. Incorporating quality data gives the possibility to explicitly influence the sewage network and manipulate the system to ensure better performance, which is possible but not guaranteed using a purely volume-based approach. Improvements derived from the use of water quality data in RTC can include reducing the overflow with highly concentrated wastewater and increasing the load being directed to WWTP.

Therefore, efforts have been made to improve RTC using pollution-based approaches as seen in the works of [19, 23, 34]. In addition, studies are available on the prediction and assessment of water quality in sewer systems [35–37]. In this domain, the estimated cumulative number of publications is greater than 200 articles by July 2025, following the same database provided by [30], as can be seen in Figure 6.2. Although in the literature there are reviews on water quality modelling [38], water quality dynamics and in-sewer processes [39], a search through SCOPUS and Google Scholar revealed a lack of studies reviewing specifically Pollution-based Real-Time Control (PRTC). As a result, a review paper was designed and published to provide a review of PRTC [11], focusing on the models used to describe pollution in UDS for control purposes and related control techniques that have been developed so far. Firstly, a brief review of the different software used for the modelling of UDS is discussed and a more detailed description of the tool used in this research is achieved.

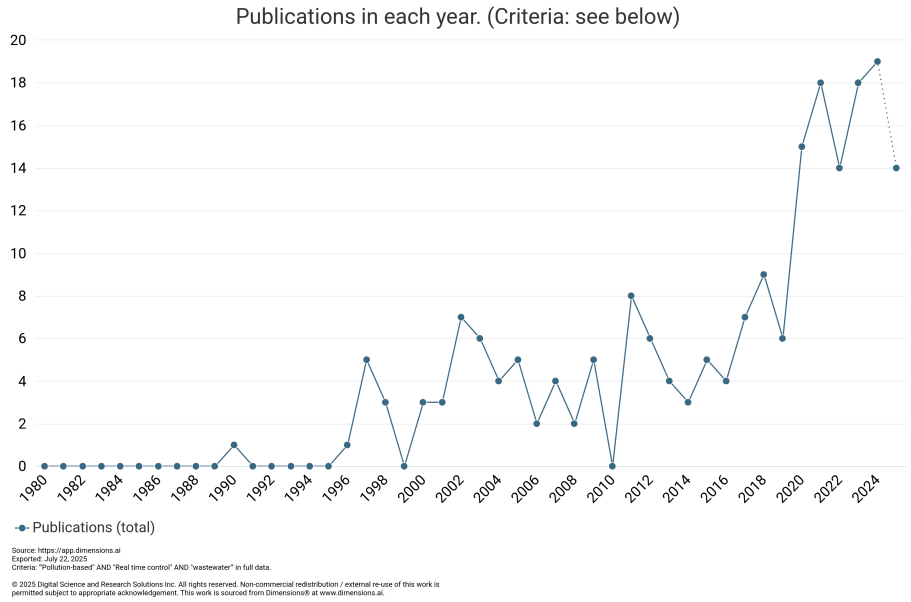

Figure 6.2: Total publications per year from 1980 to 2025, estimated by searching the key words "Pollution-based" and "Real time control" and "Wastewater" in the data-set provided by [30].

6.2 Software for Modelling Urban Drainage Systems

The challenges of implementing and validating a control system in real applications are made easier by using virtual representations of the reality. Mimicking reality in urban drainage systems is not easy, as the description of such a system is highly complex. Therefore, the virtual reality needs to cope with complexity, while also providing enough resources to be able to correctly represent and simulate reality. There are many software tools used for the simulation of urban drainage systems:

1. EPA Storm Water Management Model (SWMM) [40]: Developed by the U.S. Environmental Protection Agency, SWMM is a widely used tool to model urban stormwater and wastewater drainage systems. It supports hydrological and hydraulic simulation, allowing analysis of stormwater runoff, infiltration, sewer flow, and other features.

2. Bentley SewerGEMS [41]: A software solution for designing, modelling, and analysing complex sewer networks. SewerGEMS supports steady-state and dynamic modelling of wastewater and stormwater systems with advanced features for scenario management and optimisation.

3. MIKE URBAN [42]: Developed by DHI, MIKE URBAN is a fully integrated tool for modelling urban water systems, including stormwater, wastewater, and water distribution networks. It provides advanced simulation capabilities for both hydraulic and water quality analysis.

4. InfoSWMM [43]: A GIS-based extension of SWMM, InfoSWMM offers enhanced capabilities for dynamic hydraulic and water quality modelling of stormwater and wastewater collection systems.

5. PCSWMM [44]: A user-friendly and professional interface built on EPA SWMM, PCSWMM includes additional tools for scenario management, statistical analysis, and automated calibration, making it accessible for users with varying levels of expertise.

6. H2OMAP Sewer [45]: A modelling platform for the planning, analysis, and design of sewer systems. It offers dynamic simulation capabilities to evaluate system performance under various flow conditions, including dry weather and wet weather scenarios.

7. SewerCAD [46]: Bentley Systems software tool designed for the analysis, design and operation of sanitary sewer systems. It provides a straightforward environment for calculating the hydraulics of the gravity and pressure sewer system.

8. WASP [47]: A dynamic modelling tool for simulating water quality in surface water systems. WASP is used to predict the transport and transformation of pollutants in rivers, lakes, estuaries, and coastal waters.

9. OpenFlows STORMCAD [48]: Another Bentley software, STORMCAD is tailored for the design and analysis of stormwater drainage systems. specialises in steady-state calculations for pipe sizing and system layout optimisation.

10. Aquarius [49]: A suite of tools designed for the management of water and hydrological data. Aquarius is used for real-time data collection, storage, and analysis to support decision-making in water resource management.

11. OpenFlows SewerCAD [48]: A rebranded version of SewerCAD by Bentley Systems, this tool continues to offer robust capabilities for the design and operation of sanitary sewer systems with a focus on efficiency and cost-effectiveness.

These software tools provide many capabilities for modelling stormwater, wastewater and other fluid systems, each suited for specific applications ranging from hydrology and hydraulics to water quality. In this research, SWMM is used for modelling purposes due to the possibility to connect with RTC systems and simulate the control of UDS in real time. The next section provides a brief description of the main elements of SWMM.

6.2.1 EPA Storm Water Management Model

The EPA SWMM is an open-source software designed to simulate dynamic rainfall-runoff processes for both single events and long-term continuous scenarios, focusing on runoff quantity and quality in primarily urban environments. Runoff is modelled through the use of subcatchment areas that transport precipitation, generating runoff and pollutant loads. The generated runoff enters the model and is distributed through a system of pipes, channels, storage/treatment devices, pumps, and regulators. During the simulation period predefined by the user, SWMM monitors in each routing step the quantity and quality of runoff from each subcatchment, while also tracking flow rates, flow depth, quality of the water transported through the network, and several other important variables [40].

SWMM can be described as composed of several visual objects that represent a specific element of the sewage system and that actively and dynamically interact. Each of these visual objects has their own function and configuration, which are detailed below.

Visual Objects

The tool is used by aggregating a collection of SWMM visual objects as depicted in Figure 6.3. Using the workspace provided in the software, those objects are arranged together to resemble the urban drainage system and enable the modelling of the scenario using the parameter to configure the simulation.

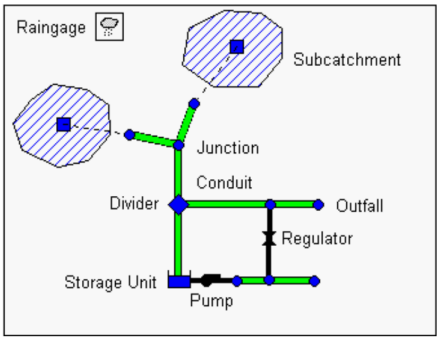

Figure 6.3: Physical objects used to model a drainage system [40].

- **Rain Gages** represent the source of precipitation data for subcatchment areas in a given region. The rainfall data is provided either by an external file or a user-defined time series. The rainfall data can be a standard format defined by the user or a classic rainfall file format already supported by SWMM.
- **Subcatchments** are hydrologic units of land characterized by topography and drainage system elements that channel surface runoff to a single discharge point. Each subcatchment is further divided into pervious and impervious sub-areas. While surface runoff in pervious areas can infiltrate into the upper soil zone, this process does not occur in impervious areas. Impervious sub-areas are subdivided into two categories: those with depression storage and those without. Runoff from one subarea can be routed to the other or directed directly to the subcatchment outlet.
- **Junction Nodes** serve as points in a drainage system where multiple links converge. Physically, they can represent features such as the confluence of natural surface channels, sewer manholes, or pipe connection fittings. Junctions also provide entry points for external inflows into the system. In cases where excess water causes connecting conduits to become surcharged, the junction may become partially pressurized. This excess water can either be lost from the system or allowed to accumulate above the junction, forming a pond that drains back into the system once conditions permit.
- **Outfall Nodes** are the terminal points of a drainage system, used to define the final downstream boundaries when employing Dynamic Wave flow routing. For other flow routing methods, outfall nodes function similarly to junctions. Each outfall node can accommodate only a single connecting link, with the option to discharge flow directly onto the surface of a subcatchment.

- **Flow Divider Nodes** are components of a drainage system that direct inflows into specific conduits based on predefined criteria. Each flow divider can have a maximum of two conduit links on its discharge side. These nodes are active only when using Steady Flow or Kinematic Wave routing and are treated as standard junctions under Dynamic Wave routing.

- **Storage Units** (SU) are nodes within a drainage system that provide capacity for water storage. They can represent a range of physical structures, from small catch basins to large lakes. The volumetric properties of a storage unit are defined by a surface area versus height function or table. In addition to receiving inflows and discharging outflows to other nodes in the network, storage units can lose water through surface evaporation or seepage into the underlying soil. SUs are also commonly known as CSO tanks, but in this thesis, they will be explicitly called Storage Units to relate to SWMM nomenclature.

- **Conduits** are the pipes or channels that convey water between nodes in a drainage system. They can be designed with a variety of cross-sectional shapes, including both standard open and closed geometries, to accommodate different hydraulic requirements.

- **Pumps** are links in the drainage system used to lift water to higher elevations. The performance of a pump is defined by a pump curve, which relates the flow rate to the hydraulic conditions at the inlet and outlet nodes.

- **Orifices** are components used to model outlet and diversion structures in drainage systems. Typically, they represent openings in the walls of manholes, storage facilities, or control gates. In SWMM, orifices are modelled as links connecting two nodes. They can be circular or rectangular in shape, positioned either at the bottom or along the side of the upstream node, and may include a flap gate to prevent backflow.

- **Weirs**, like orifices, are used to simulate outlet and diversion structures in a drainage system. They are typically placed in manholes, along the sides of channels, or within storage units. In SWMM, weirs are modelled as links connecting two nodes, with the weir located at the upstream node. A flap gate can also be included to prevent backflow.

- **Outlets** are flow control devices that regulate outflows from storage units. They are used to model unique head-discharge relationships that cannot be represented by pumps, orifices, or weirs. In SWMM, outlets are modelled as links connecting two nodes, and they can include a flap gate to restrict flow to a single direction.

In addition, the software provides a number of parameters for the various elements, allowing a detailed characterisation of the UDS. Many tools were also developed to integrate the capabilities of SWMM in other environments, such as PySWMM [50], which was created to enable access the SWMM data model using Python. This facilitates rapid prototyping and allows users to interact with the model during simulation. Furthermore, PySWMM allows the implementation of RTC systems and interaction with SWMM simulations.

6.2.2 Urban Drainage System Modelling with SWMM

This section illustrates simple cases of sewage networks to exemplify the use of SWMM and its elements. In the following chapters detailing MPC methods, these same models will be used for validation of the control strategies.

Single Storage Unit Configuration

The first case presented is the simplest sewage network possible. This structure is composed of a single SU that receives sewage from human activity (households or industry), normally called the Dry Weather Flow (DWF), combined with rain runoff, also known as Wet Weather Flow (WWF). The system is represented in Figure 6.4a.

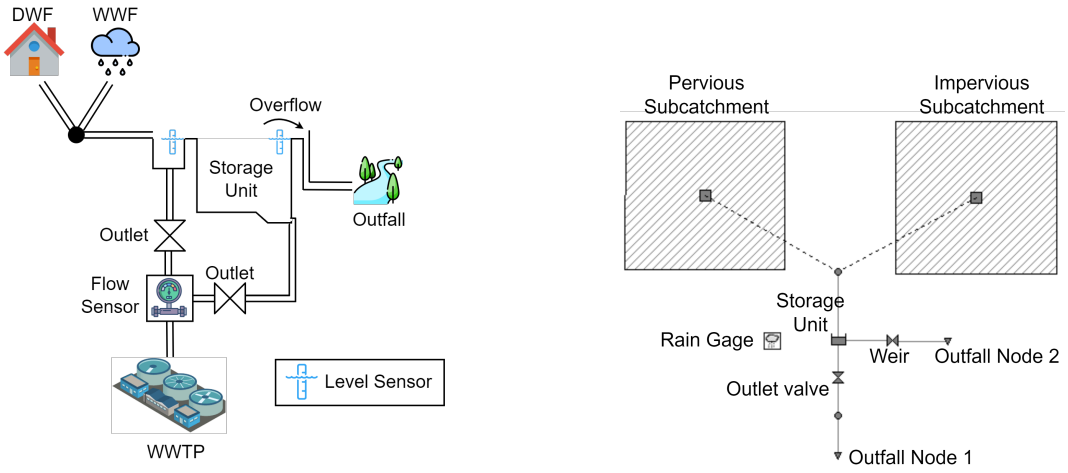

(a) Conceptual Model for Single SU. *(b)* SWMM Model for Single SU.

Figure 6.4: Single SU configuration: Conceptual and SWMM model.

A single outlet connects SU to WWTP and if maximum storage is reached, an overflow occurs and excess sewage is discharged to a receiving water body. The single SU system was modelled in SWMM as shown in Figure 6.4b, which diverges slightly from Figure 6.4a, where the two SUs are approximated by a single one. The system is composed by a pervious Subcatchment with an area of 90 ha, an impervious Subcatchment with an area of 21.78 ha and a SU with maximum volume of 2417.5 m^3. Besides, it has a Rain Gage, an Outlet with a maximum outflow of 120 L/s, an Weir, Outfall Node 1 corresponding to the WWTP and Outfall Node 2 corresponding to the overflow node. A constant infiltration flow of 39.5 L/s is added to the SU.

The input data for the simulation is divided into two parts: the precipitation recorded by the Rain Gage, which generates runoff and corresponds to the WWF, and the inflow from pervious and impervious Subcatchments, representing the DWF. The data used for the precipitation is a replica of the rain measured at Trier, Germany in Station 5100 for the period from 13/04/2023 to 14/10/2024, collected from [51] with 10 minutes resolution and shown in Figure 6.5 for a period of one year in mm/hr.

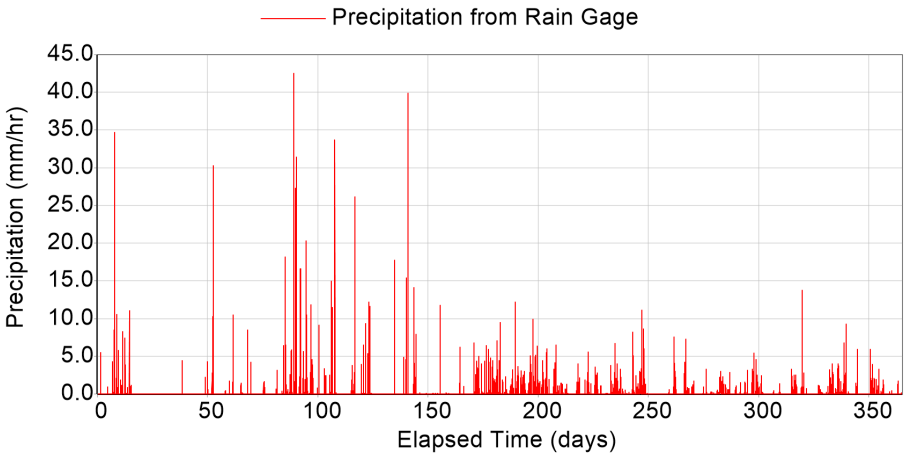

Figure 6.5: Single SU configuration - precipitation.

A dry weather flow pattern (Figure 6.6) is defined for the SU, which is sampled every hour for a year of data, where LPS is 'Litres per second'.

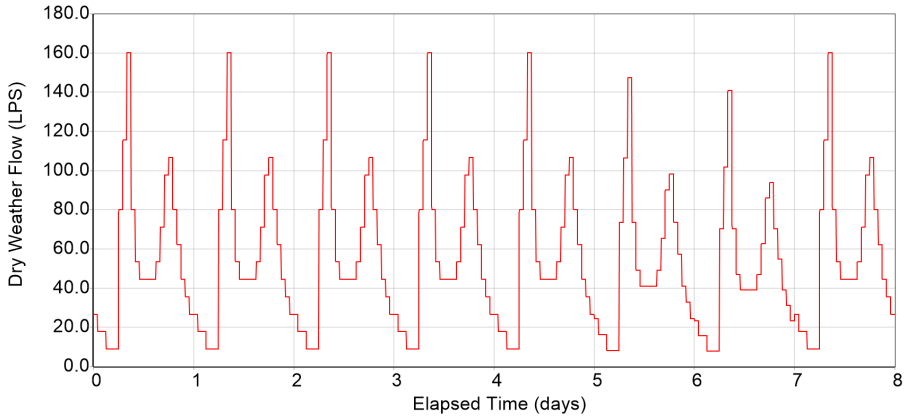

Figure 6.6: Single SU configuration - dry weather flow.

The dry weather daily pattern for the concentration of COD and NH_4^+ is shown in Figure 6.7, where the average daily concentration is 42 mg/L and 600 mg/L, respectively.

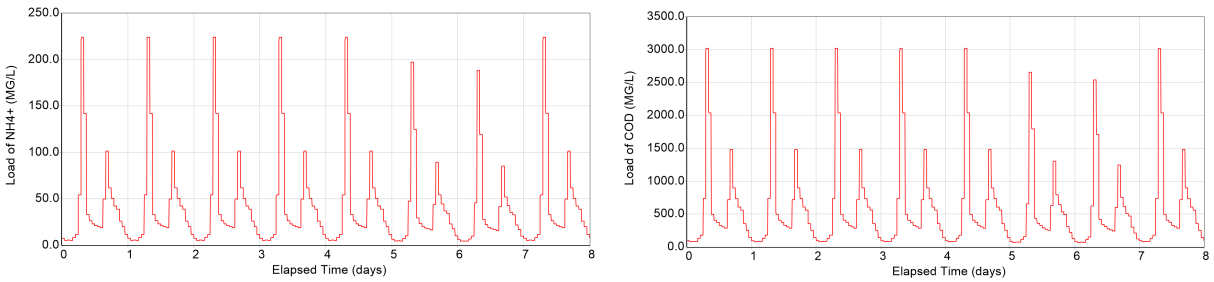

(a) Dry weather concentration for COD. *(b)* Dry weather concentration for NH_4^+.

Figure 6.7: Single SU configuration - dry weather load.

The single SU model is simulated using the input data with one year duration. The Outlet is kept open at the maximum to use the full capacity of the actuator, therefore, when the SU has enough volume, the outflow will be at the maximum of 120 L/s, as shown in Figure 6.8.

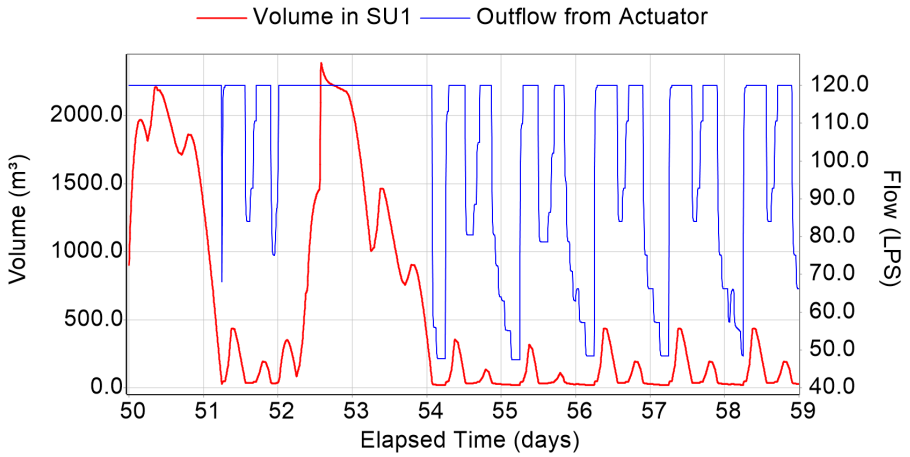

Figure 6.8: Single SU system - Volume (left y-axis, red) and Outflow (right y-axis, blue).

In Figure 6.9 the total volume and overflow occurrences for the one year period are shown. In total, the SU has an overflow of 490.2 ML, whereas the inflow to the WWTP is 3287.1 ML. Therefore approximately 15% of the total inflow to the sewage system is overflowing. Regarding the load, the overflow contains 89268 kg of COD and the inflow to the WWTP contains 1454629 kg, while having 6294 kg of NH_4^+ in the overflow, with an inflow containing 102617 kg to the WWTP, which corresponds to approximately 6% of overflow from the total inflow to the sewage system for both pollutant indicators.

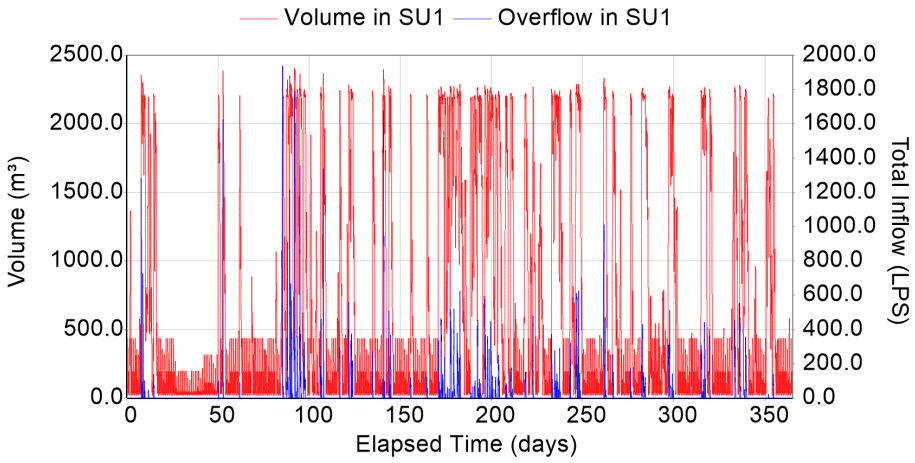

Figure 6.9: Single SU configuration - Volume (left y-axis, red) and Overflow (right y-axis, blue).

Applying RTC systems in this situation is not beneficial for improving performance since it is already using the maximum capacity of the outlet. The optimal operation of the SU is already set by the current settings, therefore such a system is too simplistic to analyse and make any conclusions about the performance of a RTC. However, it is an interesting configuration to check if the RTC is able to, at least, find the optimal behaviour which corresponds to the operation of the static control.

Parallel Storage Units Configuration

The parallel configuration can be seen in Figure 6.10a. The main difference in this case study is that there is an additional unit, SU2, in parallel to SU1, which collects sewage and runoff from a different area. Each SU is controlled independently at the outlet and the outflow from each outlet is combined and delivered to the WWTP.

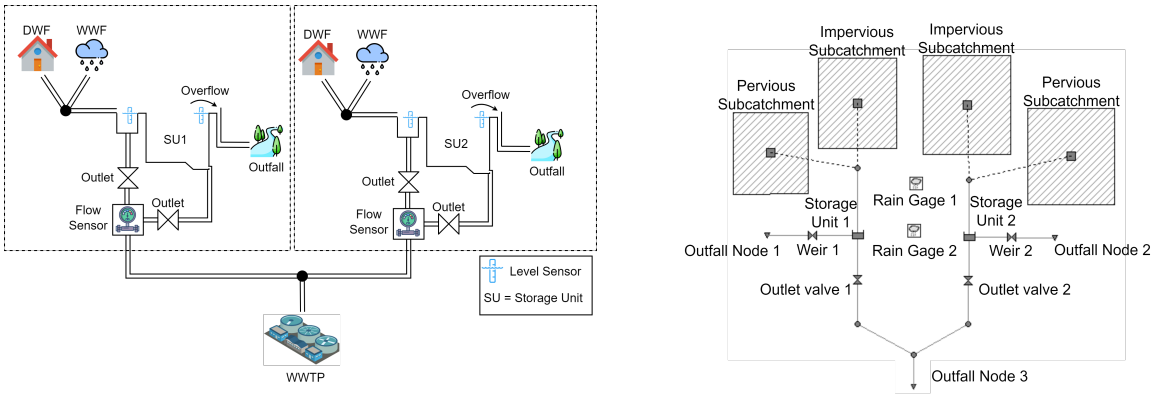

(a) Conceptual Model for Parallel SU configuration. *(b)* SWMM Model for Parallel SU configuration.

Figure 6.10: Parallel SU configuration: Conceptual and SWMM model.

In Figure 6.10b, the version modelled in SWMM is presented. The maximum volumes for SU1 and SU2 are 1450.5 m^3 and 967 m^3, respectively. Their associated pervious Subcatchment areas are 50 ha and 40 ha, while the impervious areas are 10.875 ha for both. A constant infiltration flow of 14.7 L/s is applied to each SU. The outlet flow rates are set to 65 L/s for SU1 and 55 L/s for SU2, with the aim of achieving a maximal combined inflow of 120 L/s at the WWTP, represented by Outfall Node 3.

Each SU is equipped with an independent Rain Gage, using different rainfall scenarios. The precipitation data were collected from Trier, Germany (Stations 5100 and 5099) over the period from 13/04/2023 to 14/10/2024, with a temporal resolution of 10 minutes. This data is illustrated in Figure 6.11 in mm/hr.

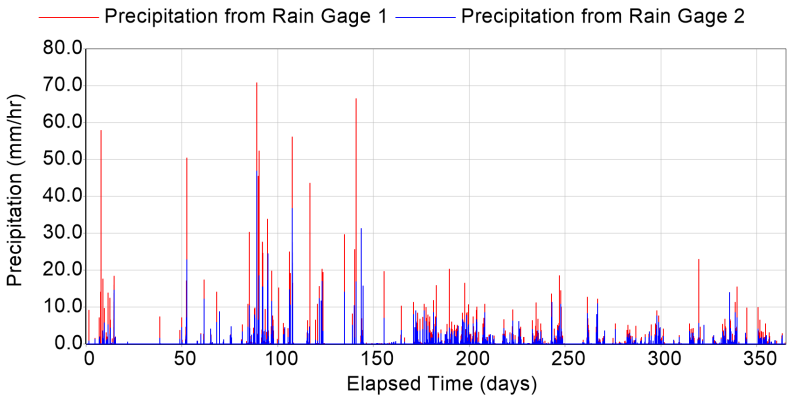

Figure 6.11: Parallel SU configuration - precipitation.

The dry weather flow for each SU is shown in Figure 6.12. The dry weather patterns for COD and NH_4^+ follow the same profile used in the single SU case, as illustrated in Figure 6.7, and are applied to both SU1 and SU2.

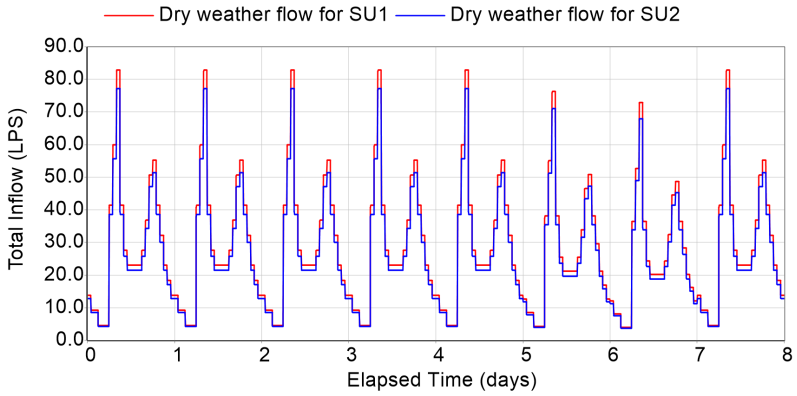

Figure 6.12: Parallel SU configuration - dry weather flow.

The system is simulated using the input data with one year of duration. In Figure 6.13, the volume and outflow are observed for a 10 day period, which shows that the Outflow from both SUs are often at their maximum outflow of 65 L/s and 55 L/s when there is volume available at the unit. This allows the desired inflow to the WWTP to reach the 120 L/s.

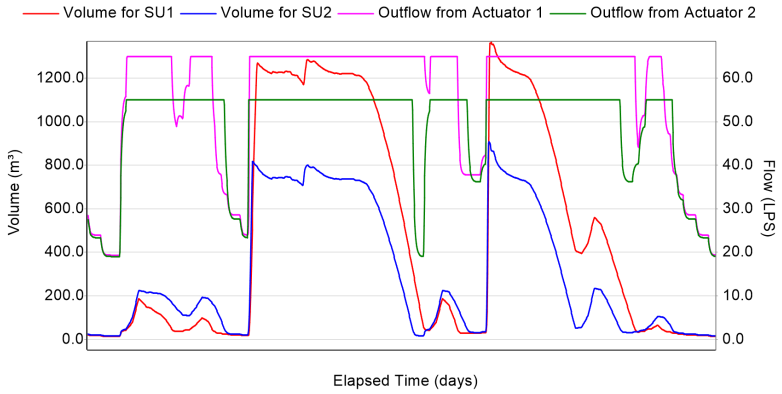

Figure 6.13: Parallel SU configuration - Volume (left axis, red) and Outflow (right axis, blue).

However, Figure 6.14a and Figure 6.14b show that both units have overflows. For the one year period, the overflow for SU1 is 240 ML and the overflow load is 34429 kg of COD and 2425 kg of NH_4^+ and in SU2 the overflow is 242 ML, 40387 kg of COD and 2850 kg of NH_4^+. In this scenario, without changing the settings of the actuators, improvements are really difficult to achieve even with an optimal control due to the constrained situation.

Similarly to the single SU configuration, the use of a RTC system in this scenario may not necessarily lead to performance improvements in the sewer network. The effectiveness of such control depends on the WWF generated in each SU and the maximum outflow capacity of their respective outlets, which together determine the system's ability to meet the reference inflow at the WWTP while avoiding overflow.

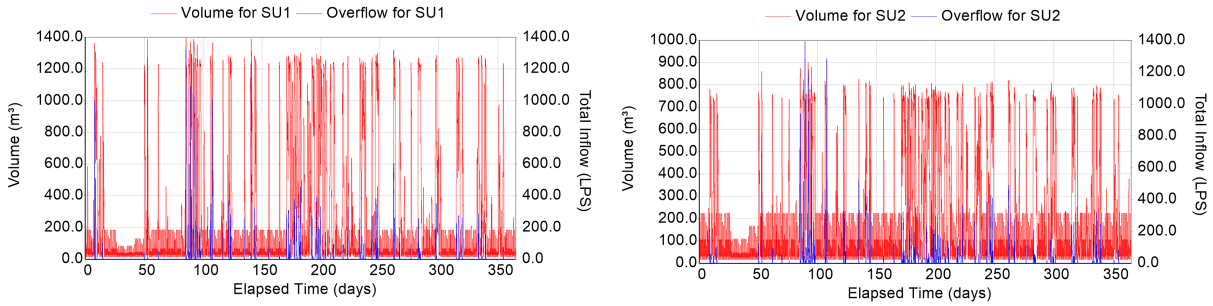

(a) SU1. *(b)* SU2.

Figure 6.14: Parallel SU configuration - Volume (red) and Overflow (blue).

In this case, although the rainfall intensities differ between the catchments, the rain events occur simultaneously, an outcome likely when the units and their drainage areas are geographically close. However, in situations where rainfall events are not synchronized, meaning the WWF varies not only in intensity but also in timing across SUs, an RTC system could potentially enhance performance. By dynamically adjusting the outflows from each SU, the system may better align with the desired inflow profile at the WWTP and reduce overflow occurrences.

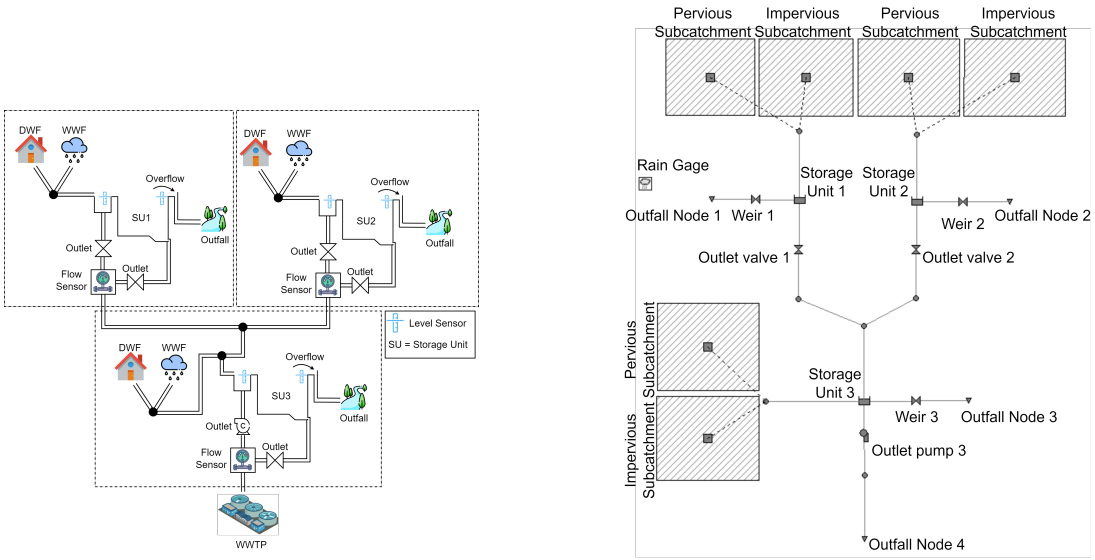

(a) Conceptual Model for Parallel+Series SU configuration. *(b)* SWMM Model for Parallel+Series SU configuration.

Figure 6.15: Parallel+Series SU configuration: Conceptual and SWMM model.

Parallel + Series Storage Units Configuration

The last configuration presented is formed by two parallel SUs (SU1 and SU2) in series (also "in cascade") with a single SU (SU3) with a pump as an actuator, as shown in Figure 6.15a. In this situation, SU3 is connected to the WWTP, receiving the combined flow from SU1, SU2 and its own catchment inflow

(DWF + WWF). As before, each unit is controlled independently by an Outlet with the exception of SU3, which is controlled by a Pump. A third Rain Gage is also added with data collected at Station 5433 at Weiskirchen, Germany with resolution of 10 minutes from 13/04/2023 to 14/10/2024.

The resulting SWMM model is in Figure 6.15b. For SU1, SU2 and SU3, the maximum volumes are 967 m^3, 483.5 m^3 and 1450.5 m^3, respectively. The pervious Subcatchment area is 26.52 ha, 16.62 ha and 36.62 ha for SU1, SU2 and SU3, while the impervious Subcatchment is 7.26 ha for all units. A constant infiltration flow of 6.2 L/s, 3.2 L/s and 15.2 L/s is added to SU1, SU2 and SU3, respectively. The Outlets are set to 40 L/s, for SU1 and SU2 and 120 L/s for SU3, aiming to reach the WWTP reference inflow of 120 L/s when possible, which is represented by the Outfall Node 4. The dry weather load for COD and NH_4^+ is the same as in Figure 6.7 for all SUs.

This structure will be the benchmark for the test of the optimal control in Chapters 7, 8 and 9. The following sections review modelling for prediction for control systems, giving extensive details about the different types of models and examples from literature.

6.3 Water Quality Models for Prediction

The infrastructure of the sewage system is designed to cope with the inflow of wastewater originating from the daily use of the water discarded from households and industry, which is defined as DWF. However, during rain events, a secondary inflow enters the sewer system, also known as WWF, and the capacity to store the volume of water may exceed the maximum storage volume of a retention structure (pipe or tank). As can be seen in Figure 6.16, this then results in a CSO event.

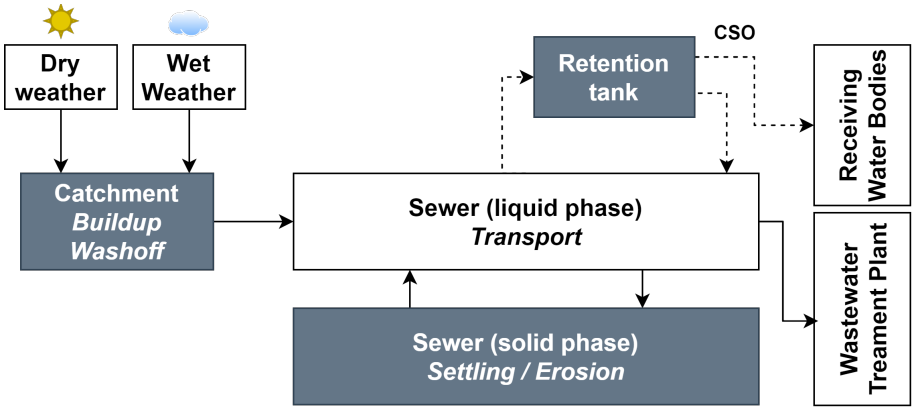

Figure 6.16: General characterisation of the sewage system [52].

The composition of the sewage network includes complex features, such as subsystems with non-linear dynamics and delays such as open-flow channels, pressured pipes, weirs, siphons, and flow joints/dividers. In addition, control of sewer networks is achieved through a combination of continuous variables (flows and volumes), and discrete variables (on-off control devices and overflow events) [53]. In general, the available storage volume in retention tanks is the main controlled variable in the network, which is manipulated by an actuator (valve or pump) located at the outlet of each retention tank that controls

the outflow. Normally, sensors are included for level and flow measurements, but estimators are often seen in their absence [54].

Sewage has both liquid and solid phases and they can be described using parameters such as Total Suspended Solids (TSS), Biochemical Oxygen Demand (BOD), Chemical Oxygen Demand (COD), Oxides of Nitrogen (NO_X), Total Kjedahl Nitrogen (TKN), Total Phosphorus (TP) and Dissolved Oxygen (DO) [4] as well as concentration of specific compounds such as Ammonium Ion (NH_4^+). The chemical and biological process of the sewage system is often viewed as a reactor where all phases interact [55] and solid particles undergo dynamic behaviours as described in [24] and [56].

Mathematical descriptions of pollutants and their known behaviour are important to understand these phenomena and to improve sewage systems models.

6.3.1 Modelling Taxonomy

Several papers developed strategies for modelling wastewater systems. In [57], a comprehensive review of mathematical descriptions of pollutants is presented, which summarises the mathematical-based models as in Figure 6.17.

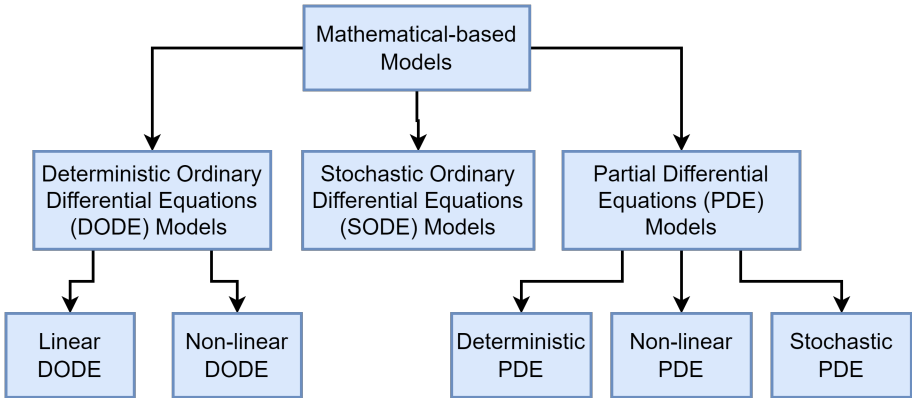

Figure 6.17: Mathematical-based model Taxonomy by [57].

In [57] a more detailed analysis for the mathematical modelling methods is provided, focussing on the methods below:

1. Deterministic Ordinary Differential Equations Models (DODE)
2. Stochastic Ordinary Differential Equations (SODE)
3. Partial Differential Equations (PDE)

These methods are used to describe the space-time evolution of pollutants dynamically, and the author presents several approaches, from a simple linear DODE, to the highly complex stochastic PDE. The final remark of the author expresses the high computational requirements for the complex methods proposed.

A more general classification was proposed in [3] based on a literature review, as seen in Figure 6.18. This taxonomy is more relevant for this thesis, because it focuses on modelling techniques applied specifically for RTC design and application, considering the time constraints, computational requirements, and acceptance that RTC systems do not require highly complex descriptions of the infrastructure. Therefore, complex models such as DODE, SODE and PDE are beyond the scope of this research. For further information on these models, the reader is encouraged to seek [58], [59], [60], [24], and [57].

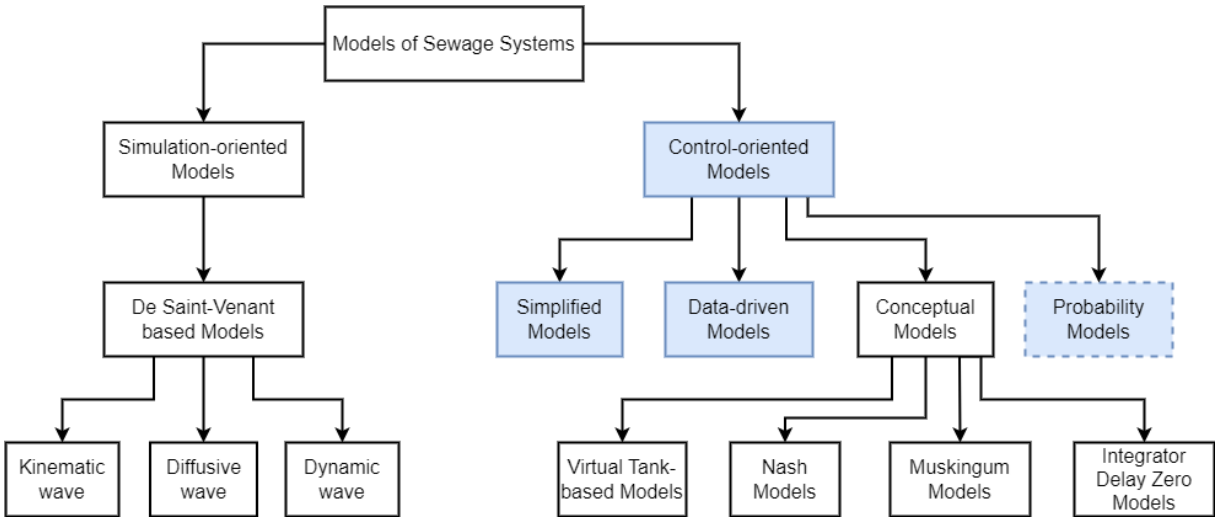

Figure 6.18: Sewage system model taxonomy proposed by [3].

The taxonomy in Figure 6.18 separates the models based on their purpose: simulation-oriented or control-oriented. In this research the focus is on water quality models needed for control implementations, and the analysis of simulation-oriented models is disregarded, though checked upon.

Control-oriented models are specifically designed to be used with control systems, which also need to factor in the relationship between accuracy and the type of controller applied. They are separated here in three main classes:

- **Simplified models** are mathematical formulations of the sewage network with simplified dynamics for the sake of a reduced computational burden. These models are characterised by a set of equations that provide an approximate behaviour of the real system.

- **Data-driven models** use process data and machine learning techniques that provide the output of the system without any knowledge of the behaviour of the sewage network. Data-driven models are commonly known as "black-box" models, since the actual mathematical model does not have physical meaning. The main use of data-driven models for control is, therefore, prediction, especially in methods where future predictions are essential for good performance.

- **Conceptual models** describe the system through a parametrisation of the SUs in the network. Each sub-category shown in Figure 6.18 represents a different way the SU is parametrised. Conceptual models are commonly used for volume-based control algorithms. Since no related conceptual model was found in the literature, this type of model is not further reviewed.

Literature research revealed methods for defining a quality model based on probability [61] that are not contemplated in the current taxonomy and, therefore, a new branch is proposed as shown in Figure 6.19.

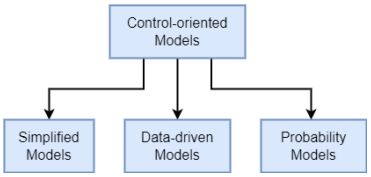

Figure 6.19: Proposed sewage system control-oriented model taxonomy.

- **Probability models** consider that not every variable of the process is deterministic and a solution is to describe the nondeterministic variable with a statistical representation [62].

The literature on pollution-based control showed that the current modelling approaches fit the proposed taxonomy. There are several important pollution-based modelling topics, such as sewer corrosion [35] [63] and greenhouse gas emission models [64], however, this thesis focuses on hydrological models and details different examples of models for each taxonomy.

6.3.2 Simplified Models

The complexity of modelling a system using phenomenological non-linear equations might prevent the model from being used for controlling the network, due to high computational cost to calculate the model's output in real time or difficult calibration of the variables to generate a reliable model. In addition, a complex model, in general, also turns the controller design into a much more complicated task. A solution is an approximation, which can be achieved by linearisation of a non-linear model or by assuming a simplified dynamic behaviour.

In a sewage network, an example of a simplified model is to approximate hydraulic elements, such as valves, pumps, pipes, and SUs with simple functions. The dynamics of pumps and valves are commonly simplified due to their relative fast action compared to the slower overall dynamic of the sewage network. Pipes and SUs can also be simplified, for example, using a plug-flow method which considers the pollutant flow with constant velocity, volume and concentration through partially filled pipes, defined by a simple time-delay. Similarly, a SU is normally approximated as a fully-mixed reactor. In the next sections, simplified models used for pollution-based control and their application are reviewed.

Concentration Balance Model

In [19], Mahmoodian defines a quality model for the sewage system, where a simple SU-based model is used with three assumptions for the pollution within the description: (i) one global indicator for pollution, (ii) a simple dilution effect and (iii) homogeneous concentrations in the SU.

Mahmoodian describes the sewage system in terms of a simple SU-based quantity model where the outflow of the SU is controlled. Each SU is modelled individually and contains a sensor for measuring the level, as depicted in Figure 6.20.

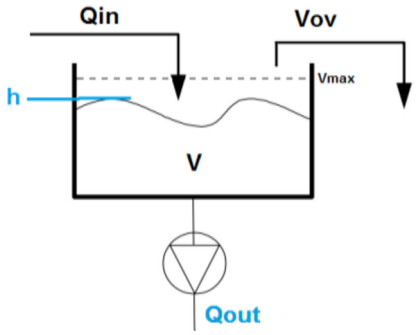

Figure 6.20: SU model for wastewater quantity modelling [19].

The inflow Q_{in}, at time t, can be derived either by measurements or by using a mass balance equation in a SU by knowing the outflow in the SU, Q_{out}, the volume V calculated using the level measurement and the volume overflow V_{ov}, as seen in Equation 6.1:

$$V(t) = V(t - \Delta t) + Q_{\text{in}}(t)\Delta t - Q_{\text{out}}(t)\Delta t - V_{\text{ov}}(t) \tag{6.1}$$

Subsequently, by connecting each SU using plug flow, the network is fully described. This mathematical formulation of the SU model can be extended to consider the concentration of the wastewater entering and leaving the SU, as presented in Figure 6.21.

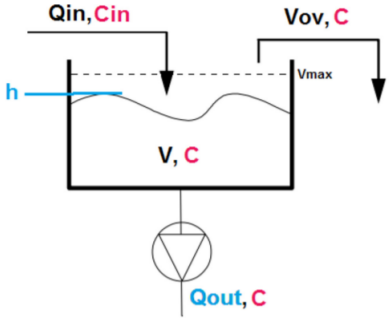

Figure 6.21: SU model for wastewater quality modelling [19].

Similarly to volume, the concentration C is calculated using the mass balance:

$$m(t) = m(t - \Delta t) + m_{\text{in}}(t)\Delta t - m_{\text{out}}(t)\Delta t - m_{\text{ov}}(t) \tag{6.2}$$

where m is the mass. By considering $m(t) = C(t)V(t)$, where C is the concentration in the SU and C_{in} is the concentration of the inflow, and $V(t) = \Delta t Q(t)$, Equation 6.2 can be written as Equation 6.3:

$$\begin{aligned} C(t)V(t) = {} & C(t - \Delta t)V(t - \Delta t) + C_{\text{in}}(t)Q_{\text{in}}(t)\Delta t \\ & - C(t - \Delta t)Q_{\text{out}}(t)\Delta t - C(t - \Delta t)V_{\text{ov}}(t) \end{aligned} \tag{6.3}$$

By manipulating Equations 6.1 and 6.3, and isolating $C(t)$, the concentration is modelled as Equation 6.4:

$$C(t) = \frac{C(t-\Delta t)V(t-\Delta t) + C_{\text{in}}(t)Q_{\text{in}}(t)\Delta t}{V(t-\Delta t) + [Q_{\text{in}} - Q_{\text{out}}]\Delta t - V_{\text{ov}}(t)} - \frac{C(t-\Delta t)Q_{\text{out}}(t)\Delta t - C(t-\Delta t)V_{\text{ov}}(t)}{V(t-\Delta t) + [Q_{\text{in}}(t) - Q_{\text{out}}(t)]\Delta t - V_{\text{ov}}(t)} \tag{6.4}$$

The author mentions that this model does not rely on measurements of concentration, which is beneficial for applications since it is not required to change the real network for the purpose of a pollution-based RTC [19]. However, it is necessary to estimate the concentration and, therefore, Mahmoodian proposes the use of a first order Taylor series to estimate C_{in} and calculate the uncertainty propagation from the derived approximation. The Taylor series uncertainty propagation is characterised by a U_X, which is the standard deviation of X such that variance of X is $Var(X) = U_X^2$. Therefore, the standard deviation for the concentration is given by Equation 6.5:

$$Var(C(t)) = U_{C(t)}^2 = \sum_{i=1}^{6} \left(\frac{\partial C(t)}{\partial A_i}\right)^2 U_{A_i}^2 \tag{6.5}$$

where A_i indicates each variable of the system.

$$A_1 = C(t-\Delta t),\ A_2 = V(t-\Delta t),\ A_3 = Q_{\text{in}}(t),$$
$$A_4 = C_{\text{in}}(t-\Delta t),\ A_5 = Q_{\text{out}}(t),\ A_6 = V_{\text{ov}}(t-\Delta t)$$

Hence, to avoid the need for measurements, the concentration can be approximated using a Taylor series and the uncertainty model from Equation 6.5 results in Equation 6.6:

$$U_{C(t)}^2 = U_{C(t-\Delta t)}^2 \left(1 - \frac{Q_{\text{in}}(t)\Delta t}{V(t)}\right)^2 + U_{C_{\text{in}}(t-\Delta t)}^2 \left(1 - \frac{Q_{\text{in}}(t)\Delta t}{V(t)}\right)^2 \tag{6.6}$$

Moreover, considering $Q_{\text{in}}(t) = Q_{\text{DW}}(t) + Q_{\text{WW}}(t)$, of which Q_{DW} is the inflow derived from dry weather and Q_{WW} is the inflow from wet weather, resulting in the uncertainty model in Equation 6.7:

$$U_{C_{\text{in}}(t)}^2 = U_{C_{\text{DW}}(t)}^2 \left(\frac{Q_{\text{DW}}(t)}{Q_{\text{in}}(t)}\right)^2 + U_{C_{\text{WW}}(t)}^2 \left(\frac{Q_{\text{WW}}(t)}{Q_{\text{in}}(t)}\right)^2 \tag{6.7}$$

Using Equations 6.6 and 6.7 it is possible to calculate the uncertainty of the unmeasured concentration in the SU and use this information for controlling the sewage system with a pollution-based RTC. This modelling is relatively straightforward, easily incorporated in a optimisation algorithm, however the assumptions of a global concentration indicator overly simplifies the model in that it makes no distinction between soluble compounds and particulate matter.

Total Suspended Solids Balance Model

Instead of modelling the concentration using a global indicator, some authors propose the use of specific analytes, such as TSS or COD. This is the case for the model in [52], which initially defines a hydraulic

model assuming a water SU container as in Figure 6.22.

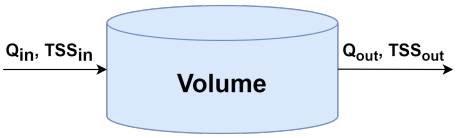

Figure 6.22: Water SU container [52].

Sun proposes three different modelling equations for the TSS:

$$\textbf{Model 1:} \quad m_{\text{out}}^{\text{TSS}}(k+1) = (1-c)m_{\text{out}}^{\text{TSS}}(k) + cm_{\text{in}}^{\text{TSS}}(k) \tag{6.8}$$

where $m_{\text{in}}^{\text{TSS}}$ and $m_{\text{out}}^{\text{TSS}}$ are the TSS entering the structure and the TSS leaving the structure, respectively. Equation 6.8 can be generalised such that the calibration parameter c can be independent for $m_{\text{in}}^{\text{TSS}}$ and $m_{\text{out}}^{\text{TSS}}$, showed in Equation 6.9:

$$\textbf{Model 2:} \quad m_{\text{out}}^{\text{TSS}}(k+1) = c_1 m_{\text{out}}^{\text{TSS}}(k) + c_2 m_{\text{in}}^{\text{TSS}}(k) \tag{6.9}$$

which c_1 and c_2 are calibration parameters for $m_{\text{out}}^{\text{TSS}}$ and $m_{\text{in}}^{\text{TSS}}$ respectively. Furthermore, as mentioned previously, the TSS is affected by sedimentation, erosion and time delays in its dynamics. Thus, Sun upgraded the model to add this information and improve the characterisation, resulting in Equation 6.10a and 6.10b:

$$\textbf{Model 3:} \quad m_{\text{out}}^{\text{TSS}}(k) = c_{vc} m_{\text{in}}^{\text{TSS}}(k-d) + e_p \tag{6.10a}$$

$$Q_{\text{out}}(k) = t_{vc} Q_{\text{in}}(k-d') \tag{6.10b}$$

where d is the delay of TSS, d' is the delay of the flow and c_{vc}, t_{vc} and e_p are parameters that need calibration. Sun et al discusses that, using these modelling methodologies, it is possible to develop a pollution-based RTC, although it is necessary to have an online calibration of several parameters, which are done via a general algebraic modelling system (GAMS) using historic or real-time data from telemetry systems. In a comparison between the three proposed models, all three behaved similarly, whereas Model 2 was slightly better. It is suggested to use a simulation software such as SWMM [40] for the real-time calibration of parameters. For that reason, these models are highly sensitive to changes in the sewer system and need to be actively calibrated to guarantee a reliable prediction.

Effluent Quality Index Model

The last simplified model presented establishes an effluent quality index that is used to measure the pollution load, integrating the following pollutants together: TSS, BOD, COD, NO_X, TKN, and TP. The model characterisation can be seen in [65] and is further described in [4]. It is a unique approach, modelling several types of pollutants simultaneously, allowing a more complex understanding of the sewage system. The effluent quality index (EQI) is defined by Equation 6.11:

$$EQI = \frac{1}{1000(t_f - t_0)} \int_{t_0}^{t_f} C_t Q_{\text{ov}}(t) dt \tag{6.11}$$

where t_f and t_0 are the final and initial instants, respectively, and:

$$C_t = \beta_{\text{TSS}} C_{\text{TSS}} + \beta_{\text{COD}} C_{\text{COD}} + \beta_{\text{BOD}} C_{\text{BOD}} + \beta_{\text{NOX}} C_{\text{NOX}} + \beta_{\text{TKN}} C_{\text{TKN}} + \beta_{\text{TP}} C_{\text{TP}}$$

where C_x and β_x corresponds to the concentration and weights for each pollutant x, respectively. The quality index modelling increases the complexity of the optimisation by increasing the number of variables, while also requiring measurement (or estimation) of several concentration parameters. This introduces more uncertainties to the optimisation where those measurements are unreliable or non-existent, degrading the control of the network. However, this technique greatly improves the versatility of the algorithm, allowing to control different types of pollutants independently. The model also enables the control algorithm to be customised depending on the requirements of the network, increasing the importance of certain pollutants for the controller.

Section Summary

Simplified models are generally used in sewage system applications which have highly non-linear and complex dynamics, approximating the system with sufficient accuracy for control. Although the assumptions needed for a simplified model might seem excessively simplistic, for real time control, these models are attractive because of their low computational effort and easy implementation.

6.3.3 Data-driven Models

The use of data and machine learning techniques is the foundation of data-driven models. When using simplified models, information of the behaviour of the system is lost for the sake of faster computation and, also, the calibration of model parameters needed are hard to calculate due to uncertainties [66]. Assuming that the model is perfectly calibrated, there is no guarantee that the calibration remains unchanged over time. In fact the system is constantly changing due to shifts in wastewater patterns, seasonal runoff dependencies and land use changes [67]. An alternative is to use data-driven modelling approaches, which rely on real time data processing to represent the dynamics of different variables of the wastewater network, either by using data from software simulation, on field measurements or historical data [68].

The continuous evolution of sensors [69,70] has led to an increasing number of studies and implementations of data-driven models, encouraging their application in real-time [71]. A few papers exists that summarise data-driven models for pollution-based systems; [72] reviews detection methods and indicator parameters for quality measurements with an extensive detailing of each type of pollutant's measuring device and a short description of each; [73] reviews and proposes source identification methods for tracking illicit discharges with low cost, showing a good precision for cost-effective analytical techniques; [74] details the modelling of water quality in sewers, providing an extensive review of sewage systems including data-driven models for different purposes.

Data-driven models are easier to adjust to different types of water quality data than other models. The main reason for that is the ability to derive a suitable model regardless of the behaviour of the system

through the use of process data and algorithms that mimic human learning. In this section, data-driven models utilised in combination with RTC systems are presented. One notable work is the publication of [75], which studies different deep learning algorithms to predict several water quality parameters. The paper proposed several models used to predict sedimentation and compare the results using five deep learning algorithms: Multi Linear Regression (MLR), Multilayer Perceptron (MLP),Recurrent Neural Network (RNN), Long Short-term Memory (LSTM), Recurrent Gate Unit (GRU).

Multiple Linear Regression and Neural Network Techniques for Sediment Prediction

Al Ani [75] studied and compared two different data-driven models, a MLR based on [76] and a neural network model based on [77], where both methods are used for predicting in-sewer location and sediment deposition. It presents an assessment of these models to establish the sediment accumulation, where the models inputs and outputs are shown in Table 6.1, given that the sediment depth, d_s, is the dependant variable.

Table 6.1: Variables and their definitions [75].

Variable	Definition
d_s	Average sediment depth in a sewer (cm)
NOC	Number of connections to a sewer
D	Diameter of the sewer (m)
Q	Sewer capacity (m^3/s)
S	Sewer gradient (%)
Q_{peak}	Peak flow (m^3/s)
L	Length of the sewer (m)
V_{peak}	Velocity occurring at peak flow (m/s)
$L_{cum.}$	Cumulative sewer length (m)
d_{peak}	Depth of flow at peak flow (m)
$L_{dir.}$	Cumulative sewer length in a direction (m)
τ_{peak}	Average tractive stress at peak flow (Pa)

The methodology for both methods is similar and is generalised as shown in Figure 6.23. First, the data collection and processing is relevant to determine the variables of the process and perform preliminary analysis of the data. This processing helps to improve the quality of the data and facilitate the use of the data set. The next step is the design of the model, that comprises the selection of several methods that will use the data to create models. In sequence, the estimation and assessment of each model is done and a data set is generated specifically for testing. Finally, a model is selected and validated, defining the most efficient model and using different scenarios for the validation.

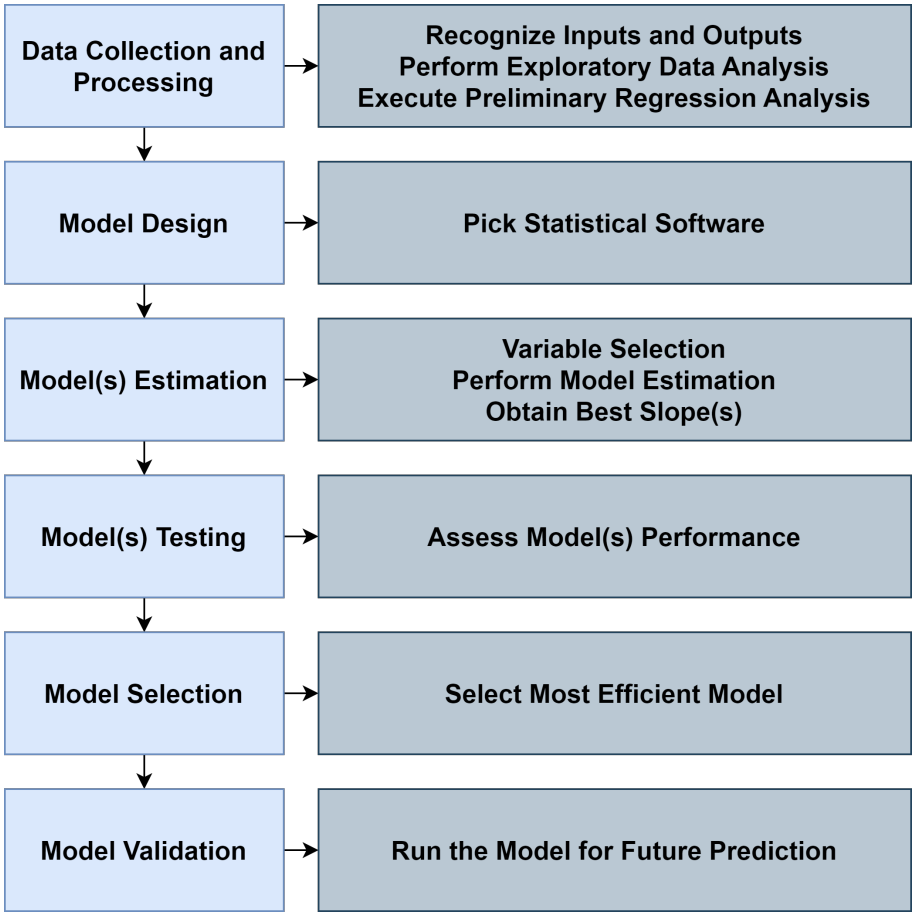

Figure 6.23: Methodology for MLR and ANN methods [75].

Multiple Linear Regression Model

The Linear Regression method is a technique where a single output variable is derived using a simple linear equation from a single input. A more generalised formulation, called Multiple Linear Regression (MLR), approximates the output by multiple inputs simultaneously. The output of the regression model, Y, is calculated by using the following model for n points collected [78]:

$$Y_i = \rho_0 + \rho_1 X_{i1} + \rho_2 X_{i2} + \rho_p X_{ip} + \chi, \quad i = 1, 2, ..., n \tag{6.12}$$

where ρ_0 is an offset variable, ρ_1, ρ_2 and ρ_p are the regression coefficients for the independent variables X_1, X_2 and X_p, respectively and χ is the error associated with the model. In order to calculated the coefficients X, the model in Equation 6.12 is rewritten to be represented in matrix form, which yields Equation 6.13:

$$Y = X\rho + \chi \tag{6.13}$$

Herein, the output Y and error χ are n-dimensional vectors, the input matrix X is $n \times (p+1)$ and the coefficient vector ρ is $(p+1)$-dimensional. Using a least-square regression, the coefficient ρ can be found by Equation 6.14:

$$\rho = (X^T X)^{-1} X^T \tag{6.14}$$

Al-Ani implemented the algorithm for a specific process in Baghdad where a sediment survey was carried out in the sewer system of the city. The implementation of the method was done using the software SPSS Neural Network [79] developed by IBM, which resulted in Equation 6.15, a linear model using the MLR algorithm as below:

$$\begin{aligned} d_s =& 0.036L_{cum.} + 0.203L + 6.685NOC \\ & - 1.142Z - 0.022L_{dir.} - 48.493 \end{aligned} \tag{6.15}$$

By using collected data, the MLR model is able to predict sediment accumulation throughout the sewer, using a simple approach with very low computational cost. An advantage of this method is that little knowledge of the behaviour of the sewer is required and as long as new data-sets are acquired, the models coefficients are easily re-identified to improve the performance, since it is known that the dynamics of a sewage network change over time. However, the main issue with this approach is the reliability of the data used for the identification and also the error inherent to measuring systems, which increases the error of the MLR method if the sensors used in the data collection are not correctly placed or calibrated.

Artificial Neural Network Model

Modelling sewage systems with Artificial Neural Network (ANN) is a method often seen in the literature. It is mainly applied for regression and classification [80]. The ANN emulates the human brain using underlying relationships between data sets, using an architecture comprised by a Input Layer, a number of Hidden Layers and an Output Layer [75]. The most common architecture is the Multilayer Perceptron (MLP), a feedforward architecture which uses backpropagation as the learning algorithm.

The data used in the MLP approach is divided into three sets: a training set which is used to find the weights of the neural network, the testing set, responsible for checking the error and avoid over-training of the network and the validation set that is used for validation of the model derived from previous training.

The MLP-ANN proposed by Al-Ani et al was identified using the tool SPSS Neural Network and the resulting model for the same sewer in Baghdad resulted in one neuron with a single hidden layer, while the weights of the network were optimised using a gradient descent method as criteria for training the neural network model. Equation 6.16 is the final result in a mathematical expression:

$$d_s = 1.716 * tanh(X) + 0.04 \tag{6.16}$$

where X is defined in Equation 6.17 below:

$$\begin{aligned} X =& 0.024 + 0.114NOC + 0.027L - 0.262S \\ & + 0.758D - 1.495Q_{peak} + 0.207V_{peak} \\ & + 0.326Q + 0.304Q_{peak}/Q \\ & + 0.325d_{peak}/D + 0.148\tau_{peak} \end{aligned} \tag{6.17}$$

There are several advantages of using a ANN-MLP, but, specifically for a sediment accumulation model, the ability to adapt to complex relationships between dependant and independent variables and to changes that occur in the process is very unique [81]. Besides that, there are many open-source software packages

available for implementing ANN´s, such as scikit-learn, a simple library of machine learning methods using python [82] and OpenNN, a neural network library for C++ [83]. The main disadvantage of using neural networks is finding the best network structure, i.e. the selection of number of layers and number of neurons in each layer, as well as the selection of other parameters of the neural network, which in most cases is done by trial and error although there are optimisation techniques that solve this issue. Another disadvantage is the lack of intuition on the model, since it is difficult to understand the reasoning behind the solution provided by the network.

Deep Learning Algorithm for Multi-Source Data Fusion to Predict Water Quality of Urban Sewer Networks

A similar solution developed in the data-driven modelling framework was proposed by [84], which also used a similar approach to the MLP proposed by Al-Ani, however with the objective of using multi-source data fusion and deep machine learning models to predict several pollutants, such as BOD, COD, NH_4^+, TKN and TP.

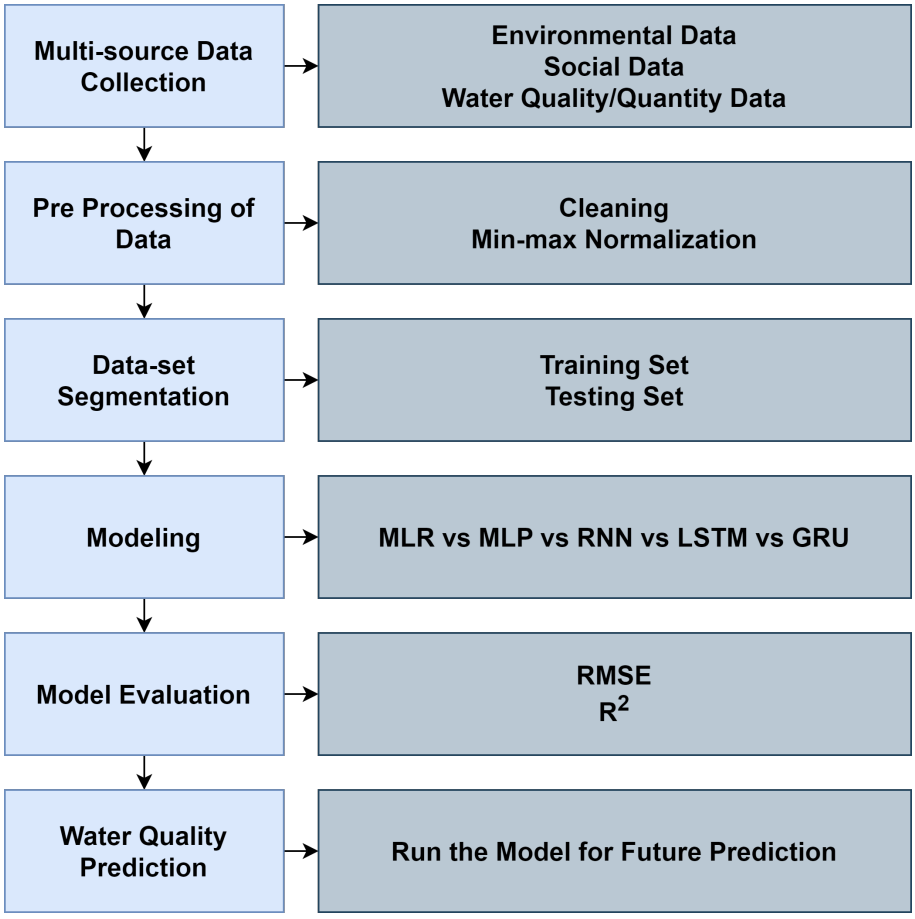

Figure 6.24: Framework for water quality prediction [74].

Jiang defines the framework as shown in Figure 6.24. The first step starts with data collection from several sources, such as (1) environmental data, (2) social data, (3) water quality data and (4) water

quantity data. Then, the multi-source data is pre-processed and separated in a training and testing set. Finally, the author compares several deep learning algorithm to predict the water quality. The algorithms the author studied are MLR, ANN-MLP, RNN, LSTM and GRU. The case study was realised using data from a southern city in China. The input dataset consists of: land area, drain pipe diameter, population, drinking water supply, flow, volume, level, pH, temperature, conductivity and suspended solids. The output indicators are BOD, COD, $NH_4{}^+$, TKN and TP. The comparison of the models was done using Root Mean Squared Error (RMSE) and R^2 metrics. The conclusions are the following:

1. MLP is more suitable for water quality prediction than MLR because traditional machine learning algorithms are better for multi-source data than linear methods.

2. RNN-based methods are better than MLP because those methods have an advantage when handling time series data.

3. Among the deep learning methods, GRU showed a significant better performance than RNN and LSTM for most indicators.

The author concludes that, although the prediction of water quality using deep learning algorithms has great potential, these models depend on the input indicator selected from the data set used and it is crucial to understand which of these indicators are key for training-learning models.

Section Summary

The exponential improvements in computer performance and artificial intelligence increases potential practical implementation of deep learning models with big data, therefore the research on water quality prediction with deep learning has a potential to be key for the future. The ability to adapt to complex dynamics without complete knowledge of such phenomena is appealing but has limitations.

6.3.4 Probability Models

The use of simplified and data-driven models introduces errors due to uncertainties, which means that the prediction using these types of model for controlling purposes might be less reliable. An alternative modelling technique is using models that factor these uncertainties using probabilistic assumptions of the system, also known as stochastic models [62]. The difference between the deterministic and stochastic model is that the later considers the description of the uncertainty within its formulation using a statistical approach.

DO and BOD Transport Model

Water quality indicators such as DO and BOD have a big impact on receiving bodies of water when there is wastewater overflow. Their transport in sewer systems is a complex process and is usually approached in modelling systems by assuming a fixed concentration or by estimation using isolated measurements [85]. However, that leads to the effect that information regarding the concentration during storm events are lost. The solution proposed by [86] is to use a probabilistic model that is able to describe the dynamics

of the process. This reduces uncertainties because it does not require a complex parametrisation of the complete sewer network and the model only needs an input value for each catchment. The catchment is shown in Figure 6.25, where the overall flow is the combination of a dry weather flow and an overland flow, which is separated as a pervious and impervious overland flow.

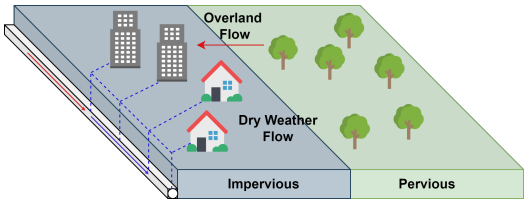

Figure 6.25: Representation of a catchment by [86].

Firstly, Morales defines the flow path using state variables, i.e, the pervious overland state ($x_{o_i,\text{perv}}$), impervious overland state ($x_{o_i,\text{imp}}$) and the dry weather flow state (x_{DWF_i}), as well as a series of conduit states (x_c), where $i = 1, 2, ..., n$ and n is the number of catchments. Then, in Equation 6.18 is shown the probability of the load in each flow:

$$\begin{aligned} P_{x_{o_i,\text{perv}}}(t) &= \frac{\Xi_{i,\text{perv}}(t)}{\Xi_T(t)} \\ P_{x_{o_i,\text{imp}}}(t) &= \frac{\Xi_{i,\text{imp}}(t)}{\Xi_T(t)} \\ P_{x_{\text{DWF}_i}}(t) &= \frac{\Xi_{\text{DWF}_i}(t)}{\Xi_T(t)} \end{aligned} \tag{6.18}$$

where $\Xi_{i,\text{perv}}$, $\Xi_{i,\text{imp}}$ and Ξ_{DWF_i} are the total constituent loads from the ith pervious, impervious and dry weather flow regions at time t, respectively.

Morales then describes a travel time probability distribution $f(t')$, where t' is a random variable associated with the travel time of a drop of water in the network, and where $f(t')$ allows to derive the concentration in the outlet, by propagating the concentration through the network. The calculation of $f(t')$ extends the work of [87] by taking into account non-conservation of mass in the BOD and DO during the travel time. Finally, the combined pollutograph at the outlet of the sewer network is calculated by convolving the travel time probability distribution and the total load, given by Equation 6.19:

$$\Xi(t) = \sum_{t'=1}^{\infty} [f(t, t') \times \Xi_T(t)] \tag{6.19}$$

The model proposed proved to be an alternative formulation for prediction of BOD and DO in control systems. When comparing with the benchmark software SWMM, the performance of the model showed a good accuracy while requiring less information and time for the implementation. However, this method is much less intuitive and the use of probabilistic variables are not a straightforward approach as the estimation of such variables are complex and harder to grasp.

Bayesian multi-objective calibration for TSS predictions

The representation proposed by [88] is a stochastic model for TSS prediction where the goal is to improve the model errors by using statistical description of the bias. It uses an auto-regressive error model to provide more reliable estimation of TSS and reduce the uncertainty of TSS using a Bayesian multi-objective approach to improve calibration of the model. The general mathematical description of a stochastic model is given by Equation 6.20:

$$\tilde{\boldsymbol{Y}}(\boldsymbol{X}, \boldsymbol{\theta^M}, \boldsymbol{\theta^\epsilon}) = \boldsymbol{Y_M}(\boldsymbol{X}, \boldsymbol{\theta^M}) + \tilde{\boldsymbol{B}}_{\boldsymbol{M}}(\boldsymbol{X}, \boldsymbol{\theta^\epsilon}) + \tilde{\boldsymbol{E}}(\boldsymbol{\theta^\epsilon}) \tag{6.20}$$

where $\boldsymbol{Y_M}(\boldsymbol{X}, \boldsymbol{\theta^M})$ is the deterministic output of the model, $\tilde{\boldsymbol{Y}}(\boldsymbol{X}, \boldsymbol{\theta^M}, \boldsymbol{\theta^\epsilon})$ is the real output of the model, i.e., the sum of the deterministic model with the error, hence $\tilde{\boldsymbol{Y}}(\boldsymbol{X}, \boldsymbol{\theta^M}, \boldsymbol{\theta^\epsilon})$ is a random variable. The inputs of the system is $\boldsymbol{X}$ the parameter of the deterministic model is represented by $\boldsymbol{\theta^M}$ and the parameter of the error is $\boldsymbol{\theta^\epsilon}$. The variable $\tilde{\boldsymbol{B}}_{\boldsymbol{M}}(\boldsymbol{X}, \boldsymbol{\theta^\epsilon})$ is used to describe the model bias and $\tilde{\boldsymbol{E}}(\boldsymbol{\theta^\epsilon})$ describe the random measurement noise.

The output $\tilde{\boldsymbol{Y}}$ is modelled as a random variable and the author defined the prediction as a predictive probability distribution $p(\tilde{\boldsymbol{Y}}|\boldsymbol{X})$, which is calculated using a Bayesian approach:

$$p(\tilde{\boldsymbol{Y}}|\boldsymbol{X}) = \int p(\boldsymbol{Y^0}|\boldsymbol{\theta}, \boldsymbol{X}) p(\boldsymbol{\theta}) d\boldsymbol{\theta} \tag{6.21}$$

where $p(\boldsymbol{\theta})$ represents the prior knowledge of the parameters $\boldsymbol{\theta}$, $p(\boldsymbol{Y^0}|\boldsymbol{\theta}, \boldsymbol{X})$ is the likelihood function of the model that measures the probability an output $\boldsymbol{Y^0}$ is generated by the model given an input $\boldsymbol{X}$ and the a parameter chosen randomly from $p(\boldsymbol{\theta})$.

Using Equation 6.21, the model proposed by Sikorska to predict the TSS can be derived, resulting in Equation 6.22:

$$\begin{aligned} \tilde{\boldsymbol{C}}_{\boldsymbol{TSS}}(\boldsymbol{P^0}, \boldsymbol{\theta}) = & \boldsymbol{C_{TSS}}(\boldsymbol{P^0}, \boldsymbol{\theta}) \\ & + \tilde{\boldsymbol{B}}_{\boldsymbol{M_{BW} \times M_{RR}}}(\boldsymbol{P^0}, \boldsymbol{\theta}) \\ & + \tilde{\boldsymbol{E}}_{\boldsymbol{TSS}}(\boldsymbol{\theta}) \end{aligned} \tag{6.22}$$

where $\tilde{\boldsymbol{B}}_{\boldsymbol{M_{BW} \times M_{RR}}}$ comprises the systematic prediction errors of the concentration of TSS, $\boldsymbol{C_{TSS}}$, due to build-up/wash-off (BW) and rainfall/runoff (RR) model components and $\tilde{\boldsymbol{E}}_{\boldsymbol{TSS}}$ describes the random errors of the prediction of TSS. The likelihood function of the TSS model is given by $p(\boldsymbol{C^0_{TSS}}|\boldsymbol{\theta}, \boldsymbol{P_0})$.

The author further discuss the model by including multiple outputs, such as flows and precipitation. This modelling approach showed an improvement in the prediction efficiency of the TSS model and the bias description led to a more reliable uncertainty estimation. The main challenge of the approach is formulating the model bias using prior information, since the bias is defined to compensate different error sources, which not always have a direct physical interpretation.

Section Summary

Probability models for quality prediction are an interesting approach to consider uncertainty in the formulation of the control. Such formulation can increase robustness and improve the performance of the

controller in scenarios where randomness is known with good accuracy.

6.4 Pollution-based Control Strategies

Generally, the main goal of PRTC is to reduce environmental impact of the wastewater network by introducing pollution information in the controller. The difference between PRTC approaches is how this information is handled within the formulation of the controller, the type of pollutant controlled and the framework used to describe the pollution. It is proposed the following PRTC methods classification:

- **Rule-based Real Time Control**: the control algorithm is defined using heuristics. These heuristics are usually in the form of rules that are imposed to the problem and expect a specific behaviour if the rules are followed. A pollution-based approach using this formulation defines several rules applied to the sewage control system, for example, the algorithm checks if the concentration in a given basin is higher than a certain a value and proposes an action depending on the output of this rule (which is generally a 'yes' or 'no' output);
- **Optimisation-based Real Time Control**: in this type of method, the overall objective is achieved by minimising (or maximising) a function using optimisation methods, which will provide an optimum operation of the system. Each method can have different objective functions depending on the desired behaviour of the system. One example is a PRTC based on MPC, which is an algorithm that optimises a cost function in order to control the system over a prediction horizon using a model to predict the behaviour of the system. In the case of a pollution-based scenario, a common objective defined in the optimisation is to minimise the concentration during overflows of SU structures.
- **Reinforcement Learning-based Real Time Control**: through a Reinforcement Learning (RL) method, an algorithm learns the behaviour of the system by a trial-and-error experience and by rewarding control actions that meet specific goals. This reward based structure will steer the algorithm towards the actions that maximise the output. For example, A RL-based RTC can be developed to improve the water quality by rewarding control actions where the concentration of overflowed wastewater is reduced [89].

6.4.1 Rule-based RTC

Due to high complexity of the dynamics of sewage systems, the definition of a model is a difficult task to be achieved. Therefore, efforts have been done to create real time control systems which avoided the use of models and one example are rule-based systems, where the control strategy is based on heuristics [32]. Control algorithms based on heuristics are usually more intuitive for operators since the control rules are based on logical statements using expert knowledge of the behaviour of the sewage system. Also, rule-based RTC systems do not require the definition of an optimisation problem and, therefore, the control is less complex and demand less computational power for computing the solution. Combining all these advantages it is clear that rule-based RTC is an attractive solution for controlling sewage systems and several researches focused their effort specifically in designing rule-based RTC systems in an pollution-based framework [32].

Water quality data-informed real-time control

The algorithm proposed by [90] adds a real time controller to the normal operation of the sewage system by adding rules to the behaviour of the system and using the available data. The author defines this controller as a water quality-informed real-time active control due to the fact that the algorithm uses quality (and rain) monitoring to derive a RTC based on rules that are applied and are actively controlling the sewage system. The author defines four possible control rules in his study, a passive control, a retention control, an on/off control and a TSS control, as can be seen in Table 6.2. Each of these rules have a different impact on the behaviour depending on the current state of the system and each control rule is dependant on different variables of the sewage system. The baseline operation is the passive control that is an operating mode where the actuator (a valve) is constantly open.

Table 6.2: Control rules implemented in [90].

Type	Description
Passive Control	Valve always open
Retention Control	If an event occurs, valve opening = 0% Else, valve opening = 100%
On/off Control	if $h < h_c$, valve opening = 0% if $h \geq h_c$, valve opening = 100%
TSS Control	if $C \geq C_c$, valve opening = 0% if $C < C_c$, valve opening = 100%

The retention control mode differs by monitoring inflow events and acting whenever a event occurs, which activates the retention controller and completely closes the valve. The valve is kept closed for a specific duration t_d, called the retention time, with the objective of storing the inflow volume into the structure. The third mode, on-off control, defines a threshold value for the level of the SU structure, called h_c, and if the water level is below h_c, the valve is remained closed, however when it reaches the threshold, is completely opened to drain the volume within the SU. These two modes are traditional volume-based algorithms, thus, to improve the quality of the sewage, Sharior proposes a fourth mode that takes into account the concentration of TSS inside the SU, called the TSS Control mode. The general idea is similar to on-off control mode, the difference is the threshold refers to the TSS concentration, called C_c, and the logic of the on-off actuation is different. In the TSS control, when the concentration of TSS is above a threshold concentration, the valve is fully closed, otherwise, it is opened. The goal of this procedure is to increase dilution when rain events occur to decrease the concentration and when the concentration reaches a specified value, the valve is opened and drains the SU, sending this volume towards the treatment plant.

The method proposed does not use an explicit model, the author clarifies that measurements were used for the formulation, implementation and simulation of the algorithm.

Quality control based on retention time

An interesting approach for controlling a urban drainage system using a rule-based algorithm was presented by [12], differing from the previous algorithm by using only a volume-based set of rules to influence

the quality of the wastewater within the drainage system during dry-weather periods. The goal of this algorithm is to control the settling process in the stormwater basin and, as a result, influence the TSS retention time using a generic formulation that considers a required volume in the basin and information regarding runoff and rainfall [12].

This algorithm is activated during dry-weather periods, whereas during wet-weather, a volume-based optimisation is implemented without any quality aspects. Therefore, since the only interest is in RTC systems that are directly impacting the pollution in the receiving water bodies, here, the only aspect discussed is the implementation of the, dry-weather, rule-based controller. The author defines four rules to control the wastewater system, as showed in Equation 6.23 below:

$$
\begin{aligned}
&\text{if } \; t_{nextrain} \leq t_e : \\
&\quad \longrightarrow Q_t = Q_{max} \\
&\text{if } \; t_e < t_{nextrain} \leq t_e + 20h : \\
&\quad \longrightarrow Q_t = Q_{max} * \frac{t_e}{t_{nextrain} - t_f} \\
&\text{if } \; t_e + 20h \leq t_{nextrain} < 40h + t_e^{max} : \\
&\quad \longrightarrow Q_t = Q_{max} * \frac{t_e + 20h}{t_{nextrain} - t_f} \\
&\text{if } \; t_{nextrain} \geq 40h + t_e^{max} : \\
&\quad \longrightarrow \begin{cases} Q_t = 0 & \forall t < 40h \\ Q_t = Q_{max} * \frac{t_e}{t_e^{max}} & \forall t \in (40h, 40h + t_e^{max}) \end{cases}
\end{aligned}
\tag{6.23}
$$

with t_e being the emptying time of the basin until availability of the storage volume V_{req} at maximum outflow $Q_{max}(s)$. The author assumes that the main characteristics of the sewage systems are known, such as the inflow to the basin, and therefore no model for control is used.

An important advantage of using this method, as mentioned by the author, is that the use of this set of rules ensures that the available volume within the basin is sufficient to handle the predicted upcoming rain event without overflow, which reduces the discharge of highly concentrated volumes. However, the main disadvantage with this approach is that the control is considered only on a local scale, the downstream areas are not considered globally. Therefore, this method is unable to find a global optimum operation for the sewer system as a whole, which would greatly increase the complexity of the overall method and new rules would need to be applied, whereas the intuitiveness commonly found in rule-based algorithms is lost due to a higher number of rules necessary.

Double-gate storage scheme based on water quality

The next rule-based RTC described was developed by [91], called a double-gate storage scheme for water quality control. The author mentions that traditional interception-storage SU control designs are unable to deal precisely with the pollution problem in combined sewer overflows, therefore, they developed a method which directly influences the variance of a pollutant with the flow-rate. In the paper, Wei presents the solution applied specifically for controlling the COD concentration, defining rules in a double-gate

scheme. The COD concentration is monitored in the system's SU and well chamber and, using this measurement, the rule-based controller will act accordingly.

The well chamber has an intercepting weir that, when opened, directs the inflow directly to a receiving body of water. Also, the chamber is connected through a intercepting pipe to the SU which will store the stormwater. During dry-weather, the double-gate is offline, the intercepting weir is closed and the inflow is directed to the municipal sewage pipe. However, when rain events occurs, the controller comes online and starts its operation depending on the current COD concentration measured.

- Firstly, a COD concentration threshold C_t is defined for the concentration within the well chamber, which indicates a value for the COD that is safe to discharge.
- If the concentration within the well chamber is below the C_t, this flow is directed to the receiving body water and safely discharged.
- However, when the current COD measurement is above C_t, the waste intercepting pipe is opened and the waste is stored in the SU while there is enough capacity.
- Eventually the waste in the SU is directed to the municipal sewage pipe.

The method developed by Wei showed a great reduction in the concentration of COD in the discharge and also a great improvement over traditional schemes commonly used for dealing with storm-water overflows. The method uses measuring devices to act directly on the concentration, which is a promising technology but which is still complex and expensive for in-situ and on-site quality assessment [33]. The tuning of this method is relatively simple, needing only the threshold COD, but similarly to the previous method, is limited to local storage control and does not provide a globally optimum solution.

Section Summary

In Table 6.3 several papers are shown with more implementations of rule-based RTC. They are separated in Local methods, indicating that each CSO is controlled individually and Local Pollution Rule-based + Global Volume-based Optimisation, that differ by integrating the pollution rule-based local RTC with a volume-based optimisation. In general, rule-based methods are simple and show improvements in local structures regarding load management. However, the capability of globally observing the network system is limited and to design a global rule-based approach requires complex interactions of rules. In the reviewed papers, water level and quality sensors are included in the formulation of the control algorithm, instead, a simplified or data-driven model could overcome situations where measurements are not available.

6.4.2 Optimisation-based RTC

Optimisation-based control is a method that relies on an optimisation problem which determines an optimum behaviour based on control objectives through a minimisation (or maximisation) [3]. The advantage is the possibility to control the system globally and the additional use of constraints, which restrict the optimum space solution to guarantee that the control will operate within physical requirements (e.g, a valve actuator will not open more than 100%). The difference between types of optimisation-based

Table 6.3: Papers on rule-based RTC methods with pollution aspects.

Authors	Year	Type of Control	Description	Type of Pollutant
[92]	1997	Local Pollution Rule-based + Global Volume-based Optimisation	Minimisation of overflow concentration and tracking of pollution discharge to WWTP using a global volume-based optimisation and rule-based local concentration-based control.	Multiple pollutants
[93]	1999	Global	Fuzzy logic control and genetic algorithms are applied to achieve improved pump operations in a combined sewer. It is concluded that current pump operations can be improved by adding the water quality to the input variables.	Global indicator
[8]	2005	Global	Rule-based control of WWTP flow overload using measurement of ammonia in the river.	NH_4^+
[94]	2005	Global	A rule interpreter was developed to make control decisions based on rules (if–then relations), which are evaluated with the aid of fuzzy logic and input values such as water levels, flows, etc.	COD
[95]	2011	Local	A real-time control strategy for separation of highly polluted storm water based on UV–Vis online measurements.	TSS using real-time water quality measurement
[96]	2013	Local	Rule-based retention control improving water quality by maximising the retention time of water in the pond to increase the TSS removal efficiency through sedimentation.	TSS
[97]	2021	Local Pollution Rule-based + Global Volume-based Optimisation	Rule-based combined with a predictive dynamic control for optimal operation of stormwater system regulators during rainfall periods, while applying heuristic control for water quality control to detain runoff in the basin during dry weather periods.	Sedimentation

RTC is the method used to solve the optimum problem, which might demand a non-linear algorithm, for example, or bayesian optimisation which relies on black-box models. The objectives defined for each method may also change, depending on the desired behaviour.

The optimisation-based RTC can be generalised in state-space representation as Equation 6.24 [98]:

$$\begin{aligned} &\min_{u(k)} J(k) \\ &\text{s.t.} \\ &h(x(k), u(k), w(k)) \geq 0 \\ &g(x(k), u(k), w(k)) = 0 \\ &x_{min} \leq x(k) \leq x_{max} \\ &u_{min} \leq u(k) \leq u_{max} \end{aligned} \tag{6.24}$$

where x, u and w are the states, controlled variables and disturbances, respectively, J is the cost function, h and g are functions that represents the inequality and equality equations, respectively, used in the constraints.

Pollution-based methods are distinct for the use of pollution information, therefore, the objectives of the optimisation problem are extended or changed to deal with water quality aspects, such as minimise load overflow or maximise the load inflow to the WWTP.

Pollution-based MPC for TSS

Policies and regulations on water quality have been made by individual environmental agencies which increase the necessity for specific pollutants to be tighter controlled and monitored. Therefore, new strategies are being studied with the objective of developing RTC systems that are capable of controlling specific pollutants in sewers. In this context, [18] proposed a MPC strategy which seeks to minimise the total amount of pollutants released to receiving bodies of water, focusing on the TSS, with the justification that this pollutant can be easily measured continuously online.

The pollution-based objective defined by Sun is given by the following function in Equation 6.25:

$$J = \sum_{i=n}^{n+N} \lambda^{\text{TSS}} \nu_1(i) + \beta^{\text{TSS}} \nu_2(i) + \alpha^{\text{TSS}} \nu_3(i) + \gamma^{\text{TSS}} \nu_4(i) \tag{6.25}$$

ν_1, in Equation 6.26, is an objective used for minimising the combined sewer overflow (CSO) in the sewage system:

$$\nu_1(k) = \Delta t \sum_{i=1}^{n_{cso}} Q^i_{\text{ov}}(k)^2 + Q_{bypass}(k)^2 \tag{6.26}$$

where n_{cso} is the number of CSO-diverting points, q^i_{cso} is the overflow from the $i-th$ point and Q_{bypass} is the bypassed overflow from the WWTP when the inflow to the treatment plant exceeded capacity. ν_2, in Equation 6.27, is an objective that tries to keep the flow incoming to the WWTP, Q_w, close to the maximum allowed inflow to the WWTP, Q^{wwtp}_{lim}:

$$\nu_2(k) = \left(Q_w(k) - Q^{wwtp}_{lim}(k)\right)^2 \tag{6.27}$$

ν_3, in Equation 6.28, is an objective to smooth variations in the output variable by minimising the

difference between the current output $u(k)$ with the previous optimum $u(k-1)$:

$$\nu_3(k) = \sum_{i=1}^{n_g} \left(u^i(k) - u^i(k-1)\right)^2 \tag{6.28}$$

where n_g is the number of controlled decision variables of the optimisation problem. Finally, ν_4, in Equation 6.29, is a quality based objective where the load in overflow of TSS is minimised:

$$\nu_4(k) = \sum_{i=1}^{n_{cso}} C^i_{\text{ov}}(k) Q^i_{\text{ov}}(k) + C^i_{bypass}(k) Q^i_{bypass}(k) \tag{6.29}$$

where C_{ov} is the TSS concentration of the CSO and $C_{bypassed}$ is the TSS concentration at the WWTP inlet. The final optimisation problem is then written in a form similar to Equation 6.24, where the constraints are established by the physical requirements of the urban drainage network and the model used internally by MPC. The method uses a simplified model as described in Section 6.3.2.

The method proposed by Sun et al is simple but effective: The addition of an objective to minimise the load during overflow impacted the behaviour of the controller to improve the quality of the water discharged in receiving waters. The complexity of this method will be relative to which model is used to calculate the predicted value for the TSS (a linear or non-linear model) and will also depend on if the monitoring of the TSS is done via measurement or estimation. The author mentioned that the method reduced the overall overflow compared to a rule-based approach. When compared to a purely volume-based MPC, the pollution-based MPC decreased the concentration of the overflowing wastewater, thus confirming that a load reduction is possible by adding a quality objective. However, it is mentioned that a certain degree of uncertainty is present and should be addressed in the optimisation to improve the control of the system. The next method reviewed suggests a solution to this uncertainty issue.

Pollution-based MPC considering uncertainty propagation

Mahmoodian [19] proposed a method for a real time controller using MPC in a pollution-based framework where a global concentration indicator is added to the optimisation problem. Using this information, the RTC implemented is able to directly affect the behaviour of the pollution within the network in an attempt to reduce the concentration of the discharged wastewater. In order to use concentration in the formulation, the model based on volumes and flow is extended to also consider the concentration and, therefore, be able to predict it. Mahmoodian designed the pollution-based MPC as in Equation 6.30:

$$\begin{aligned} \min J = \min \sum_{j=0}^{N-1} & \alpha\phi_1(k+j) + \beta\phi_2(k+j) + \gamma\phi_3(k+j) + \\ & \psi\phi_4(k+j) + \omega\phi_5(k+j) + \tau\phi_6(k+j) + \upsilon\frac{1}{\phi_7(k+j)} \end{aligned} \tag{6.30}$$

in which the cost function is represented by J and in its formulation, N defines is the prediction horizon , k represents a discrete time variable and where α, β, γ, ψ, ω, τ and υ are weights for the objectives ϕ_i, for $i = 1, ..., 7$. Each objective has a unique characteristic that will influence the behaviour of the wastewater system depending on the weights chosen for this objective. The objective ϕ_1, in Equation

6.31, is used to homogeneously store the volume within all SU structures in the sewage network.

$$\phi_1(k) = \sum_{i=1}^{N_t} \left(V^i(k) - \frac{V^i_{\max}}{\sum_{j=1}^{N} V^j_{\max}} \sum_{n=1}^{N_t} V^n(k) \right)^2 \tag{6.31}$$

where V is the volume in the SU, V_{max} the maximum volume in the SU and $i = 1, ..., N_t$ is the number of SUs in the network. ϕ_2, in Equation 6.32, keeps the flow towards the wastewater treatment plant near the operating reference value defined by Q_{ref}.

$$\phi_2(k) = \left(Q_{\text{ref}}(k) - \sum_{i \in N_t^*} Q^i_{\text{out}}(k - d^{i,t}) \right)^2 \tag{6.32}$$

where Q_{out} is the outflow from each SU, $d_{i,k}$ represents the transport time of the i^{th} SU to the destination SU k and N_t^* are all SUs draining in the destination k. ϕ_3, in Equation 6.33, is used to minimise the overflow, where NL is assigned as a negative number to keep the objective linear.

$$\phi_3(k) = \sum_{i=1}^{N_t} (Q^i_{\text{ov}}(k) - \text{NL})^2 \tag{6.33}$$

where Q_{ov} is the overflow volume. ϕ_4, in Equation 6.34, is similar to objective ϕ_1, the controller uses this objective to balance the mass over the sewage system's structures homogeneously.

$$\phi_4(k) = \sum_{i=1}^{N_t} \left(C^i(k) V^i(k) - \frac{V^i_{\max}}{\sum_{j=1}^{N} V^j_{\max}} \sum_{n=1}^{N_t} C^n(k) V^n(k) \right)^2 \tag{6.34}$$

where C is the concentration in the SU. ϕ_5, in Equation 6.35, is used to minimise the load, e.g, reduce the mass in overflow events.

$$\phi_5(k) = \sum_{i=1}^{N_t} \left(C^i(k) Q^i_{\text{ov}}(k) \right)^2 \tag{6.35}$$

ϕ_6, in Equation 6.36, is to minimise the uncertainty in the load. This objective is interesting in the case where multiple SUs are overflowing and in this scenario, the controller will prefer to let SUs with less uncertainty overflow.

$$\phi_6(k) = \sum_{i=1}^{N_t} U^i(k)^2 \tag{6.36}$$

where U is the uncertainty related to the concentration within the SU. ϕ_7, in Equation 6.37, is used to maximise the load arriving the wastewater treatment plant.

$$\phi_7(k) = \left(\sum_{i \in N_t^*} C^i(k - d^{i,t}) Q^i_{\text{out}}(k - d^{i,t}) \right)^2 \tag{6.37}$$

The final minimisation problem is than given by Equation 6.30 subject to the constraints in Equation

6.38:

$$
\begin{aligned}
&0 \leq V_i(k) \leq V_{i_{max}} \\
&0 \leq Q_{\text{out}_i}(k) \leq Q_{\text{out}_{max}} \\
&O_v(k) \geq 0 \\
&C_i(k) \geq 0 \\
&U_i(k) \geq 0 \\
&Q_{pipe_j}(k) = \sum_{i \in N_j^*} Q_{\text{out}_k}(k - d_{i,k}) \leq Q_{pipe_{jmax}}
\end{aligned}
\tag{6.38}
$$

where Q_{pipe} is the flow in a pipe and $Q_{pipe_{max}}$ is the maximum flow in a given pipe. The method uses a simplified model as described in Section 6.3.2. The pollution-based MPC reduced the mass overflowed compared to a volume-based approach [19]. This method is advantageous mainly due to the use of uncertainty, which is often disregarded during the development of a RTC system. The advantage is that, when considering uncertainty, it is assumed that there is an error related to the measurement or estimation of concentration, which is likely to occur. Therefore, the method is more robust to errors and performance is improved. However, this increased robustness comes at the cost of higher complexity and computational efforts, coupled with the need of a concentration model that requires the solution of a non-linear programming problem, increasing the complexity even further.

Multi-objective optimisation using Genetic Algorithms

Wastewater is composed of numerous pollutants and the quality of the water depends on the combination of these pollutants. The method presented by [4] is a pollution-based dynamic control algorithm for a sewer network using a multi-objective optimisation which considers different pollutants within the formulation of the problem. The author discusses the possibilities for solving the multi-objective optimisation and selects a genetic algorithm-based due to the complexity of the problem.

Genetic algorithms (GA) are an heuristic method for solving optimisation problems [99] by mimicking the search for the optimum through biological evolution. In each time step, the solutions, also known as a population of solutions, are updated. Genetic algorithms have basic features to mimic evolutionary behaviour, such as chromosome representation, fitness selection and biological-inspired operators [100]. The overall optimisation problem is similar to Equation 6.24, however the objective is separated as in Equation 6.39:

$$\min J(k) = J_1(k) + J_2(k) \tag{6.39}$$

The cost J_1 is related to the minimisation of the pollutant load discharged from a sewer chamber, as can be seen in Equation 6.40:

$$J_1 = \sum_{i=1}^{n_{cso}} EQI_i \tag{6.40}$$

where n_{cso} is the number of CSOs and EQI is the effluent quality index given by Equation 6.11.

The second objective J_2, shown in Equation 6.41, is used to minimise the cost of the treatment plant while also reducing operational costs from pumps.

$$J_2 = C_T + C_P \tag{6.41}$$

where C_T is the wastewater treatment plant cost and C_P is the operational cost of pumps in the sewer system. The calculation of both C_T and C_P are presented in [101].

The method uses a simplified model as described in Section 6.3.2. The author concludes that the genetic algorithm with the given objectives is capable of minimising the pollution load while reducing pumping costs, which is an unique approach for real time controllers, most methods are more concerned with volume reduction without actually measuring any costs. The algorithm also produced varied temporally and spatially dynamic control settings, obtained depending on regulatory requirements and the financial and environmental situation of the sewer management agency [4]. The implementation of the proposed method is simple, however the calculation of the wastewater treatment plant and pumping cost is not trivial and might lead to uncertainties. However, it is mentioned in the paper that, although GA methods have a rapid convergence, using a genetic algorithm introduces a high computational cost that scales with the size of the sewage network and more efforts are required for real applications.

Section Summary

In Table 6.4 several papers are shown with more implementations of pollution and optimisation-based RTC. The application of optimisation-based RTC is appealing for the efficient load management of urban drainage system. The high computational cost for solving optimisation problems can be an issue for network with non-linear dynamics and high number of decision variables, although this issue is diminished by advancements in computer performance.

6.4.3 Reinforcement Learning-based RTC

Reinforcement Learning (RL) is a machine learning training method in which the main idea is to mimic the human behaviour of learning through environmental interactions. A RL problem involves a trial-and-error situation where the algorithm learns what to do and derive an action of which the numerical reward from taking this action is maximised. By trying each action, the learner finds the action with most reward and influence later inputs of the system, which is why RL is a closed-loop algorithm [109].

The RL method is composed of an agent that takes actions, known as a, to interact with its environment expecting a reward, called r. During each learning step, the agent receives the state s of the environment and is rewarded depending by the quality of its actions to follow certain objectives, which can be a positive or negative reward [110]. Finally, the objective of the RL is to maximise the return function G_t as below in Equation 6.42:

$$G_t = r_t + \gamma r_{t+1} + \gamma^2 r_{t+2} + ... = \sum_{k=0}^{\infty} \gamma^k r_{t+k} \tag{6.42}$$

Table 6.4: Papers on optimisation-based RTC methods with pollution aspects.

Authors	Year	Type of Model	Type of Optimisation	Description	Type of Pollutant
[102]	1999	Model-free	MPC + GA	Non-linear MPC using Genetic Algorithm for calculating optimal solution applied to the sewer system, treatment plant and receiving water with the aim to achieve minimum effects of pollution.	DO/COD
[103]	2008	Simplified model	GA	Multi-objective quality control of urban wastewater system using NSGA-II genetic algorithm. The algorithm evaluates the performance of the system directly with regard to receiving water quality indicators, such as for ammonia, phosphorus, and dissolved oxygen.	Multiple pollutants
[104]	2010	Simplified model	MPC + Fuzzy	Investigation on fuzzy decision making for multi-criteria optimisation of sewer networks and sewage treatment works regarding the balance of ecological and economical criteria.	Global indicator
[85]	2014	Simplified model	MPC	Global water-quality optimisation with dynamic cost functions that aims to reduce the global overflow risk across the catchment. The algorithm uses hydrological models with indirect water quality considerations to improve the system performance by dynamically changing the prioritisation of discharges at different CSO structures.	TSS
[105]	2014	Simplified model	Ant Colony	Optimisation-based method designed to improve pollution load management using an ant colony algorithm. The objective is to empty retention SUs using volume and water quality data and discharge the flow to the WWTP while also avoiding exceeding the maximum capacity of the plant.	Multiple pollutants
[23]	2018	Simplified model	MPC	Model predictive control for TSS minimisation in the framework of cyber-physical systems.	TSS
[34]	2020	Model-free	Market-based	Real-time load-balancing algorithm to control distributed storage assets in the collection system to improve wet-weather flows and water quality at a receiving point.	TSS
[106]	2021	Simplified model	MPC	Integrated multi-software pollution-based control architecture using model predictive control. It proposes a methodology for a closed-loop application between the RTC module and the wastewater system for a water quality application.	TSS
[107]	2022	Simplified model	GA	Genetic algorithm optimisation with cost functions related to the volume of overflow and the overflow quality index for a sewer network, which indicates a mass of polluting units per day. The study compares five optimal control strategies using these metrics.	Multiple pollutants
[108]	2023	Simplified model	Decentralised MPC + Fuzzy	Distributed model predictive control algorithm including fuzzy negotiation among subsystems and a dynamic set-point generation method, applied to a simulated sewerage network using a hydraulic and water quality model for prediction.	TSS

where $r_t = r(s_t, a_t, s_{t+1})$ and $\gamma \in [0, 1]$ is a discount factor weighting the importance of short-term and long-term reward that depends on the current action a_t, the current and next states s_t and s_{t+1}, respectively [109]. Although research in this field is growing significantly for storm-water systems regarding flood mitigation and peak flow reduction, such as the works in [110] and [111], a reinforcement learning RTC with the goal of improving water quality is still in its infancy.

Reinforcement learning-based RTC to improve water quality

The research is a novel method using a pollution-based approach proposed by [89] using a reinforcement learning algorithm for developing the RTC. The objective of the controller is to mitigate flooding and improve water quality using a RL-based RTC, where the environment used for the learning process is executed using the software SWMM [40]. The model in SWMM provides the current states to the RL, which are:

$$s_t = \begin{cases} \text{Current depth} \\ \text{Outflow} \\ \text{Concentration of TSS} \\ \text{Current valve positions} \\ \text{Sum of 24 h rain forecast} \\ \text{Mean value of the 24 h tide forecast} \end{cases}$$

The action space (A) of the agent is manipulating the valve to any desired value. The reward (r) is calculated by how well the objectives defined are meet by the agent after taking any action within the action space, where the objectives are flood mitigation and pollutant reduction.

The author based the reinforcement learning algorithm on Deep Deterministic Policy Gradients (DDPG) [112] using a deep feed-forward neural network. The DDPG responsible to calculate the control actions (valve opening) over a continuous space while learning to control the system following the desired objectives maximising the rewards. It is presented a RL-based RTC for a sewage system with 2 sub catchments, called Pond 1 and Pond 2. Three agents were created and trained using the DDPG algorithm with the following reward system:

- Agent 1, r_{agent_1}, is rewarded for minimising total flooding and keeping target pond depths, therefore it is not used for water quality. The reward function is as follows in Equation 6.43:

$$r_{\text{ag1}} = \begin{cases} -\sum \text{Flooding}[\text{system}, \text{Pond}_1 * 1000, \text{Pond}_2] \\ \qquad\qquad F \geq \delta \\ \\ -(|\text{Pond}_{1_{\text{depth}}} - \tau_1| + |\text{Pond}_{2_{\text{depth}}} - \tau_2|) \\ \qquad\qquad F < \delta \end{cases} \tag{6.43}$$

  where Flooding[system] is the total flooding volume, $Flooding[Pond1]$ is the flooding rate at Pond 1 and Flooding[Pond_2] is the reward for having Pond 2 depth above a level that causes upstream

flooding. F and δ are the total rainfall in a 24 h window and the rainfall threshold, respectively. Finally, τ_1 and τ_2 is the reference value for the depth of Pond 1 and Pond 2, respectively.

- In the Agent 2, r_{agent_2}, is added water quality rewards, which results in it being rewarded for minimising total flooding, keeping target pond depths and minimising the outflow of TSS from the ponds as in Equation 6.44:

$$r_{\text{ag2}} = \begin{cases} -\sum \text{Flooding}[\text{system}, \text{Pond}_1 * 1000, \text{Pond}_2] \\ \quad +\text{TSS}[\text{Valve}_1, \text{Valve}_2] \qquad F \geq \delta \\ \\ -(|\text{Pond}_{1_{\text{depth}}} - \tau| + |\text{Pond}_{2_{\text{depth}}} - \tau|) \\ \quad +\text{TSS}[\text{Valve}_1, \text{Valve}_2] \\ \quad +\text{Flooding}[\text{system}/35000] \qquad F < \delta \end{cases} \tag{6.44}$$

  where $\text{TSS}[\text{Valve}_1, \text{Valve}_2]$ is the total TSS load of the controlled valves.

- Agent 3: is used as balance between Agent 1 and Agent 2. The agent is set by using the weights and memory from the trained neural network of Agent 1 as an initialisation for the reward function r_{agent_2} from Agent 2, functioning as a pre-training of Agent 3.

Bowes discusses the performance of the controller comparing the results using a RL-based RTC with each of the agents. The increased complexity of Agent 2 compared to Agent 1, due to the extra control objective for minimising the TSS load, revealed that it is harder for a single agent to effectively learn all control policies. Agent 2 was able to effectively learn a policy for minimising the TSS load, however Agent 1 had a better performance for flood mitigation, which indicates that Agent 2 compromised by increasing the flooding. The pre-training performed by Agent 3 using Agent 1's information into Agent 2's reward function resulted in a balanced performance between agents 1 and 2. [89] mentions that correctly weighting the RL is highly important to avoid reward gaming, which happens when agent's actions causes undesired behaviours in the environment.

The method uses a model based on neural networks and, therefore, inherently uses a data-driven modelling technique. The author suggests that actual physical or numerical stormwater models could be incorporated into the neural network, but further evaluation is recommended.

Section Summary

As mentioned, the use of RL for pollution-based RTC is a recent development. Mullapudi [111] discusses that there are challenges associated with RL, such as formulating rewards, choosing function approximators and deciding the complexity of the control problem. It is stated that for many fields the control is highly sensitive to the formulation of the reward function and requires both expertise and an element of subjectivity for a proper implementation. Moreover, to learn all possible relationships between rewards and control decisions becomes a complex task with high computational demands. Although the paper's statements are related to stormwater system control, the same conclusions should apply to wastewater network control but may also explain the lack of studies in the field.

6.5 Literature Gaps and Contribution

The literature review presented in this chapter highlights that research on PRTC, while still evolving, is already consolidated into many publications with promising results. However, practical implementation remains limited, mainly due to the complexity of current strategies and associated implementation challenges. With regard to MPC, which is the focus of this thesis, two key studies form the foundation of the discussion: the work by Fiorelli [5], which introduced a Volume-based MPC that does not consider water quality, and the study by Mahmoodian [19], which proposed a non-linear PMPC formulation. Both approaches are analysed in detail within this thesis. The former reveals limitations in its capacity to reduce pollutant load, while the latter demonstrates strong potential for pollution reduction but is hindered by the intrinsic complexity of solving non-linear optimisation problems, thereby affecting its practical viability. Furthermore, the review shows a noticeable gap in the literature concerning PRTC methods that explicitly incorporate uncertainty into their formulations.

In response to these gaps, this research's main goal and contribution is to provide the first steps toward a unified solution. This includes developing a novel linear-optimisation PRTC method, the implementation of a multi-layer approach to bring together the non-linear optimisation with real applications, and the creation of new pollution-based MPC approaches using a stochastic formulation to incorporate uncertainties into control strategies.

6.6 Conclusion

In this chapter, a comprehensive review of the state of art for modelling and control of Urban Drainage Systems was given. More specifically, the review focused on pollution-based real-time control and modelling, which is the main subject of this thesis. At first, a list of tools was provided for simulating different aspects of the UDS. Furthermore, a detailed description of SWMM is done, as the most common tool for modelling sewage systems integrated with control. Additionally, a few model examples are given to illustrate the use of SWMM.

Besides, a literature review was presented on modelling and control of sewage system focused on water quality. The review of the modelling for prediction revealed the strengths and weaknesses of the methods found in literature, showing that there are no base framework that is used, it depends on the application and which RTC is being implemented. A taxonomy for the models was proposed, dividing into Simplified Models, Data-driven Models and Probability Models. Finally, the pollution-based real-time control was reviewed, detailing the research that showed more relevance in the literature. A taxonomy is also proposed: Rule-based PRTC, Optimisation-based PRTC and Reinforcement Learning PRTC. The literature review revealed that publications on PRTC are still in their early stages, with the field continuing to emerge. However, the development of cost-effective and practical control systems remains largely unexplored in most existing research.

7 Volume-based Model Predictive Control

The term Model Predictive Control (MPC) is used to describe a collection of control strategies that are characterised by the application of dynamic models, which are used to predict the future behaviour of the controlled system. Furthermore, they use the minimisation of a cost function to calculate the optimal control action to be applied at the process during the control loop. The main differences in each formulation are the type of model used to represent the system, the disturbances considered during the calculation of future predictions, and the cost function used during the minimisation [113]. Although

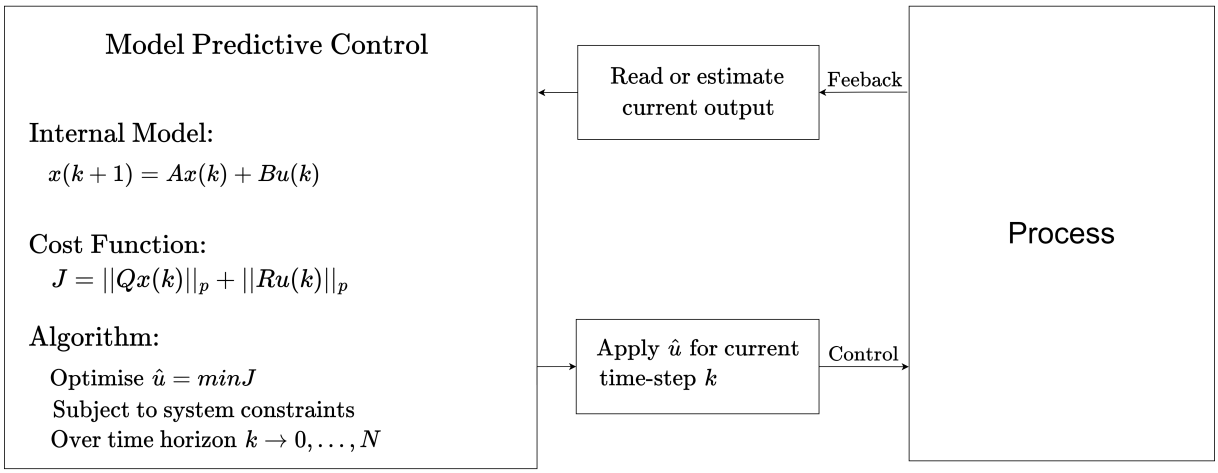

Figure 7.1: MPC scheme.

there are many formulations, the basic scheme is the same for all MPC algorithms, as demonstrated in the diagram shown in Figure 7.1. This scheme is the foundation of every MPC and could be summarised as:

- For a given system, the first step is to read the current output through a sensor or estimate it in case the measurement is unavailable;
- Then, there is the explicit use of dynamic models to predict the system output at a future time. For instance, the following model is a linear discrete state-space representation of a process (as shown in Figure 7.1):

$$\begin{aligned} x(k+1) &= Ax(k) + Bu(k) \\ y(k) &= Cx(k) + Du(k) \end{aligned} \tag{7.1}$$

where $x(k)$, $u(k)$ and $y(k)$ are the system states, inputs and outputs at discrete instant k, respectively, and where $x(k+1)$ is the successor state at instant $k+1$. Using this representation, the states may be predicted with the optimisation problem;

- A optimal control action is calculated by minimising a cost function and considering constraints of the system, which might be represented by:

$$\begin{aligned} \mathbb{P}(\hat{u}(k+j)) = \min_{\hat{u}} & \sum_{j=0}^{N-1} J(x(k+j), u(k+j)) \\ \text{subject to} \quad & A_x x(k+j) \geq b_x \\ & A_u u(k+j) \geq b_u \end{aligned} \tag{7.2}$$

where $J(x,u)$ is a cost function, $\mathbb{P}$ is the optimal control problem, $\hat{u}(k+j)$ is the optimal predicted control action, $A_x x \geq b_x$ and $A_u u \geq b_u$ are state and input constraints, respectively [114];

- In Equation 7.2, the use of the parameter N, commonly known as the prediction horizon, can be observed. It represents the prediction time used by the optimisation problem. It is called a moving horizon because each time instant the "window" of prediction is shifted and only the first control action $\hat{u}(0)$, calculated during the optimisation $\mathbb{P}(\hat{u}_k)$, is applied.

- Figure 7.2 shows the predicted time behaviour for a certain **horizon**. The MPC concept is such that, given a **reference trajectory**, the MPC controller uses the data from **past control actions** and **measured outputs** to **propose future control actions**, such that the **predicted output** converges towards the reference.

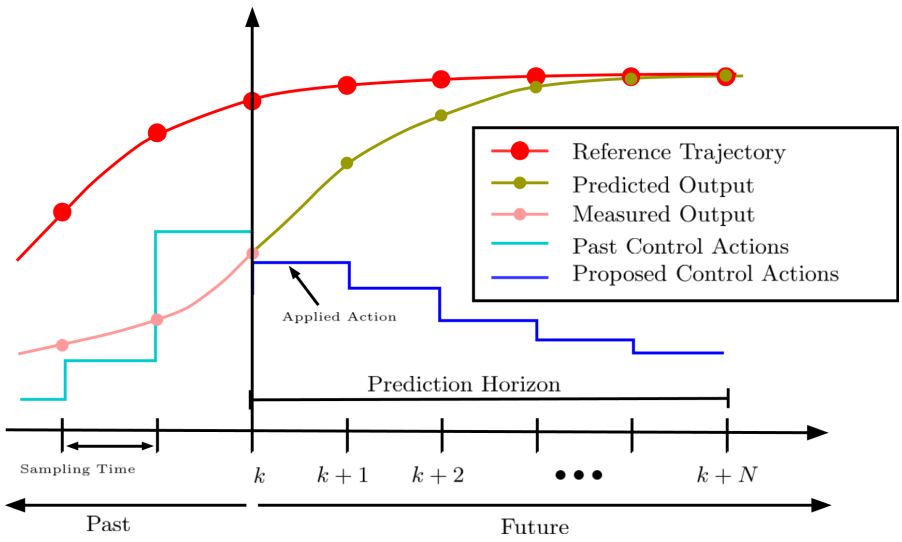

Figure 7.2: MPC strategy.

There are many advantages in using MPC compared to classical control techniques. Firstly, the main idea is very intuitive, requiring limited knowledge about control theory, indicating that the algorithm is appealing to users without strong control background. The algorithm allows to naturally define the problem for multi-variable systems and complex dynamics, such as dead-time and non-minimum phase, are intrinsically dealt with by the controller without major changes.

Also, the tuning of MPC controllers is in the time-domain, which is intuitive to understand, and constraints are easily incorporated in the optimisation problem. A controller that incorporates constraints is advantageous because the most profitable operating point is usually near the constraint region and MPC finds the optimal control actions to operate in this situation. A controller that operates at an economical optimum value, considering physical constraints, is highly desirable and, for that reason, the popularity of MPC controllers in industry is increasing.

However, all these advantages have a cost to the controller. For example, solving an optimisation problem is not an easy task and requires considerable computational power depending on the situation, resulting in a controller with a much higher computational cost compared to classical controllers that do not need optimisation. Also, the tuning of the MPC is not as simple as the concept of the MPC formulation and it is usual for operators to start the controllers with arbitrary tuning parameters and finish with a "fine-adjustment" to improve performance. The next section details the state-space formulation of MPC, explaining the most important variables used.

7.1 Description of Model Predictive Control

In a vast majority of the cases, the nominal system's dynamics are non-linear, and the most common descriptions for these are represented by continuous non-linear differential equations such as:

$$\begin{aligned} \frac{dx}{dt} &= f(x,u,t) \\ y &= h(x,u,t) \end{aligned} \tag{7.3}$$

where $x \in \mathbb{R}^n$ is an n-dimensional state vector, $u \in \mathbb{R}^m$ is an m-dimensional input vector, $y \in \mathbb{R}^p$ is a p-dimensional output vector, and $t \in \mathbb{R}$ is the time. Using non-linear equations to represent the system increases the complexity of the controller, therefore, it is common to approximate the problem using linear models in an operating point, which reduces the calculation needed for advanced controllers as MPC.

7.1.1 Linear State-Space Dynamic Models

Although the system in Equation 7.3 is written in continuous-time, models are generally sampled at discrete times. The reason to describe the model in discrete form is that the controllers are digitally implemented, and, provided that the sampling time is properly chosen, the behaviour of the sampled model is a good approximation of the system.

- **Time-varying discrete model**. Using this model the system is represented more generically by:

$$\begin{aligned} x(k+1) &= A_k x(k) + B_k u(k) \\ y(k) &= C_k x(k) + D_k u(k) \end{aligned} \tag{7.4}$$

where $A_k \in \mathbb{R}^{n\times n}$ is the state transition matrix, $B_k \in \mathbb{R}^{n\times m}$ is the input distribution matrix, $C_k \in \mathbb{R}^{p\times n}$ is the output matrix and $D_k \in \mathbb{R}^{p\times m}$ is a matrix relating directly the input and output.

- **Time-invariant discrete model**. Considering that the system is invariant at each sample time, the model is redefined as:

$$\begin{aligned} x(k+1) &= Ax(k) + Bu(k) \\ y(k) &= Cx(k) + Du(k) \end{aligned} \tag{7.5}$$

Typically, the time-invariant model is used for simplicity of representation. As expected, approximating nonlinear systems with linear models yields errors, referred to as model uncertainty, which is mentioned later in this section.

7.1.2 Optimisation Problem

As mentioned previously, the optimal control action applied to the system is calculated by solving an optimisation problem $\mathbb{P}$, which basically consists of minimising a cost function, as observed in Equation 7.6:

$$\begin{aligned} \hat{u}(k+j) = \arg\min_{u} & \sum_{j=0}^{\infty} J(x(k+j), u(k+j)) \\ \text{s.t.} \quad & x \in \mathbf{X} \\ & u \in \mathbf{U} \end{aligned} \tag{7.6}$$

where $\mathbf{X}$ is the state constraint set and $\mathbf{U}$ the input constraint set, $\hat{u}(k+j)$ is the optimal control sequence and J is called the stage cost. For practical reasons, the cost is defined over a horizon N, to ensure an optimal control problem that is solved fast and efficiently. Since the problem is reduced to N steps, a terminal cost V_f could be included to approximate the semi-infinite solution [114], which results in Equation 7.7.

$$\begin{aligned} \mathbb{P}(x,u) = \min_{\hat{u}(k+j)} & \sum_{j=0}^{N-1} J(x(k+j), u(k+j)) + V_f(x_N) \\ \text{s.t.} \quad & x \in \mathbf{X} \\ & u \in \mathbf{U} \\ & x_N \in \mathbf{X_N} \end{aligned} \tag{7.7}$$

where x_N is the state at instant N and $\mathbf{X_N}$ is the terminal constraint set. The optimisation problem from Equation 7.7 is quite complex, with many aspects and variables that influence the outcome of the optimisation, such as:

- **Prediction horizon**: The horizon N is a tuning parameter of the MPC controller that determines the window in which the predicted behaviour of the system is calculated. Choosing a large horizon compared to the settling time of the system indicates a preference over the steady-state response, while decreasing the value of N changes the priority to transient response.

- **Cost function**: The stage cost J is used to obtain the control law and can be defined as:

$$J(x,u) = (x - x_r)'Q(x - x_r) + (u - u_r)'R(u - u_r) \tag{7.8}$$

which depends on the input vector u, an input vector reference u_r, the state vector x and state vector reference x_r. The tuning parameters are the weights Q and R. When Q has a higher value than R, the controller is focused on steering the state to the reference value x_r at the expense of a higher control action. However, for higher R values, when compared to Q, the control action is reduced and the rate at which the state approaches x_r is slowed down [114]. The cost function is entirely customizable to fit the system's requirements. Here it is introduced just as an example of a generic cost function.

- **Terminal cost**: The terminal cost V_f is commonly used to guarantee stability, by approximating the infinite horizon MPC to a finite horizon. The stability is guaranteed by choosing a terminal weight P, such that:

$$J_f(x_N) = x'_N P x_N \tag{7.9}$$

and P is the solution of the Ricatti equation that proves the controller's stability [115]. The Ricatti equation is derived from the Lyapunov stability theory, which affirms that, given the function J_f from Equation 7.9, the stability is guaranteed if $P > 0$ and [116]:

$$\begin{aligned} &J_f(x_N) > 0, \\ &J_f(x_N) - J_f(x_{N-1}) < 0 \end{aligned} \tag{7.10}$$

- **Constraints**: In general, most systems are physically restricted and constraints are used to represent these limitations. For example, the control signal u applied to the system is bound by a given set $\mathbf{U}$ which establishes the field of actuation permitted. These constraints are related to physical limitations of actuators, safety or environmental issues and even the range of sensors [117].

- **Terminal set constraint**: A terminal constraint is used to steer the system towards a desirable region at the end of the horizon during the prediction. It adds another condition to stabilise the system if the terminal set $\mathbf{X_N}$ is chosen correctly.

$$x_N \in \mathbf{X_N} \tag{7.11}$$

Usually, the terminal set constraint is composed by a large number of inequality equations, which increases the optimisation problem's complexity and the computational effort to solve it. A solution is to reduce the number the terminal constraint, as proposed in [118], which defines the terminal constraint only in the unstable states of the system.

Thus, the basic algorithm of the MPC can be summarised as:

Basic Algorithm

(a) Initialise $x(k) = x(0)$, where $x(0)$ is the current state of the system;

(b) Calculate the predictions $\hat{x}(k+j)$ of the system;

(c) Solve the optimisation problem as in Equation 7.7 and obtain the optimal control sequence $\hat{u}(k+j)$;

(d) At time k, apply the first input $u(k)$ of the optimal control sequence to the plant;

(e) Measure $x(k)$ and return to Step (b).

Previously, it was noted that real processes are modelled using mathematical equations. In fact, mathematical models are often used as approximations of the reality that essentially attempts to contemplate as many aspects of reality as possible. Simplifications are assumed when using models for control objectives to keep the MPC structure simple for real-time applications, and therefore much of the process information is lost due to approximations and the dynamic of the system is not completely described.

Therefore, the design and performance of the control depend completely on the model. It is usual to apply a nominal model structure in most control techniques where no external disturbances are considered, such as in Equations 7.4 and 7.5. However, the condition in which the control model matches the process and there are no external disturbances is not correct in most situations, requiring a controller that is capable of preserving stability and performance despite model inaccuracies or uncertainties in real processes [117].

The dependency on model descriptions is an important issue, and the controller's performance is often highly sensitive to errors between the real process and the model used. These uncertainties are critical in control applications.

7.2 Model Predictive Control for Urban Drainage Systems

In the following chapters, the details of the MPC algorithms used in this research are described. Each algorithm is specifically tailored for a desired behaviour of the urban drainage system, with its own objectives and constraints. The MPC methods used in this thesis are as follows:

- ***Volume-based Model Predictive Control*** *(VMPC)*:
- ***Pollution-weighted Model Predictive Control*** *(PWMPC)*
- ***Nonlinear Pollution-based Model Predictive Control*** *(NPMPC)*
- ***Stochastic Volume-based Model Predictive Control*** *(SVMPC)*:
- ***Stochastic Pollution-weighted Model Predictive Control*** *(SPWMPC)*
- ***Stochastic Nonlinear Pollution-based Model Predictive Control*** *(SNPMPC)*

The similarities between the MPC algorithms are:

1. The manipulated variable is the flow leaving the Storage Units, aiming to optimally use the available storage within the SU to reach the controller's objectives.
2. The methods share a few state variables, such as the volumes, outflows, overflows, and inflows.
3. The available measurements are the level and the outflow of the valves and pumps of the SU .
4. The wastewater volume is calculated from the level measurement using a volume-level map determined from the geometry of the SU.

5. Inflows are estimated using a volume-based mass-balance equation.

6. Locally, in the UDS, the outlet valve or pump is controlled by a local controller, called Programmable Logic Controller (PLC), normally a Proportional-Integral-Derivative (PID) control. The set-point outflow for the local controller is calculated by MPC as the result of the optimisation algorithm.

The main differences between the MPC methods are as follows:

1. Different optimisation problems, specifically a different set of objective functions.

2. Additional state variables in Pollution-based MPC methods.

3. Estimation of concentrations in Pollution-based MPC methods.

4. Use of non-linear equality constraints for the internal model of the concentration for Non-linear Pollution-based MPC and Stochastic Non-linear Pollution-based MPC.

5. Probabilistic formulation for Stochastic MPC methods.

To begin with, in this chapter, a detailed description of VMPC is provided as an initial introduction to an MPC applied to urban drainage systems.

7.3 Volume-based Model Predictive Control

The purpose of urban drainage systems is to properly handle rainwater, surface runoff, and sewage, to minimise flooding, prevent discharge of pollution into receiving water bodies, and other health hazards. The drainage infrastructure in the case where both wet-weather flow (rainwater runoff) and dry-weather flow (domestic wastewater from toilets, sinks, and industrial processes) are combined in the same pipe network is called Combined Sewer Overflow (CSO) system.

Today, most of the infrastructure developed is outdated (mid to late 19^{th} century), as it is not built for the current rate of changes in the urban environment, caused mainly by population growth and climate change. Those changes are causing an increase in the number of overflow events in SUs and efforts to reduce the occurrence of overflow events are many [2]. The use of Real-Time Control systems is one such approach to deal with CSOs and, more specifically, MPC has proved to be a powerful tool for CSO mitigation, as elaborated in Chapter 6. For more detailed information on how climate change and population growth affect urban drainage systems, refer to [119].

7.3.1 Description

Volume-based Model Predictive Control is a type of Real-Time Control that incorporates the CSO mitigation directly into an optimisation routine. Using the measured and estimated variables in each SU, VMPC is capable of predicting the future behaviour of the system and detects potential overflow events. In order to accomplish this, the algorithm needs an internal model that relates the measurement and estimated variables, and more specifically, it needs the actual inflow (Q_{in}), and outflow (Q_{out}), the overflow in the previous step (Q_{ov}) and the volume (V).

The control algorithm scheme is illustrated in Figure 7.3 and is based on the method proposed by [5,27]. The VMPC receives feedback from the UDS through measurement devices, typically one or more level sensors in each SU. These measurements are used to estimate V, based on the known geometry of the SU, along with the Q_{out} measured at the actuator, which is generally a pump or valve. The internal model then predicts the future volume and possible overflow events. Importantly, this overflow prediction is entirely based on the internal model of VMPC, which in turn requires the estimation of both Q_{in} and Q_{ov}.

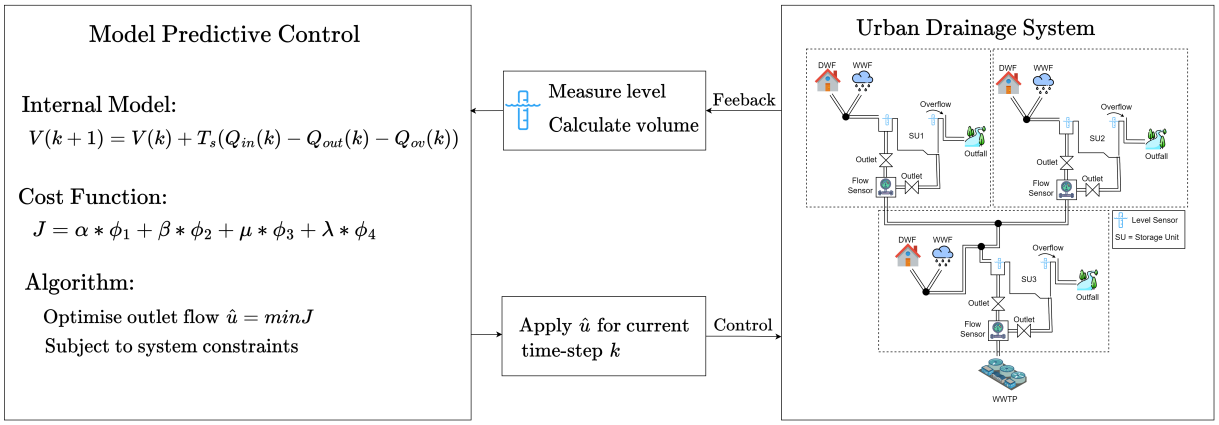

Figure 7.3: VMPC scheme for Urban Drainage Systems.

Thus, the equation for the estimation of the overflow Q_{ov} can be seen below:

$$Q_{\text{ov}}(k) = C_w \left(f H_w\right)^{1.5}, \quad f = \frac{Q_{\text{weir}_{\text{in}}}(k) - Q_{\text{min}}}{Q_{\text{max}} - Q_{\text{min}}} \tag{7.12}$$

where Q_{ov} is the diverted flow (overflow), C_w is the weir coefficient, H_w is the weir height, $Q_{\text{weir}_{\text{in}}}$ is the inflow to the weir, Q_{min} is the flow in which the overflow begins, and $Q_{\text{max}} = C_w H_w^{1.5}$. The inflow to the SU, Q_{in}, is estimated using the mass flow balance equation:

$$Q_{\text{in}}(k) = \frac{\Delta V(k)}{T_s} + Q_{\text{out}}(k) + Q_{\text{ov}}(k) \tag{7.13}$$

where $\Delta V(k) = V(k) - V(k-1)$ and T_s is the sampling time of the discretised model for the UDS.

Combining the measurements of Q_{out} and (indirectly) V with the calculated values for Q_{ov} and Q_{in} from Equations 7.12 and 7.13, the necessary information is collected to calculate the predictions. The internal

model for VMPC is shown in Equation 7.14.

$$V(k+1) = V(k) + T_s[Q_{\text{in}}(k) - Q_{\text{out}}(k) - Q_{\text{ov}}(k)] \tag{7.14}$$

Using Equation 7.14, the algorithm is able to calculate the future behaviour of the system and predict overflow events. The estimated inflow is kept constant through the prediction horizon for both WWF and DWF, although it is possible to use a weather forecast for a better prediction of WWF, but this forecast is not evaluated in this research.

7.3.2 Optimisation Problem

Let the state and input vectors be defined as:

$$\boldsymbol{x}(k) = \begin{bmatrix} \boldsymbol{V}(k) \\ \boldsymbol{Q}_{\text{ov}}(k) \\ \boldsymbol{\theta}(k) \\ \boldsymbol{Q}_{\text{in}}(k) \end{bmatrix}, \qquad \boldsymbol{u}(k) = \begin{bmatrix} \boldsymbol{Q}_{\text{out}}(k) \end{bmatrix}.$$

Considering N_t as the number of controlled SU, the vectors are defined as $\boldsymbol{V} \in \mathbb{R}^{N_t \times 1}$ (volume), $\boldsymbol{Q}_{\text{ov}} \in \mathbb{R}^{N_t \times 1}$ (overflow), $\boldsymbol{\theta} \in \mathbb{R}^{N_t \times 1}$ (slack variable), $\boldsymbol{Q}_{\text{in}} \in \mathbb{R}^{N_t \times 1}$ (inflow), and $\boldsymbol{Q}_{\text{out}} \in \mathbb{R}^{N_t \times 1}$ (outflow). The optimisation problem, with $\hat{\boldsymbol{u}}(k)$ denoting the optimal control output, is then formulated as:

$$\hat{\boldsymbol{u}}(k) = \arg\min_{\boldsymbol{u}} \sum_{j=0}^{N-1} J(\boldsymbol{x}(k+j), \boldsymbol{u}(k+j)) \tag{7.15a}$$

subject to

$$V^t(k+j+1) = V^t(k+j) + T_s(Q^t_{\text{in}}(k) - Q^t_{\text{out}}(k+j) - Q^t_{\text{ov}}(k+j)), \qquad t = 1, 2, ..., N_t \tag{7.15b}$$

$$Q^t_{in}(k+j) = Q^t_{catchment}(k+j) + \sum_{i \in N^*_{\text{in}}} Q^i_{out}(k+j), \qquad t = 1, 2, ..., N_t \tag{7.15c}$$

$$0 \leq V^t(k+j) \leq V^t_{\max} + \theta^t(k+j), , \qquad t = 1, 2, ..., N_t \tag{7.15d}$$

$$0 \leq Q^t_{\text{out}}(k+j) \leq Q^t_{\text{out}_{\max}}, , \qquad t = 1, 2, ..., N_t \tag{7.15e}$$

$$0 \leq \sum_{i \in N^*_{\text{wwtp}}} Q^i_{\text{out}}(k+j) \leq Q_{\text{wwtp}_{\max}}, \tag{7.15f}$$

$$Q^t_{\text{ov}}(k+j) \geq 0, \qquad t = 1, 2, ..., N_t \tag{7.15g}$$

$$\theta^t(k+j) \geq 0, \qquad t = 1, 2, ..., N_t \tag{7.15h}$$

where $V_{\max} \in \mathbb{R}^{N_t \times 1}$ represents the maximum volume for the SUs, $Q_{\text{out}_{\max}} \in \mathbb{R}^{N_t \times 1}$ is the maximum outflow of the SU's actuator, $j \in [0, N-1]$ is the future time instant, and N is the prediction horizon. Moreover, Equation 7.15c indicates the inflow of a SU in the context of the network's topology, where N^*_{in} indicates all SUs that are draining in a downstream SU. Furthermore, θ is a slack variable used to help guarantee the feasibility of optimisation, $Q_{\text{wwtp}_{\max}}$ is the maximum inflow to the WWTP and N^*_{wwtp} are all SUs draining in the WWTP. Equation 7.15b is the model equality constraint that is used to calculate

future predictions. The mass balance equation shows that the inflow, Q_{in}, remains constant throughout the prediction horizon and, although inflow estimates could be projected into future predictions using weather forecasts for WWF or pattern predictions for DWF, this initial formulation does not account for these scenarios.

The cost function, often called the objective function, is the part of the algorithm that steers the system to a desired behaviour. In VMPC, the goal is to improve the dynamic management of UDS, and more specifically to reduce overflow events while keeping the inflow to the WWTP close to the designed reference. Overall, four main objective functions are used in VMPC:

- Objective ϕ_1: Maintain volume **homogeneity** within each SU. The homogenisation of storage capacity in the network forces structures to fill and empty.
- Objective ϕ_2: Minimise the error between the **reference inflow to the WWTP** and the sum of the outflow from all actuators upstream of the WWTP.
- Objective ϕ_3: Minimise **overflow** events. Normally, this objective has the highest priority in the optimisation to avoid as much overflows as possible.
- Objective ϕ_4: Designed to give slightly higher degree of freedom to the optimization by allowing it to violate bound constraints by a very small margin.

Thus, to implement those objectives, J is defined as:

$$J(x(k), u(k)) = \alpha\phi_1(k) + \beta\phi_2(k) + \gamma\phi_3(k) + \epsilon\phi_4(k) \tag{7.16}$$

where (α, β, γ, ϵ) are the weights for the objectives (ϕ_1, ϕ_2, ϕ_3, ϕ_4), which are defined as:

- ϕ_1, in Equation 7.17, is used to homogeneously store the volume within all storage units in the sewer network.

$$\phi_1(k) = \sum_{i=1}^{N_t} \left(V^i(k) - \frac{V_{\max_i}}{\sum_{j=1}^{N} V_{\max_j}} \sum_{n=1}^{N_t} V^n(k) \right)^2 \tag{7.17}$$

  which N_t is the number of SUs in the network.

- ϕ_2, in Equation 7.18, keeps the flow toward the wastewater treatment plant close to the operating reference value defined by Q_{ref}.

$$\phi_2(k) = \sum_{j \in N_{up}} \left(Q^j_{\text{ref}}(k) - \sum_{i \in N^*_t} Q^i_{\text{out}}(k - d_{i,t}) \right)^2 \tag{7.18}$$

  where Q_{ref} is the reference flow for the i^{th} SU, which includes $Q_{\text{wwtp}_{\text{ref}}}$ as the inflow reference to the WWTP, Q_{out} is the outflow from each SU, $d_{i,t}$ represents the transport time of the i^{th} unit to the destination m, N^*_t are all units draining in the destination t and N_{up} are all units that have an upstream structure and the wastewater treatment plant.

- ϕ_3, in Equation 7.19, is used to minimise the overflow, where NL is assigned as a negative number to keep the objective linear; see [19, 120].

$$\phi_3(k) = \sum_{i=1}^{N_t} (Q_{\text{ov}}^i(k) - \text{NL})^2 \tag{7.19}$$

- ϕ_4, in Equation 7.20, is used to minimise the slack variable θ.

$$\phi_4(k) = \sum_{i=1}^{N_t} (\theta^i)^2 \tag{7.20}$$

For all MPC methods presented in this thesis, the prediction horizon N is set equal to the longest travel time between a SU and the WWTP, unless explicitly stated otherwise, in which case an alternative approach to determine N is described. Finally, the control loop algorithm for VMPC can be summarised as below:

Control Algorithm

(a) Initialise $\boldsymbol{x}(k) = \boldsymbol{x}(0)$, where $\boldsymbol{x}(0) = \{\boldsymbol{V}(0), \boldsymbol{Q}_{\text{ov}}(0), \boldsymbol{\theta}(0)\}$ and $\boldsymbol{u}(0) = \boldsymbol{Q}_{\text{out}}(0)$, are the current state and input of the system;

(b) Estimate $\boldsymbol{Q}_{\text{in}}(k)$ using Equation 7.13;

(c) Solve the optimisation problem as in Equation 7.15a and obtain the optimal control sequence $\hat{\boldsymbol{u}}(k)$;

(d) At time k, apply the first input $\boldsymbol{u}(k) = \boldsymbol{Q}_{\text{out}}(k)$ of the optimal control sequence to the UDS;

(e) Wait for next control loop $k = k + 1$;

(f) Measure $\boldsymbol{V}(k)$ and $\boldsymbol{Q}_{\text{out}}(k)$, calculate $\boldsymbol{Q}_{\text{ov}}(k)$ and return to Step (b).

The following section evaluates the performance of VMPC for different UDS configurations.

7.3.3 Methodology Validation - Single Storage Unit Configuration

Firstly, the analysis of the behaviour of VMPC is performed in the system configurations presented in Section 6.2.2 given the performance metrics. The metrics used are:

- **The total overflow** $Q_{\text{ov}_{\text{total}}}$, in ML, as in Equation 7.21. This metric indicates how the controller dynamically manages the storages to avoid CSO events to happen;

$$Q_{\text{ov}_{\text{total}}} = \sum_{i=1}^{T} \sum_{n=1}^{N_t} Q_{\text{ov}_n}^i(k) \tag{7.21}$$

where T is the total number of iterations in the simulated scenario and N_t is the number of Storage Units.

- **The mean error**, ξ, between the reference inflow, $Q_{\text{wwtp}_{\text{ref}}}$, and actual inflow, Q_{wwtp}, to the WWTP in L/s, shown in Equation 7.22. The desired inflow, $Q_{\text{wwtp}_{\text{ref}}}$, represents the optimal inflow rate for the WWTP to achieve the best treatment performance. Therefore, during normal operation, it is preferable for the inflow to remain as close as possible to $Q_{\text{wwtp}_{\text{ref}}}$.

$$\xi = \frac{\sum_{i=1}^{T}(Q^{i}_{\text{wwtp}}(k) - Q_{\text{wwtp}_{\text{ref}}})}{T} \tag{7.22}$$

A variant of this metric is ξ_{rain}, which filters the data to consider only the inflow during rain events, such that:

$$\xi_{\text{rain}} = \frac{\sum_{i=1}^{T_{\text{rain}}}(Q^{i}_{\text{wwtp}}(k) - Q_{\text{wwtp}_{\text{ref}}})}{T_{\text{rain}}} \tag{7.23}$$

where T_{rain} is the number of control loops during rain events with the data filtered.

- **The total inflow arriving at the WWTP**, $Q_{\text{wwtp}_{\text{total}}}$, in ML. This metric represents the volume of flow directed to the WWTP and complements the overflow metric. An increase in inflow to the WWTP might indicate a reduction in overflow, thereby resulting in a higher volume of treated wastewater.

$$Q_{\text{wwtp}_{\text{total}}} = \sum_{i=1}^{T} Q_{\text{wwtp}}(k+i) \tag{7.24}$$

The metrics are used to compare the performance of the simulated system under static control with that of VMPC. The first configuration analysed is the single Storage Unit as shown in Figure 6.4. In Section 6.2.2, it is explained that such a configuration is interesting to check whether VMPC is capable of achieving optimal behaviour, which occurs when the outlet is at its maximum output. The same parameters are used for this simulation, as shown in Table 7.1, where the designed outlet flow, Q_{design}, is a fixed outflow rate established by engineers to allow regular operation of the local controller in the sewage network with static control.

The input data for the DWF and WWF are also equal to Section 6.2.2, however the analysis is done for the period of 01/05 to 01/06 for a better visualisation of the data. The control period for VMPC in this scenario is 240 seconds, while the simulated model has a routing time step of 5 seconds. Two simulations were conducted: the first represents a static control scenario, in which the outflow is set to Q_{design}, while the second applies VMPC, with the weights α, β, γ and ϵ selected through trial and error to achieve the desired result.

Intuitively, the optimum output for this system clearly is to keep the outlet flow, Q_{out}, as close to $Q_{\text{wwtp}_{\text{max}}}$ as possible at any given time, which is achieved by the scenario with static control as shown in Figure 7.4. This guarantees that the system will always reach the objective $Q_{\text{wwtp}_{\text{ref}}}$ when there is volume availability, since $Q_{\text{wwtp}_{\text{ref}}} = Q_{\text{wwtp}_{\text{max}}}$.

Table 7.1: Single SU configuration - Urban Drainage System Parameters.

Model Parameter	Description	Value
$V_{\max}$	Maximum storage volume in m^3	2417.5
Q_{design}	Outlet designed outflow in L/s	120
$Q_{\text{out}_{\max}}$	Outlet maximum outflow in L/s	120
$Q_{\text{wwtp}_{\text{ref}}}$	Reference inflow to the WWTP in L/s	120
$Q_{\text{wwtp}_{\max}}$	Maximum inflow to the WWTP in L/s	120
VMPC Parameter	**Description**	**Value**
Control loop in s	240	
Optimisation weights (α, β, γ, ϵ)	(1, 1000, 50, 100)	

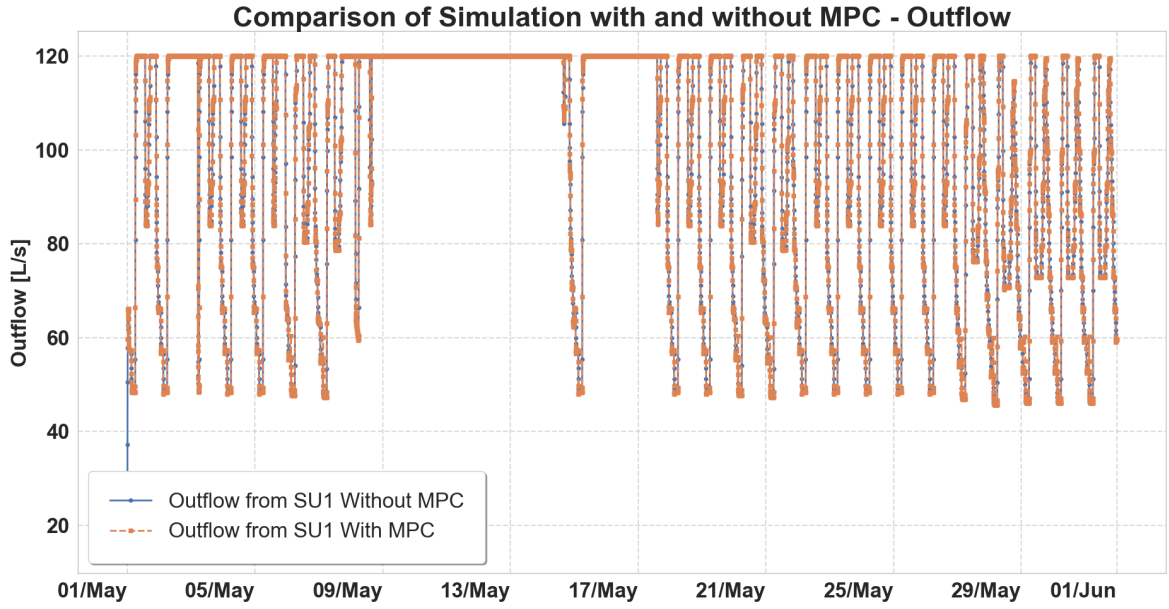

Figure 7.4: Single SU configuration - outflow comparison between static control and VMPC.

The graph also reveals that the optimum outflow calculated by VMPC is the same as the scenario with static control, as desired in this scenario. The optimal behaviour for VMPC was achieved for the single Storage Unit configuration, which is also confirmed by checking the dynamics of the volume in the Storage Unit and the total overflow for both scenarios, as can be seen in Figure 7.5.

In Table 7.2 the metrics for the simulation are displayed, where the total overflow for both methods is $19.83ML$, the total volume entering the WWTP is $267.83ML$ and the mean error for the inflow to the WWTP ξ is $20.01L/s$, whereas ξ_{rain} is $0.9L/s$.

The next steps to validate the methodology are to increase the complexity of the network configuration and to verify the strengths and weaknesses of VMPC. Therefore, the first complexity change is the addition of a parallel Storage Unit to the UDS, similar to Section 6.2.2. The goal is to change the parameters of this configuration, such as the WWF in each Storage Unit, or the outlet's reference and

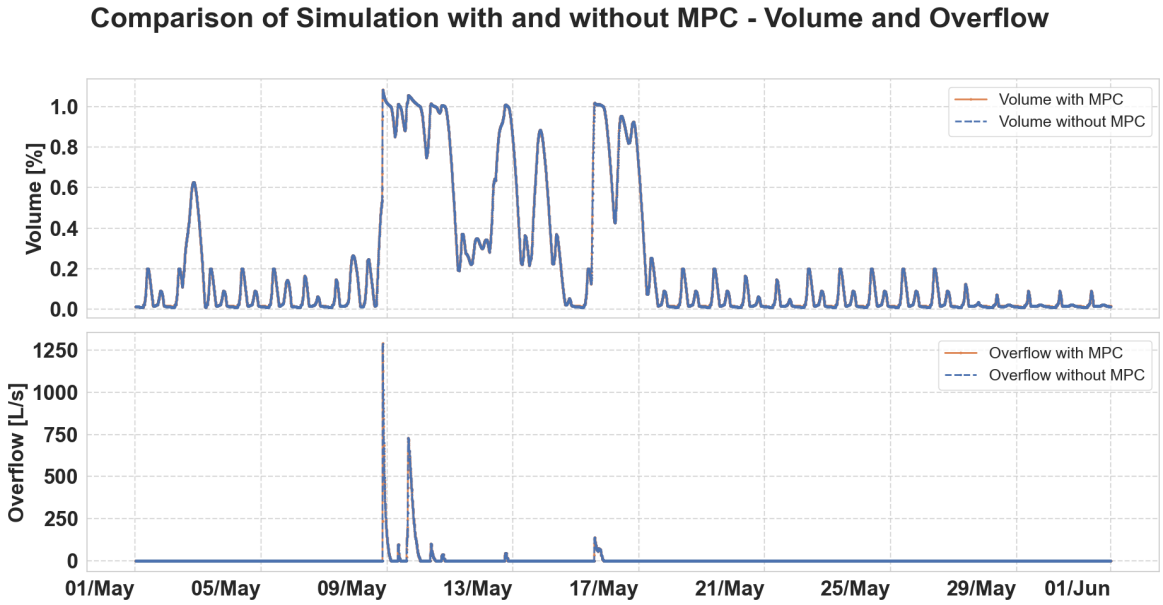

Figure 7.5: Single SU configuration - overflow comparison between static control and VMPC.

Table 7.2: Metric results for 1-month simulation with Single SU configuration.

Metric	Description	Static Control	With VMPC
$Q_{\text{ov}_{\text{total}}}$	Total overflow in ML	19.83	19.83
ξ	Inflow error in L/s	20.01	20.01
ξ_{rain}	Inflow error during WWF in L/s	0.9	0.9
$Q_{\text{wwtp}_{\text{total}}}$	Total volume arriving at WWTP in ML	267.83	267.83

maximum outflow, and to check the performance of VMPC compared to the scenario with static control using the same metrics utilised for the Single SU configuration.

7.3.4 Methodology Validation - Parallel Storage Units Configuration

The parallel storage unit configuration can be seen in Figure 6.10. The first scenario is similar to the Single SU configuration, VMPC has limited possibilities due to the constraints of the network, but should still be as good as the static control system. The initial parameters are shown in Table 7.3, the DWF and WWF are the same as in Section 6.2.2. In order to explore how the flexibility of the actuator affects the behaviour of the system, two scenarios are discussed, where the first is where $Q_{\text{out}_{\text{max}}} = Q_{\text{design}}$ and the second where $Q_{\text{out}_{\text{max}}} \geq Q_{\text{design}}$ for all SU.

Table 7.3: Parallel SU configuration - Urban Drainage System parameters.

Model Parameter	Description	Value
$(V_{\max_1}, V_{\max_2})$	Maximum storage volume for SU1 and SU2 in m^3	(1450.5, 967)
$(Q_{\text{design}_1}, Q_{\text{design}_2})$	Outlet 1 and 2 designed outflow in L/s	(65, 55)
$(Q_{\text{out}_{\max_1}}, Q_{\text{out}_{\max_2}})$	Outlet 1 maximum outflow in L/s	(65, 55)
$Q_{\text{wwtp}_{\text{ref}}}$	Reference inflow to the WWTP in L/s	120
$Q_{\text{wwtp}_{\max}}$	Maximum inflow to the WWTP in L/s	120

Scenario 1: $Q_{\text{out}_{\max}} = Q_{\text{design}}$

The simulation scenario lasts one month, from 01/05 until 01/06. The VMPC runs every 240 seconds in this scenario, while the simulated model runs every 5 seconds. The results with VMPC and static control can be seen in Table 7.4.

Table 7.4: Metric results for 1-month simulation with Parallel SU configuration.

Metric	Description	Static control	With VMPC
$Q_{\text{ov}_{\text{total}}}$	Total overflow in ML	12.64	12.64
ξ	Inflow error in L/s	26.63	26.63
ξ_{rain}	Inflow error during WWF in L/s	0.90	0.90
$Q_{\text{wwtp}_{\text{total}}}$	Total volume arriving at WWTP in ML	250.12	250.12

The outflow can be seen in Figure 7.6, whereas the volume and overflow of each Storage Unit is presented in Figure 7.7 for the simulation with static control and with VMPC, respectively.

For both static control and VMPC, the total volume overflow is $12.64ML$, ξ is $26.63L/s$, $\xi_{\text{rain}} = 0.9L/s$, and the total volume entering the WWTP is $250.12ML$. Analysing the results, this scenario reveals that VMPC is not capable of improving dynamic management with such a restricted setup for the UDS. Although VMPC is still capable of controlling the UDS, the system performance does not improve compared to the scenario without it, mainly because the maximum outflow, $Q_{\text{out}_{\max}}$, from both Storage Units is exactly the same as the designed outflow. Assuming that $Q_{\text{out}_{\max}}$ is higher than Q_{design}, keeping $Q_{\text{wwtp}_{\text{ref}}}$ as the same desired inflow to the WWTP, the flexibility of the system increases, enabling the outflow from a specific storage unit to be adjusted so that $Q_{\text{wwtp}_{\text{ref}}}$ is still maintained, while allowing adjustments in Q_{out} to reduce possible overflows.

Scenario 2: $Q_{\text{out}_{\max}} \geq Q_{\text{design}}$

In the next scenario, the maximum outflow for both actuators increases by $20L/s$, as shown in Table 7.5 and the simulation period remains the same as in Scenario 1, from 1$^{\text{st}}$ of May to 1$^{\text{st}}$ of June.

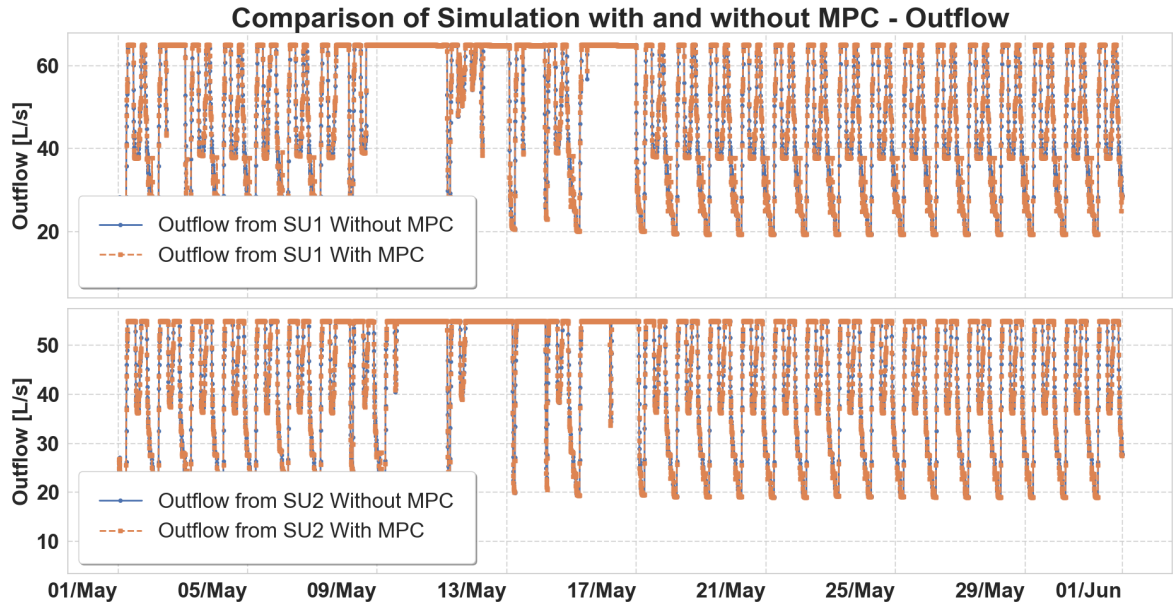

Figure 7.6: Parallel SU configuration - outflow comparison between static control and VMPC.

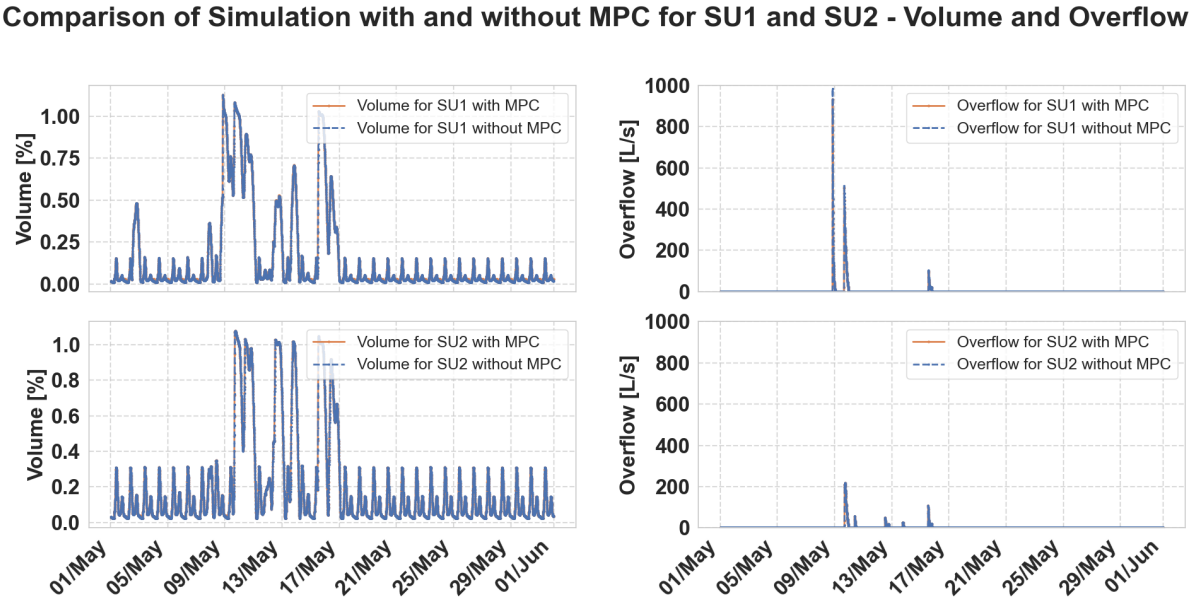

Figure 7.7: Parallel SU configuration - overflow comparison between static control and VMPC.

Although the maximum outflow capacity from actuators has been increased, the maximum inflow to the WWTP, $Q_{\mathrm{wwtp}_{\max}}$ remains capped at $120 L/s$, This change means that, while the inflow to the WWTP cannot exceed $120 L/s$, each outlet can now handle a higher outflow, providing greater flexibility, rather than being limited to just $55 L/s$ and $65 L/s$. Now, when VMPC detects that an overflow occurred in a specific Storage Unit, it utilises this additional flexibility to reduce or prevent the overflow. The optimal outflows calculated by VMPC are compared to the outflows of the static control system in Figure 7.8, showing that the outlet's behaviour changed considerably when applying VMPC.

Table 7.5: Parallel SU configuration - Urban Drainage System parameters.

Model Parameter	Description	Value
$(V_{\max_1}, V_{\max_2})$	Maximum storage volume for SU1 and SU2 in m^3	(1450.5, 967)
$(Q_{\text{design}_1}, Q_{\text{design}_2})$	Outlet 1 and 2 designed outflow in L/s	(65, 55)
$(Q_{\text{out}_{\max_1}}, Q_{\text{out}_{\max_2}})$	Outlet 1 and 2 maximum outflow in L/s	(85, 75)
$Q_{\text{wwtp}_{\text{ref}}}$	Reference inflow to the WWTP in L/s	120
$Q_{\text{wwtp}_{\max}}$	Maximum inflow to the WWTP in L/s	120

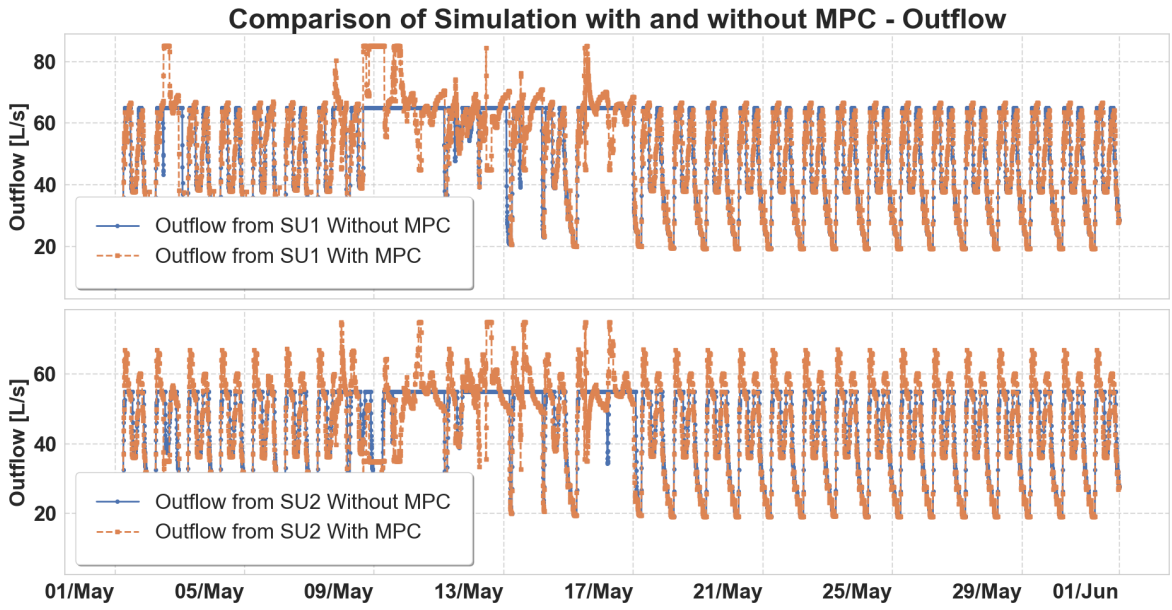

Figure 7.8: VMPC scheme for Urban Drainage Systems.

At certain times, the controller increases the outflow from one Storage Unit while reducing it from another to make the most of the system's storage. In Figure 7.9 the volumes are displayed and, evidently, the additional outflow capacity allows for a more adaptable distribution of the outflows and, therefore, allowed VMPC to improve dynamic management and decrease overflow, while staying within the constraint $Q_{\text{wwtp}_{\max}} \leq 120 L/s$.

In general, during the one-month simulation period, VMPC reduced the total overflow, $Q_{\text{ov}_{\text{total}}}$, by 12.5%, as can be seen in Table 7.6. During this time, ξ is $26.0 L/s$ with VMPC and $26.55 L/s$ without it, representing an improvement of 3%. To achieve this, the controller used the full capacity of the WWTP more often.

Figures 7.10 and 7.11 provide a zoomed view of the results between 12$^{\text{nd}}$ and 14$^{\text{th}}$ of May, highlighting a specific scenario where VMPC successfully prevents an overflow event in Storage Unit 2. During this interval, the outflow from Storage Unit 1 was reduced to allow Storage Unit 2 to operate at its maximum capacity, preventing the overflow event.

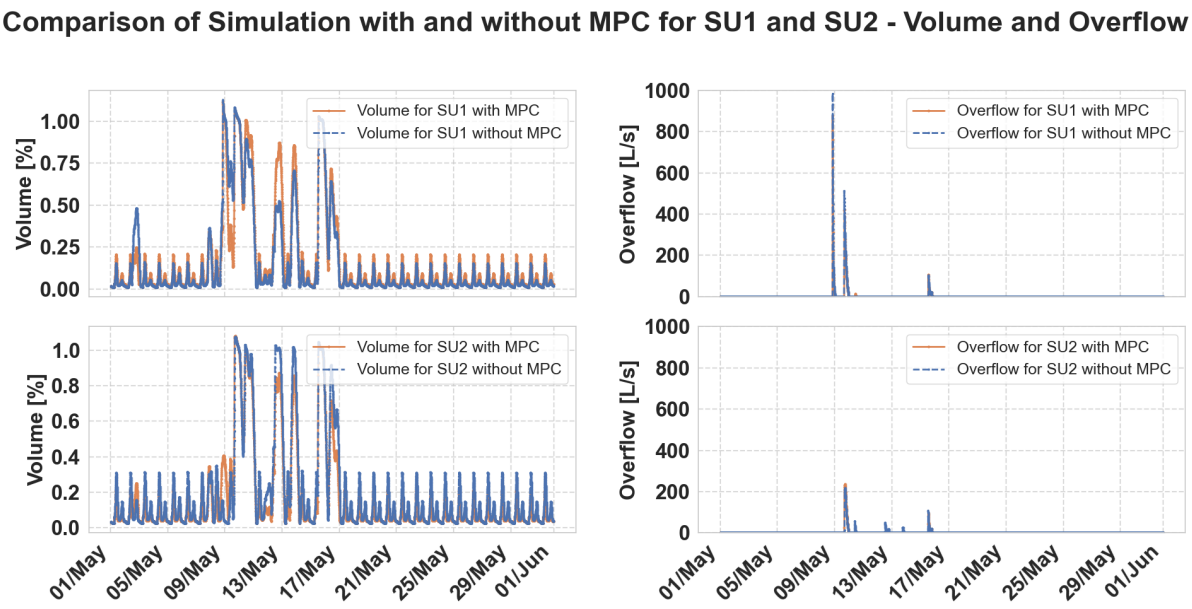

Figure 7.9: Parallel SU configuration - overflow comparison between static control and VMPC with $Q_{\text{out}_{\text{max}}} \geq Q_{\text{design}}$.

Table 7.6: Metric results for 1-month simulation with Parallel SU configuration.

Metric	Description	Static control	With VMPC
$Q_{\text{ov}_{\text{total}}}$	Total overflow in ML	12.64	11.06
ξ	Inflow error in L/s	26.63	26.00
ξ_{rain}	Inflow error during WWF in L/s	0.90	0.01
$Q_{\text{wwtp}_{\text{total}}}$	Total volume arriving at WWTP in ML	250.12	251.69

From a mathematical perspective, the system is constrained by Equation 7.15f to keep the inflow to the WWTP at $Q_{\text{wwtp}_{\text{max}}} = 120L/s$, which translates to the Parallel SU configuration as:

$$Q_{out_1} + Q_{out_2} \leq 120 \tag{7.25}$$

The static control scenario obeys this constraint because when both outlets are at maximum outflow, they comply with Equation 7.25, such that $Q_{out_1} + Q_{out_2} = 65 + 55 = 120L/s$. However, VMPC is capable of using different combinations of Q_{out_1} and Q_{out_2}, for instance $(Q_{out_1}, Q_{out_2}) = (85, 35)L/s$ or $(Q_{out_1}, Q_{out_2}) = (45, 75)L/s$, allowing higher outflows and faster emptying of specific storage units depending where the threat of overflowing is most critical. Therefore, the application of VMPC enables more effective volume management by using the potential of the actuators while still complying with the constraints of the WWTP.

Nevertheless, this configuration is still quite simple and is heavily restricted in the VMPC so that it cannot achieve a greater impact. $Q_{\text{wwtp}_{\text{ref}}}$ and $Q_{\text{wwtp}_{\text{max}}}$ are the same in this instance, so VMPC is

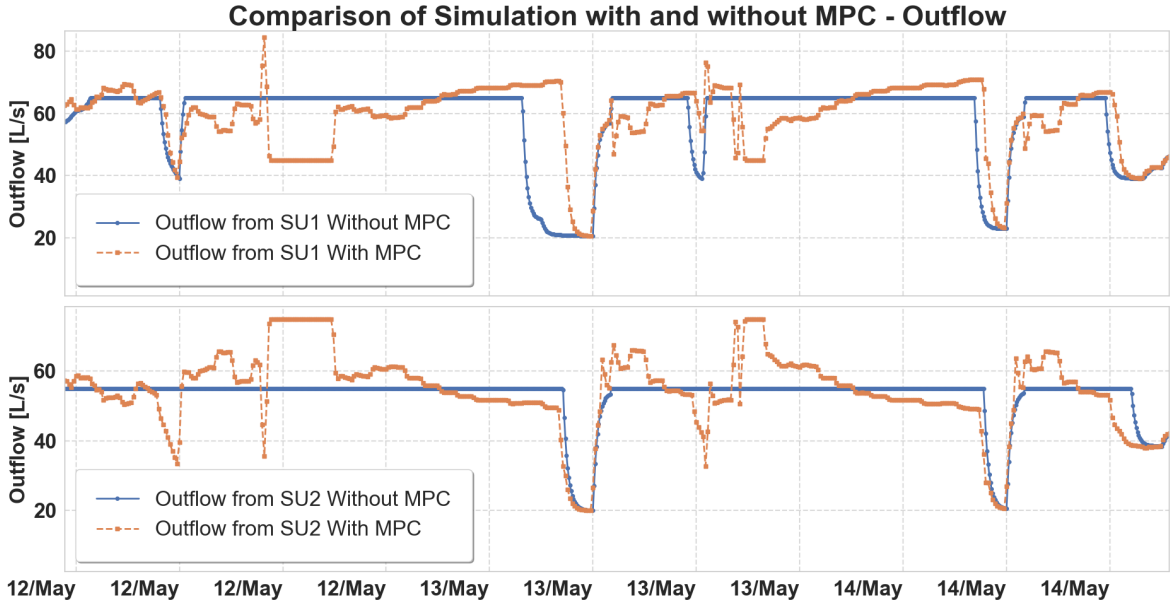

Figure 7.10: Parallel SU configuration - outflow comparison between static control and VMPC - 12nd of May to 14th of May.

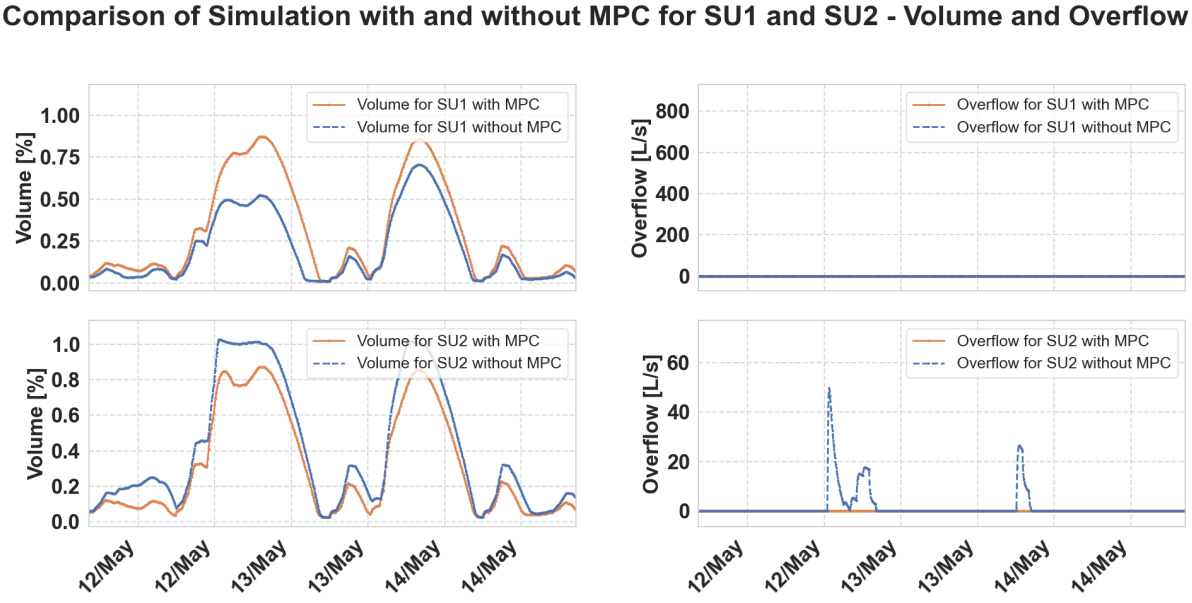

Figure 7.11: Parallel SU configuration - overflow comparison between static control and VMPC - 12nd of May to 14th of May.

constrained to $Q_{\text{wwtp}_{\text{ref}}}$ as the maximum inflow. However, it is possible that the WWTP allows higher inflows than the reference, which provides an additional degree of freedom for VMPC to optimise the system. For example, assuming a pump outlet, $Q_{\text{wwtp}_{\text{ref}}}$ could be interpreted as the optimal operating point of the pump derived from the efficiency curve, but the pump still allows higher flows, losing efficiency but increasing the possible range. To illustrate this example, the next section extends the parallel configuration by adding a SU in series with the current parallel configuration, while also using a

pump outlet. Furthermore, in this section, the importance of the weights of VMPC is investigated and how these weights affect the algorithm behaviour by applying a sensitivity analysis, ultimately providing a methodology to choose those weights using the sensitivity analysis.

7.3.5 Methodology Validation - Parallel + Series Storage Units Configuration

As introduced in Section 6.2.2, this configuration increases the complexity of the network by introducing a third Storage Unit in series with the parallel configuration. The new addition collects the outflow from both SU1 and SU2 while also handling its own DWF and WWF. Moreover, the outlet from SU3 is a pump capable of reaching a maximum outflow of $130 L/s$. This pump is speed controlled, allowing VMPC to freely adjust the flow for the calculated optimum value, given the constraints.

In this scenario, the simulation was conducted over the course of one year (from January 1 to December 31), where the precipitation data is collected from three different rain stations in Germany for a more realistic rain simulation. The weights for VMPC were initially selected to have a higher α and slightly higher γ to try to focus the optimisation to maintain good volume homogeneity and overflow minimisation, resulting in α, β, γ, ϵ = (60, 2, 10, 153). The prediction horizon is 1200 seconds. Table 7.7 shows the simulation parameters, while the results are shown in Table 7.8. Later in this section, a more effective method for determining the weights is discussed; one that takes into account the objectives of the control system.

Table 7.7: Parallel + Series SU configuration - Urban Drainage System parameters.

Model Parameter	Description	Value
$(V_{\max_1}, V_{\max_2}, V_{\max_3})$	Maximum storage volume for SU1, SU2 and SU3 in m^3	(967, 483.5, 1450.5)
$(Q_{\text{design}_1}, Q_{\text{design}_2}, Q_{\text{design}_3})$	Outlet 1,2 and 3 Designed outflow in L/s	(40, 40, 120)
$(Q_{\text{out}_{\max_1}}, Q_{\text{out}_{\max_2}}, Q_{\text{out}_{\max_3}})$	Outlet 1, 2 and 3 Maximum outflow in L/s	(60, 60, 130)
$Q_{\text{wwtp}_{\text{ref}}}$	Reference inflow to the WWTP in L/s	120
$Q_{\text{wwtp}_{\max}}$	Maximum inflow to the WWTP in L/s	130

In this scenario, VMPC led to a 52.4% increase in the system's total overflow compared to its performance without optimal control. The volume reaching the WWTP was also significantly reduced, and the higher value of ξ indicates that the controller was not close to $Q_{\text{wwtp}_{\text{ref}}}$. This poor outcome is the result of the choice of weights, as demonstrated by the metrics, indicating that these weights need to be adjusted. Manually tuning weights is not only tedious, but is also unlikely to yield optimal or even reasonable results, and without a structured approach, manual tuning relies heavily on trial and error, because there is no systematic knowledge into how each weight impacts performance. Consequently, it can easily lead to situations that underutilise the system's potential or even worsen its behaviour, as illustrated by this simulation.

Since this method is clearly not ideal, as it does not ensure optimal performance, a more systematic approach is needed to evaluate the influence of the weights on the desired behaviour of the system. A

Table 7.8: Overall results for first scenario.

Metric	Description	Static control	With VMPC
Q_{ov_1}	Overflow at SU1 in ML	94.522	161.899
Q_{ov_2}	Overflow at SU2 in ML	62.785	122.931
Q_{ov_3}	Overflow at SU3 in ML	430.079	610.366
$Q_{\text{ov}_{\text{total}}}$	Total overflow in ML	587.398	895.196
ξ	Inflow error in L/s	32.32	42.17
ξ_{rain}	Inflow error in L/s	0.06	9.86
$Q_{\text{wwtp}_{\text{total}}}$	Volume arriving at WWTP in ML	2764.913	2454.389

common method is to analyse the sensitivity of the metrics to variations in the weights. The Sensitivity Analysis (SA) of a system examines how the behavioural changes in a system's output can be attributed to variations in its input factors [121] and it can be divided into Local Sensitivity Analysis (LSA) and Global Sensitivity Analysis (GSA). LSA examines how output varies in response to small changes in inputs around a specific point, while GSA evaluates the impact on output variability across the entire range of possible values on inputs [122].

7.3.6 Weight Sensitivity Analysis

Two sensitivity analysis are evaluated in this research, as detailed below:

1. The **Local Sensitivity Analysis** method used in this research is based on the **Morris screening** method in [123]. A parameter x, (e.g. the weights α, β, γ and ϵ), is perturbed by a small value Δ, and the system's output $f(x)$ (e.g. $Q_{\text{ov}_{\text{total}}}$ and ξ) is calculated with and without the perturbation. The sensitivity factor, also called the elementary effect EE, for the i-th parameter is calculated by:

$$EE_i = \frac{f(x_1, x_2, ..., x_{i-1}, x_i + \Delta, x_{i+1}, ..., x_k) - f(\mathbf{x})}{\Delta} \tag{7.26}$$

where $\mathbf{x} = [x_1, x_2, ..., x_k]$ is the parameter input vector, k is the total number of input parameter and where $\mathbf{x}$ denotes a randomly drawn sample out of the random variable vector $\mathbf{X}$. The step size Δ is defined over a p-level grid in the input parameter space Ω, commonly set as $\Delta = \frac{p}{2(p-1)}$ if p is an even number [121]. Morris [123] defined a scheme to define trajectories for the input parameters space randomly and reducing the computational burden: The starting vector $\mathbf{x}^*$ is randomly sampled from $\mathbf{X}$ in the p-level grid and the first trajectory point $x^{(1)}$ is generated by increasing one input parameter by Δ. The second trajectory point is obtained by increasing or decreasing (randomly chosen) by Δ the i-th input parameter of $x^{(1)}$, such that $x^{(2)} = x^{(1)} + e_i\Delta$ or $x^{(2)} = x^{(1)} - e_i\Delta$, where i is randomly chosen from the set $1, 2, ..., k$. The third trajectory is defined as $x^{(3)} = x^{(2)} + e_j\Delta$ or $x^{(3)} = x^{(2)} - e_j\Delta$, where $j \neq i$, continuing this procedure until $x^{(k+1)}$. The trajectory is, therefore, defined for each input parameter $\mathbf{x} = [x_1, x_2, ..., x_k]$. However, the procedure provides only one sensitivity factor EE for each input parameter and the solution is to

produce r different input trajectories following the same procedure. The final computation of the sensitivity factor is then calculated over all trajectories, resulting in $N_m = r(k+1)$ simulations [124]. At the end, the mean of the absolute value (μ) and the standard deviation (σ) is calculated for the i-th parameter as below:

$$\mu_i = \frac{1}{r}\sum_{j=1}^{r} EE_i^j, \qquad \sigma_i = \sqrt{\frac{1}{r-1}\sum_{j=1}^{r}(EE_i^j - \mu_i)^2} \tag{7.27}$$

By iterating using this method over a range of trajectory weights, μ_i indicates the overall influence of the parameter on $f(x)$. Basically, the values of μ in relation to other parameters suggests the importance of the parameter on the output, e.g., higher values indicate that significant impact of the parameter on $f(x)$. Furthermore, σ_i estimates non-linear or interaction effects and thus provides a qualitative insight into the model structure. In the end, the aim of performing the Morris Screening is to evaluate which inputs have higher effect on the output, screening those inputs in order of importance.

2. The **Global Sensitivity Analysis** provides a broader view of the relationship between inputs and outputs over a large range of values, usually defining an input variability space. Typically, such analysis is done to support model calibration, verification, diagnostic evaluation or simplification; to prioritize efforts for uncertainty reduction; to analyse the dominant controls of a system; and to support robust decision-making [122]. Two examples of GSA are **Grid Search** SA, often called sampling method, and **Random Search** SA, both methods commonly used for hyper-parameter optimisation [125].

   In both grid search and random search, the sensitivity analysis evaluates how a set of combinations of input parameters changes the output, defining a parameter space set Ω. However, these methods differ in how they determine Ω. For instance, the grid search evaluates a specific subset of the input space by exhaustively testing predetermined values for each parameter, creating a structured grid of all possible combinations. It is simpler to implement and parallelizing the computation is trivial. Although this approach ensures thorough coverage within the chosen subset, it can be computationally expensive, especially as the number of parameters grows, therefore is more suitable for 1-D, 2-D or 3-D parameter searches [126].

   In contrast, random search defines parameter values randomly from within specified ranges, without following a predefined grid. This randomness allows random search to cover a broader range of possible values, potentially finding better-performing configurations with fewer evaluations. Besides, random search is more efficient in high dimensional spaces, however, it may not explore certain regions of the input space as thoroughly as grid search [126]. In both methods, the graphical representation used in this research is a 2-D scatter plot with a heatmap, where the x and y axis are two input parameters and the color represents the output value, as shown in Figure 7.12a and Figure 7.12b.

In the context of VMPC sensitivity analysis, the inputs are the weights of the cost function J in Equation 7.15a, therefore the input parameter vector $\mathbf{x} = [\alpha, \beta, \gamma, \epsilon]$. The output of the analysis is the total volume overflow throughout the wastewater network and the error between the reference inflow and the actual

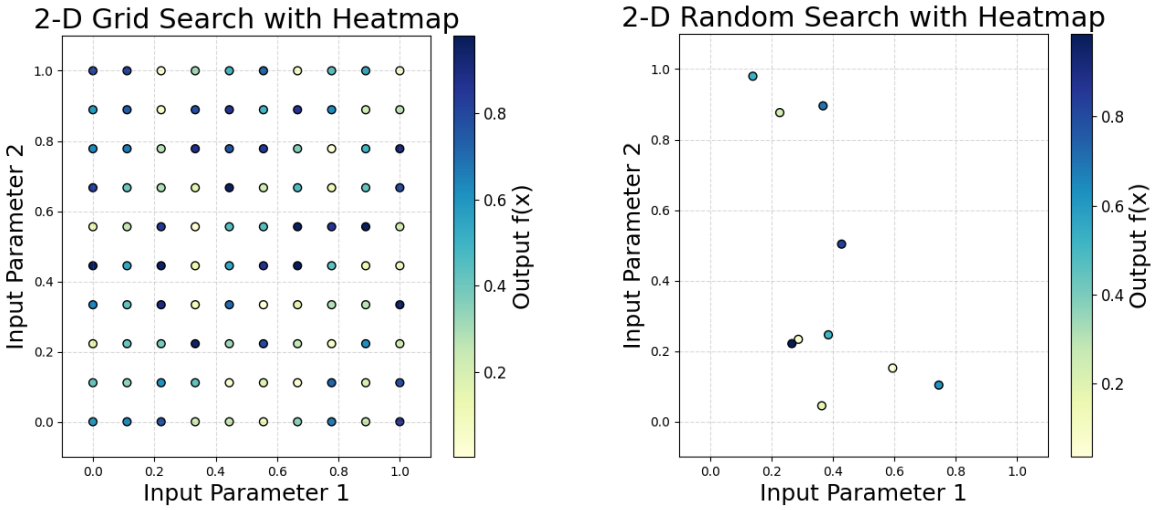

(a) Grid Search with heatmap. *(b)* Random Search with heatmap.

Figure 7.12: Global Sensitivity Analysis [125].

inflow entering the WWTP, which establishes $f(x) = (Q_{\text{ov}_{\text{total}}}, \xi)$. The goal is to determine the influence of the weights on the total overflow during rain events and also on the error in the inflow to the WWTP.

The first analysis introduced is the LSA using the Morris screening method, followed by two GSA using the Grid search and Random search methods. The Morris screening is helpful to study the individual influence of each weights and possible non-linearity interactions with the output, while the GSA methods are interesting to discover regions where the interaction between the weights are more important and have higher influence over the outputs. The Grid Search is applied to a more restricted parameter space Ω compared to the Random Search to examine specific weight configurations in greater detail. This allows for a more exhaustive search within a focused area where values are more likely to be relevant. The Random Search is defined over a broader parameter space to uncover potential areas that the Grid Search might have missed but that could still be relevant for exploration.

For all analysis, a shorter duration for the simulation was selected to reduce computational effort, since a longer simulation would be more computationally demanding. Since the rain scenario dictates the behaviour of the UDS, this analysis is highly dependent on the intensity of rain events that occur during the period. In order to assess different rain events, two scenarios with one month duration were chosen:

1. Analysis from 1$^{\text{st}}$ of May to 1$^{\text{st}}$ of June with distributed rain events with low, medium, and high intensities, as shown in Figure 7.13.

2. Analysis from 24$^{\text{th}}$ of March to 24$^{\text{th}}$ of April with higher frequency in short periods and high-intensity rain, while also with a few small and medium events, as shown in Figure 7.14.

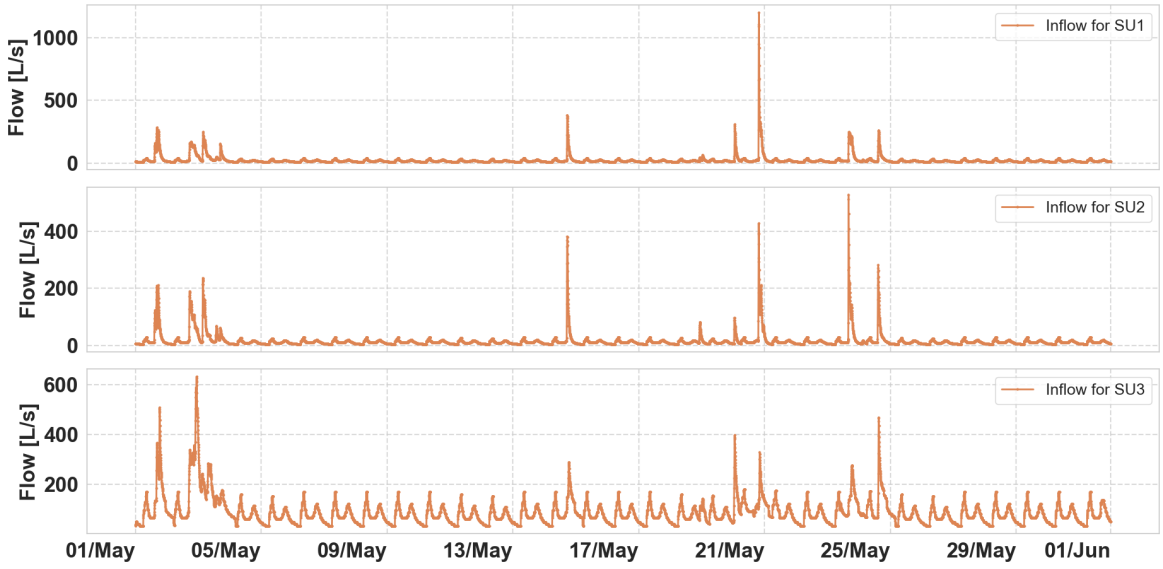

Figure 7.13: DWF + WWF data for sensitivity analysis from 1st of May to 1st of June.

Figure 7.14: DWF + WWF data for sensitivity analysis from 24th of March to 24th of April.

Local Sensitivity Analysis - Morris Screening

As mentioned above, Morris Screening provides knowledge on how each individual input influences a given output. Since Morris screening is only a qualitative method, the absolute values of μ and σ are not essential, however, the relationship between μ and σ are more interesting to obtain more valuable information about the parameters. For example, this study attempts to convey how each input parameter in $\mathbf{x} = [\alpha, \beta, \gamma, \epsilon]$ influences the output $f(x) = (Q_{\mathrm{ov}_{\mathrm{total}}}, \xi)$. Given the set $\mathbf{x}$, the number of input

parameters is $k = 4$, while the space set for the input parameters from which the trajectories are taken randomly is $\Omega = \{(\alpha, \beta, \gamma, \epsilon) \mid \alpha \in \Omega_1, \beta \in \Omega_2, \gamma \in \Omega_3, \epsilon \in \Omega_4\}$, where the lower and upper bounds of Ω_i are set to $(1, 200)$ for $i = (1, 2, 3, 4)$. The increment $\Delta = 1$ when creating the points in each trajectory. The number of trajectories is $r = 600$ for each simulated period; therefore, the total number of simulation runs necessary is $N_m = r(k + 1) = 600 * (4 + 1) = 3000$ for a single period, corresponding to 6000 simulations combining both scenarios.

The Morris screening LSA is outlined in Figure 7.15 for both inflow scenarios. The results are similar in both scenarios, the weights ϵ and γ have the least impact on the output compared to the other parameters, with γ having a slightly higher impact, while α and β showed a greater influence on the output. For α, β and γ, the parameters $\sigma \gg \mu$, which indicates a non-linear dependency between the analysed parameters and the outputs, however, the interactions between ϵ is less significant than $\sigma \approx \mu$.

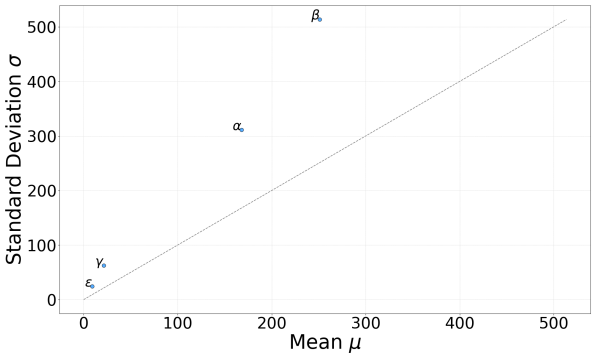

(a) LSA - $Q_{\text{ov}_{\text{total}}}$ - 1st of May to 1st of June.

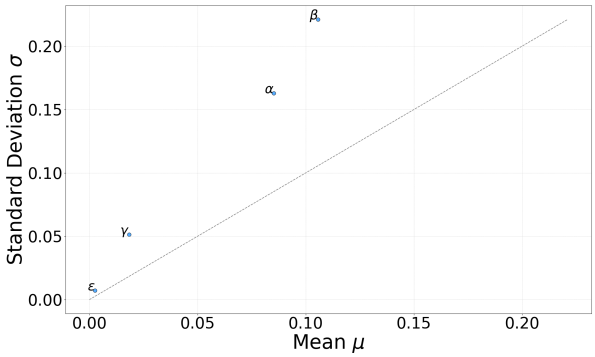

(b) LSA - ξ - 1st of May to 1st of June.

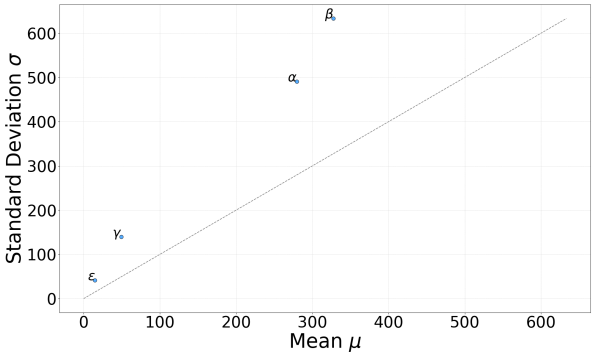

(c) LSA - $Q_{\text{ov}_{\text{total}}}$ - 24th of March to 24th of April.

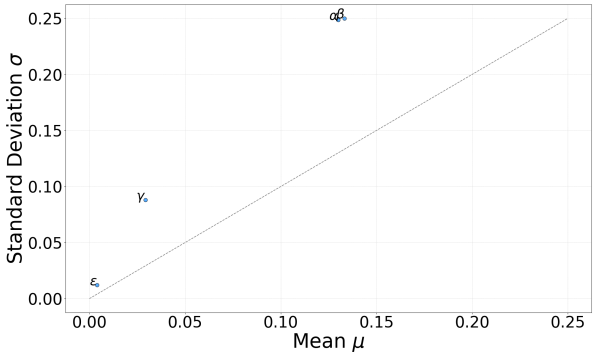

(d) LSA - ξ - 24th of March to 24th of April.

Figure 7.15: Morris Screening LSA for Parallel+Series SU configuration.

In summary, the Morris screening revealed that the weight ϵ is not as impactful on the optimisation outcome, as expected because it is mainly implemented to improve the feasibility of the algorithms. The non-linear dependency of the parameters explains the difficulties in the tuning of the MPC, although the intuition on how to select the weights is not complex, the interactions between the parameter and the output are not straightforward. The choice of α and β, for example, is decisive in the outcome and should be considered with care. Since this analysis is mostly qualitative, in the next section, GSA is performed to provide further insight into the impacts of the weights with more quantitative data.

Global Sensitivity Analysis - Grid Search

The Grid search is a method that iterates exhaustively through a specific set and because of that, it can be computationally expensive to be used. Since the input parameter vector is 4-dimensional, the number of iterations to define a relevant grid can be too large, and the graphical representation could be difficult to grasp. In this case, the analysis is divided into several 3-D grid heatmaps by fixing the value of one of the inputs, creating n 3-D grids, where n is the total number of values defined for the input fixed in each iteration. The input ϵ was chosen to be separated from the grid, as a result from the Morris screening, which revealed that ϵ is less impactul on the performance. The algorithm steps were defined as follows: a set is first specified for the input ϵ so that $\epsilon = [\epsilon_1, \epsilon_2, ..., \epsilon_n]$. Next, the grid space Ω is created to encompass the other inputs, α, β and γ. In the initial iteration, ϵ is fixed at ϵ_1, and the 3-D grid heatmap is generated by iterating over all possible values of α, β and γ in Ω. Subsequently, ϵ is updated to ϵ_2 and a new search is performed, repeating the process n times until the grids are created for all values of ϵ.

The analysis is conducted with the following setup: Six grids are defined, resulting in $n = 6$, with arbitrarily chosen values of $\epsilon = [3, 21, 52, 89, 102, 153]$. The set Ω is defined as $\Omega = \{(\alpha, \beta, \gamma) \mid \alpha \in \Omega_1, \beta \in \Omega_2, \gamma \in \Omega_3\}$, where each Ω_i has the lower and upper bounds set to $(1, 200)$ for $i = (1, 2, 3)$. Each input in the grid includes 12 equally spaced points, creating six 3-D grid heatmaps with a size of $12 \times 12 \times 12 = 1728$ points. The colours in the heatmap represent one output, specifically $Q_{\text{ov}_{\text{total}}}$ or ξ. This scenario is evaluated using inflow data presented in Figures 7.13 and 7.14.

The initial analysis is performed over the period of 1st of May to 1st of June. In Figure 7.16, one of the grid search results is displayed to demonstrate the graph; the remaining 3D heatmaps are in Appendix A.1. Firstly, the influence of the weight ϵ on the outputs $Q_{\text{ov}_{\text{total}}}$ and ξ becomes clear when comparing the heatmaps for each output across different ϵ values. The graphs reveal that changes in ϵ did not significantly modify the heatmap. The output values were kept very close when varying ϵ, however, by examining the best results of $Q_{\text{ov}_{\text{total}}}$, it is evident that the lower values of ϵ showed slightly reduced performance, with around 5% reduced performance for the output $Q_{\text{ov}_{\text{total}}}$ when $\epsilon = 3$ compared to $\epsilon = 153$.

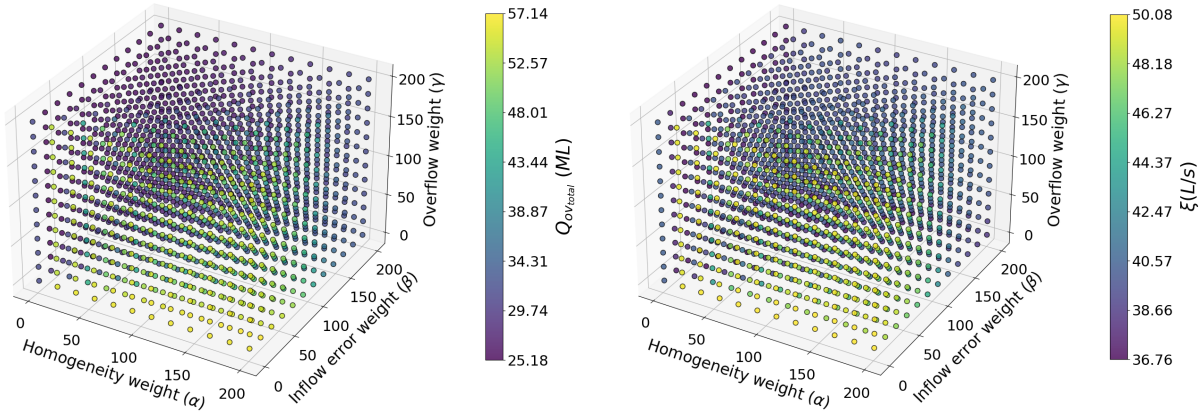

(a) $Q_{\text{ov}_{\text{total}}}$ for $\epsilon = 153$. *(b)* ξ for $\epsilon = 153$.

Figure 7.16: Grid Search SA for the total overflow in the system from 1st of May to 1st of June for $\epsilon = 153$.

Observing individual heatmaps, the 3-D grid reveals that increasing the value of α leads to poorer controller performance, while the opposite effect is shown by the other weights. The sensitivity analysis does not clearly identify what is the best combination of α, β, γ and ϵ for optimal system performance. Instead, it gives insight into a region where it is more preferable to keep the weights. The value of β affected the output ξ more strongly than for $Q_{\text{ov}_{\text{total}}}$, as indicated by the heat map. For this analysis, the weights are reasonably chosen for the values $\alpha \in (0, 20)$ and $\beta, \gamma \in (20, 200)$, while keeping $\epsilon \geq 50$.

In the next scenario, the validity of these choices is further evaluated to understand if a different rain input scenario significantly changes this outcome. The parameters used in the previous simulation are replicated, only changing the period in which the simulation is conducted, now from 24^{th} of March to 24^{th} of April, to analyse a different WWF profile. The results are displayed in Appendix A.1 for the outputs $Q_{\text{ov}_{\text{total}}}$ and ξ, respectively, where several 3D heatmaps are presented for different values of ϵ.

Compared with the analysis for the first rain scenario, the outcome is exactly the same. The value of ϵ does not greatly affect the output, although higher values are desirable. The weight α used for homogeneity minimisation is preferably chosen to be small, while the other weights can have a greater range. It can be argued that the influence of the weights did not change noticeably for different rain scenarios, which correlates to the Morris Screening. Therefore, rain scenarios need to be representative enough so that information can be extracted from the simulation, but when applied in real applications where the rain will definitely be different, a well chosen set of parameters will have a good performance over a wide range of rain events.

Global Sensitivity Analysis - Random Search

A Random Search was performed similarly to the Grid Search, where 3D heatmaps representing how α, β and γ affected a given output, whereas in this analysis fewer grids are generated and the value for ϵ is now fixed to $\epsilon = 153$ as it was already shown that it has only a small influence on the output. The lower and upper bounds of Ω_i was increased to $(1, 1000)$ to cover a wider range of values. In addition, the number of points for each input is increased to 15, therefore the grid has $15 \times 15 \times 15 = 3375$ points, randomly chosen from Ω_i. The resulting heatmaps are shown in Appendix A.1.

The results reveal a similar trend to the Grid Search analysis, where it was observed that increasing the homogeneity weight (α) leads to a deterioration in the performance of both outputs. On the other hand, β and γ presented a wider range of values where the performance is favourable. However, choosing optimal weights solely based on this analysis remains a challenge. Instead, it is more important to evaluate the unsuitable regions for the weights. The increase in the bounds of the variables to 1000 did not significantly change the outcome, and the values of the outputs, as indicated by the heatmap colour bars, remain similar within those observed using the original bounds. This suggests that the upper bound previously chosen for the Grid Search was already sufficient large.

The analysis can also help to understand whether a chosen set of weights is positioned in a region in the heatmap where the output's performance is more stable. For instance, the scenario presented in Section 7.3.5 compared the system performance of static control with a VMPC where $(\alpha, \beta, \gamma, \epsilon)$ equals $(60, 2, 10, 153)$. The comparison resulted in an unfavourable performance by VMPC due to poor weight selection. Identifying the weight vector $(60, 2, 10, 153)$ in the Grid Search from Figure A.3b and Figure A.6b, as shown in Figure 7.17, it is evident that the choice of weights was poor.

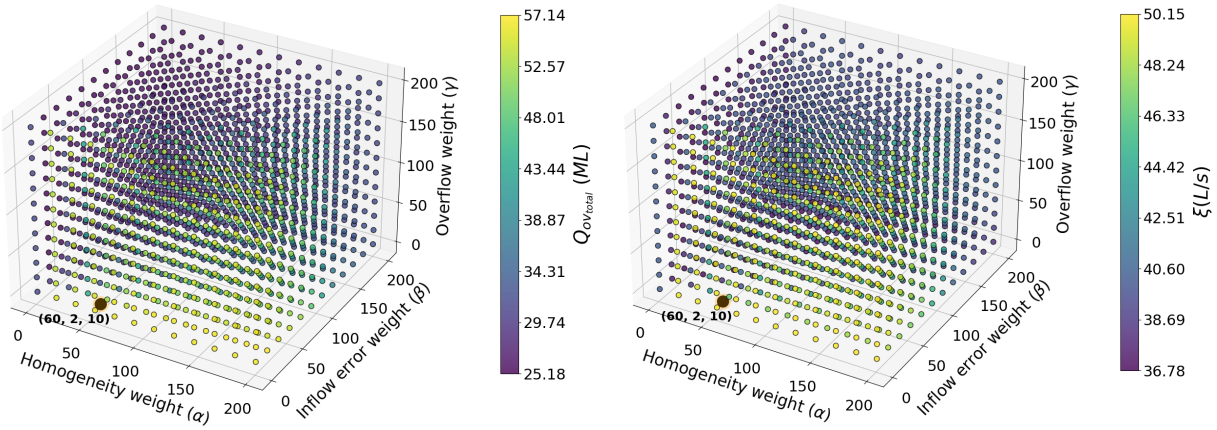

(a) Weights (60, 2, 10, 153) in grid from Figure 7.16a.

(b) Weights (60, 2, 10, 153) in grid from Figure 7.16b.

Figure 7.17: Representation in the grid of the weights chosen in Section 7.3.5.

The weights could have been chosen more wisely by selecting them in a region more favourable. However, this method consists of a trial an error methodology subject to errors. Thus, to eliminate this type of error, a methodology is suggested in the next section for sub-optimal weight selection using an optimisation algorithm to identify a Pareto-front, balancing the trade-offs between the weights and outputs.

7.3.7 Genetic Algorithm for weight optimisation

The proposed method for selecting the weights uses a Genetic Algorithm (GA) to optimise a multi-objective cost function given input constraints. The implementation of GA to choose MPC's weights is not a novel approach: in [127] the strategy is applied in a Motion cueing algorithm where the weights are optimized using a multi-objective GA, with the objective of minimizing motion inputs (linear acceleration and angular velocity), input rates, output displacements and the sensed motion errors; the study proposed by [128] defined an automated tuning algorithm for MPC that is numerically based and combines a genetic algorithm with multi-objective fuzzy decision-making; and in the research of [129] which uses an automated tuning procedure with GA to reduce the manual operations in the industrial cement kiln process.

As mentioned in Chapter 6, GA is an heuristic method for solving optimisation problems [99] by mimicking the search for the optimum through biological evolution. In each time step, the solutions, also known as the population, are updated. Genetic algorithms have basic characteristics to mimic evolutionary behaviour, such as chromosome representation, fitness selection, and biologically inspired operators [100]. In the context of the Urban Drainage System controlled by an MPC, the aim is to develop a GA to find a set of weights that will provide a pareto-front for the weights in relation to the output, obtaining a reasonable compromise between the minimisation of $Q_{\mathrm{ov}_{\mathrm{total}}}$ and ξ.

In essence, the Genetic algorithm runs a simulation with either random initial weights or a selected initial-guess as the starting point and each individual in the population iteratively increments one or

more weight randomly to explore the most regions possible, storing in each run the output and verifying the outcome with previous solutions. The algorithm can be summarised as follows:

1. Initialisation of GA's parameters.
   a) Population size (p);
   b) Maximum number of evaluations (n);
   c) Initial guess for α, β, γ and ϵ (optional);
   d) Termination criteria for the algorithm's convergence;
2. Given the chosen parameters, the algorithm either randomly selects the starting points for the weights or a initial guess is provided given prior knowledge of the system.
3. A first simulation is run using the starting point. At the end of the simulation, the outputs $Q_{\text{ov}_{\text{total}}}$ and ξ are stored.
4. Each individual in the population changes the weights by randomly varying one or more weights from the starting point, restarting the simulation with the same period duration.
5. At the end of every individual run, the output is stored and compared to previous solutions. The genetic algorithm chooses individuals from the current population with the best solutions to be parents and selects them to create children for the next iteration. Depending on the implementation used for the GA, the algorithm utilises different features during the evolution of the optimisation, such as mutations or information crossover.
6. Step 5 is repeated n times or if a stop criteria is selected, the algorithm determines in each step if the criteria is met and stops the optimisation.
7. The final solution is a pareto-front with a set of solutions for the weights. This means that the final result is not necessarily a single optimal output, since it is a multi-objective optimisation, the solution could be the best for a given objective but worse for the other. Therefore, the algorithm proposes a set of solutions to visualise the possibilities and compromises between the outputs.

An important contribution of this research is to integrate the sensitivity analysis with the GA optimisation. The goal is to use the information gathered through the sensitivity analysis to have prior knowledge of the behaviour of the system, identifying regions where the performance of the controller is adequate and, thereby, narrowing the search space where the Genetic Algorithm is applied. Morris Screening showed that ϵ, for example, does not have a considerable impact on the results, therefore, it increases the efficiency of the algorithm if ϵ is fixed and removed from the optimisation as a decision variable. Furthermore, the grid and random search showed that α should be restricted to a lower value compared to β and γ, while the lower and upper limits for β, γ could be narrowed to $(20, 200)$, for example.

Therefore, the Genetic Algorithm is studied for different scenarios to evaluate the contribution of the sensitivity analysis integrated with the GA optimisation. Three simulations are performed: (1) Simulation 1 is an optimisation of the weights of VMPC without using any prior knowledge of the sensitivity analysis and using a termination criterion with tolerance equal to 10^{-8}; (2) Simulation 2 increases the tolerance to 10^{-1}; (3) Simulation 3 uses the prior knowledge provided by SA, while keeping the tolerance equal

to 10^{-1}. The scenarios were simulated between 24$^{\text{th}}$ of March to 24$^{\text{th}}$ of April, as it showed a higher incidence of overflow events, and a summary is shown in Table 7.9.

Table 7.9: GA Simulations.

	Period	Tolerance value	Use of SA
Simulation 1	24$^{\text{th}}$ of March to 24$^{\text{th}}$ of April	10^{-8}	False
Simulation 2	24$^{\text{th}}$ of March to 24$^{\text{th}}$ of April	10^{-1}	False
Simulation 3	24$^{\text{th}}$ of March to 24$^{\text{th}}$ of April	10^{-1}	True

The GA algorithm is simulated in the UDS with the Parallel+Series SU configuration. The parameters for optimisation are: population size $p = 35$, maximum number of evaluations eval $= 3000$. For the simulation using SA results, the value of ϵ is fixed at 153, while an initial guess of the weights is set to $\alpha, \beta, \gamma = (10, 100, 100)$. Furthermore, the lower and upper bounds for the optimised variables are $(\alpha, \beta, \gamma, \epsilon) \in \{(0.01, 1000), (0.01, 1000), (0.01, 1000), (0.01, 1000)\}$ for non-restricted simulations and $(\alpha, \beta, \gamma) \in \{(20, 25), (20, 200), (0.01, 200)\}$ for the simulation using the SA.

The first important aspect evaluated is the pareto-front, which indicates the trade-offs between Q_{ov_total} and ξ across the simulations. Figure 7.18 shows that as the value of ξ increases, $Q_{\text{ov}_{\text{total}}}$ decreases. Simulation 2 stands out for achieving the lowest ξ ($\xi < 27\,\text{L/s}$) but at the cost of a higher overflow ($Q_{ov_total} > 130\,\text{ML}$). Simulations 1 and 3 dominate in the low-overflow region ($Q_{ov_total} \approx 126 - 127.5\,\text{ML}$), with Simulation 3 slightly outperforming Simulation 1 by providing lower error values for the lowest overflow level. For applications requiring a balance between overflow and error, solutions near $Q_{ov_total} = 126.5 - 127\,\text{ML}$ offer optimal trade-offs, where all simulations overlap. The choice of weights depends on whether minimising overflow, error, or achieving balance is the main goal.

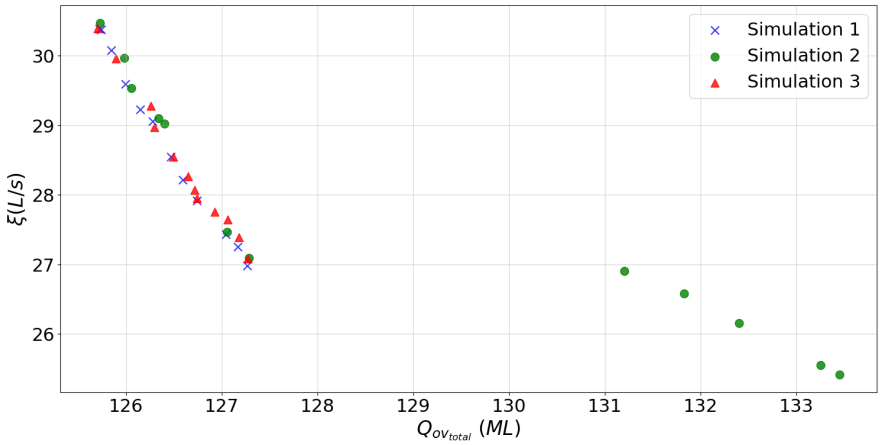

Figure 7.18: Pareto-front for all simulations.

Another important analysis is the convergence of the method and the computational effort to reach convergence. The computation time of the optimisation is important because, in many applications, the number of Storage Units is quite large, demanding a longer time for the calculations of the optimal weights. Therefore, reducing the time required to run the GA optimisation is desired. A metric commonly used

to assess the convergence and diversity of solutions in a multi-objective optimisation is the hypervolume [130], which quantifies the volume of the objective space that is "dominated" by the solutions on the Pareto front, with respect to a specified reference point. A higher hypervolume value indicates that the solutions are closer to the optimal front and well distributed, covering a larger portion of the feasible objective space. Moreover, the absolute value of the hypervolume itself is less meaningful than changes in hypervolume over generations. By comparing hypervolume values across generations, the convergence of the algorithm towards the Pareto front is analysed, and an increase in hypervolume across generations suggests improvement in the solutions' optimality and diversity, while stabilisation of the hypervolume indicates convergence. The results of the simulations are shown in Figures 7.19a, 7.19b and 7.19c.

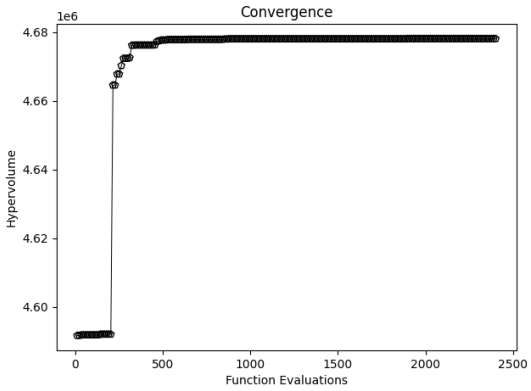

(a) Hypervolume for Simulation 1.

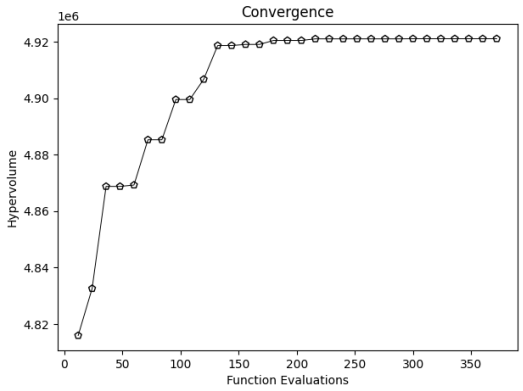

(b) Hypervolume for Simulation 2.

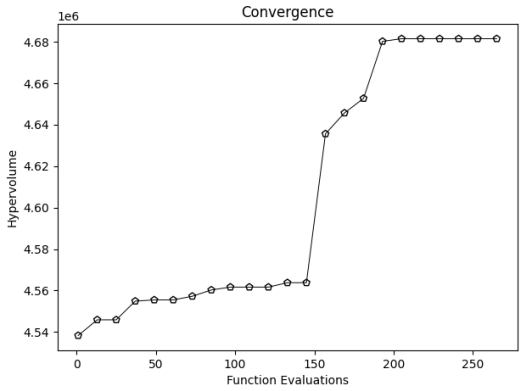

(c) Hypervolume for Simulation 3.

Figure 7.19: Hypervolume for all simulations.

Observing the hypervolume graphs, clearly Simulation 1 presents the slowest convergence speed with 2372 evaluations, which is obvious due to the reduced tolerance compared to the other simulations. Simulation 3 presented the fastest convergence, with around 265 evaluations compared to 372 evaluations from Simulation 2, although Simulation 2 shows a higher hypervolume, indicating a better trade-off in the pareto-front. This becomes clearer when observing the pareto-front in Figure 7.18, where Simulation 2 showed the lowest ξ at the cost of higher $Q_{\mathrm{ov}_{\mathrm{total}}}$. Overall, the best trade-off between the results achieved by the optimisation and the computational effort is Simulation 3, which showed a great pareto-front while also reducing the effort due to the use of the sensitivity analysis.

The final step in this analysis is to determine the weights and compare them to the simulation without using MPC. It is considered a hypothetical scenario where the most important objective is minimising the overflow at all costs. The weights are chosen from Simulation 3, where the optimal weights for the smallest $Q_{\text{ov}_{\text{total}}}$ are α, β, γ, $\epsilon = (6.9, 56.5, 106.4, 153.0)$. The analysis is carried out for the same 1 year period from Table 7.8 and the results are shown in Table 7.10.

Table 7.10: Results for optimised weights α, β, γ, $\epsilon = (6.9, 56.5, 106.4, 153.0)$.

Metric	Description	Static control	With VMPC
Q_{ov_1}	Overflow at CSO 1 in ML	94.5	101.3
Q_{ov_2}	Overflow at CSO 2 in ML	62.8	73.8
Q_{ov_3}	Overflow at CSO 3 in ML	430.1	331.2
$Q_{\text{ov}_{\text{total}}}$	Total overflow in ML	587.4	506.3
ξ	Inflow error in L/s	32.3	29.7
ξ_{rain}	Inflow error during WWF in L/s	0.06	8.95
$Q_{\text{wwtp}_{\text{total}}}$	Volume arriving at WWTP in ML	2764.9	2846.9

The optimal weights led to a 14% reduction in overflow, although ξ_{rain} remains higher than in the system without MPC control. This is expected, as VMPC uses the full capacity of the WWTP to minimise overflow. By applying insights from the sensitivity analysis, the computational cost of the GA optimisation was reduced while still identifying an effective weight configuration that improved the performance of the UDS. The combined use of SA and GA is a valuable method for tuning any MPC, or more generally any RTC system that requires parameter calibration. The method can be adapted to different objectives, such as reducing the total pollutant load reaching the WWTP or the total load discharged during CSO events.

7.3.8 Computation Time Analysis

The computation time analysis is an important evaluation of the performance and feasibility of application for MPC systems. Since MPC relies on solving an optimisation problem at each control step, the prediction horizon, system complexity, and control loop frequency are important to determine the computational burden and if the controller is applicable in real situations. Therefore, analysing computation times examines whether the MPC can operate within the constraints of real-time systems, particularly when dealing with complex systems such as the UDS.

For this analysis, the computation time for each individual control loop is calculated over a period of simulation, and both the mean and standard deviation of the combined computation times are recorded. The goal is to repeat the analysis, but increase the number of Storage Units and the prediction horizon to evaluate the impact on the computation time. Here, the number of SUs is varied from 1 unit to 5 units, while the prediction horizon is considered from 4 to 12 steps. The simulation was performed over a 6-month period with 4 minutes between control loops, which provided a total of 65520 recorded points. The hardware setup is: 2 x DELL Intel Xeon Silver 4310 2.1 GHz, 12C/24T, 10.4 GT/s, 18 MB Cache,

Turbo, HT (120 W) DDR4-2666, with 4 x DELL 16 GB RDIMM, 3.200 MT/s, Dual Rank. The results are shown in Table 7.11.

As expected, the computation time increases with the number of SUs for any given prediction horizon, which is due to the addition of more decision variables and constraints to the optimisation problem. Figure 7.20 evidences another interesting aspect of the results, showing that the variability (standard deviation) grows with both number of SUs and prediction horizon, presumably because it increases the difficulty of solving the optimisation problem consistently.

Table 7.11: Comparison of Computation Times in seconds (Mean ± Std) for VMPC.

N	1 SU	2 SUs	3 SUs	4 SUs	5 SUs
4.0	0.028 ± 0.007	0.045 ± 0.012	0.059 ± 0.011	0.076 ± 0.015	0.084 ± 0.024
5.0	0.031 ± 0.007	0.052 ± 0.016	0.071 ± 0.015	0.086 ± 0.014	0.164 ± 0.026
6.0	0.035 ± 0.008	0.059 ± 0.013	0.083 ± 0.017	0.161 ± 0.027	0.183 ± 0.028
7.0	0.039 ± 0.013	0.068 ± 0.016	0.096 ± 0.024	0.179 ± 0.030	0.216 ± 0.041
8.0	0.042 ± 0.011	0.075 ± 0.017	0.149 ± 0.021	0.194 ± 0.033	0.234 ± 0.039
9.0	0.046 ± 0.012	0.083 ± 0.016	0.173 ± 0.025	0.216 ± 0.037	0.271 ± 0.045
10.0	0.049 ± 0.012	0.090 ± 0.024	0.189 ± 0.028	0.242 ± 0.041	0.295 ± 0.053
11.0	0.057 ± 0.018	0.095 ± 0.021	0.199 ± 0.031	0.266 ± 0.045	0.318 ± 0.054
12.0	0.063 ± 0.020	0.157 ± 0.024	0.216 ± 0.033	0.292 ± 0.057	0.339 ± 0.046

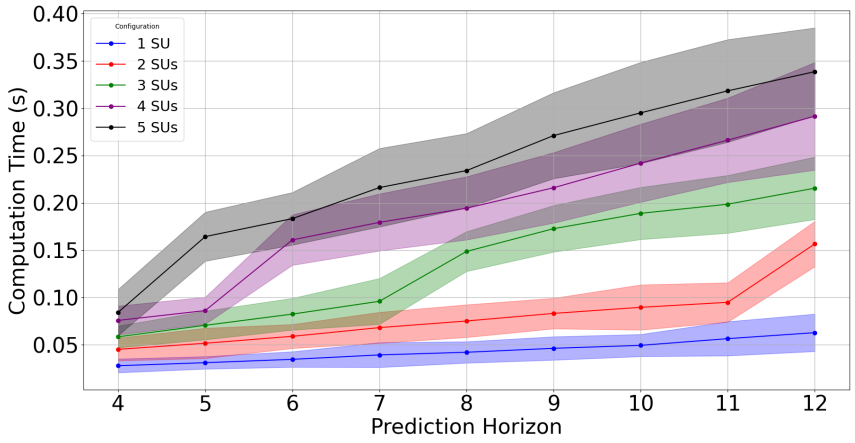

Figure 7.20: Comparison of Computation Times for VMPC - Line plot represents mean and shaded area the standard deviation.

Besides this, the graph shows that for simpler configurations, the computation time increases steadily across horizons, however, for complex configurations, the growth rate accelerates significantly as the prediction horizon increases. In all simulated scenarios, the computation time remains well below the duration of the 4-minute control loop, demonstrating that VMPC is capable of handling systems with even larger configurations and extended prediction horizons.

When running the Genetic Algorithm, the convergence time is highly influenced by the control loop computation time. Consequently, an important aspect of this analysis is to assess whether the GA opti-

misation process to determine the weights of MPC is feasible in a reasonable time frame. Although the GA is executed offline rather than in real-time, certain configurations of the UDS and the prediction horizon may result in prohibitively large convergence times, making the optimisation impractical. Therefore, it is necessary to minimise the number of steps required for GA convergence. Incorporating sensitivity analysis into the GA method might reduce convergence steps, although there is only empiric evidence.

7.3.9 Water Quality Analysis

The implementation of VMPC does not implicitly consider the pollution load (or concentration), which is only feasible using more complex models with water quality information. The advantage of considering pollution loads in MPC is that it allows the controller, when an overflow is unavoidable, to manipulate the network in a way that sends heavily contaminated wastewater to the treatment plant while, at the same time, discharges cleaner waste into the environment.

This behaviour is analysed in the Parallel+Series SU configuration from Section 6.2.2 considering two different scenarios where the total volume entering the wastewater network is exactly the same, however the COD load is different between scenarios. This can be visualised by considering that in Scenario 2, part of the dry weather originally considered coming from households in Storage Unit 3 also comes from industrial activity, as illustrated by Figure 7.21.

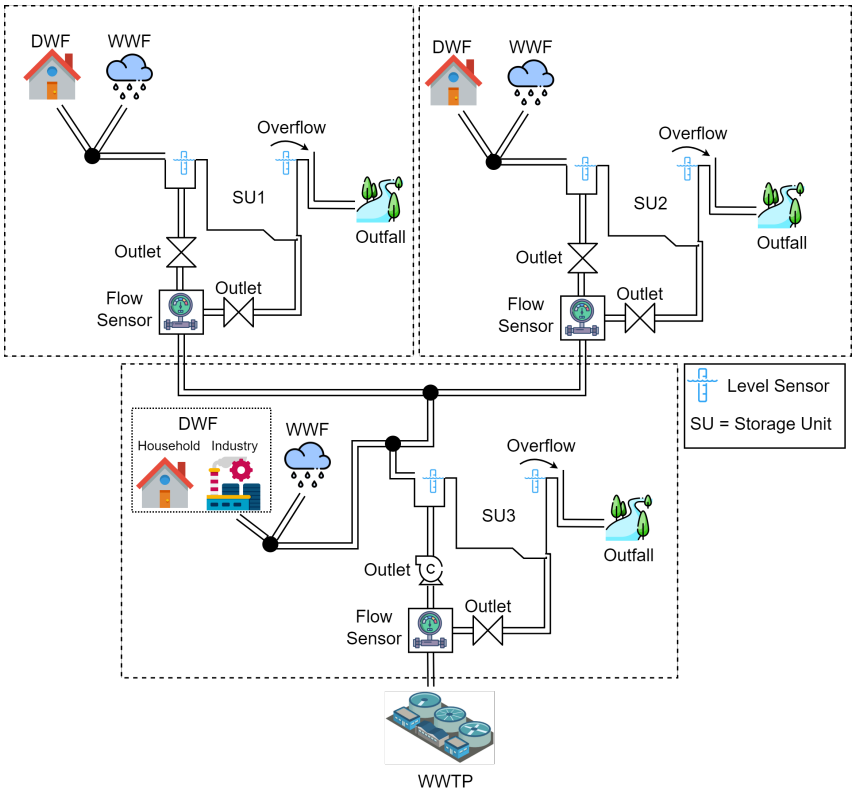

Figure 7.21: Urban Drainage System with and without industrial activity in SU3.

In summary, the second scenario has two sewage sources for SU3: a Source 1 coming from industrial activity with an average daily COD load of 1500 mg/L and a Source 2 generated by households with an average daily COD load of 600 mg/L, as shown in Figure 7.22 for a week period.

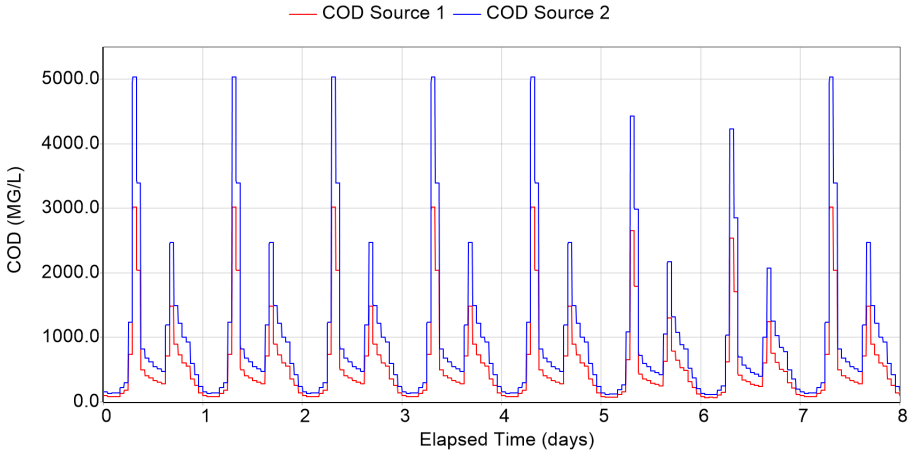

Figure 7.22: COD Load from two different sources.

Both scenarios are simulated to compare the amount of overflow in terms of volume (m^3) and the total mass of COD in the overflow (kg). The simulation period is one month, from 24^{th} of March to 24^{th} of April, and the weights for both scenarios are the values resulting from the GA optimisation (α, β, γ, $\epsilon = (6.863, 56.512, 106.387, 153.0)$).

The results are shown in Table 7.12. The overflow during the period is, evidently, the same for both scenarios. This is expected since in both scenarios the exact same MPC is implemented and the total inflow (DWF + WWF) between the scenarios is exactly equal.

Table 7.12: Comparison of results for scenarios with and without industry.

Metric	Description	Scenario 1	Scenario 2
Q_{ov_1}	Overflow at SU1 in ML	32.1	32.1
Q_{ov_2}	Overflow at SU2 in ML	24.2	24.2
Q_{ov_3}	Overflow at SU3 in ML	69.4	69.4
$Q_{ov_{total}}$	Total overflow in ML	125.7	125.7
$m^{COD}_{ov_1}$	Overflow of COD at SU1 in kg	1729.3	1729.3
$m^{COD}_{ov_2}$	Overflow of COD at SU2 in kg	1500.6	1500.6
$m^{COD}_{ov_3}$	Overflow of COD at SU2 in kg	7814.2	14335.5
$m^{COD}_{ov_{total}}$	Total COD load overflow in kg	11044.2	17561.6

However, the overflow total mass of COD for SU3 in Scenario 2 is almost twice the amount of Scenario 1, which is a consequence of the industrial activity and the inability of VMPC to act to reduce load. In this research, it is hypothesised that the incorporation of load information into the optimisation process could enable the minimisation of pollutant loads. Therefore, the next section explores the hypothesis that by using the load/concentration of pollutants within MPC, it is feasible to reduce overflowing untreated

sewage into the environment and guarantee that concentrated sewage is being sent to the treatment plant.

8 Pollution-based Model Predictive Control

One of the main limitations of volume-based strategies is their lack of consideration of pollution. Although effective in reducing overflow volume, this approach does not account for the discharge of pollutant load, leaving the control system unaware of the environmental impact caused by the overflows. To address this, a more comprehensive strategy incorporates water quality, either as a pollutant concentration or total load, directly into the optimisation problem. By doing so, the controller can prioritise reducing the discharge of highly polluted water, potentially leading to significantly lower environmental harm than volume-based methods alone. Several approaches have been proposed to integrate water quality into MPC formulations. Among them, the work of [19] introduces a more complex pollution-based MPC as already summarised in Section 6.4.2, which serves as a starting point for the discussion presented in this chapter.

8.1 Non-linear Pollution-based Model Predictive Control

The Nonlinear Pollution-based Model Predictive Control (NPMPC) is a type of RTC strategy that integrates CSO load mitigation directly into an optimisation routine with additional objectives. Using the measured and estimated variables within each SU, NPMPC can predict the future behaviour of the system, identifying potential overflow events and how polluted they would be. To achieve this, the algorithm requires an internal model that links these variables, which includes the inflow (Q_{in}), the outflow (Q_{out}), the overflow (Q_{ov}), the volume (V) and the concentration (C).

This control algorithm scheme is illustrated in Figure 8.1. The NPMPC receives real-time feedback from the UDS through measurement devices, typically consisting of one or more level measurements from each SU. This information is used to determine the volume based on the shape of the unit, along with the outflow measurements obtained from the actuator. Besides, the concentration within the SU is estimated using available measurements and certain assumptions. The NPMPC presents two internal models to predict the behaviour of the system, one to predict the volume and the other to predict the concentration.

The pollutant load mass (m) represents the mass transported through the sewer network. By estimating m, it becomes possible to assess the sewage concentration, C, and consequently evaluate the overflow concentration. To estimate m, the mass balance law is first established:

$$m(k+1) = m(k) + m_{in}(k) - m_{out}(k) - m_{ov}(k) \tag{8.1}$$

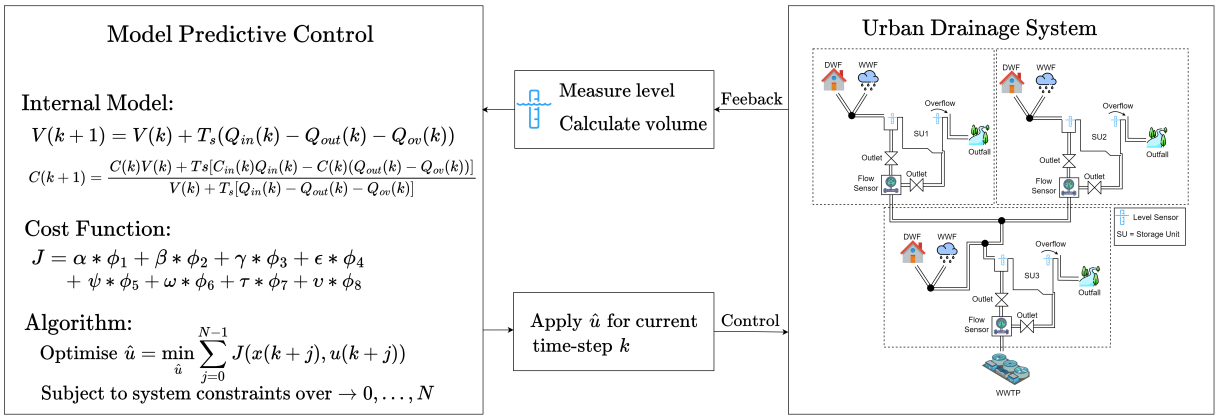

Figure 8.1: NPMPC scheme for Urban Drainage Systems.

where m_{in}, m_{out} and m_{ov} are the pollutant load mass inflow, outflow and overflow, respectively. Assuming that the concentration is C, the load is represented as $m(k) = C(k)V(k)$, resulting in Equation 8.1 converted to:

$$C(k+1)V(k+1) = C(k)V(k) + C_{in}(k)V_{in}(k) - C_{out}(k)V_{out}(k) - C_{ov}(k)V_{ov}(k) \tag{8.2}$$

where $C_{in}(k)$ denotes the concentration of sewage entering the SU, $C_{out}(k)$ the concentration of sewage exiting the SU, and $C_{ov}(k)$ the concentration associated with an overflow event. The variable $C(k)$ is from now on referred to as the concentration within the SU. It is important to note that $C_{out}(k) = C(k)$ and $C_{ov}(k) = C(k)$, as illustrated in Figure 8.2, since the concentration of sewage is assumed to be homogenous in the storage units.

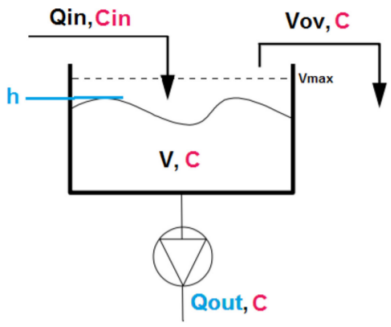

Figure 8.2: Storage Unit model for water quality [19].

Therefore, Equation 8.2 can be rewritten as:

$$C(k+1)V(k+1) = C(k)V(k) + C_{in}(k)V_{in}(k) - C(k)V_{out}(k) - C(k)V_{ov}(k) \tag{8.3}$$

Considering $V_{in}(k) = T_sQ_{in}(k)$, $V_{out}(k) = T_sQ_{out}(k)$, $V_{ov}(k) = T_sQ_{ov}(k)$ and using Equation 7.14 to substitute $V(k+1)$, the following equation for $C(k+1)$ is identified:

$$C(k+1) = \frac{C(k)V(k) + T_s[C_{in}(k)Q_{in}(k) - C(k)Q_{out}(k) - C(k)Q_{ov}(k)]}{V(k) + T_s[Q_{in}(k) - Q_{out}(k) - Q_{ov}(k)]} \tag{8.4}$$

By applying Equation 8.4, the concentration can be incorporated into the MPC formulation, transforming the Volume-based MPC into a Pollution-based MPC. However, from this formulation arise new challenges:

1. There is a necessity of measuring or estimating $C_{in}(k)$ to be able to calculate the concentration or load within the SU; This is extremely challenging, however, since $C_{in}(k)$ is divided into dry and wet weather components, a basic estimation is possible using an average sewage generation pattern for DWF and defining low concentration values for WWF.

2. The optimisation problem becomes non-linear when Equation 8.4 is used as part of the system's internal model, due to the presence of products between decision variables, such as the term $C(k)V(k)$. Although non-linear optimisation solvers are well-established, finding an optimal solution remains more complex and may not guarantee convergence to the global optimum. Furthermore, non-linear problems typically require more computational effort, which can pose challenges for applications with real-time constraints.

3. In addition, the estimation of concentration is subject to uncertainty, as it relies on several assumptions. To address this, NPMPC explicitly incorporates the uncertainty in $C(k)$ and includes its minimisation within the optimisation process to reduce potential estimation errors.

Therefore, in the next section NPMPC is proposed with the estimation of concentration and uncertainty. The first issue addressed is the estimation of $C_{\text{in}}(k)$.

8.1.1 Estimation of $C_{\text{in}}(k)$ and $C(k)$

Inflow into a SU can generally be classified into three main sources: (1) catchment inflow, denoted as $Q_{\text{incatchment}}$, which includes both surface runoff from precipitation and sewage generated by human activity; (2) cascade inflow, Qincascade, representing the outflow from an upstream SU entering a downstream unit; and (3) infiltration, $Q\text{in}_{\text{infiltration}}$, which is often a significant component that influences both volume and concentration. The total inflow is thus represented by the following equation:

$$Q_{\text{in}}(k) = Q_{\text{in}_{\text{cascade}}}(k) + Q_{\text{in}_{\text{catchment}}}(k) + Q_{\text{in}_{\text{infiltration}}}(k) \tag{8.5}$$

The inflow concentration can be derived by first considering that the total mass (m) entering the SU per unit time is the sum of the masses coming from all the sources, which can be written as:

$$m_{\text{in}}(k) = m_{\text{in}_{\text{cascade}}}(k) + m_{\text{in}_{\text{catchment}}}(k) + m_{\text{in}_{\text{infiltration}}}(k) \tag{8.6}$$

and by substituting $m(k) = Q(k)C(k)$, the result is:

$$C_{\text{in}}(k)Q_{\text{in}}(k) = Q_{\text{in}_{\text{cascade}}}(k)C_{\text{in}_{\text{cascade}}}(k) + Q_{\text{in}_{\text{catchment}}}(k)C_{\text{in}_{\text{catchment}}}(k) + Q_{\text{in}_{\text{infiltration}}}(k)C_{\text{in}_{\text{infiltration}}}(k) \tag{8.7}$$

where $C_{\text{in}_{\text{catchment}}}$ is the catchment's inflow concentration, $C_{\text{in}_{\text{cascade}}}$ is the concentration leaving the upstream SUs, when there are SUs in cascade and $C_{\text{in}_{\text{infiltration}}}$ is the concentration of infiltration. Finally,

rearranging Equation 8.7 and combining with Equation 8.5, the concentration of the inflow in a SU is defined:

$$C_{\text{in}}(k) = \frac{Q_{\text{in}_{\text{cascade}}}(k)C_{\text{in}_{\text{cascade}}}(k) + Q_{\text{in}_{\text{catchment}}}(k)C_{\text{in}_{\text{catchment}}}(k) + Q_{\text{in}_{\text{infiltration}}}(k)C_{\text{in}_{\text{infiltration}}}(k)}{Q_{\text{in}_{\text{cascade}}}(k) + Q_{\text{in}_{\text{catchment}}}(k) + Q_{\text{in}_{\text{infiltration}}}(k)} \tag{8.8}$$

The concentration of the infiltration $C_{\text{in}_{\text{infiltration}}}$ is not always known, but can be estimated depending on the source of the infiltration, for example, if the source is groundwater, it will have a low concentration of NH_4 and COD, but a fair amount of TSS. The value of $Q_{\text{in}_{\text{cascade}}}$ is a measured actuator information, which is equal to Q_{out} from the upstream SU delayed by the time it takes for the outflow to reach the source. Furthermore, the catchment's inflow $Q_{\text{in}_{\text{catchment}}}$ is calculated using Equation 7.13 combined with Equation 8.5, however the concentration $C_{\text{in}_{\text{catchment}}}$ is not known. The solution is to estimate considering that the catchment flow is the combination of DWF and WWF,

$$Q_{\text{in}_{\text{catchment}}}(k) = Q_{\text{DW}}(k) + Q_{\text{WW}}(k) \tag{8.9}$$

Using the total mass relationship, $C_{\text{in}_{\text{catchment}}}$ can be calculated as follows:

$$C_{\text{in}_{\text{catchment}}}(k) = \frac{Q_{\text{DW}}(k)C_{\text{DW}}(k) + Q_{\text{WW}}(k)C_{\text{WW}}(k)}{Q_{\text{DW}}(k) + Q_{\text{WW}}(k)} \tag{8.10}$$

Moreover, research ([74, 131–134]) shows that it is feasible to connect human daily habits with how much domestic wastewater is produced and at what time of the day, creating a pattern of these habits. Those patterns could be used to find an average daily Q_{DW} and C_{DW} to calculate $C_{\text{in}_{\text{catchment}}}$. Thus, the first step to estimate $C_{\text{in}_{\text{catchment}}}$ is to specify a generic pattern for DWF. More specifically, the pattern indicates how much volume of wastewater is generated and collected by a SU over a period of time, such as hourly, daily, monthly, yearly or even seasonal, and how much is the concentration for a given pollutant in this wastewater [135]. The amount of detail in the pattern depends on the availability of data from catchments, human activity, and measurements. For instance, in Figure 8.3 two typical normalised daily patterns, sampled hourly, represent the mean behaviour of a person over the course of the day in two different instances. In general, daily flow patterns become apparent with a high morning peak and a lower evening peak corresponding to getting-up and dinner [135].

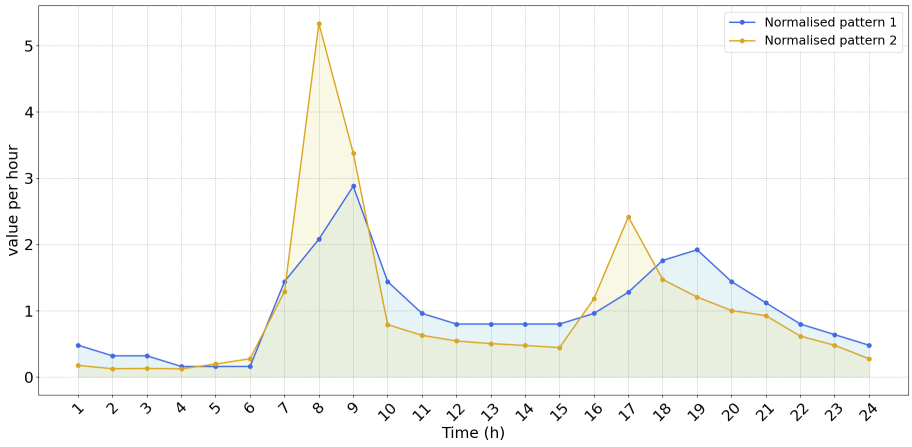

Figure 8.3: Two different normalized daily patterns sampled hourly.

A flow pattern profile can be created by multiplying a daily pattern with a wastewater generation flow rate per People Equivalent (PE) (Q_{perPE}) with the PE connected to the catchment of the SU [20]. The result is a dry weather flow $Q_{\text{DW}} = \text{Daily Pattern} \cdot Q_{\text{perPE}} \cdot \text{PE}$. For example, assuming a catchment with PE = 1000 and an average flow rate generation $Q_{\text{perPE}} = 0.202$ m^3/day, the resulting Q_{DW} profile using the normalised pattern 1 in Figure 8.4.

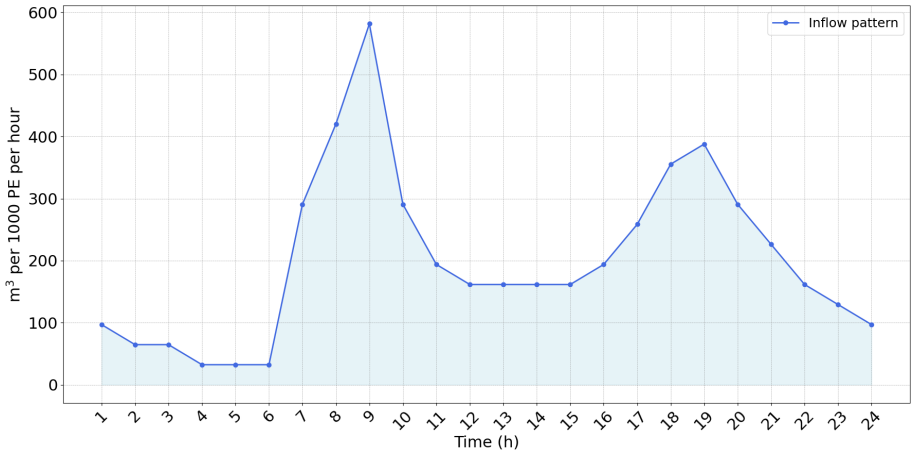

Figure 8.4: Flow daily pattern sampled hourly.

Pollutant concentration profiles (units of mg/L or g/m^3) are generated by multiplying the average concentration rates per People Equivalent (PE) (C_{perPE}), for a given pollutant with a daily pattern, resulting in a dry weather concentration profile, C_{DW}, defined as $C_{\text{DW}} = \text{Daily Pattern} \cdot C_{\text{perPE}}$. For instance, assuming a catchment with an average daily concentration rate generation $C_{\text{perPE}} = 42$ g/m^3 for a generic pollutant indicator, the resulting C_{DW} profile using the normalised pattern 2 in Figure 8.5.

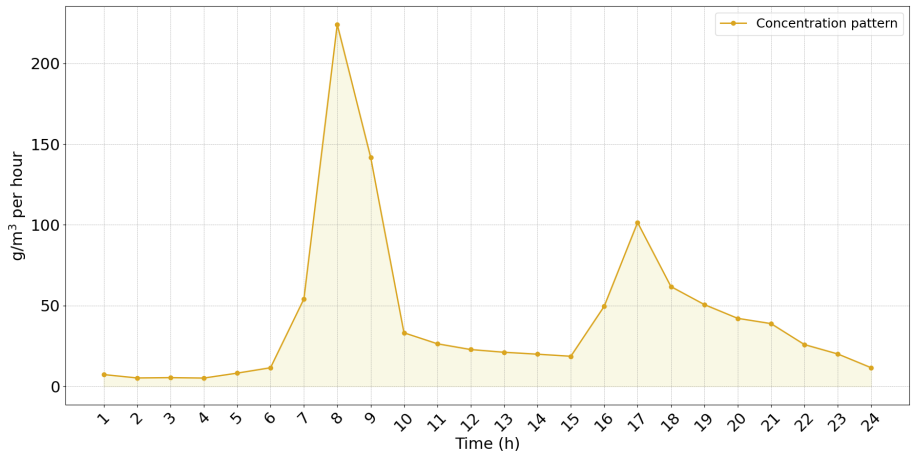

Figure 8.5: Concentration daily pattern sampled hourly.

The last step is to calculate the WWF both Q_{WW} and C_{WW}. The wet weather inflow, Q_{WW}, is determined through Equation 8.9, where Q_{DW} is derived from the daily pattern, and the concentration C_{WW} is typically fixed to low concentration values. By deriving Q_{DW} and C_{DW} using daily patterns,

the estimation of concentration entering the SU, C_{in}, can be calculated using Equation 8.8. Finally, the concentration within the SU can be estimated as below:

$$C(k) = \frac{C(k-1)V(k) + T_s C_{\text{in}}(k) Q_{\text{in}}(k)}{V(k) + T_s Q_{\text{in}}(k)} \tag{8.11}$$

In summary, the estimation of the concentration in a SU can be described as below:

1. **Identify the inflow sources:**
   - Catchment inflow: $Q_{\text{in}_{\text{catchment}}}(k)$;
   - Cascade inflow from upstream units: $Q_{\text{in}_{\text{cascade}}}(k)$;
   - Infiltration: $Q_{\text{in}_{\text{infiltration}}}(k)$.
2. **Measure cascade flow and calculate cascade concentration.**
3. **Measure or estimate infiltration flow and concentration.**
4. **Estimate catchment flow and concentration:**
   - Split catchment flow into dry weather flow (DWF) and wet weather flow (WWF) as in Equation 8.9:
     a) **Determine dry weather flow and concentration:**
        – Use daily patterns for flow and concentration:

$$Q_{\text{DW}}(k) = \text{Flow Daily Pattern} \times Q_{\text{perPE}} \times \text{PE},$$

$$C_{\text{DW}}(k) = \text{Pollutant Daily Pattern} \times C_{\text{perPE}}.$$

     b) **Determine wet weather flow and concentration:**
        – Compute $Q_{\text{WW}}(k)$ from rainfall data and, typically, low values for $C_{\text{WW}}(k)$.
   - Estimate the catchment inflow concentration using Equation 8.10
5. **Calculate the total inflow:** Using Equation 8.5 determine the inflow $Q_{\text{in}}(k)$.
6. **Apply the mass balance principle for concentration:** Using the flow and concentration of each source, calculate the total inflow concentration $C_{\text{in}}(k)$ using Equation 8.8.
7. **Estimate the concentration within the SU:** Apply the dynamic mass balance in Equation 8.11 to estimate $C(k)$.

Estimation allows incorporation of concentration into the optimisation problem using Equation 8.4 for the internal model for concentration in NPMPC combined with Equation 7.14 for the internal model of volume mass balance.

8.1.2 Uncertainty Estimation

By definition, a model is an abstraction of reality. Models rarely reflect real-world behaviour perfectly, as they simplify the system information, introducing uncertainty in the process, a concept discussed in detail by Warmink [136]. Uncertainty is defined by Walker as: "any deviation from the unachievable ideal of completely deterministic knowledge of the relevant system" [137]. Consequently, analysing uncertainty becomes essential to ensure robust decisions in any modelling process [138]. Warmink provides a structured framework for identifying and categorising uncertainties in environmental models [136], while [138] offers a review study of 14 methodologies to assess and characterise uncertainty. The main goal of this section is to identify the behaviour of an uncertain and unmeasured variable: the concentration of pollutants in network structures. This analysis defines an uncertainty propagation method for a simple quality model based on Equations 8.11 and 8.8.

The uncertainty propagation in urban rainfall-runoff models was first investigated by Lei in 1996 [139]. The study identified three main methods for uncertainty propagation: a sensitivity analysis, the Monte Carlo method, and the Taylor series. This research adopts the Taylor method because of its applicability to differentiable and non-linear models. Various assumptions have been made to simplify the calculations. In particular, the variables associated with concentration are considered uncorrelated. Thus, the Taylor series approximation for concentration in the SU can be expressed as:

$$\mathrm{Var}(C(k)) = U^2_{C(k)} = \sum_{i=1}^{6} \left(\frac{\partial C(k)}{\partial A_i} \right)^2 U^2_{A_i} \tag{8.12}$$

where:

$$A_1 = C(k-1),\ A_2 = V(k-1),\ A_3 = Q_{\mathrm{in}}(k),\ A_4 = C_{\mathrm{in}}(k-1),\ A_5 = Q_{\mathrm{out}}(k),\ A_6 = V_{\mathrm{ov}}(k-1)$$

After calculating the partial derivatives, the following assumptions were made:

1. $V(k-1)$ and $Q_{\mathrm{out}}(k)$ originate from measurements and are negligible compared to the uncertainties on $C_{\mathrm{in}}(k-1)$ and $C(k-1)$ which are unknown terms. So we can make the approximation that:

$$U_{V(k-1)} = U_{Q_{\mathrm{out}}(k)} = 0 \tag{8.13}$$

2. Similarly, $V_{\mathrm{ov}}(k-1)$ and $Q_{\mathrm{in}}(k)$ derived directly from prior measurements, are negligible:

$$U_{V_{\mathrm{ov}}(k-1)} = U_{Q_{\mathrm{in}}(k)} = 0 \tag{8.14}$$

3. Let U_{X} represent the standard deviation of X such that $\mathrm{Var(X)} = U^2_{\mathrm{X}}$. Then Equation 8.12 simplifies to:

$$U^2_{C(k)} = U^2_{C(k-1)}(\mathrm{X}(k-1))^2 + U^2_{C_{\mathrm{in}}(k-1)}(1-\mathrm{X}(k-1))^2 \tag{8.15}$$

where

$$\mathrm{X}(k-1) = \frac{V(k-1) - Q_{\mathrm{out}}(k)T_s - V_{\mathrm{ov}}(k)}{V(k)} = \frac{V(k) - Q_{\mathrm{in}}(k)T_s}{V(k)} = 1 - \frac{Q_{\mathrm{in}}(k)T_s}{V(k)} \tag{8.16}$$

The uncertainty propagation equation strongly depends on $\mathrm{X}(k-1)$. By conservation of volume and physical model constraints, it can be demonstrated that $0 \leq \mathrm{X}(k-1) \leq 1$. For probability distribution laws associated with SU load concentrations, uniform uncertainty (rectangular) and Gaussian laws (normal distribution) are commonly used. In this method, a uniform distribution is used as shown in Figure 8.6, as an unmeasured concentration value is equally probable within the interval [-a ; a].

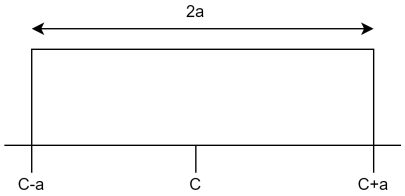

Figure 8.6: Uniform uncertainty law.

For uniform distributions, the standard deviation is $U_{\mathrm{X}} = \dfrac{a}{\sqrt{3}}$ and the variance is $\mathrm{Var}(\mathrm{X}) = \dfrac{a^2}{3}$. Using the first-order Taylor approximation and the same assumptions regarding flow uncertainty, the uncertainty propagation for the incoming load concentration can be expressed as follows:

$$U^2_{C_{\mathrm{in}}(k)} = U^2_{C_{\mathrm{DW}}(k)} \left(\frac{Q_{\mathrm{DW}}(k)}{Q_{\mathrm{in}}(k)} \right)^2 + U^2_{C_{\mathrm{WW}}(k)} \left(\frac{Q_{\mathrm{WW}}(k)}{Q_{\mathrm{in}}(k)} \right)^2 \tag{8.17}$$

For computational simplicity, the initial uncertainty of the concentration is approximated as equal to the uncertainty of the incoming concentration: $U_C(0) = U_{C_{\mathrm{in}}}(0)$. In summary, the proposed approach enables the calculation of the propagation of the concentration uncertainty in the SU combining Equations 8.15 and 8.17.

8.1.3 Optimisation Problem

The cost function for NPMPC integrates volume-related objectives with pollution aspects. The purpose of the controller is to predict both the volume and concentration of the overflow and to use both variables to make a decision regarding control actions. The manipulated variable does not change from VMPC, the optimal output is the outflow from the SUs. In summary, the objectives are separated as:

- Objective ϕ_1: Maintain volume **homogeneity** within each SU. The homogenisation of storage capacity in the network forces structures to fill and deplete in the same pattern.
- Objective ϕ_2: Minimise the error between the **reference inflow to the WWTP** and the sum of the outflow from all actuators upstream of the WWTP.
- Objective ϕ_3: Minimise **overflow** events.
- Objective ϕ_4: Defined to help reach feasibility when calculating the optimum output.
- Objective ϕ_5: Maintain mass **homogeneity** within each SU. The homogenisation of storage capacity in the network tries to keep the mass of pollutants within the network at similar levels.

- Objective ϕ_6: Minimise load **overflow** events. Normally, this objective has the highest priority in the optimisation to avoid as much load in the overflow as possible.

- Objective ϕ_7: Minimise the uncertainty estimation by adjusting the decision variables to achieve the lowest possible uncertainty.

- Objective ϕ_8: Maximise the load entering the WWTP.

Let the state and input vectors be defined as

$$\boldsymbol{x}(k) = \begin{bmatrix} \boldsymbol{V}(k) \\ \boldsymbol{Q}_{\text{ov}}(k) \\ \boldsymbol{C}(k) \\ \boldsymbol{\theta}(k) \\ \boldsymbol{U}(k) \\ \boldsymbol{Q}_{\text{in}}(k) \end{bmatrix}, \qquad \boldsymbol{u}(k) = \begin{bmatrix} \boldsymbol{Q}_{\text{out}}(k) \end{bmatrix}.$$

Considering N_t as the number of controlled SU, the vectors are defined as $\boldsymbol{V} \in \mathbb{R}^{N_t \times 1}$ (volume), $\boldsymbol{Q}_{\text{ov}} \in \mathbb{R}^{N_t \times 1}$ (overflow), $\boldsymbol{C} \in \mathbb{R}^{N_t \times 1}$ (concentration), $\boldsymbol{\theta} \in \mathbb{R}^{N_t \times 1}$ (slack variable), $\boldsymbol{U} \in \mathbb{R}^{N_t \times 1}$ (input variable), $\boldsymbol{Q}_{\text{in}} \in \mathbb{R}^{N_t \times 1}$ (inflow), and $\boldsymbol{Q}_{\text{out}} \in \mathbb{R}^{N_t \times 1}$ (outflow). The optimisation problem, with $\hat{\boldsymbol{u}}(k)$ denoting the optimal control output, is then formulated as:

$$\hat{u}(k) = \arg\min_{u} \sum_{j=0}^{N-1} J(x(k+j), u(k+j)) \tag{8.18a}$$

subject to

$$V^t(k+j+1) = V^t(k+j) + T_s\big(Q^t_{\text{in}}(k) - Q^t_{\text{out}}(k+j) - Q^t_{\text{ov}}(k+j)\big), \qquad t = 1, 2, ..., N_t \tag{8.18b}$$

$$Q^t_{in}(k+j) = Q^t_{catchment}(k+j) + \sum_{i \in N^*_{\text{in}}} Q^i_{out}(k+j), \qquad t = 1, 2, ..., N_t \tag{8.18c}$$

$$C^t(k+j+1) = \frac{C^t(k+j)V^t(k+j) + T_s\big[C^t_{\text{in}}(k)Q^t_{\text{in}}(k) - C^t(k+j)\big(Q^t_{\text{out}}(k+j) + Q^t_{\text{ov}}(k+j)\big)\big]}{V^t(k+j) + T_s\big[Q^t_{\text{in}}(k+j) - Q^t_{\text{out}}(k+j) - Q^t_{\text{ov}}(k+j)\big]}, \tag{8.18d}$$

$$t = 1, 2, ..., N_t$$

$$U^t_{C(k)} = \sqrt{{U^t_{C(k-1)}}^2 X^t(k-1)^2 + {U^t_{C_{\text{in}}(k-1)}}^2\big(1 - X^t(k-1)^2\big)}, \qquad t = 1, 2, ..., N_t \tag{8.18e}$$

$$0 \leq V^t(k+j) \leq V^t_{\max} + \theta^t(k+j), \qquad t = 1, 2, ..., N_t \tag{8.18f}$$

$$0 \leq Q^t_{\text{out}}(k+j) \leq Q^t_{\text{out}_{\max}}, \qquad t = 1, 2, ..., N_t \tag{8.18g}$$

$$0 \leq \sum_{i \in N^*_{\text{wwtp}}} Q^i_{\text{out}}(k+j) \leq Q^t_{\text{wwtp}_{\max}} \tag{8.18h}$$

$$Q^t_{\text{ov}}(k+j) \geq 0, \qquad t = 1, 2, ..., N_t \tag{8.18i}$$

$$C^t(k+j) \geq 0, \qquad t = 1, 2, ..., N_t \tag{8.18j}$$

$$\theta^t(k+j) \geq 0, \qquad t = 1, 2, ..., N_t \tag{8.18k}$$

$$U^t_{C(k)} \geq 0, \qquad t = 1, 2, ..., N_t \tag{8.18l}$$

where $V_{\max}$ is the maximum volume in a SU, $Q_{\text{out}_{\max}}$ is the maximum outflow from the actuator, $Q_{\text{wwtp}_{\max}}$ is the maximum inflow to the WWTP and N^*_{wwtp} are all SUs draining in the WWTP. Finally, U_C corresponds to the estimated concentration uncertainty within a SU and $U_{C_{in}}$ is the estimated concentration uncertainty of the inflow. Equations 8.18b and 8.18d are the model equality constraints that are used to calculate future predictions. The mass balance equations show that the inflow, Q_{in} and C_{in}, remains constant throughout the prediction horizon.

The cost function J is calculated by:

$$J(x(k), u(k)) = J(V(k), Q_{\text{out}}(k), Q_{\text{in}}(k), C(k), U(k), \theta(k), Q_{\text{out}}(k)) \tag{8.19}$$

$$= \alpha\phi_1(k) + \beta\phi_2(k) + \gamma\phi_3(k) + \epsilon\phi_4(k) + \psi\phi_5(k) + \omega\phi_6(k) + \tau\phi_7(k) + \upsilon\frac{1}{\phi_8(k)} \tag{8.20}$$

where $(\alpha, \beta, \gamma, \epsilon, \psi, \omega, \tau, \upsilon)$ are the weights for the objectives $(\phi_1, \phi_2, \phi_3, \phi_4, \phi_5, \phi_6, \phi_7, \phi_8)$, respectively. The objectives are defined as:

- ϕ_1, in Equation 8.21, is used to homogeneously store the volume within all SU structures in the sewage network.

$$\phi_1(k) = \sum_{i=1}^{N_t} \left(V^i(k) - \frac{V^i_{\max}}{\sum_{j=1}^{N} V^j_{\max}} \sum_{n=1}^{N_t} V^n(k) \right)^2 \tag{8.21}$$

  which N_t is the number of SUs in the network.

- ϕ_2, in Equation 8.22, keeps the flow toward the wastewater treatment plant close to the operating reference value defined by Q_{ref}.

$$\phi_2(k) = \sum_{j \in N_{up}} \left(Q^j_{\text{ref}}(k) - \sum_{i \in N^*_t} Q^i_{\text{out}}(k - d^{i,t}) \right)^2 \tag{8.22}$$

  where Q_{ref} is the reference flow for the i^{th} SU, which includes $Q_{\text{wwtp}_{\text{ref}}}$ as the inflow reference to the WWTP, Q_{out} is the outflow from each SU, $d_{i,t}$ represents the transport time of the i^{th} SU to the destination SU m, N^*_t are all SUs draining in the destination t and N_{up} are all SUs that have an upstream SU and the wastewater treatment plant.

- ϕ_3, in Equation 8.23, is used to minimise the overflow.

$$\phi_3(k) = \sum_{i=1}^{N_t} (Q^i_{\text{ov}}(k) - \text{NL})^2 \tag{8.23}$$

- ϕ_4, in Equation 8.24, is used to minimise the slack variable θ.

$$\phi_4(k) = \sum_{i=1}^{N_t} (\theta^i)^2 \tag{8.24}$$

- ϕ_5, in Equation 8.25, is used to homogeneously store the pollutant load within all SU structures

in the sewage network.

$$\phi_5(k) = \sum_{i=1}^{N_t} \left(C^i(k)V^i(k) - \frac{V^i_{\max}}{\sum_{j=1}^{N} V^j_{\max}} \sum_{n=1}^{N_t} C^n(k)V^n(k) \right)^2 \tag{8.25}$$

- ϕ_6, in Equation 8.26, is used to minimise the load overflow.

$$\phi_6(k) = \sum_{i=1}^{N_t} \left(C^i(k)Q^i_{\text{ov}}(k) \right)^2 \tag{8.26}$$

- ϕ_7, in Equation 8.27, is used to minimise the uncertainty value.

$$\phi_7(k) = \sum_{i=1}^{N_t} U^i(k)^2 \tag{8.27}$$

- ϕ_8, in Equation 8.28, is to force the maximum possible load to reach the WWTP.

$$\phi_8(k) = \left(\sum_{i \in N_t^*} C^i(k - d^{i,t})Q^i_{\text{out}}(k - d^{i,t}) \right)^2 \tag{8.28}$$

Since the objective is to maximise ϕ_8, it is used in the form $\frac{1}{\phi_8}$ in the cost function. Finally, the control loop's algorithm for NPMPC can summarised as below:

Control Algorithm

(a) Initialise $\boldsymbol{x}(k) = \boldsymbol{x}(0)$, where $\boldsymbol{x}(0) = \{\boldsymbol{V}(0), \boldsymbol{Q}_{\text{in}}(0), \boldsymbol{Q}_{\text{ov}}(0), \boldsymbol{C}(0), \boldsymbol{U}(0), \boldsymbol{\theta}(0)\}$ and $\boldsymbol{u}(0) = \boldsymbol{Q_{out}}(0)$ are the current state and input of the system;

(b) Estimate $\boldsymbol{Q}_{\text{in}}(k)$ using Equation 7.13, $\boldsymbol{C}_{\text{in}}(k)$ using Equation 8.8 and $\boldsymbol{C}(k)$ using Equation 8.11;

(c) Solve the optimisation problem as in Equation 8.18a and obtain the optimal control sequence $\hat{\boldsymbol{u}}(k)$;

(d) At time k, apply the first input $\boldsymbol{u}(k) = \boldsymbol{Q}_{\text{out}}(k)$ of the optimal control sequence to the UDS;

(e) Wait for next control loop $k = k + 1$;

(f) Measure $\boldsymbol{V}(k)$ and $\boldsymbol{Q}_{\text{out}}(k)$, calculate $\boldsymbol{Q}_{\text{ov}}(k)$ and return to Step (b).

8.1.4 Methodology Validation - Parallel + Series Configuration

In this section, the hypothesis is evaluated that NPMPC can improve the performance over VMPC regarding load minimisation. Therefore, in this section, the performance of NPMPC, where the weights were selected by trial and error and that uses $NH_4{}^+$ as the pollutant indicator in the control optimisation, is compared with the system with static control and with VMPC. The Parallel + Series configuration from Figure 6.15 is used for the evaluation, with the same parameters as presented in Section 7.3.5. The first scenario is an extension of the results obtained by VMPC shown in Table 7.10, including the load overflow of $NH_4{}^+$ in the analysis.

The results are shown in Table 8.1, where NPMPC displays a worse volume overflow performance, increasing the total overflow by 3% compared to VMPC, however NPMPC is slightly better at load reduction compared to VMPC by 1%. The results of the first scenario demonstrate only a slight improvement in the reduction of the pollutant load when using NPMPC compared to VMPC. This limited improvement can be attributed to the weights used in NPMPC formulation. In this case, the weights were determined through a trial-and-error approach, which does not guarantee an optimal behaviour of the UDS regarding the objectives. However, it already showed the potential of applying NPMPC to improve load management in the network.

Table 8.1: Results for weights $\alpha, \beta, \gamma, \epsilon, \psi, \omega, \tau, \upsilon = (64.6, 148.6, 91.0, 189.0, 28.0, 76.2, 28.3, 0.8)$.

Metric	Description	Static control	VMPC	NPMPC
Q_{ov_1}	Overflow at SU1 in ML	94.5	101.3	100.2
Q_{ov_2}	Overflow at SU2 in ML	62.8	73.8	63.9
Q_{ov_3}	Overflow at SU3 in ML	430.1	331.2	358.3
$Q_{\mathrm{ov}_{\mathrm{total}}}$	Total overflow in ML	587.4	506.3	522.4
ξ	Inflow error in L/s	32.3	29.9	30.2
$Q_{\mathrm{wwtp}_{\mathrm{total}}}$	Volume arriving at WWTP in ML	2764.9	2842.2	2830.7
$m^{\mathrm{NH_4}}_{\mathrm{ov}_1}$	Overflow of NH_4 at SU1 in kg	461.0	663.8	561.4
$m^{\mathrm{NH_4}}_{\mathrm{ov}_2}$	Overflow of NH_4 at SU2 in kg	298.0	554.1	330.6
$m^{\mathrm{NH_4}}_{\mathrm{ov}_3}$	Overflow of NH_4 at SU3 in kg	5399.1	3515.4	3794.8
$m^{\mathrm{NH_4}}_{\mathrm{ov}_{\mathrm{total}}}$	Total NH_4 load overflow in kg	6158.1	4733.4	4686.8
$m^{\mathrm{NH_4}}_{\mathrm{wwtp}_{\mathrm{total}}}$	Load of NH_4 arriving at WWTP in kg	93427.6	95045.3	95083.6

The lack of a methodology for weight selection highlights the need for a sensitivity analysis of NPMPC's weights. Therefore, in the following section, a detailed sensitivity analysis of the weighting factors will be conducted to better understand their influence on the objectives. For NPMPC, an additional output variable is analysed, the total load overflowed during rain events of $NH_4{}^+$, $m^{\mathrm{NH_4}}_{\mathrm{ov}_{\mathrm{total}}}$.

8.1.5 Weight Sensitivity Analysis

The sensitivity analysis for NPMPC uses the same framework presented in Section 7.3.6, which described GSA using Grid and Random Search algorithms and LSA with the Morris detection method. The NPMPC is composed by 8 weights (α, β, γ, ϵ, ψ, ω, τ, υ), which makes the analysis more challenging. However, by using the Morris Screening it is possible to identify the most relevant weights and restrict the global analysis for the most important variables. Therefore, NPMPC is evaluated using the Morris screening, where the outputs analysed are $m^{\mathrm{NH_4}}_{\mathrm{OV_{total}}}$ and ξ, and the inputs are α, β, γ, ϵ, ψ, ω, τ and υ.

Local Sensitivity Analysis - Morris Screening

The Morris screening analyses the impact of input parameters on model outputs by varying one factor at a time across a defined range. For NPMPC, the inputs are the weights for each objective function, which results in $k = 8$. The number of trajectories for this simulation is $r = 75$ with a $\Delta = 1$, which leads to a total number of simulation runs of $N_m = r(k + 1) = 75 * (8 + 1) = 675$. The analysis is realized on the Parallel + Series configuration and the period for the simulation is March 24 to April 10.

The result from the Morris Screening is shown in Figure 8.7. Two weights stand out for the most impact on the outputs: (1) weight ψ, which is used for minimising the mass homogeneity (ϕ_5), and (2) weight ω, which is used to minimise the overflow load (ϕ_6). In addition, the weight υ, which corresponds to maximising the load into the WWTP (ϕ_8), also shows a relevant impact for both outputs. An interesting result is that the weight for the minimisation of uncertainty, τ, does not impact the outputs in any meaningful way, mostly due to low uncertainties in this scenario. The relationship between the variance and the mean of the weights is characterised by $\sigma \gg \mu$, which indicates a non-linear interaction between the inputs and the outputs.

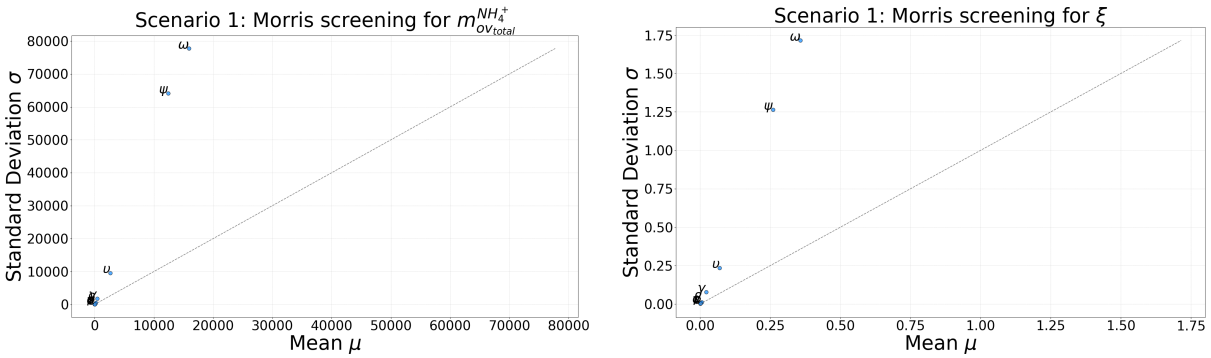

(a) Morris screening for the output $m^{\mathrm{NH_4}}_{\mathrm{OV_{total}}}$.

(b) Morris screening for the output ξ.

Figure 8.7: Morris screening for NPMPC.

The Morris screening provided insights to potentially reduce the complexity of the Grid and Random Search analysis, mainly by determining which variables have the higher impact over the outputs. Given the challenge of visualizing the global analysis with eight input parameters, the screening identified five weights as having minimal influence, corresponding to α, β, γ, ϵ, and τ.

Global Sensitivity Analysis - Grid Search

To refine the weight selection, the analysis began with the initial assignment of $\alpha = 33$, $\beta = 226$, $\gamma = 33$, $\epsilon = 189$, and $\tau = 84$, while focusing on the grid and random searches for the most impactful weights ψ, ω, and υ. Therefore, a series of targeted grid searches were conducted:

1. The initial weights were set as $\alpha = 33$, $\beta = 226$, $\gamma = 33$, $\epsilon = 189$, and $\tau = 84$, but several simulations were performed to determine the appropriate ranges for these variables.

2. The value of α varied across $(1, 33, 66)$, while β, γ, ϵ, and τ were kept constant at their initial values. For each configuration, a Grid Search is performed for $\psi, \omega, \upsilon \in [1, 50]$, with 9 equally spaced points for each variable, generating 729 points in total.

3. The process was repeated with β varying across $(1, 113, 226)$, with all other weights held constant.

4. The same approach was applied for γ, varying between $(1, 33, 66)$, ϵ was tested in the range $(98, 198)$, and τ was explored with the values $(42, 84)$.

This process is used to generate a set of graphs, which are visualized using similar 3D heatmaps from Section 7.3.6. In this case, the heatmaps represented ψ, ω, and υ along the x, y, and z axes, respectively, with a colour-bar illustrating the outputs $m^{\mathrm{NH_4}}_{\mathrm{ov_{total}}}$ or ξ. With this approach, a more manageable and focused exploration of the parameter space is ensured. In Figure 8.8, the grid search analysis for α varied across $(1, 33, 66)$ for the outputs $m^{\mathrm{NH_4}}_{\mathrm{ov_{total}}}$ and ξ is presented. The analysis for α shows an outcome similar to VMPC where α has a better performance for lower values ($\alpha < 30$).

The difference between the lowest output (when $\alpha = 1$) to the highest (when $\alpha = 66$) is around 2%, providing more evidence for the results of the Morris screening that α does not have a high impact. The values of ψ, ω, and υ show a different behaviour depending on their combination. Specifically, υ showed a better performance when $\upsilon < 20$, although the range is not very evident, while ω performed well for $\omega > 20$. In this case, ψ is not clear, although it indicates that an intermediate value could improve the outputs. The remaining Grid Search GSA graphs for β, γ, ϵ and τ are shown in Appendix A.2, while their overall observations can be summarised as:

- The value of β influenced the outputs positively, whereas ($\beta > 113$) improved the performance of the outputs. In this scenario, the lowest output value for $\beta = 1$ to $\beta = 226$ is reduced by around 3%, providing more evidence for the results in the Morris screening that β does not have a high impact on the output. The inputs ψ, ω, and υ demonstrated the same behaviour in this scenario for the values of β, where $\upsilon < 20$, while $\omega > 20$ performed well and ψ showed an improvement in intermediate values in some cases.

- The analysis for γ is not really conclusive, later the random search analysis is done specifically on γ to have a better estimation.

- The weight ϵ kept the same behaviour from VMPC, while for τ is also difficult to have a conclusion without more data.

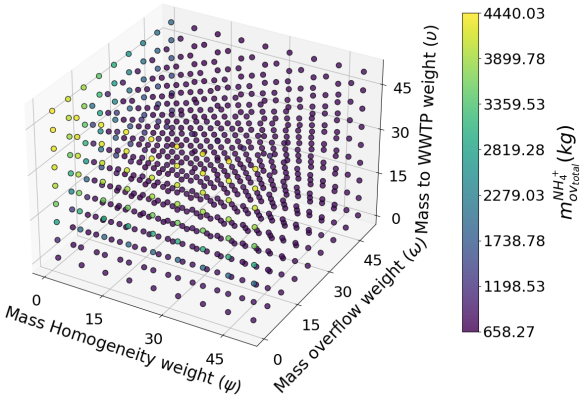

(a) $\alpha = 1$ for $m^{\mathrm{NH_4}}_{\mathrm{OV_{total}}}$.

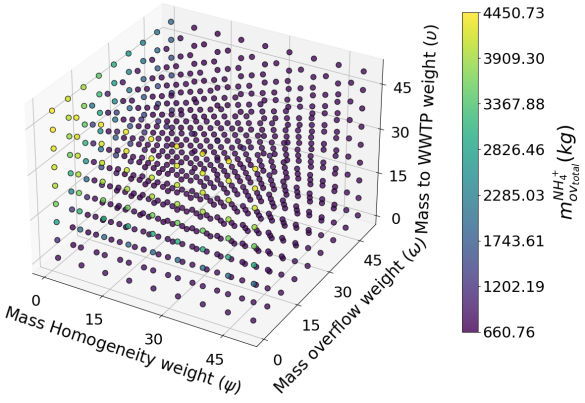

(b) $\alpha = 33$ for $m^{\mathrm{NH_4}}_{\mathrm{OV_{total}}}$.

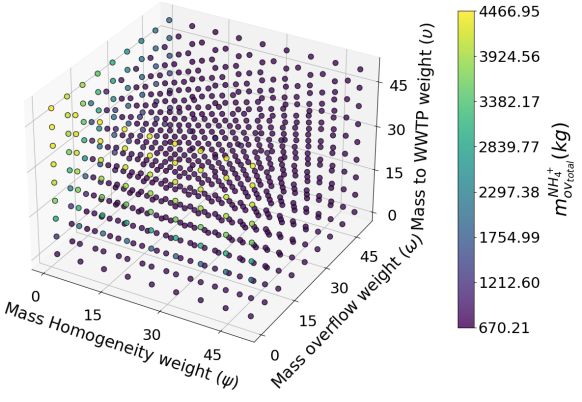

(c) $\alpha = 66$ for $m^{\mathrm{NH_4}}_{\mathrm{OV_{total}}}$.

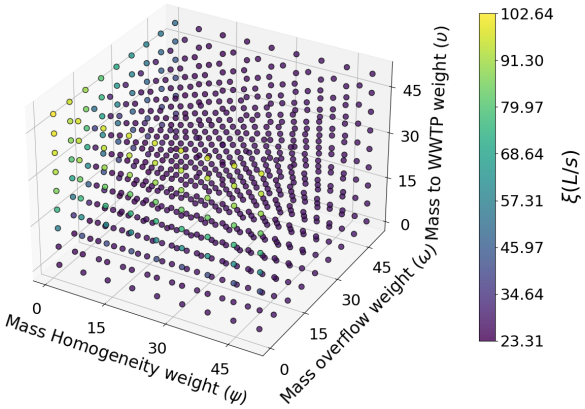

(d) $\alpha = 1$ for ξ.

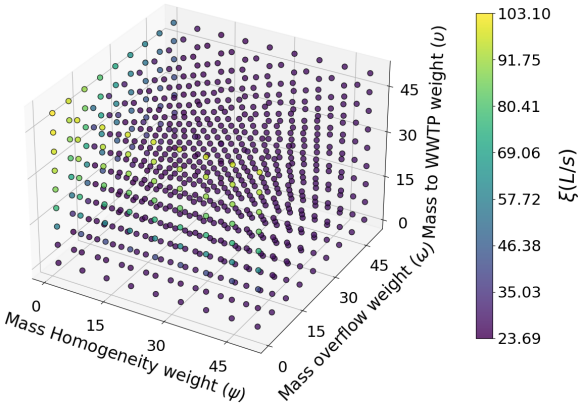

(e) $\alpha = 33$ for ξ.

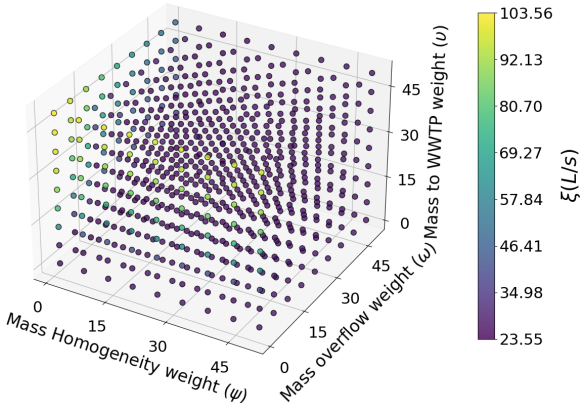

(f) $\alpha = 66$ for ξ.

Figure 8.8: Grid Search SA for the total load overflow in the system.

- Overall, the analysis revealed that α, β and ϵ, exhibit a notably lower influence on the outputs compared to ψ, ω, and υ, which demonstrated consistent behaviour across varying ranges of the other weights. Specifically, υ required lower values, as expected given the objective of maximisation, but the range is unclear, whereas ψ and ω performed optimally in regions exceeding 20, with ω in regions with higher values. Furthermore, α and γ produced better results at lower values (< 30), while β showed superior performance at higher values (> 113). In contrast, ϵ and τ had

negligible impact on the result, indicating minimal sensitivity to changes in these parameters.

To further analyse γ, τ, and υ, a random search was carried out to gain more knowledge of the ranges of these weights and identify the regions where they are most effective.

8.1.6 Global Sensitivity Analysis - Random Search

Given the assessment in the Grid Search, the following weights are fixed in the Random Search: $\alpha = 20$, $\beta = 200$, $\epsilon = 190$, $\psi = 30$, $\omega = 100$. Furthermore, the random search varies γ, τ and υ in the sets: $\gamma \in [1, 200]$, $\tau \in [1, 50]$ and $\upsilon \in [0.01, 5]$. The search is performed with 12 equally spaced points for each variable, generating 1728 points in total.

The results for $m^{\mathrm{NH_4}}_{\mathrm{ov_{total}}}$ and ξ are presented in Figure 8.9, where the random search analysis revealed that, for γ, intermediate values of around 100 are commonly observed in better-performing solutions. In contrast, the weight τ demonstrates a preference for lower to moderate values, particularly in the range of 10 to 30. Lastly, random search fails to provide more detailed knowledge on which region υ is most effective; however, intuitively, υ is strongly suited for very low values, because it is used to maximise load inflow to the WWTP. Therefore, keeping υ close to zero allows the system to prioritise other objectives while maximising the flow to the WWTP.

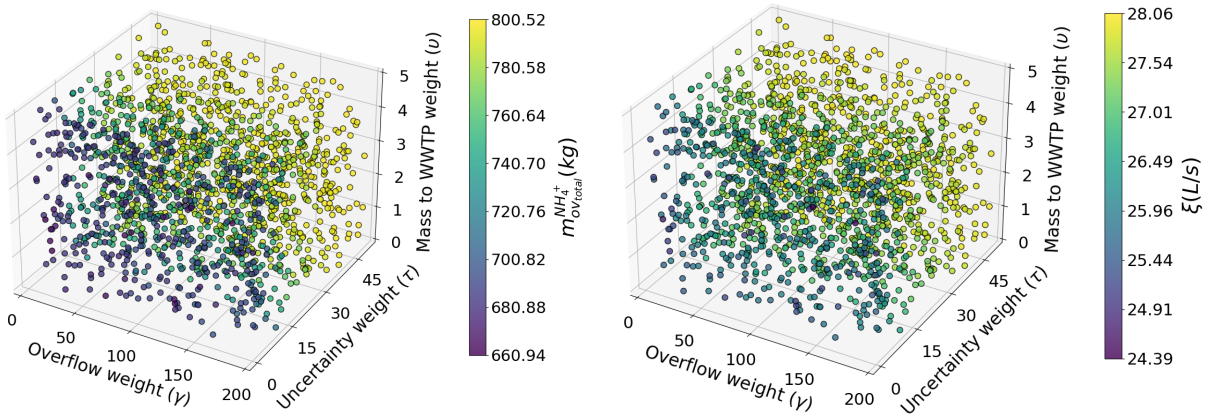

(a) Random Search for the output $m^{\mathrm{NH_4}}_{\mathrm{ov_{total}}}$.

(b) Random Search for the output ξ.

Figure 8.9: Random Search for NPMPC.

The final assessment for the Sensitivity Analysis is:

- Volume homogeneity weight: $\alpha < 30$
- Inflow error to the WWTP weight: $\beta \in [100, 250]$
- Volume overflow weight: $\gamma \in [50, 150]$
- Slack variable weight: $\epsilon = 190$
- Mass homogeneity weight: $\psi \in [10, 100]$

- Load overflow weight: $\omega \in [50, 250]$
- Uncertainty weight: $\tau \in [10, 30]$
- Load to the WWTP weight: $\upsilon < 0.5$

In the next section, the GA optimisation is executed to identify a Pareto front, effectively balancing the trade-offs between the weights and outputs for sub-optimal weight selection.

8.1.7 Genetic Algorithm for weight optimisation

As in the previous section, the GA is evaluated under different conditions to analyse the benefits of integrating SA into the optimisation process. Two simulation scenarios are conducted: (1) optimisation of the MPC weights without incorporating prior sensitivity analysis, and (2) optimisation that uses the insights gained from the SA. For Simulation 2, the initial guess for the weights is set as α, β, γ, ϵ, ψ, ω, τ, $\upsilon = (20, 150, 100, 190, 50, 100, 20, 0.1)$. Both scenarios adopt a convergence tolerance of 10^{-1} and are simulated over the period from March 24 to April 10, which is characterised by a higher frequency of overflow events. The genetic algorithm was configured with a population size of 20 and a maximum of 2000 iterations for each simulation.

The Pareto front for both simulations is shown in Figure 8.10, which, as for VMPC, demonstrates that Simulation 2 achieves lower values for both objectives compared to Simulation 1, indicating that it generally performs better. Simulation 1 presents more points in the Pareto-front, but it is not capable to reach the same potential weights Simulation 2 was able to identify. A possible explanation is that the algorithm got stuck at a local-optima and was unable to scan enough different regions. The use of SA significantly impacted the performance of the GA, most likely avoiding getting locked in the local-optima region as happened with Simulation 1. By narrowing the input ranges, the search space was reduced, enabling the algorithm to concentrate on a more relevant subset of solutions while preventing the exploration of less optimal regions.

The convergence of both scenarios is presented in Figure 8.11, where the hypervolume is used to measure the convergence. Both simulations achieve a similar hypervolume (2.10×10^7 against) compared to Simulation 2 ($2.05 \times 10^7 4$), where the slightly higher value for Simulation 1 might be explained by the better distribution and number of points at the Pareto-front.

Regarding the number of steps for convergence, Simulation 2 is higher (around 1200 evaluations) compared to Simulation 1 (around 1000 evaluations), showing a gradual improvement of the Pareto front as better solutions are found, albeit slowly.

The final step is repeat the simulation realized in Section 8.1.4 and assess the improvement given by the new set of weights. For this scenario, the decision was to choose the weights that provided the least amount of $m^{\mathrm{NH_4}}_{\mathrm{ov_{total}}}$ from the Pareto-front, resulting in α, β, γ, ϵ, ψ, ω, τ, υ = (11.2, 228.6, 90.7, 190.0, 10.0, 241.4, 19.4, 0.04). For the same 1-year period, the outcome is shown in Table 8.2.

In this instance, NPMPC with optimised weights improved the system's total load overflow by around 6% compared to VMPC, which is 253.4 kg of $NH_4{}^+$ less being discharged to the environment. Comparing to the scenario with static control, NPMPC improved the load overflow by 28%. For such a constrained

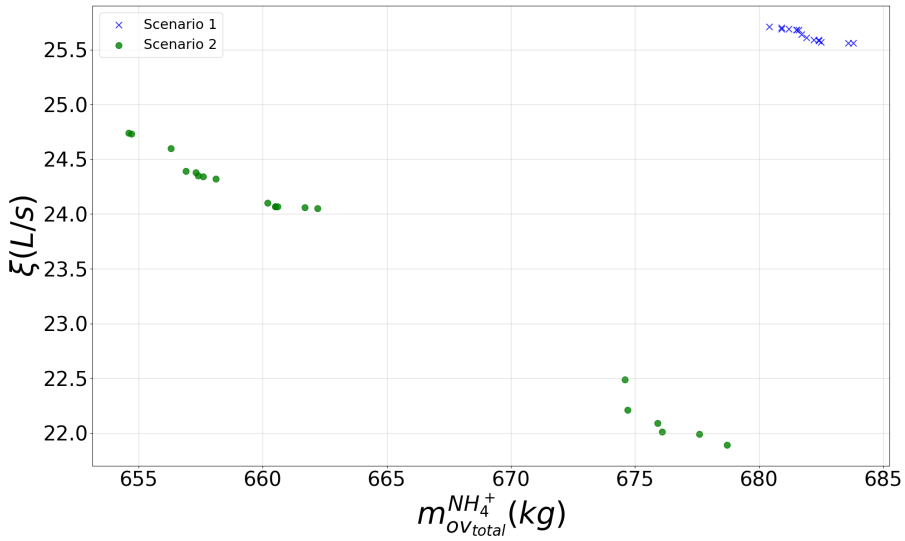

Figure 8.10: Pareto-front for all simulations.

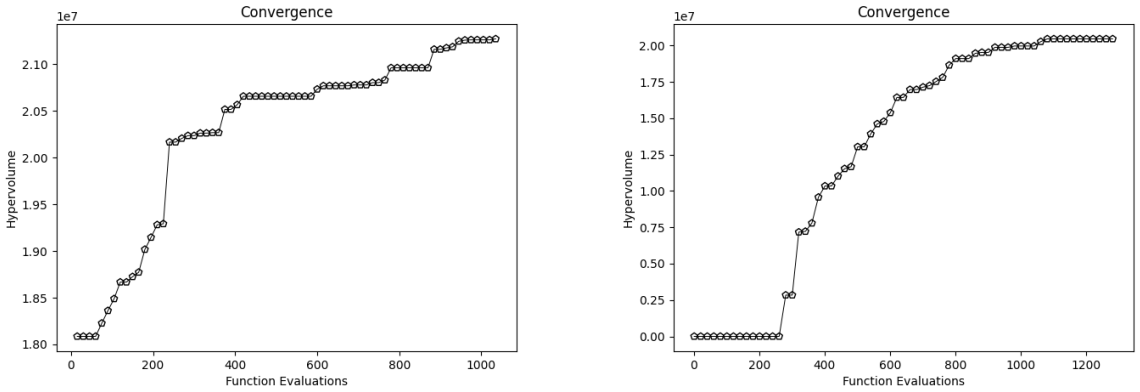

(a) Hypervolume for Simulation 1.

(b) Hypervolume for Simulation 2.

Figure 8.11: Hypervolume for all simulations.

network, the improvement is very good and indicates the potential for using a more detailed Pollution-based RTC system. The overall performance of the controller is evident, but many factors influence the utilisation of the method. The network used for the experiment is small and without much complexity compared to real applications, therefore the application of a non-linear method is feasible. In addition, NPMPC proposed has more complexity in the optimisation problem, especially with the non-linear equality constraint, which also escalates the computational burden of the method when the network has more SUs s. Hence, the computational cost of the method needs to be analysed to understand the applicability of the controller.

Table 8.2: Results for weights α, β, γ, ϵ, ψ, ω, τ, υ = (11.2, 228.6, 90.7, 190.0, 10.0, 241.4, 19.4, 0.04).

Metric	Description	Static control	VMPC	NPMPC
Q_{ov_1}	Overflow at SU1 in ML	94.5	101.3	101.3
Q_{ov_2}	Overflow at SU2 in ML	62.8	73.8	70.9
Q_{ov_3}	Overflow at SU3 in ML	430.1	331.2	334.5
$Q_{\text{ov}_{\text{total}}}$	Total overflow in ML	587.4	506.3	506.7
ξ	Inflow error in L/s	32.3	29.9	30.2
$Q_{\text{wwtp}_{\text{total}}}$	Volume arriving at WWTP in ML	2764.9	2842.2	2846.3
$m^{\text{NH}_4}_{\text{ov}_1}$	Overflow of NH_4 at SU1 in kg	461.0	663.8	641.8
$m^{\text{NH}_4}_{\text{ov}_2}$	Overflow of NH_4 at SU2 in kg	298.0	554.1	445.1
$m^{\text{NH}_4}_{\text{ov}_3}$	Overflow of NH_4 at SU3 in kg	5399.1	3515.4	3393.1
$m^{\text{NH}_4}_{\text{ov}_{\text{total}}}$	Total NH_4 load overflow in kg	6158.1	4733.4	4480.0
$m^{\text{NH}_4}_{\text{wwtp}_{\text{total}}}$	Load of NH_4 arriving at WWTP in kg	93427.6	95045.3	95338.6

8.1.8 Computation Time Analysis

The setup for the analysis is the same as for VMPC in Section 7.3.8, where the number of SUs is varied from 1 unit to 5 units, while the prediction horizon is considered from 4 to 12 steps, for a 6 months period with 4 minutes of control loop. The results for NPMPC are shown in Table 8.3. Compared to Table 7.11, for small prediction horizons ($N = 4, 5, 6$), VMPC and NPMPC have relatively similar mean computation times across all SU configurations, however as the prediction horizon increases ($N \geq 7$), NPMPC computation time increases more rapidly than VMPC for larger numbers of SUs. For 5 SUs s, the difference is more noticeable at higher prediction horizons.

Table 8.3: Comparison of Computation Times in seconds (Mean ± Std) for NPMPC.

N	1 SU	2 SUs	3 SUs	4 SUs	5 SUs
4.0	0.032 ± 0.009	0.064 ± 0.029	0.072 ± 0.051	0.101 ± 0.057	0.139 ± 0.079
5.0	0.036 ± 0.011	0.075 ± 0.031	0.093 ± 0.076	0.172 ± 0.167	0.300 ± 0.232
6.0	0.040 ± 0.012	0.087 ± 0.037	0.112 ± 0.107	0.276 ± 0.266	0.410 ± 0.500
7.0	0.043 ± 0.013	0.099 ± 0.044	0.185 ± 0.283	0.341 ± 0.748	0.499 ± 1.086
8.0	0.047 ± 0.017	0.111 ± 0.050	0.248 ± 0.472	0.411 ± 1.130	0.582 ± 1.399
9.0	0.050 ± 0.016	0.121 ± 0.056	0.281 ± 0.761	0.504 ± 1.593	0.698 ± 1.918
10.0	0.055 ± 0.019	0.199 ± 0.105	0.314 ± 0.986	0.508 ± 1.745	0.798 ± 2.447
11.0	0.064 ± 0.029	0.211 ± 0.112	0.328 ± 1.212	0.671 ± 2.529	1.077 ± 3.345
12.0	0.062 ± 0.022	0.145 ± 0.067	0.234 ± 0.869	0.827 ± 3.190	1.085 ± 3.438

For instance:

- At $N = 10$, VMPC takes 0.295s, while NPMPC takes 0.798s—about 2.7 times longer.
- At $N = 12$, VMPC takes 0.339s, while NPMPC takes 1.085s—about 3.2 times longer.

Furthermore, VMPC has a much more stable computation time, with smaller standard deviations across all configurations. In contrast, NPMPC shows significantly higher variation, especially for:

- 3 SUs and above, where the standard deviation grows rapidly. This is even more evident for 4 SUs and 5 SUs, where fluctuations are extreme at higher horizons.
- At $N = 10$, NPMPC has a standard deviation of 2.447s for 5 SUs, whereas VMPC has only 0.053s.
- At $N = 12$, NPMPC has 3.438s standard deviation for 5 SUs, meaning computation time can vary drastically between runs.

In Figure 8.12, the variability of the standard deviation is more evident as the shaded areas increase greatly with the number of SUs and the prediction horizon.

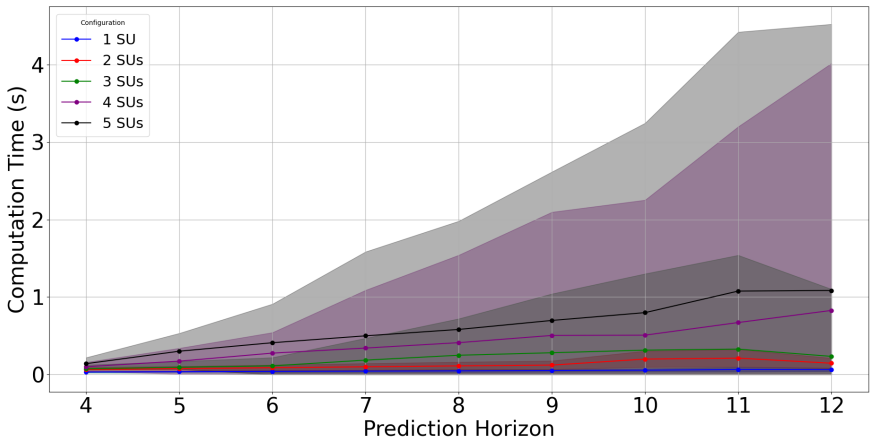

Figure 8.12: Comparison of Computation Times for NPMPC - Line plot represents mean and shaded area the standard deviation.

The significantly higher standard deviation observed in the computation times of NPMPC, especially at higher prediction horizons and units, is a consequence of the non-linear optimisation process and the additional complexity. Unlike VMPC, which follows a more predictable optimisation, NPMPC relies on an iterative solver that can often reach the maximum number of evaluations in a single control loop, especially if convergence is more difficult. When this happens, the solver terminates without fully converging, leading to longer computation times. This explains the large variability in standard deviation, as some iterations may finish quickly, while others take longer times depending on the solver's convergence behaviour. The instability suggests that NPMPC may require careful consideration for real-time applications, where the choice and tuning of the solver is important to reduce such problems.

Evidently, NPMPC presents a higher computational cost compared to VMPC. In the next section, a novel pollution-based method is presented to address such issues, where a linear alternative is proposed to be a trade-off between computational cost, although at the cost of a slightly higher load overflow reduction compared to NPMPC.

8.2 Pollution-weighted Model Predictive Control

The NPMPC showed promising results in reducing load discharges to the environment. However, the method presents some implementation challenges due to its non-linear nature. Thus, in this section, a novel pollution-based method is proposed that avoids non-linearities and, consequently, reduces the computational time for the optimisation of the UDS.

8.2.1 Description

The proposed method is called Pollution-weighted Model Predictive Control (PWMPC), which describes a linear pollution-based MPC capable of minimising load overflow while maintaining computational efforts similar to VMPC. The volume-based algorithm is modified to incorporate water quality by adjusting the weights of MPC in each control loop, estimating the concentration of a given pollutant within the SU and prioritising the units where the concentration is higher. More specifically, the concentration is used as a weighting factor for the overflow minimisation, thereby naming the method Pollution-weighted Model Predictive Control. The method is kept linear because the concentration is not considered a decision variable, just a weighting factor, named φ, for the objective, as shown in Figure 8.13 where the controller scheme is presented.

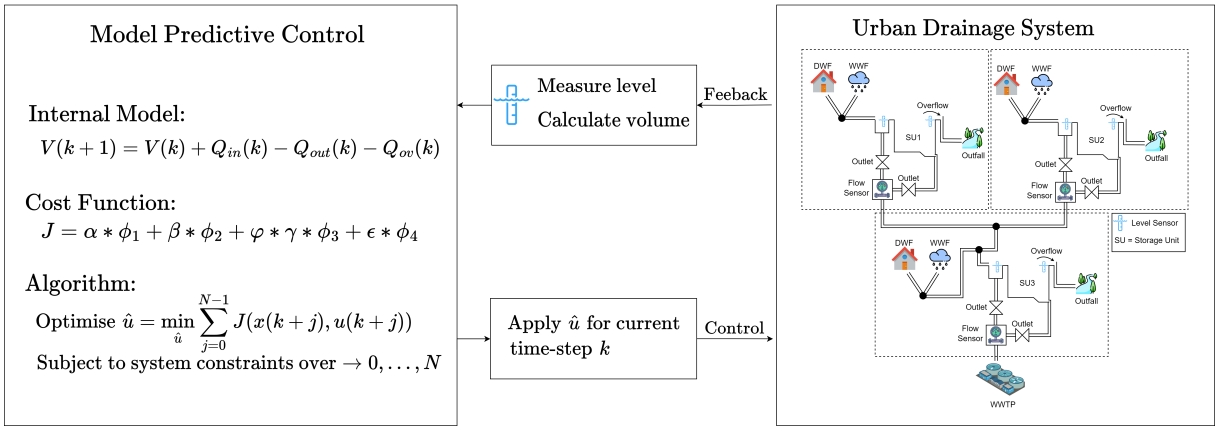

Figure 8.13: PWMPC scheme for Urban Drainage Systems.

In general, the main differences between PWMPC and NPMPC are:

- The internal model for the concentration in Equation 8.18d is removed from the constraints in the formulation. Therefore, PWMPC does not consider future predictions for the concentration, and the non-linear element in the constraints is removed.
- The objectives ϕ_5, ϕ_6, ϕ_7 and ϕ_8 are removed from the objective function, which reduces the complexity of the optimisation problem.

Nevertheless, the concentration C is still necessary for the optimisation as it is used in the weighting factor φ, which is defined as:

$$\varphi^i(k) = C^i(k) \tag{8.29}$$

where $i = (1, 2, ..., N_t)$ is a given SU. The concentration is considered constant through the prediction horizon. The weighting factor φ contains the concentration of a given pollutant for each Storage Unit, which in turn is added to the objective of minimising the overflow. φ is updated in each control loop using the new estimated concentration. Therefore, by multiplying φ in the objective, SUs with higher load will have more priority in reducing the overflow over lower pollutant load SUs. The optimisation problem is very similar to VMPC, it only adds φ, which requires the estimation of the concentration in each control loop. The estimation is done using the same principles from Section 8.1.1, resulting in the following:

$$C_{\text{in}}(k) = \frac{Q_{\text{in}_{\text{cascade}}}(k)C_{\text{in}_{\text{cascade}}}(k) + Q_{\text{in}_{\text{catchment}}}(k)C_{\text{in}_{\text{catchment}}}(k) + Q_{\text{in}_{\text{infiltration}}}(k)C_{\text{in}_{\text{infiltration}}}(k)}{Q_{\text{in}_{\text{cascade}}}(k) + Q_{\text{in}_{\text{catchment}}}(k) + Q_{\text{in}_{\text{infiltration}}}(k)} \tag{8.30}$$

and

$$C(k) = \frac{C(k-1)V(k) + T_s C_{\text{in}}(k)Q_{\text{in}}(k)}{V(k) + T_s Q_{\text{in}}(k)} \tag{8.31}$$

Hence, the optimisation problem from VMPC is redefined to add φ to the objective function.

8.2.2 Optimisation Problem

Given that the states and input are

$$\boldsymbol{x}(k) = \begin{bmatrix} \boldsymbol{V}(k) \\ \boldsymbol{Q}_{\text{ov}}(k) \\ \boldsymbol{\theta}(k) \\ \boldsymbol{Q}_{\text{in}}(k) \\ \boldsymbol{C}(k) \end{bmatrix}, \qquad \boldsymbol{u}(k) = \begin{bmatrix} \boldsymbol{Q}_{\text{out}}(k) \end{bmatrix},$$

the optimisation problem, where $\hat{\boldsymbol{u}}(k)$ is the optimal output, is defined as:

$$\hat{\boldsymbol{u}}(k) = \arg\min_{\boldsymbol{u}} \sum_{j=0}^{N-1} J(\boldsymbol{x}(k+j), \boldsymbol{u}(k+j)) \tag{8.32a}$$

subject to

$$V^t(k+j+1) = V^t(k+j) + T_s(Q^t_{\text{in}}(k) - Q^t_{\text{out}}(k+j) - Q^t_{\text{ov}}(k+j)), \qquad t = 1, 2, ..., N_t \tag{8.32b}$$

$$Q^t_{in}(k+j) = Q^t_{catchment}(k+j) + \sum_{i \in N^*_{\text{in}}} Q^i_{out}(k+j), \qquad t = 1, 2, ..., N_t \tag{8.32c}$$

$$0 \leq V^t(k+j) \leq V^t_{\max} + \theta^t(k+j), , \qquad t = 1, 2, ..., N_t \tag{8.32d}$$

$$0 \leq Q^t_{\text{out}}(k+j) \leq Q^t_{\text{out}_{\max}}, , \qquad t = 1, 2, ..., N_t \tag{8.32e}$$

$$0 \leq \sum_{i \in N^*_{\text{wwtp}}} Q^i_{\text{out}}(k+j) \leq Q_{\text{wwtp}_{\max}}, \tag{8.32f}$$

$$Q^t_{\text{ov}}(k+j) \geq 0, , \qquad t = 1, 2, ..., N_t \tag{8.32g}$$

$$\theta^t(k+j) \geq 0, \qquad t = 1, 2, ..., N_t \tag{8.32h}$$

where $V_{\max} \in \mathbb{R}^{N_t \times 1}$ represents the maximum volume for the SUs, $Q_{\text{out}_{\max}} \in \mathbb{R}^{N_t \times 1}$ is the maximum outflow of the SU's actuator, $j \in [0, N-1]$ is the future time instant, and N is the prediction horizon. Moreover, Equation 8.32c indicates the inflow of a SU in the context of the network's topology, where N^*_{in} indicates all SUs that are draining in a downstream SU. Furthermore, θ is a slack variable used to help guarantee the feasibility of optimisation, $Q_{\text{wwtp}_{\max}}$ is the maximum inflow to the WWTP and N^*_{wwtp} are all SUs draining in the WWTP.

The cost function J is calculated as follows:

$$J(x(k), u(k)) = J(V(k), Q_{\text{out}}(k), Q_{\text{in}}(k), \theta(k), Q_{\text{out}}(k)) \tag{8.33}$$

$$= \alpha\phi_1(k) + \beta\phi_2(k) + \gamma\phi_3(k) + \epsilon\phi_4(k) \tag{8.34}$$

where (α, β, γ, ϵ) are the weights for the objectives (ϕ_1, ϕ_2, ϕ_3, ϕ_4). In addition, φ is included as a weighting factor that contains the concentration of each SU for a given pollutant, which is added to ϕ_3. Summarising:

- ϕ_1, in Equation 7.17, is used to homogeneously store the volume within all SU structures in the sewage network.

$$\phi_1(k) = \sum_{i=1}^{N_t} \left(V^i(k) - \frac{V^i_{\max}}{\sum_{j=1}^{N} V^j_{\max}} \sum_{n=1}^{N_t} V^n(k) \right)^2 \tag{8.35}$$

  which N_t is the number of SUs in the network.

- ϕ_2, in Equation 7.18, keeps the flow toward the wastewater treatment plant close to the operating reference value defined by Q_{ref}.

$$\phi_2(k) = \sum_{j \in N_{up}} \left(Q^j_{\text{ref}}(k) - \sum_{i \in N^*_t} Q^i_{\text{out}}(k - d^{i,t}) \right)^2 \tag{8.36}$$

  where Q_{ref} is the reference flow for the i^{th} SU, which includes $Q_{\text{wwtp}_{\text{ref}}}$ as the inflow reference to the WWTP, Q_{out} is the outflow from each SU, $d_{i,t}$ represents the transport time of the i^{th} SU to the destination m, N^*_t are all SUs draining in the destination t and N_{up} are all SUs that have an upstream and the wastewater treatment plant.

- ϕ_3, in Equation 7.19, is used to minimise the overflow. For PWMPC, φ is included to transform this objective into a load overflow minimisation.

$$\phi_3(k) = \sum_{i=1}^{N_t} (\varphi^i(k) Q^i_{\text{ov}}(k) - \text{NL})^2 \tag{8.37}$$

- ϕ_4, in Equation 7.20, is used to minimise the slack variable θ.

$$\phi_4(k) = \sum_{i=1}^{N_t} (\theta^i)^2 \tag{8.38}$$

Finally, the control algorithm for PWMPC can be summarised as follows:

Control Algorithm

(a) Initialise $\boldsymbol{x}(k) = \boldsymbol{x}(0)$, where $\boldsymbol{x}(0) = \{\boldsymbol{V}(0), \boldsymbol{Q}_{\text{in}}(0), \boldsymbol{Q}_{\text{ov}}(0), \boldsymbol{\theta}(0)\}$ and $\boldsymbol{u}(0) = \boldsymbol{Q_{out}}(0)$ are the current state and input of the system;

(b) Estimate $\boldsymbol{Q}_{\text{in}}(k)$ using Equation 7.13, $\boldsymbol{C}_{\text{in}}(k)$ using Equation 8.30 and $\boldsymbol{C}(k)$ using Equation 8.31;

(c) Solve the optimisation problem as in Equation 8.32a and obtain the optimal control sequence $\hat{\boldsymbol{u}}(k)$;

(d) At time k, apply the first input $\boldsymbol{u}(k) = \boldsymbol{Q}_{\text{out}}(k)$ of the optimal control sequence to the UDS;

(e) Wait for next control loop $k = k + 1$;

(f) Measure $\boldsymbol{V}(k)$ and $\boldsymbol{Q}_{\text{out}}(k)$, calculate $\boldsymbol{Q}_{\text{ov}}(k)$ and return to Step (b).

8.2.3 Methodology Validation - Parallel + Series Configuration

The performance of PWMPC is evaluated in the Parallel + Series configuration. The controller is compared to the algorithms proposed previously in this chapter, aiming to prove that PWMPC can be better at load reduction than VMPC, while also comparing the performance with NPMPC. At first glance, it is expected that the new method proposed in this section performs worse than the non-linear MPC.

The scenario simulated is the same as in Section 8.1.4. The weights α, β, γ, $\epsilon = (33, 126, 38, 150)$ for PWMPC were chosen by trial and error. The results are shown in Table 8.4, which reveals that PWMPC is, in fact, slightly worse in volume overflow than VMPC with 1% more, however, the total load overflow decreased by 2% in PWMPC. Compared to NPMPC, PWMPC has around the same volume overflow reduction compared to the static control scenario; however, it performed around 4% worse when comparing the load overflow.

The results already indicate that PWMPC has potential to improve load management. The scenario can be improved using the GA methodology to find a more appropriate weight configuration. Therefore, the next sections present the sensitivity analysis, followed by the GA optimisation to understand the relationship between the weights with the error ξ and the total load overflow $m^{\text{P}}_{\text{ov}_{\text{total}}}$.

8.2.4 Weight Sensitivity Analysis

The sensitivity analysis for PWMPC uses the same framework presented in Section 7.3.6, which described GSA and LSA. Firstly, PWMPC is evaluated using the Morris screening, where the outputs analysed are $m^{\text{NH}_4^+}_{\text{ov}_{\text{total}}}$ and ξ and the inputs are α, β, γ, ϵ. The weighting factor φ is not a parameter, it results from the estimation of the concentration, thus, it is not an input for the sensitivity analysis.

Table 8.4: Results for weights α, β, γ, $\epsilon = (33, 126, 38, 150)$.

Metric	Description	Static control	VMPC	NPMPC	PWMPC
Q_{ov_1}	Overflow at SU1 in ML	94.5	101.3	101.3	111.4
Q_{ov_2}	Overflow at SU2 in ML	62.8	73.8	70.9	80.8
Q_{ov_3}	Overflow at SU3 in ML	430.1	331.2	334.5	315.7
$Q_{\mathrm{ov}_{\mathrm{total}}}$	Total overflow in ML	587.4	506.3	506.7	508.0
ξ	Inflow error in L/s	32.3	29.9	29.7	29.8
$Q_{\mathrm{wwtp}_{\mathrm{total}}}$	Volume arriving at WWTP in ML	2764.9	2842.2	2846.3	2845.2
$m^{\mathrm{NH}_4}_{\mathrm{ov}_1}$	Overflow of NH_4 at SU1 in kg	461.0	663.8	641.8	861.9
$m^{\mathrm{NH}_4}_{\mathrm{ov}_2}$	Overflow of NH_4 at SU2 in kg	298.0	554.1	445.1	715.7
$m^{\mathrm{NH}_4}_{\mathrm{ov}_3}$	Overflow of NH_4 at SU3 in kg	5399.1	3515.4	3393.1	3080.3
$m^{\mathrm{NH}_4}_{\mathrm{ov}_{\mathrm{total}}}$	Total NH_4 load overflow in kg	6158.1	4733.4	4480.0	4657.8
$m^{\mathrm{NH}_4}_{\mathrm{wwtp}_{\mathrm{total}}}$	Load of NH_4 arriving at WWTP in kg	93427.6	95045.3	95338.6	95139.4

Local Sensitivity Analysis - Morris Screening

The Morris screening for PWMPC is executed with a number of trajectories of $r = 600$ with a $\Delta = 1$, which leads to a total number of simulation runs of $N_m = r(k+1) = 600 * (4+1) = 3000$. The analysis is performed in the Parallel + Series configuration and the period for the simulation is March 24 to April 10. The result of the Morris Screening presented in Figure 8.14 shows that, very similarly to VMPC, the weight ϵ does not have a relevant impact on the outputs compared to α, β and γ. The influence of α and β is significant, demonstrating that the choice of these weights requires careful consideration. In addition, γ, which is the weight used to minimise overflow, also has some influence, being also an important factor in optimisation.

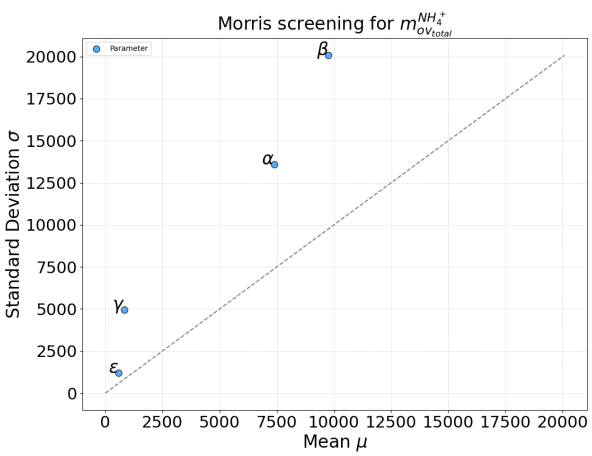

(a) Morris screening for the output $m^{p}_{\mathrm{ov}_{\mathrm{total}}}$.

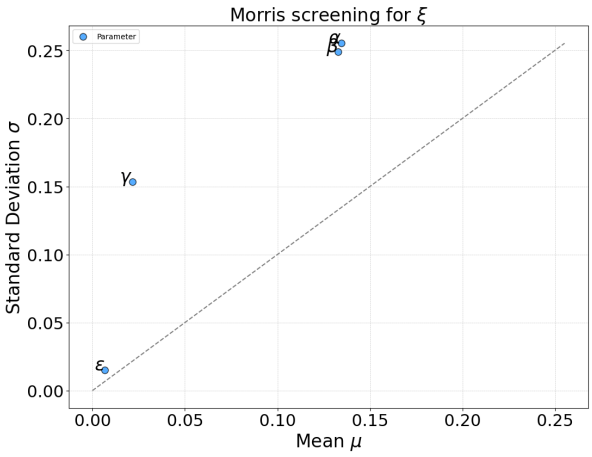

(b) Morris screening for the output ξ.

Figure 8.14: Morris screening for PWMPC.

The Morris screening provided important knowledge for the random search and grid analysis of PWMPC. It showed that the relationship between the weights and the outputs is almost the same as for VMPC, thus GSA can be shortened using the information collected for VMPC.

Global Sensitivity Analysis - Grid Search

Similarly to VMPC, the value of ϵ is fixed for the analysis, since it showed the least impact on the output. Then, GSA is divided to provide several 3-D grid heatmaps by fixing the value of ϵ, creating n 3-D grids, where n is the total number of values defined for ϵ. The analysis is conducted with the following setup: Six grids are defined, resulting in $n = 3$, with arbitrarily chosen values of $\epsilon = [3, 89, 150]$. The set Ω is defined as $\Omega = \{(\alpha, \beta, \gamma) \mid \alpha \in \Omega_1, \beta \in \Omega_2, \gamma \in \Omega_3\}$, where each Ω_i has the lower and upper bounds set to $(1, 200)$ for $i = (1, 2, 3)$. Each input in the grid includes 12 equally spaced points, creating three 3-D grid heatmaps with a size of $12 \times 12 \times 12 = 1728$ points. The colours in the heatmap represent one output, specifically $m_{\mathrm{ov}_{\mathrm{total}}}^{\mathrm{NH}_4^+}$ or ξ. This scenario is evaluated using inflow data presented in Figures 7.13 and 7.14.

The result for the Grid Search analysis is shown in Figure 8.15, which shows an a behaviour closely resembles that of VMPC, since, for PWMPC, the output is the total load in overflow events, which is correlated to the volume in overflow events. The parameter ϵ had minimal impact on the overall outputs, although slightly better results were observed with higher values, yielding an improvement of approximately 4% for the load and a negligible effect on ξ. In general, the algorithm performed better with $\alpha < 20$ and $\beta, \gamma \in [30, 200]$. The original choice for the weights in 8.2.3 are α, β, γ, $\epsilon = (33, 126, 38, 150)$, fall close to this range. However, further fine-tuning could potentially increase performance.

Global Sensitivity Analysis - Random Search

The Random Search GSA is realized to identify possible unexplored regions where the weights could also be applied. In this case, the analysis is only realized for $\epsilon = 150$. The weights are varied such that $\Omega = \{(\alpha, \beta, \gamma) \mid \alpha \in \Omega_1, \beta \in \Omega_2, \gamma \in \Omega_3\}$, where each Ω_i has lower and upper bounds set to $(1, 1000)$ for $i = (1, 2, 3)$. The upper bounds is elevated to 1000 to cover a higher range of values. Besides, the number of points for each input is increased to 15, therefore the grid has $15 \times 15 \times 15 = 3375$ points, randomly chosen from Ω_i.

The result is shown in Figure 8.16. The 3-D heatmap indicates no additional region is found by increasing the range of the weights to 1000, in fact, a similar trend to the Grid Search analysis is observed. GSA showed that increasing the homogeneity minimisation weight (α) leads to a deterioration of the output value, while the weights to minimise the inflow error to the WWTP (β) and the overflow (γ) have a wider favourable range. An interesting observation is that the Random Search obtained a worse minimum value for both outputs, which is explained by the randomness of the algorithm and the broader range of search. This grid search analysis was more focused in the region where the best solutions appeared, therefore, it reached a better minimum value.

The results obtained from the sensitivity analysis suggest that the control performance of PWMPC can be further improved. Therefore, the Genetic Algorithm for PWMPC is applied to identify a Pareto-front

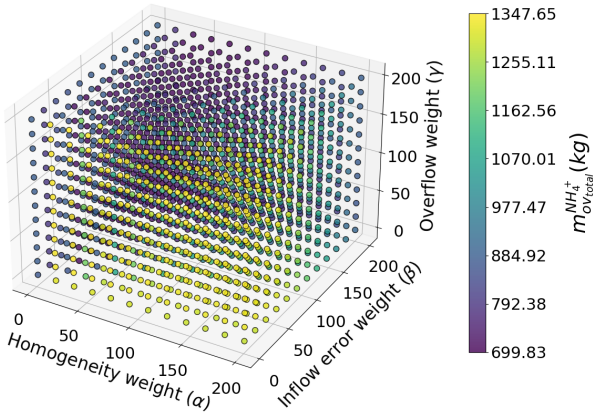

(a) Grid Search with $\epsilon = 1$ for the output $m^{\mathrm{NH}_4^+}_{\mathrm{ov_{total}}}$.

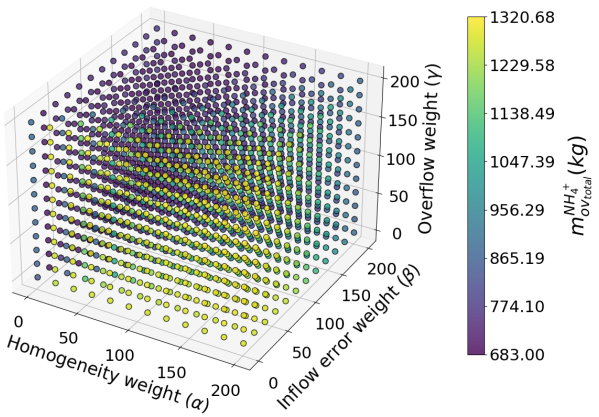

(b) Grid Search with $\epsilon = 89$ for the output $m^{\mathrm{NH}_4^+}_{\mathrm{ov_{total}}}$.

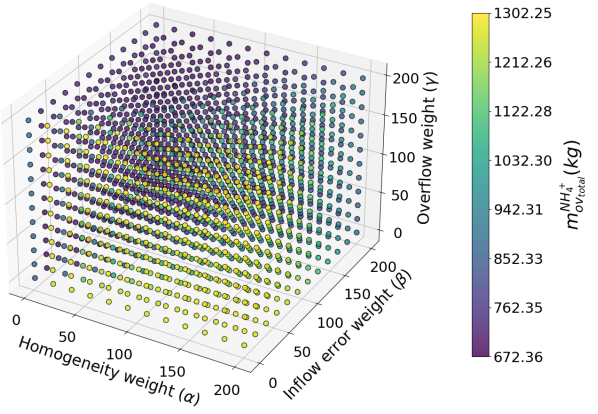

(c) Grid Search with $\epsilon = 150$ for the output $m^{\mathrm{NH}_4^+}_{\mathrm{ov_{total}}}$.

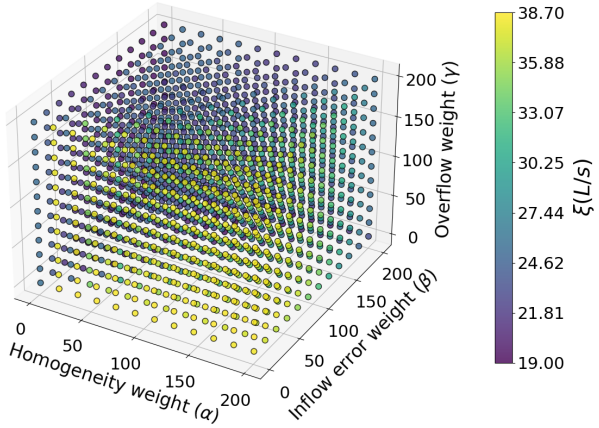

(d) Grid Search with $\epsilon = 1$ for the output ξ.

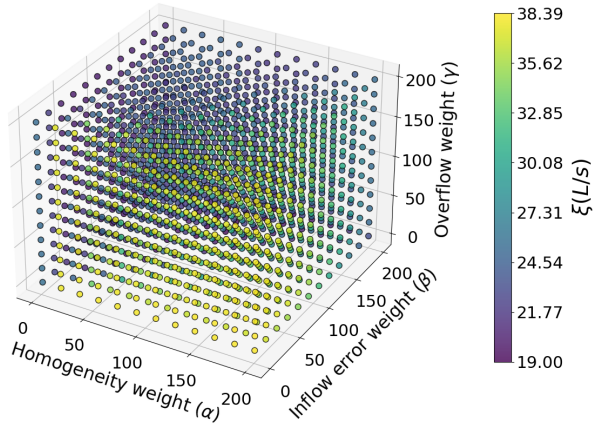

(e) Grid Search with $\epsilon = 89$ for the output ξ.

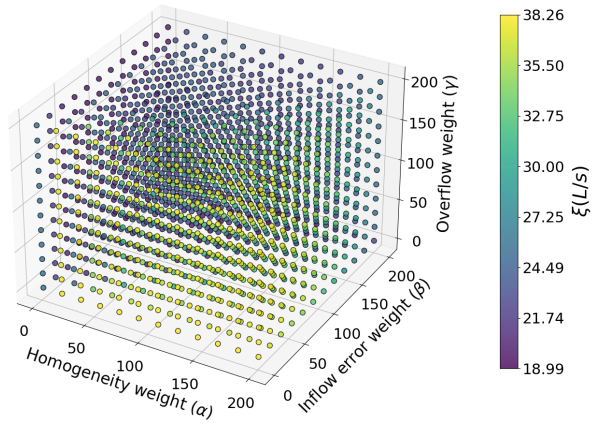

(f) Grid Search with $\epsilon = 150$ for the output ξ.

Figure 8.15: Grid Search Analysis for PWMPC.

for the outputs $m^{\mathrm{NH}_4^+}_{\mathrm{ov_{total}}}$ and ξ, using the result of the sensitivity analysis to increase the efficiency of the optimisation.

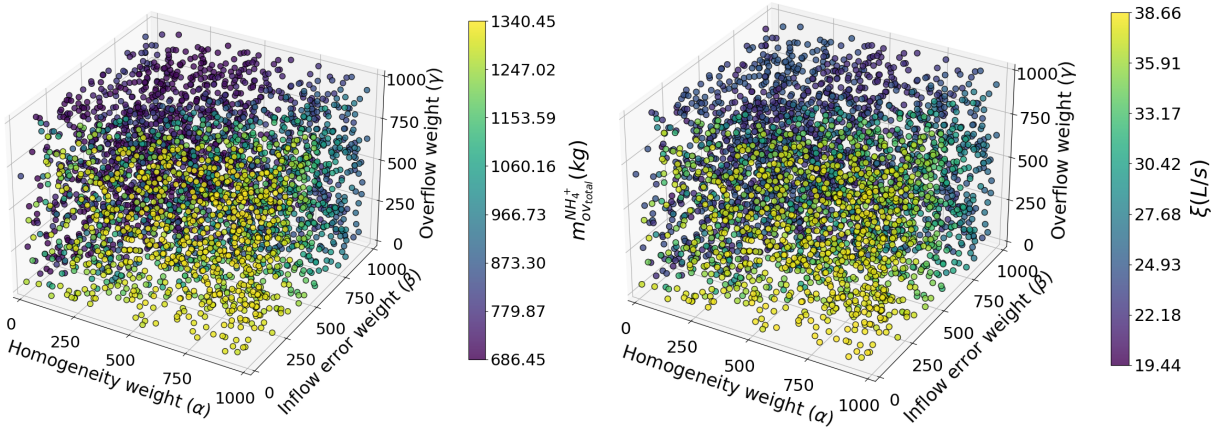

(a) Random Search for the output $m^{\mathrm{NH}_4^+}_{\mathrm{ov_{total}}}$. *(b)* Random Search for the output xi.

Figure 8.16: Random Search Analysis for PWMPC.

8.2.5 Genetic Algorithm for weight optimisation

Firstly, the weights are analysed in two different scenarios to evaluate the influence of incorporating sensitivity analysis into the GA optimisation process. Two simulations are conducted: (1) optimisation of the MPC weights without prior knowledge of the sensitivity analysis, (2) optimisation which incorporates prior knowledge from the SA, where $\alpha < 20$, $\beta, \gamma \in [30, 200]$ and $\epsilon = 190$. The initial guess for Simulation 2 is $\alpha, \beta, \gamma = (20, 150, 50)$. Both scenarios maintained a tolerance of 10^{-1}. These scenarios are simulated over the period from March 24 to April 24, a period characterised by a higher frequency of overflow events, and both optimisations had a population size of 20 with 2000 maximum iterations.

The Pareto-front for both simulation is displayed in Figure 8.17, which shows that Simulation 2 achieves lower values for both objectives compared to Simulation 1, indicating that it generally performs better.

Simulation 1 was able to find the best solution for ξ, but the total load in this situation is not suitable, as it is extremely high. In general, the use of SA significantly impacted the performance of the GA and the resulting Pareto front, as can be seen from the outcome of Simulation 2. By reducing the input ranges, the search space was narrowed, allowing the algorithm to focus on a more relevant subset of potential solutions and avoided exploring less optimal regions.

The convergence of both scenarios is presented in Figure 8.18, where the hypervolume is used to measure the convergence. Simulation 1 achieves a higher hypervolume (3.425×10^7 against) compared to Simulation 2 (3.08×10^7), which is due to the set of weights that had the lowest value of ξ, even though it produced a higher $m^{\mathrm{NH}_4^+}_{\mathrm{ov_{total}}}$.

The hypervolume graph indicates that the optimisation in Simulation 2 appears to have converged prematurely, likely due to the lower tolerance specified for that scenario. Additionally, the significantly higher number of evaluations in Simulation 2 suggests a more gradual progression of the Pareto front, reflecting the slow discovery of improved solutions over time.

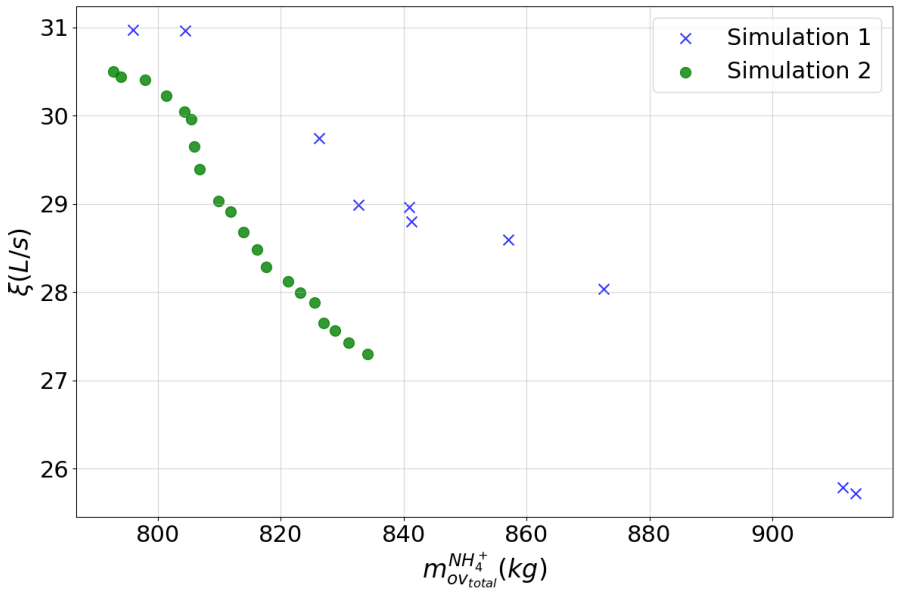

Figure 8.17: Pareto-front for all simulations.

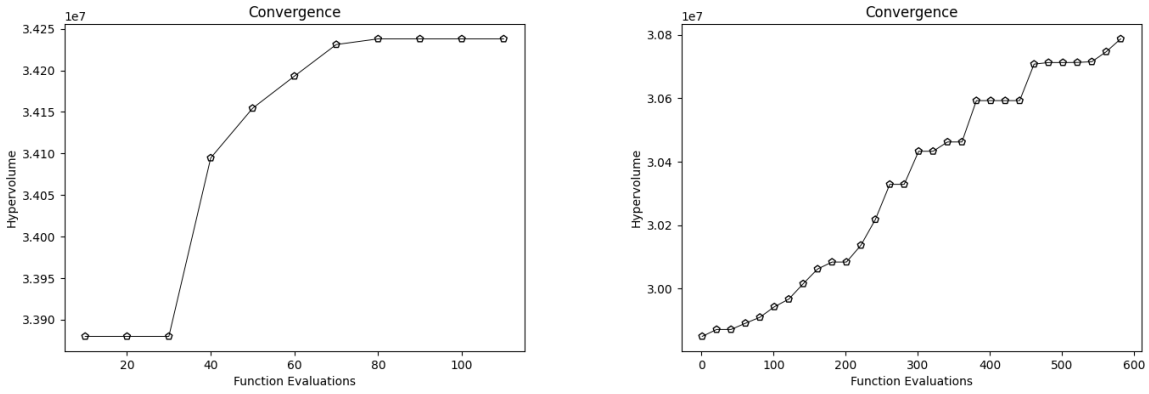

(a) Hypervolume for Simulation 1.

(b) Hypervolume for Simulation 2.

Figure 8.18: Hypervolume for all simulations.

The weights chosen for the optimisation are $\alpha, \beta, \gamma, \epsilon = (19.1, 149.1, 30.1, 190.0)$, which resulted in the lowest $m^{\mathrm{NH}_4^+}_{\mathrm{ov_{total}}} = 810$kg and still a reasonable value for ξ at 29L/s. These weights are then used in the same scenario as in Section 8.2.3 to see the improvements over the old weights and compared to other MPC methods, which is shown in Table 8.5. The optimised weights are approximately 4% better in load reduction than VMPC with a reduction of 26% compared to the uncontrolled scenario. However, NPMPC stills performs better, with 2% less load overflow compared to PWMPC.

Clearly, the use of PWMPC improved load reduction, however not as effective as a NPMPC. Although the model used for evaluation of the methods is valid, in such a constrained simple system, the room for improvement is not really high. The NPMPC could struggle in systems with more complex dynamics and configurations, while also possibly being unsuitable for real application in systems with a higher number of Storage Units. In subsequent chapters, more complex networks are explored and analysed, so that the

Table 8.5: Results for weights α, β, γ, $\epsilon = (19.1, 149.1, 30.1, 190.0)$.

Metric	Description	Static control	VMPC	NPMPC	PWMPC
Q_{ov_1}	Overflow at SU1 in ML	94.5	101.3	101.3	102.7
Q_{ov_2}	Overflow at SU2 in ML	62.8	73.8	70.9	71.7
Q_{ov_3}	Overflow at SU3 in ML	430.1	331.2	334.5	337.0
$Q_{\text{ov}_{\text{total}}}$	Total overflow in ML	587.4	506.3	506.7	511.4
ξ	Inflow error in L/s	32.3	29.9	29.7	29.9
$Q_{\text{wwtp}_{\text{total}}}$	Volume arriving at WWTP in ML	2764.9	2842.2	2846.3	2845.2
$m^{\text{NH}_4}_{\text{ov}_1}$	Overflow of NH_4 at SU1 in kg	461.0	663.8	641.8	736.8
$m^{\text{NH}_4}_{\text{ov}_2}$	Overflow of NH_4 at SU2 in kg	298.0	554.1	445.1	589.0
$m^{\text{NH}_4}_{\text{ov}_3}$	Overflow of NH_4 at SU3 in kg	5399.1	3515.4	3393.1	3227.6
$m^{\text{NH}_4}_{\text{ov}_{\text{total}}}$	Total NH_4 load overflow in kg	6158.1	4733.4	4480.0	4553.4
$m^{\text{NH}_4}_{\text{wwtp}_{\text{total}}}$	Load of NH_4 arriving at WWTP in kg	93427.6	95045.3	95338.6	95225.0

effectiveness of the methods can be dimensioned more correctly. However, the computational burden of PWMPC could justify the use of the method over NPMPC, and, hence this chapter concludes with a final computation time analysis to support this hypotheses.

8.2.6 Computation Time Analysis

Firstly, the computation time analysis for PWMPC is executed. The scenario is equal to VMPC and NPMPC in Sections 7.3.8 and 8.1.8. The result is shown in Table 8.6, which demonstrates that PWMPC has a computational burden matching the results for VMPC, which is expected since the optimisation problem is almost exactly the same. The difference between the methods is in the update of the weights in PWMPC, which does not substantially alter the computational requirement. Figure 8.19 illustrates that the behaviour is quite similar between VMPC and PWMPC.

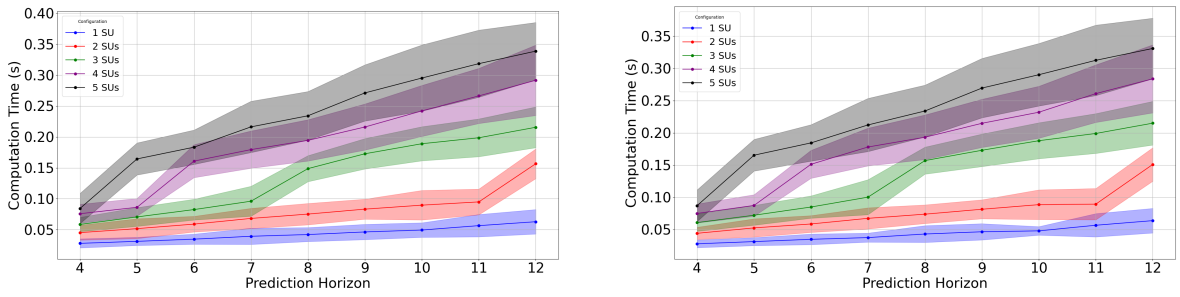

(a) Computation Times for VMPC. *(b)* Computation Times for PWMPC.

Figure 8.19: Computation time for PWMPC and VMPC - Line plot represents mean and shaded area the standard deviation.

Table 8.6: Comparison of Computation Times (Mean ± Std) for PWMPC.

N	1 SU	2 SUs	3 SUs	4 SUs	5 SUs
4.0	0.028 ± 0.006	0.044 ± 0.009	0.061 ± 0.013	0.075 ± 0.015	0.087 ± 0.024
5.0	0.031 ± 0.006	0.053 ± 0.014	0.072 ± 0.015	0.087 ± 0.017	0.165 ± 0.025
6.0	0.035 ± 0.008	0.059 ± 0.013	0.085 ± 0.017	0.151 ± 0.022	0.184 ± 0.028
7.0	0.038 ± 0.007	0.067 ± 0.016	0.100 ± 0.027	0.178 ± 0.029	0.212 ± 0.041
8.0	0.043 ± 0.013	0.074 ± 0.014	0.157 ± 0.021	0.193 ± 0.035	0.234 ± 0.040
9.0	0.047 ± 0.013	0.081 ± 0.015	0.173 ± 0.025	0.215 ± 0.037	0.269 ± 0.046
10.0	0.048 ± 0.007	0.089 ± 0.023	0.188 ± 0.028	0.232 ± 0.040	0.290 ± 0.048
11.0	0.057 ± 0.018	0.089 ± 0.024	0.199 ± 0.031	0.261 ± 0.045	0.313 ± 0.055
12.0	0.064 ± 0.019	0.151 ± 0.026	0.215 ± 0.034	0.284 ± 0.053	0.331 ± 0.047

The comparison between the different MPC approaches is shown in Figure 8.20, where the computation time is analysed against the prediction horizon while fixing the number of SUs to 4, and Figure 8.21, which evaluates the computation time as a function of the number of SUs with a fixed prediction horizon of 10.

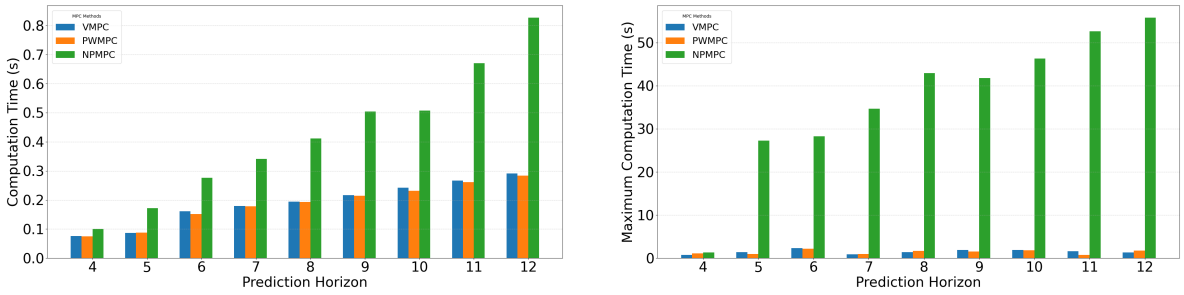

(a) Average computation time for each MPC against prediction horizon.

(b) Maximum computation time for each MPC against prediction horizon.

Figure 8.20: Computation time for each MPC against the Prediction Horizon with fixed SUs = 4.

The results highlight the comparatively extreme computational demand of NPMPC, where, in the worst case, its execution time exceeds that of VMPC and PWMPC by more than 50 times. The maximum computational time of NPMPC is still below the 4-minute control loop requirement, however its scalability presents concerns for practical applications. The implementation of PWMPC allows pollution-based real-time control with computation performance comparable to or even better than VMPC, reinforcing the great potential for practical implementation.

To conclude, while the computational cost of different MPC approaches has been thoroughly analysed, it is equally important to assess the impact of uncertainty on the system's performance. Given that practical applications are inherently subject to various sources of uncertainty, the next chapter starts with an uncertainty analysis for urban drainage systems and examines potential strategies to address these challenges, including the application of a Stochastic Model Predictive Control as an alternative to improved control performance under uncertainty.

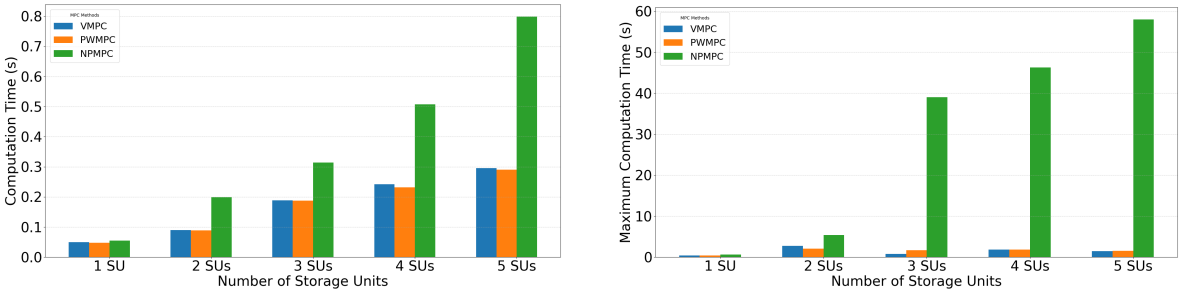

(a) Average computation time for each MPC against number of MPCs.

(b) Maximum computation time for each MPC against number of MPCs.

Figure 8.21: Computation time for each MPC against the number of MPCs with fixed $N = 10$.

9 Uncertainty Analysis and Stochastic Model Predictive Control

Robustness is a highly valued property of process control systems, ensuring reliable performance even under deviations from nominal conditions. Qualitatively, a controller is considered robust if the actual closed-loop behaviour remains acceptably close to the nominal closed-loop response, which itself corresponds to the desired process behaviour [140]. For instance, a model-based controller demonstrates robust closed-loop stability if the system remains stable despite discrepancies between the controller's model and the actual behaviour of the process [140]. The degree of robustness of a controller corresponds to the extent of such discrepancies it can tolerate while keeping closed-loop stability.

However, robust stability alone is typically insufficient to achieve good control performance. Additional closed-loop properties must be preserved despite differences between the nominal and actual process behaviours. For example, the magnitude of the regulation error in a feedback loop must remain within acceptable limits under such discrepancies. This requirement is often referred to as robust performance [140–142].

In the context of a constrained MPC, robustness takes on another dimension: the ability to ensure that inequality constraints defined in the online optimisation problem are satisfied by the actual system. Although constraints on process input can generally be enforced directly, constraints on process outputs are more difficult to guarantee [143]. This difficulty is derived from the fact that future process outputs within the moving horizon of an MPC must be predicted using a process model that accounts for the effects of manipulated inputs and disturbances. Since the model itself is subject to uncertainty, these output predictions are inherently uncertain. As a result, output constraints may be violated in the actual closed-loop system, even if the predicted outputs satisfy them within the optimisation horizon [140]. To address this issue, incorporating model uncertainty into the output constraints of the online optimisation process is essential. Such an approach would improve the robustness of constrained MPC [140, 144]. In addition, uncertainty analysis can be a powerful tool to understand possible weaknesses of the controller and identify gaps that could be fulfilled by changing the MPC formulation. Therefore, in the next section, an uncertainty analysis is performed for urban drainage systems.

9.1 Uncertainty Analysis

Uncertainty is intrinsic in any modelling process and originates from a wide range of sources, from model formulation to the collection of data to be used for calibration and verification. Uncertainties cannot be eliminated, but their amplitude should be estimated and, if possible, reduced. It is also necessary to

understand their sources and impact on model predictions. However, not all sources of uncertainty can be quantified with acceptable levels of precision, and the sources of uncertainty that are ignored may be considerable in environmental modelling [145]. From the literature on hydrological modelling, four sources of uncertainty occur in deterministic flow modelling [146] [147]:

- Type 1: Random or systematic errors in model input (boundary or initial conditions) [145].
- Type 2: Random or systematic errors in recorded output data used to measure simulation accuracy [148].
- Type 3: Uncertainties due to sub-optimal parameter values [149, 150].
- Type 4: Uncertainties due to an incomplete or biased model structure [151].

To assert the possible uncertainties on MPC and their impacts on its performance, researchers studied the influence of uncertainties on RTC systems [31] [152]. For instance, taking into account precipitation forecast, several methods have been proposed to account for precipitation uncertainty in an RTC [153]. Furthermore, it has been argued that the precipitation uncertainty will not significantly influence the final MPC performance due to the re-updating of the initial conditions at every optimisation interval [5]. However, in reality, dynamic models using rainfall forecasts would include uncertainties that could affect UDS operation, which could result in more CSO events and consequent pollution of the environment [151].

Therefore, evaluating the performance of MPC on different types of uncertainties is imperative to ensure robustness, stability, and reliability in actual applications, allowing the controller to deal with variations in system dynamics under external disturbances [154]. So far, the methods proposed in this research have one common feature: the estimation of the inflow through the equation $Q_{\text{in}}(k) = \frac{\Delta V(k)}{T_s} + Q_{\text{out}}(k) + Q_{\text{ov}}(k)$. Estimation of inflow plays an important role as the main input for optimisation, thus, it represents a major source of uncertainty that affects MPC. From within the equation to estimate the inflow, three variables stand out as possible sources of uncertainty:

1. $V(k)$ represents the volume within SUs during each control loop. The volume is determined by measuring the wastewater level within the SU using a level sensor and, knowing the geometry of the unit, the volume can be computed. However, the level sensor is prone to inaccuracies due to sensor drift, resolution limitations, calibration issues, environmental factors from the system or installation and placement issues. Here, it is assumed that these uncertainties follow a truncated Gaussian distribution, with appropriate bounds applied to prevent (unrealistic) negative values or excessively high volume estimation [155].

   Additionally, the random variables in this context are heteroscedastic, meaning their variance is not constant across different values. This effect is explained by the differences in low and high values of the measured volume. Specifically, when the volume is low, the sensor measurement is more susceptible to uncertainty. Therefore, if X is a random variable, the truncated Gaussian distribution bounded by $[a, b]$ can be expressed as follows:

   $$X \sim \mathcal{N}(\mu, \sigma^2, a, b) \tag{9.1}$$

   where:

- The mean value μ is

$$\mu = u_{\text{sc}} * \mathbb{E}\{V(k)\} + u_{\text{offset}} * V_{\max}$$

Here, $\mathbb{E}\{V(k)\}$ represents the expected value of $V(k)$, normally equal to the measured value. The term u_{sc} scales the range of the distribution, and u_{offset} shifts the distribution by a fraction of the maximum volume $V_{\max}$.

- The standard deviation σ is

$$\sigma = u_p * (V_{\max} - V(k))$$

where u_p is a scaling factor that adjusts the standard deviation based on the difference between the maximum volume and the measured volume $V(k)$.

- The bounds $[a, b]$ are defined as:

$$[a, b] = [0, \mu + u_p * V(k)]$$

- To standardize the distribution to a standard normal form, the bounds are transformed as follows:

$$a_{\text{trunc}} = \frac{a - \mathbb{E}\{V(k)\}}{\sigma}, \qquad b_{\text{trunc}} = \frac{b - \mathbb{E}\{V(k)\}}{\sigma}$$

The heteroscedasticity appears in σ by using the distance between the maximum volume and the measured volume in its calculation. As a result, lower measured volumes are associated with higher variability and, consequently, higher variance.

2. $Q_{\text{out}}(k)$ represents the outflow from SUs, which is collected through a flow measurement located on the actuator that controls locally the unit (such as valve or pump). Such systems are also under uncertainties, which arises from multiple factors, including sensor errors with resolution, time delays, malfunctioning; hydraulic variability, mechanical degradation, environmental influences, and data transmission issues. An important consideration for outflow uncertainties is that they follow the same truncated Gaussian distribution as the volume uncertainties, where for lower outflows, the uncertainty increases. Thus, for $Q_{\text{out}}(k)$ the uncertainty is formulated exactly as for $V(k)$ with the only difference being the substitution of the variable $V(k)$ with $Q_{\text{out}}(k)$ and $V_{\max}$ to $Q_{out_{\max}}$.

3. $Q_{\text{ov}}(k)$ represents the overflow from SUs, which is determined either through direct measurements using level or flow meters installed at overflow structures, or indirect methods that use hydraulic modelling or historical data [156], [25]. Similar to the volume and outflow measurements, overflow measurements are also subject to uncertainties arising from sensor inaccuracies, including drift, resolution limitations, and noise caused by electrical or mechanical effects. Additionally, infrastructure's variability can introduce further errors, such as incorrect weir coefficients or misplacement of measurement devices, leading to inaccurate readings. Nevertheless, the overflow's uncertainties can be assumed to follow a truncated Gaussian distribution as in Equation 9.1, with bounds calculated in a similar manner to the other uncertainties. However, contrary to the volume and outflow uncertainties, the overflow's standard deviation variability increases with higher overflow measurements, hence, for overflow measurements, the standard deviation is given by:

$$\sigma = u_p * Q_{\text{ov}}(k)$$

In Figure 9.1 a simplified control diagram is shown that includes the uncertainty added to the measurements to illustrate how the uncertainty interacts with the controller and the system.

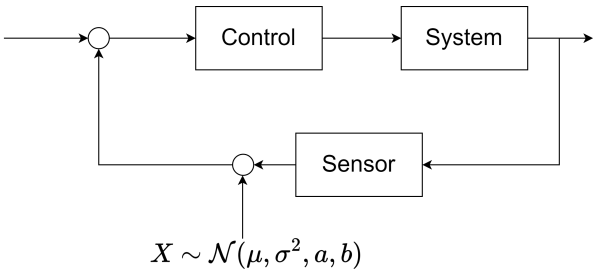

Figure 9.1: Control diagram including uncertainty measurements.

Taking into account these three variables as potential sources of uncertainties, an analysis of the robustness of the MPC methods studied so far is performed in different ranges of uncertainties. The analysis is done for uncertainties in $V(k)$, $Q_{\text{out}}(k)$ and $Q_{\text{ov}}(k)$, varying u_{offset} and u_p in different ranges, according to each type of uncertainty. For clarity, the underestimations (i.e., $u_{\text{offset}} < 0$) of $V(k)$, $Q_{\text{out}}(k)$ and $Q_{\text{ov}}(k)$ are denoted as $u_{\text{offset}}^{\text{vol-}}$, $u_{\text{offset}}^{\text{out-}}$, and $u_{\text{offset}}^{\text{ov-}}$, respectively. Conversely, overestimations (i.e., $u_{\text{offset}} > 0$) are represented as $u_{\text{offset}}^{\text{vol+}}$, $u_{\text{offset}}^{\text{out+}}$, and $u_{\text{offset}}^{\text{ov+}}$. The UDS used for the analysis is the Parallel + Series configuration as in Section 7.3.5, simulated over a 5-month period. The weights of each MPC are the optimal weights calculated using the GA algorithm in the previous chapter.

9.1.1 Uncertainty on $V(k)$

The base values for the parameters in the simulations are as follows: $u_{\text{sc}} = 1$, $u_{\text{offset}} = 0\%$, and $u_p = 1\%$. The first simulation explores different uncertainty bounds by varying u_p to 0% (no uncertainty), 5%, 10%, 25%, 50%, and 75%, while keeping the base values for u_{sc} and u_{offset} unchanged. In Figure 9.2, the uncertainties for all SUs are displayed, showing how the variability increases with different values of u_p in each scenario. In Figure 9.3 provides a closer view, illustrating that, as expected, the variability increases with higher values of u_p. It also shows that, for higher volumes, the variability is reduced because of the heteroscedasticity attributed to the uncertainty.

The metrics used for the comparison are the total volume overflow, $Q_{\text{ov}_{\text{total}}}$, in ML, the total load overflow of $NH_4{}^+$, $m_{\text{ov}_{\text{total}}}^{\text{NH}_4}$, in kg, %F represents the relative performance degradation (or improvement) of a given MPC when uncertainty is introduced, compared to its performance under ideal conditions (without uncertainty, hence $u_p = 0\%$), for a specific metric. Essentially, it quantifies the percentage difference in controller performance due to the presence of uncertainty. ξ_{rain}, which represents the average deviation between the inflow to the WWTP only during rain events and the reference inflow to the WWTP, $Q_{\text{wwtp}_{\text{ref}}}$. Table 9.1 presents the results for each MPC.

The results show that as the uncertainty parameter u_p increases, both overflow metrics increase across all MPC methods. Specifically, VMPC and PWMPC show similar increases in volume and load overflow as the uncertainty increases, with increases of up to 3.9% for volume and 7.5% for load at $u_p = 75\%$. NPMPC, however, consistently outperforms both VMPC and PWMPC, resulting in lower overflows under

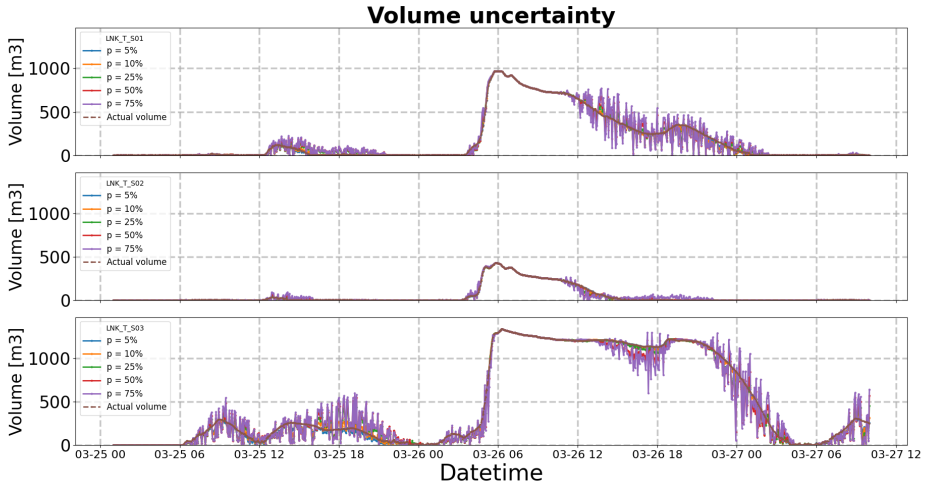

Figure 9.2: Volume for a range of u_p.

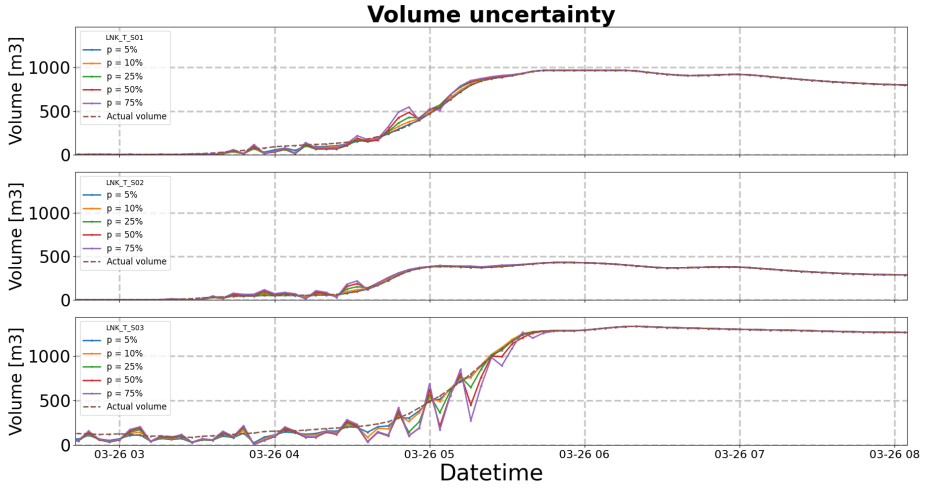

Figure 9.3: Volume for a range of u_p zoomed in.

the same uncertainty conditions. For instance, at $u_p = 75\%$, NPMPC has the smallest volume and load overflow compared to the other two MPCs. With respect to the error ξ_{rain}, all strategies exhibited a consistent decrease as variability increased. This indicates that the system operated closer to $Q_{\text{wwtp}_{\text{ref}}}$, which may explain the rise in overflow due to underutilisation of the WWTP's maximum inflow capacity. Furthermore, higher uncertainty may lead the MPC to incorrectly predict potential overflows, causing it to fail to mitigate those that actually occur. In summary, the results indicate that increasing uncertainty impacts the system's performance, and NPMPC offers a more robust control approach, better handling the uncertainty compared to the other methods.

The next simulations checked the influence of varying the offset u_{off} first by varying $u_{\text{offset}}^{\text{vol+}}$ across $[5\%, 10\%, 25\%, 50\%, 75\%]$, and then $u_{\text{offset}}^{\text{vol-}}$ in the interval $[-5\%, -10\%, -25\%, -50\%, -75\%]$. In addition, u_p is kept constant at the base value. In Figures 9.4 and 9.5, the $u_{\text{offset}}^{\text{vol+}}$ and $u_{\text{offset}}^{\text{vol-}}$ are displayed in more detail.

The results for $u_{\text{offset}}^{\text{vol+}}$ are shown in Table 9.2. A similar behaviour is displayed by VMPC compared to

Table 9.1: Volume uncertainty: Analysis of ξ_{rain}, volume and load overflow for u_p.

VMPC						
u_p	0%	5%	10%	25%	50%	75%
$Q_{\text{ov}_{\text{total}}}$	167.434	168.971	169.771	171.595	173.193	174.031
$\%\mathbf{F}_Q$		0.92%	1.4%	2.49%	3.44%	3.94%
$m^{\text{NH}_4}_{\text{ov}_{\text{total}}}$	1072.366	1088.102	1094.839	1118.461	1136.925	1152.927
$\%\mathbf{F}_m$		1.47%	2.1%	4.3%	6.02%	7.51%
ξ_{rain}	7.926	6.221	4.853	2.314	1.222	1.152
PWMPC						
u_p	0%	5%	10%	25%	50%	75%
$Q_{\text{ov}_{\text{total}}}$	168.77	170.499	171.351	172.923	174.078	174.463
$\%\mathbf{F}_Q$		1.02%	1.53%	2.46%	3.15%	3.37%
$m^{\text{NH}_4}_{\text{ov}_{\text{total}}}$	1034.79	1052.8	1062.468	1078.114	1090.945	1100.189
$\%\mathbf{F}_m$		1.74%	2.67%	4.19%	5.43%	6.32%
ξ_{rain}	7.629	5.715	4.323	1.789	0.883	0.933
NPMPC						
u_p	0%	5%	10%	25%	50%	75%
$Q_{\text{ov}_{\text{total}}}$	166.872	167.963	168.49	169.591	170.61	171.03
$\%\mathbf{F}_Q$		0.65%	0.97%	1.63%	2.24%	2.49%
$m^{\text{NH}_4}_{\text{ov}_{\text{total}}}$	1009.773	1021.104	1028.821	1037.617	1048.43	1053.341
$\%\mathbf{F}_m$		1.12%	1.89%	2.76%	3.83%	4.31%
ξ_{rain}	9.539	8.319	7.363	5.723	4.964	4.495

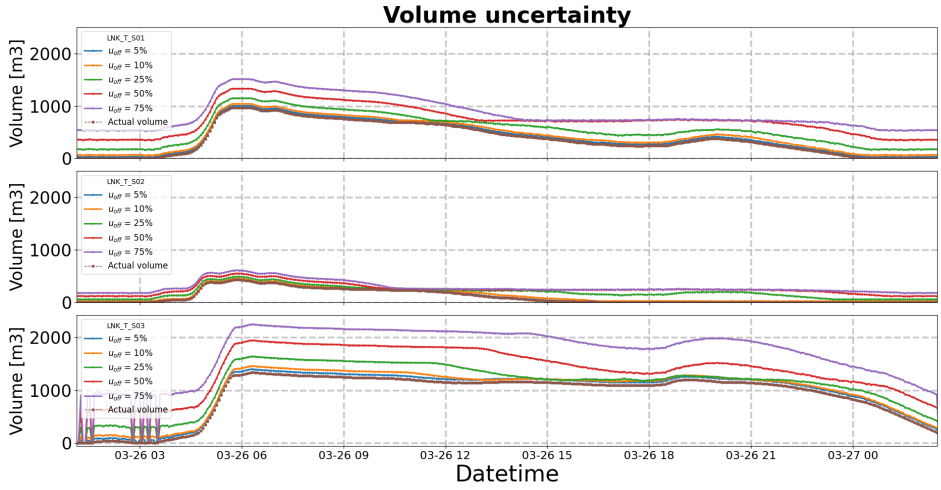

Figure 9.4: Overestimation of u_{off}.

the scenario varying u_p, while, on the contrary, NPMPC consistently performs poorly, demonstrating the worst results among algorithms. This suggests that NPMPC struggles to handle the uncertainty, in fact, it fails to converge to an optimal solution more often. On the other hand, PWMPC stands out as a very robust controller option. It slightly outperforms the scenario without uncertainty, and observing the behaviour of the controller, the reason for the improvement is that specifically in this scenario, PWMPC prioritised reducing overflow in SU3, while the other MPC focused on reducing overflow on SU1 and SU2.

More specifically, the table shows that the volume overflow in VMPC at $u_{\text{off}} = 5\%$ and $u_{\text{off}} = 10\%$ is slightly better than in $u_{\text{off}} = 0\%$, however, it grows steadily, reaching 172.8 ML in $u_{\text{off}} = 75\%$ with a 3.2% increase in volume overflow. Similarly, NPMPC's volume increases constantly reaching a 4.2% increase

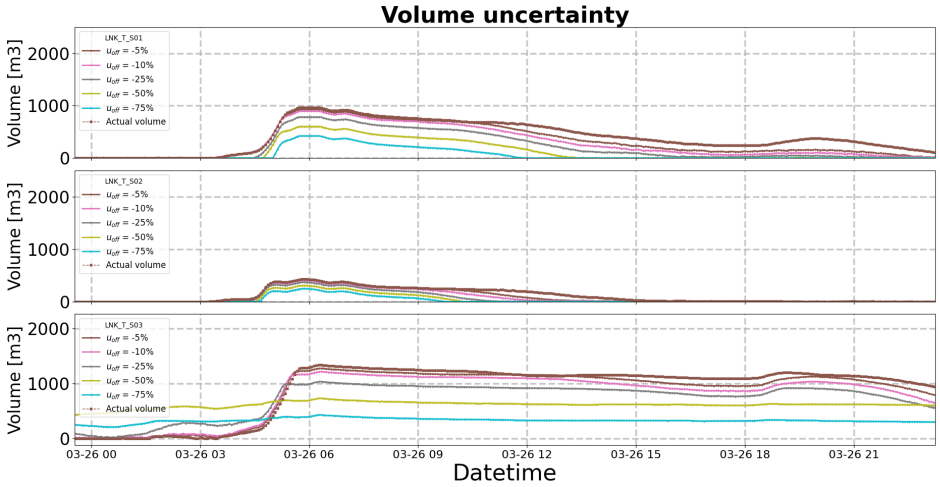

Figure 9.5: Underestimation of u_{off}.

Table 9.2: Volume uncertainty: Analysis of ξ_{rain}, volume and load overflow for $u^{\text{vol+}}_{\text{offset}}$.

VMPC						
u_{off}	0%	5%	10%	25%	50%	75%
$Q_{\text{ov}_{\text{total}}}$	167.434	166.782	167.017	168.22	170.44	172.75
$\%\mathbf{F}_Q$		-0.39%	-0.25%	0.47%	1.8%	3.17%
$m^{\text{NH}_4}_{\text{ov}_{\text{total}}}$	1072.366	1066.461	1071.089	1086.543	1129.77	1181.609
$\%\mathbf{F}_m$		-0.55%	-0.12%	1.32%	5.35%	10.19%
ξ_{rain}	7.926	8.573	9.062	9.594	9.849	9.909
PWMPC						
u_{off}	0%	5%	10%	25%	50%	75%
$Q_{\text{ov}_{\text{total}}}$	168.77	167.127	166.82	167.079	168.232	169.528
$\%\mathbf{F}_Q$		-0.97%	-1.16%	-1.0%	-0.32%	0.45%
$m^{\text{NH}_4}_{\text{ov}_{\text{total}}}$	1034.79	1011.539	1010.532	1007.75	1017.285	1028.648
$\%\mathbf{F}_m$		-2.25%	-2.34%	-2.61%	-1.69%	-0.59%
ξ_{rain}	7.629	8.364	8.892	9.6	9.875	9.899
NPMPC						
u_{off}	0%	5%	10%	25%	50%	75%
$Q_{\text{ov}_{\text{total}}}$	166.872	166.845	167.543	169.337	171.927	173.933
$\%\mathbf{F}_Q$		-0.02%	0.4%	1.48%	3.03%	4.23%
$m^{\text{NH}_4}_{\text{ov}_{\text{total}}}$	1009.773	1027.146	1043.661	1090.992	1149.691	1204.124
$\%\mathbf{F}_m$		1.72%	3.36%	8.04%	13.86%	19.25%
ξ_{rain}	9.539	9.587	9.629	9.813	9.831	9.837

in volume. However, PWMPC only begins to show a poorer performance at $u_{\text{off}} = 75\%$, although not a significant increase (0.4%). Observing the results for load, VMPC and NPMPC had a larger increase at $u_{\text{off}} = 75\%$, increasing the load by 10.2% and 19.2%, respectively. In terms of volume, PWMPC presents an improved load performance, even at $u_{\text{off}} = 75\%$, reducing the load overflow by 0.6% with this uncertainty. In this scenario, an interesting outcome observed across all MPC strategies is the positive increase in error ξ_{rain}, indicating that the maximum capacity of the WWTP is being reached more frequently as uncertainty increases. Despite this, overflow levels still increased. This suggests that reducing overflow at SU1 and SU2 led to a higher inflow into SU3, requiring its outflow to operate near its maximum capacity more often, yet, eventually, this was insufficient to avoid overflow.

In contrast, the result for $u^{\text{vol-}}_{\text{offset}}$ presented in Table 9.3 reveals a significant degradation in the performance

of all controllers. Although NPMPC outperforms the other strategies, it still shows a considerable increase in volume and load overflow, while VMPC and PWMPC are dramatically worse. The result suggests that underestimations of the volume lead to poorer prediction of overflow, reducing the reaction time of the controllers when a rain event occurs, leading to higher overflows. This type of scenario is not far from reality as the level sensor can be easily displaced or blocked, which impedes it from properly measuring the level.

Table 9.3: Volume uncertainty: Analysis of ξ_{rain}, volume and load overflow for $u_{\text{offset}}^{\text{vol-}}$.

VMPC						
u_{off}	0%	-5%	-10%	-25%	-50%	-75%
$Q_{\text{ov}_{\text{total}}}$	167.434	175.95	182.162	201.263	259.73	444.554
$\%\mathbf{F}_Q$		5.09%	8.8%	20.2%	55.12%	165.51%
$m_{\text{ov}_{\text{total}}}^{\text{NH}_4}$	1072.366	1196.528	1266.674	1571.667	2852.361	10867.604
$\%\mathbf{F}_m$		11.58%	18.12%	46.56%	165.99%	913.42%
ξ_{rain}	7.926	6.132	3.52	-6.714	-31.339	-59.93
PWMPC						
u_{off}	0%	-5%	-10%	-25%	-50%	-75%
$Q_{\text{ov}_{\text{total}}}$	168.77	176.55	182.521	203.081	268.19	485.907
$\%\mathbf{F}_Q$		4.61%	8.15%	20.33%	58.91%	187.91%
$m_{\text{ov}_{\text{total}}}^{\text{NH}_4}$	1034.79	1160.127	1247.463	1588.802	3057.457	12442.546
$\%\mathbf{F}_m$		12.11%	20.55%	53.54%	195.47%	1102.42%
ξ_{rain}	7.629	5.884	3.317	-7.805	-34.407	-65.611
NPMPC						
u_{off}	0%	-5%	-10%	-25%	-50%	-75%
$Q_{\text{ov}_{\text{total}}}$	166.872	170.477	173.849	181.875	194.091	218.174
$\%\mathbf{F}_Q$		2.16%	4.18%	8.99%	16.31%	30.74%
$m_{\text{ov}_{\text{total}}}^{\text{NH}_4}$	1009.773	1040.733	1070.63	1173.591	1319.062	1808.97
$\%\mathbf{F}_m$		3.07%	6.03%	16.22%	30.63%	79.15%
ξ_{rain}	9.539	9.188	8.616	7.348	4.424	-2.084

As uncertainty increases, particularly with negative offsets, both the volume overflow and the load overflow increase substantially, suggesting that the controllers struggle to minimise the overflow. For instance, in the case of VMPC, the volume overflow at $u_{\text{off}} = 75\%$ reaches 444.5 ML, a significant increase from 167.4 ML at $u_{\text{off}} = 0\%$, experiencing an increase of 165.5% in volume overflow. Similarly, PWMPC and NPMPC show increased overflows, reaching 485.9 ML and 218.2 ML, respectively, at $u_{\text{off}} = 75\%$, seeing an increase of 187.9% and 30.7%, respectively. The load overflow increases massively in all scenarios, increasing by 913.4% for VMPC, 1102.4% for PWMPC and 79.1% for NPMPC, and, evidently, NPMPC is more robust to the presence of large uncertainties. The value of ξ_{rain} exhibits that the error is constantly decreasing with lower values of u_{off}, reaching extremely low values with $\xi = -59.93$ and $\xi = -65.51$ L/s for VMPC and PWMPC, respectively. This suggests that the strategies did not correctly predict the overflow and, as a result, did not use the full capacity of the actuator. Although ξ_{rain} is also diminishing for NPMPC, it is not as critical as for the other methods.

9.1.2 Uncertainty on $Q_{\text{out}}(k)$

The next scenario considers the uncertainty applied to the outflow, $Q_{\text{out}}(k)$. The base value of each parameter in the simulations is: $u_{\text{sc}} = 1$, $u_{\text{offset}} = 0\%$ and $u_p = 25\%$. The first simulation varies the uncertainty bounds choosing u_p to 0%, 25%, 75%, 100%, 125% and 175% and using the base values for

u_{sc} and u_{offset}. The metrics chosen for comparison are the same as in the previous section. In Figure 9.6, the outflow uncertainty is shown for all SUs, revealing that the variability increases with different values of u_p in each scenario. Moreover, Figure 9.7 illustrates the uncertainty distribution, where for lower measured values the variability is higher.

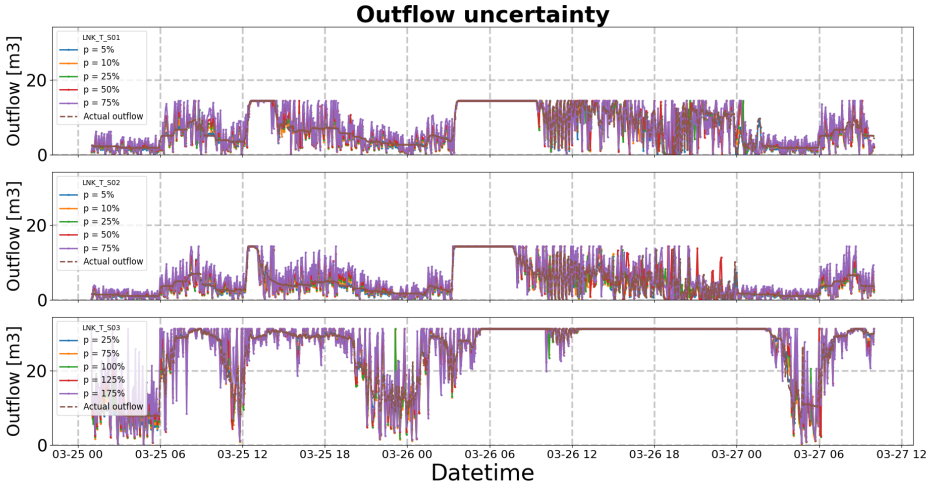

Figure 9.6: Outflow for a range of u_p.

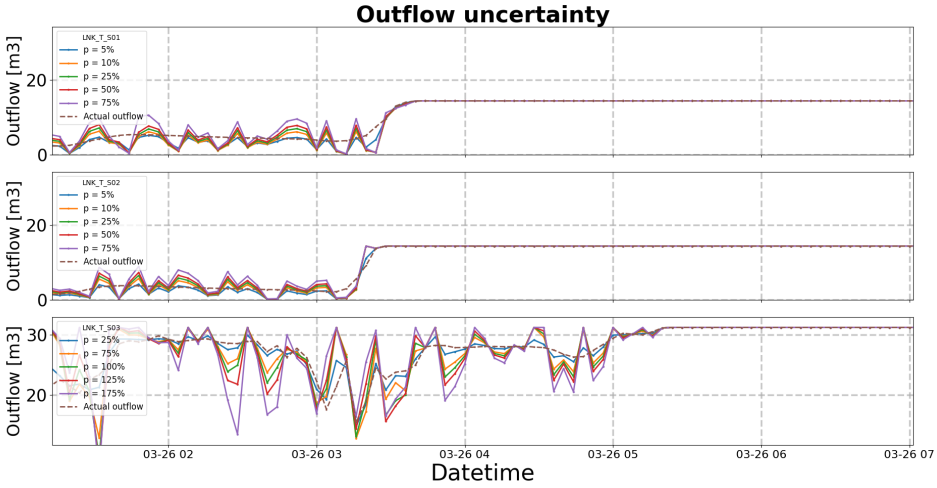

Figure 9.7: Outflow for a range of u_p zoomed in.

The results are shown in Table 9.4, which suggests that the volume and load overflow are not significantly affected by increasing the variability of the uncertainty. In the worst case scenario, $m^{NH_4}_{ov_{total}}$ increased only by 1.1% for PWMPC for $u_p = 175\%$, indicating great robustness for all MPC methods when there is variability in Q_{out}. In addition, ξ_{rain} also does not change considerably, the variability in actuator measurement does not affect the behaviour mainly because they are already close to operating in their maximum capacity. A different choice of weights for each MPC could result in different behaviours, since the weights were chosen to focus on minimising overflow.

The second simulation checked the influence of varying the offset u_{off} similarly to the volume uncertainty scenario. Hence, u^{out+}_{offset} is in the interval $[5\%, 10\%, 25\%, 50\%, 75\%]$, and u^{out-}_{offset} is varied between

Table 9.4: Outflow uncertainty: Analysis of ξ_{rain}, volume and load overflow for u_p.

VMPC						
u_p	0%	25%	75%	100%	125%	175%
$Q_{\text{ov}_{\text{total}}}$	167.434	167.463	167.692	167.749	167.808	168.03
$\%\mathbf{F}_Q$		0.02%	0.15%	0.19%	0.22%	0.36%
$m^{\text{NH}_4}_{\text{ov}_{\text{total}}}$	1072.366	1074.472	1078.197	1077.432	1077.661	1082.022
$\%\mathbf{F}_m$		0.2%	0.54%	0.47%	0.49%	0.9%
ξ_{rain}	7.926	7.866	7.824	7.815	7.808	7.777
PWMPC						
u_p	0%	25%	75%	100%	125%	175%
$Q_{\text{ov}_{\text{total}}}$	168.77	168.765	168.883	168.933	169.025	169.167
$\%\mathbf{F}_Q$		-0.0%	0.07%	0.1%	0.15%	0.24%
$m^{\text{NH}_4}_{\text{ov}_{\text{total}}}$	1034.79	1036.351	1038.948	1041.474	1043.092	1045.685
$\%\mathbf{F}_m$		0.15%	0.4%	0.65%	0.8%	1.05%
ξ_{rain}	7.629	7.508	7.449	7.469	7.482	7.458
NPMPC						
u_p	0%	25%	75%	100%	125%	175%
$Q_{\text{ov}_{\text{total}}}$	166.872	166.989	167.107	167.135	167.058	167.121
$\%\mathbf{F}_Q$		0.07%	0.14%	0.16%	0.11%	0.15%
$m^{\text{NH}_4}_{\text{ov}_{\text{total}}}$	1009.773	1014.373	1018.229	1018.637	1016.685	1017.137
$\%\mathbf{F}_m$		0.46%	0.84%	0.88%	0.68%	0.73%
ξ_{rain}	9.539	9.399	9.278	9.3	9.329	9.308

$[-5\%, -10\%, -25\%, -50\%, -75\%]$. The behaviour of the outflow is shown in Figures 9.8 and 9.9, where it can be seen that the uncertainties clearly affect the outflow measurements.

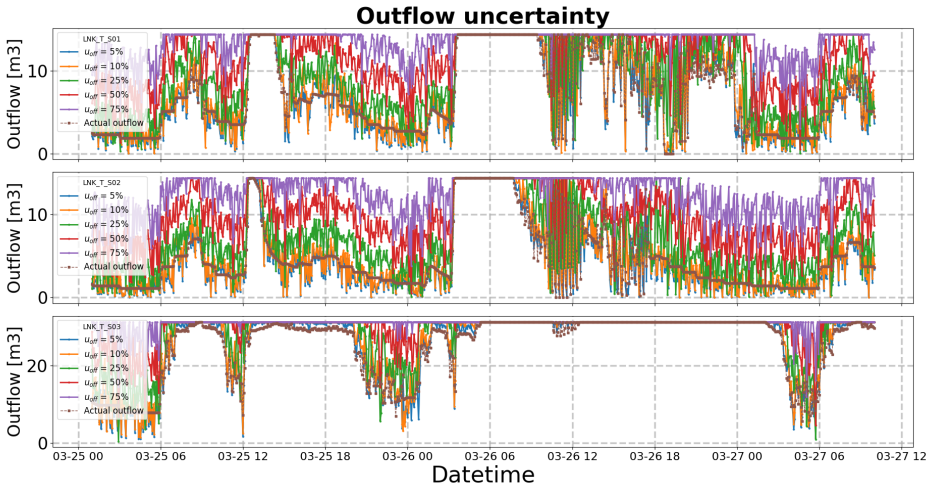

Figure 9.8: Overestimation of u_{off}.

In Table 9.5 the results for $u^{\text{out+}}_{\text{offset}}$. Volume overflows are, similarly to the uncertainty u_p, barely affected by disturbances caused by u_{off}. For VMPC and PWMPC, the overflow in terms of load is more directly affected by the uncertainty, showing an increase in load of 3.1% and 3.9% for u_p equal to 75%, respectively. In this scenario, NPMPC is more robust, with a maximum increase of 1.8% in load. The error ξ_{rain} also does not change significantly, all MPC strategies were capable of handling uncertainties without compromising performance greatly.

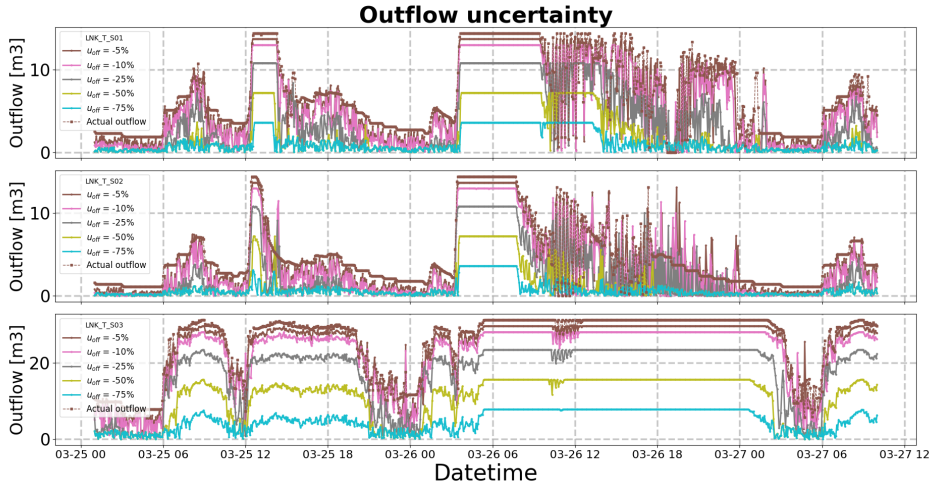

Figure 9.9: Underestimation of u_{off}.

Table 9.5: Outflow uncertainty: Analysis of ξ_{rain}, volume and load overflow for $u^{\text{out+}}_{\text{offset}}$.

VMPC						
u_{off}	0%	5%	10%	25%	50%	75%
$Q_{\text{ov}_{\text{total}}}$	167.434	167.497	167.45	167.621	168.324	169.353
$\%\mathbf{F}_Q$		0.04%	0.01%	0.11%	0.53%	1.15%
$m^{\text{NH}_4}_{\text{ov}_{\text{total}}}$	1072.366	1075.368	1075.381	1075.443	1086.521	1105.802
$\%\mathbf{F}_m$		0.28%	0.28%	0.29%	1.32%	3.12%
ξ_{rain}	7.926	7.886	7.854	7.824	7.71	7.699
PWMPC						
u_{off}	0%	5%	10%	25%	50%	75%
$Q_{\text{ov}_{\text{total}}}$	168.77	168.782	168.72	168.752	169.243	170.009
$\%\mathbf{F}_Q$		0.01%	-0.03%	-0.01%	0.28%	0.73%
$m^{\text{NH}_4}_{\text{ov}_{\text{total}}}$	1034.79	1035.825	1037.897	1043.013	1056.523	1075.083
$\%\mathbf{F}_m$		0.1%	0.3%	0.79%	2.1%	3.89%
ξ_{rain}	7.629	7.575	7.56	7.513	7.446	7.477
NPMPC						
u_{off}	0%	5%	10%	25%	50%	75%
$Q_{\text{ov}_{\text{total}}}$	166.872	166.902	166.815	166.592	166.845	167.097
$\%\mathbf{F}_Q$		0.02%	-0.03%	-0.17%	-0.02%	0.13%
$m^{\text{NH}_4}_{\text{ov}_{\text{total}}}$	1009.773	1012.038	1013.581	1010.963	1020.763	1028.285
$\%\mathbf{F}_m$		0.22%	0.38%	0.12%	1.09%	1.83%
ξ_{rain}	9.539	9.361	9.304	9.367	9.41	9.415

Looking at the results for $u^{\text{out-}}_{\text{offset}}$ in Figure 9.6, similar to $u^{\text{vol-}}_{\text{offset}}$, the results show a greater impact over the MPC strategies in terms of volume and load overflow. The performance for both VMPC and PWMPC stands out negatively, reaching a load increase of 15% and 16.3%, respectively, at $u_p = 75\%$, while NPMPC kept at a reasonable 1.8% increase. However, ξ_{rain} is fairly consistent and does not change dramatically. Increased uncertainties did not affect the behaviour of the SU connected to the WWTP, which remains consistent in its outflow. This suggests that the prediction in this SU did not anticipate an overflow, or that this structure was not prioritised in the optimisation.

In summary, the MPC strategies showed great performance for increased variability of the outflow, handling the uncertainty without compromising the performance. However, an offset uncertainty does affect the controllers, mainly when the outflow measurements are underestimated, resulting in higher

Table 9.6: Outflow uncertainty: Analysis of ξ_{rain}, volume and load overflow for $u_{\text{offset}}^{\text{out-}}$.

VMPC						
u_{off}	0%	-5%	-10%	-25%	-50%	-75%
$Q_{\text{ov}_{\text{total}}}$	167.434	167.791	168.256	170.937	174.586	176.381
$\%\mathbf{F}_Q$		0.21%	0.49%	2.09%	4.27%	5.34%
$m_{\text{ov}_{\text{total}}}^{\text{NH}_4}$	1072.366	1081.025	1087.939	1139.193	1200.527	1232.686
$\%\mathbf{F}_m$		0.81%	1.45%	6.23%	11.95%	14.95%
ξ_{rain}	7.926	7.737	7.675	7.622	7.483	7.203
PWMPC						
u_{off}	0%	-5%	-10%	-25%	-50%	-75%
$Q_{\text{ov}_{\text{total}}}$	168.77	169.149	169.697	172.141	175.228	176.585
$\%\mathbf{F}_Q$		0.22%	0.55%	2.0%	3.83%	4.63%
$m_{\text{ov}_{\text{total}}}^{\text{NH}_4}$	1034.79	1044.777	1056.727	1110.921	1170.809	1203.465
$\%\mathbf{F}_m$		0.97%	2.12%	7.36%	13.14%	16.3%
ξ_{rain}	7.629	7.417	7.401	7.451	7.46	7.108
NPMPC						
u_{off}	0%	-5%	-10%	-25%	-50%	-75%
$Q_{\text{ov}_{\text{total}}}$	166.872	167.296	167.761	168.456	168.169	167.211
$\%\mathbf{F}_Q$		0.25%	0.53%	0.95%	0.78%	0.2%
$m_{\text{ov}_{\text{total}}}^{\text{NH}_4}$	1009.773	1021.37	1030.344	1042.714	1041.437	1027.929
$\%\mathbf{F}_m$		1.15%	2.04%	3.26%	3.14%	1.8%
ξ_{rain}	9.539	9.479	9.521	9.465	9.383	9.455

overflows.

9.1.3 Uncertainty on $Q_{\text{ov}}(k)$

Finally, the uncertainties are considered in the overflow, $Q_{\text{ov}}(k)$. The base value of each parameter in the simulations is: $u_{\text{sc}} = 1$, $u_{\text{offset}} = 0\%$ and $u_p = 10\%$. The first simulation varies the uncertainties' limits by choosing u_p to 0%, 50%, 100%, 150%, 175%, and 200% and using the base values for u_{sc} and u_{offset}. The behaviour of the uncertainties for the changes in u_p is shown in Figure 9.10.

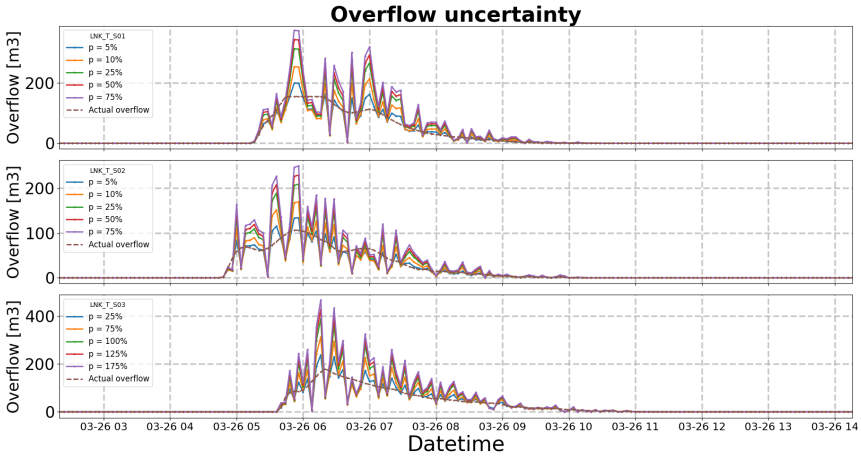

Figure 9.10: Overflow uncertainty for u_p in different ranges.

The results are presented in Table 9.7, which shows that the overflow variability does not have a strong

impact on any MPC strategies in any metrics. The choice of weights basically forces the system to always keep the actuators at high outflows when overflows are predicted, therefore, as long as the system is able to predict the overflow, the variability in $Q_{\text{ov}}(k)$ measurements will not influence the outcome.

Table 9.7: Overflow uncertainty: Analysis of volume and load overflow for u_p.

VMPC						
u_p	0%	50%	100%	150%	175%	200%
$Q_{\text{ov}_{\text{total}}}$	167.434	167.682	167.661	167.609	167.595	167.552
$\%\mathbf{F}_Q$		0.15%	0.14%	0.1%	0.1%	0.07%
$m^{\text{NH}_4}_{\text{ov}_{\text{total}}}$	1072.366	1074.136	1071.316	1068.024	1066.955	1064.954
$\%\mathbf{F}_m$		0.17%	-0.1%	-0.4%	-0.5%	-0.69%
ξ_{rain}	7.926	7.889	7.876	7.872	7.868	7.871
PWMPC						
u_p	0%	50%	100%	150%	175%	200%
$Q_{\text{ov}_{\text{total}}}$	168.77	169.002	169.009	168.967	168.957	168.926
$\%\mathbf{F}_Q$		0.14%	0.14%	0.12%	0.11%	0.09%
$m^{\text{NH}_4}_{\text{ov}_{\text{total}}}$	1034.79	1041.701	1038.929	1034.501	1032.897	1030.976
$\%\mathbf{F}_m$		0.67%	0.4%	-0.03%	-0.18%	-0.37%
ξ_{rain}	7.629	7.602	7.554	7.533	7.532	7.527
NPMPC						
u_p	0%	50%	100%	150%	175%	200%
$Q_{\text{ov}_{\text{total}}}$	166.872	167.01	166.973	166.957	166.981	166.915
$\%\mathbf{F}_Q$		0.08%	0.06%	0.05%	0.07%	0.03%
$m^{\text{NH}_4}_{\text{ov}_{\text{total}}}$	1009.773	1017.832	1015.81	1010.548	1010.759	1008.569
$\%\mathbf{F}_m$		0.8%	0.6%	0.08%	0.1%	-0.12%
ξ_{rain}	9.539	9.541	9.542	9.54	9.536	9.534

The next scenario checked whether $Q_{\text{ov}_{\text{total}}}$, $m^{\text{NH}_4}_{\text{ov}_{\text{total}}}$, and ξ_{rain} are impacted by offset uncertainties in the overflow. The value of u_{off} is varied in two ranges, first in the interval $[5\%, 10\%, 25\%, 50\%, 75\%]$, and second in $[-5\%, -10\%, -25\%, -50\%, -75\%]$, as can be seen in Figures 9.11 and 9.12, and the results are shown in Table 9.8 and Table 9.9.

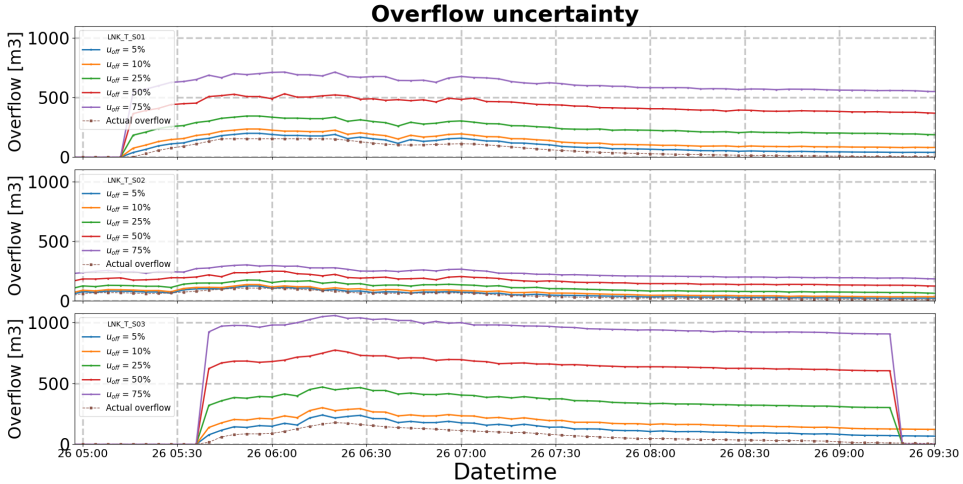

Figure 9.11: Overestimation of u_{off}.

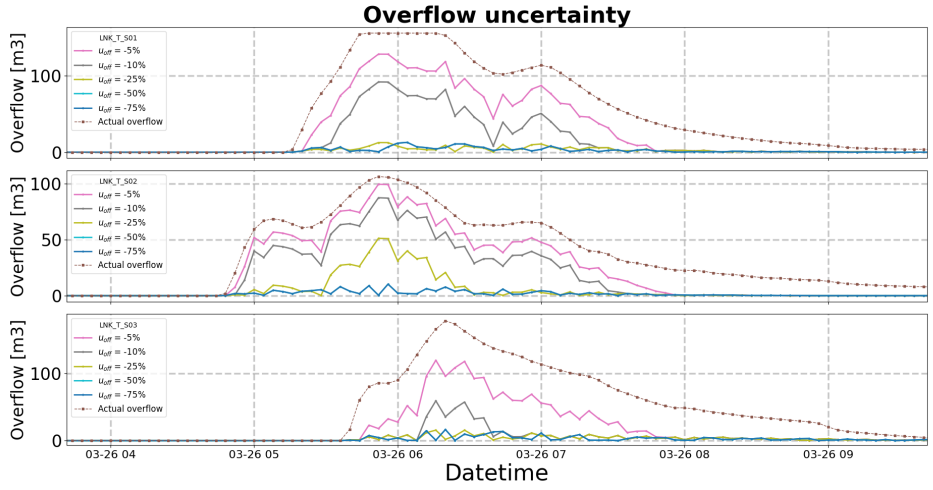

Figure 9.12: Underestimation of u_{off}.

Table 9.8: Overflow uncertainty: Analysis of volume and load overflow for $u^{\text{ov+}}_{\text{offset}}$.

VMPC						
u_{off}	0%	5%	10%	25%	50%	75%
$Q_{\text{ov}_{\text{total}}}$	167.434	167.099	167.368	167.516	167.466	167.332
$\%\mathbf{F}_Q$		-0.2%	-0.04%	0.05%	0.02%	-0.06%
$m^{\text{NH}_4}_{\text{ov}_{\text{total}}}$	1072.366	1058.702	1037.079	1015.923	1010.801	1010.258
$\%\mathbf{F}_m$		-1.27%	-3.29%	-5.26%	-5.74%	-5.79%
ξ_{rain}	7.926	7.702	7.621	7.553	7.535	7.535
PWMPC						
u_{off}	0%	5%	10%	25%	50%	75%
$Q_{\text{ov}_{\text{total}}}$	168.77	168.375	168.297	168.223	168.104	168.024
$\%\mathbf{F}_Q$		-0.23%	-0.28%	-0.32%	-0.39%	-0.44%
$m^{\text{NH}_4}_{\text{ov}_{\text{total}}}$	1034.79	998.634	993.176	998.199	1009.106	1016.806
$\%\mathbf{F}_m$		-3.49%	-4.02%	-3.54%	-2.48%	-1.74%
ξ_{rain}	7.629	7.546	7.641	7.672	7.645	7.662
NPMPC						
u_{off}	0%	5%	10%	25%	50%	75%
$Q_{\text{ov}_{\text{total}}}$	166.872	167.053	168.237	169.605	170.313	170.356
$\%\mathbf{F}_Q$		0.11%	0.82%	1.64%	2.06%	2.09%
$m^{\text{NH}_4}_{\text{ov}_{\text{total}}}$	1009.773	991.537	1008.578	1037.051	1060.8	1062.015
$\%\mathbf{F}_m$		-1.81%	-0.12%	2.7%	5.05%	5.17%
ξ_{rain}	9.539	9.486	9.47	9.458	9.456	9.458

The overflow affected by an offset uncertainty shows less impact than other uncertainties, although non-negligible. In fact, for the overestimation, NPMPC displays a 5% increase in load overflow for $u_{\text{off}} = 75\%$, while VMPC and PWMPC surprisingly reduce it by 5.8% and by 1.7%, respectively. The value of ξ_{rain} is barely changing in both scenarios, again suggesting that, if the system is able to predict the overflow, the uncertainty will not greatly alter the behaviour of the controller. For underestimation, all MPC are underperforming, highlighting PWMPC with an increase 1.1% and 4.8% in the volume and load overflow, respectively.

In general, the analysis of the uncertainties shows that the MPC algorithms are robust to uncertainty up to a certain level and depending on the type of uncertainty, for which an offset uncertainty stands out as the one affecting the control performance the most. Due to the choice of weights, the MPCs are

Table 9.9: Overflow uncertainty: Analysis of volume and load overflow for $u_{\text{offset}}^{\text{ov-}}$.

VMPC						
u_{off}	0%	-5%	-10%	-25%	-50%	-75%
$Q_{\text{ov}_{\text{total}}}$	167.434	169.609	169.572	169.599	169.561	169.561
$\%\mathbf{F}_Q$		1.3%	1.28%	1.29%	1.27%	1.27%
$m_{\text{ov}_{\text{total}}}^{\text{NH}_4}$	1072.366	1099.018	1097.333	1096.522	1094.832	1094.832
$\%\mathbf{F}_m$		2.49%	2.33%	2.25%	2.09%	2.09%
ξ_{rain}	7.926	7.485	7.501	7.488	7.476	7.476
PWMPC						
u_{off}	0%	-5%	-10%	-25%	-50%	-75%
$Q_{\text{ov}_{\text{total}}}$	168.77	170.831	170.866	170.747	170.67	170.617
$\%\mathbf{F}_Q$		1.22%	1.24%	1.17%	1.13%	1.09%
$m_{\text{ov}_{\text{total}}}^{\text{NH}_4}$	1034.79	1088.107	1089.487	1086.525	1085.304	1084.129
$\%\mathbf{F}_m$		5.15%	5.29%	5.0%	4.88%	4.77%
ξ_{rain}	7.629	7.264	7.256	7.278	7.258	7.271
NPMPC						
u_{off}	0%	-5%	-10%	-25%	-50%	-75%
$Q_{\text{ov}_{\text{total}}}$	166.872	167.406	167.358	167.442	167.307	167.414
$\%\mathbf{F}_Q$		0.32%	0.29%	0.34%	0.26%	0.32%
$m_{\text{ov}_{\text{total}}}^{\text{NH}_4}$	1009.773	1043.906	1043.317	1047.655	1041.86	1046.62
$\%\mathbf{F}_m$		3.38%	3.32%	3.75%	3.18%	3.65%
ξ_{rain}	9.539	9.524	9.535	9.532	9.528	9.533

prioritising overflow reduction and, therefore, they tend to compensate more to reduce overflows.

9.2 Stochastic Model Predictive Control

A promising approach to address uncertainty in MPC is through Stochastic Model Predictive Control (SMPC) schemes aiming to exploit the stochastic nature of uncertainty and, where available, its statistical characterisation. Within this framework, hard constraints on system variables are reformulated as stochastic constraints, permitting controlled violations in predefined probabilistic terms [157]. This approach is particularly effective when disturbances or uncertainties, such as those following a Gaussian distribution, are unbounded. A notable example of SMPC is the Chance-Constrained Model Predictive Control (CC-MPC) [158], which reformulates the output constraints of the form $y_{\min} \leq y \leq y_{\max}$ as chance constraints, where the constraint is assumed to have a probability ζ to be true. The chance constraint can be described by:

$$Pr(y_{\min} \leq y \leq y_{\max}) \geq \zeta \tag{9.2}$$

In CC-MPC, the internal model accounts for uncertainties by incorporating them directly into the formulation. Constraints are reformulated as either expectations of the constraints or probabilistic constraints with a chosen probability of being true, as in Equation 9.2, depending on the application. Generally, expectation-based constraints are used for equality constraints, while probabilistic constraints are applied to inequality constraints. Probabilistic constraints are introduced to restrict deterministic constraints, to statistically avoid unwanted behaviours, where this tightening is achieved by using quantiles, which transform probabilistic constraints into their deterministic counterparts [153]. The main scheme for CC-MPC is shown in Figure 9.13, which uses the expectation of the states and inputs, $\mathbb{E}\{x\}$ and $\mathbb{E}\{u\}$.

The scheme can be summarised as follows:

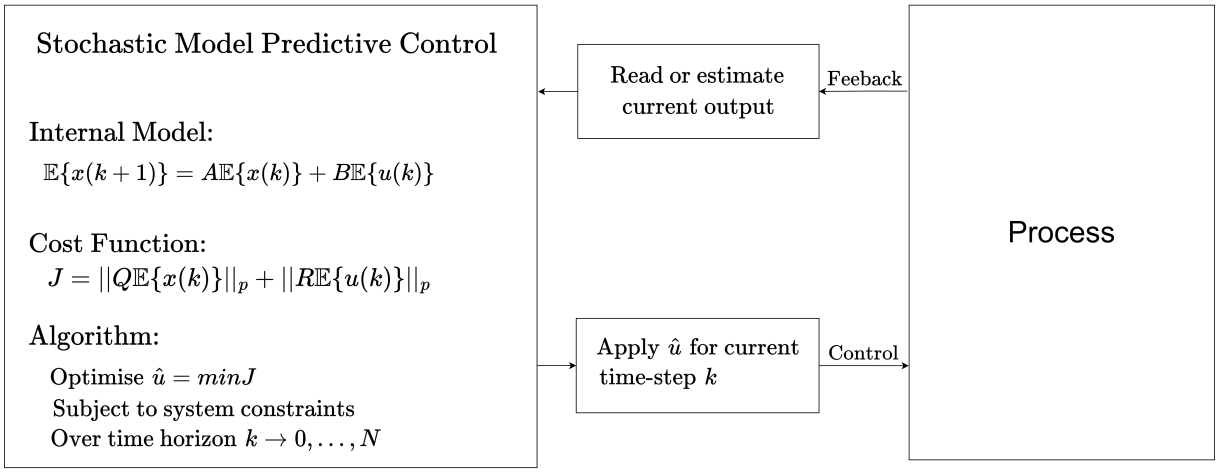

Figure 9.13: CC-MPC scheme.

- For a given system, the first step is to read the current output through a sensor or estimate it in the case of unavailable measurements;

- Then, there is the explicit use of dynamic models to predict the system output at future time instants. For this formulation, the following model is a linear stochastic discrete state-space representation of a process:

$$\begin{aligned} \mathbb{E}\{x(k+1)\} &= A\mathbb{E}\{x(k)\} + B\mathbb{E}\{u(k) \\ \mathbb{E}\{y(k)\} &= C\mathbb{E}\{x(k)\} + D\mathbb{E}\{u(k)\} \end{aligned} \tag{9.3}$$

  where $\mathbb{E}\{x(k)\}$, $\mathbb{E}\{u(k)\}$ and $\mathbb{E}\{y(k)\}$ are the expectations of system's states, input and output at instant k, respectively, and $\mathbb{E}\{x(k+1)\}$ is the successor expected state at instant $k+1$. Using this representation, the states might be predicted during the optimisation problem;

- A optimal control action is calculated by minimising a cost function and considering physical constraints of the system, which might be represented in many forms, such as:

$$\hat{u}(k) = \arg\min_{u} \sum_{j=0}^{N-1} J(\mathbb{E}\{x(k+j)\}, \mathbb{E}\{u(k+j)\}) \tag{9.4}$$

$$\text{subject to} \quad \mathbb{E}\{x(k)\} + \sigma\{x(k)\}\Phi^{-1}(\zeta) \tag{9.5}$$

$$\mathbb{E}\{u(k)\} + \sigma\{u(k)\}\Phi^{-1}(\zeta) \tag{9.6}$$

  where $J(\mathbb{E}\{x\}, \mathbb{E}\{u\})$ is a cost function, $\hat{u}(k)$ is the optimal predicted control action, Equation 9.5 is the chance-constraint for the state and Equation 9.6 is the chance-constraint for the input, both written in its deterministic form. For more details on how to reformulate probabilistic constraints into deterministic ones, the following studies are suggested: [151, 153, 159]. The deterministic part includes the expectation $\mathbb{E}\{.\}$, the standard deviation $\sigma\{.\}$, a quantile function of the standard normal distribution $\Phi^{-1}(\zeta)$ and ζ is the confidence level, which indicates the probability for the constraint to hold.

- The CC-MPC also uses a prediction horizon, N, which represents the number of future steps considered during optimisation to calculate the control actions.

In summary, SMPC explicitly accounts for uncertainties in the system model or measurements by formulating constraints as probabilistic (chance) constraints. The probability level for chance constraints defines the acceptable likelihood of violating the constraint. For example, setting $\zeta = 95\%$ assumes that constraints are satisfied at least 95% of the time. The adjustment of ζ involves a trade-off between constraint satisfaction and controller conservatism. Lower probability levels may result in more aggressive control but increase the risk of constraint violations. In addition, the deterministic approximation using quantiles is used to convert probabilistic constraints into tractable optimisation problems. ζ is kept between (0.5, 1] due to $\Phi^{-1}(\zeta)$ representing the quantile of a standard normal distribution with mean 0 and standard deviation 1. Allowing $\zeta < 0.5$ would, in fact, relax the stochastic constraint, which is an undesirable behaviour for the control application.

Although the use of SMPC is appealing as most systems are susceptible to uncertainties, the methodology faces some challenges. For instance, an accurate statistical characterisation of uncertainties is very important for the performance, which can degrade considerably if the stochastic model is defined incorrectly. Moreover, over-conservatism can reduce the system's performance, while under-conservatism can lead to unacceptable risks due to unforeseen constraint violations [142, 160]. Assessment of uncertainties is imperative for the success of the technique, otherwise, a deterministic MPC or other methods are more relevant. Specifically for urban drainage systems, Section 9.1 analysed some situations where the deterministic MPC showed reduced performance when there are uncertainties present in the system's behaviour. Therefore, in the following sections, a group of novel algorithms is proposed to handle uncertainties as an alternative to VMPC, PWMPC and NPMPC.

9.3 Stochastic Volume-based Model Predictive Control

The first method proposed in this chapter is the Stochastic Volume-based Model Predictive Control (SVMPC), which is inspired by works in [151, 153, 155] that applied and implemented a stochastic CC-MPC method considering the uncertainty that exists in the forecast of rain. The main differences between previous works and the methodology in this thesis are the different objectives in the cost function of the stochastic MPC and the consideration of different types of uncertainties based on Section 9.1.

9.3.1 Description

The SVMPC is a method that transforms VMPC from Section 7.3 into a stochastic control method using the same formulation as in [151, 153, 155]. Since VMPC is a deterministic controller, a few assumptions are necessary to change it into a stochastic method:

1. The variables are reformulated as expectations of the variable $\mathbb{E}\{.\}$, e.g., volume $V(k)$, outflow $Q_{\text{out}}(k)$, overflow $Q_{\text{ov}}(k)$, and inflow $Q_{\text{in}}(k)$ are reformulated as $\mathbb{E}\{V(k)\}$, $\mathbb{E}\{Q_{\text{out}}(k)\}$, $\mathbb{E}\{Q_{\text{ov}}(k)\}$, and $\mathbb{E}\{Q_{\text{in}}(k)\}$.

2. They also include a standard deviation $\sigma^2\{V(k)\}$, $\sigma^2\{Q_{\text{out}}(k)\}$, $\sigma^2\{Q_{\text{in}}(k)\}$ and $\sigma^2\{Q_{\text{ov}}(k)\}$

3. Uncertainties are considered truncated Gaussian distributed with heteroscedastic behaviour.

The scheme for the control algorithm is presented in Figure 9.14.

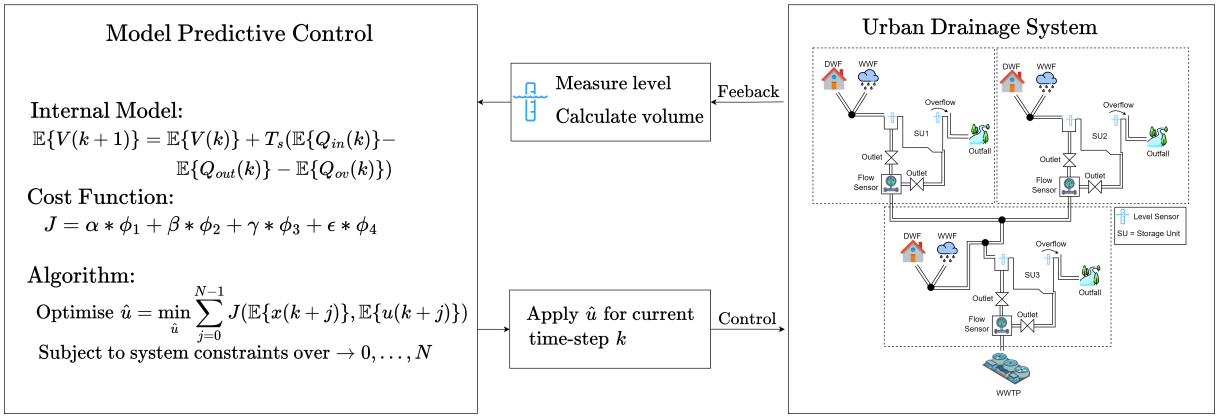

Figure 9.14: SVMPC scheme for Urban Drainage Systems.

SVMPC receives feedback information from the UDS through the measurement devices and the expectations and standard deviations are estimated given a pre-determined probabilistic distribution. The internal model is used to predict the expected volume in the prediction horizon, where the objective is to estimate the expected overflow in the future.

The main difference is the characterisation of the constraints in the optimisation, where, for equality constraints, the internal model is substituted by the expectation of the constraint and their standard deviation. Assuming that the different sources of uncertainties are independently distributed, the equality constraint of VMPC represented in Equation 7.15b is reformulated to:

$$\mathbb{E}\{Q_{\text{in}}(k)\} = \frac{\Delta\mathbb{E}\{V(k)\}}{T_s} + \mathbb{E}\{Q_{\text{out}}\}(k) + \mathbb{E}\{Q_{\text{ov}}\}(k) \tag{9.7}$$

$$\mathbb{E}\{V(k+1)\} = \mathbb{E}\{V(k)\} + T_s[\mathbb{E}\{Q_{\text{in}}(k)\} - \mathbb{E}\{Q_{\text{out}}(k)\} - \mathbb{E}\{Q_{\text{ov}}(k)\}] \tag{9.8}$$

where T_s is the sampling time. In addition, the standard deviation must also be propagated during the prediction. The general formulation to calculate the standard deviation is given below:

$$\sigma^2\{f(X_1, X_2, \ldots, X_n)\} = \sum_{i=1}^{n} \left(\frac{\partial f}{\partial X_i}\right)^2 \sigma^2(X_i)$$

where $f(X)$ represents a stochastic function, X_i represents each stochastic variable in the equation, and n is the number of stochastic variables. For SVMPC, those variables are $V(k)$, $Q_{\text{in}}(k)$, $Q_{\text{out}}(k)$, $Q_{\text{ov}}(k)$ and $n = 4$. The next step is to compute the partial derivative for each variable:

$$\frac{\partial\mathbb{E}\{V(k+1)\}}{\partial V(k)} = 1, \qquad \frac{\partial\mathbb{E}\{V(k+1)\}}{\partial Q_{\text{in}}(k)} = T_s$$

$$\frac{\partial\mathbb{E}\{V(k+1)\}}{\partial Q_{\text{out}}(k)} = -T_s, \qquad \frac{\partial\mathbb{E}\{V(k+1)\}}{\partial Q_{\text{ov}}(k)} = -T_s$$

Resulting in:

$$\sigma^2\{V(k+1)\} = \sigma^2\{V(k)\} + T_s^2(\sigma^2\{Q_{\text{in}}(k)\} + \sigma^2\{Q_{\text{out}}(k)\} + \sigma^2\{Q_{\text{ov}}(k)\})$$

The inequality constraints from Equation 7.15d to 7.15g are also reformulated, where Equation 7.15d is rewritten as a chance-constrained constraint. The constraints are separated into two sets, when $Q_{\text{ov}}(k) = 0$ and $Q_{\text{ov}}(k) > 0$:

- Lower bound considering $Q_{\text{ov}}(k) = 0$:

$$\mathbb{E}\{V(k)\} + T_s(\mathbb{E}\{Q_{\text{in}}(k)\} - \mathbb{E}\{Q_{\text{out}}(k)\}) \geq \sigma\{V(k) + T_s(Q_{\text{in}}(k) + Q_{\text{out}}(k))\}\Phi^{-1}(\zeta) - \theta_{\min} \quad (9.9)$$

- Lower bound considering $Q_{\text{ov}}(k) > 0$:

$$\mathbb{E}\{V(k)\} + T_s(\mathbb{E}\{Q_{\text{in}}(k)\} - \mathbb{E}\{Q_{\text{out}}(k)\} - \mathbb{E}\{Q_{\text{ov}}(k)\}) \geq 0 \quad (9.10)$$

- Upper bound considering $Q_{\text{ov}}(k) = 0$:

$$\mathbb{E}\{V(k)\} + T_s(\mathbb{E}\{Q_{\text{in}}(k)\}\} - \mathbb{E}\{Q_{\text{out}}(k)\}\}) \leq V_{\max} - \sigma\{V(k) + T_s(Q_{\text{in}}(k) + Q_{\text{out}}(k))\}\Phi^{-1}(\zeta) + \theta_{\max} \quad (9.11)$$

- Upper bound considering $Q_{\text{ov}}(k) > 0$:

$$\mathbb{E}\{V(k)\} + T_s(\mathbb{E}\{Q_{\text{in}}\}(k)\} - \mathbb{E}\{Q_{\text{out}}\}(k)\} - \mathbb{E}\{Q_{\text{ov}}\}(k)\}) \leq V_{\max} \quad (9.12)$$

where ζ is the desired probability confidence level, $\theta_{\min}$ is a slack variable for the lower bound and $\theta_{\max}$ is a slack variable for the upper bound. The interpretation here is that the term $\sigma\{V(k) + T_s(Q_{\text{in}}(k) - Q_{\text{out}}(k))\}\Phi^{-1}(\zeta)$ restricts the bounds to account for possible uncertainties. This term ensures that, with a certain confidence level (determined by ζ), the volume of the system will not exceed the maximum volume $V_{\max}$, accounting for the uncertainty in the inflows and outflows. When $Q_{\text{ov}}(k) = 0$, both Equations 9.9 and 9.10 are true, so feasibility is maintained. The same applies to Equations 9.11 and 9.12.

However, as soon as an overflow is measured or calculated, the constraint of Equations 9.10 and 9.12 prevents the volume from exceeding the system's capacity with a harder constraint, trying to force the system to avoid the overflow. The higher the standard deviation, the more restricted the bounds are. Furthermore, the slack variables are limited by:

$$0 \leq \theta_{\min} \leq \sigma\{V(k) + T_s(Q_{\text{in}}(k) + Q_{\text{out}}(k))\}\Phi^{-1}(\zeta) \qquad \text{and} \qquad 0 \leq \theta_{\max}$$

And, finally, $Q_{\text{out}}(k)$ and $Q_{\text{ov}}(k)$ are constrained following the equations below:

$$0 \leq \mathbb{E}\{Q_{\text{out}}(k)\} \leq Q_{\text{out}_{\max}} \qquad \text{and} \qquad 0 \leq \mathbb{E}\{Q_{\text{ov}}(k)\}$$

9.3.2 Optimisation Problem

Given the stochastic constraints and that the states $\boldsymbol{x}(k)$, and input $\boldsymbol{u}(k)$, are

$$\boldsymbol{x}(k) = [\mathbb{E}\{\boldsymbol{V}(k)\},\ \mathbb{E}\{\boldsymbol{Q}_{\text{ov}}(k)\},\ \mathbb{E}\{\boldsymbol{Q}_{\text{in}}(k)\},\ \boldsymbol{\theta}_{\min}(k),\ \boldsymbol{\theta}_{\max}(k)] \qquad \text{and} \qquad \boldsymbol{u}(k) = [\mathbb{E}\{\boldsymbol{Q}_{\text{out}}(k)\}]$$

the optimisation problem, where $\hat{\boldsymbol{u}}(k)$ is the optimal output, is defined as:

$$\hat{u}(k) = \arg\min_{u} \sum_{j=0}^{N-1} J(x(k+j), u(k+j)) \tag{9.13a}$$

subject to

$$\mathbb{E}\{V^t(k+j+1)\} = \mathbb{E}\{V^t(k+j)\} + T_s\big[\mathbb{E}\{Q^t_{\text{in}}(k+j)\} - \mathbb{E}\{Q^t_{\text{out}}(k+j)\} - \mathbb{E}\{Q^t_{\text{ov}}(k+j)\}\big], \qquad t = 1, 2, ..., N_t \tag{9.13b}$$

$$\sigma^2\{V^t(k+j+1)\} = \sigma^2\{V^t(k+j)\} + T_s^2\big(\sigma^2\{Q^t_{\text{in}}(k+j)\} + \sigma^2\{Q^t_{\text{out}}(k+j)\} + \sigma^2\{Q^t_{\text{ov}}(k+j)\}\big), \qquad t = 1, 2, ..., N_t \tag{9.13c}$$

$$\mathbb{E}\{Q^t_{in}\} = \mathbb{E}\{Q^t_{catchment}\} + \sum_{i \in N^*_{\text{in}}} \mathbb{E}\{Q^i_{out}\}, \qquad t = 1, 2, ..., N_t \tag{9.13d}$$

$$\mathbb{E}\{V^t(k+j)\} + T_s\big(\mathbb{E}\{Q^t_{\text{in}}(k+j)\} + \mathbb{E}\{Q^t_{\text{out}}(k+j)\}\big) \geq \sigma\{V^t(k+j) + T_s(Q^t_{\text{in}}(k+j) + Q^t_{\text{out}}(k+j))\}\Phi^{-1}(\zeta) - \theta^t_{\min}, \qquad t = 1, 2, ..., N_t \tag{9.13e}$$

$$\mathbb{E}\{V^t(k+j)\} + T_s\big(\mathbb{E}\{Q^t_{\text{in}}(k+j)\} - \mathbb{E}\{Q^t_{\text{out}}(k+j)\} - \mathbb{E}\{Q^t_{\text{ov}}(k+j)\}\big) \geq 0, \qquad t = 1, 2, ..., N_t \tag{9.13f}$$

$$\mathbb{E}\{V^t(k+j)\} + T_s\big(\mathbb{E}\{Q^t_{\text{in}}(k+j)\} - \mathbb{E}\{Q^t_{\text{out}}(k+j)\}\big) \leq V^t_{\max} - \sigma\{V^t(k+j) + T_s(Q^t_{\text{in}}(k+j) + Q^t_{\text{out}}(k+j))\}\Phi^{-1}(\zeta) + \theta^t_{\max}, \qquad t = 1, 2, ..., N_t \tag{9.13g}$$

$$\mathbb{E}\{V^t(k+j)\} + T_s\big(\mathbb{E}\{Q^t_{\text{in}}(k+j)\} - \mathbb{E}\{Q^t_{\text{out}}(k+j)\} - \mathbb{E}\{Q^t_{\text{ov}}(k+j)\}\big) \leq V^t_{\max}, \qquad t = 1, 2, ..., N_t \tag{9.13h}$$

$$0 \leq \sum_{i \in N^*_{\text{wwtp}}} \mathbb{E}\{Q^i_{\text{out}}(k+j)\} \leq Q_{\text{wwtp}_{\max}}, \qquad t = 1, 2, ..., N_t \tag{9.13i}$$

$$0 \leq \mathbb{E}\{Q^t_{\text{out}}(k)\} \leq Q^t_{\text{out}_{\max}}, \qquad t = 1, 2, ..., N_t \tag{9.13j}$$

$$\mathbb{E}\{Q^t_{\text{ov}}(k+j)\} \geq 0, \qquad t = 1, 2, ..., N_t \tag{9.13k}$$

$$0 \leq \theta^t_{\min}(k+j) \leq \sigma\{V^t(k+j) + T_s(Q^t_{\text{in}}(k+j) + Q_{\text{out}}(k+j))\}\Phi^{-1}(\zeta), \qquad t = 1, 2, ..., N_t \tag{9.13l}$$

$$0 \leq \theta^t_{\max}(k+j), \qquad t = 1, 2, ..., N_t \tag{9.13m}$$

The internal model used for the prediction can be seen in Equation 9.13b, including the propagation of the standard deviation in future steps in Equation 9.13c. In addition, the cost function for SVMPC closely resembles that of VMPC, with the only difference being that the stochastic method includes an additional slack variable for the lower bound. However, both slack variables are minimised using the same weight, ϵ, maintaining the number of weights to choose constant. Hence, the cost function J is calculated by:

$$J(x(k), u(k)) = J(\mathbb{E}\{V(k)\}, \mathbb{E}\{Q_{\text{out}}(k)\}, \mathbb{E}\{Q_{\text{in}}(k)\}, \theta_{\min}(k), \theta_{\max}(k), \mathbb{E}\{Q_{\text{out}}(k)\}) \tag{9.14}$$

$$= \alpha\phi_1(k) + \beta\phi_2(k) + \gamma\phi_3(k) + \epsilon(\phi_4(k) + \phi_5(k)) \tag{9.15}$$

where (α, β, γ, ϵ) are the weights for the objectives (ϕ_1, ϕ_2, ϕ_3, (ϕ_4, ϕ_5)), which are described below:

- ϕ_1, in Equation 9.16, is used to homogeneously store the volume within all tank structures in the wastewater network.

$$\phi_1(k) = \sum_{i=1}^{N_t} \left(\mathbb{E}\{V^i(k)\} - \frac{V^i_{\max}}{\sum_{j=1}^{N} V^j_{\max}} \sum_{n=1}^{N_t} \mathbb{E}\{V_n(k)\} \right)^2 \tag{9.16}$$

- ϕ_2, in Equation 9.17, keeps the flow towards the wastewater treatment plant near the operating reference value defined by Q_{ref}.

$$\phi_2(k) = \sum_{j \in N_{up}} \left(Q^j_{\text{ref}} - \sum_{i \in N^*_t} \mathbb{E}\{Q^i_{\text{out}}(k - d^{i,t})\} \right)^2 \tag{9.17}$$

  where Q_{ref} is the reference flow for the i^{th} tank, which includes $Q_{\text{wwtp}_{\text{ref}}}$ as the inflow reference to the WWTP, Q_{out} is the outflow from each tank, $d_{i,t}$ represents the transport time of the i^{th} tank to the destination tank m, N^*_t are all tanks draining in the destination t and N_{up} are all tanks that have an upstream tank and the wastewater treatment plant.

- ϕ_3, in Equation 9.18, is used to minimise the overflow.

$$\phi_3(k) = \sum_{i=1}^{N_t} (\mathbb{E}\{Q^i_{\text{ov}}(k)\} - \text{NL})^2 \tag{9.18}$$

- ϕ_4, in Equation 9.19, is used to minimise the slack variable $\theta_{\min}$.

$$\phi_4(k) = \sum_{i=1}^{N_t} (\theta^i_{\min})^2 \tag{9.19}$$

- ϕ_5, in Equation 9.20, is used to minimise the slack variable $\theta_{\max}$.

$$\phi_5(k) = \sum_{i=1}^{N_t} (\theta^i_{\max})^2 \tag{9.20}$$

Finally, the control loop's algorithm for the SVMPC can summarised as below:

Control Algorithm

(a) Initialise $\boldsymbol{x}(k) = \boldsymbol{x}(0)$, where $\boldsymbol{x}(0) = [\mathbb{E}\{\boldsymbol{V}(0)\},\ \mathbb{E}\{\boldsymbol{Q}_{\text{ov}}(0)\},\ \boldsymbol{\theta}_{\min}(0),\ \boldsymbol{\theta}_{\max}(0)]$ is the current state of the system, and the standard deviations $\sigma\{\boldsymbol{V}(k)\}$, $\sigma\{\boldsymbol{Q}_{\text{in}}(k)\}$, $\sigma\{\boldsymbol{Q}_{\text{out}}(k)\}$, $\sigma\{\boldsymbol{Q}_{\text{ov}}(k)\}$;

(b) Estimate $\mathbb{E}\{\boldsymbol{Q}_{\text{in}}(k)\}$ using Equation 9.7;

(c) Solve the optimisation problem as in Equation 9.13a and obtain the optimal control sequence $\hat{\boldsymbol{u}}(k)$;

(d) At time k, apply the first input $\boldsymbol{u}(k) = \boldsymbol{Q}_{\text{out}}(k)$ of the optimal control sequence to the UDS;

(e) Wait for next control loop $k = k + 1$;

(f) Measure $\boldsymbol{V}(k)$ and $\boldsymbol{Q}_{\text{out}}(k)$, calculate $\boldsymbol{Q}_{\text{ov}}(k)$, and update the expected values as $\mathbb{E}\{\boldsymbol{V}(k)\} = u_s \cdot \boldsymbol{V}(k) + u_{\text{off}}$, $\mathbb{E}\{\boldsymbol{Q}_{\text{out}}(k)\} = u_s \cdot \boldsymbol{Q}_{\text{out}}(k) + u_{\text{off}}$, and $\mathbb{E}\{\boldsymbol{Q}_{\text{ov}}(k)\} = u_s \cdot \boldsymbol{Q}_{\text{ov}}(k) + u_{\text{off}}$, then return to Step (b).

The following scenarios are considered for standard deviations:

- In all scenarios, a standard deviation for the inflow $Q_{\text{in}}(k)$ is determined to ascertain possible errors in the estimation during the control loop:

$$\sigma\{Q_{\text{in}}(k)\} = u_p * \frac{Q_{\text{in}}(k)}{n}$$

  where n represents a fraction of the actual value.

- The first scenario considers uncertainties on the volume, therefore $\sigma\{Q_{\text{out}}(k)\} = 0$, $\sigma\{Q_{\text{ov}}(k)\} = 0$ and

$$\sigma\{V(k)\} = u_p * (V_{\max} - V(k))$$

- The second scenario considers uncertainties on the outflow, therefore, at $k = 0$, $\sigma\{V(0)\} = 0$ and $\sigma\{Q_{\text{ov}}(k)\} = 0$ and

$$\sigma\{Q_{\text{out}}(k)\} = u_p * (Q_{\text{out}_{\max}} - Q_{\text{out}}(k))$$

- The third scenario considers uncertainties on the overflow, therefore, at $k = 0$, $\sigma\{V(0)\} = 0$ and $\sigma\{Q_{\text{out}}(k)\} = 0$ and

$$\sigma\{Q_{\text{ov}}(k)\} = u_p * Q_{\text{ov}}(k)$$

For practical purposes, in future simulations $n = 3$, therefore, the input standard deviation is a third of the actual value. Moreover, SVMPC introduces a new parameter: the confidence level ζ. The confidence level represents the probability with which it is desired to ensure that a certain constraint is satisfied. Specifically, it indicates the probability that the controlled system will not exceed its constraints, e.g. the probability that the maximum volume of a SU is reached. For instance, if $\zeta = 0.95$, it means that it is expected that 95% of the time the constraint is violated. In the context of urban drainage systems, such as controlling the volume in a SU, higher confidence level, such as $\zeta = 0.99$, would ensure that the volume of the unit remains below its maximum capacity 99% of the time, taking into account uncertainties. This allows the system to minimise the risk of overflow while maintaining efficient operation.

Additionally, the standard deviation is propagated across the future horizon to account for errors in subsequent predictions. For example, considering that the upper bound for $V(k+1)$ when there are no overflows is defined by the constraint in Equation 9.13e, the upper bound can be expressed as:

$$\text{upper bound} = V_{\max} - \sigma\{V(k+j) + T_s(Q_{\text{in}}(k) + Q_{\text{out}}(k+j))\}\Phi^{-1}(\zeta)$$

The equation accounts for the uncertainties in both inflows and outflows, and the upper bound is adjusted accordingly to ensure that the system remains within its capacity while accommodating these uncertainties. In the case where the uncertainty in the outflow is $u_p = 0.25$ (a 25% variation of the difference between the maximum outflow and the expected outflow), Figure 9.15 illustrates the behaviour of the

upper bound for a storage unit for $\zeta = (0.6, 0.7, 0.8, 0.9, 0.95)$, looking at four steps in the prediction.

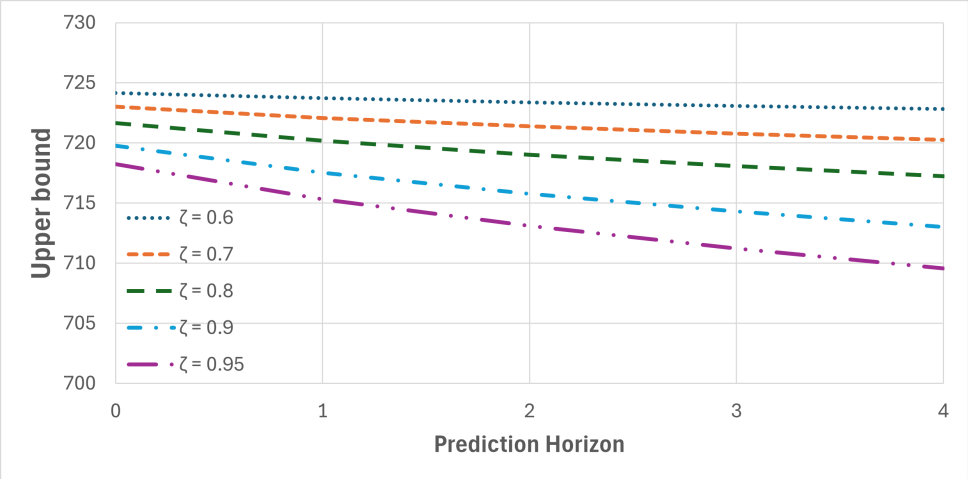

Figure 9.15: Confidence level.

As shown in the graph, the upper bound decreases as ζ increases. This is due to the fact that a higher ζ value corresponds to a higher probability of violating the constraint. Consequently, the system must adopt a more conservative approach, lowering the upper bound to prevent exceeding the maximum allowable volume ($V_{\max}$) with a higher degree of confidence. This illustrates how the algorithm adjusts its predictions to ensure robust performance under uncertain conditions, where the confidence level influences the system's tolerance for violations. In essence, the higher the confidence level ζ, the more conservative the controller becomes in managing the upper bound, reducing the risk of overflow. This behaviour is particularly important for ensuring that the system can operate safely in various uncertainty scenarios.

In the next section, the performance of the SVMPC is assessed through validation methodology, comparing the results with VMPC for different metrics.

9.3.3 Methodology Validation

The validation of the SVMPC is conducted by evaluating its control performance under the same conditions presented in Section 9.1. Given that the initial weights of the objective function are unknown, they are chosen to match those used in VMPC since the overall objectives of both controllers are similar, thus the weights are α, β, γ, $\epsilon = (6.9, 56.5, 106.4, 153.0)$ and ζ is varied across $[0.6, 0.8, 0.95]$. In this evaluation, the metrics are the volume overflow, $Q_{\text{ov}_{\text{total}}}$, the load overflow, $m^{\text{NH}_4}_{\text{ov}_{\text{total}}}$, the error coefficient $\%\mathbf{F}_Q$ and $\%\mathbf{F}_m$ for both types of overflow, and ξ_{rain}. In each scenario, the uncertainty is isolated, e.g. if the uncertainty is considered in the volume, $\sigma\{Q_{\text{out}}(k)\} = 0$ and $\sigma\{Q_{\text{ov}}(k)\} = 0$. A key performance indicator is the controller's ability to remain stable under increasing uncertainties, keeping $\%\mathbf{F}_Q$ and $\%\mathbf{F}_m$ at low values. Since the weights were not optimised to reach minimal overflow values, the main objective of the validation is not to compare the absolute overflow values between SVMPC and VMPC, but rather assess the stability and robustness of SVMPC. A more detailed analysis of how to define the weights for SVMPC will be presented later in this chapter.

Uncertainty on $V(k)$

Firstly, SVMPC is evaluated considering the uncertainty in $V(k)$. The analysis begins by comparing u_p and evaluating the performance of SVMPC against VMPC for varying values of ζ, across $u_p = [0\%, 5\%, 10\%, 25\%, 50\%, 75\%]$. The results presented in Table 9.10 show that, in general, SVMPC does not outperform VMPC in any of the scenarios analysed. Specifically, as ζ increases, the stochastic method demonstrates a notable performance decrease, reaching an increase in volume and load overflow of 8. 2% and 14. 1% for $\zeta = 0.95$ and $u_p = 75\%$.

Table 9.10: Volume uncertainty: Comparison between VMPC and SVMPC for u_p.

	VMPC					
u_p	0%	5%	10%	25%	50%	75%
$Q_{\text{ov}_{\text{total}}}$	167.434	168.971	169.771	171.595	173.193	174.031
$\%\mathbf{F}_Q$		0.92%	1.4%	2.49%	3.44%	3.94%
$m^{\text{NH}_4}_{\text{ov}_{\text{total}}}$	1072.366	1088.102	1094.839	1118.461	1136.925	1152.927
$\%\mathbf{F}_m$		1.47%	2.1%	4.3%	6.02%	7.51%
ξ_{rain}	7.926	6.221	4.853	2.314	1.222	1.152
	SVMPC - $\zeta = 0.60$					
u_p	0%	5%	10%	25%	50%	75%
$Q_{\text{ov}_{\text{total}}}$	177.352	179.109	180.339	182.989	185.564	187.094
$\%\mathbf{F}_Q$		0.99%	1.68%	3.18%	4.63%	5.49%
$m^{\text{NH}_4}_{\text{ov}_{\text{total}}}$	1276.828	1292.962	1305.568	1331.697	1359.346	1376.410
$\%\mathbf{F}_m$		1.26%	2.25%	4.3%	6.46%	7.8%
ξ_{rain}	8.495	7.398	6.852	5.661	5.750	5.937
	SVMPC - $\zeta = 0.80$					
u_p	0%	5%	10%	25%	50%	75%
$Q_{\text{ov}_{\text{total}}}$	177.605	179.862	181.981	186.824	191.057	192.190
$\%\mathbf{F}_Q$		1.27%	2.46%	5.19%	7.57%	8.21%
$m^{\text{NH}_4}_{\text{ov}_{\text{total}}}$	1278.572	1300.931	1317.646	1371.800	1439.533	1456.452
$\%\mathbf{F}_m$		1.75%	3.06%	7.29%	12.59%	13.91%
ξ_{rain}	8.576	7.724	7.432	7.029	6.728	6.253
	SVMPC - $\zeta = 0.95$					
u_p	0%	5%	10%	25%	50%	75%
$Q_{\text{ov}_{\text{total}}}$	178.115	180.832	184.031	189.964	192.346	192.718
$\%\mathbf{F}_Q$		1.53%	3.32%	6.65%	7.99%	8.2%
$m^{\text{NH}_4}_{\text{ov}_{\text{total}}}$	1282.477	1307.181	1339.221	1422.861	1458.449	1463.838
$\%\mathbf{F}_m$		1.93%	4.42%	10.95%	13.72%	14.14%
ξ_{rain}	8.643	7.957	7.708	7.708	6.973	6.244

Naturally, for scenarios without uncertainty ($u_p = 0\%$), a worse performance is expected by SVMPC since the algorithm is inherently more conservative in its approach. It could also be due to the poor choice of weights α, β, γ and ϵ, which were originally selected based on the sensitivity analysis conducted

for VMPC. This indicates that the stochastic controller's parameters may need further optimisation for better adaptation to uncertainty.

The next set of simulations compares the performance of the controllers, focusing on the impact of u_{off} for both $u^{\text{vol+}}_{\text{offset}}$ and $u^{\text{vol-}}_{\text{offset}}$ across the sets: u_{off} = [0%, 5%, 10%, 25%, 50%, 75%] and u_{off} = [0%, -5%, -10%, -25%, -50%, -75%], respectively. The results for $u^{\text{vol+}}_{\text{offset}}$ are presented in Table 9.11. In this case, although SVMPC shows slightly worse performance in terms of absolute volume and load overflow values compared to VMPC, the stochastic method demonstrates superior robustness under higher uncertainties in the network. As the uncertainty level increases, SVMPC becomes more resilient, the method is even improving its performance under higher uncertainties for volume and load overflow metrics. In contrast, VMPC reached a 3.2% and 10.2% increase in volume and load overflow, respectively, a percentage much higher than SVMPC, highlighting the ability of the stochastic method to better handle uncertainty.

Table 9.11: Volume uncertainty: Comparison between VMPC and SVMPC for $u^{\text{vol+}}_{\text{offset}}$.

	VMPC					
u_{off}	0%	5%	10%	25%	50%	75%
$Q_{\text{ov}_{\text{total}}}$	167.434	166.782	167.017	168.22	170.44	172.75
$\%\mathbf{F}_Q$		-0.39%	-0.25%	0.47%	1.8%	3.17%
$m^{\text{NH}_4}_{\text{ov}_{\text{total}}}$	1072.366	1066.461	1071.089	1086.543	1129.77	1181.609
$\%\mathbf{F}_m$		-0.55%	-0.12%	1.32%	5.35%	10.19%
ξ_{rain}	7.926	8.573	9.062	9.594	9.849	9.909
	SVMPC - $\zeta = 0.60$					
u_{off}	0%	5%	10%	25%	50%	75%
$Q_{\text{ov}_{\text{total}}}$	177.352	176.486	176.149	175.717	175.582	175.571
$\%\mathbf{F}_Q$		-0.49%	-0.68%	-0.92%	-1.0%	-1.0%
$m^{\text{NH}_4}_{\text{ov}_{\text{total}}}$	1276.828	1269.181	1264.995	1261.414	1259.812	1258.673
$\%\mathbf{F}_m$		-0.6%	-0.93%	-1.21%	-1.33%	-1.42%
ξ_{rain}	8.495	8.904	9.27	9.694	9.919	9.949
	SVMPC - $\zeta = 0.80$					
u_{off}	0%	5%	10%	25%	50%	75%
$Q_{\text{ov}_{\text{total}}}$	177.605	176.63	176.15	175.718	175.582	175.57
$\%\mathbf{F}_Q$		-0.55%	-0.82%	-1.06%	-1.14%	-1.15%
$m^{\text{NH}_4}_{\text{ov}_{\text{total}}}$	1278.572	1270.898	1265.249	1261.417	1259.809	1258.673
$\%\mathbf{F}_m$		-0.6%	-1.04%	-1.34%	-1.47%	-1.56%
ξ_{rain}	8.576	8.839	9.283	9.694	9.92	9.949
	SVMPC - $\zeta = 0.95$					
u_{off}	0%	5%	10%	25%	50%	75%
$Q_{\text{ov}_{\text{total}}}$	178.115	176.624	176.207	175.718	175.583	175.58
$\%\mathbf{F}_Q$		-0.84%	-1.07%	-1.35%	-1.42%	-1.42%
$m^{\text{NH}_4}_{\text{ov}_{\text{total}}}$	1282.477	1270.333	1265.667	1261.421	1259.794	1258.895
$\%\mathbf{F}_m$		-0.95%	-1.31%	-1.64%	-1.77%	-1.84%
ξ_{rain}	8.643	8.942	9.276	9.694	9.919	9.919

Further analysis, presented in Table 9.12, investigates $u^{\text{vol-}}_{\text{offset}}$. For SVMPC with $\zeta = 0.6$, the performance

is comparable to that of VMPC in terms of absolute volume and load overflow values. In fact, when comparing the percentage increase with the base case ($u_{\text{off}} = 0\%$), SVMPC slightly outperforms VMPC. This indicates that the stochastic controller at this confidence level can handle underestimation effectively, providing a robust solution in such scenarios. However, as the confidence level ζ increases, the controller becomes excessively conservative and restrictive. This behaviour is evident in the results for $\zeta = 0.8$ and $\zeta = 0.95$, where the performance is hindered by the controller's increased caution in handling uncertainty. his over-conservatism leads to a significant increase in overflow values, especially for larger uncertainties, suggesting that while higher confidence levels might improve stability in some cases, they can also deteriorate performance by under-utilising the system's capacity.

Table 9.12: Volume uncertainty: Comparison between VMPC and SVMPC for $u_{\text{offset}}^{\text{vol-}}$.

	VMPC					
u_{off}	0%	−5%	−10%	−25%	−50%	−75%
$Q_{\text{ov}_{\text{total}}}$	167.43	175.95	182.16	201.26	259.73	444.55
$\%\mathbf{F}_Q$		5.09%	8.80%	20.2%	55.12%	165.51%
$m_{\text{ov}_{\text{total}}}^{\text{NH}_4}$	1072.37	1196.53	1266.67	1571.67	2852.36	10867.60
$\%\mathbf{F}_m$		11.58%	18.12%	46.56%	165.99%	913.42%
ξ_{rain}	7.93	6.13	3.52	-6.71	-31.34	-59.93
	SVMPC - $\zeta = 0.60$					
u_{off}	0%	−5%	−10%	−25%	−50%	−75%
$Q_{\text{ov}_{\text{total}}}$	177.35	180.26	183.16	192.51	221.55	464.07
$\%\mathbf{F}_Q$		1.64%	3.28%	8.55%	24.92%	161.66%
$m_{\text{ov}_{\text{total}}}^{\text{NH}_4}$	1276.83	1307.45	1345.88	1489.57	2356.58	11448.42
$\%\mathbf{F}_m$		2.40%	5.41%	16.66%	84.56%	796.63%
ξ_{rain}	8.50	7.26	6.02	2.74	2.58	-61.73
	SVMPC - $\zeta = 0.80$					
u_{off}	0%	−5%	−10%	−25%	−50%	−75%
$Q_{\text{ov}_{\text{total}}}$	177.61	180.52	183.53	193.95	255.20	715.08
$\%\mathbf{F}_Q$		1.64%	3.34%	9.20%	43.69%	302.62%
$m_{\text{ov}_{\text{total}}}^{\text{NH}_4}$	1278.57	1311.34	1348.74	1513.54	3891.63	21221.87
$\%\mathbf{F}_m$		2.56%	5.49%	18.38%	204.37%	1559.81%
ξ_{rain}	8.58	7.18	5.80	2.16	4.16	-72.65
	SVMPC - $\zeta = 0.95$					
u_{off}	0%	−5%	−10%	−25%	−50%	−75%
$Q_{\text{ov}_{\text{total}}}$	178.12	180.92	183.76	194.08	258.86	873.24
$\%\mathbf{F}_Q$		1.57%	3.17%	8.96%	45.33%	390.27%
$m_{\text{ov}_{\text{total}}}^{\text{NH}_4}$	1282.48	1315.22	1350.74	1514.67	4073.72	26649.29
$\%\mathbf{F}_m$		2.55%	5.32%	18.10%	217.64%	1977.95%
ξ_{rain}	8.64	7.12	5.89	2.28	7.07	-78.18

Uncertainty on $Q_{\text{out}}(k)$

The next analysis compares SVMPC with VMPC for the outflow uncertainties in terms of u_p and u_{off} varied across different ranges. In Table 9.13 the results for the variation of u_p, show that, in this instance, it is slightly more stable than VMPC for $\zeta = 0.6$ and $\zeta = 0.8$, and comparable with $\zeta = 0.95$, although the increase in all metrics is not substantial, reaching an increase of less than 1%. The results for ξ_{rain} also reveal a slight increase in sensitivity for SVMPC. Specifically, the variation of ξ_{rain} for SVMPC with $\zeta = 0.6$ is 0.07, while for VMPC it is 0.15. This suggests that SVMPC is slightly less sensitive to variability in the inflows, yet this increase in deviation is minimal and does not significantly affect the overall performance of the system.

Table 9.13: Outflow uncertainty: Comparison between VMPC and SVMPC for u_p.

	VMPC					
u_p	0%	25%	75%	100%	125%	175%
$Q_{\text{ov}_{\text{total}}}$	167.434	167.463	167.692	167.749	167.808	168.03
$\%\mathbf{F}_Q$		0.02%	0.15%	0.19%	0.22%	0.36%
$m^{\text{NH}_4}_{\text{ov}_{\text{total}}}$	1072.366	1074.472	1078.197	1077.432	1077.661	1082.022
$\%\mathbf{F}_m$		0.2%	0.54%	0.47%	0.49%	0.9%
ξ_{rain}	7.926	7.866	7.824	7.815	7.808	7.777
	SVMPC - $\zeta = 0.60$					
u_p	0%	25%	75%	100%	125%	175%
$Q_{\text{ov}_{\text{total}}}$	177.352	177.202	177.374	177.473	177.511	177.551
$\%\mathbf{F}_Q$		-0.08%	0.01%	0.07%	0.09%	0.11%
$m^{\text{NH}_4}_{\text{ov}_{\text{total}}}$	1276.828	1274.96	1277.835	1278.389	1278.681	1276.082
$\%\mathbf{F}_m$		-0.15%	0.08%	0.12%	0.15%	-0.06%
ξ_{rain}	8.495	8.431	8.418	8.404	8.403	8.422
	SVMPC - $\zeta = 0.80$					
u_p	0%	25%	75%	100%	125%	175%
$Q_{\text{ov}_{\text{total}}}$	177.605	177.249	177.574	177.724	177.881	178.347
$\%\mathbf{F}_Q$		-0.2%	-0.02%	0.07%	0.16%	0.42%
$m^{\text{NH}_4}_{\text{ov}_{\text{total}}}$	1278.572	1275.174	1279.241	1281.139	1282.073	1286.669
$\%\mathbf{F}_m$		-0.27%	0.05%	0.2%	0.27%	0.63%
ξ_{rain}	8.576	8.425	8.306	8.199	8.127	8.141
	SVMPC - $\zeta = 0.95$					
u_p	0%	25%	75%	100%	125%	175%
$Q_{\text{ov}_{\text{total}}}$	178.115	177.325	178.045	178.178	178.532	179.386
$\%\mathbf{F}_Q$		-0.44%	-0.04%	0.04%	0.23%	0.71%
$m^{\text{NH}_4}_{\text{ov}_{\text{total}}}$	1282.477	1275.738	1282.922	1284.401	1287.449	1292.745
$\%\mathbf{F}_m$		-0.53%	0.03%	0.15%	0.39%	0.8%
ξ_{rain}	8.643	8.419	8.118	7.944	7.996	7.817

In the scenario for $u^{\text{out+}}_{\text{offset}}$, shown in Table 9.14, the stochastic controller demonstrates a better performance against VMPC. In this case, VMPC experiences a 1.1% and 3.1% higher volume and load overflow,

respectively, while stochastic MPC improved the system performance. The more conservative nature of SVMPC in this overestimation scenario allows better control and stability, preventing larger fluctuations in the system's behaviour.

Table 9.14: Outflow uncertainty: Comparison between VMPC and SVMPC for $u_{\text{offset}}^{\text{out+}}$.

	VMPC					
u_{off}	0%	5%	10%	25%	50%	75%
$Q_{\text{ov}_{\text{total}}}$	167.434	167.497	167.45	167.621	168.324	169.353
$\%\mathbf{F}_Q$		0.04%	0.01%	0.11%	0.53%	1.15%
$m_{\text{ov}_{\text{total}}}^{\text{NH}_4}$	1072.366	1075.368	1075.381	1075.443	1086.521	1105.802
$\%\mathbf{F}_m$		0.28%	0.28%	0.29%	1.32%	3.12%
ξ_{rain}	7.926	7.886	7.854	7.824	7.71	7.699
	SVMPC - $\zeta = 0.60$					
u_{off}	0%	5%	10%	25%	50%	75%
$Q_{\text{ov}_{\text{total}}}$	177.352	177.159	177.125	177.069	177.083	177.037
$\%\mathbf{F}_Q$		-0.11%	-0.13%	-0.16%	-0.15%	-0.18%
$m_{\text{ov}_{\text{total}}}^{\text{NH}_4}$	1276.828	1275.209	1274.705	1273.574	1270.735	1265.138
$\%\mathbf{F}_m$		-0.13%	-0.17%	-0.25%	-0.48%	-0.92%
ξ_{rain}	8.495	8.43	8.399	8.378	8.347	8.35
	SVMPC - $\zeta = 0.80$					
u_{off}	0%	5%	10%	25%	50%	75%
$Q_{\text{ov}_{\text{total}}}$	177.605	177.212	177.172	177.116	177.119	177.076
$\%\mathbf{F}_Q$		-0.22%	-0.24%	-0.28%	-0.27%	-0.3%
$m_{\text{ov}_{\text{total}}}^{\text{NH}_4}$	1278.572	1275.688	1275.246	1274.071	1271.089	1265.647
$\%\mathbf{F}_m$		-0.23%	-0.26%	-0.35%	-0.59%	-1.01%
ξ_{rain}	8.576	8.45	8.393	8.37	8.353	8.362
	SVMPC - $\zeta = 0.95$					
u_{off}	0%	5%	10%	25%	50%	75%
$Q_{\text{ov}_{\text{total}}}$	178.115	177.289	177.252	177.18	177.172	177.131
$\%\mathbf{F}_Q$		-0.46%	-0.48%	-0.52%	-0.53%	-0.55%
$m_{\text{ov}_{\text{total}}}^{\text{NH}_4}$	1282.477	1276.453	1275.994	1274.687	1271.321	1266.621
$\%\mathbf{F}_m$		-0.47%	-0.51%	-0.61%	-0.87%	-1.24%
ξ_{rain}	8.643	8.487	8.393	8.365	8.354	8.378

The final analysis for $u_{\text{offset}}^{\text{out-}}$, shown in Table 9.15, reveals that SVMPC in these scenarios is considerably more stable against increased uncertainties. It maintains performance similar to the base scenario with $u_{\text{off}} = 0\%$, while VMPC shows up to a 5.3% and 15.0% increase in volume and load overflow. The stochastic framework in the face of this uncertainty shows the advantage of SVMPC in handling unpredictable conditions, preventing potential underperformance as observed in VMPC.

Table 9.15: Outflow uncertainty: Comparison between VMPC and SVMPC for $u_{\text{offset}}^{\text{out-}}$.

	VMPC					
u_{off}	0%	−5%	−10%	−25%	−50%	−75%
$Q_{\text{ov}_{\text{total}}}$	167.434	167.791	168.256	170.937	174.586	176.381
$\%\mathbf{F}_Q$		0.21%	0.49%	2.09%	4.27%	5.34%
$m_{\text{ov}_{\text{total}}}^{\text{NH}_4}$	1072.366	1081.025	1087.939	1139.193	1200.527	1232.686
$\%\mathbf{F}_m$		0.81%	1.45%	6.23%	11.95%	14.95%
ξ_{rain}	7.926	7.737	7.675	7.622	7.483	7.203
	SVMPC - $\zeta = 0.60$					
u_{off}	0%	−5%	−10%	−25%	−50%	−75%
$Q_{\text{ov}_{\text{total}}}$	177.352	177.237	177.256	177.7	178.477	178.933
$\%\mathbf{F}_Q$		-0.06%	-0.05%	0.2%	0.63%	0.89%
$m_{\text{ov}_{\text{total}}}^{\text{NH}_4}$	1276.828	1275.548	1275.18	1278.754	1286.943	1292.018
$\%\mathbf{F}_m$		-0.1%	-0.13%	0.15%	0.79%	1.19%
ξ_{rain}	8.495	8.334	8.284	8.008	7.285	6.295
	SVMPC - $\zeta = 0.80$					
u_{off}	0%	−5%	−10%	−25%	−50%	−75%
$Q_{\text{ov}_{\text{total}}}$	177.605	177.271	177.41	177.909	178.641	179.134
$\%\mathbf{F}_Q$		-0.19%	-0.11%	0.17%	0.58%	0.86%
$m_{\text{ov}_{\text{total}}}^{\text{NH}_4}$	1278.572	1275.838	1276.372	1283.836	1292.32	1299.352
$\%\mathbf{F}_m$		-0.21%	-0.17%	0.41%	1.08%	1.63%
ξ_{rain}	8.576	8.345	8.295	8.258	8.147	7.701
	SVMPC - $\zeta = 0.95$					
u_{off}	0%	−5%	−10%	−25%	−50%	−75%
$Q_{\text{ov}_{\text{total}}}$	178.115	177.445	177.506	177.965	178.675	179.176
$\%\mathbf{F}_Q$		-0.38%	-0.34%	-0.08%	0.31%	0.6%
$m_{\text{ov}_{\text{total}}}^{\text{NH}_4}$	1282.477	1276.938	1276.855	1283.16	1292.389	1299.64
$\%\mathbf{F}_m$		-0.43%	-0.44%	0.05%	0.77%	1.34%
ξ_{rain}	8.643	8.366	8.306	8.294	8.193	7.78

Uncertainty on $Q_{\mathbf{ov}}(k)$

The final uncertainty evaluation investigates the effects of varying both u_p and u_{off}, comparing SVMPC with VMPC. The results are shown in Tables 9.16, 9.17, and 9.18. In general, SVMPC consistently demonstrates more stable performance when uncertainty increases, although VMPC also shows a relatively stable behaviour. Specifically, for $u^{\text{ov+}}_{\text{offset}}$, SVMPC shows a significant improvement over VMPC. For instance, the load overflow decreases by up to 13.9% for SVMPC with $\zeta = 0.8$, while VMPC only achieves a reduction of 5.8% in the same scenario. The main reason for the improvement with the overestimation of the overflow is that the controller predicts the overflow earlier, which means that the actuator moves to $Q_{\text{out}_{\text{max}}}$ more often.

Table 9.16: Overflow uncertainty: Comparison between VMPC and SVMPC for u_p.

	VMPC					
u_p	0%	50%	100%	150%	175%	200%
$Q_{\text{ov}_{\text{total}}}$	167.434	167.682	167.661	167.609	167.595	167.552
$\%\mathbf{F}_Q$		0.15%	0.14%	0.10%	0.10%	0.07%
$m^{\text{NH}_4}_{\text{ov}_{\text{total}}}$	1072.366	1074.136	1071.316	1068.024	1066.955	1064.954
$\%\mathbf{F}_m$		0.17%	-0.10%	-0.40%	-0.50%	-0.69%
ξ_{rain}	7.926	7.889	7.876	7.872	7.868	7.871
	SVMPC - $\zeta = 0.60$					
u_p	0%	50%	100%	150%	175%	200%
$Q_{\text{ov}_{\text{total}}}$	177.352	177.283	177.274	177.284	177.291	177.290
$\%\mathbf{F}_Q$		-0.04%	-0.04%	-0.04%	-0.03%	-0.03%
$m^{\text{NH}_4}_{\text{ov}_{\text{total}}}$	1276.828	1275.935	1275.945	1275.404	1275.199	1275.175
$\%\mathbf{F}_m$		-0.07%	-0.07%	-0.11%	-0.13%	-0.13%
ξ_{rain}	8.495	8.478	8.485	8.491	8.491	8.492
	SVMPC - $\zeta = 0.80$					
u_p	0%	50%	100%	150%	175%	200%
$Q_{\text{ov}_{\text{total}}}$	177.605	177.312	177.361	177.403	177.416	177.459
$\%\mathbf{F}_Q$		-0.16%	-0.14%	-0.11%	-0.11%	-0.08%
$m^{\text{NH}_4}_{\text{ov}_{\text{total}}}$	1278.572	1276.302	1276.191	1275.813	1275.392	1275.008
$\%\mathbf{F}_m$		-0.18%	-0.19%	-0.22%	-0.25%	-0.28%
ξ_{rain}	8.576	8.491	8.497	8.527	8.538	8.544
	SVMPC - $\zeta = 0.95$					
u_p	0%	50%	100%	150%	175%	200%
$Q_{\text{ov}_{\text{total}}}$	178.115	177.360	177.477	177.586	177.646	177.689
$\%\mathbf{F}_Q$		-0.42%	-0.36%	-0.30%	-0.26%	-0.24%
$m^{\text{NH}_4}_{\text{ov}_{\text{total}}}$	1282.477	1276.576	1276.908	1276.135	1276.478	1275.044
$\%\mathbf{F}_m$		-0.46%	-0.43%	-0.49%	-0.47%	-0.58%
ξ_{rain}	8.643	8.496	8.538	8.573	8.594	8.602

Table 9.17: Overflow uncertainty: Comparison between VMPC and SVMPC for $u_{\text{offset}}^{\text{ov+}}$.

	VMPC					
u_{off}	0%	5%	10%	25%	50%	75%
$Q_{\text{ov}_{\text{total}}}$	167.434	167.099	167.368	167.516	167.466	167.332
$\%\mathbf{F}_Q$		-0.20%	-0.04%	0.05%	0.02%	-0.06%
$m_{\text{ov}_{\text{total}}}^{\text{NH}_4}$	1072.366	1058.702	1037.079	1015.923	1010.801	1010.258
$\%\mathbf{F}_m$		-1.27%	-3.29%	-5.26%	-5.74%	-5.79%
ξ_{rain}	7.926	7.702	7.621	7.553	7.535	7.535
	SVMPC - $\zeta = 0.60$					
u_{off}	0%	5%	10%	25%	50%	75%
$Q_{\text{ov}_{\text{total}}}$	177.352	177.14	176.652	171.992	169.783	168.61
$\%\mathbf{F}_Q$		-0.12%	-0.39%	-3.02%	-4.27%	-4.93%
$m_{\text{ov}_{\text{total}}}^{\text{NH}_4}$	1276.828	1270.825	1252.372	1152.906	1123.733	1102.935
$\%\mathbf{F}_m$		-0.47%	-1.92%	-9.71%	-11.99%	-13.62%
ξ_{rain}	8.495	8.469	8.468	8.423	8.409	8.415
	SVMPC - $\zeta = 0.80$					
u_{off}	0%	5%	10%	25%	50%	75%
$Q_{\text{ov}_{\text{total}}}$	177.605	177.144	176.657	171.975	169.79	168.557
$\%\mathbf{F}_Q$		-0.26%	-0.53%	-3.17%	-4.40%	-5.09%
$m_{\text{ov}_{\text{total}}}^{\text{NH}_4}$	1278.572	1270.874	1252.55	1152.762	1123.803	1101.452
$\%\mathbf{F}_m$		-0.60%	-2.04%	-9.84%	-12.10%	-13.85%
ξ_{rain}	8.576	8.471	8.470	8.427	8.413	8.418
	SVMPC - $\zeta = 0.95$					
u_{off}	0%	5%	10%	25%	50%	75%
$Q_{\text{ov}_{\text{total}}}$	178.115	177.153	176.670	171.958	169.776	168.494
$\%\mathbf{F}_Q$		-0.54%	-0.81%	-3.46%	-4.68%	-5.40%
$m_{\text{ov}_{\text{total}}}^{\text{NH}_4}$	1282.477	1271.028	1252.716	1152.633	1123.963	1100.994
$\%\mathbf{F}_m$		-0.89%	-2.32%	-10.12%	-12.36%	-14.15%
ξ_{rain}	8.643	8.481	8.480	8.437	8.422	8.426

Table 9.18: Overflow uncertainty: Comparison between VMPC and SVMPC for $u_{\text{offset}}^{\text{ov-}}$.

	VMPC					
u_{off}	0%	−5%	−10%	−25%	−50%	−75%
$Q_{\text{ov}_{\text{total}}}$	167.434	169.609	169.572	169.599	169.561	169.561
$\%\mathbf{F}_Q$		1.30%	1.28%	1.29%	1.27%	1.27%
$m_{\text{ov}_{\text{total}}}^{\text{NH}_4}$	1072.366	1099.018	1097.333	1096.522	1094.832	1094.832
$\%\mathbf{F}_m$		2.49%	2.33%	2.25%	2.09%	2.09%
ξ_{rain}	7.926	7.485	7.501	7.488	7.476	7.476
	SVMPC - $\zeta = 0.60$					
u_{off}	0%	−5%	−10%	−25%	−50%	−75%
$Q_{\text{ov}_{\text{total}}}$	177.352	177.266	177.289	177.334	177.363	177.363
$\%\mathbf{F}_Q$		-0.05%	-0.04%	-0.01%	0.01%	0.01%
$m_{\text{ov}_{\text{total}}}^{\text{NH}_4}$	1276.828	1276.238	1276.160	1276.181	1276.195	1276.195
$\%\mathbf{F}_m$		-0.05%	-0.05%	-0.05%	-0.05%	-0.05%
ξ_{rain}	8.495	8.464	8.463	8.463	8.463	8.463
	SVMPC - $\zeta = 0.80$					
u_{off}	0%	−5%	−10%	−25%	−50%	−75%
$Q_{\text{ov}_{\text{total}}}$	177.605	177.271	177.294	177.338	177.367	177.367
$\%\mathbf{F}_Q$		-0.19%	-0.18%	-0.15%	-0.13%	-0.13%
$m_{\text{ov}_{\text{total}}}^{\text{NH}_4}$	1278.572	1276.304	1276.227	1276.250	1276.263	1276.263
$\%\mathbf{F}_m$		-0.18%	-0.18%	-0.18%	-0.18%	-0.18%
ξ_{rain}	8.576	8.466	8.466	8.465	8.465	8.465
	SVMPC - $\zeta = 0.95$					
u_{off}	0%	−5%	−10%	−25%	−50%	−75%
$Q_{\text{ov}_{\text{total}}}$	178.115	177.279	177.302	177.335	177.375	177.375
$\%\mathbf{F}_Q$		-0.47%	-0.46%	-0.44%	-0.42%	-0.42%
$m_{\text{ov}_{\text{total}}}^{\text{NH}_4}$	1282.477	1276.422	1276.346	1276.357	1276.381	1276.381
$\%\mathbf{F}_m$		-0.47%	-0.48%	-0.48%	-0.48%	-0.48%
ξ_{rain}	8.643	8.476	8.475	8.475	8.475	8.475

In summary, for most scenarios, SVMPC demonstrated good robustness against uncertainties in most scenarios, particularly for outflow and overflow uncertainties. However, for volume variations, SVMPC underperformed in comparison to VMPC, specifically for u_p and negative values of u_{off}. This underperformance may be attributed to suboptimal control parameters. In absolute terms, the SVMPC performance was inferior. Therefore, the next section establishes the methodology for weight selection in the stochastic framework, following the same principles as in Chapter 7. The main difference is the inclusion of the confidence level in the sensitivity analysis to assess the impact of ζ, although ζ itself is not optimised through the Genetic Algorithm with the weights. Nevertheless, it is important to understand the contribution of ζ. In addition, the slack variable, ϵ, is also slightly different as it is included in the lower bound constraint, as seen in Equation 9.13e. Thus, the first step is to evaluate the parameters of SVMPC through both LSA and GSA. The next section introduces the Morris screening LSA applied to the SVMPC.

9.3.4 Local Sensitivity Analysis - Morris screening

The Morris screening is useful to understand the impact of parameters at a local level, i.e., how the inputs of SVMPC impact the objectives of the control. The only additional parameter included for this analysis compared to VMPC is the confidence level ζ, thus the number of parameters k is $k = 5$. The number of trajectories r chosen for the analysis is $r = 400$, hence the total number of simulation runs necessary are $N_m = r(k + 1) = 400 * (5 + 1) = 2400$. The value of $\Delta = 1$ for α, β, γ and ϵ, whereas $\Delta = 0.1$ for ζ. Moreover, the analysis is realized on the Parallel + Series configuration and the period for the simulation is March 24 to April 10, as in Section 8.2.4. Finally, the scenarios selected for the analysis were those with uncertainties that had the greatest overall impact on the system, shown in Table 9.19, including the scenario without uncertainties.

Scenario	Type	u_p	u_{off}
1	No uncertainty	-	-
2	Volume	25%	0%
3	Volume	25%	-50%
4	Outflow	25%	-50%

Table 9.19: Scenarios for Morris screening Sensitivity Analysis.

The Morris screening for SVMPC is shown in Figure 9.16 for $Q_{\text{ov}_{\text{total}}}$ and Figure 9.17 for ξ. In the first scenario without uncertainties, the confidence level ζ yields a value μ of approximately 523.5 for $Q_{\text{ov}_{\text{total}}}$ and 0.35 for ξ. For the other parameters (α, β, γ and ϵ), the contribution is significantly reduced, with μ below 200 and 0.1 for $Q_{\text{ov}_{\text{total}}}$ and ξ, respectively. The outcome emphasises the higher impact of the confidence level on the other parameters. For the standard deviation, the difference is also present, where for ζ the value of σ is 1120.9 and 0.84, for $Q_{\text{ov}_{\text{total}}}$ and ξ, respectively, and for the other parameters, σ is less than 400 and 0.2. For all parameters, $\sigma \gg \mu$, indicating a non-linear relationship between the parameters and the outputs $Q_{\text{ov}_{\text{total}}}$ and ξ.

In the second scenario, where uncertainties are included in the volume with $u_p = 25\%$, the influence of ζ becomes even more pronounced. The value of μ and σ for ζ increases to 6866.6 and 13859.2 for $Q_{\text{ov}_{\text{total}}}$ and 5.1 and 9.8 for ξ, respectively. The weights maintain mean values below 35 for $Q_{\text{ov}_{\text{total}}}$ and below

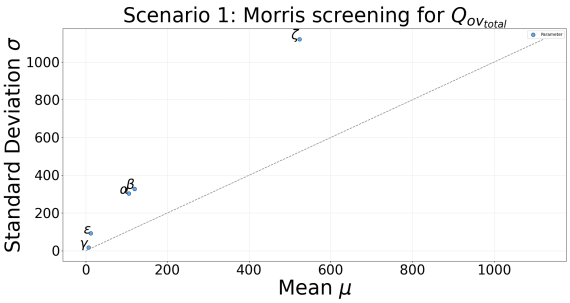

(a) Scenario 1 - No uncertainty.

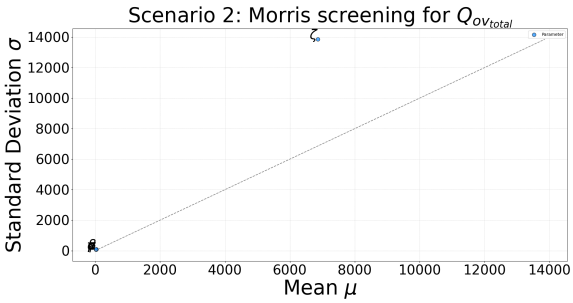

(b) Scenario 2 - Volume uncertainty (25%, 0%).

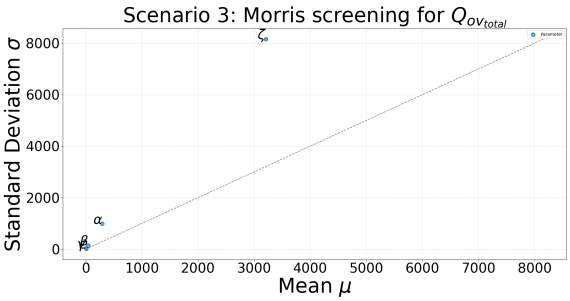

(c) Scenario 3 - Volume uncertainty (25%, -50%).

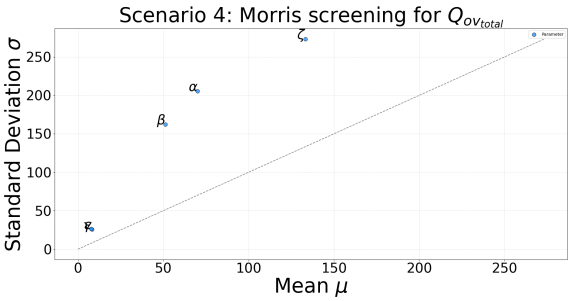

(d) Scenario 4 - Outflow uncertainty (25%, -50%).

Figure 9.16: Morris screening for SVMPC - $Q_{\mathrm{ov_{total}}}$.

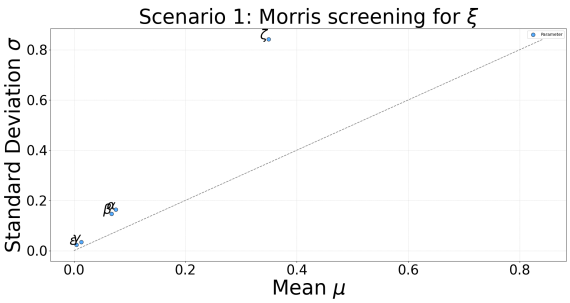

(a) Scenario 1 - No uncertainty.

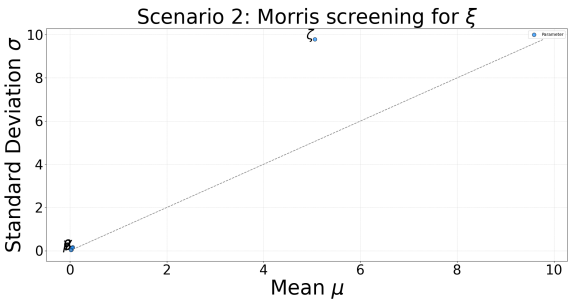

(b) Scenario 2 - Volume uncertainty (25%, 0%).

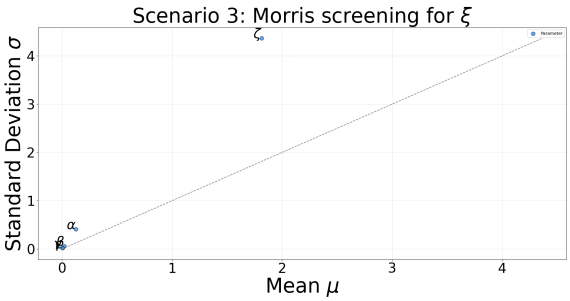

(c) Scenario 3 - Volume uncertainty (25%, -50%).

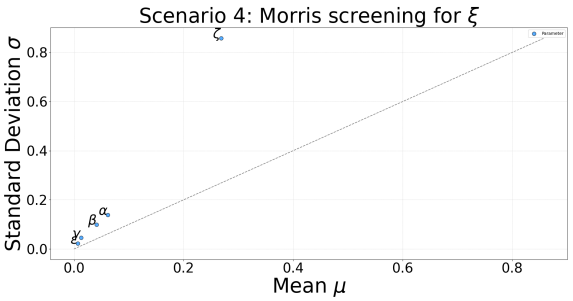

(d) Scenario 4 - Outflow uncertainty (25%, -50%).

Figure 9.17: Morris screening for SVMPC - ξ.

0.05 standard deviation for ξ, suggesting a major impact of ζ even compared to the scenario without uncertainty. This significant increase suggests that, when uncertainties are introduced, the confidence

level not only keeps its importance, but also becomes increasingly meaningful. These findings emphasise the need to carefully consider ζ in the model, especially when handling uncertainties.

Moreover, for scenario 3, ζ continues to show a greater impact compared to the other weights, however μ in this instance is considerably reduced (around 3000), which indicates more influence of other parameters, especially by α with $\mu = 400$. Finally, for scenario 4, the effect of ζ reduced even further, highlighting more the influence of other parameters such as α and β. In general, ζ show a more significant influence on the uncertainties in the volume, which is due to ζ being directly related to the constraint on the maximum volume of SU (Equations 9.13e and 9.13l).

Since ζ has such a dominant effect, it would be valuable to investigate whether there is a possibility of fine-tuning or optimising the confidence level to balance between stability and performance, possibly even introducing a dynamic ζ that adapts depending on the conditions, which could allow the model to retain stability while improving performance. However, this is not explored in this research. The author suggests tuning the confidence level to match the variability of the uncertainty when they are known. Otherwise, the value of ζ could be chosen globally at 0.8, making a compromise between conservativeness and performance. In contrast to VMPC, the weight ϵ has the same influence on the output as the other parameters, with values of μ and σ comparable to those of the other weights. Hence, for SVMPC, it is recommended to include ϵ in the Genetic Algorithm optimisation, although the appropriate range for each variable is still unclear.

9.3.5 Global Sensitivity Analysis - Grid and Random Search

The aim of the next analysis is to assess the global interaction between the weights of the MPC via Grid Search and to identify the regions where they are suited the best. Similarly to the Morris screening, the outputs for the Grid Search analysis are $Q_{\text{ov}_{\text{total}}}$ and ξ. In addition, the analysis is performed on the Parallel + Series configuration, and the simulation period is March 24 to April 10 and the same scenarios from Table 9.19 are considered. In contrast to the Morris screening, the Grid Search is performed only for the weights α, β, γ, and ϵ, fixing ζ at 0.8.

Firstly, a more detailed analysis is done for Scenario 1 without uncertainties, and later a summary of the results for all scenarios is provided. For this instance, the Grid Search is conducted similarly to VMPC, with the following setup: three grids are defined, resulting in $n = 3$, where $\epsilon = [3, 89, 153]$. The set Ω is defined as $\Omega = \{(\alpha, \beta, \gamma) \mid \alpha \in \Omega_1, \beta \in \Omega_2, \gamma \in \Omega_3\}$, where each Ω_i has the lower and upper bounds set to $(1, 200)$ for $i = (1, 2, 3)$. Each input in the grid includes 12 equally spaced points, creating in total six 3-D grid heatmaps with a size of $12 \times 12 \times 12 = 1728$ points. The colours in the heatmap represent one output, $Q_{\text{ov}_{\text{total}}}$ or ξ. For this scenario, the result of the grid search for both $Q_{\text{ov}_{\text{total}}}$ and ξ can be seen in Figure 9.18.

By analysing the heatmap, the influence of the weights can be assessed. The result shows that, for $Q_{\text{ov}_{\text{total}}}$, although the difference is almost negligible, the lower values of ϵ are slightly better, where for $\epsilon = 3$, $Q_{\text{ov}_{\text{total}}}$ is 111.82 ML, steadily increasing with higher ϵ, reaching 111.93 ML for $\epsilon = 153$, a difference of only 0.1%. However, for the output ξ, the influence is more significant, resulting in $\xi = 18.80$ L/s for $\epsilon = 3$, while an increase of 20.2% is observed compared to $\epsilon = 153$ which has $\xi = 22.60$ L/s. Analysing the data, it suggests that ϵ is better suited around 3, although the range is still difficult to identify. Finally, in terms of α, β, and γ, the weights were better suited to the following ranges: $\alpha \in (0, 100]$ and

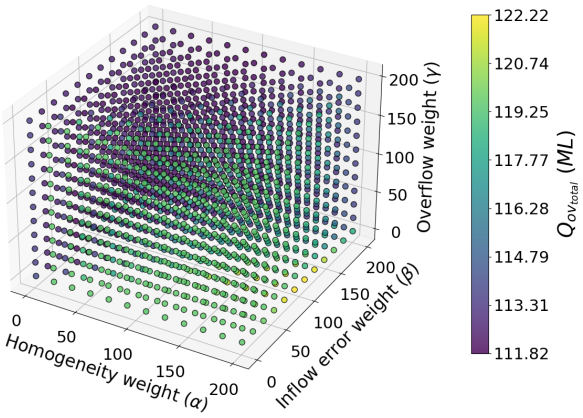

(a) $Q_{\mathrm{ov_{total}}}$ for $\epsilon = 3$.

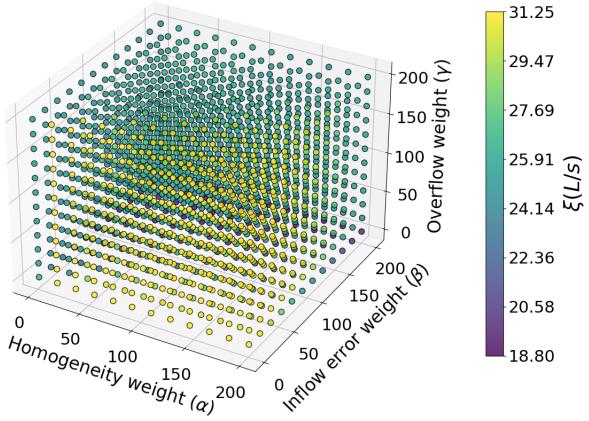

(b) ξ for $\epsilon = 3$.

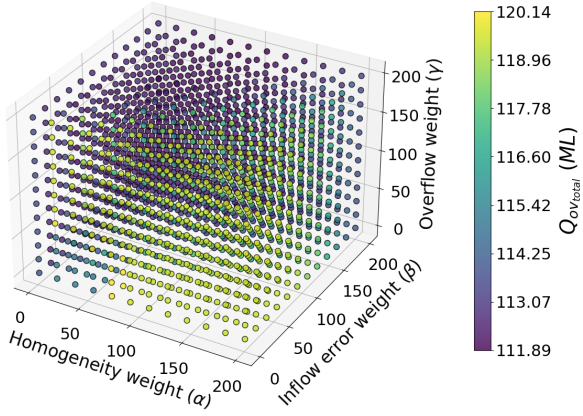

(c) $Q_{\mathrm{ov_{total}}}$ for $\epsilon = 89$.

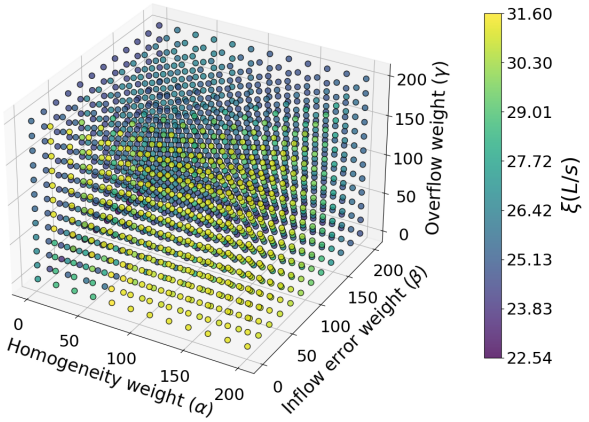

(d) ξ for $\epsilon = 89$.

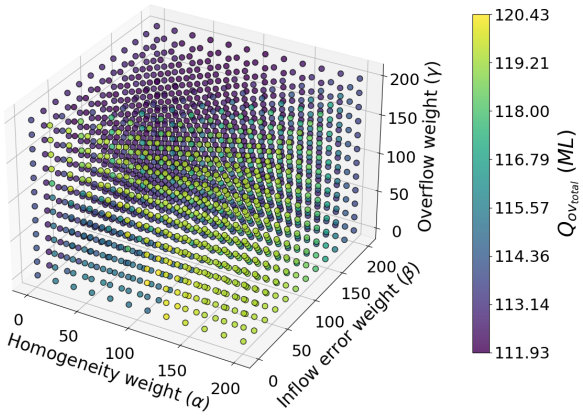

(e) $Q_{\mathrm{ov_{total}}}$ for $\epsilon = 153$.

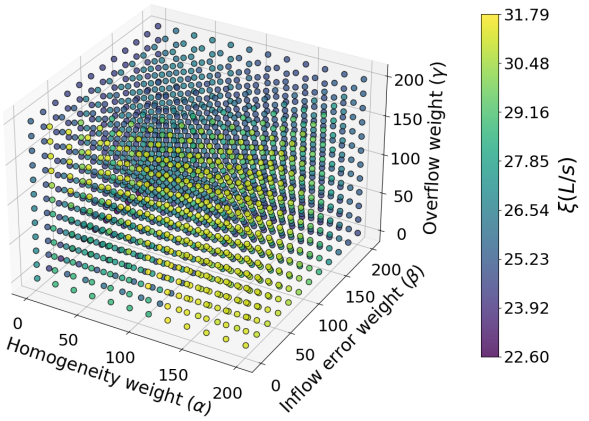

(f) ξ for $\epsilon = 153$.

Figure 9.18: Grid Search SA for SVMPC for Scenario 1.

$\beta, \gamma \in [20, 200]$. A more detailed analysis of the heatmap for $\epsilon = 3$, which presents the best solution overall, reveals that lower values of α (below 50) are better suited to minimise $Q_{\mathrm{ov_{total}}}$, while the opposite

is better suited to minimise ξ.

The outcome for all scenarios is summarised in Table 9.20, highlighting the minimum and maximum values of $Q_{\text{ov}_{\text{total}}}$ and ξ in the different scenarios and for $\epsilon = [3, 89, 153]$. The value of ϵ had a greater influence on $Q_{\text{ov}_{\text{total}}}$ when uncertainty in volume was considered. The minimum value for $Q_{\text{ov}_{\text{total}}}$ increased by 2% and 3.5% for Scenario 2 and 3, respectively, when ϵ increased from 3 to 153, while ξ increased 23.7% and 15.9%. This reinforces the previous analysis, where lower values of ϵ consistently show better performance for both outputs.

Table 9.20: Grid Search applied for all scenarios.

	$\epsilon = 3$				$\epsilon = 89$				$\epsilon = 153$			
	$Q_{\text{ov}_{\text{total}}}$		ξ		$Q_{\text{ov}_{\text{total}}}$		ξ		$Q_{\text{ov}_{\text{total}}}$		ξ	
Scenario	Minimum	Maximum	Minimum	Maximum	Minimum	Maximum	Minimum	Maximum	Minimum	Maximum	Minimum	Maximum
1	111.82	122.22	18.80	31.25	111.89	120.14	22.54	31.60	111.93	120.43	22.60	31.79
2	113.30	120.44	19.84	34.13	115.36	117.49	24.35	34.48	115.39	117.50	24.55	34.48
3	116.39	138.67	20.94	38.97	120.31	134.83	24.10	38.98	120.55	134.69	24.28	38.98
4	112.41	123.79	19.27	31.40	112.50	119.93	22.58	31.54	112.51	120.39	22.73	31.83

The weight ranges remain quite similar, showing consistent behaviour between the different types of uncertainty, showing $\alpha \in (0, 50]$ and $\beta, \gamma \in (0, 200]$ as an adequate range. Specifically for Scenario 3 where the degradation in the validation of the methodology was the highest between all uncertainty scenarios, a low value of α (below 20) results in better overflow and ξ. Consequently, since the system's dynamics is affected by the uncertainties, the overall behaviour of the algorithm changes considerably between different uncertainties.

Finally, a random search is applied to more easily identify the regions where ϵ is the most suitable. In this approach α is fixed at 30, while β, γ, and ϵ are randomly varied. The analysis is performed exclusively for Scenario 2, where $u_p = 25\%$ and $u_{\text{off}} = 0$. The ranges are $\beta, \gamma \in [30, 200]$, $\epsilon < 20$ and the results are shown in Figure 9.19. The graph demonstrates that β is the most influential weight among the three explored in the search, with optimal values above 30. In addition, α is also best suited at values greater than 30, although its impact is less pronounced. A closer examination of ϵ reveals that it performs better when below 5 for ξ, although at the cost of increased overflow. Using the GA optimisation to identify the Pareto-front would definitely be beneficial to determine a good combination of weights.

Although the sensitivity analysis provided an in-depth understanding of the behaviour of the parameters of SVMPC, the choice of parameters is still unclear. Therefore, as discussed, an optimisation using the Genetic Algorithm is interesting to identify the best Pareto-front for the weights of SVMPC and decide whether $Q_{\text{ov}_{\text{total}}}$ or ξ is more important for the application.

9.3.6 Genetic Algorithm for weight optimisation

The next step involves determining the optimal weights for SVMPC. To achieve this, the sensitivity analysis is combined with the Genetic Algorithm to identify a Pareto front for the weights, which are simulated for the same uncertainty scenarios in Table 9.19. Based on the SA results, independent of the type of uncertainty, the following ranges are determined: $\alpha \in (0, 50]$, $\beta, \gamma \in (30, 200]$, and $\epsilon \in (0, 5]$. The initial guess for the simulation is set as $\alpha = 20$, $\beta = 100$, $\gamma = 100$, and $\epsilon = 1$, with a tolerance of 10^{-1}.

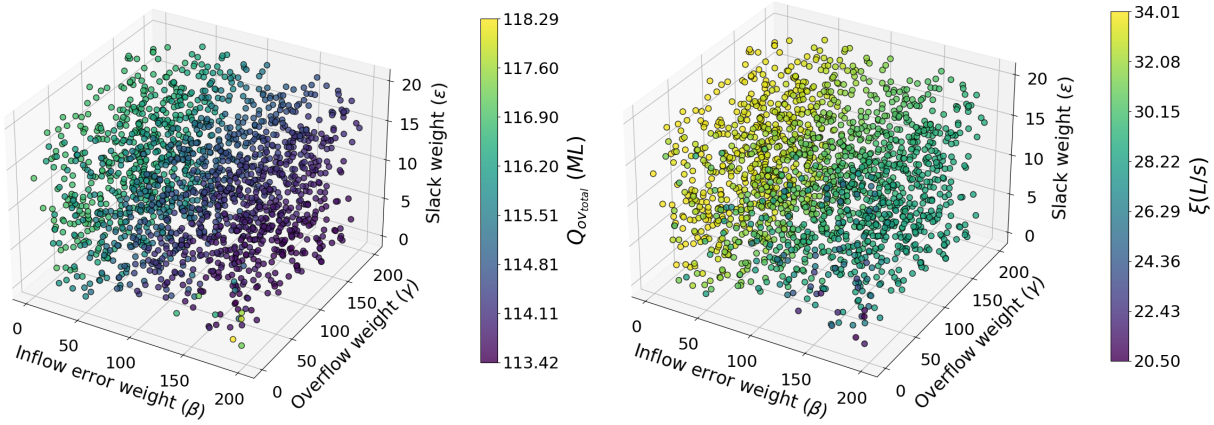

(a) Random Search for $Q_{\mathrm{ov_{total}}}$.

(b) Random Search for ξ.

Figure 9.19: Random Search applied to Scenario 2.

These scenarios were simulated over the period from March 24 to April 10, using a population size of 10 and a maximum of 300 iterations.

The Pareto front for the scenarios is shown in Figure 9.20, which demonstrates different answers for each scenario, as expected, since they have different impacts on the network. The pareto front for Scenario 1 presents the best pareto front for the overflow, reaching a minimum overflow of 112.6 ML. Since this simulation does not consider uncertainties, the controller is not hindered by the presence of uncertainties and performs better. In general, Scenarios 1, 2 and 4 are similar, following the same behaviour from the methodology validation in Section 9.3.3. In particular, scenario 4 presents a more discontinuous pareto, which might be explained by the genetic algorithm having two different populations not crossing their information and creating these separate areas. Finally, scenario 3 showed the poorest performance, although it is also expected, since offset uncertainties in the volume had the worst impact on the wastewater network in general. For all cases, the Pareto front highlighted the threshold beyond which MPC performance could be further improved for each type of uncertainty. Since the sensitivity analysis narrows the search for an optimal solution, the Pareto front often corresponds to a more restricted set of input parameters.

In Table 9.21 the optimal weights for each scenario and different criteria are presented based on which objective is more desirable. Scenario 3, which showed the worst pareto, for all criteria the algorithm converged to an optimal with very low α and higher β and γ. In contrast, the other scenarios clearly indicate that higher values of α were more effective in minimising the overflow, while lower values of α were more suitable for reducing ξ. Specifically for Scenario 2, α is lower than for Scenario 1 and 4.

Table 9.21: Optimal (α, β, γ, ϵ) for each uncertainty scenario.

Scenario	Best weights for $Q_{\mathrm{ov_{total}}}$	Best weights for ξ	Best compromise
1	(38.56, 80.94, 92.44, 2.69))	(0.01, 114.40, 92.44, 1.06)	(45.08, 59.75, 93.78, 1.51)
2	(4.34, 125.39, 101.88, 1.78)	(0.23, 142.37, 101.88, 1.78)	(2.60, 125.40, 106.53, 1.78)
3	(0.02, 109.50, 49.73, 1.48)	(0.05, 143.50, 33.05, 2.01)	(0.02, 115.60, 31.08, 1.47)
4	(21.50, 74.79, 100.44, 1.14)	(3.02, 127.34, 100.22, 1.05)	(23.71, 74.79, 88.35, 0.56)

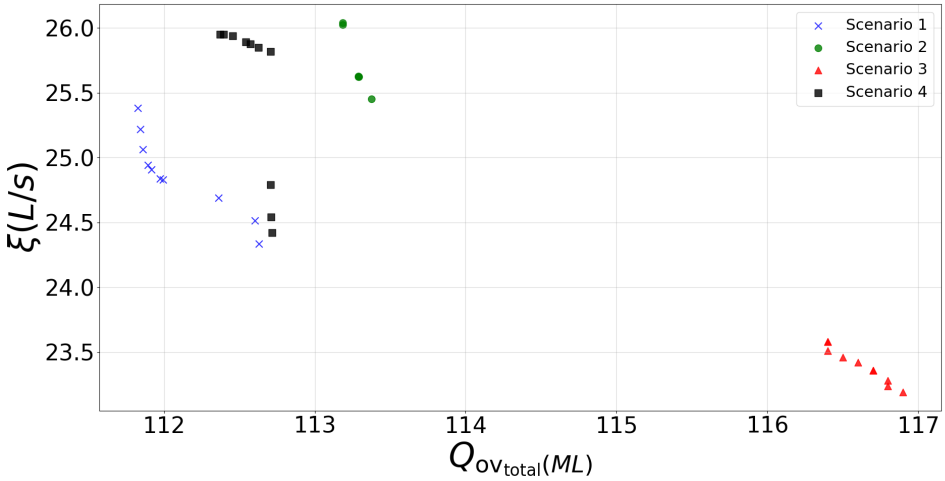

Figure 9.20: Pareto front SVMPC.

Since Scenario 3 exhibited the worst performance, the final optimal weight for SVMPC was selected from this scenario using the minimisation overflow criteria. The weights chosen are $\alpha = 0.02$, $\beta = 109.50$, $\gamma = 49.73$, and $\epsilon = 1.48$. The performance of SVMPC with these optimal weights is then evaluated and compared against VMPC with its optimal weights, also considering the effect of the confidence level ζ. The evaluation is performed in the same scenarios as in Section 9.3.3. An additional metric, denoted as $\%\mathbf{F}_Q^*$, $\%\mathbf{F}_m^*$ and $\%\mathbf{F}_\xi^*$, is introduced into the evaluation to compare the performance of non-optimal SVMPC (from Table 9.10) with optimal SVMPC. Essentially, those variables represent the percentage of a given metric for the optimal SVMPC relative to the non-optimal version. A negative value indicates an improvement, while a positive value suggests that the optimal SVMPC performs worse.

Uncertainty on $V(k)$

Firstly, the performance of volume uncertainty is analysed changing the variability through the parameter u_p, shown in Table 9.22. The new weights for SVMPC clearly improved the stability and overall performance of the controller, maintaining the overflow stable for increased uncertainty, while VMPC reaches 4% worse performance. However, it still did not improve the performance against VMPC in terms of absolute value. In terms of the output ξ_{rain}, VMPC has an overall better performance. Another interesting result is that, for the optimal weights, the confidence level has much less influence on the objectives.

The second instance of the evaluation targeted $u_{\text{offset}}^{\text{vol+}}$, as shown in Table 9.23, which exhibits a behaviour similar to the previous scenario, where SVMPC is more stable than VMPC with increasing uncertainty; however, it still performs poorly in absolute terms of overflow. In this scenario, both methods have a similar ξ_{rain}. When comparing $\%\mathbf{F}_m^*$, the optimal SVMPC did not change significantly.

The final evaluation of volume uncertainty compared the performance for $u_{\text{offset}}^{\text{vol-}}$. For this scenario, the performance of the SVMPC is outstanding, it is able to maintain a reasonable stability by limiting the overflow to 208.3 ML and 1813 kg for volume and load, respectively, when $u_{\text{off}} = -75\%$, an increase of 17.55% and 41.62%. The result is outstanding compared to VMPC which increases up to 165%

Table 9.22: Volume uncertainty: Comparison between VMPC and optimal SVMPC with u_p.

	VMPC					
u_p	0%	5%	10%	25%	50%	75%
$Q_{\mathrm{ov_{total}}}$	167.434	168.971	169.771	171.595	173.193	174.031
$\%\mathbf{F}_Q$		**0.92%**	**1.4%**	**2.49%**	**3.44%**	**3.94%**
$m^{\mathrm{NH_4}}_{\mathrm{ov_{total}}}$	1072.366	1088.102	1094.839	1118.461	1136.925	1152.927
$\%\mathbf{F}_m$		**1.47%**	**2.1%**	**4.3%**	**6.02%**	**7.51%**
ξ_{rain}	7.926	6.221	4.853	2.314	1.222	1.152
	SVMPC - $\zeta = 0.60$					
u_p	0%	5%	10%	25%	50%	75%
$Q_{\mathrm{ov_{total}}}$	177.244	178.757	178.943	179.152	178.911	179.227
$\%\mathbf{F}_Q$		**0.85%**	**0.96%**	**1.08%**	**0.94%**	**1.12%**
$\%\mathbf{F}^*_Q$	**-0.06%**	**-0.2%**	**-0.77%**	**-2.1%**	**-3.59%**	**-4.2%**
$m^{\mathrm{NH_4}}_{\mathrm{ov_{total}}}$	1280.512	1297.819	1299.71	1290.295	1289.422	1291.225
$\%\mathbf{F}_m$		**1.35%**	**1.5%**	**0.76%**	**0.7%**	**0.84%**
$\%\mathbf{F}^*_m$	**0.29%**	**0.38%**	**-0.45%**	**-3.11%**	**-5.14%**	**-6.19%**
ξ_{rain}	6.564	6.491	5.845	4.438	4.196	3.987
$\%\mathbf{F}^*_\xi$	**-22.73%**	**-12.26%**	**-14.7%**	**-21.6%**	**-27.03%**	**-32.84%**
	SVMPC - $\zeta = 0.80$					
u_p	0%	5%	10%	25%	50%	75%
$Q_{\mathrm{ov_{total}}}$	177.245	178.632	178.972	179.03	179.247	179.306
$\%\mathbf{F}_Q$		**0.78%**	**0.97%**	**1.01%**	**1.13%**	**1.16%**
$\%\mathbf{F}^*_Q$	**-0.2%**	**-0.68%**	**-1.65%**	**-4.17%**	**-6.18%**	**-6.7%**
$m^{\mathrm{NH_4}}_{\mathrm{ov_{total}}}$	1280.479	1296.922	1300.53	1291.305	1288.328	1290.704
$\%\mathbf{F}_m$		**1.28%**	**1.57%**	**0.85%**	**0.61%**	**0.8%**
$\%\mathbf{F}^*_m$	**0.15%**	**-0.31%**	**-1.3%**	**-5.87%**	**-10.5%**	**-11.38%**
ξ_{rain}	6.564	6.493	5.893	4.44	4.052	3.929
$\%\mathbf{F}^*_\xi$	**-23.46%**	**-15.94%**	**-20.71%**	**-36.83%**	**-39.77%**	**-37.17%**
	SVMPC - $\zeta = 0.95$					
u_p	0%	5%	10%	25%	50%	75%
$Q_{\mathrm{ov_{total}}}$	177.246	178.524	178.865	179.157	179.329	179.228
$\%\mathbf{F}_Q$		**0.72%**	**0.91%**	**1.08%**	**1.18%**	**1.12%**
$\%\mathbf{F}^*_Q$	**-0.49%**	**-1.28%**	**-2.81%**	**-5.69%**	**-6.77%**	**-7.0%**
$m^{\mathrm{NH_4}}_{\mathrm{ov_{total}}}$	1280.496	1292.315	1299.821	1295.94	1290.629	1289.96
$\%\mathbf{F}_m$		**0.92%**	**1.51%**	**1.21%**	**0.79%**	**0.74%**
$\%\mathbf{F}^*_m$	**-0.15%**	**-1.14%**	**-2.94%**	**-8.92%**	**-11.51%**	**-11.88%**
ξ_{rain}	6.564	6.408	5.974	4.631	3.989	3.903
$\%\mathbf{F}^*_\xi$	**-24.05%**	**-19.47%**	**-22.5%**	**-39.92%**	**-42.79%**	**-37.49%**

and 913% for volume and load overflow, evidently having a much better result. Analysing $\%\mathbf{F}^*_m$, the new simulation reduced $Q_{\mathrm{ov_{total}}}$ by 55% and $m^{\mathrm{NH_4}}_{\mathrm{ov_{total}}}$ by 84%, demonstrating the effectiveness of the GA optimisation to find better weights. Regarding ξ_{rain}, SVMPC is also performing remarkably well, almost reaching $\xi_{\mathrm{rain}} = 0$ for $u_{\mathrm{off}} = -75\%$.

Table 9.23: Volume uncertainty: Comparison between VMPC and optimal SVMPC for $u^{\text{vol+}}_{\text{offset}}$.

	VMPC					
u_{off}	0%	5%	10%	25%	50%	75%
$Q_{\text{ov}_{\text{total}}}$	167.434	166.782	167.017	168.22	170.44	172.75
$\%\mathbf{F}_Q$		**-0.39%**	**-0.25%**	**0.47%**	**1.8%**	**3.17%**
$m^{\text{NH}_4}_{\text{ov}_{\text{total}}}$	1072.366	1066.461	1071.089	1086.543	1129.77	1181.609
$\%\mathbf{F}_m$		**-0.55%**	**-0.12%**	**1.32%**	**5.35%**	**10.19%**
ξ_{rain}	7.926	8.573	9.062	9.594	9.849	9.909
	SVMPC - $\zeta = 0.60$					
u_{off}	0%	5%	10%	25%	50%	75%
$Q_{\text{ov}_{\text{total}}}$	177.244	176.928	176.719	176.45	175.626	175.611
$\%\mathbf{F}_Q$		**-0.18%**	**-0.3%**	**-0.45%**	**-0.91%**	**-0.92%**
$\%\mathbf{F}^*_Q$	**-0.06%**	**0.25%**	**0.32%**	**0.42%**	**0.03%**	**0.02%**
$m^{\text{NH}_4}_{\text{ov}_{\text{total}}}$	1280.512	1278.782	1276.397	1272.054	1260.564	1259.833
$\%\mathbf{F}_m$		**-0.14%**	**-0.32%**	**-0.66%**	**-1.56%**	**-1.61%**
$\%\mathbf{F}^*_m$	**0.29%**	**0.76%**	**0.9%**	**0.84%**	**0.06%**	**0.09%**
ξ_{rain}	6.564	6.588	6.596	6.975	9.913	9.949
$\%\mathbf{F}^*_\xi$	**-22.73%**	**-26.01%**	**-28.85%**	**-28.05%**	**-0.06%**	**0.0%**
	SVMPC - $\zeta = 0.80$					
u_{off}	0%	5%	10%	25%	50%	75%
$Q_{\text{ov}_{\text{total}}}$	177.245	176.928	176.719	176.45	175.626	175.611
$\%\mathbf{F}_Q$		**-0.18%**	**-0.3%**	**-0.45%**	**-0.91%**	**-0.92%**
$\%\mathbf{F}^*_Q$	**-0.2%**	**0.17%**	**0.32%**	**0.42%**	**0.03%**	**0.02%**
$m^{\text{NH}_4}_{\text{ov}_{\text{total}}}$	1280.479	1278.785	1276.404	1272.058	1260.564	1259.833
$\%\mathbf{F}_m$		**-0.13%**	**-0.32%**	**-0.66%**	**-1.56%**	**-1.61%**
$\%\mathbf{F}^*_m$	**0.15%**	**0.62%**	**0.88%**	**0.84%**	**0.06%**	**0.09%**
ξ_{rain}	6.564	6.588	6.596	6.975	9.913	9.949
$\%\mathbf{F}^*_\xi$	**-23.46%**	**-25.47%**	**-28.95%**	**-28.05%**	**-0.07%**	**0.0%**
	SVMPC - $\zeta = 0.95$					
u_{off}	0%	5%	10%	25%	50%	75%
$Q_{\text{ov}_{\text{total}}}$	177.246	176.928	176.714	176.449	175.626	175.611
$\%\mathbf{F}_Q$		**-0.18%**	**-0.3%**	**-0.45%**	**-0.91%**	**-0.92%**
$\%\mathbf{F}^*_Q$	**-0.49%**	**0.17%**	**0.29%**	**0.42%**	**0.02%**	**0.02%**
$m^{\text{NH}_4}_{\text{ov}_{\text{total}}}$	1280.496	1278.771	1276.084	1272.056	1260.563	1259.833
$\%\mathbf{F}_m$		**-0.13%**	**-0.34%**	**-0.66%**	**-1.56%**	**-1.61%**
$\%\mathbf{F}^*_m$	**-0.15%**	**0.66%**	**0.82%**	**0.84%**	**0.06%**	**0.07%**
ξ_{rain}	6.564	6.588	6.626	6.975	9.913	9.949
$\%\mathbf{F}^*_\xi$	**-24.05%**	**-26.33%**	**-28.57%**	**-28.05%**	**-0.06%**	**0.3%**

Table 9.24: Volume uncertainty: Comparison between VMPC and optimal SVMPC for $u_{\text{offset}}^{\text{vol-}}$.

	VMPC					
u_{off}	0%	−5%	−10%	−25%	−50%	−75%
$Q_{\text{ov}_{\text{total}}}$	167.434	175.95	182.162	201.263	259.73	444.554
$\%\mathbf{F}_Q$		**5.09%**	**8.8%**	**20.2%**	**55.12%**	**165.51%**
$m_{\text{ov}_{\text{total}}}^{\text{NH}_4}$	1072.366	1196.528	1266.674	1571.667	2852.361	10867.604
$\%\mathbf{F}_m$		**11.58%**	**18.12%**	**46.56%**	**165.99%**	**913.42%**
ξ_{rain}	7.926	6.132	3.52	-6.714	-31.339	-59.93
	SVMPC - $\zeta = 0.60$					
u_{off}	0%	−5%	−10%	−25%	−50%	−75%
$Q_{\text{ov}_{\text{total}}}$	177.244	179.037	180.521	185.157	194.027	208.349
$\%\mathbf{F}_Q$		**1.01%**	**1.85%**	**4.46%**	**9.47%**	**17.55%**
$\%\mathbf{F}_Q^*$	**-0.06%**	**-0.68%**	**-1.44%**	**-3.82%**	**-12.42%**	**-55.1%**
$m_{\text{ov}_{\text{total}}}^{\text{NH}_4}$	1280.512	1295.601	1312.086	1367.071	1507.522	1813.373
$\%\mathbf{F}_m$		**1.18%**	**2.47%**	**6.76%**	**17.73%**	**41.61%**
$\%\mathbf{F}_m^*$	**0.29%**	**-0.91%**	**-2.51%**	**-8.22%**	**-36.03%**	**-84.16%**
ξ_{rain}	6.564	6.516	6.499	6.358	6.279	0.105
$\%\mathbf{F}_\xi^*$	**-22.73%**	**-10.27%**	**8.01%**	**131.87%**	**143.66%**	**-100.17%**
	SVMPC - $\zeta = 0.80$					
u_{off}	0%	−5%	−10%	−25%	−50%	−75%
$Q_{\text{ov}_{\text{total}}}$	177.245	179.038	180.52	185.156	194.028	208.348
$\%\mathbf{F}_Q$		**1.01%**	**1.85%**	**4.46%**	**9.47%**	**17.55%**
$\%\mathbf{F}_Q^*$	**-0.2%**	**-0.82%**	**-1.64%**	**-4.53%**	**-23.97%**	**-70.86%**
$m_{\text{ov}_{\text{total}}}^{\text{NH}_4}$	1280.479	1295.597	1312.074	1367.055	1507.547	1813.355
$\%\mathbf{F}_m$		**1.18%**	**2.47%**	**6.76%**	**17.73%**	**41.62%**
$\%\mathbf{F}_m^*$	**0.15%**	**-1.2%**	**-2.72%**	**-9.68%**	**-61.26%**	**-91.46%**
ξ_{rain}	6.564	6.514	6.499	6.358	6.279	0.105
$\%\mathbf{F}_\xi^*$	**-23.46%**	**-9.31%**	**12.11%**	**194.9%**	**51.08%**	**-100.14%**
	SVMPC - $\zeta = 0.95$					
u_{off}	0%	−5%	−10%	−25%	−50%	−75%
$Q_{\text{ov}_{\text{total}}}$	177.246	179.037	180.52	185.156	194.028	208.348
$\%\mathbf{F}_Q$		**1.01%**	**1.85%**	**4.46%**	**9.47%**	**17.55%**
$\%\mathbf{F}_Q^*$	**-0.49%**	**-1.04%**	**-1.76%**	**-4.6%**	**-25.05%**	**-76.14%**
$m_{\text{ov}_{\text{total}}}^{\text{NH}_4}$	1280.496	1295.58	1312.069	1367.091	1507.56	1813.322
$\%\mathbf{F}_m$		**1.18%**	**2.47%**	**6.76%**	**17.73%**	**41.61%**
$\%\mathbf{F}_m^*$	**-0.15%**	**-1.49%**	**-2.86%**	**-9.74%**	**-62.99%**	**-93.2%**
ξ_{rain}	6.564	6.514	6.498	6.358	6.279	0.105
$\%\mathbf{F}_\xi^*$	**-24.05%**	**-8.56%**	**10.3%**	**179.1%**	**-11.19%**	**-100.13%**

Uncertainty on $Q_{\text{out}}(k)$

Continuing for the outflow uncertainty, the results for increased variability between different u_p are seen in Table 9.25.

Table 9.25: Outflow uncertainty: Comparison between VMPC and optimal SVMPC for u_p.

	VMPC					
u_p	0%	25%	75%	100%	125%	175%
$Q_{\text{ov}_{\text{total}}}$	167.434	167.463	167.692	167.749	167.808	168.03
$\%\mathbf{F}_Q$		**0.02%**	**0.15%**	**0.19%**	**0.22%**	**0.36%**
$m^{\text{NH}_4}_{\text{ov}_{\text{total}}}$	1072.366	1074.472	1078.197	1077.432	1077.661	1082.022
$\%\mathbf{F}_m$		**0.2%**	**0.54%**	**0.47%**	**0.49%**	**0.9%**
ξ_{rain}	7.926	7.866	7.824	7.815	7.808	7.777
	SVMPC - $\zeta = 0.60$					
u_p	0%	25%	75%	100%	125%	175%
$Q_{\text{ov}_{\text{total}}}$	177.244	177.211	177.33	177.408	177.465	177.551
$\%\mathbf{F}_Q$		**-0.02%**	**0.05%**	**0.09%**	**0.12%**	**0.17%**
$\%\mathbf{F}^*_Q$	**-0.06%**	**0.01%**	**-0.02%**	**-0.04%**	**-0.03%**	**0.0%**
$m^{\text{NH}_4}_{\text{ov}_{\text{total}}}$	1280.512	1280.001	1281.509	1283.233	1284.554	1286.636
$\%\mathbf{F}_m$		**-0.04%**	**0.08%**	**0.21%**	**0.32%**	**0.48%**
$\%\mathbf{F}^*_m$	**0.29%**	**0.4%**	**0.29%**	**0.38%**	**0.46%**	**0.83%**
ξ_{rain}	6.564	6.608	6.644	6.633	6.643	6.614
$\%\mathbf{F}^*_\xi$	**-22.73%**	**-21.62%**	**-21.07%**	**-21.07%**	**-20.94%**	**-21.47%**
	SVMPC - $\zeta = 0.80$					
u_p	0%	25%	75%	100%	125%	175%
$Q_{\text{ov}_{\text{total}}}$	177.245	177.212	177.331	177.409	177.466	177.551
$\%\mathbf{F}_Q$		**-0.02%**	**0.05%**	**0.09%**	**0.12%**	**0.17%**
$\%\mathbf{F}^*_Q$	**-0.2%**	**-0.02%**	**-0.14%**	**-0.18%**	**-0.23%**	**-0.45%**
$m^{\text{NH}_4}_{\text{ov}_{\text{total}}}$	1280.479	1279.997	1281.51	1283.236	1284.551	1286.657
$\%\mathbf{F}_m$		**-0.04%**	**0.08%**	**0.22%**	**0.32%**	**0.48%**
$\%\mathbf{F}^*_m$	**0.15%**	**0.38%**	**0.18%**	**0.16%**	**0.19%**	**-0.0%**
ξ_{rain}	6.564	6.608	6.644	6.633	6.643	6.614
$\%\mathbf{F}^*_\xi$	**-23.46%**	**-21.57%**	**-20.01%**	**-19.1%**	**-18.26%**	**-18.76%**
	SVMPC - $\zeta = 0.95$					
u_p	0%	25%	75%	100%	125%	175%
$Q_{\text{ov}_{\text{total}}}$	177.246	177.212	177.331	177.408	177.466	177.552
$\%\mathbf{F}_Q$		**-0.02%**	**0.05%**	**0.09%**	**0.12%**	**0.17%**
$\%\mathbf{F}^*_Q$	**-0.49%**	**-0.06%**	**-0.4%**	**-0.43%**	**-0.6%**	**-1.02%**
$m^{\text{NH}_4}_{\text{ov}_{\text{total}}}$	1280.496	1279.996	1281.504	1283.22	1284.545	1286.661
$\%\mathbf{F}_m$		**-0.04%**	**0.08%**	**0.21%**	**0.32%**	**0.48%**
$\%\mathbf{F}^*_m$	**-0.15%**	**0.33%**	**-0.11%**	**-0.09%**	**-0.23%**	**-0.47%**
ξ_{rain}	6.564	6.608	6.645	6.633	6.643	6.616
$\%\mathbf{F}^*_\xi$	**-24.05%**	**-21.51%**	**-18.14%**	**-16.5%**	**-16.92%**	**-15.36%**

In this scenario, both VMPC and SVMPC are stable, although in absolute terms, VMPC outperforms SVMPC in all u_p values when observing both overflow, although ξ_{rain} is better for SVMPC. For $u_{\text{offset}}^{\text{out+}}$ as shown in Table 9.26, the results are similar to those varying u_p.

Table 9.26: Outflow uncertainty: Comparison between VMPC and optimal SVMPC for $u_{\text{offset}}^{\text{out+}}$.

	VMPC					
u_{off}	0%	5%	10%	25%	50%	75%
$Q_{\text{ov}_{\text{total}}}$	167.434	167.497	167.45	167.621	168.324	169.353
$\%\mathbf{F}_Q$		**0.04%**	**0.01%**	**0.11%**	**0.53%**	**1.15%**
$m_{\text{ov}_{\text{total}}}^{\text{NH}_4}$	1072.366	1075.368	1075.381	1075.443	1086.521	1105.802
$\%\mathbf{F}_m$		**0.28%**	**0.28%**	**0.29%**	**1.32%**	**3.12%**
ξ_{rain}	7.926	7.886	7.854	7.824	7.71	7.699
	SVMPC - $\zeta = 0.60$					
u_{off}	0%	5%	10%	25%	50%	75%
$Q_{\text{ov}_{\text{total}}}$	177.244	177.196	177.173	177.199	177.367	177.576
$\%\mathbf{F}_Q$		**-0.03%**	**-0.04%**	**-0.03%**	**0.07%**	**0.19%**
$\%\mathbf{F}_Q^*$	**-0.06%**	**0.02%**	**0.03%**	**0.07%**	**0.16%**	**0.3%**
$m_{\text{ov}_{\text{total}}}^{\text{NH}_4}$	1280.512	1280.113	1280.045	1281.628	1285.004	1288.515
$\%\mathbf{F}_m$		**-0.03%**	**-0.04%**	**0.09%**	**0.35%**	**0.62%**
$\%\mathbf{F}_m^*$	**0.29%**	**0.38%**	**0.42%**	**0.63%**	**1.12%**	**1.85%**
ξ_{rain}	6.564	6.545	6.465	6.426	6.453	6.486
$\%\mathbf{F}_\xi^*$	**-22.73%**	**-22.36%**	**-23.03%**	**-23.3%**	**-22.69%**	**-22.32%**
	SVMPC - $\zeta = 0.80$					
u_{off}	0%	5%	10%	25%	50%	75%
$Q_{\text{ov}_{\text{total}}}$	177.245	177.197	177.172	177.199	177.367	177.575
$\%\mathbf{F}_Q$		**-0.03%**	**-0.04%**	**-0.03%**	**0.07%**	**0.19%**
$\%\mathbf{F}_Q^*$	**-0.2%**	**-0.01%**	**0.0%**	**0.05%**	**0.14%**	**0.28%**
$m_{\text{ov}_{\text{total}}}^{\text{NH}_4}$	1280.479	1280.116	1280.047	1281.628	1285.004	1288.516
$\%\mathbf{F}_m$		**-0.03%**	**-0.03%**	**0.09%**	**0.35%**	**0.63%**
$\%\mathbf{F}_m^*$	**0.15%**	**0.35%**	**0.38%**	**0.59%**	**1.09%**	**1.81%**
ξ_{rain}	6.564	6.545	6.465	6.426	6.453	6.486
$\%\mathbf{F}_\xi^*$	**-23.46%**	**-22.54%**	**-22.97%**	**-23.23%**	**-22.75%**	**-22.43%**
	SVMPC - $\zeta = 0.95$					
u_{off}	0%	5%	10%	25%	50%	75%
$Q_{\text{ov}_{\text{total}}}$	177.246	177.197	177.172	177.199	177.367	177.575
$\%\mathbf{F}_Q$		**-0.03%**	**-0.04%**	**-0.03%**	**0.07%**	**0.19%**
$\%\mathbf{F}_Q^*$	**-0.49%**	**-0.05%**	**-0.05%**	**0.01%**	**0.11%**	**0.25%**
$m_{\text{ov}_{\text{total}}}^{\text{NH}_4}$	1280.496	1280.115	1280.047	1281.628	1285.003	1288.516
$\%\mathbf{F}_m$		**-0.03%**	**-0.04%**	**0.09%**	**0.35%**	**0.63%**
$\%\mathbf{F}_m^*$	**-0.15%**	**0.29%**	**0.32%**	**0.54%**	**1.08%**	**1.73%**
ξ_{rain}	6.564	6.545	6.465	6.426	6.453	6.486
$\%\mathbf{F}_\xi^*$	**-24.05%**	**-22.88%**	**-22.97%**	**-23.18%**	**-22.76%**	**-22.58%**

Finally, the last outflow uncertainty analysed is $u^{\text{out-}}_{\text{offset}}$ shown in Table 9.27, which in this scenario showed a better robustness of SVMPC compared to VMPC. Although the overflow is still overall higher, ξ_{rain} is lower for SVMPC, indicating that the WWTP is more often at their design inflow.

Table 9.27: Outflow uncertainty: Comparison between VMPC and optimal SVMPC for $u^{\text{out-}}_{\text{offset}}$.

	VMPC					
u_{off}	0%	−5%	−10%	−25%	−50%	−75%
$Q_{\text{ov}_{\text{total}}}$	167.434	167.791	168.256	170.937	174.586	176.381
$\%\mathbf{F}_Q$		**0.21%**	**0.49%**	**2.09%**	**4.27%**	**5.34%**
$m^{\text{NH}_4}_{\text{ov}_{\text{total}}}$	1072.366	1081.025	1087.939	1139.193	1200.527	1232.686
$\%\mathbf{F}_m$		**0.81%**	**1.45%**	**6.23%**	**11.95%**	**14.95%**
ξ_{rain}	7.926	7.737	7.675	7.622	7.483	7.203
	SVMPC - $\zeta = 0.60$					
u_{off}	0%	−5%	−10%	−25%	−50%	−75%
$Q_{\text{ov}_{\text{total}}}$	177.244	177.181	177.101	177.088	177.708	178.052
$\%\mathbf{F}_Q$		**-0.04%**	**-0.08%**	**-0.09%**	**0.26%**	**0.46%**
$\%\mathbf{F}^*_Q$	**-0.06%**	**-0.03%**	**-0.09%**	**-0.34%**	**-0.43%**	**-0.49%**
$m^{\text{NH}_4}_{\text{ov}_{\text{total}}}$	1280.512	1279.2	1278.267	1275.608	1281.233	1285.073
$\%\mathbf{F}_m$		**-0.1%**	**-0.18%**	**-0.38%**	**0.06%**	**0.36%**
$\%\mathbf{F}^*_m$	**0.29%**	**0.29%**	**0.24%**	**-0.25%**	**-0.44%**	**-0.54%**
ξ_{rain}	6.564	6.619	6.55	6.51	6.626	6.283
$\%\mathbf{F}^*_\xi$	**-22.73%**	**-20.58%**	**-20.93%**	**-18.71%**	**-9.05%**	**-0.19%**
	SVMPC - $\zeta = 0.80$					
u_{off}	0%	−5%	−10%	−25%	−50%	−75%
$Q_{\text{ov}_{\text{total}}}$	177.245	177.183	177.101	177.085	177.707	178.051
$\%\mathbf{F}_Q$		**-0.03%**	**-0.08%**	**-0.09%**	**0.26%**	**0.45%**
$\%\mathbf{F}^*_Q$	**-0.2%**	**-0.05%**	**-0.17%**	**-0.46%**	**-0.52%**	**-0.6%**
$m^{\text{NH}_4}_{\text{ov}_{\text{total}}}$	1280.479	1279.193	1278.265	1275.549	1281.223	1285.076
$\%\mathbf{F}_m$		**-0.1%**	**-0.17%**	**-0.39%**	**0.06%**	**0.36%**
$\%\mathbf{F}^*_m$	**0.15%**	**0.26%**	**0.15%**	**-0.65%**	**-0.86%**	**-1.1%**
ξ_{rain}	6.564	6.619	6.55	6.51	6.626	6.281
$\%\mathbf{F}^*_\xi$	**-23.46%**	**-20.68%**	**-21.04%**	**-21.17%**	**-18.67%**	**-18.44%**
	SVMPC - $\zeta = 0.95$					
u_{off}	0%	−5%	−10%	−25%	−50%	−75%
$Q_{\text{ov}_{\text{total}}}$	177.246	177.182	177.1	177.085	177.707	178.05
$\%\mathbf{F}_Q$		**-0.04%**	**-0.08%**	**-0.09%**	**0.26%**	**0.45%**
$\%\mathbf{F}^*_Q$	**-0.49%**	**-0.15%**	**-0.23%**	**-0.49%**	**-0.54%**	**-0.63%**
$m^{\text{NH}_4}_{\text{ov}_{\text{total}}}$	1280.496	1279.198	1278.267	1275.547	1281.228	1285.069
$\%\mathbf{F}_m$		**-0.1%**	**-0.17%**	**-0.39%**	**0.06%**	**0.36%**
$\%\mathbf{F}^*_m$	**-0.15%**	**0.18%**	**0.11%**	**-0.59%**	**-0.86%**	**-1.12%**
ξ_{rain}	6.564	6.619	6.55	6.512	6.626	6.282
$\%\mathbf{F}^*_\xi$	**-24.05%**	**-20.88%**	**-21.14%**	**-21.49%**	**-19.13%**	**-19.25%**

Uncertainty on $Q_{ov}(k)$

The last type of uncertainty evaluated is the overflow, starting with the variability shown in Table 9.28. The results are similar to the outflow uncertainty as VMPC is already robust for this uncertainty.

Table 9.28: Overflow uncertainty: Comparison between VMPC and optimal SVMPC for u_p.

	VMPC					
u_p	0%	50%	100%	150%	175%	200%
$Q_{\mathrm{ov}_{\mathrm{total}}}$	167.434	167.682	167.661	167.609	167.595	167.552
$\%\mathbf{F}_Q$		**0.15%**	**0.14%**	**0.1%**	**0.1%**	**0.07%**
$m^{\mathrm{NH_4}}_{\mathrm{ov}_{\mathrm{total}}}$	1072.366	1074.136	1071.316	1068.024	1066.955	1064.954
$\%\mathbf{F}_m$		**0.17%**	**-0.1%**	**-0.4%**	**-0.5%**	**-0.69%**
ξ_{rain}	7.926	7.889	7.876	7.872	7.868	7.871
	SVMPC - $\zeta = 0.60$					
u_p	0%	50%	100%	150%	175%	200%
$Q_{\mathrm{ov}_{\mathrm{total}}}$	177.244	177.258	177.264	177.246	177.243	177.233
$\%\mathbf{F}_Q$		**0.01%**	**0.01%**	**0.0%**	**-0.0%**	**-0.01%**
$\%\mathbf{F}^*_Q$	**-0.06%**	**-0.01%**	**-0.01%**	**-0.02%**	**-0.03%**	**-0.03%**
$m^{\mathrm{NH_4}}_{\mathrm{ov}_{\mathrm{total}}}$	1280.512	1280.489	1280.423	1280.157	1279.957	1279.61
$\%\mathbf{F}_m$		**-0.0%**	**-0.01%**	**-0.03%**	**-0.04%**	**-0.07%**
$\%\mathbf{F}^*_m$	**0.29%**	**0.36%**	**0.35%**	**0.37%**	**0.37%**	**0.35%**
ξ_{rain}	6.564	6.564	6.564	6.564	6.565	6.566
$\%\mathbf{F}^*_\xi$	**-22.73%**	**-22.58%**	**-22.64%**	**-22.69%**	**-22.68%**	**-22.68%**
	SVMPC - $\zeta = 0.80$					
u_p	0%	50%	100%	150%	175%	200%
$Q_{\mathrm{ov}_{\mathrm{total}}}$	177.245	177.258	177.263	177.247	177.242	177.233
$\%\mathbf{F}_Q$		**0.01%**	**0.01%**	**0.0%**	**-0.0%**	**-0.01%**
$\%\mathbf{F}^*_Q$	**-0.2%**	**-0.03%**	**-0.06%**	**-0.09%**	**-0.1%**	**-0.13%**
$m^{\mathrm{NH_4}}_{\mathrm{ov}_{\mathrm{total}}}$	1280.479	1280.491	1280.399	1280.135	1279.911	1279.566
$\%\mathbf{F}_m$		**0.0%**	**-0.01%**	**-0.03%**	**-0.04%**	**-0.07%**
$\%\mathbf{F}^*_m$	**0.15%**	**0.33%**	**0.33%**	**0.34%**	**0.35%**	**0.36%**
ξ_{rain}	6.564	6.564	6.564	6.564	6.565	6.566
$\%\mathbf{F}^*_\xi$	**-23.46%**	**-22.69%**	**-22.75%**	**-23.02%**	**-23.11%**	**-23.15%**
	SVMPC - $\zeta = 0.95$					
u_p	0%	50%	100%	150%	175%	200%
$Q_{\mathrm{ov}_{\mathrm{total}}}$	177.246	177.258	177.263	177.247	177.243	177.235
$\%\mathbf{F}_Q$		**0.01%**	**0.01%**	**0.0%**	**-0.0%**	**-0.01%**
$\%\mathbf{F}^*_Q$	**-0.49%**	**-0.06%**	**-0.12%**	**-0.19%**	**-0.23%**	**-0.26%**
$m^{\mathrm{NH_4}}_{\mathrm{ov}_{\mathrm{total}}}$	1280.496	1280.486	1280.395	1280.095	1279.867	1279.461
$\%\mathbf{F}_m$		**-0.0%**	**-0.01%**	**-0.03%**	**-0.05%**	**-0.08%**
$\%\mathbf{F}^*_m$	**-0.15%**	**0.31%**	**0.27%**	**0.31%**	**0.27%**	**0.35%**
ξ_{rain}	6.564	6.564	6.564	6.564	6.565	6.566
$\%\mathbf{F}^*_\xi$	**-24.05%**	**-22.74%**	**-23.12%**	**-23.43%**	**-23.61%**	**-23.67%**

The second scenario shown in Table 9.29 presents $u^{\text{ov+}}_{\text{offset}}$. For this example, SVMPC is capable of reaching the same overflow ranges of VMPC, while also having an improved ξ_{rain} compared to the deterministic approach.

Table 9.29: Overflow uncertainty: Comparison between VMPC and optimal SVMPC for $u^{\text{ov+}}_{\text{offset}}$.

	VMPC					
u_{off}	0%	5%	10%	25%	50%	75%
$Q_{\text{ov}_{\text{total}}}$	167.434	167.099	167.368	167.516	167.466	167.332
$\%\mathbf{F}_Q$		**-0.2%**	**-0.04%**	**0.05%**	**0.02%**	**-0.06%**
$m^{\text{NH}_4}_{\text{ov}_{\text{total}}}$	1072.366	1058.702	1037.079	1015.923	1010.801	1010.258
$\%\mathbf{F}_m$		**-1.27%**	**-3.29%**	**-5.26%**	**-5.74%**	**-5.79%**
ξ_{rain}	7.926	7.702	7.621	7.553	7.535	7.535
	SVMPC - $\zeta = 0.60$					
u_{off}	0%	5%	10%	25%	50%	75%
$Q_{\text{ov}_{\text{total}}}$	177.244	177.232	177.052	172.511	168.052	167.508
$\%\mathbf{F}_Q$		**-0.01%**	**-0.11%**	**-2.67%**	**-5.19%**	**-5.49%**
$\%\mathbf{F}^*_Q$	**-0.06%**	**0.05%**	**0.23%**	**0.3%**	**-1.02%**	**-0.65%**
$m^{\text{NH}_4}_{\text{ov}_{\text{total}}}$	1280.512	1279.946	1272.521	1163.15	1100.962	1096.66
$\%\mathbf{F}_m$		**-0.04%**	**-0.62%**	**-9.17%**	**-14.02%**	**-14.36%**
$\%\mathbf{F}^*_m$	**0.29%**	**0.72%**	**1.61%**	**0.89%**	**-2.03%**	**-0.57%**
ξ_{rain}	6.564	6.566	6.578	6.423	6.328	6.158
$\%\mathbf{F}^*_\xi$	**-22.73%**	**-22.47%**	**-22.32%**	**-23.74%**	**-24.75%**	**-26.82%**
	SVMPC - $\zeta = 0.80$					
u_{off}	0%	5%	10%	25%	50%	75%
$Q_{\text{ov}_{\text{total}}}$	177.245	177.233	177.054	172.531	168.072	167.508
$\%\mathbf{F}_Q$		**-0.01%**	**-0.11%**	**-2.66%**	**-5.18%**	**-5.49%**
$\%\mathbf{F}^*_Q$	**-0.2%**	**0.05%**	**0.22%**	**0.32%**	**-1.01%**	**-0.62%**
$m^{\text{NH}_4}_{\text{ov}_{\text{total}}}$	1280.479	1279.926	1272.413	1163.481	1102.038	1096.661
$\%\mathbf{F}_m$		**-0.04%**	**-0.63%**	**-9.14%**	**-13.94%**	**-14.36%**
$\%\mathbf{F}^*_m$	**0.15%**	**0.71%**	**1.59%**	**0.93%**	**-1.94%**	**-0.43%**
ξ_{rain}	6.564	6.565	6.579	6.423	6.339	6.158
$\%\mathbf{F}^*_\xi$	**-23.46%**	**-22.5%**	**-22.33%**	**-23.78%**	**-24.65%**	**-26.85%**
	SVMPC - $\zeta = 0.95$					
u_{off}	0%	5%	10%	25%	50%	75%
$Q_{\text{ov}_{\text{total}}}$	177.246	177.231	177.053	172.531	168.073	167.511
$\%\mathbf{F}_Q$		**-0.01%**	**-0.11%**	**-2.66%**	**-5.18%**	**-5.49%**
$\%\mathbf{F}^*_Q$	**-0.49%**	**0.04%**	**0.22%**	**0.33%**	**-1.0%**	**-0.58%**
$m^{\text{NH}_4}_{\text{ov}_{\text{total}}}$	1280.496	1279.961	1272.417	1163.428	1102.644	1097.681
$\%\mathbf{F}_m$		**-0.04%**	**-0.63%**	**-9.14%**	**-13.89%**	**-14.28%**
$\%\mathbf{F}^*_m$	**-0.15%**	**0.7%**	**1.57%**	**0.94%**	**-1.9%**	**-0.3%**
ξ_{rain}	6.564	6.566	6.579	6.423	6.335	6.156
$\%\mathbf{F}^*_\xi$	**-24.05%**	**-22.58%**	**-22.42%**	**-23.87%**	**-24.78%**	**-26.94%**

Lastly, the performance of $u^{\text{ov-}}_{\text{offset}}$ shown in Table 9.30 did not change much in terms of overflow, but ξ_{rain} is reduced by approximately 22%.

Table 9.30: Overflow uncertainty: Comparison between VMPC and optimal SVMPC for $u^{\text{ov-}}_{\text{offset}}$.

	VMPC					
u_{off}	0%	−5%	−10%	−25%	−50%	−75%
$Q_{\text{ov}_{\text{total}}}$	167.434	169.609	169.572	169.599	169.561	169.561
$\%\mathbf{F}_Q$		**1.3%**	**1.28%**	**1.29%**	**1.27%**	**1.27%**
$m^{\text{NH}_4}_{\text{ov}_{\text{total}}}$	1072.366	1099.018	1097.333	1096.522	1094.832	1094.832
$\%\mathbf{F}_m$		**2.49%**	**2.33%**	**2.25%**	**2.09%**	**2.09%**
ξ_{rain}	7.926	7.485	7.501	7.488	7.476	7.476
	SVMPC - $\zeta = 0.60$					
u_{off}	0%	−5%	−10%	−25%	−50%	−75%
$Q_{\text{ov}_{\text{total}}}$	177.244	177.255	177.277	177.34	177.355	177.355
$\%\mathbf{F}_Q$		**0.01%**	**0.02%**	**0.05%**	**0.06%**	**0.06%**
$\%\mathbf{F}^*_Q$	**-0.06%**	**-0.01%**	**-0.01%**	**0.0%**	**-0.0%**	**-0.0%**
$m^{\text{NH}_4}_{\text{ov}_{\text{total}}}$	1280.512	1280.842	1280.927	1280.967	1280.975	1280.975
$\%\mathbf{F}_m$		**0.03%**	**0.03%**	**0.04%**	**0.04%**	**0.04%**
$\%\mathbf{F}^*_m$	**0.29%**	**0.36%**	**0.37%**	**0.38%**	**0.37%**	**0.37%**
ξ_{rain}	6.564	6.564	6.564	6.564	6.564	6.564
$\%\mathbf{F}^*_\xi$	**-22.73%**	**-22.45%**	**-22.44%**	**-22.44%**	**-22.44%**	**-22.44%**
	SVMPC - $\zeta = 0.80$					
u_{off}	0%	−5%	−10%	−25%	−50%	−75%
$Q_{\text{ov}_{\text{total}}}$	177.245	177.255	177.277	177.34	177.355	177.355
$\%\mathbf{F}_Q$		**0.01%**	**0.02%**	**0.05%**	**0.06%**	**0.06%**
$\%\mathbf{F}^*_Q$	**-0.2%**	**-0.01%**	**-0.01%**	**0.0%**	**-0.01%**	**-0.01%**
$m^{\text{NH}_4}_{\text{ov}_{\text{total}}}$	1280.479	1280.842	1280.927	1280.967	1280.975	1280.975
$\%\mathbf{F}_m$		**0.03%**	**0.03%**	**0.04%**	**0.04%**	**0.04%**
$\%\mathbf{F}^*_m$	**0.15%**	**0.36%**	**0.37%**	**0.37%**	**0.37%**	**0.37%**
ξ_{rain}	6.564	6.564	6.564	6.564	6.564	6.564
$\%\mathbf{F}^*_\xi$	**-23.46%**	**-22.47%**	**-22.47%**	**-22.46%**	**-22.46%**	**-22.46%**
	SVMPC - $\zeta = 0.95$					
u_{off}	0%	−5%	−10%	−25%	−50%	−75%
$Q_{\text{ov}_{\text{total}}}$	177.246	177.255	177.277	177.341	177.355	177.355
$\%\mathbf{F}_Q$		**0.01%**	**0.02%**	**0.05%**	**0.06%**	**0.06%**
$\%\mathbf{F}^*_Q$	**-0.49%**	**-0.01%**	**-0.01%**	**0.0%**	**-0.01%**	**-0.01%**
$m^{\text{NH}_4}_{\text{ov}_{\text{total}}}$	1280.496	1280.842	1280.927	1280.967	1280.975	1280.975
$\%\mathbf{F}_m$		**0.03%**	**0.03%**	**0.04%**	**0.04%**	**0.04%**
$\%\mathbf{F}^*_m$	**-0.15%**	**0.35%**	**0.36%**	**0.36%**	**0.36%**	**0.36%**
ξ_{rain}	6.564	6.564	6.564	6.564	6.564	6.564
$\%\mathbf{F}^*_\xi$	**-24.05%**	**-22.56%**	**-22.55%**	**-22.55%**	**-22.55%**	**-22.55%**

In summary, optimal weights introduced more overflow stability to SVMPC, while reducing ξ_{rain} in most

scenarios. In particular, the most critical uncertainty, $u_{\text{offset}}^{\text{vol-}}$, demonstrated a significant improvement, especially when compared to both the non-optimal SVMPC and VMPC. In general, VMPC still outperforms SVMPC in terms of reducing overflow load and volume, while SVMPC offers more stability when managing uncertainties and a overall reduced value of ξ_{rain}. This discrepancy could be attributed to the simplicity of the network used to validate the method. The relatively straightforward structure of the network may not provide enough complexity to fully reveal the potential benefits of the stochastic approach. Specifically, the conservative behaviour of SVMPC might not allow enough flexibility for the controller to optimise performance as effectively as the deterministic VMPC, which may have more freedom to adjust to the system dynamics. In simpler networks, this conservative approach could lead to overly cautious control actions, which could limit performance improvements. In contrast, more complex systems with diverse dynamics could potentially offer SVMPC greater opportunities to showcase its strengths. In the next chapter, the controllers will be reevaluated in systems with higher complexity to assess whether the impact of the stochastic method can be more effectively realised and its performance better compared.

However, the next sections present a similar stochastic formulation using the CC-MPC framework, now reformulating the pollution-based methods PWMPC and NPMPC into a stochastic MPC.

9.4 Stochastic Pollution-weighted Model Predictive Control

The next method proposed in this chapter is the Stochastic Pollution-weighted Model Predictive Control (SPWMPC), which is also inspired by the papers in [151, 153, 155], although implemented in a pollution-based framework. The SPWMPC can be described as a linear pollution-based MPC capable of minimising load overflow while keeping computational efforts similar to SVMPC. It incorporates water quality by adjusting the weights of the MPC in each control loop, estimating the concentration of a given pollutant within the SU and prioritising the units where the concentration is higher. The reformulation to turn the controller into a stochastic MPC is performed by using the CC-MPC method, considering that the uncertainty follows the same principles as in Section 9.1.

9.4.1 Description

The SPWMPC is a method that transforms PWMPC from Section 8.2 into a stochastic control method using the techniques in [151, 153, 155], but considering a pollution-based algorithm. Since PWMPC is a deterministic controller, a few assumptions are necessary to change it to a stochastic method.

1. As for stochastic volume-based formulation, the variables are reformulated as expectations of the variable $\mathbb{E}\{.\}$, e.g. volume $V(k)$, outflow $Q_{\text{out}}(k)$, overflow $Q_{\text{ov}}(k)$, and inflow $Q_{\text{in}}(k)$ are reformulated as $\mathbb{E}\{V(k)\}$, $\mathbb{E}\{Q_{\text{out}}(k)\}$, $\mathbb{E}\{Q_{\text{ov}}(k)\}$ and $\mathbb{E}\{Q_{\text{in}}(k)\}$.

2. Additionally, the concentration within the SU, $C(k)$ is reformulated as $\mathbb{E}\{C(k)\}$.

3. They also include a standard deviation $\sigma^2\{V(k)\}$, $\sigma^2\{Q_{\text{out}}(k)\}$, $\sigma^2\{Q_{\text{in}}(k)\}$ and $\sigma^2\{Q_{\text{ov}}(k)\}$.

4. Since the concentration is propagated as a constant value, $\sigma^2\{C(k)\} = 0$ and $\mathbb{E}\{C(k)\} = C(k)$.

5. Uncertainties are considered to be truncated Gaussian distributed with heteroscedastic behaviour.

The scheme for the control algorithm is presented in Figure 9.21. SPWMPC receives feedback information from the UDS through the measurement devices and the expectations and standard deviations are estimated given a pre-determined probabilistic distribution. The internal model is used to predict the expected volume in the prediction horizon, where the objective is to estimate the expected overflow in the future.

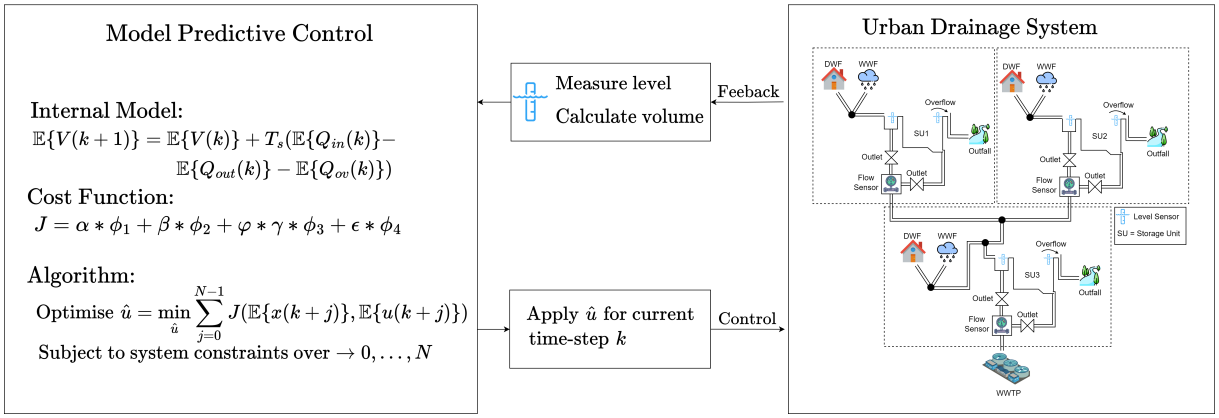

Figure 9.21: SPWMPC scheme for Urban Drainage Systems.

The chance-constraints added to the formulation are the same as for SVMPC in Equations 9.9, 9.10, 9.11 and 9.12, where the maximum volume is considered to have a probability of being violated. The estimation of $C(k)$ is done following the deterministic approach, as in Equations 8.30 and 8.31.

9.4.2 Optimisation Problem

Given the stochastic constraints and that the states $\boldsymbol{x}(k)$, and input $\boldsymbol{u}(k)$, are

$$\boldsymbol{x}(k) = [\mathbb{E}\{\boldsymbol{V}(k)\},\ \mathbb{E}\{\boldsymbol{Q}_{\text{ov}}(k)\},\ \mathbb{E}\{\boldsymbol{Q}_{\text{in}}(k)\},\ \boldsymbol{\theta}_{\min}(k),\ \boldsymbol{\theta}_{\max}(k)] \qquad \text{and} \qquad \boldsymbol{u}(k) = [\mathbb{E}\{\boldsymbol{Q}_{\text{out}}(k)\}]$$

the optimisation problem, where $\hat{\boldsymbol{u}}(k)$ is the optimal output, is defined as:

$$\hat{u}(k) = \arg\min_{u} \sum_{j=0}^{N-1} J(x(k+j), u(k+j)) \tag{9.21a}$$

subject to

$$\mathbb{E}\{V^t(k+j+1)\} = \mathbb{E}\{V^t(k+j)\} + T_s\big[\mathbb{E}\{Q^t_{\text{in}}(k+j)\} - \mathbb{E}\{Q^t_{\text{out}}(k+j)\} - \mathbb{E}\{Q^t_{\text{ov}}(k+j)\}\big], \qquad t = 1, 2, ..., N_t \tag{9.21b}$$

$$\sigma^2\{V^t(k+j+1)\} = \sigma^2\{V^t(k+j)\} + T_s^2\big(\sigma^2\{Q^t_{\text{in}}(k+j)\} + \sigma^2\{Q^t_{\text{out}}(k+j)\} + \sigma^2\{Q^t_{\text{ov}}(k+j)\}\big), \qquad t = 1, 2, ..., N_t \tag{9.21c}$$

$$\mathbb{E}\{Q^t_{in}(k+j)\} = \mathbb{E}\{Q^t_{catchment}(k+j)\} + \sum_{i \in N^*_{\text{in}}} \mathbb{E}\{Q^i_{out}(k+j)\}, \qquad t = 1, 2, ..., N_t \tag{9.21d}$$

$$\mathbb{E}\{V^t(k+j)\} + T_s\big(\mathbb{E}\{Q^t_{\text{in}}(k+j)\} + \mathbb{E}\{Q^t_{\text{out}}(k+j)\}\big) \geq \sigma\{V^t(k+j) + T_s(Q^t_{\text{in}}(k+j) + Q^t_{\text{out}}(k+j))\}\Phi^{-1}(\zeta) - \theta^t_{\min}, \qquad t = 1, 2, ..., N_t \tag{9.21e}$$

$$\mathbb{E}\{V^t(k+j)\} + T_s\big(\mathbb{E}\{Q^t_{\text{in}}(k+j)\} - \mathbb{E}\{Q^t_{\text{out}}(k+j)\} - \mathbb{E}\{Q^t_{\text{ov}}(k+j)\}\big) \geq 0, \qquad t = 1, 2, ..., N_t \tag{9.21f}$$

$$\mathbb{E}\{V^t(k+j)\} + T_s\big(\mathbb{E}\{Q^t_{\text{in}}(k+j)\} - \mathbb{E}\{Q^t_{\text{out}}(k+j)\}\big) \leq V^t_{\max} - \sigma\{V^t(k+j) + T_s(Q^t_{\text{in}}(k+j) + Q^t_{\text{out}}(k+j))\}\Phi^{-1}(\zeta) + \theta^t_{\max}, \qquad t = 1, 2, ..., N_t \tag{9.21g}$$

$$\mathbb{E}\{V^t(k+j)\} + T_s\big(\mathbb{E}\{Q^t_{\text{in}}(k+j)\} - \mathbb{E}\{Q^t_{\text{out}}(k+j)\} - \mathbb{E}\{Q^t_{\text{ov}}(k+j)\}\big) \leq V^t_{\max}, \qquad t = 1, 2, ..., N_t \tag{9.21h}$$

$$0 \leq \sum_{i \in N^*_{\text{wwtp}}} \mathbb{E}\{Q^i_{\text{out}}(k+j)\} \leq Q_{\text{wwtp}_{\max}}, \qquad t = 1, 2, ..., N_t \tag{9.21i}$$

$$0 \leq \mathbb{E}\{Q^t_{\text{out}}(k)\} \leq Q^t_{\text{out}_{\max}}, \qquad t = 1, 2, ..., N_t \tag{9.21j}$$

$$\mathbb{E}\{Q^t_{\text{ov}}(k+j)\} \geq 0, \qquad t = 1, 2, ..., N_t \tag{9.21k}$$

$$0 \leq \theta^t_{\min}(k+j) \leq \sigma\{V^t(k+j) + T_s(Q^t_{\text{in}}(k+j) + Q_{\text{out}}(k+j))\}\Phi^{-1}(\zeta), \qquad t = 1, 2, ..., N_t \tag{9.21l}$$

$$0 \leq \theta^t_{\max}(k+j), \qquad t = 1, 2, ..., N_t \tag{9.21m}$$

The cost function J is calculated as follows:

$$J(x(k), u(k)) = J(\mathbb{E}\{V(k)\}, \mathbb{E}\{Q_{\text{out}}(k)\}, \mathbb{E}\{Q_{\text{in}}(k)\}, \theta_{\min}(k), \theta_{\max}(k), \mathbb{E}\{Q_{\text{out}}(k)\}) \tag{9.22}$$

$$= \alpha\phi_1(k) + \beta\phi_2(k) + \gamma\phi_3(k) + \epsilon\phi_4(k) + \epsilon\phi_5(k) \tag{9.23}$$

where (α, β, γ, ϵ) are the weights for the objectives (ϕ_1, ϕ_2, ϕ_3, (ϕ_4, ϕ_5)), and φ is defined as the weighting factor φ that is equal to the concentration C at time k for N_t storage units, hence $\varphi^i(k) = C^i(k)$. The objectives can be defined as follows:

- ϕ_1, in Equation 9.24, is used to homogeneously store the volume within all SI structures in the sewage network.

$$\phi_1(k) = \sum_{i=1}^{N_t} \left(\mathbb{E}\{V^i(k)\} - \frac{V^i_{\max}}{\sum_{j=1}^{N} V^j_{\max}} \sum_{n=1}^{N_t} \mathbb{E}\{V_n(k)\} \right)^2 \tag{9.24}$$

- ϕ_2, in Equation 9.25, keeps the flow towards the wastewater treatment plant near the operating reference value defined by Q_{ref}.

$$\phi_2(k) = \sum_{j \in N_{up}} \left(Q^j_{\text{ref}} - \sum_{i \in N^*_t} \mathbb{E}\{Q^i_{\text{out}}(k - d^{i,t})\} \right)^2 \tag{9.25}$$

where Q_{ref} is the reference flow for the i^{th} SI, which includes $Q_{\text{wwtp}_{\text{ref}}}$ as the inflow reference to the WWTP, Q_{out} is the outflow from each SI, $d_{i,t}$ represents the transport time of the i^{th} SI to

the destination SI m, N_t^* are all SIs draining in the destination t and N_{up} are all SIs that have an upstream SI and the wastewater treatment plant.

- ϕ_3, in Equation 9.26, is used to minimise the overflow.

$$\phi_3(k) = \sum_{i=1}^{N_t} (\varphi^i(k)\mathbb{E}\{Q_{\text{ov}}^i(k)\} - \text{NL})^2 \tag{9.26}$$

- ϕ_4, in Equation 9.27, is used to minimise the slack variable $\theta_{\min}$.

$$\phi_4(k) = \sum_{i=1}^{N_t} (\theta_{\min}^i)^2 \tag{9.27}$$

- ϕ_5, in Equation 9.28, is used to minimise the slack variable $\theta_{\max}$.

$$\phi_5(k) = \sum_{i=1}^{N_t} (\theta_{\max}^i)^2 \tag{9.28}$$

Finally, the control loop algorithm for the PWMPC can summarised as below:

Control Algorithm

(a) Initialise $\boldsymbol{x}(k) = \boldsymbol{x}(0)$, where $\boldsymbol{x}(0) = [\mathbb{E}\{\boldsymbol{V}(0)\},\ \mathbb{E}\{\boldsymbol{Q}_{\text{ov}}(0)\},\ \boldsymbol{\theta}_{\min}(0),\ \boldsymbol{\theta}_{\max}(0)]$ is the current state of the system, and the standard deviations $\sigma\{\boldsymbol{V}(k)\}$, $\sigma\{\boldsymbol{Q}_{\text{in}}(k)\}$, $\sigma\{\boldsymbol{Q}_{\text{out}}(k)\}$, $\sigma\{\boldsymbol{Q}_{\text{ov}}(k)\}$;

(b) Estimate $\mathbb{E}\{\boldsymbol{Q}_{\text{in}}(k)\}$ using Equation 9.7, $\boldsymbol{C}_{\text{in}}(k)$ using Equation 8.30, and $\mathbb{E}\{\boldsymbol{C}(k)\} = \boldsymbol{C}(k)$ using Equation 8.31;

(c) Solve the optimisation problem as in Equation 9.21a and obtain the optimal control sequence $\hat{\boldsymbol{u}}(k)$;

(d) At time k, apply the first input $\boldsymbol{u}(k) = \boldsymbol{Q}_{\text{out}}(k)$ of the optimal control sequence to the UDS;

(e) Wait for next control loop $k = k + 1$;

(f) Measure $\boldsymbol{V}(k)$ and $\boldsymbol{Q}_{\text{out}}(k)$, calculate $\boldsymbol{Q}_{\text{ov}}(k)$, and update the expected values as $\mathbb{E}\{\boldsymbol{V}(k)\} = u_s \cdot \boldsymbol{V}(k) + u_{\text{off}}$, $\mathbb{E}\{\boldsymbol{Q}_{\text{out}}(k)\} = u_s \cdot \boldsymbol{Q}_{\text{out}}(k) + u_{\text{off}}$, and $\mathbb{E}\{\boldsymbol{Q}_{\text{ov}}(k)\} = u_s \cdot \boldsymbol{Q}_{\text{ov}}(k) + u_{\text{off}}$, then return to Step (b).

The following scenarios are considered for standard deviations:

- In all scenarios, a standard deviation for the inflow $Q_{\text{in}}(k)$ is determined to ascertain possible errors in the estimation during the control loop:

$$\sigma\{Q_{\text{in}}(k)\} = u_p * \frac{Q_{\text{in}}(k)}{n}$$

where n represents a fraction of the actual value.

- The first scenario considers uncertainties on the Volume, therefore $\sigma\{Q_{\text{out}}(k)\} = 0$, $\sigma\{Q_{\text{ov}}(k)\} = 0$ and
$$\sigma\{V(k)\} = u_p * (V_{\max} - V(k))$$

- The second scenario considers uncertainties on the Outflow, therefore, at $k = 0$, $\sigma\{V(0)\} = 0$ and $\sigma\{Q_{\text{ov}}(k)\} = 0$ and
$$\sigma\{Q_{\text{out}}(k)\} = u_p * (Q_{\text{out}_{\max}} - Q_{\text{out}}(k))$$

- The third scenario considers uncertainties on the Overflow, therefore, at $k = 0$, $\sigma\{V(0)\} = 0$ and $\sigma\{Q_{\text{out}}(k)\} = 0$ and
$$\sigma\{Q_{\text{ov}}(k)\} = u_p * Q_{\text{ov}}(k)$$

For practical purposes, in future simulations $n = 3$, therefore, the inflow standard deviation is a third of the actual value. In the next section, the performance of SPWMPC is assessed through validation methodology, comparing the results with PWMPC for different metrics.

9.4.3 Methodology Validation

The validation of the SPWMPC is carried out by evaluating its control performance under the same conditions presented in Section 9.1. However, for SPWMPC, only a few scenarios were chosen: (1) Volume uncertainty: changes in u_p, (2) Volume uncertainty: negative changes in u_{off} and (3) Outflow uncertainty: negative changes in u_{off}. The other scenarios are added to Appendix A.3 as complementary results. In each scenario, only one type of uncertainty is considered at a time. The weights for SPWMPC are α, β, γ, $\epsilon = (19.1, 149.1, 30.1, 190.0)$ and ζ vary between $[0.6, 0.8, 0.95]$.

Uncertainty on $V(k)$

Firstly, SPWMPC is evaluated considering the uncertainty in $V(k)$. The analysis begins by comparing u_p and evaluating the performance of SPWMPC against PWMPC for varying values of ζ, across u_p = [0%, 5%, 10%, 25%, 50%, 75%]. The results presented in Table 9.31 show that, in general, SPWMPC does not outperform PWMPC in any of the scenarios analysed. Specifically, as ζ increases, the stochastic method demonstrates a notable performance decrease, reaching an increase in volume and load overflow of 8.1% and 14.9% for $\zeta = 0.95$ and $u_p = 75\%$.

For $u_{\text{offset}}^{\text{vol+}}$ as shown in Table 9.32, the results show that, for $\zeta = 0.6$, SPWMPC is more stable than the other configurations, reaching similar load and volume overflow values compared to PWMPC with increased uncertainty, even outperforming it for u_{off} equal to -25% and -50%. However, for ζ equal to 0.8 and 0.95, SPWMPC underperformed considerably, with an increase in overflow of approximately 368% and 1878% for volume and load, respectively, for ζ equal to 0.95.

Table 9.31: Volume uncertainty: Comparison between PWMPC and SPWMPC for u_p.

	PWMPC					
u_p	0%	5%	10%	25%	50%	75%
$Q_{\text{ov}_{\text{total}}}$	168.77	170.499	171.351	172.923	174.078	174.463
$\%\mathbf{F}_Q$		**1.02%**	**1.53%**	**2.46%**	**3.15%**	**3.37%**
$m^{\text{NH}_4}_{\text{ov}_{\text{total}}}$	1034.79	1052.8	1062.468	1078.114	1090.945	1100.189
$\%\mathbf{F}_m$		**1.74%**	**2.67%**	**4.19%**	**5.43%**	**6.32%**
ξ_{rain}	7.629	5.715	4.323	1.789	0.883	0.933
	SPWMPC - $\zeta = 0.60$					
u_p	0%	5%	10%	25%	50%	75%
$Q_{\text{ov}_{\text{total}}}$	177.238	179.027	180.373	183.121	185.151	186.577
$\%\mathbf{F}_Q$		**1.01%**	**1.77%**	**3.32%**	**4.46%**	**5.27%**
$m^{\text{NH}_4}_{\text{ov}_{\text{total}}}$	1267.61	1286.737	1301.862	1327.721	1344.533	1365.298
$\%\mathbf{F}_m$		**1.51%**	**2.7%**	**4.74%**	**6.07%**	**7.71%**
ξ_{rain}	8.508	7.283	6.595	5.543	5.952	5.993
	SPWMPC - $\zeta = 0.80$					
u_p	0%	5%	10%	25%	50%	75%
$Q_{\text{ov}_{\text{total}}}$	177.45	179.831	181.769	186.347	190.466	191.757
$\%\mathbf{F}_Q$		**1.34%**	**2.43%**	**5.01%**	**7.34%**	**8.06%**
$m^{\text{NH}_4}_{\text{ov}_{\text{total}}}$	1268.455	1294.767	1308.873	1364.385	1429.57	1451.283
$\%\mathbf{F}_m$		**2.07%**	**3.19%**	**7.56%**	**12.7%**	**14.41%**
ξ_{rain}	8.614	7.825	7.409	7.06	6.883	6.532
	SPWMPC - $\zeta = 0.95$					
u_p	0%	5%	10%	25%	50%	75%
$Q_{\text{ov}_{\text{total}}}$	177.937	180.66	183.842	189.609	192.011	192.356
$\%\mathbf{F}_Q$		**1.53%**	**3.32%**	**6.56%**	**7.91%**	**8.1%**
$m^{\text{NH}_4}_{\text{ov}_{\text{total}}}$	1271.773	1298.785	1331.293	1415.478	1455.232	1461.078
$\%\mathbf{F}_m$		**2.12%**	**4.68%**	**11.3%**	**14.43%**	**14.89%**
ξ_{rain}	8.653	7.875	7.718	7.766	7.242	6.616

Uncertainty on $Q_{\text{out}}(k)$

The last uncertainty analysed is applied to the outflow measurement of the storage unit. For $u^{\text{out-}}_{\text{offset}}$ as shown in Table 9.33, globally SPWMPC exhibited a much more stable performance when raising the value of the uncertainty, in contrast with PWMPC that underperforms significantly compared to the scenario without uncertainty. However, the controller is still not improving the total overflow.

The results are similar to SVMPC, which showed a performance in absolute terms that is worse than the stochastic method, indicating room for improvement. For most scenarios, SPWMPC demonstrated stability comparable to PWMPC. This underperformance could be linked to suboptimal weight selection, which was not optimised and, despite the stability it offers, the method's performance could be enhanced. To improve this, a sensitivity analysis of the weights, along with the Genetic Algorithm optimisation, is realised. The next section will outline the methodology for weight selection in the context of SPWMPC, utilising the principles from Chapter 7.

Table 9.32: Volume uncertainty: Comparison between PWMPC and SPWMPC for $u_{\text{offset}}^{\text{vol-}}$.

	PWMPC					
u_{off}	0%	−5%	−10%	−25%	−50%	−75%
$Q_{\text{ov}_{\text{total}}}$	168.77	176.55	182.521	203.081	268.19	485.907
$\%\mathbf{F}_Q$		**4.61%**	**8.15%**	**20.33%**	**58.91%**	**187.91%**
$m_{\text{ov}_{\text{total}}}^{\text{NH}_4}$	1034.79	1160.127	1247.463	1588.802	3057.457	12442.546
$\%\mathbf{F}_m$		**12.11%**	**20.55%**	**53.54%**	**195.47%**	**1102.42%**
ξ_{rain}	7.629	5.884	3.317	-7.805	-34.407	-65.611
	SPWMPC - $\zeta = 0.60$					
u_{off}	0%	−5%	−10%	−25%	−50%	−75%
$Q_{\text{ov}_{\text{total}}}$	177.238	180.023	182.457	189.528	227.655	498.509
$\%\mathbf{F}_Q$		**1.57%**	**2.94%**	**6.93%**	**28.45%**	**181.27%**
$m_{\text{ov}_{\text{total}}}^{\text{NH}_4}$	1267.61	1297.776	1327.413	1430.485	2563.912	12837.951
$\%\mathbf{F}_m$		**2.38%**	**4.72%**	**12.85%**	**102.26%**	**912.77%**
ξ_{rain}	8.508	7.364	6.402	3.837	3.004	-66.661
	SPWMPC - $\zeta = 0.80$					
u_{off}	0%	−5%	−10%	−25%	−50%	−75%
$Q_{\text{ov}_{\text{total}}}$	177.45	180.423	183.13	193.176	246.339	740.775
$\%\mathbf{F}_Q$		**1.68%**	**3.2%**	**8.86%**	**38.82%**	**317.46%**
$m_{\text{ov}_{\text{total}}}^{\text{NH}_4}$	1268.455	1300.837	1332.406	1489.349	3441.148	22609.536
$\%\mathbf{F}_m$		**2.55%**	**5.04%**	**17.41%**	**171.29%**	**1682.45%**
ξ_{rain}	8.614	7.147	5.962	2.794	5.354	-78.653
	SPWMPC - $\zeta = 0.95$					
u_{off}	0%	−5%	−10%	−25%	−50%	−75%
$Q_{\text{ov}_{\text{total}}}$	177.937	180.647	183.614	194.444	264.212	833.195
$\%\mathbf{F}_Q$		**1.52%**	**3.19%**	**9.28%**	**48.49%**	**368.25%**
$m_{\text{ov}_{\text{total}}}^{\text{NH}_4}$	1271.773	1303.175	1339.055	1516.472	4348.56	25167.883
$\%\mathbf{F}_m$		**2.47%**	**5.29%**	**19.24%**	**241.93%**	**1878.96%**
ξ_{rain}	8.653	7.191	5.84	2.199	7.663	-80.297

Table 9.33: Outflow uncertainty: Comparison between PWMPC and SPWMPC for $u_{\text{offset}}^{\text{out-}}$.

	PWMPC					
u_{off}	0%	−5%	−10%	−25%	−50%	−75%
$Q_{\text{ov}_{\text{total}}}$	168.77	169.149	169.697	172.141	175.228	176.585
$\%\mathbf{F}_Q$		**0.22%**	**0.55%**	**2.0%**	**3.83%**	**4.63%**
$m_{\text{ov}_{\text{total}}}^{\text{NH}_4}$	1034.79	1044.777	1056.727	1110.921	1170.809	1203.465
$\%\mathbf{F}_m$		**0.97%**	**2.12%**	**7.36%**	**13.14%**	**16.3%**
ξ_{rain}	7.629	7.417	7.401	7.451	7.46	7.108
	SPWMPC - $\zeta = 0.60$					
u_{off}	0%	−5%	−10%	−25%	−50%	−75%
$Q_{\text{ov}_{\text{total}}}$	177.238	177.229	177.273	177.609	178.43	178.809
$\%\mathbf{F}_Q$		**-0.01%**	**0.02%**	**0.21%**	**0.67%**	**0.89%**
$m_{\text{ov}_{\text{total}}}^{\text{NH}_4}$	1267.61	1269.103	1270.431	1273.087	1281.319	1287.443
$\%\mathbf{F}_m$		**0.12%**	**0.22%**	**0.43%**	**1.08%**	**1.56%**
ξ_{rain}	8.508	8.322	8.272	7.973	7.272	6.268
	SPWMPC - $\zeta = 0.80$					
u_{off}	0%	−5%	−10%	−25%	−50%	−75%
$Q_{\text{ov}_{\text{total}}}$	177.45	177.265	177.336	177.806	178.55	179.029
$\%\mathbf{F}_Q$		**-0.1%**	**-0.06%**	**0.2%**	**0.62%**	**0.89%**
$m_{\text{ov}_{\text{total}}}^{\text{NH}_4}$	1268.455	1269.29	1270.958	1275.709	1286.135	1294.081
$\%\mathbf{F}_m$		**0.07%**	**0.2%**	**0.57%**	**1.39%**	**2.02%**
ξ_{rain}	8.614	8.339	8.294	8.173	7.968	7.412
	SPWMPC - $\zeta = 0.95$					
u_{off}	0%	−5%	−10%	−25%	−50%	−75%
$Q_{\text{ov}_{\text{total}}}$	177.937	177.302	177.377	177.824	178.589	179.1
$\%\mathbf{F}_Q$		**-0.36%**	**-0.31%**	**-0.06%**	**0.37%**	**0.65%**
$m_{\text{ov}_{\text{total}}}^{\text{NH}_4}$	1271.773	1269.231	1269.825	1276.57	1285.92	1294.388
$\%\mathbf{F}_m$		**-0.2%**	**-0.15%**	**0.38%**	**1.11%**	**1.78%**
ξ_{rain}	8.653	8.35	8.307	8.321	8.233	7.825

9.4.4 Local Sensitivity Analysis - Morris Screening

The local sensitivity analysis begins with a Morris screening, similar to the one conducted for SVMPC, where the number of parameters k is equal to 5, which includes the weights α, β, γ and ϵ, and the confidence level ζ. The number of trajectories r chosen for the analysis is 400, hence the total number of simulation runs necessary is $N_m = r(k+1) = 400 * (5+1) = 2400$. The value of Δ is set to 1 for the weights α, β, γ, and ϵ, and to 0.1 for ζ. Moreover, the analysis is performed on the Parallel + Series configuration, and the simulation period is March 24 to April 10, as in Section 8.2.4. The scenarios selected for the analysis were those with uncertainties that had the greatest overall impact on the system, as in Table 9.19, including the scenario without uncertainties, observing the impact of the inputs on the outputs $m^{\mathrm{NH_4}}_{\mathrm{ov_{total}}}$ and ξ.

In fact, the outcome of the Morris screening for $m^{\mathrm{NH_4}}_{\mathrm{ov_{total}}}$ is quite similar to that of $Q_{\mathrm{ov_{total}}}$ in SVMPC, as shown in Figure 9.22. The confidence level, ζ, had the greatest impact compared to other parameters, for all scenarios, resulting, approximately, μ = (8213, 165357, 90200, 3071) and σ = (16450, 320485, 23116, 7071) for each scenario. When comparing the values with the weights, ζ has a much higher impact. Furthermore, ϵ is more impactful in the stochastic formulation compared to its performance in the deterministic approach. α and β exhibit a higher influence between the weights, especially for Scenarios 1 and 4, showing higher μ and σ.

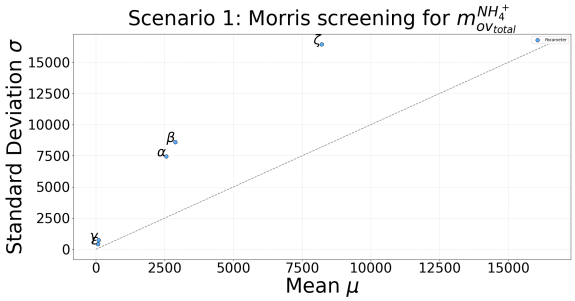

(a) Scenario 1.

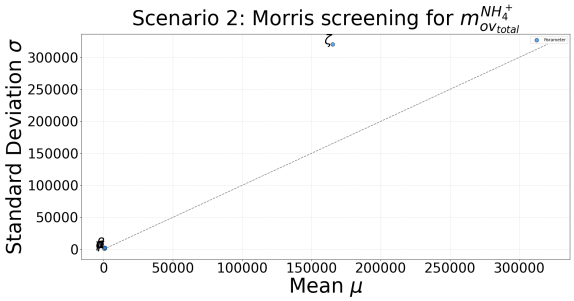

(b) Scenario 2.

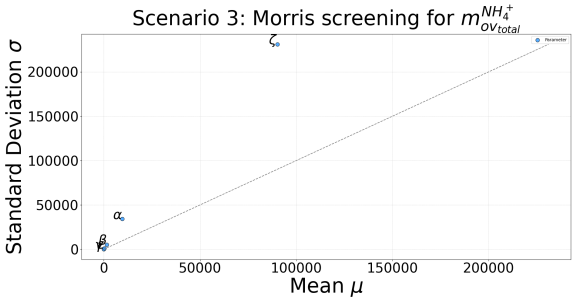

(c) Scenario 3.

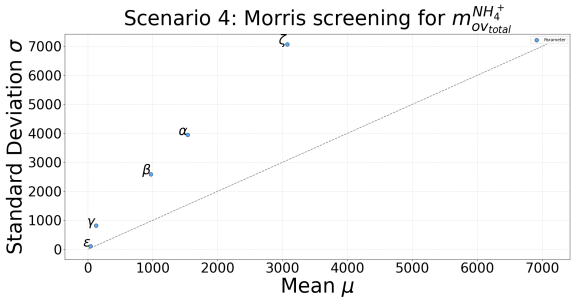

(d) Scenario 4.

Figure 9.22: Morris screening for $m^{\mathrm{NH_4}}_{\mathrm{ov_{total}}}$.

The analysis of the output ξ is presented in Figure 9.23. The impact of ζ on the output ξ is particularly pronounced, regardless of the uncertainty scenario. In Scenarios 2 and 3, the confidence level plays a significant role, as these are the scenarios most affected by uncertainties, which in turn influences the

control performance. Globally, the parameters exhibit $\sigma \gg \mu$, which suggests that non-linearities are present in the relationship between parameters and both outputs $m^{\mathrm{NH_4}}_{\mathrm{OV_{total}}}$ and ξ.

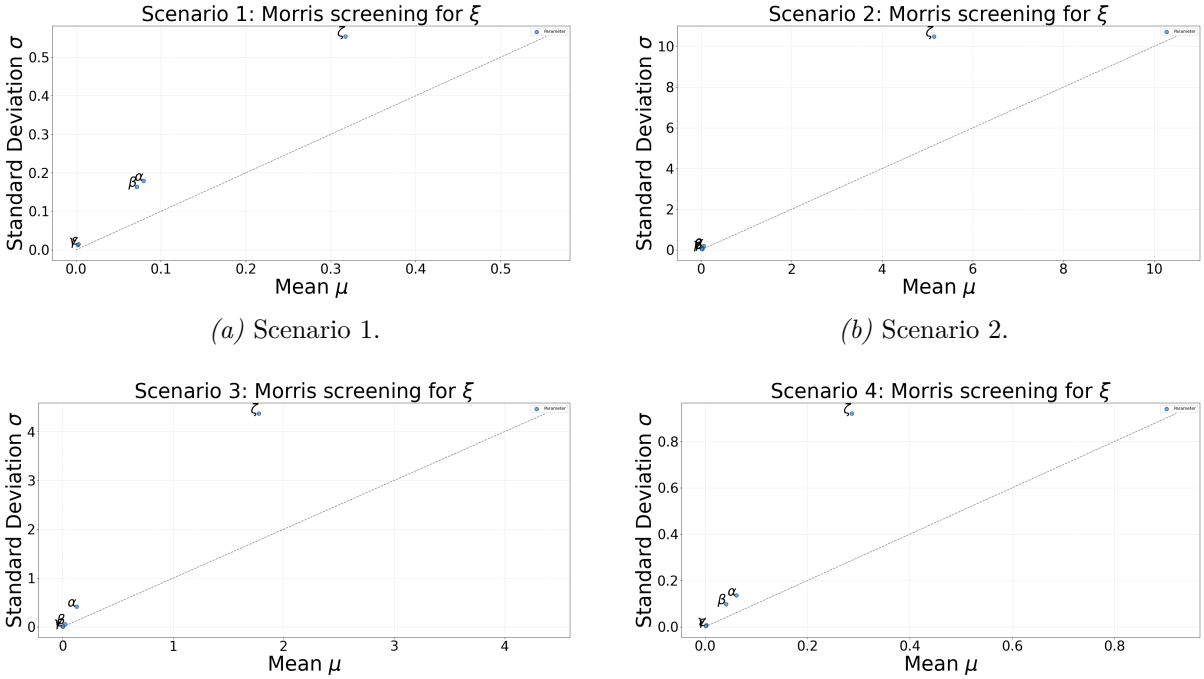

(a) Scenario 1.

(b) Scenario 2.

(c) Scenario 3.

(d) Scenario 4.

Figure 9.23: Morris screening for ξ.

The value of ζ depends on the uncertainty present in the system. Given that it is primarily influenced by the uncertainty, it would be inappropriate to treat it as a decision variable within the Genetic Algorithm, as it does not require such fine-tuning. Instead, ζ should be chosen more intuitively, based on the nature of the uncertainty. Consequently, similar to SVMPC, the confidence level is excluded from the GA optimisation. In the following section, a detailed analysis using Grid and Random search techniques will be performed to determine the appropriate ranges for each weight, providing the initial conditions necessary to begin the GA optimisation process.

9.4.5 Global Sensitivity Analysis - Grid and Random Search

In order to assess the global interaction between the weights of the MPC, the Grid Search is conducted to identify the regions where the parameters are best suited. The outputs used for the Grid Search analysis are also $m^{\mathrm{NH_4}}_{\mathrm{OV_{total}}}$ and ξ. In addition, the analysis is performed on the Parallel + Series configuration, and the period for the simulation is March 24 to April 10. As mentioned previously, the grid search is performed only for the weights α, β, γ and ϵ, fixing ζ at 0.8 and running simulations for the uncertainty scenarios in Table 9.19.

Firstly, a more detailed analysis is done for Scenario 1 without uncertainties and fixing $\epsilon = 3$, later a summary of the results for all scenarios is provided. For this instance, the Grid Search is performed considering two grids, resulting in $n = 2$. The set Ω is defined as $\Omega = \{(\alpha, \beta, \gamma) \mid \alpha \in \Omega_1, \beta \in \Omega_2, \gamma \in \Omega_3\}$,

where each Ω_i has the lower and upper bounds set to $(1, 200)$ for $i = (1, 2, 3)$. Each input in the grid includes 12 equally spaced points, creating in total two 3-D grid heatmaps with a size of $12 \times 12 \times 12 = 1728$ points. For this scenario, the outcome of the grid search for both $m^{\mathrm{NH_4}}_{\mathrm{ov_{total}}}$ and ξ can be seen in Figure 9.24. The results for the non-optimal weights used in the methodology validation are added to the heatmap to give perspective on its performance.

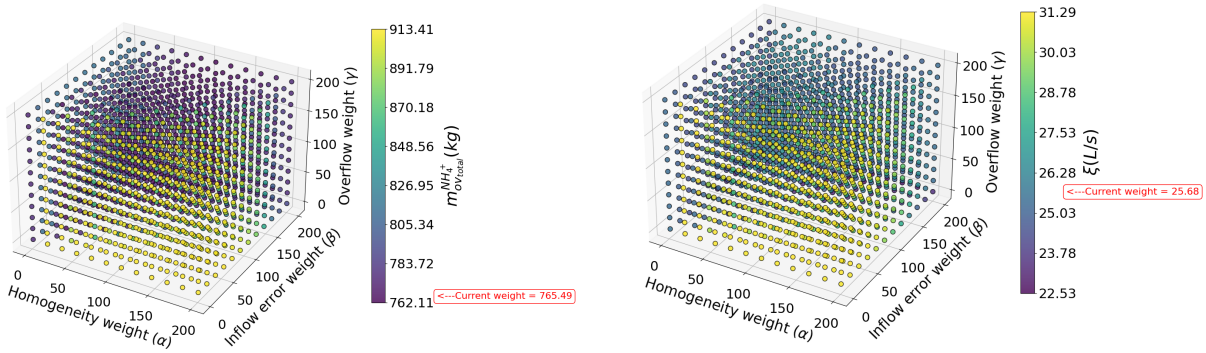

(a) $m^{\mathrm{NH_4}}_{\mathrm{ov_{total}}}$ for $\epsilon = 3$. *(b)* ξ for $\epsilon = 3$.

Figure 9.24: Grid Search SA for SPWMPC for Scenario 1.

The first impression of the heatmap is that α is most effective when set to values in the lower to mid range, particularly when α is below 100. The interaction between β and γ decides which of the objectives will have the highest priority, which has been consistently observed across the linear methods explored in this thesis. The graph also shows that the original weight values used in the methodology validation are very close to the best solution found in this specific grid search. A more detailed examination of the results for all scenarios is presented in Table 9.34. There, it suggests that, for all scenarios, a value of ϵ close to 3 is better. However, the exact range of values for ϵ remains unclear, therefore an additional random search is performed to evaluate the effects of ϵ, as shown in Figure 9.25, varying it between 0 and 100, while also evaluating β and γ between a larger range of 0 to 1000.

Table 9.34: Grid Search applied for all scenarios.

	$\epsilon = 3$				$\epsilon = 89$				$\epsilon = 153$			
	$m^{\mathrm{NH_4}}_{\mathrm{ov_{total}}}$		ξ		$m^{\mathrm{NH_4}}_{\mathrm{ov_{total}}}$		ξ		$m^{\mathrm{NH_4}}_{\mathrm{ov_{total}}}$		ξ	
Scenario	Minimum	Maximum	Minimum	Maximum	Minimum	Maximum	Minimum	Maximum	Minimum	Maximum	Minimum	Maximum
1	762.11	913.41	22.53	31.29	763.24	911.77	24.17	31.35	763.31	930.43	24.2	31.62
2	796.3	854.83	22.82	34.42	824.38	863.18	26.11	34.43	826.61	872.87	26.19	34.53
3	864.7	1372.71	21.47	38.98	913.57	1334.43	24.98	38.98	917.79	1331.31	25.16	38.98
4	777.75	917.82	23.03	31.41	777.8	914.84	24.18	31.44	777.89	931.41	24.24	31.74

The random search highlights a stronger influence of β on the heatmap, while also suggesting that ϵ values below 50 yield better results. Furthermore, the optimal outcomes were found in this case when β and γ ranged between 30 and 300. However, the random search has limitations in its applicability as it explores the parameter space randomly. In larger search areas, regions with the best results for specific metrics may be overlooked. This is evident in the results of this random search, where the best solution for m^{NH4}total is 795.22 kg, significantly higher than the 762.11 kg found in the grid search. Despite this, the random search is still valuable for identifying regions where the parameter settings are suboptimal.

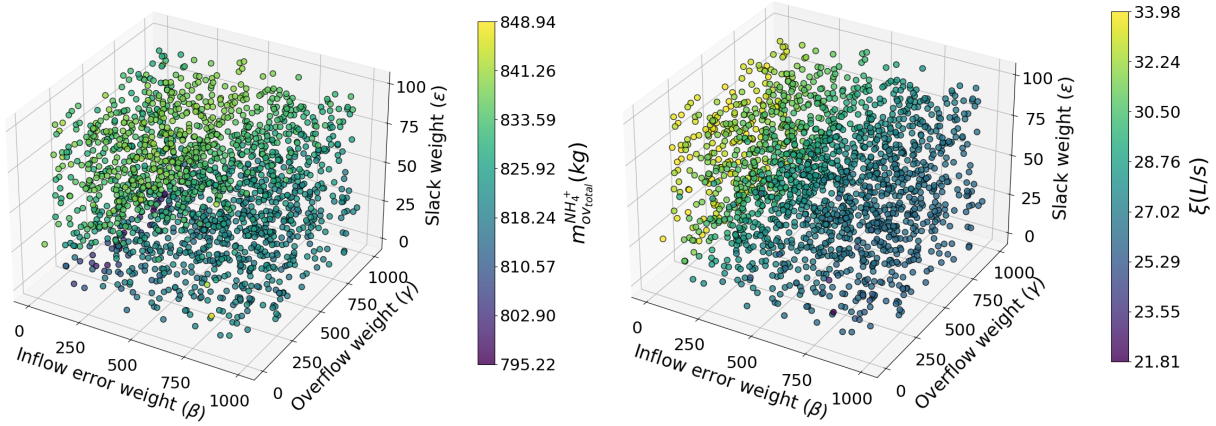

(a) Random Search for $m^{\mathrm{NH_4}}_{\mathrm{OV_{total}}}$.

(b) Random Search for ξ.

Figure 9.25: Random Search applied to Scenario 2.

Given the results of both local and global sensitivity analysis, the final assessment is $\alpha < 100$, $\beta, \gamma \in [30, 300]$, and $\epsilon < 5$. This information is used in the GA optimisation to improve the convergence of the algorithm and find an optimal Pareto-front.

9.4.6 Genetic Algorithm for weight optimisation

The next step involves determining the optimal weights for SPWMPC. To achieve this, the sensitivity analysis is combined with the Genetic Algorithm to identify a Pareto front for the weights, which are simulated for the same uncertainty scenarios in Table 9.19. Based on the SA results, independent of the type of uncertainty, the following ranges are determined: $\alpha \in (0, 50]$, $\beta, \gamma \in (30, 200]$, and $\epsilon \in (0, 5]$. The initial guess for the simulation is set as $\alpha = 73$, $\beta = 127$, $\gamma = 200$, and $\epsilon = 3$, with a tolerance of 10^{-1}. These scenarios were simulated over the period from March 24 to April 10, using a population size of 7 and a maximum of 300 iterations.

Figure 9.26 illustrates the Pareto front for each scenario, showing different outcomes as expected due to the varying impacts on the network.

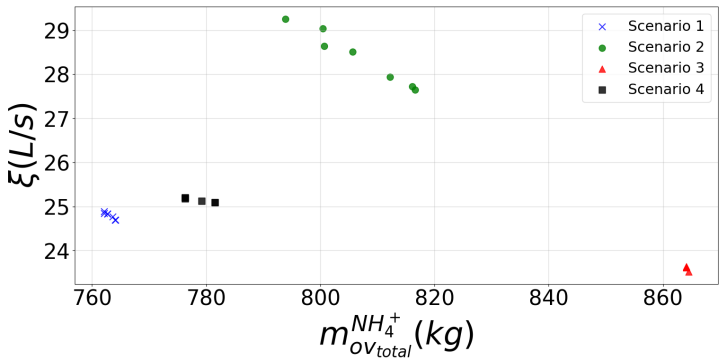

Figure 9.26: Pareto front SPWMPC.

Scenario 1 presents the most favourable Pareto front for overflow, achieving a minimum load overflow of 762.06 kg, which represents a minimal improvement over the results from the weight validation methodology. In Scenario 2, $m^{NH_4}_{OV_{total}}$ also only slightly improved in the Pareto front, while ξ remains at similar levels. Scenario 3 exhibits the poorest performance in terms of $m^{NH_4}_{OV_{total}}$, as expected since this uncertainty had the highest effect on performance, however, it has the best performance for ξ.

In Table 9.35, the optimal weights for each scenario are presented, based on different criteria for which objective is more desirable. Scenario 3 shows that for all criteria, the algorithm converged to an optimal solution with very low values for α and higher values of β and γ. In contrast, for the other scenarios, higher values of α were more effective in minimising overflow, while lower values of α were better suited to reduce ξ.

Scenario	Best weights for $m^{NH_4}_{OV_{total}}$	Best weights for ξ	Best compromise
1	(73.36, 126.63, 248.56, 3.04)	(75.17, 102.67, 218.08, 2.51)	(73.29, 103.09, 230.52, 2.51)
2	(56.48, 238.47, 201.87, 1.82)	(23.84, 296.63, 212.58, 2.23)	(30.00, 208.79, 191.37, 2.56)
3	(0.12, 249.95, 245.63, 2.58)	(0.02, 252.31, 115.27, 3.63)	(0.02, 283.49, 120.68, 3.65)
4	(72.52, 127.63, 212.27, 3.20)	(72.52, 127.63, 277.80, 3.20)	(64.80, 127.63, 202.54, 3.64)

Table 9.35: Optimal (α, β, γ, ϵ) for each uncertainty scenario.

When comparing the results with SVMPC, the optimal weight selection for SPWMPC in Scenario 3 shares a very low trend α. However, the outcomes of other scenarios vary significantly between the two controllers, highlighting the importance of how each controller adapts to different uncertainties. The differences observed between the scenarios, especially for Scenario 3, indicate that the weight parameters in SPWMPC are highly sensitive to the type of uncertainty in the system.

Since Scenario 3 demonstrated the poorest performance in the evaluation, the final optimal weight for SPWMPC was selected from this scenario, using the criterion of minimising overflow. The weights chosen are $\alpha = 0.12$, $\beta = 249.95$, $\gamma = 245.63$, and $\epsilon = 2.58$. The performance of SPWMPC with these optimal weights is then evaluated and compared against PWMPC with its own optimal weights, taking into account the effect of the confidence level. This evaluation is carried out using the same scenarios presented in Section 9.4.3.

Uncertainty on $V(k)$

The first evaluation in this section for SPWMPC begins with the analysis of performance with volume uncertainty changing the variability through the parameter u_p, shown in Table 9.36. The new weights for SPWMPC clearly improved the stability and overall performance of the controller, maintaining the overflow stable for increased uncertainty with $\%F$ between -0.3% and 0.55% for load, depending on the confidence level. In addition, there was a noticeable improvement in the performance of the stochastic controller for higher uncertainties, especially for ξ_{rain}. Nevertheless, although PWMPC reached up to 11.4% worse performance for $m^{NH_4}_{OV_{total}}$, SPWMPC still did not improve the performance against PWMPC in terms of absolute value for both overflows and ξ_{rain}, where PWMPC has an overall better performance.

Table 9.36: Volume uncertainty: Comparison between PWMPC and optimal SPWMPC for u_p.

	PWMPC					
u_p	0%	5%	10%	25%	50%	75%
$Q_{\mathrm{ov_{total}}}$	168.77	168.971	169.771	171.595	173.193	174.031
$\%\mathbf{F}_Q$		**0.12%**	**0.59%**	**1.67%**	**2.62%**	**3.12%**
$m^{\mathrm{NH_4}}_{\mathrm{ov_{total}}}$	1034.79	1088.102	1094.839	1118.461	1136.925	1152.927
$\%\mathbf{F}_m$		**5.15%**	**5.8%**	**8.09%**	**9.87%**	**11.42%**
ξ_{rain}	7.629	6.221	4.853	2.314	1.222	1.152
	SPWMPC - $\zeta = 0.60$					
u_p	0%	5%	10%	25%	50%	75%
$Q_{\mathrm{ov_{total}}}$	177.244	178.615	178.98	179.138	179.032	178.831
$\%\mathbf{F}_Q$		**0.77%**	**0.98%**	**1.07%**	**1.01%**	**0.9%**
$\%\mathbf{F}^*_Q$	**0.0%**	**-0.23%**	**-0.77%**	**-2.18%**	**-3.3%**	**-4.15%**
$m^{\mathrm{NH_4}}_{\mathrm{ov_{total}}}$	1279.872	1293.069	1299.031	1291.753	1279.998	1276.08
$\%\mathbf{F}_m$		**1.03%**	**1.5%**	**0.93%**	**0.01%**	**-0.3%**
$\%\mathbf{F}^*_m$	**0.97%**	**0.49%**	**-0.22%**	**-2.71%**	**-4.8%**	**-6.53%**
ξ_{rain}	6.566	6.447	5.848	4.609	4.069	4.229
$\%\mathbf{F}^*_\xi$	**-22.83%**	**-11.48%**	**-11.33%**	**-16.85%**	**-31.64%**	**-29.43%**
	SPWMPC - $\zeta = 0.80$					
u_p	0%	5%	10%	25%	50%	75%
$Q_{\mathrm{ov_{total}}}$	177.243	178.541	178.888	179.269	179.077	179.332
$\%\mathbf{F}_Q$		**0.73%**	**0.93%**	**1.14%**	**1.03%**	**1.18%**
$\%\mathbf{F}^*_Q$	**-0.12%**	**-0.72%**	**-1.58%**	**-3.8%**	**-5.98%**	**-6.48%**
$m^{\mathrm{NH_4}}_{\mathrm{ov_{total}}}$	1279.876	1290.707	1297.448	1287.976	1280.958	1282.262
$\%\mathbf{F}_m$		**0.85%**	**1.37%**	**0.63%**	**0.08%**	**0.19%**
$\%\mathbf{F}^*_m$	**0.9%**	**-0.31%**	**-0.87%**	**-5.6%**	**-10.4%**	**-11.65%**
ξ_{rain}	6.566	6.516	5.944	4.578	4.283	4.442
$\%\mathbf{F}^*_\xi$	**-23.78%**	**-16.73%**	**-19.77%**	**-35.16%**	**-37.77%**	**-32.0%**
	SPWMPC - $\zeta = 0.95$					
u_p	0%	5%	10%	25%	50%	75%
$Q_{\mathrm{ov_{total}}}$	177.245	178.576	179.025	179.217	179.221	179.369
$\%\mathbf{F}_Q$		**0.75%**	**1.0%**	**1.11%**	**1.11%**	**1.2%**
$\%\mathbf{F}^*_Q$	**-0.39%**	**-1.15%**	**-2.62%**	**-5.48%**	**-6.66%**	**-6.75%**
$m^{\mathrm{NH_4}}_{\mathrm{ov_{total}}}$	1279.891	1291.891	1300.602	1288.684	1292.496	1286.895
$\%\mathbf{F}_m$		**0.94%**	**1.62%**	**0.69%**	**0.98%**	**0.55%**
$\%\mathbf{F}^*_m$	**0.64%**	**-0.53%**	**-2.31%**	**-8.96%**	**-11.18%**	**-11.92%**
ξ_{rain}	6.566	6.596	5.859	4.539	4.114	4.203
$\%\mathbf{F}^*_\xi$	**-24.12%**	**-16.24%**	**-24.09%**	**-41.55%**	**-43.19%**	**-36.47%**

Lastly, for the optimal weights identified, the confidence level has much less influence over the objectives.

The following analysis evaluates the volume uncertainty resulting from $u^{\mathrm{vol-}}_{\mathrm{offset}}$, as presented in Table 9.37.

In this scenario, the performance of SPWMPC is outstanding, closely resembling that of SVMPC. The controller manages to maintain a stable operation, limiting the overflow to 208.3 ML in volume and 1804 kg in load, even when $u_{\text{off}} = -75\%$. This represents an increase of 17.55% for volume and 41.76% for load, which is a significant improvement over PWMPC. In contrast, PWMPC experiences a dramatic increase of 163% in volume and 950% in load overflow, showing much worse performance. A closer look at the $\%\mathbf{F}_m^*$ metric reveals that the new simulation successfully reduces $Q_{\text{ov}_{\text{total}}}$ by 58% and $m_{\text{ov}_{\text{total}}}^{\text{NH}_4}$ by 85% for $\zeta = 0.6$ and $Q_{\text{ov}_{\text{total}}}$ by 75% and $m_{\text{ov}_{\text{total}}}^{\text{NH}_4}$ by 93% for $\zeta = 0.95$, demonstrating the effectiveness of the GA optimisation to find better weights. Additionally, SPWMPC performs exceptionally well in terms of ξrain, almost reaching a value of 0 for $u_{\text{off}} = -75\%$.

Uncertainty on $Q_{\text{out}}(k)$

The final analysis in this section examines $u_{\text{offset}}^{\text{out-}}$, presented in Table 9.33. demonstrates that SPWMPC is significantly more stable when faced with increased uncertainties. In these scenarios, SPWMPC maintains performance similar to the baseline scenario with $u_{\text{off}} = 0\%$, while PWMPC experiences up to a 4.5% increase in volume overflow and a 19.1% increase in load overflow.

The conclusion is essentially the same as for SVMPC, the stability that the stochastic method offers is quite robust facing extreme uncertainties. Moreover, it is capable of better handling ξ_{rain} and, as a result, keep the inflow to the WWTP closer to the designed flow. However, it still underperformed compared to the deterministic method in such simple 3-SU system, where its conservative nature can be excessive and hinder the controller's performance. The upcoming section presents the last stochastic formulation using the CC-MPC framework, changing the framework designed to NPMPC into a stochastic MPC.

Table 9.37: Volume uncertainty: Comparison between PWMPC and optimal SPWMPC for $u_{\text{offset}}^{\text{vol-}}$.

	PWMPC					
u_{off}	0%	−5%	−10%	−25%	−50%	−75%
$Q_{\text{ov}_{\text{total}}}$	168.77	175.95	182.162	201.263	259.73	444.554
$\%\mathbf{F}_Q$		**4.25%**	**7.94%**	**19.25%**	**53.9%**	**163.41%**
$m_{\text{ov}_{\text{total}}}^{\text{NH}_4}$	1034.79	1196.528	1266.674	1571.667	2852.361	10867.604
$\%\mathbf{F}_m$		**15.63%**	**22.41%**	**51.88%**	**175.65%**	**950.22%**
ξ_{rain}	7.629	6.132	3.52	-6.714	-31.339	-59.93
	SPWMPC - $\zeta = 0.60$					
u_{off}	0%	−5%	−10%	−25%	−50%	−75%
$Q_{\text{ov}_{\text{total}}}$	177.244	178.981	180.433	184.984	194.01	208.351
$\%\mathbf{F}_Q$		**0.98%**	**1.8%**	**4.37%**	**9.46%**	**17.55%**
$\%\mathbf{F}_Q^*$	**0.0%**	**-0.58%**	**-1.11%**	**-2.4%**	**-14.78%**	**-58.21%**
$m_{\text{ov}_{\text{total}}}^{\text{NH}_4}$	1279.872	1293.495	1308.187	1358.416	1506.897	1814.334
$\%\mathbf{F}_m$		**1.06%**	**2.21%**	**6.14%**	**17.74%**	**41.76%**
$\%\mathbf{F}_m^*$	**0.97%**	**-0.33%**	**-1.45%**	**-5.04%**	**-41.23%**	**-85.87%**
ξ_{rain}	6.566	6.517	6.495	6.359	6.281	0.101
$\%\mathbf{F}_\xi^*$	**-22.83%**	**-11.5%**	**1.45%**	**65.73%**	**109.09%**	**-100.15%**
	SPWMPC - $\zeta = 0.80$					
u_{off}	0%	−5%	−10%	−25%	−50%	−75%
$Q_{\text{ov}_{\text{total}}}$	177.243	178.979	180.404	184.966	194.01	208.351
$\%\mathbf{F}_Q$		**0.98%**	**1.78%**	**4.36%**	**9.46%**	**17.55%**
$\%\mathbf{F}_Q^*$	**-0.12%**	**-0.8%**	**-1.49%**	**-4.25%**	**-21.24%**	**-71.87%**
$m_{\text{ov}_{\text{total}}}^{\text{NH}_4}$	1279.876	1293.116	1307.301	1357.548	1506.88	1814.33
$\%\mathbf{F}_m$		**1.03%**	**2.14%**	**6.07%**	**17.74%**	**41.76%**
$\%\mathbf{F}_m^*$	**0.9%**	**-0.59%**	**-1.88%**	**-8.85%**	**-56.21%**	**-91.98%**
ξ_{rain}	6.566	6.514	6.495	6.36	6.282	0.101
$\%\mathbf{F}_\xi^*$	**-23.78%**	**-8.86%**	**8.94%**	**127.63%**	**17.33%**	**-100.13%**
	SPWMPC - $\zeta = 0.95$					
u_{off}	0%	−5%	−10%	−25%	−50%	−75%
$Q_{\text{ov}_{\text{total}}}$	177.245	178.98	180.402	184.966	194.008	208.352
$\%\mathbf{F}_Q$		**0.98%**	**1.78%**	**4.36%**	**9.46%**	**17.55%**
$\%\mathbf{F}_Q^*$	**-0.39%**	**-0.92%**	**-1.75%**	**-4.87%**	**-26.57%**	**-74.99%**
$m_{\text{ov}_{\text{total}}}^{\text{NH}_4}$	1279.891	1293.161	1307.191	1358.248	1506.839	1814.329
$\%\mathbf{F}_m$		**1.04%**	**2.13%**	**6.12%**	**17.73%**	**41.76%**
$\%\mathbf{F}_m^*$	**0.64%**	**-0.77%**	**-2.38%**	**-10.43%**	**-65.35%**	**-92.79%**
ξ_{rain}	6.566	6.514	6.495	6.36	6.281	0.101
$\%\mathbf{F}_\xi^*$	**-24.12%**	**-9.41%**	**11.22%**	**189.22%**	**-18.03%**	**-100.13%**

Table 9.38: Outflow uncertainty: Comparison between PWMPC and optimal SPWMPC for $u_{\text{offset}}^{\text{out-}}$.

	PWMPC					
u_{off}	0%	−5%	−10%	−25%	−50%	−75%
$Q_{\text{ov}_{\text{total}}}$	168.77	167.791	168.256	170.937	174.586	176.381
$\%\mathbf{F}_Q$		**-0.58%**	**-0.3%**	**1.28%**	**3.45%**	**4.51%**
$m_{\text{ov}_{\text{total}}}^{\text{NH}_4}$	1034.79	1081.025	1087.939	1139.193	1200.527	1232.686
$\%\mathbf{F}_m$		**4.47%**	**5.14%**	**10.09%**	**16.02%**	**19.12%**
ξ_{rain}	7.629	7.737	7.675	7.622	7.483	7.203
	SPWMPC - $\zeta = 0.60$					
u_{off}	0%	−5%	−10%	−25%	−50%	−75%
$Q_{\text{ov}_{\text{total}}}$	177.244	177.175	177.109	177.113	177.699	178.034
$\%\mathbf{F}_Q$		**-0.04%**	**-0.08%**	**-0.07%**	**0.26%**	**0.45%**
$\%\mathbf{F}_Q^*$	**0.0%**	**-0.03%**	**-0.09%**	**-0.28%**	**-0.41%**	**-0.43%**
$m_{\text{ov}_{\text{total}}}^{\text{NH}_4}$	1279.872	1279.154	1277.901	1275.807	1280.852	1284.44
$\%\mathbf{F}_m$		**-0.06%**	**-0.15%**	**-0.32%**	**0.08%**	**0.36%**
$\%\mathbf{F}_m^*$	**0.97%**	**0.79%**	**0.59%**	**0.21%**	**-0.04%**	**-0.23%**
ξ_{rain}	6.566	6.646	6.563	6.553	6.63	6.285
$\%\mathbf{F}_\xi^*$	**-22.83%**	**-20.14%**	**-20.66%**	**-17.81%**	**-8.83%**	**0.27%**
	SPWMPC - $\zeta = 0.80$					
u_{off}	0%	−5%	−10%	−25%	−50%	−75%
$Q_{\text{ov}_{\text{total}}}$	177.243	177.175	177.104	177.114	177.7	178.035
$\%\mathbf{F}_Q$		**-0.04%**	**-0.08%**	**-0.07%**	**0.26%**	**0.45%**
$\%\mathbf{F}_Q^*$	**-0.12%**	**-0.05%**	**-0.13%**	**-0.39%**	**-0.48%**	**-0.56%**
$m_{\text{ov}_{\text{total}}}^{\text{NH}_4}$	1279.876	1279.144	1277.741	1275.788	1280.861	1284.439
$\%\mathbf{F}_m$		**-0.06%**	**-0.17%**	**-0.32%**	**0.08%**	**0.36%**
$\%\mathbf{F}_m^*$	**0.9%**	**0.78%**	**0.53%**	**0.01%**	**-0.41%**	**-0.75%**
ξ_{rain}	6.566	6.646	6.562	6.553	6.63	6.285
$\%\mathbf{F}_\xi^*$	**-23.78%**	**-20.3%**	**-20.88%**	**-19.82%**	**-16.79%**	**-15.21%**
	SPWMPC - $\zeta = 0.95$					
u_{off}	0%	−5%	−10%	−25%	−50%	−75%
$Q_{\text{ov}_{\text{total}}}$	177.245	177.174	177.104	177.114	177.699	178.034
$\%\mathbf{F}_Q$		**-0.04%**	**-0.08%**	**-0.07%**	**0.26%**	**0.45%**
$\%\mathbf{F}_Q^*$	**-0.39%**	**-0.07%**	**-0.15%**	**-0.4%**	**-0.5%**	**-0.6%**
$m_{\text{ov}_{\text{total}}}^{\text{NH}_4}$	1279.891	1279.131	1277.747	1275.787	1280.863	1284.437
$\%\mathbf{F}_m$		**-0.06%**	**-0.17%**	**-0.32%**	**0.08%**	**0.36%**
$\%\mathbf{F}_m^*$	**0.64%**	**0.78%**	**0.62%**	**-0.06%**	**-0.39%**	**-0.77%**
ξ_{rain}	6.566	6.646	6.562	6.553	6.63	6.285
$\%\mathbf{F}_\xi^*$	**-24.12%**	**-20.41%**	**-21.01%**	**-21.25%**	**-19.47%**	**-19.68%**

9.5 Stochastic Non-linear Pollution-based Model Predictive Control

The last method proposed in this chapter is the Stochastic Nonlinear Pollution-based Model Predictive Control (SNPMPC), again inspired by the papers in [151, 153, 155] and implemented in a pollution-based framework based on Nonlinear Pollution-based Model Predictive Control. Hence, it uses the same principles as the CC-MPC method, considering that the uncertainty follows the same principles as in Section 9.1 and adding the concentration of a given pollutant in the formulation.

9.5.1 Description

SNPMPC is a method that transforms NPMPC from Section 8.1 into a stochastic control method using the techniques in [151, 153, 155]. Since NPMPC is a deterministic controller, a few assumptions are necessary to change it to a stochastic method.

1. As for stochastic volume-based formulation, the variables are reformulated as expectations of the variable $\mathbb{E}\{.\}$, e.g. volume $V(k)$, outflow $Q_{\text{out}}(k)$, overflow $Q_{\text{ov}}(k)$, and inflow $Q_{\text{in}}(k)$ are reformulated as $\mathbb{E}\{V(k)\}$, $\mathbb{E}\{Q_{\text{out}}(k)\}$, $\mathbb{E}\{Q_{\text{ov}}(k)\}$ and $\mathbb{E}\{Q_{\text{in}}(k)\}$.

2. Additionally, the concentration within the SU, $C(k)$, and the concentration of volume entering the SU, $C_{in}(k)$, are reformulated as $\mathbb{E}\{C(k)\}$ and $\mathbb{E}\{C_{in}(k)\}$, respectively.

3. They also include a standard deviation $\sigma^2\{V(k)\}$, $\sigma^2\{Q_{\text{out}}(k)\}$, $\sigma^2\{Q_{\text{in}}(k)\}$, $\sigma^2\{Q_{\text{ov}}(k)\}$ and $\sigma^2\{C_{\text{in}}(k)\}$, $\sigma^2\{C(k)\}$.

4. Uncertainties are considered to be truncated Gaussian distributed with heteroscedastic behaviour.

The scheme for the control algorithm is presented in Figure 9.27. SNPMPC receives feedback information from the UDS through the measurement devices and the expectations and standard deviations are estimated given a pre-determined probabilistic distribution. The internal model is used to predict the expected volume and concentration in the prediction horizon, where the objective is to estimate the expected overflow volume and load in the future.

Including the internal model presented for SVMPC in Equation 9.8, the additional internal model to predict concentration is given below:

$$\begin{aligned}\mathbb{E}\{C(k+1)\} = &\frac{\mathbb{E}\{C(k)\}\mathbb{E}\{V(k)\} + T_s\mathbb{E}\{C_{\text{in}}(k)\}\mathbb{E}\{Q_{\text{in}}(k)\}}{\mathbb{E}\{V(k)\} + T_s[\mathbb{E}\{Q_{\text{in}}(k)\} - \mathbb{E}\{Q_{\text{out}}(k)\} - \mathbb{E}\{Q_{\text{ov}}(k)\}]} \\ &- \frac{\mathbb{E}\{C(k)\}(\mathbb{E}\{Q_{\text{out}}(k)\} + \mathbb{E}\{Q_{\text{ov}}(k)\})]}{\mathbb{E}\{V(k)\} + T_s[\mathbb{E}\{Q_{\text{in}}(k)\} - \mathbb{E}\{Q_{\text{out}}(k)\} - \mathbb{E}\{Q_{\text{ov}}(k)\}]}\end{aligned} \tag{9.29}$$

The standard deviation of the concentration is also included in the formulation as it needs to be propagated in future steps. The formula for calculating the standard deviation of independent variables is as follows:

$$\sigma^2\{f(X_1, X_2, \ldots, X_n)\} = \sum_{i=1}^{n} \left(\frac{\partial f}{\partial X_i}\right)^2 \sigma^2(X_i)$$

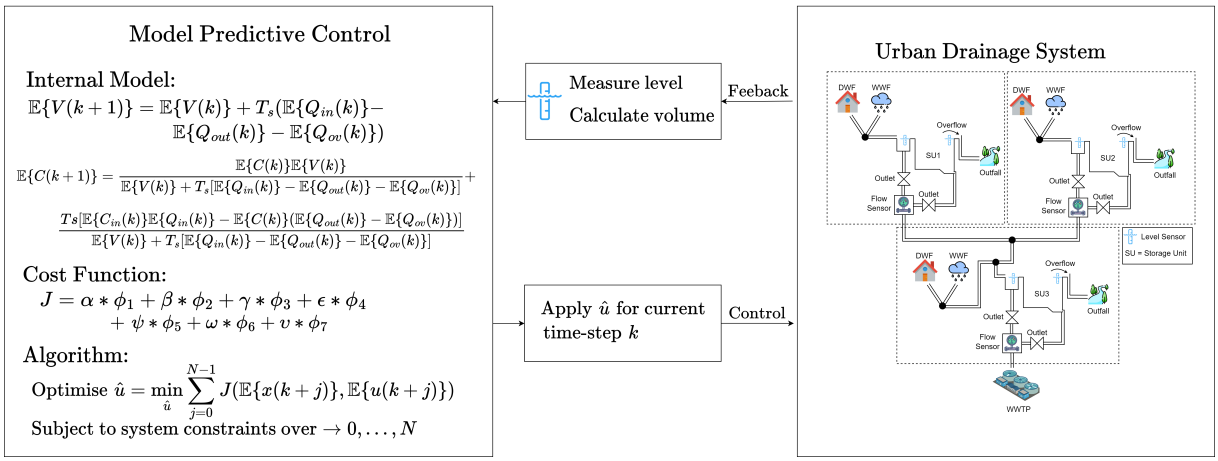

Figure 9.27: SNPMPC scheme for Urban Drainage Systems.

where $f(X)$ represents a stochastic function and X_i represents each stochastic variable in the equation (e.g. $C(k)$, $V(k)$, $C_{\text{in}}(k)$, $Q_{\text{in}}(k)$, $Q_{\text{out}}(k)$, $Q_{\text{ov}}(k)$). Firstly, for simplicity of visualisation, the elements are separated as follows:

$$X_1 = \mathbb{E}\{C(k)\}, \quad X_2 = \mathbb{E}\{V(k)\}, \quad X_3 = \mathbb{E}\{C_{\text{in}}(k)\},$$

$$X_4 = \mathbb{E}\{Q_{\text{in}}(k)\}, \quad X_5 = \mathbb{E}\{Q_{\text{out}}(k)\}, \quad X_6 = \mathbb{E}\{Q_{\text{ov}}(k)\}$$

The next step is to compute the partial derivative for each variable:

$$\frac{\partial \mathbb{E}\{C(k+1)\}}{\partial X_1} = \frac{X_2 - T_s(X_5 + X_6)}{X_2 + T_s(X_4 - X_5 - X_6)}, \qquad \frac{\partial \mathbb{E}\{C(k+1)\}}{\partial X_2} = \frac{X_1}{X_2 + T_s(X_4 - X_5 - X_6)}$$

$$\frac{\partial \mathbb{E}\{C(k+1)\}}{\partial X_3} = \frac{T_s X_4}{X_2 + T_s(X_4 - X_5 - X_6)}, \qquad \frac{\partial \mathbb{E}\{C(k+1)\}}{\partial X_4} = \frac{T_s X_3}{X_2 + T_s(X_4 - X_5 - X_6)}$$

$$\frac{\partial \mathbb{E}\{C(k+1)\}}{\partial X_5} = \frac{-T_s X_1}{X_2 + T_s(X_4 - X_5 - X_6)}, \qquad \frac{\partial \mathbb{E}\{C(k+1)\}}{\partial X_6} = \frac{-T_s X_1}{X_2 + T_s(X_4 - X_5 - X_6)}$$

Therefore, the standard deviation $\sigma(C(k+1))$ can be defined as:

$$\begin{aligned}\sigma^2\{C(k+1)\} = &\left(\frac{X_2 - T_s(X_5 + X_6)}{X_2 + T_s(X_4 - X_5 - X_6)}\right)^2 \sigma^2\{X_1\} + \left(\frac{X_1}{X_2 + T_s(X_4 - X_5 - X_6)}\right)^2 \sigma^2\{X_2\} \\ &+ \left(\frac{T_s X_4}{X_2 + T_s(X_4 - X_5 - X_6)}\right)^2 \sigma^2\{X_3\} + \left(\frac{T_s X_3}{X_2 + T_s(X_4 - X_5 - X_6)}\right)^2 \sigma^2\{X_4\} \\ &+ \left(\frac{-T_s X_1}{X_2 + T_s(X_4 - X_5 - X_6)}\right)^2 \sigma^2\{X_5\} + \left(\frac{-T_s X_1}{X_2 + T_s(X_4 - X_5 - X_6)}\right)^2 \sigma^2\{X_6\} \end{aligned} \tag{9.30}$$

The chance-constraints added to the formulation are a combination of Equations 9.9, 9.10, 9.11 and 9.12 with an additional chance-constraint for the upper bound of the concentration, as given in Equation 9.31, which includes a slack variable for the bound in $\theta^c_{\max}$. Besides, as the uncertainty is now handled

differently with the chance-constraint, the variable $U(k)$ is removed from the original formulation of the NPMPC, as well as the objective ϕ_7 in Equation 8.27.

$$\mathbb{E}\{C(k+1)\} \leq C_{\max} - \sigma\{C(k+1)\}\Phi^{-1}(\zeta) + \theta^{c}_{\max}(k) \tag{9.31}$$

9.5.2 Optimisation Problem

Given the stochastic constraints and that the states $\boldsymbol{x}(k)$, and input $\boldsymbol{u}(k)$, are

$$\boldsymbol{x}(k) = [\mathbb{E}\{\boldsymbol{V}(k)\},\ \mathbb{E}\{\boldsymbol{Q}_{\text{ov}}(k)\},\ \mathbb{E}\{\boldsymbol{Q}_{\text{in}}(k)\},\ \mathbb{E}\{\boldsymbol{C}(k)\},\ \mathbb{E}\{\boldsymbol{C}_{\text{in}}(k)\},\ \boldsymbol{\theta}_{\min}(k),\ \boldsymbol{\theta}_{\max}(k),\ \boldsymbol{\theta}^{c}_{\max}(k)]$$

and

$$\boldsymbol{u}(k) = [\mathbb{E}\{\boldsymbol{Q}_{\text{out}}(k)\}]$$

the optimisation problem, where $\hat{\boldsymbol{u}}(k)$ is the optimal output, is defined as:

$$\hat{u}(k) = \arg\min_{u} \sum_{j=0}^{N-1} J(x(k+j), u(k+j)) \tag{9.32a}$$

subject to

$$\mathbb{E}\{V^t(k+j+1)\} = \mathbb{E}\{V^t(k+j)\} + T_s\big[\mathbb{E}\{Q^t_{\text{in}}(k+j)\} - \mathbb{E}\{Q^t_{\text{out}}(k+j)\} - \mathbb{E}\{Q^t_{\text{ov}}(k+j)\}\big],$$
$$t = 1, 2, ..., N_t \tag{9.32b}$$

$$\sigma^2\{V^t(k+j+1)\} = \sigma^2\{V^t(k+j)\} + T_s^2\big(\sigma^2\{Q^t_{\text{in}}(k+j)\} + \sigma^2\{Q^t_{\text{out}}(k+j)\} + \sigma^2\{Q^t_{\text{ov}}(k+j)\}\big),$$
$$t = 1, 2, ..., N_t \tag{9.32c}$$

$$\mathbb{E}\{Q^t_{in}(k+j)\} = \mathbb{E}\{Q^t_{catchment}(k+j)\} + \sum_{i \in N^*_{\text{in}}} \mathbb{E}\{Q^i_{out}(k+j)\}, \qquad t = 1, 2, ..., N_t \tag{9.32d}$$

$$\mathbb{E}\{C^t(k+j+1)\} = \frac{\mathbb{E}\{C^t(k+j)\}\mathbb{E}\{V^t(k+j)\} + T_s\mathbb{E}\{C^t_{\text{in}}(k+j)\}\mathbb{E}\{Q^t_{\text{in}}(k+j)\}}{\mathbb{E}\{V^t(k+j)\} + T_s\big[\mathbb{E}\{Q^t_{\text{in}}(k+j)\} - \mathbb{E}\{Q^t_{\text{out}}(k+j)\} - \mathbb{E}\{Q^t_{\text{ov}}(k+j)\}\big]}$$
$$- \frac{T_s\big[\mathbb{E}\{C^t(k+j)\}\big(\mathbb{E}\{Q^t_{\text{out}}(k+j)\} + \mathbb{E}\{Q^t_{\text{ov}}(k+j)\}\big)\big]}{\mathbb{E}\{V^t(k+j)\} + T_s\big[\mathbb{E}\{Q^t_{\text{in}}(k+j)\} - \mathbb{E}\{Q^t_{\text{out}}(k+j)\} - \mathbb{E}\{Q^t_{\text{ov}}(k+j)\}\big]},$$
$$t = 1, 2, ..., N_t \tag{9.32e}$$

$$\sigma^2\{C^t(k+j+1)\} = \left(\frac{X_2 - T_s(X_5+X_6)}{X_2 + T_s(X_4 - X_5 - X_6)}\right)^2 \sigma^2\{X_1\} + \left(\frac{X_1}{X_2 + T_s(X_4 - X_5 - X_6)}\right)^2 \sigma^2\{X_2\}$$
$$+ \left(\frac{T_s X_4}{X_2 + T_s(X_4 - X_5 - X_6)}\right)^2 \sigma^2\{X_3\} + \left(\frac{T_s X_3}{X_2 + T_s(X_4 - X_5 - X_6)}\right)^2 \sigma^2\{X_4\}$$
$$+ \left(\frac{-T_s X_1}{X_2 + T_s(X_4 - X_5 - X_6)}\right)^2 \sigma^2\{X_5\} + \left(\frac{-T_s X_1}{X_2 + T_s(X_4 - X_5 - X_6)}\right)^2 \sigma^2\{X_6\},$$
$$t = 1, 2, ..., N_t \tag{9.32f}$$

$$\mathbb{E}\{V^t(k+j)\} + T_s\big(\mathbb{E}\{Q^t_{\text{in}}(k+j)\} + \mathbb{E}\{Q^t_{\text{out}}(k+j)\}\big) \geq \sigma\{V^t(k+j) + T_s(Q^t_{\text{in}}(k+j) + Q^t_{\text{out}}(k+j))\}\Phi^{-1}(\zeta) - \theta^t_{\min},$$
$$t = 1, 2, ..., N_t \tag{9.32g}$$

$$\mathbb{E}\{V^t(k+j)\} + T_s\big(\mathbb{E}\{Q^t_{\text{in}}(k+j)\} - \mathbb{E}\{Q^t_{\text{out}}(k+j)\} - \mathbb{E}\{Q^t_{\text{ov}}(k+j)\}\big) \geq 0, \qquad t = 1, 2, ..., N_t \tag{9.32h}$$

$$\begin{aligned}\mathbb{E}\{V^t(k+j)\} + T_s\big(\mathbb{E}\{Q^t_{\text{in}}(k+j)\} - \mathbb{E}\{Q^t_{\text{out}}(k+j)\}\big) \\ \leq V^t_{\max} - \sigma\{V^t(k+j) + T_s(Q^t_{\text{in}}(k) + Q^t_{\text{out}}(k+j))\}\Phi^{-1}(\zeta) + \theta^t_{\max}, \\ t = 1, 2, ..., N_t\end{aligned} \tag{9.32i}$$

$$\begin{aligned}\mathbb{E}\{V^t(k+j)\} + T_s\big(\mathbb{E}\{Q^t_{\text{in}}(k+j)\} - \mathbb{E}\{Q^t_{\text{out}}(k+j)\} - \mathbb{E}\{Q^t_{\text{ov}}(k+j)\}\big) \leq V^t_{\max}, \\ t = 1, 2, ..., N_t\end{aligned} \tag{9.32j}$$

$$\mathbb{E}\{C^t(k+j+1)\} \leq C^t_{\max} - \sigma\{C^t(k+j+1)\}\Phi^{-1}(\zeta) + {\theta^t_{\max}}^c, \qquad t = 1, 2, ..., N_t \tag{9.32k}$$

$$0 \leq \sum_{i \in N^*_{\text{wwtp}}} \mathbb{E}\{Q^i_{\text{out}}(k+j)\} \leq Q_{\text{wwtp}_{\max}}, \qquad t = 1, 2, ..., N_t \tag{9.32l}$$

$$0 \leq \mathbb{E}\{Q^t_{\text{out}}(k)\} \leq Q^t_{\text{out}_{\max}}, \qquad t = 1, 2, ..., N_t \tag{9.32m}$$

$$\mathbb{E}\{Q^t_{\text{ov}}(k+j)\} \geq 0, \qquad t = 1, 2, ..., N_t \tag{9.32n}$$

$$\mathbb{E}\{C^t(k+j)\} \geq 0, \qquad t = 1, 2, ..., N_t \tag{9.32o}$$

$$0 \leq \theta^t_{\min}(k+j) \leq \sigma\{V^t(k+j) + T_s(Q^t_{\text{in}}(k+j) + Q^t_{\text{out}}(k+j))\}\Phi^{-1}(\zeta), \qquad t = 1, 2, ..., N_t \tag{9.32p}$$

$$0 \leq \theta^t_{\max}(k+j), \qquad t = 1, 2, ..., N_t \tag{9.32q}$$

The cost function J is calculated by:

$$J(x(k), u(k)) = \alpha\phi_1(k) + \beta\phi_2(k) + \gamma\phi_3(k) + \epsilon(\phi_4(k) + \phi_5(k) + \phi_6(k)) + \psi\phi_7(k) + \omega\phi_8(k) + \upsilon\frac{1}{\phi_9(k)} \tag{9.33}$$

where (α, β, γ, ϵ, ψ, ω, υ) are the weights for objectives (ϕ_1, ϕ_2, ϕ_3, (ϕ_4, ϕ_5), ϕ_6, ϕ_7, ϕ_8, ϕ_9), respectively. Each objective is represented as below:

- ϕ_1, in Equation 9.34, is used to homogeneously store the volume within all tank structures in the sewage network.

$$\phi_1(k) = \sum_{i=1}^{N_t} \left(\mathbb{E}\{V^i(k)\} - \frac{V^i_{\max}}{\sum_{j=1}^{N} V^j_{\max}} \sum_{n=1}^{N_t} \mathbb{E}\{V^n(k)\} \right)^2 \tag{9.34}$$

  which N_t is the number of tanks in the network.

- ϕ_2, in Equation 9.35, keeps the flow towards the wastewater treatment plant near the operating reference value defined by Q_{ref}.

$$\phi_2(k) = \sum_{j \in N_{up}} \left(Q^j_{\text{ref}}(k) - \sum_{i \in N^*_t} \mathbb{E}\{Q^i_{\text{out}}(k - d^{i,t})\} \right)^2 \tag{9.35}$$

  where Q_{ref} is the reference flow for the i^{th} tank, which includes $Q_{\text{wwtp}_{\text{ref}}}$ as the inflow reference to the WWTP, Q_{out} is the outflow from each tank, $d_{i,t}$ represents the transport time of the i^{th} tank to the destination tank m, N^*_t are all tanks draining in the destination t and N_{up} are all tanks that have an upstream tank and the wastewater treatment plant.

- ϕ_3, in Equation 9.36, is used to minimise the overflow.

$$\phi_3(k) = \sum_{i=1}^{N_t} \mathbb{E}\{Q_{\text{ov}}^i(k) - NL\}^2 \tag{9.36}$$

- ϕ_4, in Equation 9.37, is used to minimise the slack variable θ_{min}.

$$\phi_4(k) = \sum_{i=1}^{N_t} (\theta_{\text{min}}^i)^2 \tag{9.37}$$

- ϕ_5, in Equation 9.38, is used to minimise the slack variable θ_{max}.

$$\phi_5(k) = \sum_{i=1}^{N_t} (\theta_{\text{max}}^i)^2 \tag{9.38}$$

- ϕ_6, in Equation 9.39, is used to minimise the slack variable θ_{max}^c.

$$\phi_6(k) = \sum_{i=1}^{N_t} (\theta_{\text{max}}^{c^i})^2 \tag{9.39}$$

- ϕ_7, in Equation 9.40, is used to homogeneously store the pollutant load within all tank structures in the sewage network.

$$\phi_7(k) = \sum_{i=1}^{N_t} \left(\mathbb{E}\{C^i(k)\}\mathbb{E}\{V^i(k)\} - \frac{V_{\text{max}}^i}{\sum_{j=1}^{N} V_{\text{max}}^j} \sum_{n=1}^{N_t} \mathbb{E}\{C^n(k)\}\mathbb{E}\{V^n(k)\} \right)^2 \tag{9.40}$$

- ϕ_8, in Equation 9.41, is used to minimise the load overflow.

$$\phi_8(k) = \sum_{i=1}^{N_t} \left(\mathbb{E}\{C^i(k)\}\mathbb{E}\{Q_{\text{ov}}^i(k)\} \right)^2 \tag{9.41}$$

- ϕ_9, in Equation 9.42, is to force the maximum possible load to reach the WWTP.

$$\phi_9(k) = \left(\sum_{i \in N_t^*} \mathbb{E}\{C^i(k - d^{i,t})\}\mathbb{E}\{Q_{\text{out}}^i(k - d^{i,t})\} \right)^2 \tag{9.42}$$

Since the objective is to maximise ϕ_9, it is used in the form $\frac{1}{\phi_9}$ in the cost function. Finally, the control loop algorithm for NPMPC can be summarised as follows:

Control Algorithm

(a) Initialise $\boldsymbol{x}(k) = \boldsymbol{x}(0)$, where $\boldsymbol{x}(0) = \{\mathbb{E}\{\boldsymbol{V}(0)\},\ \mathbb{E}\{\boldsymbol{Q}_{\text{out}}(0)\},\ \mathbb{E}\{\boldsymbol{Q}_{\text{ov}}(0)\},\ \mathbb{E}\{\boldsymbol{C}(0)\},\ \boldsymbol{V}_{\epsilon}(0)\}$ is the current state of the system;

(b) Estimate $\mathbb{E}\{\boldsymbol{Q}_{\text{in}}(k)\}$ using Equation 7.13, $\mathbb{E}\{\boldsymbol{C}_{\text{in}}(k)\} = \boldsymbol{C}_{\text{in}}(k)$ using Equation 8.8, and $\mathbb{E}\{\boldsymbol{C}(k)\} = \boldsymbol{C}(k)$ using Equation 8.11;

(c) Solve the optimisation problem as in Equation 9.32a and obtain the optimal control sequence $\hat{\boldsymbol{u}}(k)$;

(d) At time k, apply the first input $\boldsymbol{u}(k) = \boldsymbol{Q}_{\text{out}}(k)$ of the optimal control sequence to the UDS;

(e) Wait for next control loop $k = k + 1$;

(f) Measure $\boldsymbol{V}(k)$ and $\boldsymbol{Q}_{\text{out}}(k)$, calculate $\boldsymbol{Q}_{\text{ov}}(k)$, and update the expected values as $\mathbb{E}\{\boldsymbol{V}(k)\} = u_s \cdot \boldsymbol{V}(k) + u_{\text{off}}$, $\mathbb{E}\{\boldsymbol{Q}_{\text{out}}(k)\} = u_s \cdot \boldsymbol{Q}_{\text{out}}(k) + u_{\text{off}}$, and $\mathbb{E}\{\boldsymbol{Q}_{\text{ov}}(k)\} = u_s \cdot \boldsymbol{Q}_{\text{ov}}(k) + u_{\text{off}}$, then return to Step (b).

The following scenarios are considered for standard deviations:

- In all scenarios, a standard deviation for the inflow, $Q_{\text{in}}(k)$, the concentration of the inflow, $C_{\text{in}}(k)$ and the concentration within the SU $C(k)$, are determined to ascertain possible errors in the estimation during the control loop:

$$\sigma\{Q_{\text{in}}(k)\} = u_p * \frac{Q_{\text{in}}(k)}{n}$$

$$\sigma\{C_{\text{in}}(k)\} = u_p * \frac{C_{\text{in}}(k)}{n_c}$$

$$\sigma\{C(k)\} = u_p * \frac{C(k)}{n_c}$$

  where n and n_c represents a fraction of the actual value.

- The first scenario considers uncertainties on the Volume, therefore $\sigma\{Q_{\text{out}}(k)\} = 0$, $\sigma\{Q_{\text{ov}}(k)\} = 0$ and

$$\sigma\{V(k)\} = u_p * (V_{\max} - V(k))$$

- The second scenario considers uncertainties on the Outflow, therefore, at $k = 0$, $\sigma\{V(0)\} = 0$ and $\sigma\{Q_{\text{ov}}(k)\} = 0$ and

$$\sigma\{Q_{\text{out}}(k)\} = u_p * (Q_{\text{out}_{\max}} - Q_{\text{out}}(k))$$

- The third scenario considers uncertainties on the Overflow, therefore, at $k = 0$, $\sigma\{V(0)\} = 0$ and $\sigma\{Q_{\text{out}}(k)\} = 0$ and

$$\sigma\{Q_{\text{ov}}(k)\} = u_p * Q_{\text{ov}}(k)$$

For practical purposes, in future simulations $n = 3$ and $n_c = 5$. In the next section, the performance of SNPMPC is assessed using the validation methodology, comparing the results with NPMPC for different metrics.

9.5.3 Methodology Validation

The validation of SNPMPC involves assessing its control performance under conditions outlined in Section 9.1, focusing on three primary scenarios: (1) Volume uncertainty due to changes in u_p, (2) Volume uncertainty caused by positive variations in u_{off}, (3) Volume uncertainty caused by negative variations in u_{off}. Additional scenarios are provided in Appendix A.4. For each scenario, uncertainty is isolated to a specific parameter. The initial weights for the objective function are α, β, γ, ϵ, ψ, ω, υ = (11.2, 228.6, 90.7, 190.0, 10.0, 241.4, 0.04) and the confidence level ζ is varied throughout the range $[0.6, 0.8, 0.95]$.

Uncertainty on $V(k)$

To begin, the performance of SNPMPC is assessed under conditions where uncertainty is introduced in $V(k)$. The analysis starts by examining the impact of u_p and comparing SNPMPC with NPMPC across different values of ζ, for u_p values in the range of [0%, 5%, 10%, 25%, 50%, 75%]. The results presented in Table 9.39 show that, in general, SNPMPC does not outperform NPMPC in any of the scenarios analysed. Specifically, as ζ increases, the stochastic method demonstrates a notable decline in performance, reaching 3.12% and 7.3% volume and load overflow increase for $\zeta = 0.95$ and $u_p = 75\%$.

For the second scenario shown in Table 9.40, the volume uncertainty is varied by changing u_{off} between [0%, 5%, 10%, 25%, 50%, 75%]. In general, SNPMPC produces a more stable performance when uncertainties are present, displaying greater robustness to increasing levels of uncertainties. Furthermore, the difference between the values of ζ is not significant, maintaining a similar performance. However, SNPMPC is still worse than NPMPC in all metrics in absolute terms.

The last volume uncertainty analysed varies u_{off} in [0%, -5%, -10%, -25%, -50%, -75%], as shown in Table 9.41. For this scenario, the robustness of SNPMPC is not as pronounced as for other uncertainties, although it is more stable than NPMPC. Furthermore, the confidence level does not influence the outcome in a meaningful way either. For this instance, $\%\mathbf{F}_m$ increases steadily with uncertainties, reaching 28% for volume and 65% for load overflow in all SNPMPC in the worst case.

In general, SNPMPC is displaying good robustness, but the performance suggests a poor choice of weights, since SNPMPC is not capable of outperforming NPMPC whatsoever. Therefore, the analysis of the parameters is imperative to understand if the performance can be improved. The following section will detail the methodology for selecting the weights in the context of SNPMPC, based on the principles discussed in Chapter 7. This approach presents additional complexities due to the numerous weights involved, including α, β, γ, ϵ, ψ, ω, and υ, making the analysis more challenging. Nevertheless, the process remains manageable with a few simplifying assumptions and basic considerations.

9.5.4 Local Sensitivity Analysis - Morris Screening

In contrast to the other stochastic methods, SNPMPC contains additional weights, with a total of seven weights (α, β, γ, ϵ, ψ, ω and υ), and the confidence level. Hence, for the Morris screening there are in total 8 parameters ($k = 8$). The number of trajectories for this simulation is $r = 75$, which leads to a total number of simulation runs of $N_m = r(k+1) = 75*(8+1) = 675$. Besides, $\Delta = 1$ for the weights, whereas

Table 9.39: Volume uncertainty: Comparison between NPMPC and SNPMPC for u_p.

	NPMPC					
u_p	0%	5%	10%	25%	50%	75%
$Q_{\text{ov}_{\text{total}}}$	166.872	167.963	168.49	169.591	170.61	171.03
$\%\mathbf{F}_Q$		**0.65%**	**0.97%**	**1.63%**	**2.24%**	**2.49%**
$m^{\text{NH}_4}_{\text{ov}_{\text{total}}}$	1009.773	1021.104	1028.821	1037.617	1048.43	1053.341
$\%\mathbf{F}_m$		**1.12%**	**1.89%**	**2.76%**	**3.83%**	**4.31%**
ξ_{rain}	9.539	8.319	7.363	5.723	4.964	4.495
	SNPMPC - $\zeta = 0.60$					
u_p	0%	5%	10%	25%	50%	75%
$Q_{\text{ov}_{\text{total}}}$	172.913	174.071	174.869	175.865	175.885	176.683
$\%\mathbf{F}_Q$		**0.67%**	**1.13%**	**1.71%**	**1.72%**	**2.18%**
$m^{\text{NH}_4}_{\text{ov}_{\text{total}}}$	1154.018	1171.48	1180.767	1190.519	1180.052	1192.728
$\%\mathbf{F}_m$		**1.51%**	**2.32%**	**3.16%**	**2.26%**	**3.35%**
ξ_{rain}	9.672	8.663	7.628	6.715	5.835	5.457
	SNPMPC - $\zeta = 0.80$					
u_p	0%	5%	10%	25%	50%	75%
$Q_{\text{ov}_{\text{total}}}$	172.938	174.013	175.055	176.563	177.256	177.771
$\%\mathbf{F}_Q$		**0.62%**	**1.22%**	**2.1%**	**2.5%**	**2.79%**
$m^{\text{NH}_4}_{\text{ov}_{\text{total}}}$	1154.872	1166.452	1183.975	1203.48	1212.017	1215.031
$\%\mathbf{F}_m$		**1.0%**	**2.52%**	**4.21%**	**4.95%**	**5.21%**
ξ_{rain}	9.674	8.778	7.881	6.525	6.119	5.744
	SNPMPC - $\zeta = 0.95$					
u_p	0%	5%	10%	25%	50%	75%
$Q_{\text{ov}_{\text{total}}}$	172.901	174.476	175.384	177.02	178.375	178.29
$\%\mathbf{F}_Q$		**0.91%**	**1.44%**	**2.38%**	**3.17%**	**3.12%**
$m^{\text{NH}_4}_{\text{ov}_{\text{total}}}$	1153.967	1175.47	1188.07	1205.224	1225.786	1238.156
$\%\mathbf{F}_m$		**1.86%**	**2.96%**	**4.44%**	**6.22%**	**7.3%**
ξ_{rain}	9.675	8.656	8.097	7.43	6.359	6.813

$\Delta = 0.1$ for ζ. The analysis is performed in the Parallel + Series configuration and the simulation period is March 24 to April 10, while the analysis is only realized on Scenario 1 and Scenario 2 considering the simulation without uncertainties and the one with volume uncertainties, $u_p = 25\%$ and $u_{\text{off}} = 0$.

The results are presented in Figure 9.28. Unlike other stochastic methods, the influence of the confidence level, ζ, in SNPMPC varies significantly between scenarios with and without uncertainty. When uncertainty is absent, the parameter with the most significant impact is the weight ω, responsible for scaling optimisation to minimise load overflow (ϕ_8 in Equation 9.41), with $\mu = 25496.4$ and $\sigma = 146748.9$. In this scenario, the confidence level, ζ, has the same impact as other parameters with $\mu = 4401.2$ and $\sigma = 8534.2$.

However, when uncertainties are introduced, the effect of ζ becomes much more pronounced. In this case, ζ achieves $\mu = 491376.7$ and $\sigma = 895761.5$, which is at least 8 times the second most influential parameter, ω. The result for ω in the presence of uncertainty is $\mu = 25442.6$ and $\sigma = 113580.7$, which is

Table 9.40: Volume uncertainty: Comparison between NPMPC and SNPMPC for $u_{\text{offset}}^{\text{vol+}}$.

	NPMPC					
u_{off}	0%	5%	10%	25%	50%	75%
$Q_{\text{ov}_{\text{total}}}$	166.872	166.845	167.543	169.337	171.927	173.933
$\%\mathbf{F}_Q$		**-0.02%**	**0.4%**	**1.48%**	**3.03%**	**4.23%**
$m_{\text{ov}_{\text{total}}}^{\text{NH}_4}$	1009.773	1027.146	1043.661	1090.992	1149.691	1204.124
$\%\mathbf{F}_m$		**1.72%**	**3.36%**	**8.04%**	**13.86%**	**19.25%**
ξ_{rain}	9.539	9.587	9.629	9.813	9.831	9.837
	SNPMPC - $\zeta = 0.60$					
u_{off}	0%	5%	10%	25%	50%	75%
$Q_{\text{ov}_{\text{total}}}$	172.913	172.923	173.476	174.793	175.535	175.531
$\%\mathbf{F}_Q$		**0.01%**	**0.33%**	**1.09%**	**1.52%**	**1.51%**
$m_{\text{ov}_{\text{total}}}^{\text{NH}_4}$	1154.018	1162.747	1175.884	1215.019	1259.937	1260.658
$\%\mathbf{F}_m$		**0.76%**	**1.89%**	**5.29%**	**9.18%**	**9.24%**
ξ_{rain}	9.672	9.679	9.714	9.708	9.87	9.889
	SNPMPC - $\zeta = 0.80$					
u_{off}	0%	5%	10%	25%	50%	75%
$Q_{\text{ov}_{\text{total}}}$	172.938	172.914	173.331	174.762	175.525	175.533
$\%\mathbf{F}_Q$		**-0.01%**	**0.23%**	**1.05%**	**1.5%**	**1.5%**
$m_{\text{ov}_{\text{total}}}^{\text{NH}_4}$	1154.872	1162.616	1174.661	1213.213	1260.408	1260.54
$\%\mathbf{F}_m$		**0.67%**	**1.71%**	**5.05%**	**9.14%**	**9.15%**
ξ_{rain}	9.674	9.662	9.677	9.823	9.893	9.944
	SNPMPC - $\zeta = 0.95$					
u_{off}	0%	5%	10%	25%	50%	75%
$Q_{\text{ov}_{\text{total}}}$	172.901	172.972	173.292	174.64	175.477	175.547
$\%\mathbf{F}_Q$		**0.04%**	**0.23%**	**1.01%**	**1.49%**	**1.53%**
$m_{\text{ov}_{\text{total}}}^{\text{NH}_4}$	1153.967	1160.952	1170.855	1210.133	1259.479	1260.822
$\%\mathbf{F}_m$		**0.61%**	**1.46%**	**4.87%**	**9.14%**	**9.26%**
ξ_{rain}	9.675	9.655	9.782	9.749	9.916	9.854

quite similar to its performance in scenario 1.

The Morris Screening displays a significant influence of both ω and ζ. For Scenario 2, excluding those two parameters, the effects of the remaining ones are quite similar, suggesting that all of them are important to the performance of the controller and should therefore be considered in the Genetic Algorithm. The next step is to determine the ranges within which the parameters demonstrate optimal performance through the Global Sensitivity Analysis.

9.5.5 Global Sensitivity Analysis - Grid and Random Search

To refine the weight selection, the analysis began with the initial assignment of $\alpha = 11.2$, $\beta = 228.6$, $\gamma = 90.7$, $\epsilon = 190.0$, and $\zeta = 0.8$, while focusing on the global sensitivity analysis for the most impactful

Table 9.41: Volume uncertainty: Comparison between NPMPC and SNPMPC for $u_{\text{offset}}^{\text{vol-}}$.

	NPMPC					
u_{off}	0%	−5%	−10%	−25%	−50%	−75%
$Q_{\text{ov}_{\text{total}}}$	166.872	170.477	173.849	181.875	194.091	218.174
$\%\mathbf{F}_Q$		**2.16%**	**4.18%**	**8.99%**	**16.31%**	**30.74%**
$m_{\text{ov}_{\text{total}}}^{\text{NH}_4}$	1009.773	1040.733	1070.63	1173.591	1319.062	1808.97
$\%\mathbf{F}_m$		**3.07%**	**6.03%**	**16.22%**	**30.63%**	**79.15%**
ξ_{rain}	9.539	9.188	8.616	7.348	4.424	-2.084
	SNPMPC - $\zeta = 0.60$					
u_{off}	0%	−5%	−10%	−25%	−50%	−75%
$Q_{\text{ov}_{\text{total}}}$	172.913	174.393	175.971	180.918	190.161	220.755
$\%\mathbf{F}_Q$		**0.86%**	**1.77%**	**4.63%**	**9.97%**	**27.67%**
$m_{\text{ov}_{\text{total}}}^{\text{NH}_4}$	1154.018	1164.931	1176.063	1232.584	1385.548	1901.042
$\%\mathbf{F}_m$		**0.95%**	**1.91%**	**6.81%**	**20.06%**	**64.73%**
ξ_{rain}	9.672	9.485	9.433	9.184	8.823	-3.97
	SNPMPC - $\zeta = 0.80$					
u_{off}	0%	−5%	−10%	−25%	−50%	−75%
$Q_{\text{ov}_{\text{total}}}$	172.938	174.419	176.028	180.914	190.147	220.767
$\%\mathbf{F}_Q$		**0.86%**	**1.79%**	**4.61%**	**9.95%**	**27.66%**
$m_{\text{ov}_{\text{total}}}^{\text{NH}_4}$	1154.872	1166.231	1178.422	1232.449	1384.592	1901.813
$\%\mathbf{F}_m$		**0.98%**	**2.04%**	**6.72%**	**19.89%**	**64.68%**
ξ_{rain}	9.674	9.491	9.432	9.168	8.811	-3.949
	SNPMPC - $\zeta = 0.95$					
u_{off}	0%	−5%	−10%	−25%	−50%	−75%
$Q_{\text{ov}_{\text{total}}}$	172.901	174.413	175.96	180.961	190.178	220.78
$\%\mathbf{F}_Q$		**0.87%**	**1.77%**	**4.66%**	**9.99%**	**27.69%**
$m_{\text{ov}_{\text{total}}}^{\text{NH}_4}$	1153.967	1165.977	1175.695	1233.1	1385.807	1903.594
$\%\mathbf{F}_m$		**1.04%**	**1.88%**	**6.86%**	**20.09%**	**64.96%**
ξ_{rain}	9.675	9.49	9.437	9.16	8.783	-3.951

weights ψ, ω, and υ. To explore the sensitivity of the fixed weights, a series of targeted grid searches was conducted for the same period as for the Morris screening analysis:

1. The initial weights were established as $\alpha = 11.2$, $\beta = 228.6$, $\gamma = 90.7$ and $\epsilon = 190.0$, but several simulations were performed to determine the appropriate range for these variables.

2. A first grid search is executed using the base values as in Step 1 to immediately evaluate if the weights used in Section 9.5.3 could be improved using different combinations of ψ, ω, and υ.

3. Secondly, the value of α was varied across $(1, 33, 66)$, while β, γ and ϵ were held constant at their initial values.

4. The process was repeated with β varying in $(1, 113, 226)$, with all other weights remaining constant, as well as for γ, varying in $(1, 70, 150)$, and then finally, ϵ tested throughout the range $(1, 100, 250)$.

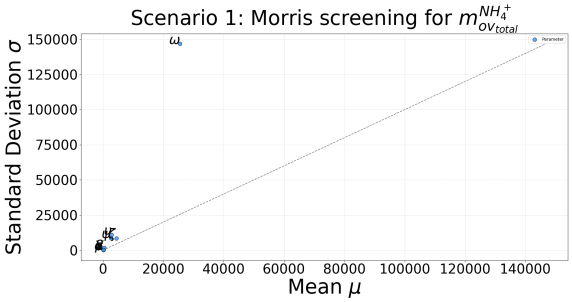

(a) $m^{\mathrm{NH_4}}_{\mathrm{OV_{total}}}$ in Scenario 1.

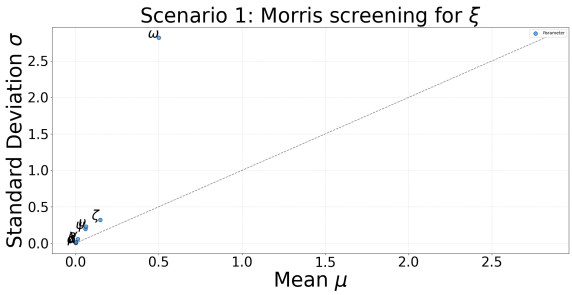

(b) ξ in Scenario 1.

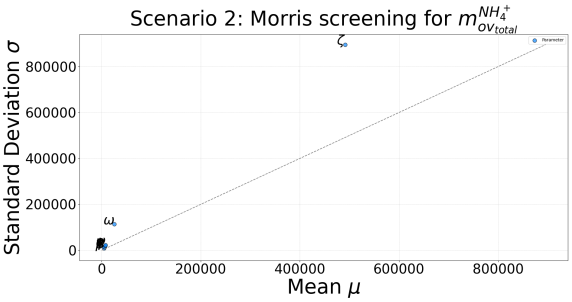

(c) $m^{\mathrm{NH_4}}_{\mathrm{OV_{total}}}$ in Scenario 2.

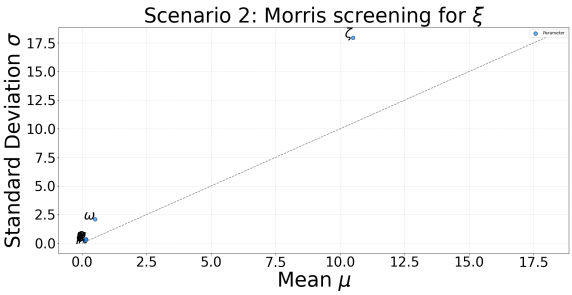

(d) ξ in Scenario 2.

Figure 9.28: Morris screening for $m^{\mathrm{NH_4}}_{\mathrm{OV_{total}}}$ and ξ.

For each configuration, a Grid Search is performed for $\psi, \omega, \upsilon \in [1, 100]$, with 10 equally spaced points for each variable, generating 1000 points in total. The grid search with base values proposed in Step 2 can be seen in Figure 9.29. .

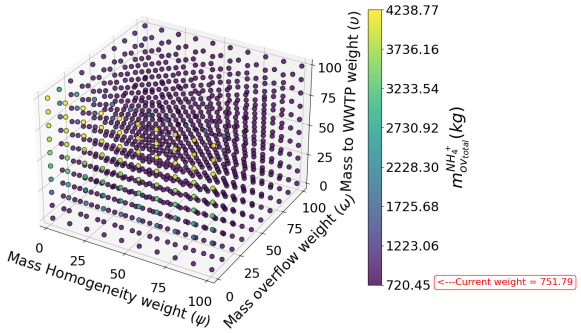

(a) $m^{\mathrm{NH_4}}_{\mathrm{OV_{total}}}$ for $\epsilon = 3$.

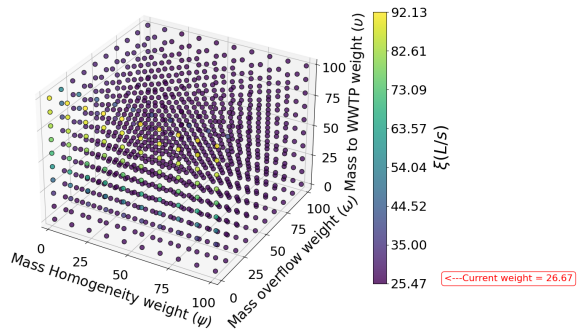

(b) ξ for $\epsilon = 3$.

Figure 9.29: Grid Search SA for SNPMPC with base values.

It reveals potential to improve the performance already in the scenario without uncertainties, although the original set of weights is already in a suitable region for the performance. The search through υ exhibits a trend toward lower values (below 40), especially when ω is also in lower ranges, which is therefore preferable in mid- to higher ranges to avoid high loads and errors. Although in the graph it is difficult to properly analyse the behaviour for ψ, the data showed that it is better in the lower to mid ranges in this scenario. The lowest load was reached with $\upsilon = 34$, $\omega = 100$ and $\psi = 78$, while the lowest

error was at $\upsilon = 12$, $\omega = 23$ and $\psi = 45$, highlighting the conclusions obtained. In summary, analysing all the grid search heatmaps, the results suggest that to minimise overflow, the lower values of γ and ϵ are the most effective. Specifically, γ should be set lower (around 1) to reduce $m^{\mathrm{NH_4}}_{\mathrm{ov_{total}}}$, while ϵ should also remain at range to avoid increasing overflow, however, this causes the ξ to increase, and thus it is suggested to keep them at mid ranges to be able to find an optimal pareto with the possible trade-offs.

Furthermore, the impact of β is less pronounced, with β showing no clear trend, while α performs similarly at all values. The overall best result obtained for $m^{\mathrm{NH_4}}_{\mathrm{ov_{total}}}$ is 720.08kg with weights $\alpha = 11.2$, $\beta = 228.6$, $\gamma = 90.7$, $\epsilon = 1.0$, $\upsilon = 25.75$, $\omega = 75.25$ and $\psi = 50.5$, while for ξ it is 25.47 L/s with $\alpha = 11.2$, $\beta = 228.6$, $\gamma = 90.7$, $\epsilon = 190.0$, $\upsilon = 12$, $\omega = 23$ and $\psi = 45$. An additional random search is performed using the same settings to try to reach a better conclusion at the values of β, ω and υ. The analysis is performed using a total of 1000 points randomly chosen, varying β from 0 to 250, ω from 0 to 200 and υ from 0 to 20. The random search heatmap, shown in Figure 9.30, displays additional information on the behaviour of the weights. It indicates that ω performs optimally within the range of 20 to 100 for both metrics, while β tends to perform best in the mid-range values. Additionally, the value of υ reveals a trade-off between $m^{\mathrm{NH4}}_{\mathrm{ov_{total}}}$ and ξ within the range explored during this search, suggesting also that it should be bounded in a higher range to encompass more combinations of weights.

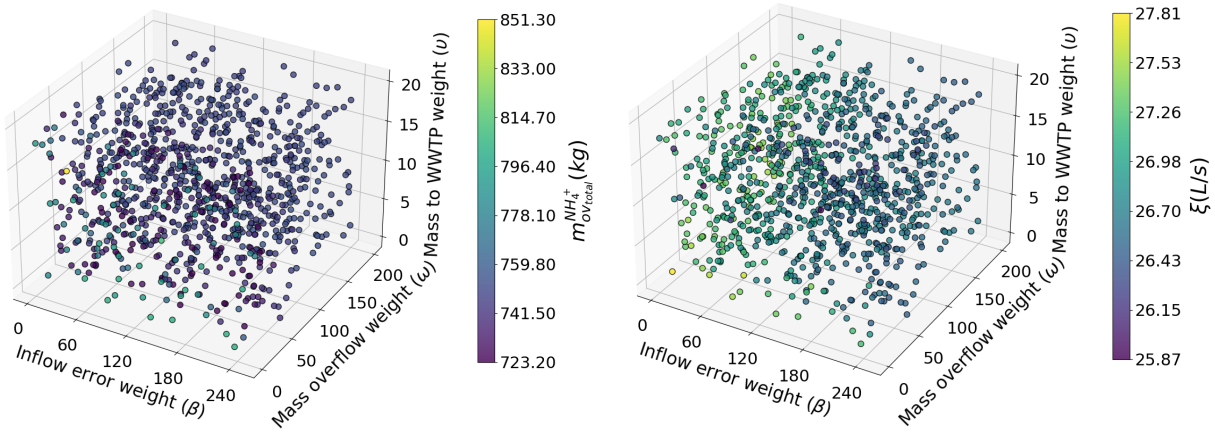

(a) Random Search for $m^{\mathrm{NH_4}}_{\mathrm{ov_{total}}}$.

(b) Random Search for ξ.

Figure 9.30: Random Search.

In general, the final assessment for the Sensitivity Analysis is $\alpha < 30$, $\beta \in [50, 300]$, $\gamma < 150]$, $\epsilon < 20$, $\psi \in [10, 100]$, $\omega \in [20, 150]$, $\upsilon < 100$. Since there are many possible combinations, it was decided to broaden the range for some variables to help the Genetic Algorithm to reach an optimal Pareto-front.

9.5.6 Genetic Algorithm for weight optimisation

The next step involves determining the optimal weights for SNPMPC. The Genetic Algorithm is simulated under the same uncertainty scenarios described in Table 9.19, except scenario 4. The initial parameter estimates for the simulation are set as follows: $\alpha = 11.2$, $\beta = 228.6$, $\gamma = 90.7$, $\epsilon = 1.0$, $\upsilon = 25.75$, $\omega = 75.25$, and $\psi = 50.5$, with a tolerance of 10^{-1}. The simulations are run over the period from March 24 to April 10, using a population size of 10 and a maximum of 300 iterations.

The Pareto front for each scenario is presented in Figure 9.31, which reveals different outcomes as expected, given the varying impacts each uncertainty has on the network. The provided Pareto plot shows three different scenarios, each highlighting a distinct relationship between the overflow load ($m_{\mathrm{OV_{total}}}^{\mathrm{NH_4}}$) and the error metric ($\xi$). Scenario 1 demonstrates generally low overflow and moderate error levels, representing the most balanced performance. Scenario 2 exhibits a clear trade-off, ranging from very low error with higher overflow to moderate overflow paired with increasing error. Scenario 3, in contrast, clearly presents the highest error levels and comparatively medium overflow levels.

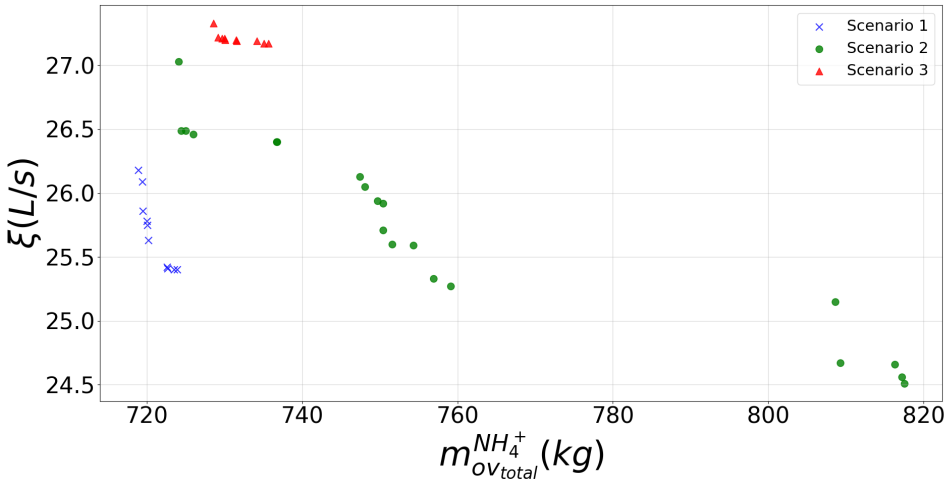

Figure 9.31: Pareto front SPWMPC.

Since each scenario represents a different type of uncertainty that impacts the wastewater network, their respective Pareto fronts naturally diverge. Scenario 1 maintains a balanced performance, which is expected since it is the scenario without uncertainties. Scenario 2 suggests a scenario where the uncertainty strongly influences the trade-off between overflow minimisation and precision, thus allowing clear optimisation directions based on each objective. Scenario 3 shows that the underestimation of the volume significantly deteriorates ξ, and the overflow is high compared to the other scenarios.

In Table 9.42 the optimal weights for each scenario are presented, selected according to various criteria based on the objectives. The weight selection is quite different for the scenarios, suggesting that the optimisation focused on each scenario might improve the performance for that specific situation.

Table 9.42: Optimal (α, β, γ, ϵ, ψ, ω, υ) for each uncertainty scenario.

Scenario	Best weights for $m_{\mathrm{OV_{total}}}^{\mathrm{NH_4}}$	Best weights for ξ	Best compromise
1	(16.69, 275.49, 73.65, 1.42, 24.23, 71.35, 54.20)	(8.66, 299.00, 73.65, 1.0, ,12.60, 42.35, 50.5)	(12.82, 299.08, 82.25, 1.0, 18.91, 55.22, 62.93)
2	(4.91, 198.63, 170.81, 20.67, 39.55, 120.26, 1.66)	(5.18, 198.63, 170.81, 1.64, 0.02, 155.73, 1.17)	(3.01, 198.63, 170.81, 1.83, 6.23, 165.59, 27.78)
3	(1.24, 299.99, 16.69, 0.01, 10.01, 38.42, 0.20)	(1.24, 299.99, 1.78, 0.14, 10.02, 32.66, 0.20)	(2.52, 298.84, 2.74, 0.01, 10.00, 32.66, 0.90)

Examining the weights, α remained consistently at lower values (below 5) in scenarios involving uncertainties, while β was maintained at higher values (above 200) in all cases. The weight γ showed greater variability without a clear pattern in all evaluated scenarios. Additionally, ϵ predominantly occupied mid to lower ranges, diverging significantly from the findings for NPMPC, which, similar to other deterministic approaches, showed significantly higher values for ϵ. Furthermore, the parameter ψ consistently fell

within intermediate ranges, contrary to ω and υ which were less consistent between scenarios, reinforcing that the choice of parameters depends on the scenario for some weights.

The choice of optimal weights for the final analysis is the best weight of Scenario 3, resulting in $m_{\text{ov}_{\text{total}}}^{\text{NH}_4}$. This resulted in $\alpha = 1.24$, $\beta = 299.99$, $\gamma = 16.69$, $\epsilon = 0.01$, $\psi = 10.01$, $\omega = 38.42$, $\upsilon = 0.20$. The performance of SNPMPC, using the optimal weights identified, is subsequently compared against NPMPC with its respective optimal parameters, while also considering the influence of the confidence level.

Uncertainty on $V(k)$

The first analysis considers volume uncertainties and varying u_p. The choice of weights considerably improved the system in both robustness of the MPC for increasing levels of uncertainty and in the performance of SNPMPC compared to NPMPC regarding the overflow load when there were higher uncertainties. For all confidence levels, the improvement over the non-optimal weights is noticeable, however, it still underperforms compared to the deterministic method. However, the best outcome is for $\zeta = 0.6$, which is most likely because higher confidence levels were too conservative in their formulation.

The second scenario where the volume is overestimated shows that SNPMPC performs slightly better compared to NPMPC for $u_{\text{off}} = 75\%$, showing a more robust and stable performance as the uncertainty increases. The optimal weights improved performance by 5% for all confidence levels, with $\zeta = 0.6$ exhibiting slightly superior behaviour for overflow load.

Lastly, the scenario in which the optimal weights were selected is analysed, where the volume is underestimated. Observing $\%\mathbf{F}_m^*$, the improvement with optimal weights is significant, resulting in a better performance of SNPMPC compared to NPMPC when the uncertainty is greater than 50%, reaching an overflow load of 1682 kg compared to 1809 kg from NPMPC. The value of ζ did not affect performance compared to its impact on u_p. Furthermore, there is a large improvement in ξ_{rain} for $u_{\text{off}} = -75\%$, although NPMPC still performed better in reducing ξ_{rain}.

The results show that a well tuned SNPMPC is capable of not just maintaining robustness of the control performance, but also over-performing their deterministic counterpart as the uncertainty increases. For all stochastic methods, the main challenge is identifying which uncertainty is affecting the system in order to properly tune the controller. This can be difficult, but using real data would help by observing the discrepancies between what the controller is assuming and what is actually happening in reality. In addition, the choice of ζ is also dependent on the level of uncertainty and the type, therefore, it needs careful consideration. In this example, the uncertainties are equal between all storage units, however, in practice, uncertainties are different between each unit, therefore, ζ should be considered independently. Finally, the conservative behaviour of stochastic methods could hinder scenarios where the uncertainty is not significant, highlighting the need for careful consideration of uncertainty.

Table 9.43: Volume uncertainty: Comparison between NPMPC and optimal SNPMPC for u_p.

	NPMPC					
u_p	0%	5%	10%	25%	50%	75%
$Q_{\mathrm{ov}_{\mathrm{total}}}$	166.872	167.963	168.49	169.591	170.61	171.03
$\%\mathbf{F}_Q$		**0.65%**	**0.97%**	**1.63%**	**2.24%**	**2.49%**
$m^{\mathrm{NH_4}}_{\mathrm{ov}_{\mathrm{total}}}$	1009.773	1021.104	1028.821	1037.617	1048.43	1053.341
$\%\mathbf{F}_m$		**1.12%**	**1.89%**	**2.76%**	**3.83%**	**4.31%**
ξ_{rain}	9.539	8.319	7.363	5.723	4.964	4.495
	SNPMPC - $\zeta = 0.60$					
u_p	0%	5%	10%	25%	50%	75%
$Q_{\mathrm{ov}_{\mathrm{total}}}$	172.511	172.932	173.541	173.833	173.628	173.583
$\%\mathbf{F}_Q$		**0.24%**	**0.6%**	**0.77%**	**0.65%**	**0.62%**
$\%\mathbf{F}^*_Q$	**-0.23%**	**-0.65%**	**-0.76%**	**-1.16%**	**-1.28%**	**-1.75%**
$m^{\mathrm{NH_4}}_{\mathrm{ov}_{\mathrm{total}}}$	1118.019	1124.548	1134.437	1137.754	1127.871	1126.246
$\%\mathbf{F}_m$		**0.58%**	**1.47%**	**1.77%**	**0.88%**	**0.74%**
$\%\mathbf{F}^*_m$	**-3.12%**	**-4.01%**	**-3.92%**	**-4.43%**	**-4.42%**	**-5.57%**
ξ_{rain}	9.613	8.531	7.531	6.371	5.977	6.176
$\%\mathbf{F}^*_\xi$	**-0.61%**	**-1.52%**	**-1.27%**	**-5.12%**	**2.43%**	**13.18%**
	SNPMPC - $\zeta = 0.80$					
u_p	0%	5%	10%	25%	50%	75%
$Q_{\mathrm{ov}_{\mathrm{total}}}$	172.507	173.091	173.921	174.075	173.955	173.812
$\%\mathbf{F}_Q$		**0.34%**	**0.82%**	**0.91%**	**0.84%**	**0.76%**
$\%\mathbf{F}^*_Q$	**-0.25%**	**-0.53%**	**-0.65%**	**-1.41%**	**-1.86%**	**-2.23%**
$m^{\mathrm{NH_4}}_{\mathrm{ov}_{\mathrm{total}}}$	1117.937	1124.992	1137.701	1134.884	1131.162	1126.437
$\%\mathbf{F}_m$		**0.63%**	**1.77%**	**1.52%**	**1.18%**	**0.76%**
$\%\mathbf{F}^*_m$	**-3.2%**	**-3.55%**	**-3.91%**	**-5.7%**	**-6.67%**	**-7.29%**
ξ_{rain}	9.612	8.294	7.415	6.026	5.449	5.224
$\%\mathbf{F}^*_\xi$	**-0.64%**	**-5.51%**	**-5.91%**	**-7.65%**	**-10.95%**	**-9.05%**
	SNPMPC - $\zeta = 0.95$					
u_p	0%	5%	10%	25%	50%	75%
$Q_{\mathrm{ov}_{\mathrm{total}}}$	172.518	173.085	173.691	174.272	174.156	174.116
$\%\mathbf{F}_Q$		**0.33%**	**0.68%**	**1.02%**	**0.95%**	**0.93%**
$\%\mathbf{F}^*_Q$	**-0.22%**	**-0.8%**	**-0.97%**	**-1.55%**	**-2.37%**	**-2.34%**
$m^{\mathrm{NH_4}}_{\mathrm{ov}_{\mathrm{total}}}$	1118.165	1129.724	1131.53	1137.022	1133.83	1136.942
$\%\mathbf{F}_m$		**1.03%**	**1.2%**	**1.69%**	**1.4%**	**1.68%**
$\%\mathbf{F}^*_m$	**-3.1%**	**-3.89%**	**-4.76%**	**-5.66%**	**-7.5%**	**-8.17%**
ξ_{rain}	9.612	8.548	7.468	6.156	5.239	5.632
$\%\mathbf{F}^*_\xi$	**-0.65%**	**-1.25%**	**-7.77%**	**-17.15%**	**-17.61%**	**-17.33%**

Table 9.44: Volume uncertainty: Comparison between NPMPC and optimal SNPMPC for $u_{\text{offset}}^{\text{vol+}}$.

	NPMPC					
u_{off}	0%	5%	10%	25%	50%	75%
$Q_{\text{ov}_{\text{total}}}$	166.872	166.845	167.543	169.337	171.927	173.933
$\%\mathbf{F}_Q$		**-0.02%**	**0.4%**	**1.48%**	**3.03%**	**4.23%**
$m_{\text{total}}^{\text{NH}_4}$	1009.773	1027.146	1043.661	1090.992	1149.691	1204.124
$\%\mathbf{F}_m$		**1.72%**	**3.36%**	**8.04%**	**13.86%**	**19.25%**
ξ_{rain}	9.539	9.587	9.629	9.813	9.831	9.837
	SNPMPC - $\zeta = 0.60$					
u_{off}	0%	5%	10%	25%	50%	75%
$Q_{\text{ov}_{\text{total}}}$	172.511	172.29	172.547	173.659	174.201	174.298
$\%\mathbf{F}_Q$		**-0.13%**	**0.02%**	**0.67%**	**0.98%**	**1.04%**
$\%\mathbf{F}_Q^*$	**-0.23%**	**-0.37%**	**-0.54%**	**-0.65%**	**-0.76%**	**-0.7%**
$m_{\text{total}}^{\text{NH}_4}$	1118.019	1123.279	1130.286	1163.28	1193.183	1197.861
$\%\mathbf{F}_m$		**0.47%**	**1.1%**	**4.05%**	**6.72%**	**7.14%**
$\%\mathbf{F}_m^*$	**-3.12%**	**-3.39%**	**-3.88%**	**-4.26%**	**-5.3%**	**-4.98%**
ξ_{rain}	9.613	9.556	9.629	9.871	9.868	9.946
$\%\mathbf{F}_\xi^*$	**-0.61%**	**-1.27%**	**-0.88%**	**1.68%**	**-0.02%**	**0.58%**
	SNPMPC - $\zeta = 0.80$					
u_{off}	0%	5%	10%	25%	50%	75%
$Q_{\text{ov}_{\text{total}}}$	172.507	172.255	172.602	173.769	174.285	174.283
$\%\mathbf{F}_Q$		**-0.15%**	**0.06%**	**0.73%**	**1.03%**	**1.03%**
$\%\mathbf{F}_Q^*$	**-0.25%**	**-0.38%**	**-0.42%**	**-0.57%**	**-0.71%**	**-0.71%**
$m_{\text{total}}^{\text{NH}_4}$	1117.937	1121.446	1131.915	1163.964	1193.654	1198.244
$\%\mathbf{F}_m$		**0.31%**	**1.25%**	**4.12%**	**6.77%**	**7.18%**
$\%\mathbf{F}_m^*$	**-3.2%**	**-3.54%**	**-3.64%**	**-4.06%**	**-5.3%**	**-4.94%**
ξ_{rain}	9.612	9.545	9.754	9.797	9.802	9.921
$\%\mathbf{F}_\xi^*$	**-0.64%**	**-1.21%**	**0.8%**	**-0.26%**	**-0.92%**	**-0.23%**
	SNPMPC - $\zeta = 0.95$					
u_{off}	0%	5%	10%	25%	50%	75%
$Q_{\text{ov}_{\text{total}}}$	172.518	172.399	172.644	173.839	174.216	174.405
$\%\mathbf{F}_Q$		**-0.07%**	**0.07%**	**0.77%**	**0.98%**	**1.09%**
$\%\mathbf{F}_Q^*$	**-0.22%**	**-0.33%**	**-0.37%**	**-0.46%**	**-0.72%**	**-0.65%**
$m_{\text{total}}^{\text{NH}_4}$	1118.165	1123.646	1130.991	1163.593	1190.392	1199.572
$\%\mathbf{F}_m$		**0.49%**	**1.15%**	**4.06%**	**6.46%**	**7.28%**
$\%\mathbf{F}_m^*$	**-3.1%**	**-3.21%**	**-3.4%**	**-3.85%**	**-5.49%**	**-4.86%**
ξ_{rain}	9.612	9.437	9.678	9.826	9.914	9.874
$\%\mathbf{F}_\xi^*$	**-0.65%**	**-2.26%**	**-1.06%**	**0.79%**	**-0.02%**	**0.2%**

Table 9.45: Volume uncertainty: Comparison between NPMPC and optimal SNPMPC for $u_{\text{offset}}^{\text{vol-}}$.

	NPMPC					
u_{off}	0%	−5%	−10%	−25%	−50%	−75%
$Q_{\text{ov}_{\text{total}}}$	166.872	170.477	173.849	181.875	194.091	218.174
$\%\mathbf{F}_Q$		**2.16%**	**4.18%**	**8.99%**	**16.31%**	**30.74%**
$m_{\text{ov}_{\text{total}}}^{\text{NH}_4}$	1009.773	1040.733	1070.63	1173.591	1319.062	1808.97
$\%\mathbf{F}_m$		**3.07%**	**6.03%**	**16.22%**	**30.63%**	**79.15%**
ξ_{rain}	9.539	9.188	8.616	7.348	4.424	-2.084
	SNPMPC - $\zeta = 0.60$					
u_{off}	0%	−5%	−10%	−25%	−50%	−75%
$Q_{\text{ov}_{\text{total}}}$	172.511	174.146	175.573	180.254	189.618	206.757
$\%\mathbf{F}_Q$		**0.95%**	**1.77%**	**4.49%**	**9.92%**	**19.85%**
$\%\mathbf{F}_Q^*$	**-0.23%**	**-0.14%**	**-0.23%**	**-0.37%**	**-0.29%**	**-6.34%**
$m_{\text{ov}_{\text{total}}}^{\text{NH}_4}$	1118.019	1134.34	1146.953	1195.866	1314.168	1680.944
$\%\mathbf{F}_m$		**1.46%**	**2.59%**	**6.96%**	**17.54%**	**50.35%**
$\%\mathbf{F}_m^*$	**-3.12%**	**-2.63%**	**-2.48%**	**-2.98%**	**-5.15%**	**-11.58%**
ξ_{rain}	9.613	9.454	9.418	9.267	8.386	3.946
$\%\mathbf{F}_\xi^*$	**-0.61%**	**-0.33%**	**-0.16%**	**0.9%**	**-4.95%**	**-199.4%**
	SNPMPC - $\zeta = 0.80$					
u_{off}	0%	−5%	−10%	−25%	−50%	−75%
$Q_{\text{ov}_{\text{total}}}$	172.507	174.145	175.607	180.235	189.638	206.788
$\%\mathbf{F}_Q$		**0.95%**	**1.8%**	**4.48%**	**9.93%**	**19.87%**
$\%\mathbf{F}_Q^*$	**-0.25%**	**-0.16%**	**-0.24%**	**-0.38%**	**-0.27%**	**-6.33%**
$m_{\text{ov}_{\text{total}}}^{\text{NH}_4}$	1117.937	1134.16	1147.618	1195.457	1315.401	1681.521
$\%\mathbf{F}_m$		**1.45%**	**2.65%**	**6.93%**	**17.66%**	**50.41%**
$\%\mathbf{F}_m^*$	**-3.2%**	**-2.75%**	**-2.61%**	**-3.0%**	**-5.0%**	**-11.58%**
ξ_{rain}	9.612	9.445	9.414	9.271	8.38	3.962
$\%\mathbf{F}_\xi^*$	**-0.64%**	**-0.48%**	**-0.19%**	**1.12%**	**-4.89%**	**-200.33%**
	SNPMPC - $\zeta = 0.95$					
u_{off}	0%	−5%	−10%	−25%	−50%	−75%
$Q_{\text{ov}_{\text{total}}}$	172.518	174.158	175.597	180.22	189.641	206.801
$\%\mathbf{F}_Q$		**0.95%**	**1.78%**	**4.46%**	**9.93%**	**19.87%**
$\%\mathbf{F}_Q^*$	**-0.22%**	**-0.15%**	**-0.21%**	**-0.41%**	**-0.28%**	**-6.33%**
$m_{\text{ov}_{\text{total}}}^{\text{NH}_4}$	1118.165	1134.453	1147.526	1195.119	1314.862	1682.53
$\%\mathbf{F}_m$		**1.46%**	**2.63%**	**6.88%**	**17.59%**	**50.47%**
$\%\mathbf{F}_m^*$	**-3.1%**	**-2.7%**	**-2.4%**	**-3.08%**	**-5.12%**	**-11.61%**
ξ_{rain}	9.612	9.451	9.424	9.267	8.359	3.891
$\%\mathbf{F}_\xi^*$	**-0.65%**	**-0.41%**	**-0.14%**	**1.17%**	**-4.83%**	**-198.48%**

9.6 Comparison between MPC methods

Finally, two scenarios were selected to globally compare the performance of all MPC methods, beginning with the scenario involving volume underestimation, where the deterministic methods previously demonstrated their weakest performance. Table 9.46 illustrates this comparison, showing the optimal results for each stochastic MPC alongside their deterministic counterparts. Under the scenario without uncertainties, NPMPC achieves the best outcomes regarding overflow volume and load, whereas PWMPC exhibits the lowest ξ_{rain}. The stochastic methods performed better than their deterministic counterparts when the uncertainty surpasses 25%, notably for SNPMPC with the lowest overflow and both SVMPC and SPWMPC for their reduced ξ_{rain}.

Table 9.46: Volume uncertainty: Analysis of $u_{\text{offset}}^{\text{vol-}}$ for all MPCs.

	VMPC					
u_{off}	0%	−5%	−10%	−25%	−50%	−75%
$Q_{\text{ov}_{\text{total}}}$	167.434	175.950	182.162	201.263	259.730	444.554
$m_{\text{ov}_{\text{total}}}^{\text{NH}_4}$	1072.366	1196.528	1266.674	1571.667	2852.361	10867.604
ξ_{rain}	7.926	6.132	3.520	-6.714	-31.339	-59.930
	PWMPC					
u_{off}	0%	−5%	−10%	−25%	−50%	−75%
$Q_{\text{ov}_{\text{total}}}$	168.770	176.550	182.521	203.081	268.190	485.907
$m_{\text{ov}_{\text{total}}}^{\text{NH}_4}$	1034.790	1160.127	1247.463	1588.802	3057.457	12442.546
ξ_{rain}	7.629	5.884	3.317	-7.805	-34.407	-65.611
	NPMPC					
u_{off}	0%	−5%	−10%	−25%	−50%	−75%
$Q_{\text{ov}_{\text{total}}}$	166.872	170.477	173.849	181.875	194.091	218.174
$m_{\text{ov}_{\text{total}}}^{\text{NH}_4}$	1009.773	1040.733	1070.630	1173.591	1319.062	1808.970
ξ_{rain}	9.539	9.188	8.616	7.348	4.424	-2.084
	SVMPC ($\zeta = 0.8$)					
u_{off}	0%	−5%	−10%	−25%	−50%	−75%
$Q_{\text{ov}_{\text{total}}}$	177.245	179.038	180.520	185.156	194.028	208.348
$m_{\text{ov}_{\text{total}}}^{\text{NH}_4}$	1280.479	1295.597	1312.074	1367.055	1507.547	1813.355
ξ_{rain}	6.564	6.514	6.499	6.358	6.279	0.105
	SPWMPC ($\zeta = 0.95$)					
u_{off}	0%	−5%	−10%	−25%	−50%	−75%
$Q_{\text{ov}_{\text{total}}}$	177.245	178.980	180.402	184.966	194.008	208.352
$m_{\text{ov}_{\text{total}}}^{\text{NH}_4}$	1279.891	1293.161	1307.191	1358.248	1506.839	1814.329
ξ_{rain}	6.566	6.514	6.495	6.360	6.281	0.101
	SNPMPC ($\zeta = 0.6$)					
u_{off}	0%	−5%	−10%	−25%	−50%	−75%
$Q_{\text{ov}_{\text{total}}}$	172.511	174.146	175.573	180.254	189.618	206.757
$m_{\text{ov}_{\text{total}}}^{\text{NH}_4}$	1118.019	1134.340	1146.953	1195.866	1314.168	1680.944
ξ_{rain}	9.612	9.451	9.424	9.267	8.359	3.891

The second scenario considers volume overestimation, as illustrated in Figure 9.47. In this case, under high uncertainty, PWMPC achieves the best performance, followed by VMPC and SNPMPC. Here, the conservative nature of the stochastic methods proved to be a limiting factor, leading to reduced performance even under high uncertainty. As a result, the stochastic approaches underperformed compared to their deterministic counterparts.

Table 9.47: Volume uncertainty: Analysis of $u_{\text{offset}}^{\text{vol+}}$ for all MPCs.

	VMPC					
u_{off}	0%	5%	10%	25%	50%	75%
$Q_{\text{ov}_{\text{total}}}$	167.434	166.782	167.017	168.22	170.44	172.75
$m_{\text{total}}^{\text{NH}_4}$	1072.366	1066.461	1071.089	1086.543	1129.77	1181.609
ξ_{rain}	7.926	8.573	9.062	9.594	9.849	9.909
	PWMPC					
u_{off}	0%	5%	10%	25%	50%	75%
$Q_{\text{ov}_{\text{total}}}$	168.77	167.127	166.82	167.079	168.232	169.528
$m_{\text{total}}^{\text{NH}_4}$	1034.79	1011.539	1010.532	1007.75	1017.285	1028.648
ξ_{rain}	7.629	8.364	8.892	9.6	9.875	9.899
	NPMPC					
u_{off}	0%	5%	10%	25%	50%	75%
$Q_{\text{ov}_{\text{total}}}$	166.872	166.845	167.543	169.337	171.927	173.933
$m_{\text{total}}^{\text{NH}_4}$	1009.773	1027.146	1043.661	1090.992	1149.691	1204.124
ξ_{rain}	9.539	9.587	9.629	9.813	9.831	9.837
	SVMPC - $\zeta = 0.6$					
u_{off}	0%	5%	10%	25%	50%	75%
$Q_{\text{ov}_{\text{total}}}$	177.244	176.928	176.719	176.45	175.626	175.611
$m_{\text{total}}^{\text{NH}_4}$	1280.512	1278.782	1276.397	1272.054	1260.564	1259.833
ξ_{rain}	6.564	6.588	6.596	6.975	9.913	9.949
	SPWMPC - $\zeta = 0.6$					
u_{off}	0%	5%	10%	25%	50%	75%
$Q_{\text{ov}_{\text{total}}}$	177.244	176.928	176.725	176.502	175.674	175.586
$m_{\text{total}}^{\text{NH}_4}$	1279.872	1278.213	1275.892	1271.644	1260.345	1259.371
ξ_{rain}	6.566	6.59	6.596	6.977	9.895	9.951
	SNPMPC - $\zeta = 0.6$					
u_{off}	0%	5%	10%	25%	50%	75%
$Q_{\text{ov}_{\text{total}}}$	172.511	172.29	172.547	173.659	174.201	174.298
$m_{\text{total}}^{\text{NH}_4}$	1118.019	1123.279	1130.286	1163.28	1193.183	1197.861
ξ_{rain}	9.613	9.556	9.629	9.871	9.868	9.946

The conclusion of the chapter is that stochastic methods are better suited to improve operation of the UDS under high uncertainty. However, for simpler systems, such as the one evaluated here, deterministic methods are sufficiently robust and tend to outperform stochastic approaches in most scenarios. In practical applications, where systems are more complex and uncertainties are both higher and less predictable, stochastic methods are strongly recommended. The next chapter explores this further by

examining more complex UDS models based on real-world MPC implementations. Before closing this chapter, a brief analysis of the computational cost of each stochastic method is presented, as this aspect is crucial for practical deployment.

10 High-Complexity Urban Drainage Simulations

The simulations performed up until now were applied to a simple representation of a urban drainage system composed of three storage units. Although this system is useful for the evaluation and validation of methods, in reality, wastewater networks are much more complex, with many more details that were neglected to simplify the initial assessment. Hence, this chapter introduces novel urban drainage systems based on actual networks that encompass a more detailed description with higher complexity. Three networks with the following general composition were selected:

1. Urban Drainage System 1 (based on Altenrhein): system with 31 storage units, where MPC control four of these SUs. The actuators for all storage units are valves with continuous actuation.

2. Urban Drainage System 2 (based on Rheinfelden): system with 16 storage units, where MPC control six of those SUs. There are two units with continuous pump actuation, whereas the rest are actuated through continuous valves.

3. Urban Drainage System 3 (based on Siden): system with 46 storage units, where MPC control 34 of those SUs. In this case, there are 10 controlled units with continuous valve actuation, 23 on-off pump actuators, and one continuous pump actuator.

Each network presents distinct characteristics, which are detailed in their respective sections. The purpose of this chapter is to assess the performance of each MPC method under varying conditions. All methods are individually tuned using a sensitivity analysis-based weight selection approach prior to evaluation. The specific uncertainties associated with each system are discussed and, when relevant, integrated into the stochastic controllers.

Additionally, four parameters—$V_{\text{controlled}}$, $V_{\text{controllable}}$, $Q_{\text{incontrolled}}$, and $Q\text{in}_{\text{controllable}}$—are introduced into the controller formulation, defined independently for each Storage Unit. These parameters are used to implement a state machine that determines whether the control action computed by the MPC is executed by the local controller. Although they do not alter the MPC's optimisation process, which continues to calculate the optimal control at each loop, they act as a filter, deciding whether the suggested action is applied based on the current state of the storage unit. This mechanism is designed to prevent the MPC from storing dry weather flow unnecessarily, instead allowing the local controller to decide when and how the actuator should respond.

Each Storage Unit can have two states regarding its relationship with MPC: **controlled** or **controllable**. Initially, each unit is considered to be in the controllable state, which indicates that MPC is calculating the

optimal control action, but it is not being implemented. The switch from **Controllable** → **Controlled** is realised when **one** of the following situations is fulfilled:

1. The volume is above $V_{\text{controllable}}$, or
2. The estimated inflow is above $Q_{\text{in}_{\text{controllable}}}$

In this state, the optimal control action calculated by MPC is actually implemented by the local controller. The switch from **Controlled** → **Controllable** is realised when **both** of the following situations are fulfilled:

1. The volume is below $V_{\text{controlled}}$, and
2. The estimated inflow is below $Q_{\text{in}_{\text{controlled}}}$

The use of two different thresholds for the change of states is to reduce constant switching between states and, therefore, guarantee smooth operation of the wastewater network. An example is provided in Figure 10.1 to illustrate the switch between states. Initially, MPC is in controllable state and changes to controlled when the inflow is greater than $Q_{\text{in}_{\text{controllable}}}$. The state is changed again to controllable when both the inflow and the volume are below $Q_{\text{in}_{\text{controlled}}}$ and $V_{\text{controlled}}$, respectively.

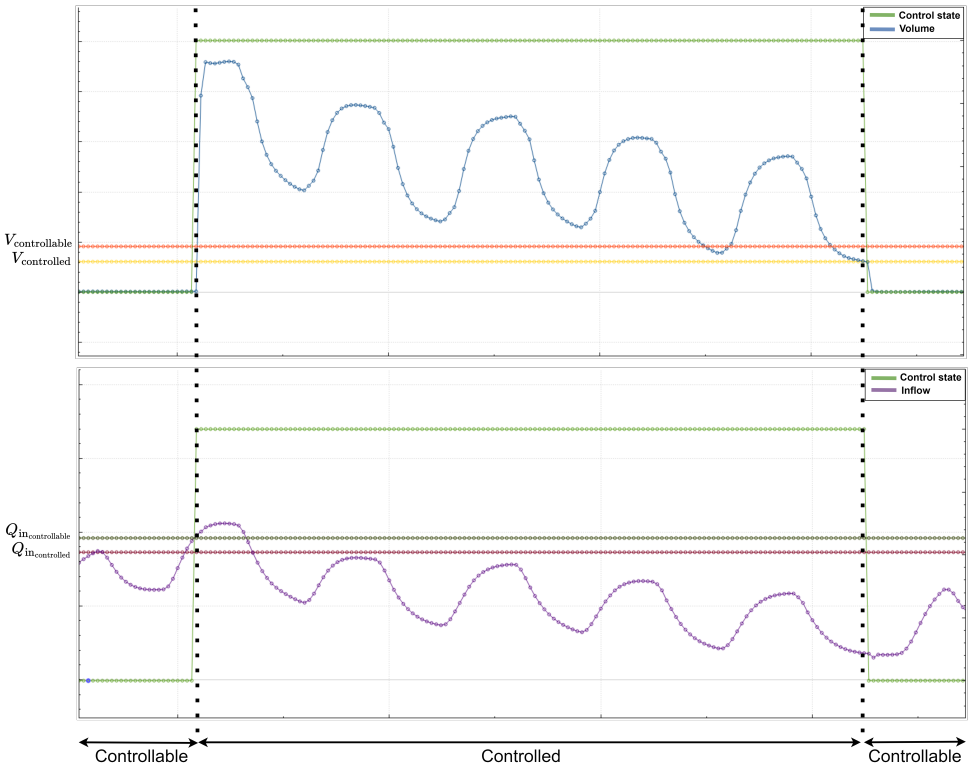

Figure 10.1: Example of State Machine with $V_{\text{controlled}}$, $V_{\text{controllable}}$, $Q_{\text{in}_{\text{controlled}}}$ and $Q_{\text{in}_{\text{controllable}}}$.

In this example, although the estimated inflow is below $Q_{\text{in}_{\text{controlled}}}$ soon after entering the **controlled** state, the change to **controllable** only occurs when both conditions are met. In the next section, an evaluation of the MPC methods for Urban Drainage System 1 is carried out, detailing the main difficulties of controlling such a network and how MPC is able to deal with them.

10.1 Urban Drainage System 1

The first drainage system analysed in this chapter consists of 31 storage units, as shown in the SWMM model in Figure 10.2. This system is responsible for collecting and distributing human activity wastewater, totalling approximately 41.000 PE, which is distributed throughout the network. In the figure, the red highlighted segments represent the areas optimised by MPC, meaning that only a part of the network is involved in the control problem.

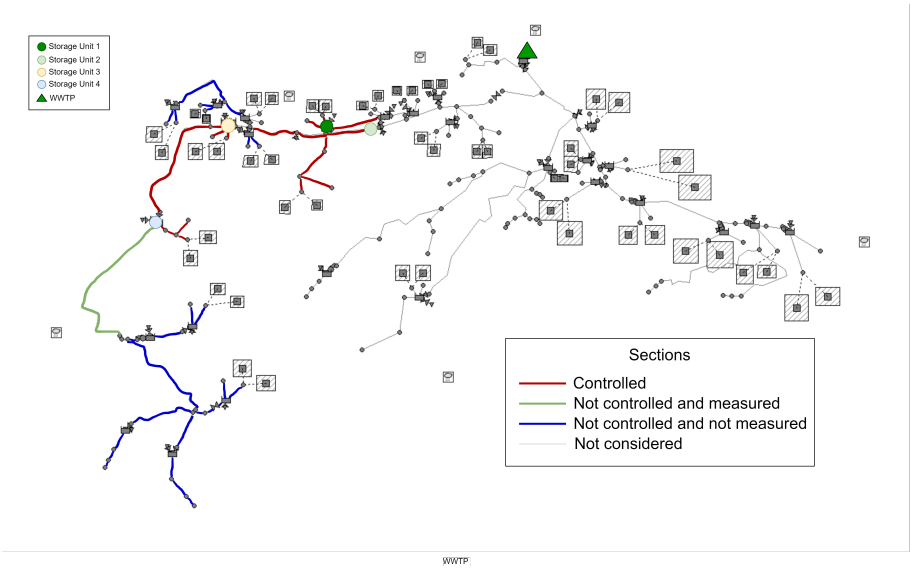

Figure 10.2: Urban Drainage System 1 - red line indicates sections that are controlled by MPC - green line indicates sections that are measured, but not controlled by MPC - blue line indicate sections that are not controlled by MPC and not measured - gray line indicates sections unknown to MPC and not considered in the formulation.

Consequently, MPC does not account for many dynamics of the entire network, potentially introducing uncertainties into the system. For example, inflows from regions outside the control scope are treated as typical dry-weather inflows with an assigned load, disregarding any dynamics of devices such as pumps and valves that are outside the red-marked area, and are therefore not observed by the MPC. This scenario is interesting to evaluate whether the MPC methods are capable of improving wastewater network management by controlling only a fraction of the system. A detailed diagram of the controlled section of the network can be seen in Figure 10.3.

The diagram shows the maximum volume, $V_{\max_i}$, the maximum outflow, $Q_{\text{out}_{i,\max}}$ and the designed outflow Q_{design_i} for the i-th SU. The maximum inflow allowed in the WWTP is represented by $Q_{\text{wwtp}_{\max}}$ and the desired reference inflow to the WWTP by $Q_{\text{wwtp}_{\text{ref}}}$. However, it is important to note that, in reality, SU1 and SU2 are not directly connected to WWTP, as can be seen in Figure 10.2. Since the downstream structures from SU1 and SU2 are unknown and not controlled, for practical purposes, it is considered that the end node is the WWTP.

The dry-weather flow included in the model is based on a hourly sampled normalised pattern combined with an average daily flow that is assumed to be generated by the human activity. This normalised dry-weather flow pattern for the storage units is assumed to be identical, as illustrated in 10.4. However,

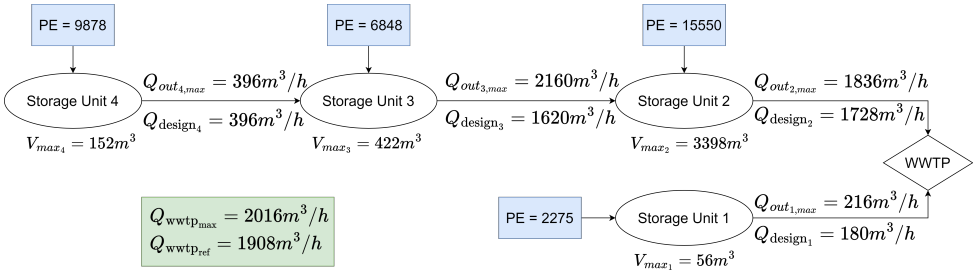

Figure 10.3: Schema for controlled section of Urban Drainage System 1.

the average flow of waste received by each storage unit varies as it depends on the number of people connected to the system. As a result, each unit experiences different inflows, both in terms of volume and pollutant load. In addition, units that are not considered in the MPC formulation are approximated in the control as additional DWF using this pattern, which is realised by including the corresponding DWF in the PE of the downstream storage unit.

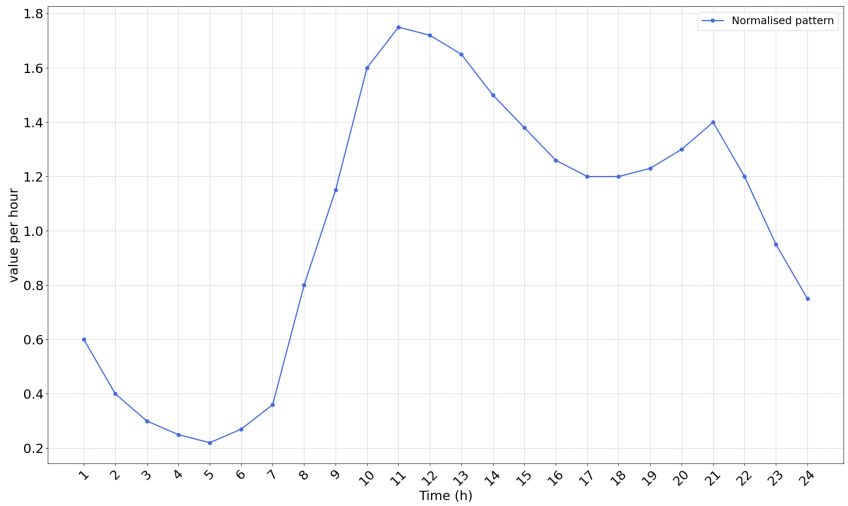

Figure 10.4: Normalized daily patterns sampled hourly.

Furthermore, in Table 10.1, the state machine limits for controllable and controlled states are displayed for each SU, including an additional variable, $Q_{\text{ov}_{\text{sensitivity}}}$, which is added to MPC to give higher priority in reducing overflows to specific SUs.

Table 10.1: Additional parameters in the model for Urban Drainage System 2.

	Storage Unit 1	Storage Unit 2	Storage Unit 3	Storage Unit 4
$V_{\text{controlled}}$	2.24 m^3	135.92 m^3	25 m^3	6.08 m^3
$V_{\text{controllable}}$	3.36 m^3	203.88 m^3	35 m^3	9.12 m^3
$Q_{\text{in}_{\text{controlled}}}$	129.6 m^3/h	1717.2 m^3/h	360 m^3/h	324 m^3/h
$Q_{\text{in}_{\text{controllable}}}$	144.0 m^3/h	1908.0 m^3/h	900 m^3/h	360 m^3/h
$Q_{\text{ov}_{\text{sensitivity}}}$	5	1	3	5

The value of $Q_{\text{ov}_{\text{sensitivity}}}$ was previewed from a discussion with the utility to understand which storage units had more impact in the environment when they overflow. Hence, from the values obtained, the priority for the system is to minimise overflows in SU1 and SU4.

A static control simulation is executed to assess the dynamics of the system, where only the red-marked controlled section is observed, while the remaining parts of the network are considered disturbances. For this simulation, the outflow of actuators is maintained equal to Q_{design_i}. Engineers typically determine the outflow of storage units based on several factors, with two main considerations being the estimated rainfall and the number of people connected to the system. These factors influence the inflow volume into the system, and the outflow is designed to manage this input to prevent or reduce overflow incidents. The values of Q_{design_i} were chosen based on these factors, thus, they can be considered as statically optimal when looking at the individual needs of the storage unit. The dry weather flow considered for each SU can be seen in Figure 10.5 for a 7-day period, which combines inflows directly at the unit and dry weather flows arriving from upstream structures.

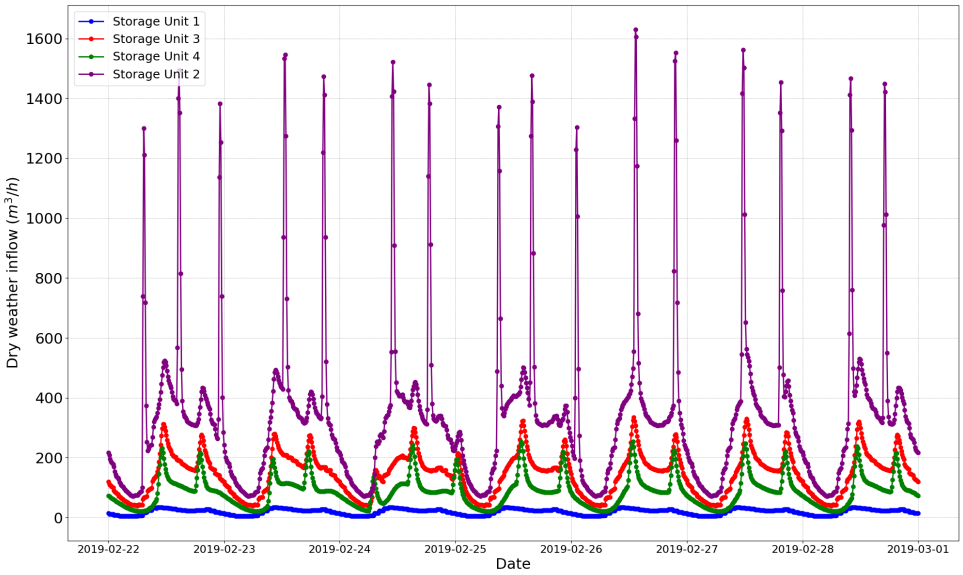

Figure 10.5: Dry weather flow for the Storage Units.

The expected behaviour of the dry weather flows in each SU follows the pattern previously presented, with different peaks depending on the PE of the unit. However, the graph reveals that Storage Units 2, 3 and 4 have sudden peaks that are above the expected. The issue arises from the blue-marked highlighted regions in Figure 10.2, where there are dynamics that slightly change the expected behaviour for the red-marked regions. In the blue-marked sections of the network, there are storage units controlled by pumps, which do not operate continuously. First, the inflow arriving at those units is stored, and the pump is activated when there is a certain amount of volume, creating a pulsed inflow in the storage units that are downstream. Thus, due to discontinuous pumping activity, the dry weather flow is affected by a disturbance not modelled by MPC. This behaviour will be studied in detail to understand if it affects the performance and robustness of the MPC methods.

The runoff, in m^3/h, for each Storage Unit is presented in Figure 10.6 for the year of 2019, where the rain data used for optimisation are derived from hydrometric stations, where, for each catchment,

the precipitation measurements are collected from the closest station. Storage Unit 2 does not have a subcatchment directly connected to its structure, but there is a subcatchment of 30.5ha connect to its main inflow pipe, thus it is considered as the subcatchment for Storage Unit 2. Besides, as the last unit in the cascade configuration, it receives runoff from all upstream storage units. Storage Unit 3 has the highest runoff, with its catchment reaching a total of 32.5ha, while Storage Units 1 and 4's catchment has 7.64ha and 3.85ha, respectively. However, unlike the other controlled SU, Storage Unit 1 does not have any upstream structures, thus combining the smaller catchment area, the number of people connected to the unit, and the absence of upstream units, the volume of the unit is considerably smaller compared to $V_{\max} = 56m^3$.

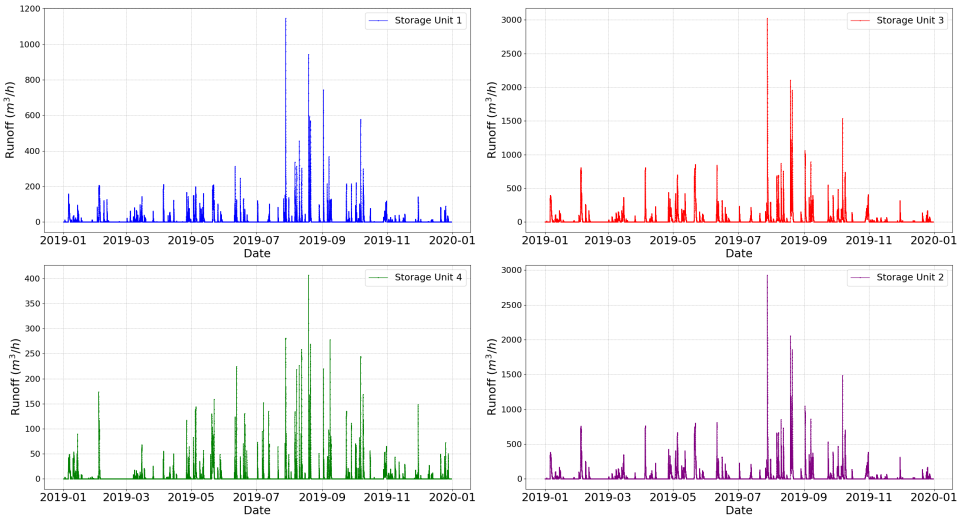

Figure 10.6: Runoff for Storage Units for the year of 2019.

The static control simulation was conducted for the previously presented 1-year rainfall scenario from 2019. Figure 10.7 illustrates the overflow for each SU in terms of both volume (left) and load (right), along with their cumulative values over time. The most intense rainfall event occurred in August, representing an extreme case where MPC would likely offer little to no performance improvement, as the resulting overflow is unavoidable due to limited storage capacity and outflow rates. Such events also reduce pollutant load within the storage unit due to dilution effects. This phenomenon is visible in Figures 10.7c and 10.7d, which present several overflow events, such as those in February, April, and June, where the overflow volume (ML) is significantly lower than in August, yet the overflow load (kg) remains at a similar level. The accumulated overflow for each storage unit, as well as the total system overflow, is presented in Table 10.2.

Table 10.2: Total overflow volume and load for Urban Drainage System 1 with static control

Metric	Storage Unit 1	Storage Unit 2	Storage Unit 3	Storage Unit 4	Total
Q_{ov} in ML	10.87	121.08	9.03	1.70	142.68
$m_{\text{ov}}^{\text{NH}_4}$ in kg	21.65	532.41	23.30	14.52	591.88

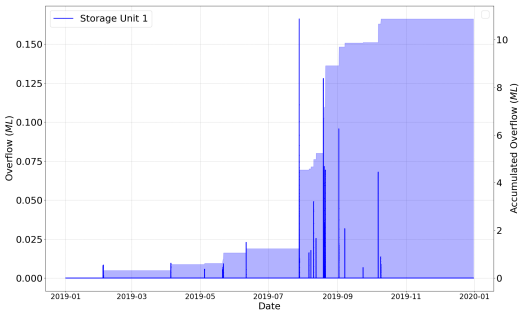

(a) Instantaneous (line) and Accumulated (shaded area) Q_{ov} for Storage Unit 1.

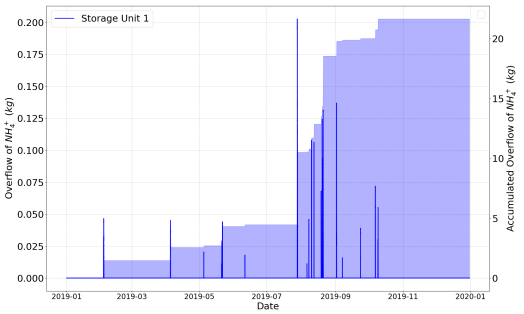

(b) Instantaneous (line) and Accumulated (shaded area) $m_{\text{ov}}^{\text{NH}_4}$ for Storage Unit 1.

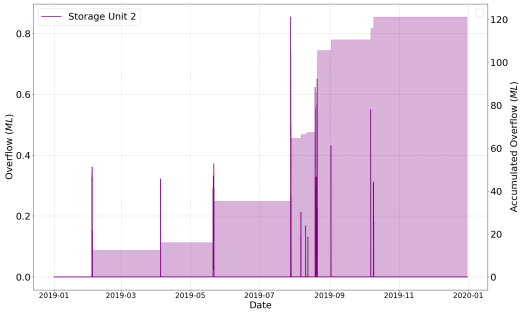

(c) Instantaneous (line) and Accumulated (shaded area) Q_{ov} for Storage Unit 2.

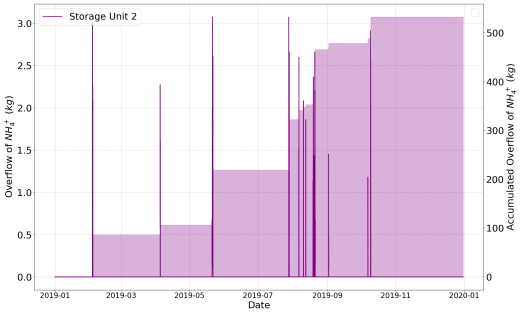

(d) Instantaneous (line) and Accumulated (shaded area) $m_{\text{ov}}^{\text{NH}_4}$ for Storage Unit 2.

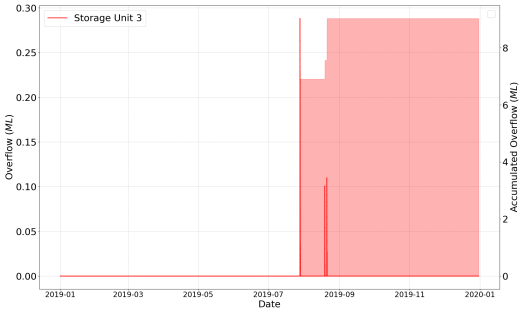

(e) Instantaneous (line) and Accumulated (shaded area) Q_{ov} for Storage Unit 3.

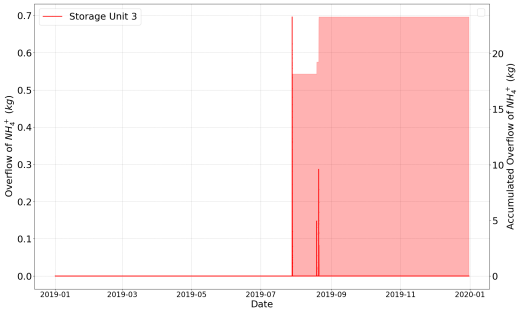

(f) Instantaneous (line) and Accumulated (shaded area) $m_{\text{ov}}^{\text{NH}_4}$ for Storage Unit 3.

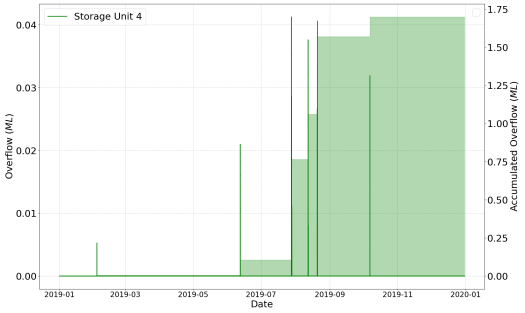

(g) Instantaneous (line) and Accumulated (shaded area) Q_{ov} for Storage Unit 4.

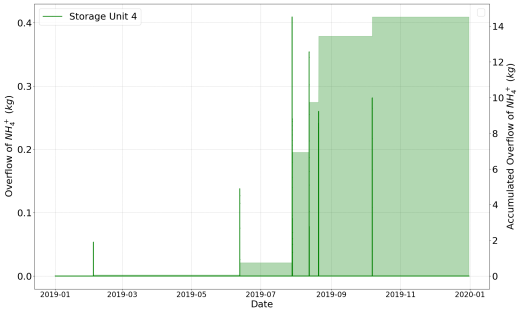

(h) Instantaneous (line) and Accumulated (shaded area) $m_{\text{ov}}^{\text{NH}_4}$ for Storage Unit 4.

Figure 10.7: Q_{ov} and $m_{\text{ov}}^{\text{NH}_4}$ for Urban Drainage System 1 with static control.

Storage Unit 2 has approximately 90% of the total overflow load of the scenario, which is expected since this unit has the highest volume and receives the highest amount of inflow. Therefore, focusing on reducing the overflow in this unit will have a greater effect on the total. However, given the sensitivity provided in Table 10.1, the priority is in reducing overflow in SU1 and SU4.

The next steps towards the MPC implementation is choosing the parameters for each method. Thus, the sensitivity analysis is performed individually for each MPC, considering two different rain periods where the impact of having MPC can be presumably higher: from February 1st to February 5th and from October 6th to October 10th. The first period was chosen because it has a single overflow event with medium runoff intensity and large overflow load, whereas the second period was selected because it shows two consecutive overflow events with high load. The purpose of having the analysis for these scenarios is to understand the impact of different rain events on the weights and whether they are similar or not, and whether the decision of optimising the weights in a single or multiple rain events impacts the performance. The information identified via the sensitivity analysis will be used to refine the Genetic Algorithm weight optimisation. A LSA using Morris Screening and a GSA through Grid Search is performed for each MPC and for both periods, with the aim of identifying the ranges for each parameter and an initial guess to help the convergence to an optimal weight combination.

10.1.1 Sensitivity Analysis and Genetic Algorithm Optimisation

The first period analysed is from February 1st to February 5th, which is characterised by a medium intensity rain event, as can be seen in Figure 10.8a.

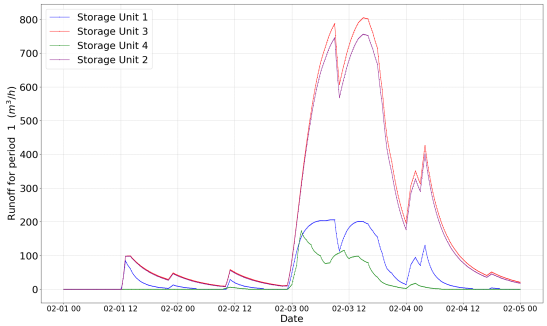

(a) Runoff for Period 1.

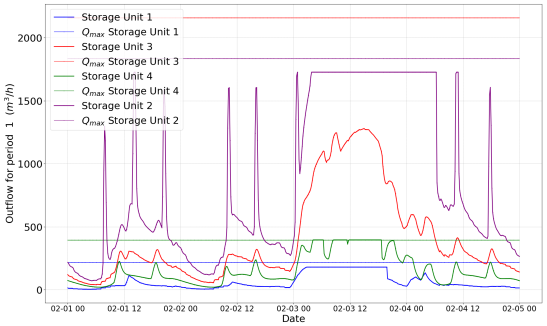

(b) Outflow for Period 1.

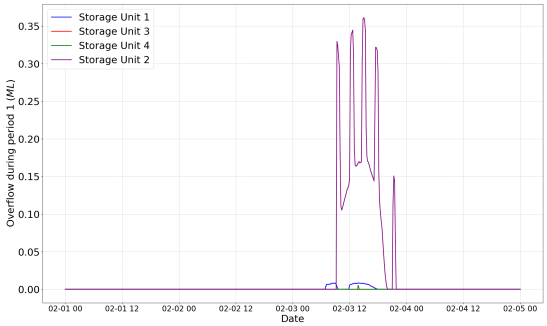

(c) Overflow for Period 1.

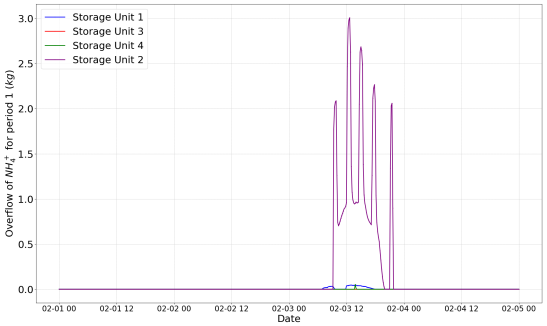

(d) Load for Period 1.

Figure 10.8: Urban Drainage System 1 with static control for Period 1.

Figure 10.8b presents the outflow for each local controller, showing that the actuators are not operating at full capacity. Although an operator could manually adjust the actuator set-points to increase outflow, this may lead to higher inflow downstream. In contrast, MPC can dynamically coordinate the system and, with accurate predictions, optimise the use of actuators to improve overall performance.

The second period analysed is from October 6 to October 10, which is characterised by two different rain events, the first with high intensity and the second with medium intensity. This causes a higher overflow in the SUs. This example is interesting as it shows that SU3 is over-dimensioned, however, its storage capability is not fully utilised. Intuitively, to avoid overflows in SU2 or SU4, the available storage in SU3 could be better handled to avoid sending that sewage to SU2 or to store excess sewage from SU4.

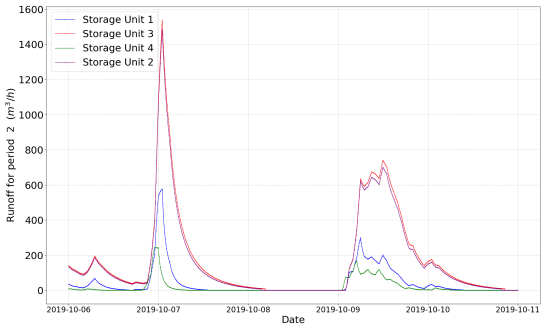

(a) Runoff for Period 2.

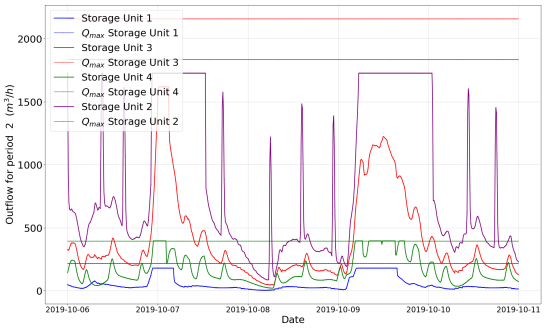

(b) Outflow for Period 2.

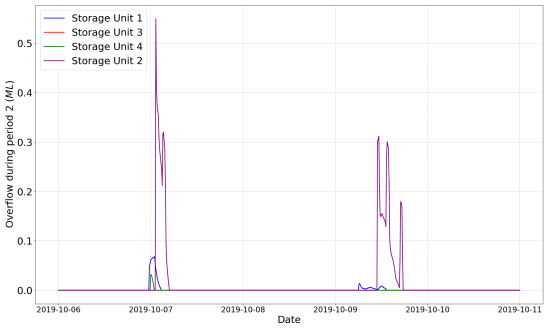

(c) Overflow for Period 2.

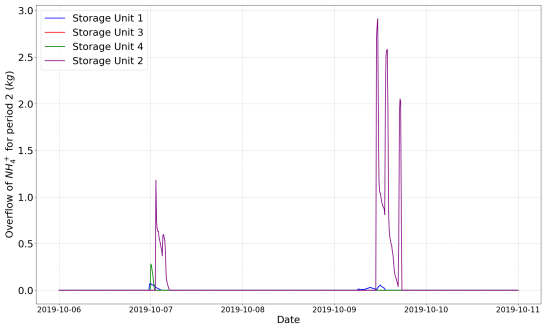

(d) Load for Period 2.

Figure 10.9: Urban Drainage System 1 with static control for Period 2.

To begin, the Morris Screening method is applied to both periods. The detailed results for each MPC are provided in Appendix A.5, Figure A.25. The sensitivity analysis is conducted with the trajectory as $r = (200, 200, 125, 170, 170, 125)$, resulting in a total number of iterations of $N = r(k+1) = (1000, 1000, 1125, 1020, 1020, 1125)$, for VMPC, PWMPC, NPMPC,SVMPC, SPWMPC and SNPMPC, respectively. The analysis uses $Q_{\text{ov}_{\text{total}}}$ and ξ as output metrics for volume-based controllers, and $m^{\text{NH}_4}_{\text{ov}_{\text{total}}}$ and ξ for pollution-based controllers. A general overview of the results for both periods is summarised below:

- VMPC: In general, all parameters show consistent influence across both periods, with β presenting slightly higher μ compared to other weights;

- PWMPC: For this instance, the influence of β is also more pronounced, specially for $m^{\text{NH}_4}_{\text{ov}_{\text{total}}}$, while for ξ there is less difference between the weights;

- NPMPC: For Period 1, ψ and τ are more pronounced, while the other parameters are more concentrated together. For Period 2, the influence of ψ and τ is reduced, specially for $m^{\mathrm{NH_4}}_{\mathrm{ov_{total}}}$, however still demonstrating more impact on both objectives;
- SVMPC, SPWMPC and SNPMPC: ζ displays a much greater influence. For SNPMPC ω is slightly more pronounced than other weights.

Overall, the analysis is consistent with that in the previous chapter. Deterministic methods display a more uniform influence across parameters, whereas stochastic methods consistently have ζ as the most influential parameters. Given that ζ is constrained to be between 0.5 and 1, its range is relatively narrow and easier to define, thus it is removed from the Genetic Algorithm. Before starting GA, a grid search is carried out to determine the appropriate weight ranges, which are summarised in Table 10.3.

Table 10.3: Weights Ranges for Urban Drainage System 1 for each MPC.

Weight	α	β	γ	ϵ	ψ	ω	τ	υ
VMPC	(0, 40]	[30, 300]	[30, 300]	(0, 300]	-	-	-	-
PWMPC	(0, 100]	[30, 300]	[30, 300]	(0, 300]	-	-	-	-
NPMPC	(0, 30]	[100, 350]	[50, 200]	(0, 300]	(0, 150]	(0, 300]	(0, 50]	(0, 50]
SVMPC	(0, 40]	[30, 300]	[30, 300]	(0, 300]	-	-	-	-
SPWMPC	(0, 40]	[30, 300]	[30, 300]	(0, 300]	-	-	-	-
SNPMPC	(0, 30]	[50, 400]	(0, 150]	(0, 50]	[10, 100]	[20, 150]	-	(0, 100]

For all MPC methods, the GA optimisation is performed using the information gathered from the SA. The number of population is equal to 10, and the maximum number of iterations is set to 500. The initial guess is defined as the best weight combination that displayed the minimum overflow (volume or load) found using the Grid Search. Volume-based methods are optimised considering $Q_{\mathrm{ov_{total}}}$ and ξ and pollution-based methods considering $m^{\mathrm{NH_4}}_{\mathrm{ov_{total}}}$ and ξ. The GA optimisation is realised for Periods 1 and 2, and their respective pareto-fronts are shown in Figures 10.10 and 10.11.

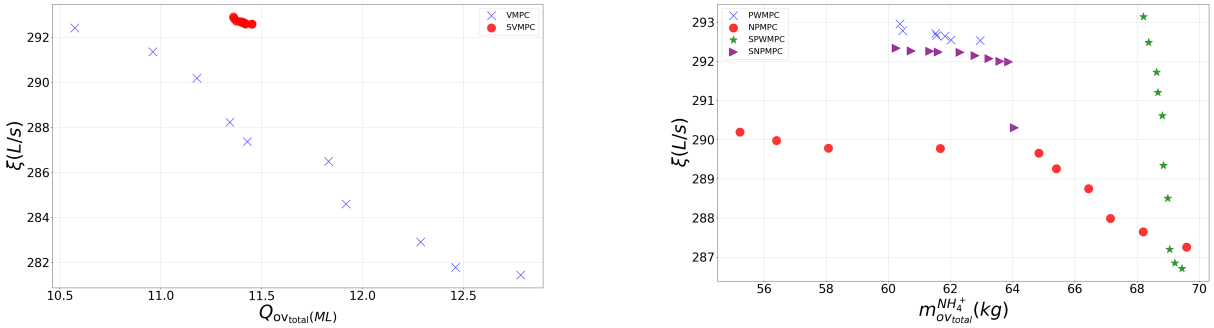

(a) Pareto front for volume-based methods on Period 1.

(b) Pareto front for pollution-based methods on Period 1.

Figure 10.10: Urban Drainage System 1 - Period 1 - Pareto front.

In Period 1, the Pareto-front generated by the deterministic VMPC is well distributed, offering a wide trade-off between $Q_{\mathrm{ov_{total}}}$ and ξ. This dispersion is desirable as it allows decision-makers to prioritise

performance objectives based on operational needs. In contrast, SVMPC produces a much narrower and clustered Pareto-front, indicating limited flexibility and generally poorer performance in both objectives. These results suggest that the inclusion of stochastic elements in SVMPC, while useful for robustness, may restrict controller responsiveness under certain conditions.

For pollution-based methods in the same period, NPMPC achieves the lowest $m^{\mathrm{NH_4}}_{\mathrm{ov_{total}}}$, signifying high effectiveness in pollution load management. Meanwhile, SNPMPC results in the lowest ξ and both PWMPC and SPWMPC fall between these extremes, representing a performance trade-off.

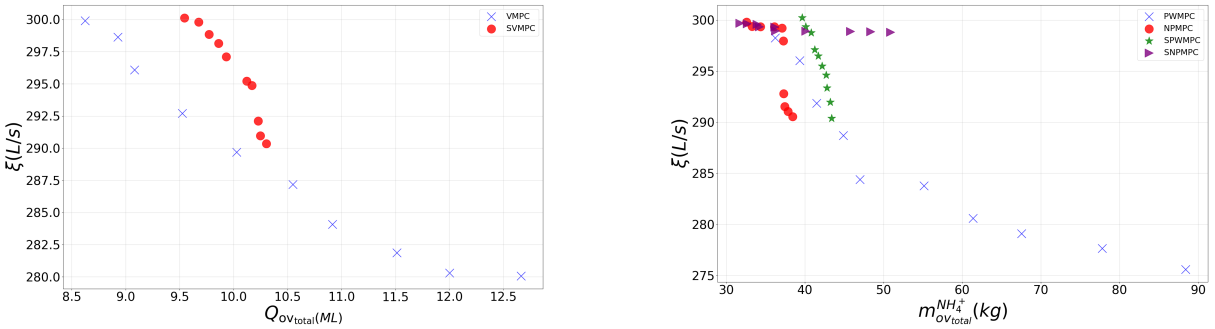

(a) Pareto front for volume-based methods on Period 2.

(b) Pareto front for pollution-based methods on Period 2.

Figure 10.11: Urban Drainage System 1 - Period 2 - Pareto front.

In Period 2, a similar trend is observed for volume-based methods. The Pareto-front for VMPC maintains its spread and effectiveness, confirming the consistency of this method in hydrological conditions. Although SVMPC performs slightly better compared to Period 1, its Pareto-front remains inferior in both metrics compared to VMPC, again pointing to reduced adaptability. For pollution-based control in Period 2, the competition among methods becomes tighter. NPMPC and SNPMPC remain front-runners, with both displaying effective trade-offs between minimising pollution overflow and error. Notably, SPWMPC shows a better reduction $m^{\mathrm{NH_4}}_{\mathrm{ov_{total}}}$ than in Period 1. Furthermore, PWMPC displayed the best distributed Pareto-front, showing that it could be effective both for the reduction of load overflow and error.

The weight combinations used in each method were selected based on the goal of minimising either overflow volume or load. The optimised weights are presented in Table 10.4, and show clear differences between Periods 1 and 2. For example, in Period 1, NPMPC prioritises minimising overflow load, as shown by high ω (155.78) and low values for ψ, τ, and υ, indicating little emphasis on load homogeneity and WWTP inflow maximisation. However, in Period 2, the weights change: ω drops to 45.22 while ψ, τ, and υ increase, suggesting a more balanced strategy to distribute the pollution more evenly and make better use of the WWTP capacity. SNPMPC maintains very low α and ϵ throughout both periods, but in Period 2, its reduced ω and increased ψ and υ reflect more load homogeneity. The results for both non-linear methods indicate that in Period 2, to reduce the overflow, a distribution of the sewage benefits the distributed system. This behaviour was not identified in Period 1 because we had a single rain event and thus it was completely focused on reducing overflow.

PWMPC shows a major shift in α and β between periods, from a low α (23.11) and moderate β (177.88) to a much higher α (74.42) and β (203.89). This indicates that in Period 2, overflow prevention becomes a stronger priority, a contrary behaviour to the non-linear methods. Oppositely, SPWMPC shows a

priority switch in β, from 190.70 in Period 1 to 119.62 in Period 2, and γ, from 90.67 in Period 1 to 150.55 in Period 2.

Table 10.4: Optimal Weights for Urban Drainage System 1 for each MPC and Period.

	Period 1								**Period 2**							
Weight	α	β	γ	ϵ	ψ	ω	τ	υ	α	β	γ	ϵ	ψ	ω	τ	υ
VMPC	33.25	64.44	185.70	141.63	-	-	-	-	26.47	103.43	180.35	127.24	-	-	-	-
PWMPC	23.11	177.88	69.75	190.0	-	-	-	-	74.42	203.89	47.2	176.38	-	-	-	-
NPMPC	10.32	228.6	90.7	213.32	16.77	155.78	2.63	14.20	11.2	228.6	90.7	190.0	84.53	45.22	23.11	18.37
SVMPC	22.05	152.66	200.0	92.24	-	-	-	-	23.11	159.75	149.45	32.09	-	-	-	-
SPWMPC	16.27	190.70	90.97	9.80	-	-	-	-	17.28	119.62	150.55	2.50	-	-	-	-
SNPMPC	1.24	297.25	9.29	1.54	100.0	150.0	-	1.0	1.24	299.99	16.69	0.011	62.74	45.22	-	1.82

VMPC maintain more stable weight configurations throughout periods, only slightly adjusting their weights, indicating robustness in its prioritisation of overflow volume control, which aligns with the broad Pareto fronts observed in both periods. In contrast, SVMPC displays lower ϵ and γ in Period 2, shifting the priority to greater homogeneity and maintaining the WWTP operation stable.

In summary, the table reveals how each method adapts its weight configuration to the specific rainfall dynamics of each period. Now that the optimal weights have been identified for each MPC throughout Period 1 and Period 2, a detailed simulation is executed to compare the performance of all control strategies, including the static control, under the same conditions. The performance of the MPC methods is assessed by considering the sensitivity value, $Q_{\text{ov}_{\text{sensitivity}}}$. To evaluate the effectiveness of these methods for each storage unit, a new metric is introduced that compares the volume of the overflow (Q_{ov}) with the total inflow to the storage unit (Q_{in}). This metric is referred to as the Relative Volume Overflow (%), denoted R_{V}. A similar metric is applied to assess the overflow in terms of load ($m_{\text{ov}}^{\text{NH}_4}$) relative to the total inflow load ($m_{\text{in}}^{\text{NH4}}$), called the Relative Load Overflow (%), denoted as R_{m}. These metrics for the i-th storage unit can be expressed as:

$$R_{\text{V}}^{i} = \frac{Q_{\text{ov}_i}}{Q_{\text{in}_i}} \quad \textit{and} \quad R_{\text{m}}^{i} = \frac{m_{\text{ov}_i}^{\text{NH}_4}}{m_{\text{in}_i}^{\text{NH}_4}} \tag{10.1}$$

Additionally, the total overflow volume and load, $Q_{\text{ov}_{\text{total}}}$ and $m_{\text{ov}_{\text{total}}}^{\text{NH4}}$, are also analysed to assess the overall performance of the entire network.

10.1.2 Comparison of MPC Methods

Initially, the weights identified from the analysis of Period 1 are applied and compared. A simulation of the year 2019 is executed, with a sampling time of 8 min for the controllers and a prediction horizon of 40 min. The value of $\zeta = 0.95$ is used for stochastic methods. Figures 10.12 and 10.13 illustrate a bar graph where each bar represents a specific MPC method. The y-axis displays the relative overflow in terms of volume (R_{V}) on the left and load (R_{m}) on the right. The x-axis corresponds to each SU, with their respective $Q_{\text{ov}_{\text{sensitivity}}}$ values highlighted. The graph demonstrates that SVMPC and SPWMPC yield the

best performance among all methods, showing the lowest R_V and R_m for SU1 and SU4, which have the highest sensitivity. Static control was effective in reducing overflow in SU4; however, this came at the cost of higher overflow in SU1 and SU2. Both VMPC and PWMPC exhibit similar performance, with the pollution-based method slightly reducing the load more. Non-linear methods, while showing lower values for SU4, exhibited significantly worse performance in SU1 and SU3 compared to other MPCs.

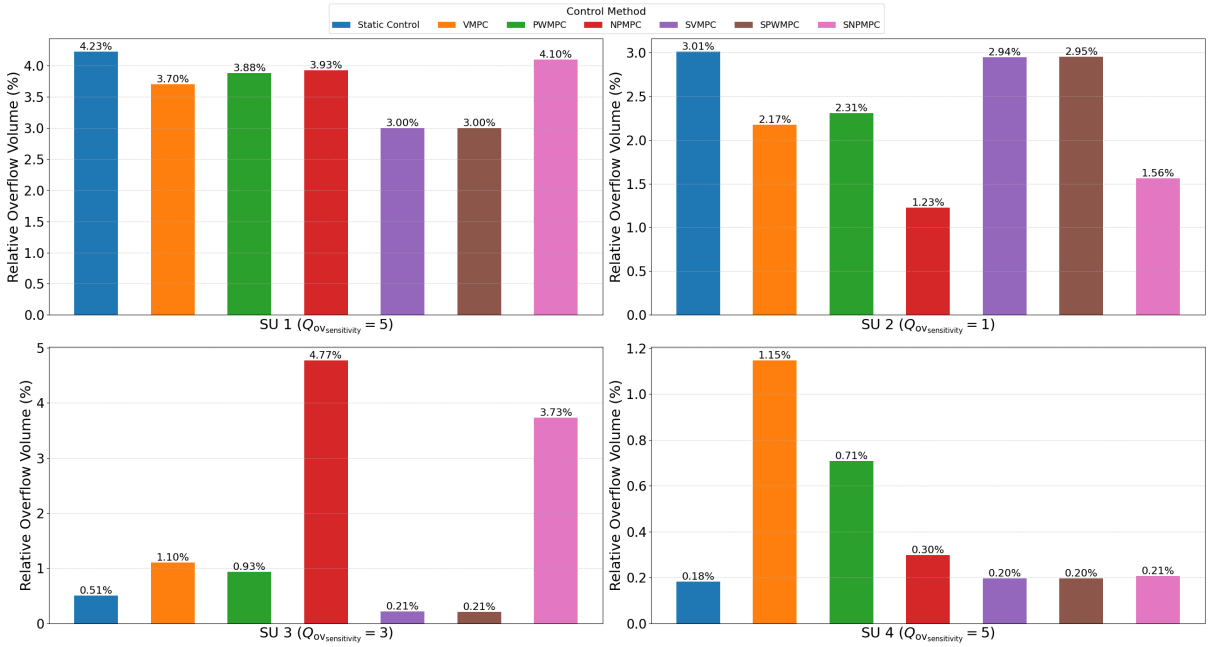

Figure 10.12: R_V - Relative Overflow Volume % using weights identified in Period 1.

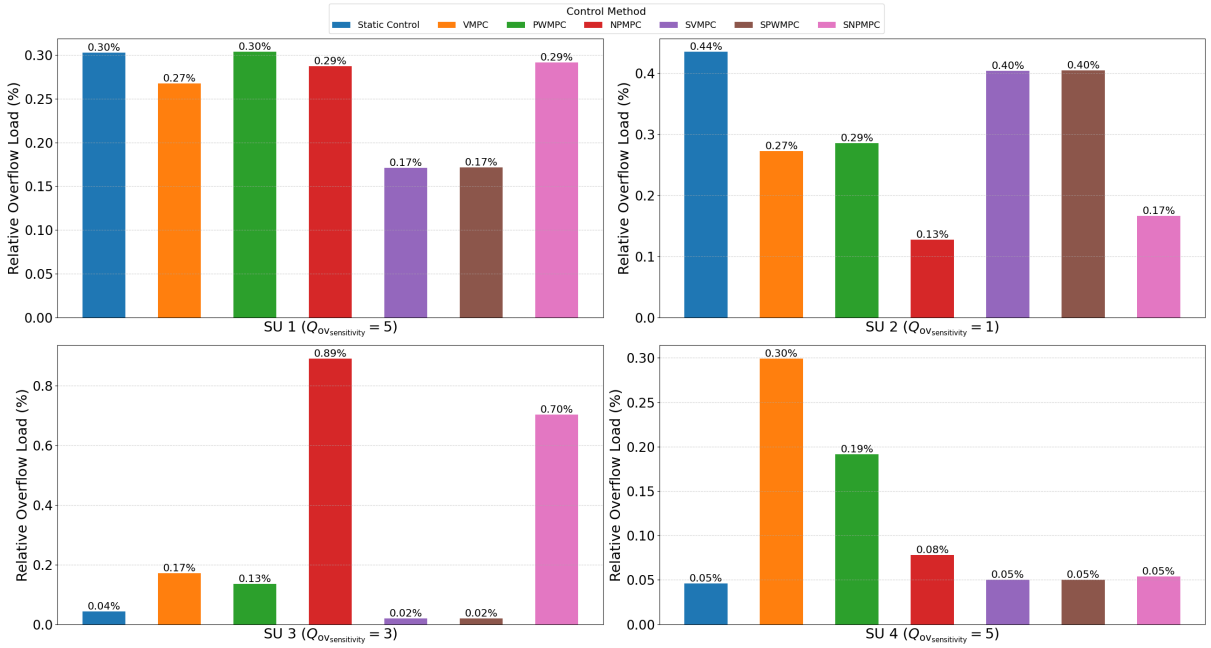

Figure 10.13: R_m - Relative Overflow Load % using weights identified in Period 1.

In Figure 10.14, the total volume of overflow (ML) and load (kg) are presented, where the bars represent various MPC methods. The results indicate that VMPC and PWMPC have the least overall overflow, while NPMPC and SNPMPC underperformed even compared to static control. The findings suggest that the rain event used for the GA optimisation is not well suited for the non-linear methods, likely due to its short duration and single occurrence. Although the non-linear methods produced a better Pareto front for Period 1, the chosen weights performed better for this specific event only, whereas their performance over the full year was not of the same standard.

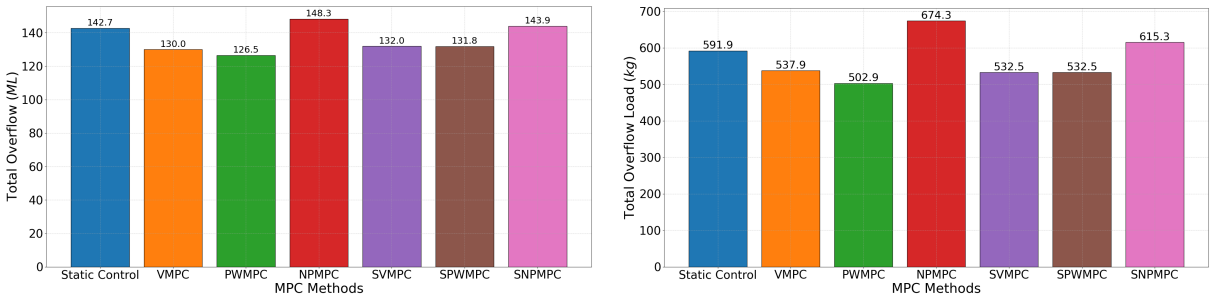

(a) $Q_{\mathrm{ov}_{\mathrm{total}}}$ - Total Overflow Volume in ML. *(b)* $m_{\mathrm{ov}_{\mathrm{total}}}$ - Total Overflow Load in kg.

Figure 10.14: Urban Drainage System 1 - Comparison of MPC in terms of total overflow volume and load using weights identified in Period 1.

The second analysis is conducted for Period 2, executing the same settings as in the previous simulation. The results are summarised in Figures 10.15 and 10.16.

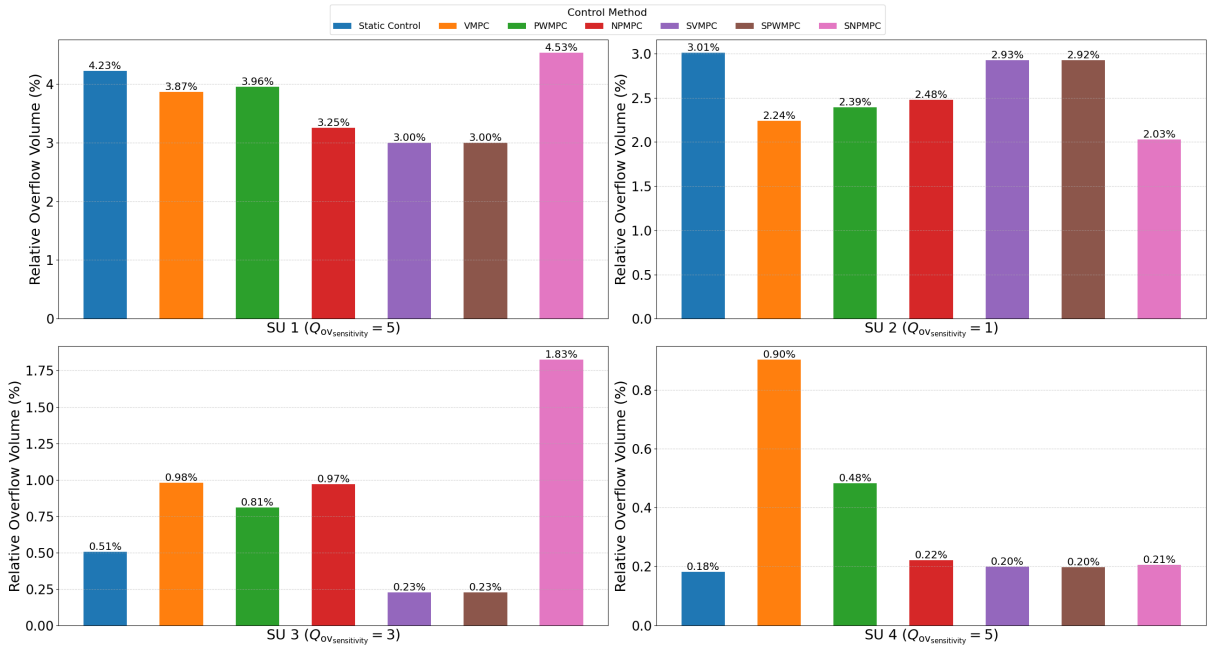

Figure 10.15: R_{V} - Relative Overflow Volume % using weights identified in Period 2.

The first notable observation is the significant improvement of both NPMPC and SNPMPC. Specifically, NPMPC, along with SVMPC and SPWMPC produced the best performance for SU1 and SU4. In

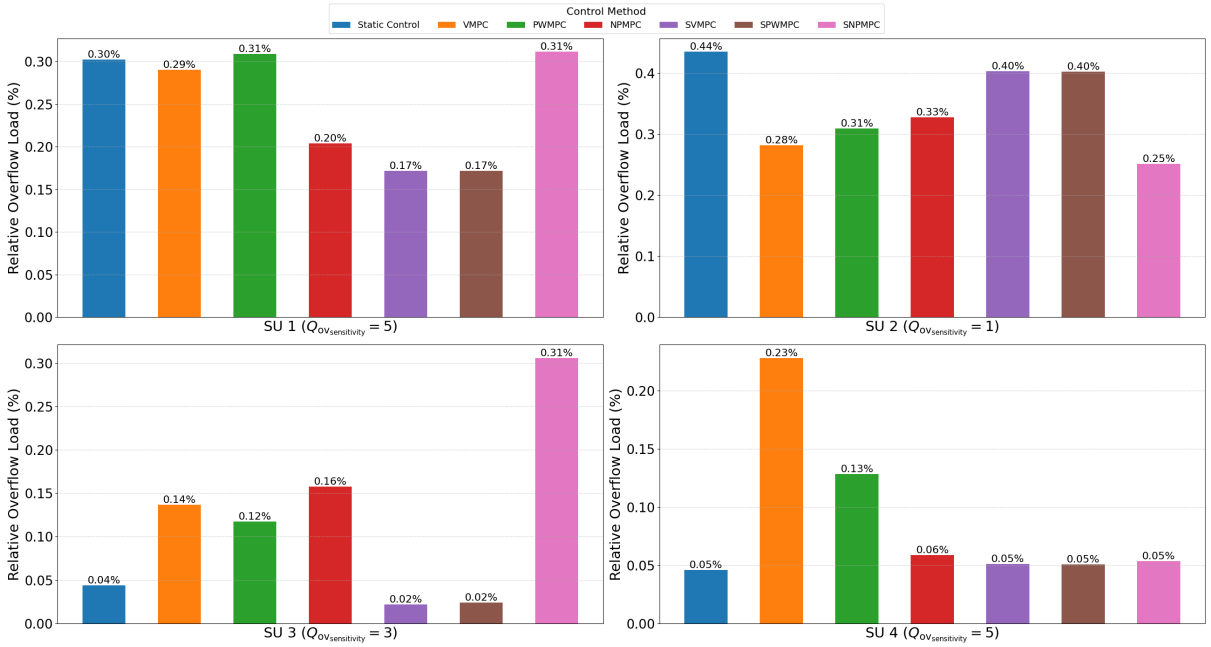

Figure 10.16: R_{m} - Relative Overflow Load % using weights identified in Period 2.

contrast, VMPC and PWMPC demonstrate the worst R_{V} and R_{m} for units with high sensitivity, with SU4 standing out negatively.

When comparing the absolute overflow results, VMPC and PWMPC actually produce the best outcomes, followed by the non-linear methods, and finally, SVMPC and SPWMPC as the worst in minimising total overflow. This suggests that the MPCs prioritising SU1 and SU4 tend to result in greater total overflow. A deeper analysis of SU2, the largest unit, clarifies this, where overflow from SU4 (and SU3) contributes to excess flow in SU2, leading to higher total overflow during rain events. Also, the difference between the weights identified using the rain in Periods 1 and 2 affected the non-linear methods more significantly. The main reason is that non-linear methods involve a greater number of weights to be tuned and therefore require more information, in this case from different rainfall events, to allow for an appropriate selection.

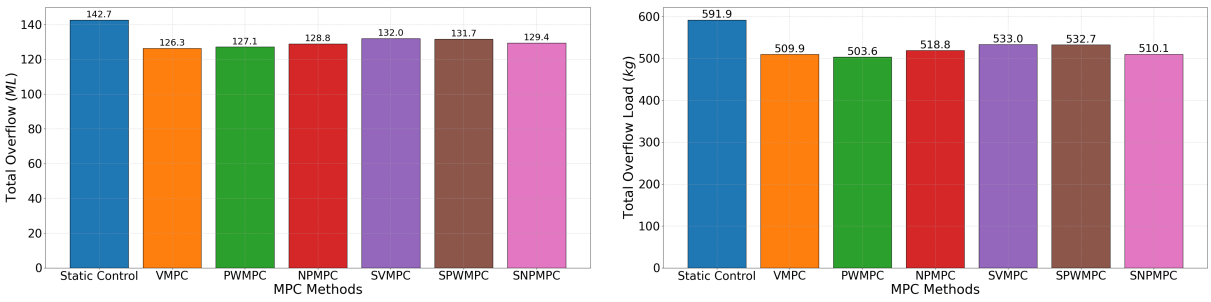

(a) $Q_{\mathrm{ov_{total}}}$ - Total Overflow Volume in ML.

(b) $m_{\mathrm{ov_{total}}}$ - Total Overflow Load in kg.

Figure 10.17: Urban Drainage System 1 - Comparison of MPC in terms of total overflow volume and load using weights identified in Period 2.

The general results emphasise the importance of carefully selecting the weights for the success of any MPC approach. Non-linear methods are particularly sensitive due to the presence of multiple weights and objectives. For GA optimisation, the recommended strategy is to select a scenario that incorporates a variety of rain events. This ensures that the method can capture the diverse dynamics of the system and adapt its behaviour accordingly. However, the main challenge is to define the appropriate range of rainfall intensities that would optimise the performance of MPC. A short analysis is performed to examine the controllers' performance, comparing it against the static control across different rain intensities.

To facilitate this comparison, the identification of rain events for the year 2019 is conducted following the steps below:

1. The runoff from the catchments connected to the SUs is aggregated into a single runoff time series that represents the entire system, along with the corresponding volume data.

2. The start of a rain event is determined by identifying the first non-zero runoff value in the time series.

3. The event is considered to end when the system's **volume** falls below a predefined threshold, indicating that the system is emptying and the rain event has ended.

4. Events are discarded if their peak runoff is below a certain threshold or if the event duration is less than 5 minutes.

The identification for Urban Drainage System 1 is shown in Figure 10.18, where the light blue shaded areas represent each identified event and the dark blue lines the runoff.

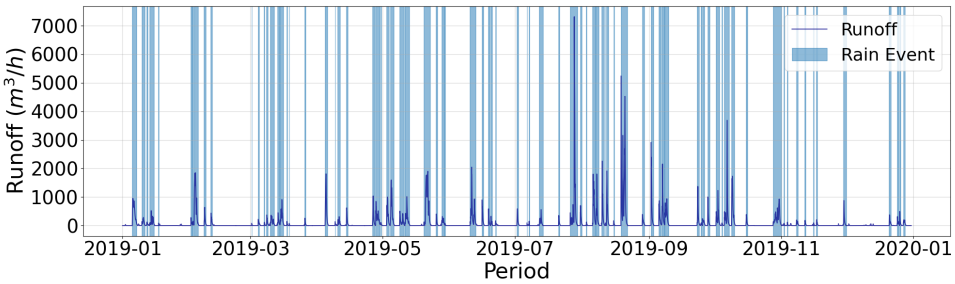

Figure 10.18: Accumulated Runoff over 1 year period.

For each rain event, the total runoff is calculated by accumulating the runoff data throughout the event. The objective is to categorise the data based on runoff intensity. To achieve this, the runoff data is sorted in ascending order. Once the data is ordered, it is divided into four regions: events with very small runoff intensity, events with low runoff intensity, events with medium runoff intensity, and events with high runoff intensity. For each accumulated runoff, the corresponding accumulated overflow volume and load are calculated to assess the impact of each event on the system. Figure 10.19 illustrates the accumulated runoff and overflow, with the regions highlighted.

There is a clear and expected relationship between runoff and overflow volume, where, on average, higher runoff intensity corresponds to greater overflow volume. However, a more detailed analysis is required for the load, as high runoff intensity often results in more diluted wastewater. For instance, the last event

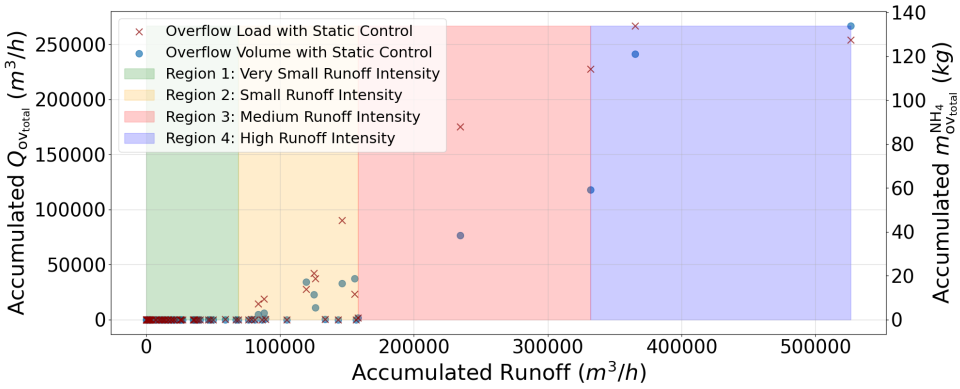

Figure 10.19: Accumulated Runoff and Overflow for the Static Control with Highlighted Regions.

in the graph in Region 4 shows that the increase in runoff also increased the total overflow in m^3/h, however, the overflow of $NH_4{}^+$ actually is reduced compared to the previous event. A deeper analysis is performed to show the improvement of each MPC by region compared to the static control scenario. The improvement for the overflow volume (I_v) and the load (I_m) is shown below, which assesses how much one method outperforms the other.

$$I_\mathrm{v} = \frac{Q^{\mathrm{MPC}}_{\mathrm{ov_{total}}} - Q^{\mathrm{static}}_{\mathrm{ov_{total}}}}{\max(Q^{\mathrm{MPC}}_{\mathrm{ov_{total}}}, Q^{\mathrm{static}}_{\mathrm{ov_{total}}})}, \qquad I_\mathrm{m} = \frac{m^{\mathrm{MPC}}_{\mathrm{ov_{total}}} - m^{\mathrm{static}}_{\mathrm{ov_{total}}}}{\max(m^{\mathrm{MPC}}_{\mathrm{ov_{total}}}, m^{\mathrm{static}}_{\mathrm{ov_{total}}})}$$

where $Q^{\mathrm{MPC}}_{\mathrm{ov_{total}}}$ and $Q^{\mathrm{static}}_{\mathrm{ov_{total}}}$ are the accumulated overflow volume of a given MPC and the static control, respectively, $m^{\mathrm{MPC}}_{\mathrm{ov_{total}}}$ and $m^{\mathrm{static}}_{\mathrm{ov_{total}}}$ are the accumulated overflow load of a given MPC and the static control, respectively. The metrics I_v and I_m were chosen because they allow a relevant comparison even when static control or MPC results in zero overflow. These indicators are calculated relative to the method with the highest overflow, where a positive value indicates that MPC outperforms static control, and a negative value indicates the opposite. The ceiling for both metrics is 100%, representing cases where one method produces significantly higher overflow than the other.

A box-plot is used to visualise I_v and I_m for each region in a single representation, to visualise the distribution, and to summarise the statistics of the data. In Figure 10.20, two box-plots compare the performance of VMPC against static control in terms of overflow load and volume improvement in the four regions. Overall, VMPC outperforms the static approach, showing positive improvements in most cases. However, Region 2 shows negative values in the 25% quartile for both metrics, indicating that, under certain conditions, the static control performed better. The spread of the data in Region 2 compared to the other regions is higher because it has more data points. Interestingly, Region 4, which corresponds to high-intensity rain scenarios, shows minimal improvement in the overflow load (less than 1%), suggesting that, in fact, higher-intensity runoff dilutes the wastewater and the load is reduced.

In general, Region 2 and Region 3 show the highest improvement with VMPC, and Region 2 shows an improvement of 70% in some scenarios. Region 1 is mostly showing no overflows in both scenarios, as expected from very small rain events.

In Figure 10.21 is presented the box-plot for NPMPC compared to static control, which a similar trend

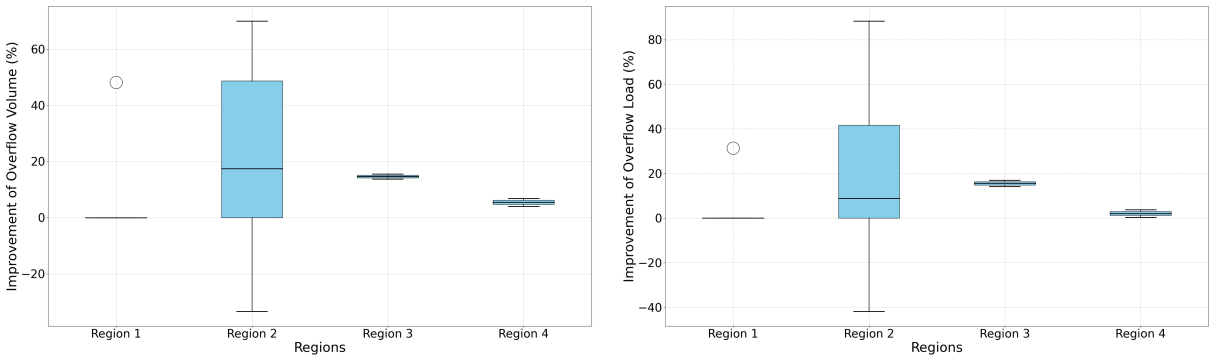

(a) Improvement of overflow volume (I_v in %) under VMPC compared to static control.

(b) Improvement of overflow load (I_m in %) under VMPC compared to static control.

Figure 10.20: Comparison of overflow load and volume improvement between VMPC and static control across four regions with varying hydrological characteristics.

where Regions 2 and 3 showed higher improvements by MPC, although in Region 2, static control outperforms in a few scenarios. Nevertheless, the box-plot does show that overall, the overflows are reduced consistently. Similarly to VMPC, Region 4 is less significant compared to Regions 2 and 3, mainly due to the dilution effects in the case of the load, but also considering the volume, high intensity runoff events usually completely burden the wastewater network and the full capacity is used, which in turn makes the overflow impossible to avoid.

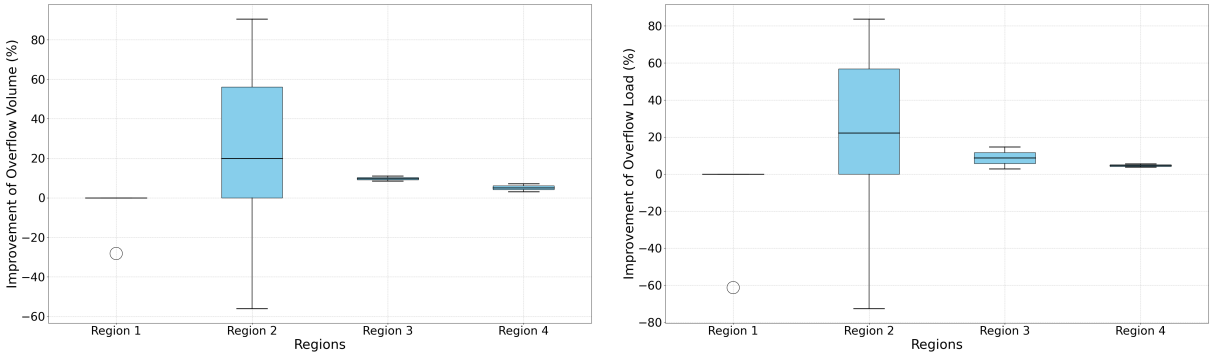

(a) Improvement of overflow volume (I_v in %) under NPMPC compared to static control.

(b) Improvement of overflow load (I_m in %) under NPMPC compared to static control.

Figure 10.21: Comparison of overflow load and volume improvement between NPMPC and static control across four regions with varying hydrological characteristics.

The box-plot for the remaining MPCs is shown in Appendix A.5. The results indicate that the impact of MPC is more pronounced during small to medium rainfall events, particularly when evaluating load. This reinforces that optimising the MPC weights using rain events from Period 2 was an appropriate choice, especially given that this period includes events from both Region 2 and Region 3. Both non-linear methods showed improved performance when the GA optimisation was performed on scenarios with a representative range of dynamics, which provide more variability and thus richer information for convergence toward a robust overall solution.

In this section, a final analysis is carried out to evaluate the effectiveness of control strategies under increased uncertainty. To this end, a disturbance is introduced in Urban Drainage System 1 by applying volume uncertainties to each SU, using the same distribution defined in Chapter 9, Section 9.1. Specifically, $V(k)$ follows a truncated normal distribution, $X(V) \sim \mathcal{N}(\mu(V), \sigma^2(V), a, b)$, where the mean is defined as $\mu = \mathbb{E}\{V(k)\} + u_{\text{offset}} * V_{\max}$, the standard deviation is defined as $\sigma = u_p * (V_{\max} - V(k))$, and the limits are defined as $[a, b] = [0, \mu + u_p * V(k)]$. For this analysis, the chosen uncertainty scenario is defined by $(u_p, u_{\text{offset}}) = (0.5, -0.5)$, applied over the same one-year period with rain events from 2019. The MPC weights are kept consistent with those identified through GA optimisation.

The results, shown in Table 10.5, reveal that SVMPC, SPWMPC, and SNPMPC outperform their deterministic counterparts in terms of both total overflow volume ($Q_{\text{ov}_{\text{total}}}$) and ammonia load ($m^{\text{NH}_4}_{\text{ov}_{\text{total}}}$). Furthermore, these stochastic controllers achieve lower overflow values for the SUs identified as having higher $Q_{\text{ov}_{\text{sensitivity}}}$, as highlighted in red in the table.

Table 10.5: Comparison of results for Urban Drainage System 1 with uncertainties and $Q_{\text{ov}_{\text{sensitivity}}} = (5, 1, 3, 5)$. Rows in red indicate SUs with higher weight sensitivity.

Metric	VMPC	PWMPC	NPMPC	SVMPC	SPWMPC	SNPMPC
Q_{ov_1}	8.042	8.344	12.861	8.115	8.072	10.561
Q_{ov_2}	490.376	185.708	70.958	212.337	163.613	69.575
Q_{ov_3}	5.389	7.151	75.804	4.93	6.639	87.23
Q_{ov_4}	6.561	6.217	11.145	5.512	4.587	3.899
$Q_{\text{ov}_{\text{total}}}$	510.369	207.42	170.768	230.895	182.911	171.265
$\%\mathbf{F}^*_Q$	**304.1%**	**63.2%**	**32.6%**	**74.9%**	**38.9%**	**32.4%**
$m^{\text{NH}_4}_{\text{ov}_1}$	13.073	13.881	29.338	13.239	13.05	20.797
$m^{\text{NH}_4}_{\text{ov}_2}$	4411.553	870.381	200.54	1035.05	734.725	209.004
$m^{\text{NH}_4}_{\text{ov}_3}$	13.265	21.022	416.812	14.328	21.264	449.351
$m^{\text{NH}_4}_{\text{ov}_4}$	59.908	57.412	117.33	51.605	42.004	35.899
$m^{\text{NH}_4}_{\text{ov}_{\text{total}}}$	4497.799	962.696	764.02	1114.221	811.043	715.051
$\%\mathbf{F}^*_m$	**782.1%**	**91.2%**	**47.3%**	**109.0%**	**50.8%**	**40.2%**

Among the tested methods, SPWMPC shows the lowest ammonia overflow load for SU1, while SNPMPC achieves the best performance for SU4 and in the total ammonia overflow metric. $\%\mathbf{F}^*_Q$ and $\%\mathbf{F}^*_m$ presented in the table quantifies the performance degradation relative to the scenario without additional uncertainties, demonstrating the improved robustness and stability of the stochastic MPC approaches. Overall, their performance outmatched their deterministic counterpart, and SNPMPC stands out for its capabilities and potential.

10.1.3 Global View of Urban Drainage System 1

One of the hypotheses of this section was that by controlling a portion of the drainage system, the global behaviour of the system would also be improved. Therefore, in this section, the performance of the static control is compared to the MPC methods investigating the 31 storage units present in the

system. In here, the total overflow is analysed together with the load of NH_4^+ reaching the WWTP and the results are displayed in Table 10.6. The results indicate that PWMPC is the only controller that consistently outperforms static control in all metrics. However, in general, MPCs perform slightly worse than static control when evaluating the entire network. This behaviour can be attributed to the fact that the MPCs are not managing the full system and therefore cannot account for the downstream impact of their decisions. As a result, flows can be redirected in ways that inadvertently affect areas outside of the controller's scope. Furthermore, when comparing the results of the isolated controlled section with those of the global network, PWMPC exhibited the weakest performance in SUs with high $Q_{\mathrm{ov}_{\mathrm{sensitivity}}}$, but achieved the best performance in terms of total overflow reduction. This suggests that while some MPCs were more effective in targeting overflows in sensitive units, this focus may come at the cost of overall network performance.

Table 10.6: Comparison of results for Urban Drainage System 1 considering the complete network.

Metric	Static control	VMPC	PWMPC	NPMPC	SVMPC	SPWMPC	SNPMPC
$Q_{\mathrm{ov}_{\mathrm{total}}}$	556.527	555.143	551.772	563.472	563.873	564.047	565.014
$\%\mathbf{F}_Q$		**-0.25%**	**-0.85%**	**1.25%**	**1.32%**	**1.35%**	**1.52%**
$Q_{\mathrm{wwtp}_{\mathrm{total}}}$	9078.1	9080.4	9082.3	9075.7	9071.4	9071.9	9073.0
$m^{\mathrm{NH_4}}_{\mathrm{ov}_{\mathrm{total}}}$	2462.065	2463.241	2421.955	2521.497	2522.174	2526.613	2530.638
$\%\mathbf{F}_m$		**0.05%**	**-1.63%**	**2.41%**	**2.44%**	**2.62%**	**2.79%**
$m^{\mathrm{NH_4}}_{\mathrm{wwtp}_{\mathrm{total}}}$	285072.3	285066.6	285080.5	285024.5	284933.0	284974.5	284987.4

In general, the decision to implement MPC in a specific section of the network or across the entire system depends on the objectives and constraints of the utility. Although full network control is undeniably the most effective approach, it is not always feasible. Nevertheless, MPC offers the flexibility to adapt to varying operational requirements and system configurations. This choice influences the overall control strategy, and the associated parameters must be selected accordingly. Any future modifications to the control framework will necessitate re-tuning to maintain optimal performance. In the following section, Urban Drainage System 2 is introduced and extends the discussion of MPC methods by incorporating additional pollutants as controlled variables, evaluating how MPC can improve UDS management under different conditions.

10.2 Urban Drainage System 2

The second drainage system studied in this chapter is composed of a total of 16 Storage Units, where the wastewater network collects and distributes sewage in a portion of a city close to a river with approximately 24000 PE. The MPC is implemented to control 6 Storage Units, distributed throughout the network, as shown in Figure 10.22 in the SWMM model. The remaining 10 units are either side storages located alongside the controlled SU, or storages within the network which are not controlled, although they have local controllers, overflow weirs and actuators.

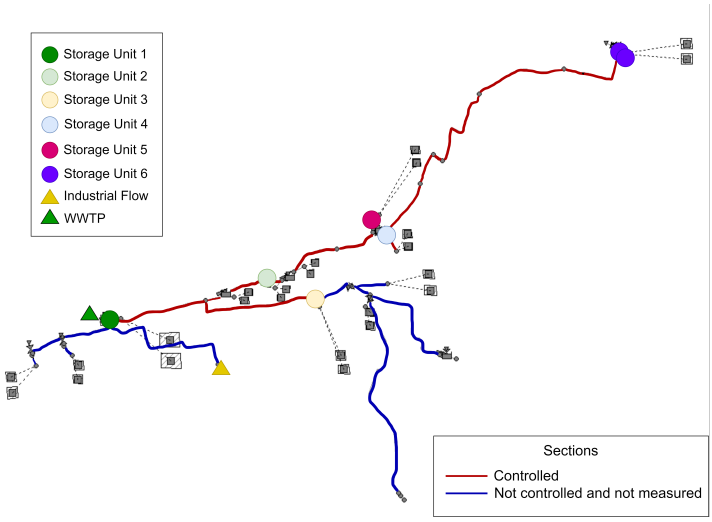

Figure 10.22: Urban Drainage System 2 - red line indicates sections that are controlled by MPC - blue line indicate sections that are not controlled by MPC and not measured - yellow triangle is an industrial flow.

A detailed diagram of the network is provided in Figure 10.23. The main infrastructural differences from Urban Drainage System 1 are the addition of two SUs, and the presence of a controlled pump as an actuator for SU5 and SU6. Moreover, there are SUs between controlled units that are unknown to MPC. These unknown structures function as buffers, delaying the flow from one unit to their respective downstream when they are between those controlled units. This causes inflow estimation errors due to delayed arrival of an expected volume from the upstream structures, and potential overflow that is not accounted for in uncontrolled structures, which reduces the inflow that is actually arriving at downstream units. Furthermore, some of those uncontrolled structures are pumping stations without continuous actuation, which can also cause discontinuity in the flow through the network and estimation errors.

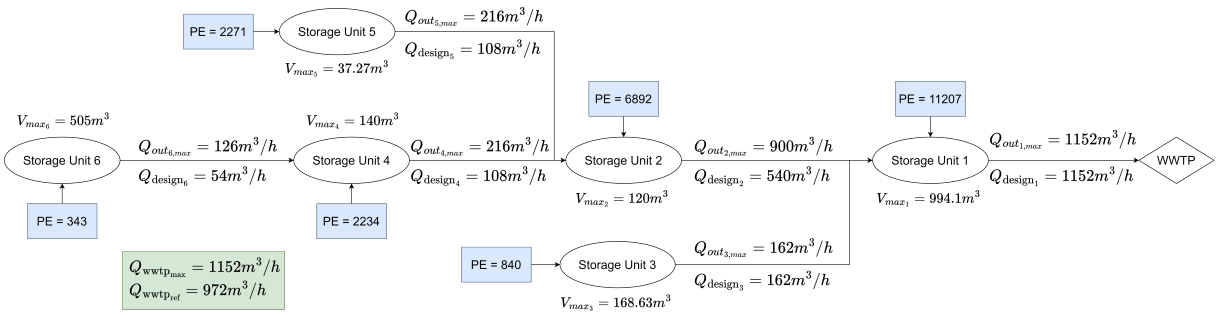

Figure 10.23: Schema for controlled section of Urban Drainage System 2.

Furthermore, Urban Drainage System 2 has two particularities compared to the previous system. Firstly, because of its location being close to a river, the network is known to have high infiltration. This is modelled in SWMM as a constant flow in specific nodes with low concentrations. The second unique feature in the system is the presence of a known industrial activity (yellow triangle in Figure 10.23) with a high concentration of COD and low concentration of NH_4^+, connected directly to the SU upstream to

the WWTP. Those particularities introduce new challenges and possibilities when controlling the system in a pollution-based framework. On one hand the infiltration dilutes the sewage, while the presence of an industrial facility raises the COD level (and decreases the NH_4^+ level) and the concentration itself, hence the scenario is quite interesting to validate the MPCs proposed in this thesis. Industrial flow is considered a constant flow with a certain concentration of COD and NH_4^+,. For practicality of implementation, this flow is included as infiltration in the model of MPC.

Similarly to Urban Drainage System 1, inflows originating from regions outside the control area are represented as typical dry-weather inflows, each associated with a specific load, without accounting for the dynamics of components such as pumps and valves, thus remaining unseen by the MPC. The dry-weather inflow modelled relies on an hourly sampled normalised flow pattern, which is scaled according to an average daily flow rate, however for the Urban Drainage System 2, the pattern is calibrated given observed data from the actual system, as shown in Figure 10.24. The calibration takes into account DWF from other structures on top of the SU own flow, resulting in a divergent pattern from the one as in Figure 10.4 for the Urban Drainage System 1.

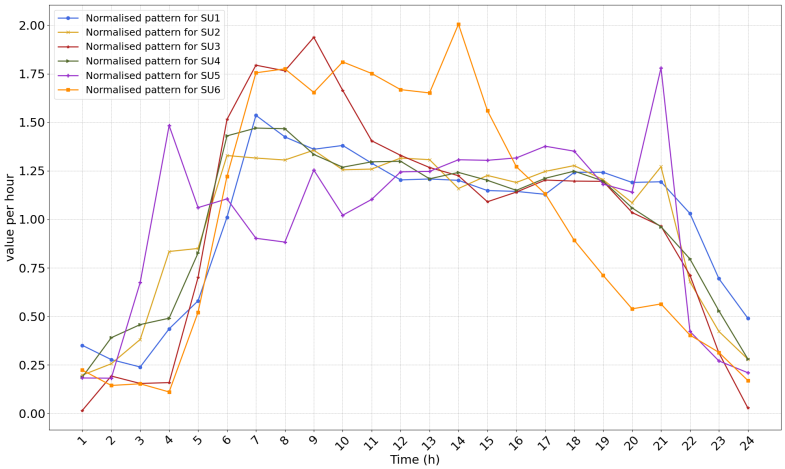

Figure 10.24: Normalized daily patterns sampled hourly.

The parameters of the controlled scenario can be seen in Table 10.7, including infiltration flow ($Q_{\text{infiltration}}$), concentration of COD ($m^{\text{COD}}_{\text{infiltration}}$) and concentration of NH_4^+ ($m^{\text{NH4}}_{\text{infiltration}}$). The limits of the state machine for controllable and controlled states are displayed for each SU, including the sensitivity, $Q_{\text{ov}_{\text{sensitivity}}}$, which is added to MPC to give higher priority in reducing overflows to specific SUs.

Firstly, a simulation with only static control is executed to assess the dynamics of the system where only the controlled red-marked section is observed, while the remaining parts of the network are considered disturbances. For this simulation, the outflow of actuators is maintained equal to Q_{design_i}. The dry weather flow considered for each SU can be seen in Figure 10.25 for a 7-day period, which combines inflows directly at the unit and dry weather flows arriving from upstream structures.

As in the previous UDS, the expected behaviour of dry-weather flows in each SU follows the predefined pattern, with peak magnitudes varying according to the PE associated with each unit. However, the graph reveals different behaviours, for instance SU4 exhibits sudden peaks that exceed expectations, while SU1 and SU2 display highly fluctuating flow patterns. The irregular peaks observed in SU4 are similar to the Urban Drainage System 1, where the storage units are managed by pumps that do not operate

Table 10.7: Additional parameters in the model.

	Storage Unit 1	Storage Unit 2	Storage Unit 3	Storage Unit 4	Storage Unit 5	Storage Unit 6
$V_{\text{controlled}}$	140.0 m^3	25.0 m^3	6.7 m^3	30.0 m^3	15.0 m^3	9.3 m^3
$V_{\text{controllable}}$	250.0 m^3	40.0 m^3	10.1 m^3	40.0 m^3	25.0 m^3	30.0 m^3
$Q_{\text{in}_{\text{controlled}}}$	720.0 m^3/h	216.0 m^3/h	64.8 m^3/h	54.0 m^3/h	72.0 m^3/h	21.6 m^3/h
$Q_{\text{in}_{\text{controllable}}}$	972.0 m^3/h	540.0 m^3/h	162.0 m^3/h	108.0 m^3/h	144.0 m^3/h	54.0 m^3/h
$Q_{\text{infiltration}}$	52.6 m^3/h	41.5 m^3/h	7.8 m^3/h	25.5 m^3/h	11.1 m^3/h	3.8 m^3/h
$Q_{\text{in}_{\text{controllable}}}$	972.0 m^3/h	540.0 m^3/h	162.0 m^3/h	108.0 m^3/h	144.0 m^3/h	54.0 m^3/h
$Q_{\text{infiltration}}$	52.6 m^3/h	41.5 m^3/h	7.8 m^3/h	25.5 m^3/h	11.1 m^3/h	3.8 m^3/h
$C^{\text{COD}}_{\text{infiltration}}$	932.9 g/m^3	40.0 g/m^3	40.0 g/m^3	40.0 g/m^3	40.0 g/m^3	40.0 g/m^3
$C^{\text{NH4}}_{\text{infiltration}}$	0.96 g/m^3	0.5 g/m^3	0.5 g/m^3	0.5 g/m^3	0.5 g/m^3	0.5 g/m^3
$Q_{\text{ov}_{\text{sensitivity}}}$	1	2	3	3	1	3

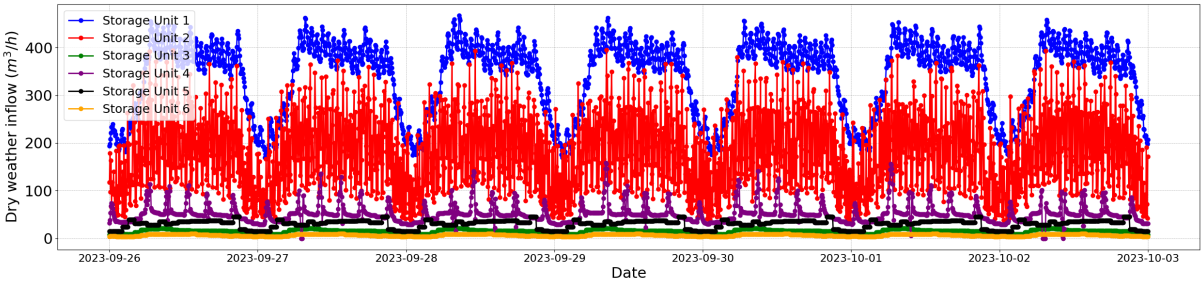

Figure 10.25: Dry weather flow for the Storage Units.

continuously. For SU1 and SU2, the irregularities come not only from intermittent pumping activity, but also from the influence of upstream structures located between units. These upstream dynamics disrupt the expected DWF profile, causing deviations from the assumed inflow pattern.

The runoff, in m^3/h, for each Storage Unit is presented in Figure 10.26 between June 1st 2023 until June 1st 2024, where the rain data used for the optimisation are derived from a single hydrometric station. Therefore, storage units have the same precipitation, while runoff differs only by their intensity (catchment size). Storage Unit 1 is connected to a 5ha catchment. Besides, as the last unit in the cascade configuration, it receives runoff from all upstream storage units. Storage Units 2 and 6 have the highest runoff, with their catchment reaching a total of 13ha and 12.2ha, respectively, while Storage Units 3, 4 and 5's catchment has 3.5ha, 6ha and 4.6ha, respectively.

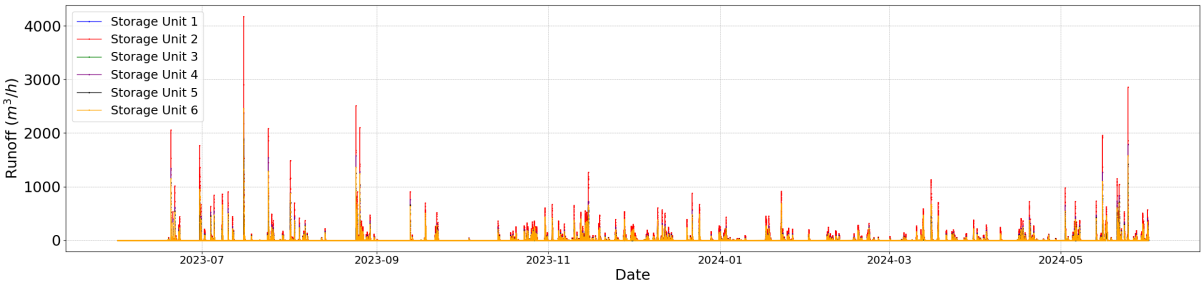

Figure 10.26: Runoff for Storage Units between June 1st 2023 until June 1st 2024.

The simulation with static control is executed for the 1 year rain scenario from June 1st 2023 until June 1st 2024. The overflow in terms of both volume (left side) and load of COD (right side) for each SU can

be seen in Figure 10.27, which includes their accumulated values over time. The biggest rain event during this period occurred in August 2023, affecting all infrastructures and causing major overflow throughout the network. In general, overflow events occur throughout the year regularly, as the current static settings are not coping with the inflow.

In summary, SU4 exhibits the highest overflow, followed by SU2, although to a significantly lesser extent. Storage Unit 4 accounts for approximately 67% of the total overflow load in the scenario. The unit receiving the industrial flow, SU1, shows reduced overflow volume, mainly due to its substantially larger storage volume. However, its COD overflow is notable, exceeding 1000 kg, due to the high pollutant load associated with the industrial inflow. Observing $Q_{\text{ov}_{\text{sensitivity}}}$, the SU with significant overflow and high sensitivity is clearly SU4, thus, intuitively MPC should focus on reducing overflows in this unit.

The accumulated overflow for each Storage Unit and the total for Urban Drainage System 2 are shown in Table 10.8, including the results for the overflow load of NH_4^+. The data shows that SU1 has higher

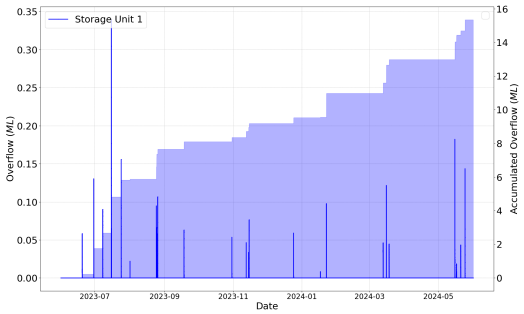

(a) Instantaneous (line) and Accumulated (shaded area) Q_{ov} for Storage Unit 1.

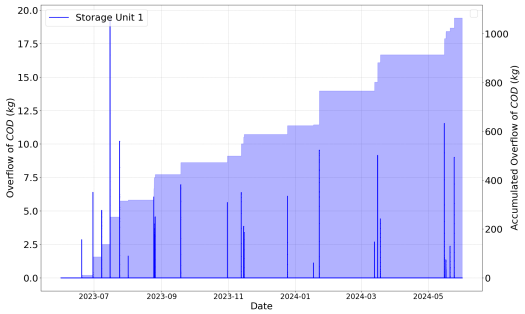

(b) Instantaneous (line) and Accumulated (shaded area) $m_{\text{ov}}^{\text{COD}}$ for Storage Unit 1.

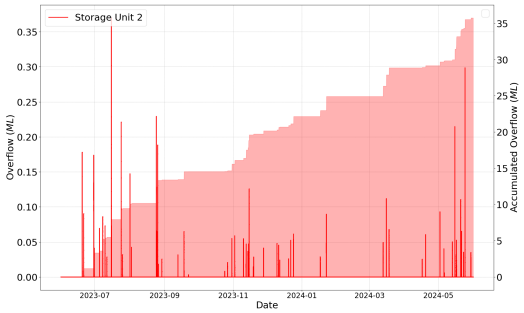

(c) Instantaneous (line) and Accumulated (shaded area) Q_{ov} for Storage Unit 2.

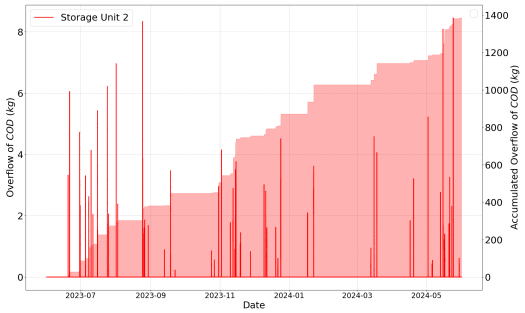

(d) Instantaneous (line) and Accumulated (shaded area) $m_{\text{ov}}^{\text{COD}}$ for Storage Unit 2.

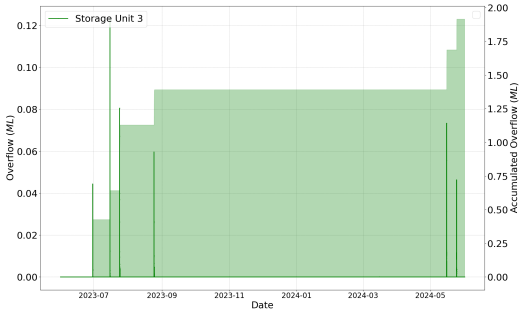

(e) Instantaneous (line) and Accumulated (shaded area) Q_{ov} for Storage Unit 3.

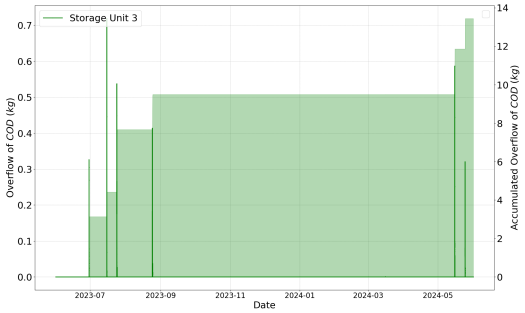

(f) Instantaneous (line) and Accumulated (shaded area) $m_{\text{ov}}^{\text{COD}}$ for Storage Unit 3.

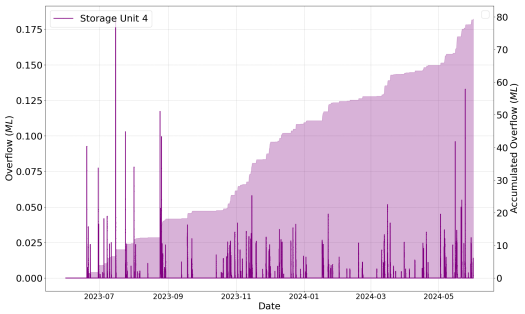

(g) Instantaneous (line) and Accumulated (shaded area) Q_{ov} for Storage Unit 4.

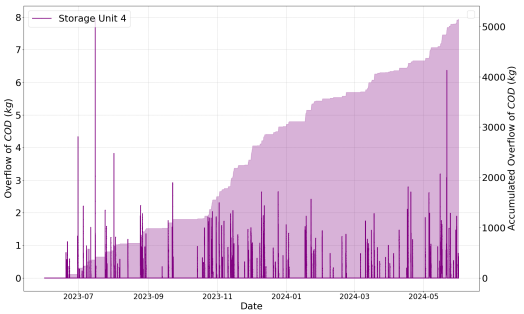

(h) Instantaneous (line) and Accumulated (shaded area) $m_{\text{ov}}^{\text{COD}}$ for Storage Unit 4.

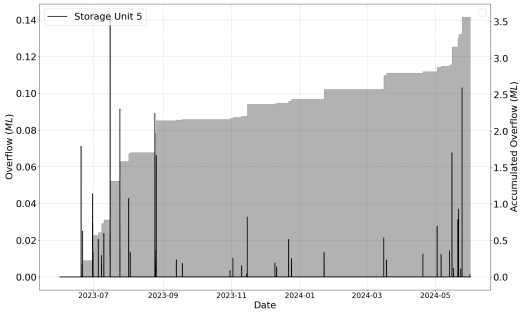

(i) Instantaneous (line) and Accumulated (shaded area) Q_{ov} for Storage Unit 5.

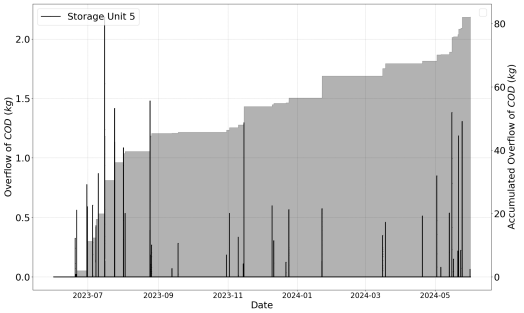

(j) Instantaneous (line) and Accumulated (shaded area) $m_{\text{ov}}^{\text{COD}}$ for Storage Unit 5.

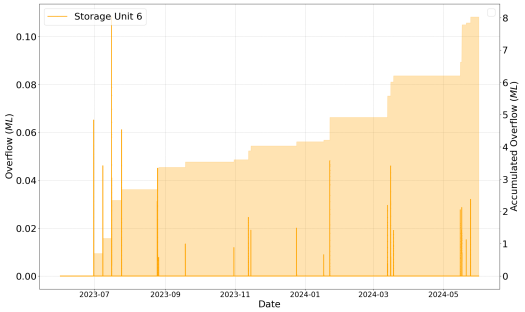

(k) Instantaneous (line) and Accumulated (shaded area) Q_{ov} for Storage Unit 6.

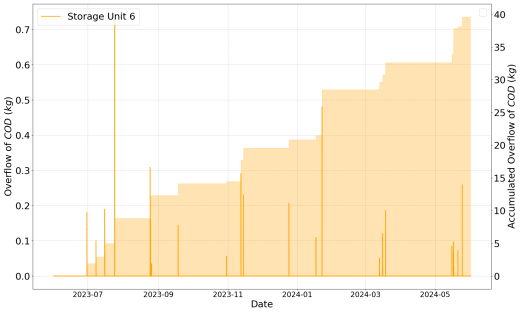

(l) Instantaneous (line) and Accumulated (shaded area) $m_{\text{ov}}^{\text{COD}}$ for Storage Unit 6.

Figure 10.27: Q_{ov} and $m_{\text{ov}}^{\text{COD}}$ for Urban Drainage System 2 with static control.

overflow of COD compared to NH_4^+, due to the industrial flow. It also demonstrated that, although SU2 displays a higher volume of overflow, the load overflow is comparable to SU1, indicating that the high infiltration on SU2 is diluting the sewage considerably. In contrast to the previous network, Urban Drainage System 2's inflow to the treatment plant is more important, where the controller should aim to reach $Q_{\text{wwtp}_{\text{ref}}}$ consistently, while also avoiding CSO events.

Furthermore, the value of $Q_{\text{ov}_{\text{sensitivity}}}$ is higher for SU3, SU4 and SU6, and the data displays that SU3 and SU6 already have low overflows, thus indicating that the static control is well designed for these structures. Dynamic management of Urban Drainage System 2 in real time can potentially mitigate overflows at SU4, using the available storage in other units more freely, while also conveying the sewage to the WWTP more promptly.

Table 10.8: Total overflow volume and load for Urban Drainage System 2 with static control.

Metric	Storage Unit 1	Storage Unit 2	Storage Unit 3	Storage Unit 4	Storage Unit 5	Storage Unit 6	Total
Q_{ov} in ML	15.34	35.75	1.92	79.39	3.56	8.03	143.99
% From the total	10.6%	24.8%	1.3%	55.1%	2.6%	5.6%	-
m_{ov}^{COD} in kg	1064.62	1385.10	13.44	5150.32	82.13	39.60	7735.21
% From the total	13.8%	17.8%	0.2%	66.6%	1.1%	0.5%	-
$m_{ov}^{NH_4}$ in kg	51.61	95.41	0.92	350.77	5.68	2.67	507.06
% From the total	10.2%	18.9%	0.2%	69.2%	1.1%	0.5%	-

Therefore, the next step is the implementation of the MPC algorithms, which involves selecting appropriate weights for each control method. To achieve this, a sensitivity analysis is carried out individually for each MPC, considering a rainfall period in which the impact of implementing MPC is expected to be more pronounced. Observing the runoff data, the period from November 9th to November 16th is selected. This period is characterised by five consecutive overflow events triggered by a series of rainfalls with varying intensities, as can be seen in Figure 10.28.

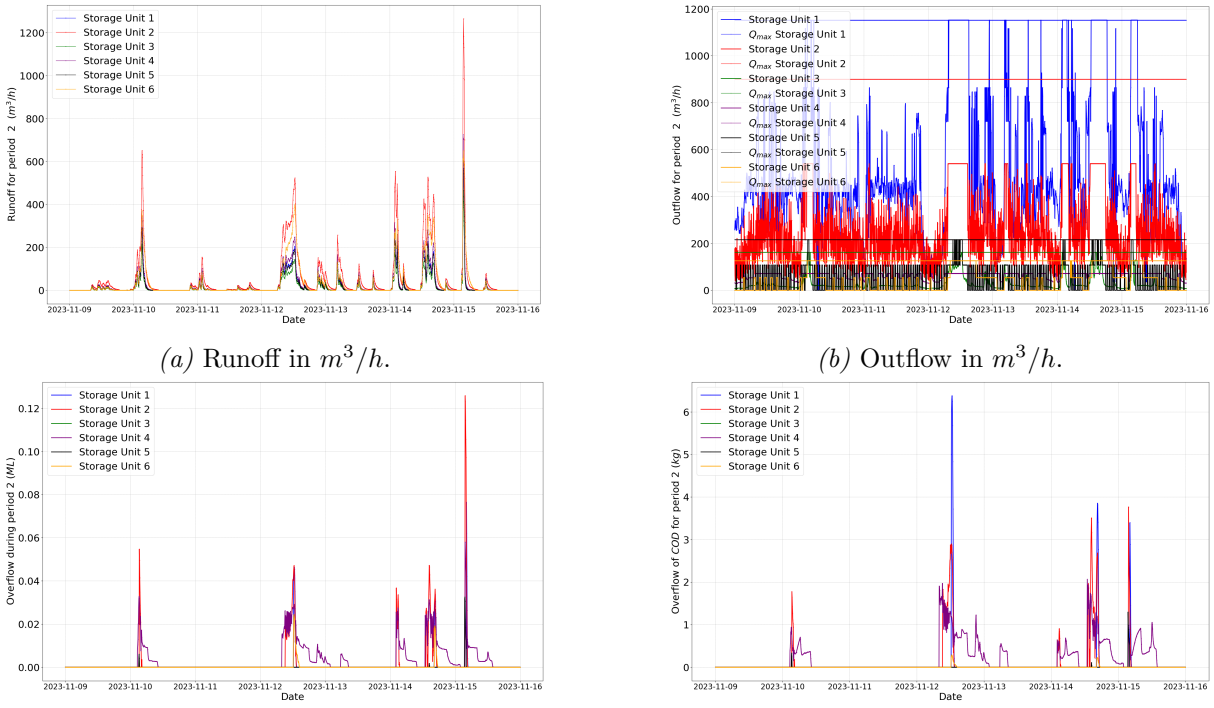

(a) Runoff in m^3/h.

(b) Outflow in m^3/h.

(c) Overflow volume in ML.

(d) Overflow load of COD in kg.

Figure 10.28: Urban Drainage System 2 with static control from November 9th to November 16th.

The previous analysis for Urban Drainage System 1 assessed whether the duration and dynamics of runoff events influence the sensitivity analysis and concluded that optimal parameter selection is best done with as much diversity as possible. Therefore, the period chosen for the analysis is suitable due to its variability in rain events. Initially, the sensitivity analysis was conducted through Morris Screening and Grid Search

for the rainfall selected and using NH_4^+ as the pollutant indicator. The results were applied to the GA optimisation, resulting in the following weights:

Table 10.9: Optimal Weights for Urban Drainage System 2 for each MPC.

Weight	α	β	γ	ϵ	ψ	ω	τ	υ
VMPC	127.34	326.14	318.37	116.35	-	-	-	-
PWMPC	69.97	160.53	84.43	264.17	-	-	-	-
NPMPC	11.2	187.36	90.7	208.51	300.0	266.02	17.2	34.22
SVMPC	44.44	83.91	177.88	1.10	-	-	-	-
SPWMPC	105.62	195.66	133.24	16.61	-	-	-	-
SNPMPC	1.24	299.99	4.20	0.011	300.0	266.77	-	1.0

These weights are used to perform two distinct simulations: (1) a scenario in which pollution-based methods use NH_4^+ as the pollutant indicator to control the system, and (2) a scenario in which the indicator is switched to COD. The primary objective is to evaluate the performance of the MPC methods under each pollutant indicator and observe how the behaviour of the UDS is influenced. A secondary objective is to evaluate whether the sensitivity analysis performed solely on NH_4^+ remains valid to control COD, or if a dedicated analysis is also required for this pollutant. Essentially, the goal is to determine whether the optimal MPC weights are interchangeable between different indicators. This analysis is presented in the following section.

10.2.1 Comparison of MPC Methods

A simulation is carried out using the weights identified from the NH_4^+ sensitivity analysis. The simulation period spans from June 1st, 2023, to June 1st, 2024, with a controller sampling time of 5 minutes and a prediction horizon of 25 minutes. For stochastic methods, a value of $\zeta = 0.95$ is applied. In the first scenario, NH_4^+ is used as the controlled pollutant indicator. Figures 10.29 and 10.30 present the results using the same bar graph format as for Urban Drainage System 1. The y-axis shows the relative overflow, with the volume (R_V) on the left and the pollutant load (R_m) on the right. The x-axis lists each SU, with their respective $Q_{ov_{sensitivity}}$ values. The priority in this control system is to reduce overflow at SU3, SU4 and SU6. The static control is performing well for SU3 and SU6, however, for SU4, the overflow is exceedingly high. Overall, the stochastic methods are performing better when analysing the relative overflows, specially SVMPC and SPWMPC, which are worse for SU1, but with great load reduction at other units. The NPMPC showed the lowest overflow at SU4, although not as good for SU4 and SU6. VMPC and PWMPC displayed an intermediate output.

In contrast to the relative overflow metric, the absolute overflow of NH_4^+, presented in Figure 10.31, reveals a different perspective on controller performance. Clearly, static control is considerably less effective in managing the UDS, with a total overflow load exceeding 507 kg over the one-year simulation period. Among MPC strategies, NPMPC achieves the lowest absolute overflow load, highlighting its superior performance in this scenario. Notably, NPMPC prioritised reducing the overflow at SU1, which has the highest inflow between all units, thus having the greatest influence on the overall performance of the system. This is further supported by the relative overflow results, which also show NPMPC yielding the lowest overflow at SU1.

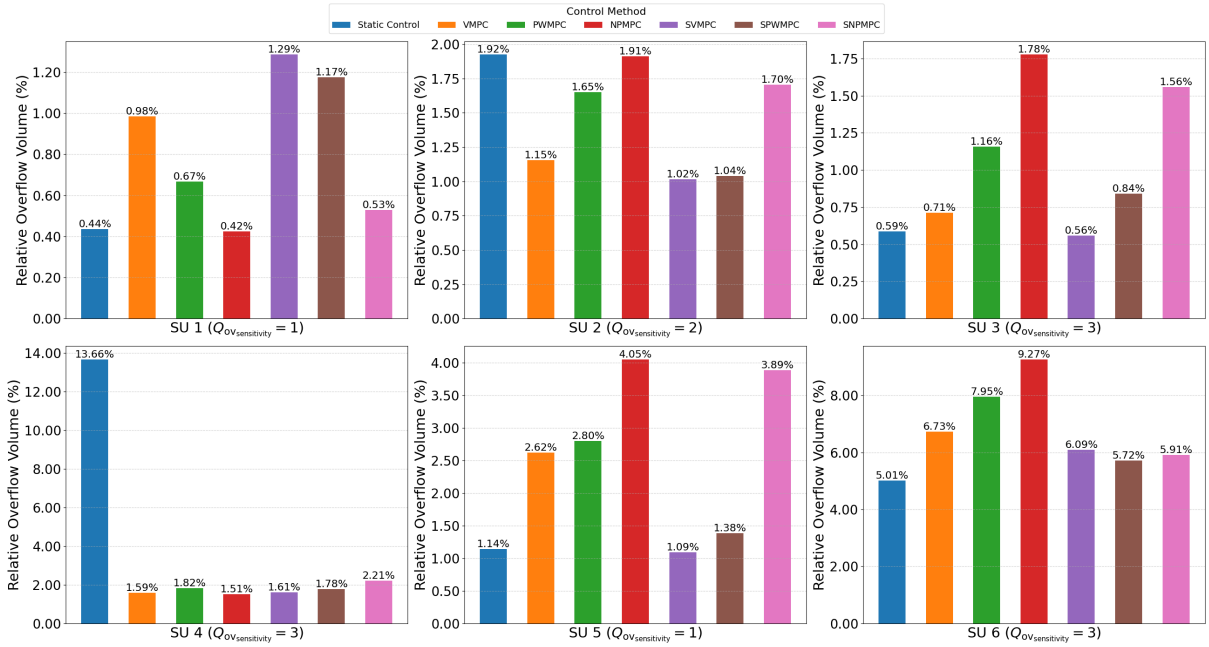

Figure 10.29: R_{V} - Relative Overflow Volume % for NH_4^+.

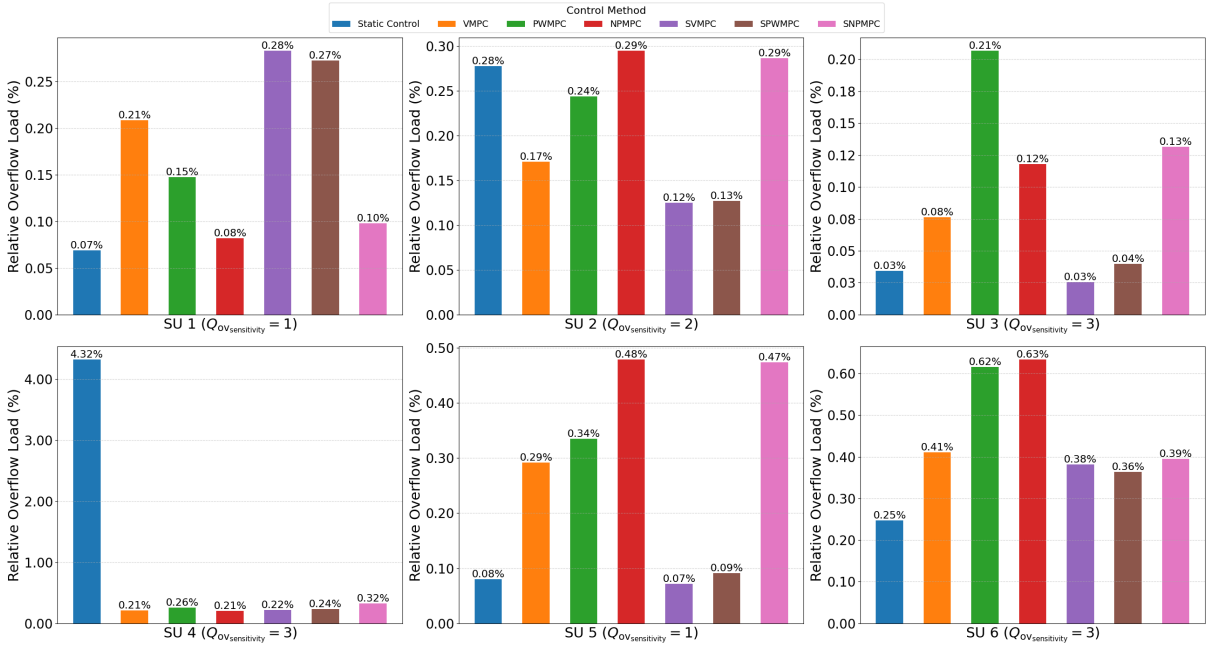

Figure 10.30: R_{m} - Relative Overflow Load % for NH_4^+.

When comparing these findings with those of Urban Drainage System 1, a consistent pattern is observed: SVMPC and SPWMPC performed better in reducing the overflow for storage units with higher $Q_{\mathrm{ov}_{\mathrm{sensitivity}}}$, although not necessarily in reducing the total overflow of the network. Conversely, SNPMPC demonstrates a well-balanced performance, achieving effective reductions in both critical units and throughout the system.

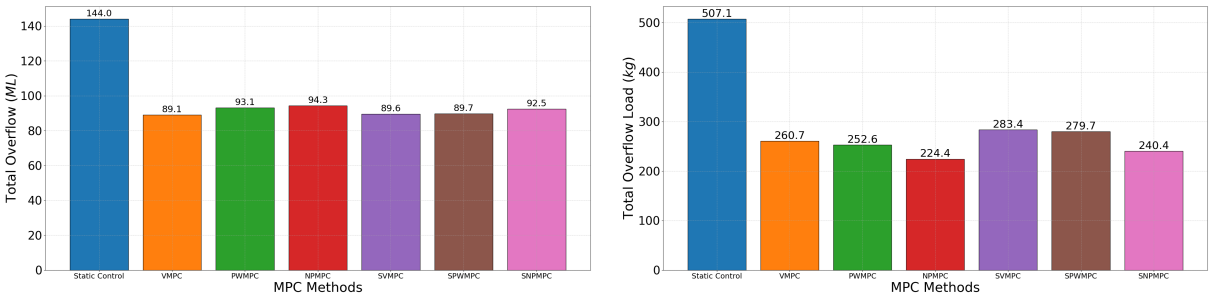

(a) $Q_{\mathrm{ov_{total}}}$ - Total Overflow Load in ML controlling $NH_4{}^+$.

(b) $m_{\mathrm{ov_{total}}}$ - Total Overflow Load in kg controlling $NH_4{}^+$.

Figure 10.31: Urban Drainage System 2 - Comparison of MPC in terms of total overflow volume and load for $NH_4{}^+$.

Using the same set of weights, a similar simulation is performed, this time using COD as the pollutant indicator for pollution-based MPC methods. In Figures 10.32 and 10.33, the results are presented for the relative overflow volume (R_{V}) and the pollutant load (R_{m}). As expected, the change in the pollutant indicator did not have an impact on the performance of VMPC and SVMPC, as they are volume-based methods. Following the trend of the previous control scenario, NPMPC continued to prioritise overflow reduction at SU1, which, in this case, resulted in a focus on the high COD inflow from industrial discharges. In general, the performance of pollution-based methods is slightly worse compared to the $NH_4{}^+$-based scenario, with SNPMPC showing a particularly worse performance.

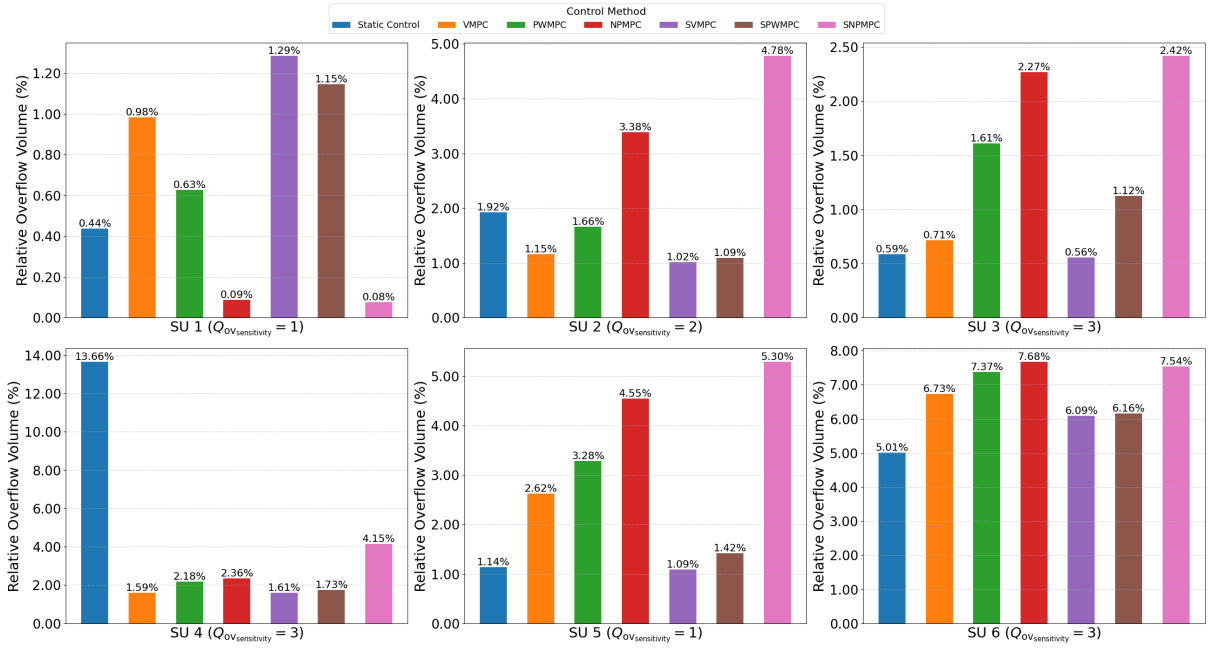

Figure 10.32: R_{V} - Relative Overflow Volume % for COD.

In Figure 10.34, the total volume of overflow (ML) and load (kg) are presented. All MPC methods outperform static control, with the exception of SNPMPC, which showed a notable performance decline. This reduced performance is mainly attributed to the fact that the controller weights were adjusted based

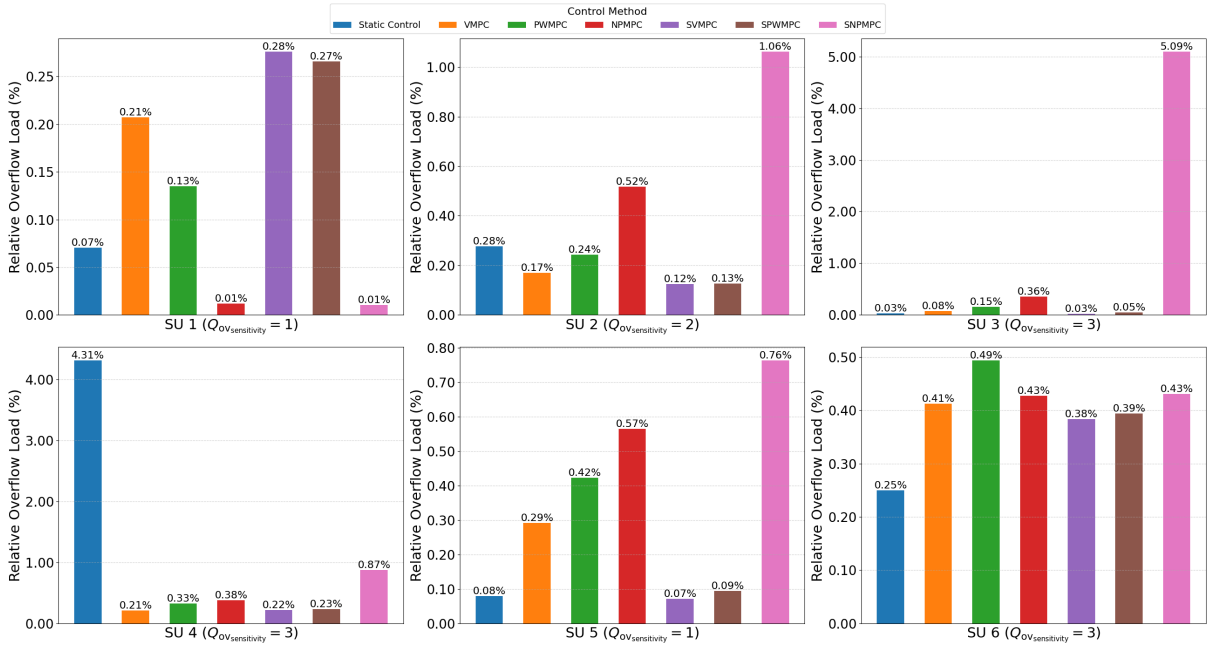

Figure 10.33: R_m - Relative Overflow Load % for COD.

on NH_4^+, and the system dynamics is different when a different pollutant indicator is used. As such, it is recommended that the controller parameters be specifically tuned to the pollutant of interest. A particularly interesting observation is that NPMPC exhibited a higher overflow volume than the other linear MPC strategies, yet achieved the lowest pollutant load. This suggests that the controller prioritised the discharge of less contaminated wastewater, better managing the storage units to avoid highly contaminated overflow events.

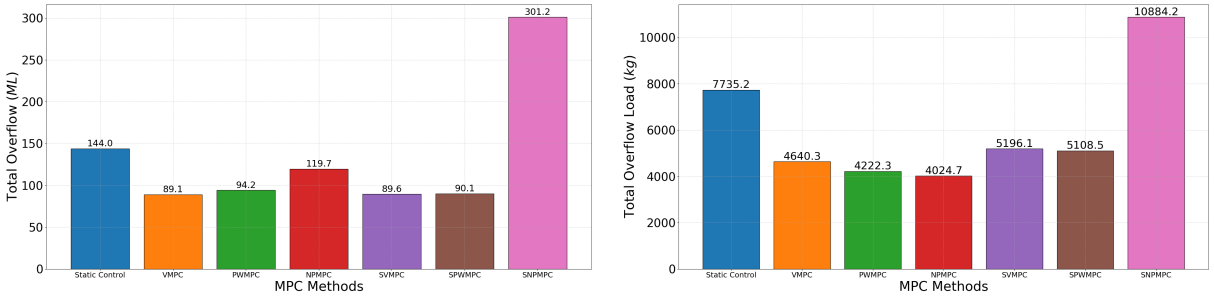

(a) $Q_{ov_{total}}$ - Total Overflow Load in ML controlling COD.

(b) $m_{ov_{total}}$ - Total Overflow Load in kg controlling COD.

Figure 10.34: Urban Drainage System 2 - Comparison of MPC in terms of total overflow volume and load for COD.

A new GA optimisation was conducted to find an updated set of weights to improve the pollution-based controller performance. Since the previous weights yielded satisfactory results for most MPC strategies,, they were used as initial guesses for GA, with the exception of SNPMPC, which was optimised without an initial guess. The updated weights are shown in Table 10.10.

The relative overflow volume and load are displayed in Figures 10.35 and 10.36, and in Table 10.11 the

Table 10.10: New Optimal Weights for Urban Drainage System 2 for each MPC to control COD.

Weight	α	β	γ	ϵ	ψ	ω	τ	υ
PWMPC	93.74	160.53	40.14	264.17	-	-	-	-
NPMPC	18.38	228.35	90.7	175.65	362.66	250.36	19.4	36.33
SPWMPC	78.85	133.66	126.18	2.58	-	-	-	-
SNPMPC	78.19	337.0	128.86	26.07	114.58	262.60	-	16.74

comparison between the previous simulation and the weights from Table 10.9 are compared to the new set of weights. The results can be generalised as follows:

- For PWMPC, the load was reduced in all SUs, with the exception of SU2. An interesting outcome is the fact that for SU4, SU5 and SU6, the relative overflow in volume increased, however, the overflow of COD actually decreased in those units. This suggests a better management of storage within those units in handling the load, allowing overflow of cleaner wastewater.
- For NPMPC, the load was reduced in all SUs, with the exception of SU4. Similarly to PWMPC, the decrease in relative load does not necessarily translate into a decrease in relative overflow volume, as can be seen in SU6.
- For SPWMPC, the new set of weights made the performance worse for all SUs, with the exception of SU1. However, SPWMPC still remains having the best performance between all controllers for units with higher $Q_{\text{ov}_{\text{sensitivity}}}$.
- Finally, for SNPMPC, the load was reduced in all SUs, with the exception of SU6. Performance improvement is notable for SU3, with a significant improvement. SNPMPC still presents the worse performance for the units with higher $Q_{\text{ov}_{\text{sensitivity}}}$.

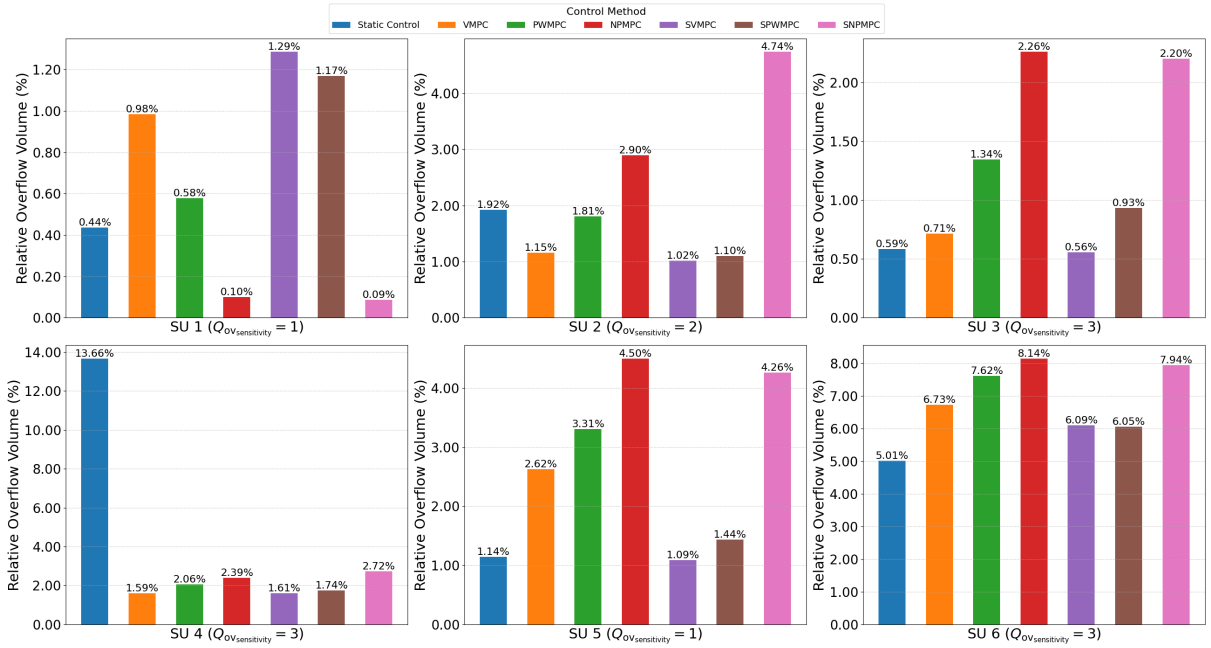

Figure 10.35: R_V - Relative Overflow Volume % for COD.

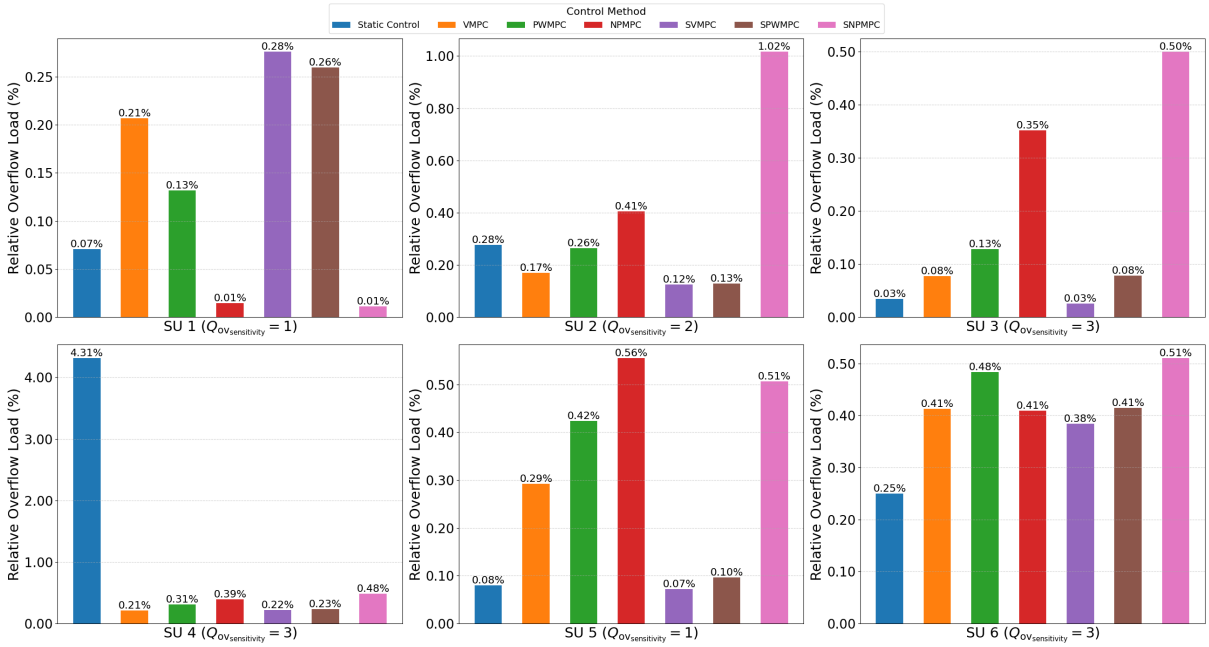

Figure 10.36: R_m - Relative Overflow Load % for COD.

Table 10.11: Comparison between MPC methods with updated weights controlling COD. Methods followed by * are the ones with updated weights. Each cell corresponds to the pair (R_V, R_m) for a MPC at a specific SU. Columns with light red colouring represent the SUs with higher $Q_{ovsensitivity}$.

MPC \ SU	SU1	SU2	SU3	SU4	SU5	SU6
PWMPC	(0.63%, 0.13%)	(1.66%, 0.24%)	(1.61%, 0.15%)	(2.18%, 0.33%)	(3.28%, 0.42%)	(7.37%, 0.49%)
PWMPC*	(0.58%, 0.13%)	(1.81%, 0.26%)	(1.34%, 0.13%)	(2.60%, 0.31%)	(3.31%, 0.42%)	(7.62%, 0.48%)
NPMPC	(0.09%, 0.01%)	(3.38%, 0.52%)	(2.27%, 0.36%)	(2.36%, 0.38%)	(4.55%, 0.57%)	(7.68%, 0.43%)
NPMPC*	(0.10%, 0.01%)	(2.90%, 0.41%)	(2.26%, 0.35%)	(2.39%, 0.39%)	(4.50%, 0.56%)	(8.14%, 0.41%)
SPWMPC	(1.15%, 0.27%)	(1.09%, 0.13%)	(1.12%, 0.05%)	(1.73%, 0.23%)	(1.42%, 0.09%)	(6.16%, 0.39%)
SPWMPC*	(1.17%, 0.26%)	(1.10%, 0.13%)	(0.93%, 0.08%)	(1.74%, 0.23%)	(1.44%, 0.10%)	(6.05%, 0.41%)
SNPMPC	(0.08%, 0.01%)	(4.78%, 1.06%)	(2.42%, 5.09%)	(4.15%, 0.87%)	(5.30%, 0.76%)	(7.54%, 0.43%)
SNPMPC*	(0.09%, 0.01%)	(4.74%, 1.02%)	(2.20%, 0.50%)	(2.72%, 0.48%)	(4.26%, 0.51%)	(7.94%, 0.51%)

In Figure 10.37, the total volume of overflow (ML) and load (kg) are presented. The MPC strategies with the best performance in terms of total load reduction are NPMPC, followed by PWMPC. Compared to the results in Figure 10.34, both NPMPC and SNPMPC show significant improvement, while SPWMPC displays a slight improvement and PWMPC performs slightly worse. The results highlight that reducing the overflow volume does not necessarily lead to an optimal reduction in the pollutant load. Notably, NPMPC exhibits the highest overflow volume among the MPCs, however, it achieves the greatest reduction in overflow load, demonstrating its effectiveness in prioritising the discharge of less contaminated water.

An interesting outcome for SNPMPC is observed when controlling NH_4^+, where the total overflow of COD in this specific scenario reached 3930.5 m^3, which is significantly better than the results obtained when controlling the COD itself. This suggests that the current weights are still not properly adjusted and that

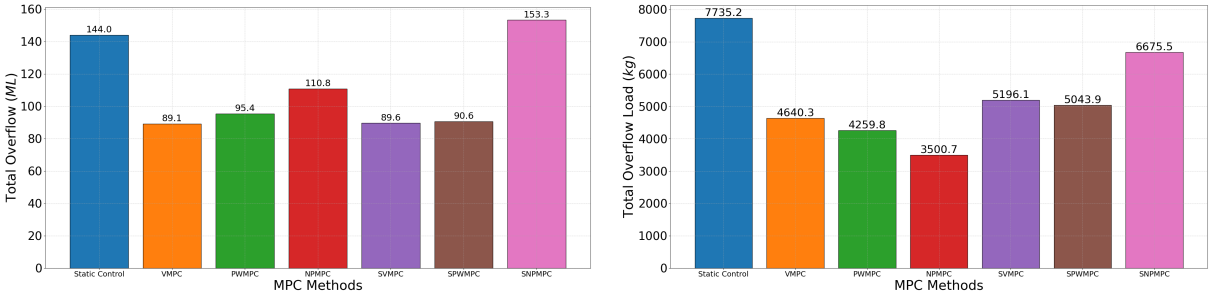

(a) $Q_{\mathrm{ov}_{\mathrm{total}}}$ - Total Overflow Load in ML controlling COD.

(b) $m_{\mathrm{ov}_{\mathrm{total}}}$ - Total Overflow Load in kg controlling COD.

Figure 10.37: Urban Drainage System 2 - Comparison of MPC in terms of total overflow volume and load for COD with updated weights.

a more in-depth analysis is needed. However, due to its high computational demands, SNPMPC is a particularly challenging controller to fine-tune using the proposed methodological approaches. Nonetheless, the improvement of the controlled is feasible, as the performance of SNPMPC for the scenario controlling $NH_4{}^+$ is quite good, arguably the most balanced when considering both relative and absolute overflow metrics.

The last analysis for Urban Drainage System 2 is the improvement of MPC methods across 4 regions of intensity of rain. This is executed to complement the results from the previous UDS. Therefore, the first step is to classify the rain events, which is done following the same procedure performed for the urban drainage system 1. The results can be seen in Figure 10.38, where the light blue shaded areas represent each identified event and the dark blue lines the runoff.

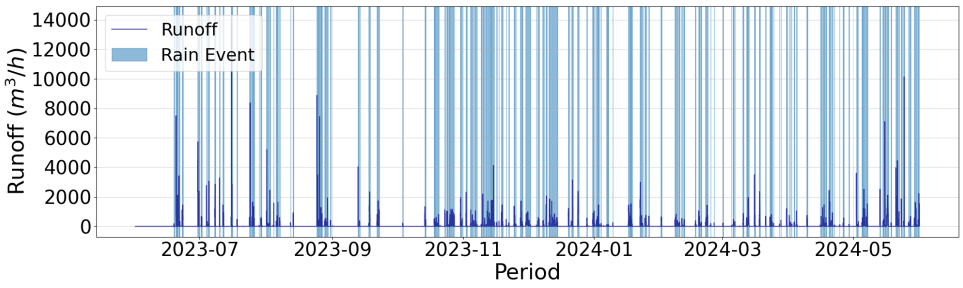

Figure 10.38: Accumulated Runoff over 1 year period.

Rain events are divided into four categories: events with very low runoff intensity, events with low runoff intensity, events with medium runoff intensity, and events with high runoff intensity. For each event, the corresponding accumulated overflow volume and the $NH_4{}^+$ load are also calculated and both are shown in Figure 10.39, with the defined runoff regions highlighted. For Urban Drainage System 2, a higher number of rain events was identified compared to the previously analysed UDS, thereby providing increased statistical relevance to the analysis.

The improvement metrics, I_{v} and I_{m}, are used again to compare the static control with the performance of MPC using a box-plot graph to present the data, where the aim is to evaluate in which regions a given MPC has a higher improvement compared to the static control. First, the box-plot for VMPC is

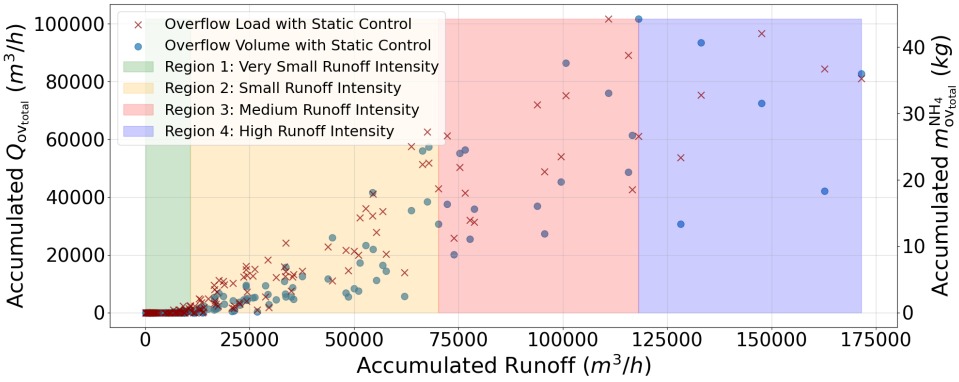

Figure 10.39: Accumulated Runoff and Overflow for the Static Control with Highlighted Regions.

presented to evaluate the performance of a volume-based approach, as shown in Figure 10.40. Clearly, the improvement is much higher for Region 2, reaching a median of almost 100% in the box-plot.

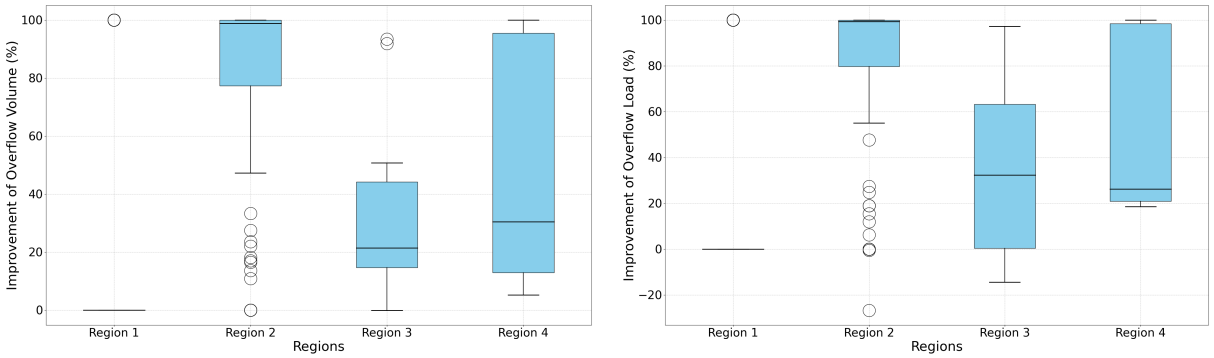

(a) Improvement of overflow volume (I_v in %) under VMPC compared to static control.

(b) Improvement of overflow load (I_m in %) under VMPC compared to static control.

Figure 10.40: Comparison of overflow load and volume improvement between VMPC and static control across four regions with varying hydrological characteristics.

In terms of volume, the improvement is higher in Region 4 than in Region 3, which for Urban Drainage System 3 is explained by long periods of rain that accumulate a considerable runoff inflow, but where the peaks are not so elevated to cause massive overflow events during the period. This pattern becomes even clearer when examining the load box-plot, where Region 3 shows greater improvement than Region 4. This outcome is a result of prolonged rainfall periods, leading to significant dilution and reduced pollutant concentration. For Region 1, most events were avoided, but there was a single outlier which overflow occurred only with the static control.

In Figure 10.41 is presented the box-plot for NPMPC compared to static control, which displays a overall similar result to VMPC. The improvement in the overflow load is more pronounced for Region 2, reaching a I_V close to 100%, while Region 3 and Region 4 have a very similar median (around 37%). For both VMPC and NPMPC, the 75% quartile of Region 4 is considerably higher, suggesting that there is much potential for reducing overflow even for high-intensity rain events.

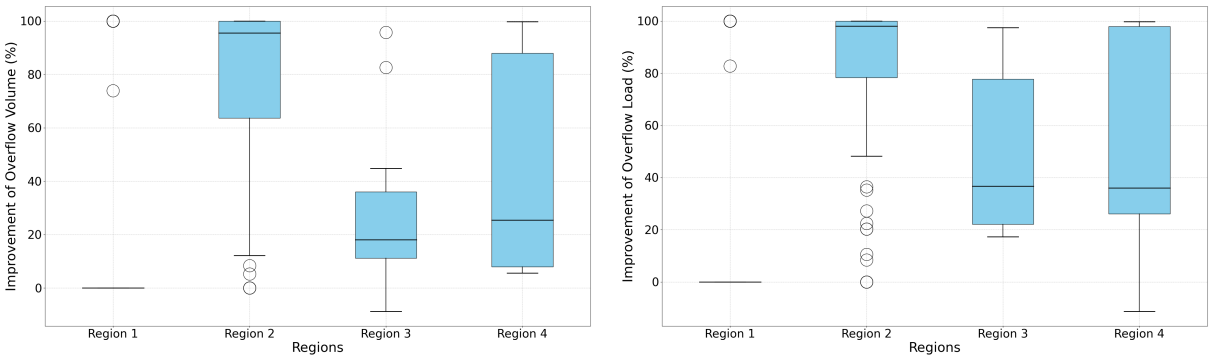

(a) Improvement of overflow volume (I_v in %) under NPMPC compared to static control.

(b) Improvement of overflow load (I_m in %) under NPMPC compared to static control.

Figure 10.41: Comparison of overflow load and volume improvement between NPMPC and static control across four regions with varying hydrological characteristics.

The box-plots for the remaining MPC methods are provided in Appendix A.6. Overall, the results are consistent with those from Urban Drainage System 1, with the analysis here benefiting from a larger dataset. The greatest improvements over static control were observed during small and medium rain events. However, high-intensity events should not be neglected, as they naturally contribute significantly to pollutant loads during overflows.

In the next section, Urban Drainage System 3 is introduced, providing a more qualitative analysis on deployment, parametrisation, and computation cost attributed to high number of storage units.

10.3 Urban Drainage System 3

The last drainage system studied in this chapter is composed by a total of 45 Storage Units, where the wastewater network collects and distributes sewage encompassing communes close to a lake, totalling approximately 7000 PE. The MPC is implemented to control 34 Storage Units, distributed around the network and the remaining 11 units are side storages located alongside the controlled SU. Given the larger number of controlled structures, this section focuses mainly on the practicality of implementing each individual MPC within a network of this scale, addressing challenges such as parameter identification, computational efforts and other potential limitations. Although the analysis in this section is centred around discussion rather than quantitative results, the full network is included to help in comprehending the system's structure and context.

The main distinction of this system compared to the previous ones is the significant increase in the number of controlled SUs. Figure 10.43 presents a detailed diagram of Urban Drainage System 3, where most units are connected directly to a single SU, namely SU16, which in turn discharges to the WWTP. The diagram shows a complex network with different connections. The network itself is close to a river that is retained by a dam, used as a drinking water reservoir, therefore, the overflow of water highly contaminated can cause potential harm to the population.

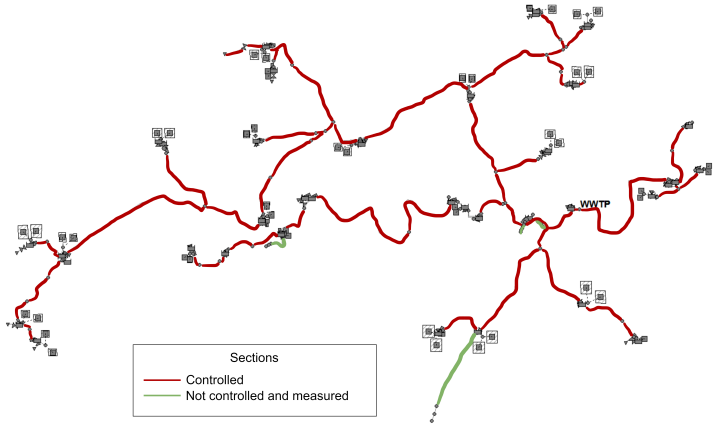

Figure 10.42: Urban Drainage System 3 - red line indicates sections that are controlled by MPC - green line indicate sections that are not controlled by MPC but are measured.

Additionally, many units are associated with low PE, indicating that they represent small sections of the network with low population density. A unique characteristic of this network is that some units do not receive inflow from catchments, meaning no surface runoff caused by precipitation in those areas enters the sewer. From those:

- SU13, SU20 and SU25 are separate sewer systems, serving exclusively as conduits for wastewater transport.
- SU5, SU11, SU18 and SU32 are seasonal camping sites with activity only during summer. Those units appear with PE equals to 0, due to not having human activity most of the year. They are considered as so for the modelling of MPC to add this layer of uncertainties to the system, but in real implementations, they could easily be incorporated with a seasonal pattern added to the estimation of dry weather flow.
- SU16, SU24 and SU34 function as intermediate pumping stations that collect and store flows from various locations. Among these, SU16 is of particular importance as it directly connects to the WWTP.

Furthermore, the dry-weather inflow is modelled using the same hourly-sampled, normalized flow pattern applied in Urban Drainage System 1, as illustrated in Figure 10.4. However, the average wastewater flow received by each storage unit varies, depending on the number of inhabitants connected to the system. Consequently, each unit experiences different inflow conditions, both in terms of volume and pollutant load. Table 10.12 presents the state machine limits for both controllable and controlled states for each SU, along with $Q_{\text{ov}_{\text{sensitivity}}}$, which is incorporated into the MPC formulation to prioritise overflow reduction in specific storage units. In Urban Drainage System 3, no additional infiltration is added to the modelling of the sewer.

A simulation using static control is carried out to evaluate the system dynamics in a 6-month period, between 1st of June of 2024 to the 11th of December of 2024. The actuator outflows are fixed at Q_{design_i}, and Figure 10.44 illustrates a 7-day segment of the DWF across each SU in Urban Drainage System 3, showing an overview without providing a detailed analysis. The SU16 presents the higher dry weather

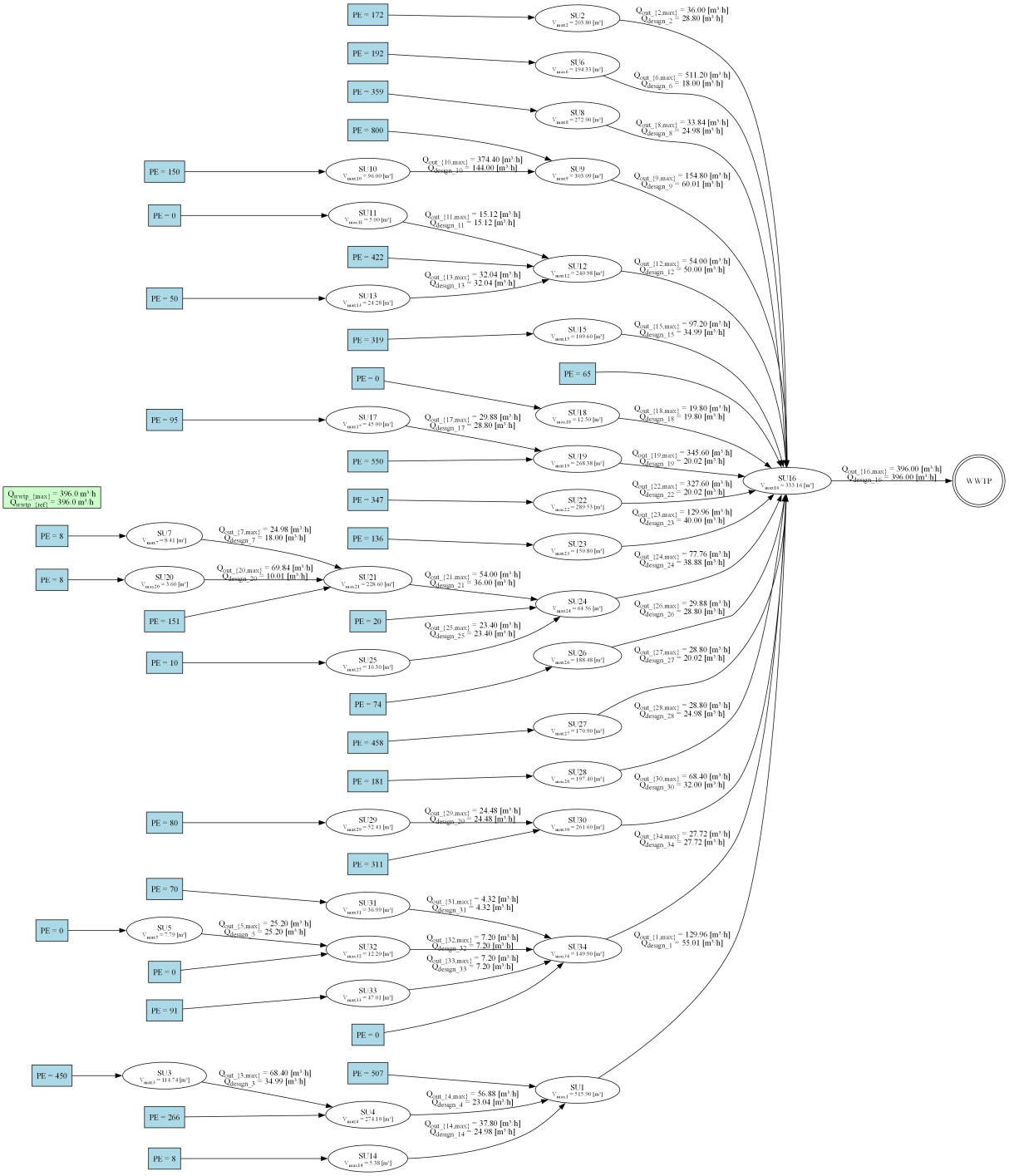

Figure 10.43: Schema for controlled section of Urban Drainage System 3.

flow, as it is the unit right before the WWTP, with a peak of up to 120 m^3/h. Considering the outflow from SU16 can reach approximately 400 m^3/h, the structure has enough capacity to handle the DWF

The precipitation input for Urban Drainage System 3 is derived from 17 rain gauges distributed throughout the network, producing the accumulated runoff shown in Figure 10.45 for the complete network. The area is served by many catchments of various sizes, where SU4 stands out with the biggest catchment of

Table 10.12: Model parameters.

	Storage Unit 1	Storage Unit 2	Storage Unit 3	Storage Unit 4	Storage Unit 5	Storage Unit 6	Storage Unit 7	Storage Unit 8
$V_{\text{controlled}}$	5.00 m^3	20.00 m^3	27.50 m^3	5.00 m^3	1.01 m^3	2.00 m^3	0.86 m^3	37.50 m^3
$V_{\text{controllable}}$	15.00 m^3	45.00 m^3	65.00 m^3	12.50 m^3	1.59 m^3	6.00 m^3	1.85 m^3	52.50 m^3
$Q_{\text{in}_{\text{controlled}}}$	18.0 m^3/h	18.0 m^3/h	9.0 m^3/h	9.0 m^3/h	3.6 m^3/h	8.1 m^3/h	7.2 m^3/h	6.6 m^3/h
$Q_{\text{in}_{\text{controllable}}}$	72.0 m^3/h	54.0 m^3/h	37.8 m^3/h	54.0 m^3/h	23.4 m^3/h	20.2 m^3/h	18.0 m^3/h	16.6 m^3/h
$Q_{\text{ov}_{\text{sensitivity}}}$	5	5	1	1	1	1	5	1
	Storage Unit 9	Storage Unit 10	Storage Unit 11	Storage Unit 12	Storage Unit 13	Storage Unit 14	Storage Unit 15	Storage Unit 16
$V_{\text{controlled}}$	5.00 m^3	4.20 m^3	0.50 m^3	12.50 m^3	2.90 m^3	1.50 m^3	7.50 m^3	30.00 m^3
$V_{\text{controllable}}$	10.00 m^3	10.00 m^3	1.50 m^3	25.00 m^3	6.80 m^3	2.20 m^3	10.00 m^3	105.00 m^3
$Q_{\text{in}_{\text{controlled}}}$	23.4 m^3/h	10.8 m^3/h	6.0 m^3/h	18.0 m^3/h	5.4 m^3/h	5.4 m^3/h	5.4 m^3/h	90.0 m^3/h
$Q_{\text{in}_{\text{controllable}}}$	90.0 m^3/h	36.0 m^3/h	15.1 m^3/h	54.0 m^3/h	12.6 m^3/h	12.6 m^3/h	12.6 m^3/h	234.0 m^3/h
$Q_{\text{ov}_{\text{sensitivity}}}$	1	1	1	5	5	5	1	1
	Storage Unit 17	Storage Unit 18	Storage Unit 19	Storage Unit 20	Storage Unit 21	Storage Unit 22	Storage Unit 23	Storage Unit 24
$V_{\text{controlled}}$	2.40 m^3	1.93 m^3	10.74 m^3	0.90 m^3	2.90 m^3	2.00 m^3	2.50 m^3	10.00 m^3
$V_{\text{controllable}}$	4.40 m^3	3.40 m^3	16.10 m^3	3.00 m^3	10.00 m^3	5.00 m^3	7.50 m^3	20.00 m^3
$Q_{\text{in}_{\text{controlled}}}$	5.4 m^3/h	1.7 m^3/h	6.2 m^3/h	4.0 m^3/h	9.0 m^3/h	5.4 m^3/h	5.4 m^3/h	27.0 m^3/h
$Q_{\text{in}_{\text{controllable}}}$	12.6 m^3/h	5.4 m^3/h	30.6 m^3/h	10.0 m^3/h	18.0 m^3/h	12.6 m^3/h	12.6 m^3/h	72.0 m^3/h
$Q_{\text{ov}_{\text{sensitivity}}}$	1	1	1	4	1	2	6	6
	Storage Unit 25	Storage Unit 26	Storage Unit 27	Storage Unit 28	Storage Unit 29	Storage Unit 30	Storage Unit 31	Storage Unit 32
$V_{\text{controlled}}$	1.50 m^3	2.50 m^3	2.50 m^3	5.00 m^3	2.50 m^3	2.50 m^3	1.50 m^3	1.00 m^3
$V_{\text{controllable}}$	4.00 m^3	5.00 m^3	5.00 m^3	9.00 m^3	5.00 m^3	5.00 m^3	3.00 m^3	2.00 m^3
$Q_{\text{in}_{\text{controlled}}}$	5.4 m^3/h	5.4 m^3/h	5.4 m^3/h	5.4 m^3/h	5.4 m^3/h	14.0 m^3/h	1.8 m^3/h	5.4 m^3/h
$Q_{\text{in}_{\text{controllable}}}$	12.6 m^3/h	12.6 m^3/h	13.0 m^3/h	12.6 m^3/h	12.6 m^3/h	35.3 m^3/h	3.6 m^3/h	28.8 m^3/h
$Q_{\text{ov}_{\text{sensitivity}}}$	5	4	1	1	5	5	1	1
	Storage Unit 33	Storage Unit 34						
$V_{\text{controlled}}$	1.00 m^3	5.00 m^3						
$V_{\text{controllable}}$	2.50 m^3	10.00 m^3						
$Q_{\text{in}_{\text{controlled}}}$	1.3 m^3/h	9.4 m^3/h						
$Q_{\text{in}_{\text{controllable}}}$	1.8 m^3/h	19.8 m^3/h						
$Q_{\text{ov}_{\text{sensitivity}}}$	1	1						

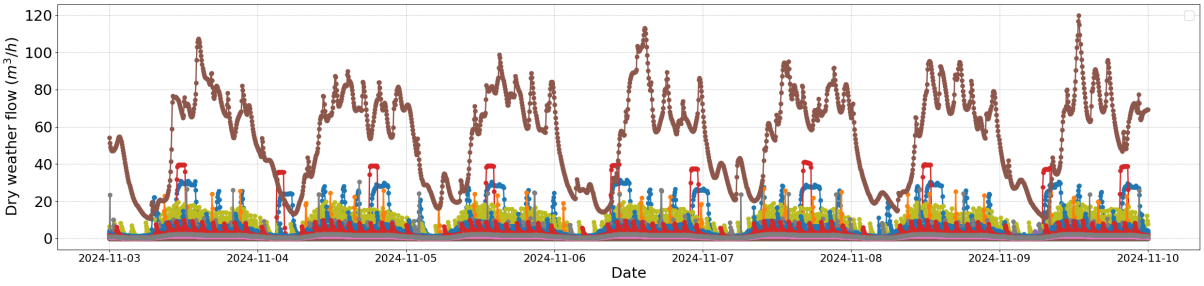

Figure 10.44: Dry weather flow for the Storage Units.

35.8ha, followed by SU2 and SU3 with 24.4ha and 18.8ha, respectively.

Hence, considering these inputs for the sewage system, a simulation with static control is executed for the 6-month period. In here, the overflow in terms of both volume (left side) and load (right side) is shown for a few selected structures: SU2, SU3, SU4 and SU16, as can be seen in Figure 10.46, which includes their accumulated values over time. SU2, SU3 and SU4 are the units with greater overflow, and SU2 stands out as having also a high $Q_{\text{ov}_{\text{sensitivity}}}$ in comparison to the others. Besides, SU16 is also important

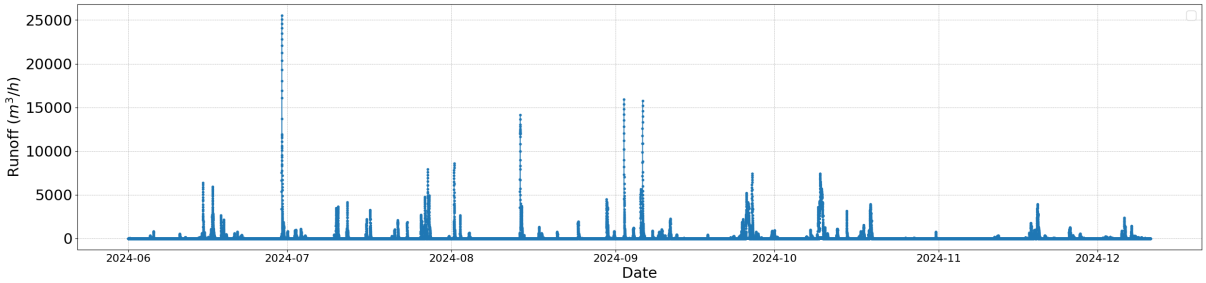

Figure 10.45: Accumulated runoff at Urban Drainage System 3.

as the unit connected to the WWTP, therefore its behaviour is also highlighted.

10.3.1 Qualitative Analysis

The deployment of MPC, or any RTC system, is inherently challenging, as it requires managing a wide range of variables to ensure effective control. Measurement devices demand regular maintenance, and in such complex systems, failures are inevitable. Therefore, controllers must be robust and adaptable to a variety of operating conditions. Additionally, reliable communication between MPC and the Supervisory Control and Data Acquisition (SCADA) system is fundamental. This connection must be properly

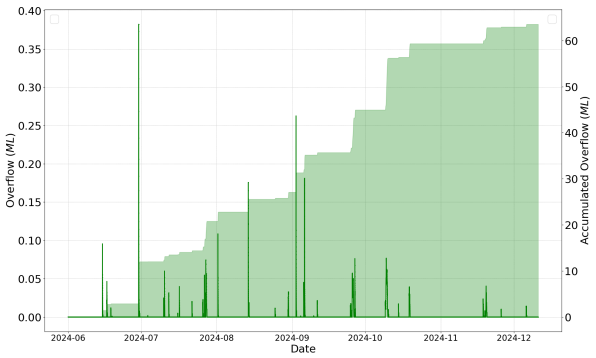

(a) Instantaneous (line) and Accumulated (shaded area) Q_{ov} for Storage Unit 2.

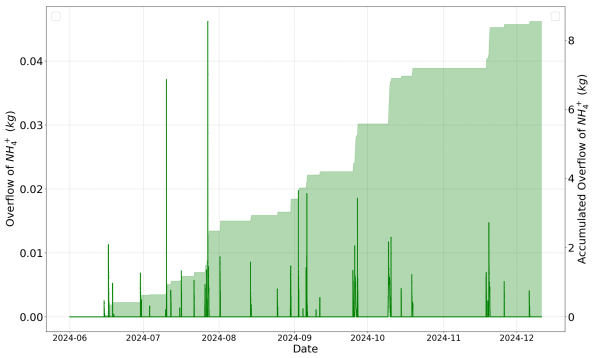

(b) Instantaneous (line) and Accumulated (shaded area) $m_{\text{ov}}^{\text{NH4}}$ for Storage Unit 2.

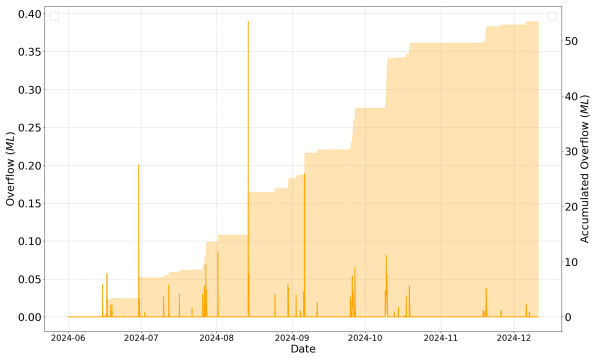

(c) Instantaneous (line) and Accumulated (shaded area) Q_{ov} for Storage Unit 3.

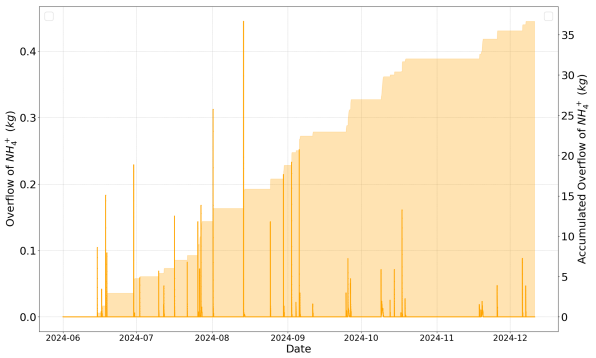

(d) Instantaneous (line) and Accumulated (shaded area) $m_{\text{ov}}^{\text{NH4}}$ for Storage Unit 3.

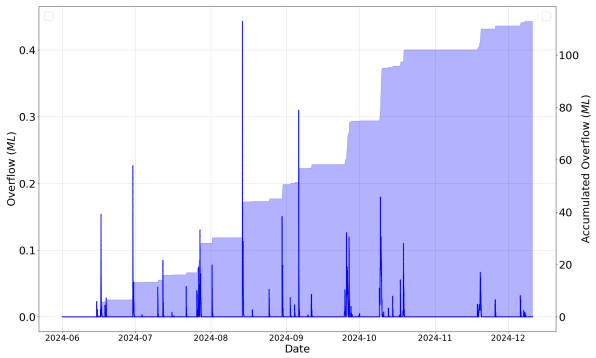

(e) Instantaneous (line) and Accumulated (shaded area) Q_{ov} for Storage Unit 4.

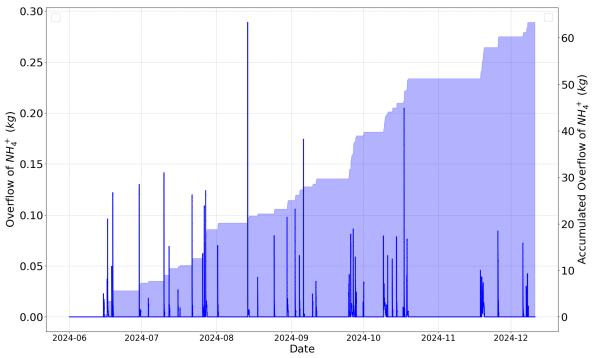

(f) Instantaneous (line) and Accumulated (shaded area) $m_{\text{ov}}^{\text{NH4}}$ for Storage Unit 4.

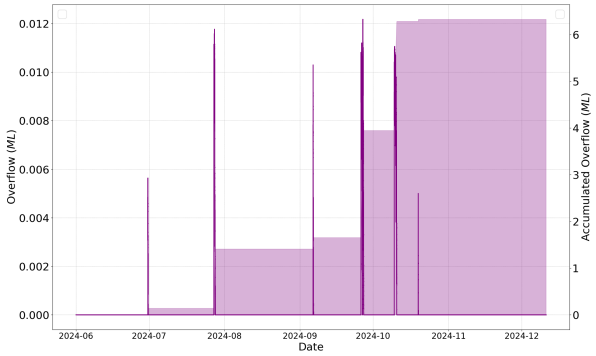

(g) Instantaneous (line) and Accumulated (shaded area) Q_{ov} for Storage Unit 16.

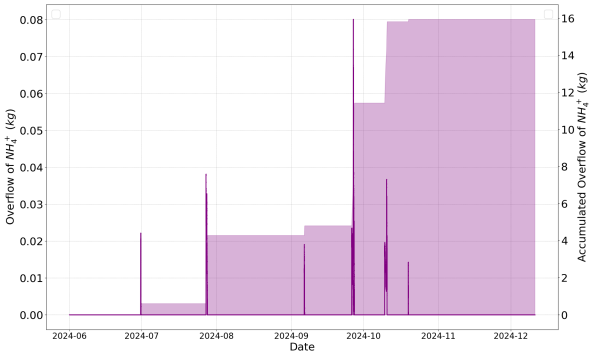

(h) Instantaneous (line) and Accumulated (shaded area) $m_{\text{ov}}^{\text{NH4}}$ for Storage Unit 16.

Figure 10.46: Q_{ov} and $m_{\text{ov}}^{\text{NH4}}$ for Urban Drainage System 3 with static control.

configured, stable, and capable of delivering real-time data to the controller without interruption. These technical demands are further complicated in networks that cover several kilometres, where environmental factors introduce additional layers of uncertainty that are characteristic of urban drainage systems. Regarding a pollution-based framework, the main obstacle towards a proper implementation is measuring pollutant concentration in real-time. This can be solved using pollutant load patterns, but this introduces another level of uncertainties, and these patterns may need to consider specific scenarios, such as commute from work to home from inhabitants or seasonal behaviours.

Specifically considering the MPC methods proposed in this thesis, the main challenges are: (1) create a proper model, which includes the simulation model for validation and the internal model of the MPC with the correct variables. For instance, MPC needs to know the maximum volume to predict overflows correctly, the maximum outflow to calculate the optimal without surpassing the physical limitations of the controllers or proper concentration patterns to predict the load as well. The simulation model needs to be as faithful to the actual system as possible, since the validation of the controller is realized through experiments in the simulated urban drainage system. (2) The computational efforts by the MPC depends on the system requirements and the size of the UDS. Often, the control loop ranges between 5 to 10 minutes, thus the calculation of the optimal output needs to be below that range.

To address the first challenge, it is recommended to conduct high-frequency measurement campaigns prior to initiating any control strategies or tuning of the MPC. The objective is to gather data from as

many relevant variables as possible, ensuring that the calibration of both the internal and simulation models is carried out with high accuracy. This process may require a considerable amount of time, as longer data collection allows for a broader range of system dynamics to be captured, including more rain events, leading to a more detailed and reliable model. For Urban Drainage System 3, the water level in the model was calibrated after the measurements were collected, increasing the reliability of the model.

The second limitation related to the computational cost is inherent to the control method. For this system, the control loop is 300 seconds, therefore, the calculation of the optimal output needs to be below this threshold. Each MPC strategy is evaluated with a prediction horizon of 50 minutes to verify their computation costs, realized by simulating the controllers at 12 days period, leading to a total of 3456 data points. A box-plot in Figure 10.47 is used to compare the MPC strategies, but the visualization is difficult due to the linear methods presenting a much lower computation time, thus, Table 10.13 summarizes the statistics.

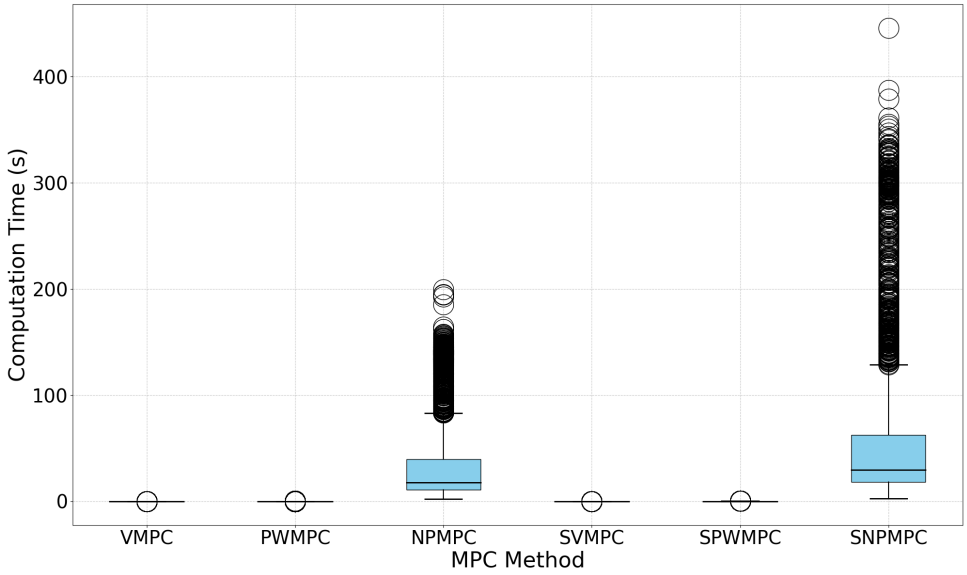

Figure 10.47: Boxplot comparing the computation cost (in seconds) of each MPC strategy.

Table 10.13: Descriptive statistics of computation time (in seconds) for each MPC method.

	Min	Q1	Median	Q3	Max	Mean	Std Dev
VMPC	0.008090	0.008390	0.008870	0.012640	0.052950	0.010730	0.003680
PWMPC	0.059650	0.061390	0.065330	0.079550	0.266880	0.077860	0.027060
NPMPC	2.295450	10.876900	17.903020	39.878600	199.779030	34.930470	38.531260
SVMPC	0.013920	0.015990	0.016710	0.026670	0.081210	0.020900	0.008050
SPWMPC	0.093910	0.096470	0.101940	0.146000	0.380930	0.124820	0.042100
SNPMPC	2.728490	18.102250	29.700140	62.435590	445.869620	59.338020	73.013290

The findings indicate that SNPMPC is, by a significant margin, the most computationally demanding method, with peak runtimes reaching 445 seconds and an average of 18.1 seconds—approximately 80% higher than NPMPC. This elevated computational burden is problematic, as SNPMPC approaches, and occasionally exceeds, the controller's sampling time of 300 seconds. Non-linear approaches are inherently slower than linear ones, meaning that as system size increases, both SNPMPC and NPMPC are likely to

struggle in maintaining computational times within acceptable margins. A more detailed examination of the optimisation problems for both controllers (Sections 8.1.3 and 9.5.2) reveals potential strategies to reduce this computational cost:

- One way to reduce computational complexity is by decreasing the number of objectives, which simplifies the optimisation problem considerably. For instance, ϕ_1, ϕ_2 and ϕ_3 could be excluded from the problem, as they are purely volume-based objectives, focusing exclusively on the pollution-based objectives. However, the drawback of this approach is that by not penalizing overflow volume, the MPC may allow overflows in situations where pollutant loads are low, as their associated cost in the optimisation would also be minimal.
- A great contributor to their high computation time is the need of solving a non-linear optimisation problem. More specifically:
  - For NPMPC, the equality constraint in Equation 8.18e, shown below, is a quadratic equality constraint. This type of non-convex equality constraint poses additional challenges for solver convergence. Although modern solvers are continually improving, handling such constraints remains a complex and demanding task.

$$U_{C(k)} = \sqrt{U_{C(k-1)}^2 X(k-1)^2 + U_{C_{in}(k-1)}^2 (1 - X(k-1)^2)}$$

  - SNPMPC faces a similar issue, where the main challenge in the formulation is in Equation 9.32c and Equation 9.32f.
  - The problem could be approximated or reformulated to reduce computational cost, as well different solvers could be used for more efficiency in the calculation [161]. For example, in [162, 163], a relaxation of equality constraints is proposed to soften the restrictions.
- Finally, the prediction horizon also influences the computation as it increases the size of the matrices, turning the problem more dense. A suggestion is adding the prediction as a parameter within the sensitivity analysis and include it in the Genetic Algorithm to find a suitable prediction horizon without reducing performance. Thus, the GA could be reformulated to find the smallest possible value for the prediction while also maintaining the effectiveness of MPC. Furthermore, transport delay compensation could also be used to reduce the prediction horizon [17].

In general, the linear methods do not encounter the same computational limitations, making them well-suited for wastewater systems with a significantly larger number of storage units, while still improving the performance of the network. Such situation reinforces the potential of using a multi-layer approach, as it will be discussed in the next chapter. In the next section, the MPCs are evaluated in a short simulation to check their impact on Urban Drainage System 3.

10.3.2 Comparison of MPC Methods

A quick simulation was performed to analyse the impact of each MPC, between June 29th and July 2nd, 2024. Initially, the weights for the MPC methods were determined using GA, with the exception of VMPC, which had already been satisfactorily tuned in previous projects. For Urban Drainage System 3,

no dedicated sensitivity analysis was carried out. Tuning this network proved particularly challenging, as the GA was executed without an initial guess, requiring the algorithm to search broadly for a suitable set of weights. The resulting weight configurations for each MPC are presented in Figure 10.14, corresponding to the optimisation period.

Table 10.14: Comparison of results for Urban Drainage System 3.

Metric	Static control	VMPC	PWMPC	NPMPC	SVMPC	SPWMPC	SNPMPC
$Q_{\text{ov}_{\text{total}}}$	38.069	37.473	36.821	43.848	38.322	38.527	40.023
$\%\mathbf{F}_Q$		**-1.57%**	**-3.28%**	**15.18%**	**0.66%**	**1.2%**	**5.13%**
$m^{\text{NH}_4}_{\text{ov}_{\text{total}}}$	6.797	8.382	5.634	54.349	8.47	6.618	11.345
$\%\mathbf{F}_m$		**23.32%**	**-17.11%**	**699.6%**	**24.61%**	**-2.63%**	**66.91%**

In terms of load management, only PWMPC and SPWMPC demonstrated improved performance compared to static control, whereas VMPC performed better in its domain than the static approach, reducing overflow volume. In contrast, both NPMPC and SNPMPC showed significant underperformance in this scenario. These results should not be interpreted as evidence that the non-linear methods are inherently less effective, but rather as a reflection of the difficulty involved in tuning them appropriately. The computational demands of executing a full SA in combination with GA for weight optimisation were substantial, rendering the process infeasible within a reasonable timeframe for this thesis. From a development perspective, achieving acceptable performance through proper tuning could require several months of effort. This highlights a key limitation of non-linear approaches: while their potential performance is high, the complexity and cost of achieving that performance can be prohibitive.

The following chapter introduces a novel strategy designed to address the main challenges related to the feasibility of non-linear methods and the impact of uncertainties in urban drainage systems.

11 Multi-layer Model Predictive Control

The continuous operation of the UDS is imperative to maintain stability and proper functioning. The static control can achieve the required level of stability, but with climate change and population growth, the demand on the wastewater system is steadily increasing, which the static control was not designed to cope with. Developing and implementing MPC proved to be a great alternative to a cost-effective solution that improves management using a global optimisation algorithm. Between the MPC methods discussed in this research, the non-linear algorithms, i.e. NPMPC and SNPMPC, exhibited the best overall performance to reduce overflow load and the operation of the UDS stable. However, one limiting factor that is not yet discussed is the feasibility of non-linear optimisation. As exhaustively discussed, non-linear MPC methods are prone to convergence issues, which can be caused by various conditions, such as discontinuity in state variables leading to wrong assumptions by the estimated inflow or load, oversimplification of the model which misses important dynamic behaviours of the system or discrepancies between MPCs internal model and the actual system.

Convex optimisation methods, which include VMPC, PWMPC, SVMPC and SPWMPC, are naturally easier to solve and guarantee to have a solution for every control loop. In certain conditions, it is preferable to use the non-linear methods, however when a failure is inevitable, linear method can keep the operation stable and ongoing, maintaining a good performance. Consequently, this thesis proposes a novel approach that combines the strong performance of non-linear MPC methods with the continuous operation of linear MPC, using the latter as a backup strategy for when infeasibility occurs with NPMPC or SNPMPC. In the first section, the feasibility of NPMPC and SNPMPC is investigated in detail to understand the causes and what effects these behaviours have on the system.

11.1 Feasibility of Non-linear MPC Strategies

This section examines the feasibility issues encountered with non-linear methods, explores their underlying causes, and ends proposing a solution to ensure continuous operation: Multi-Layer Model Predictive Control (ML-MPC). Therefore, the feasibility of NPMPC and SNPMPC is analysed for Urban Drainage System 1 and 2, both studied in the previous chapter, to assess their operational performance.

The first analysis conducted verifies the number of infeasible solutions in a simulation for each UDS, while also discussing the underlying causes of the infeasibility, starting with the Urban Drainage System 1. The chosen period is exactly the same as that evaluated in Section 10.1.2, which had a total of 65513 iterations. In Figure 11.1 the infeasible solutions for NPMPC are shown in a stepwise graph, where 1

indicates an infeasible solution. Although the graph alone does not allow for precise quantification, it indicates that infeasibilities occur with some regularity, whereas the visual density provides a general sense of their frequency. In total, there were 763 infeasible solutions, representing 1.16% of the total number of iterations.

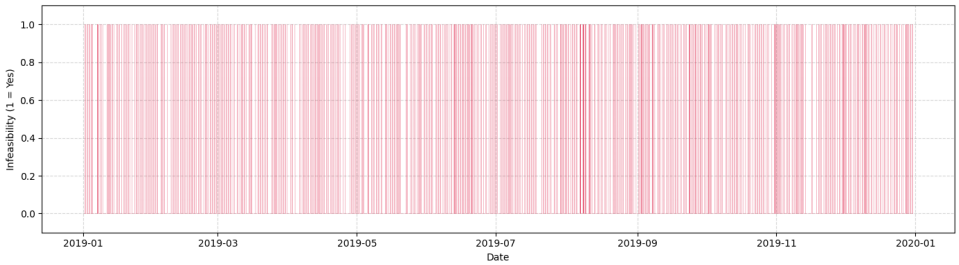

Figure 11.1: Feasibility instances for NPMPC.

SNPMPC under the same scenario shows a similar pattern, as seen in Figure 11.2, with the stochastic controller yielding 921 infeasible solutions, representing 1.4% of the total iterations. This is a slightly worse outcome than the deterministic method, which is expected given the increased complexity of the optimisation problem in SNPMPC.

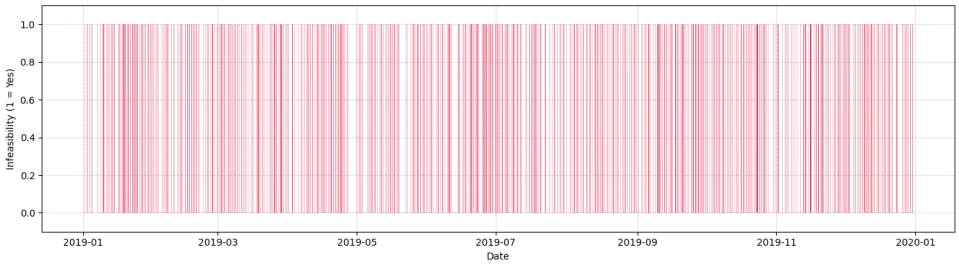

Figure 11.2: Feasibility instances for SNPMPC.

A second analysis is conducted for both NPMPC and SNPMPC, this time considering the scenario with volume uncertainty. For NPMPC, the number of infeasible instances increased significantly, reaching 3,927 cases, approximately 6% of the total iterations. Figure 11.3 illustrates the temporal distribution of these infeasible solutions, showing a denser pattern due to the elevated frequency of infeasibility.

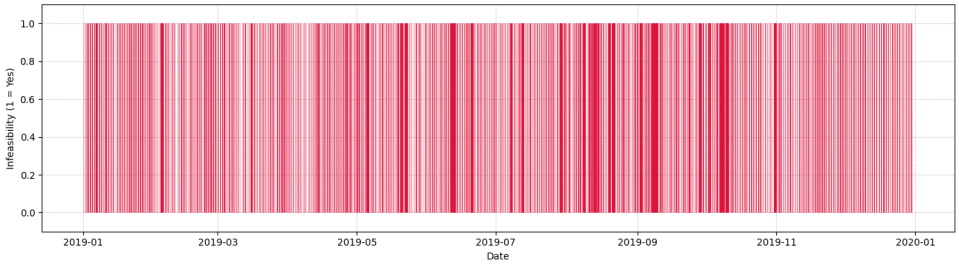

Figure 11.3: Feasibility instances for NPMPC with uncertainty $u_p = 50\%$ and $u_{\text{off}} = -50\%$.

Finally, in the scenario using SNPMPC including uncertainties, the number of infeasible solutions increases considerably, resulting in 23,081 instances, which is equivalent to 35.2% of all iterations. As shown in Figure 11.4, the graph becomes considerably denser, highlighting the alarming frequency of infeasibility under these conditions.

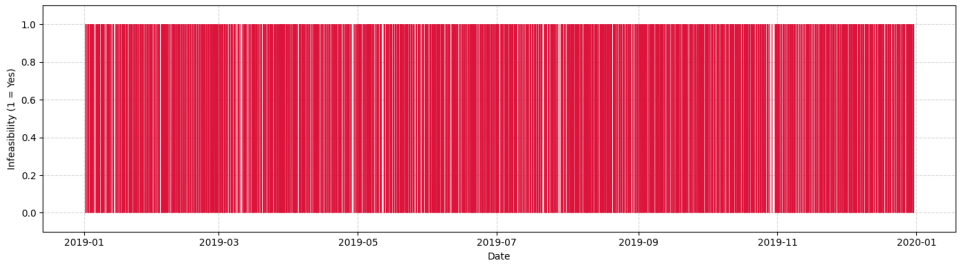

Figure 11.4: Feasibility instances for SNPMPC with uncertainty $u_p = 50\%$ and $u_{\text{off}} = -50\%$.

A comparison of the outflow from SU2 using NPMPC and SNPMPC, both with and without uncertainty, is carried out to evaluate the optimal control behaviour. In Figure 11.5, the outflows for both scenarios are shown on the left y-axis, while instances of infeasibility are indicated on the right y-axis. The results reveal that, under uncertainty, the outflow becomes significantly more oscillatory. These oscillations coincide with periods of increased infeasibility, suggesting that the introduced uncertainties are shrinking the feasible region of the optimisation problem or even turning it infeasible. The resulting control variability appears to be a consequence of the solver struggling to maintain feasibility under disturbed conditions.

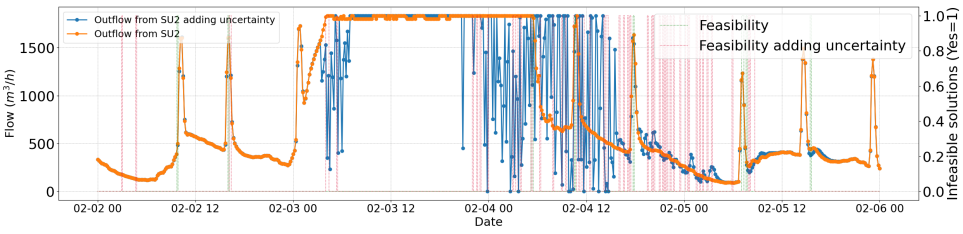

(a) Outflow comparison between for NPMPC.

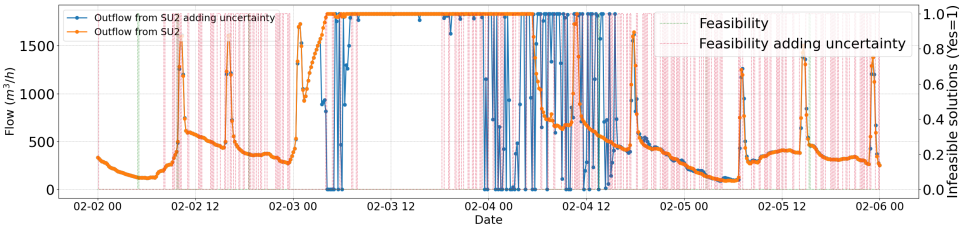

(b) Outflow comparison between for SNPMPC.

Figure 11.5: Outflow comparison (left y-axis) of controllers with and without uncertainties, including feasible solutions for uncertain scenario (right y-axis).

The same principles are applied to Urban Drainage System 2, for the scenarios utilising either NH_4^+ or COD as the controlled pollutant (Section 10.2.1). In Figure 11.6 are shown the instances of feasible

solutions during the 1-year period simulated for NH_4^+ which, for a total of 105401 simulation steps, displayed 3796 infeasible solutions, constituted 3.6%.

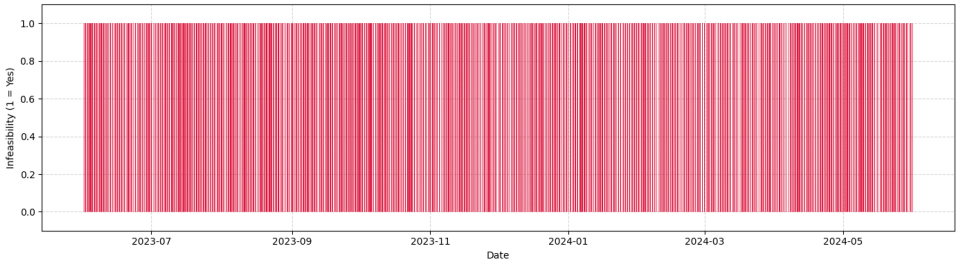

Figure 11.6: Feasibility instances for NPMPC with NH_4^+ as controlled pollutant.

The analysis is also performed for COD, which totalled 8414 infeasible solutions, thus representing approximately 8%. The tuning of NPMPC controlling COD proved to be a challenging task, although the performance was satisfactory. But the number of infeasible solutions is quite high, suggesting that the performance can still be improved.

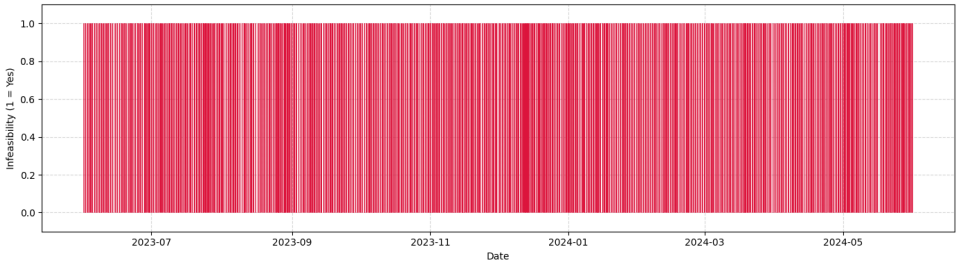

Figure 11.7: Feasibility instances for NPMPC with COD as controlled pollutant.

The results for SNPMPC are the following: 1780 and 1864 infeasible solutions controlling NH_4^+ and COD, respectively, corresponding to a 1.7% and 1.8%, as can be seen in Figure 11.8 and Figure 11.9. For Urban Drainage System 2, SNPMPC showed more stability, interestingly, it also had the worst performance. Here, the discussion is more related to the complexity of the optimisation problem, where NPMPC exhibited many issues solving the quadratic equality constraint in Equation 8.18e, specially with COD as the controlled variable.

Tuning the control parameters requires careful consideration, as the non-linear constraint can become a performance bottleneck for NPMPC. A recommended approach is to begin the sensitivity analysis, which might include other outputs such as the infeasibility, or the computation time, providing a better knowledge of how those outputs are affected by the various parameters. This analysis can help identify parameter ranges where the solver operates more reliably. However, the issue with such an approach is that feasibility is also directly related to uncertainty and it is difficult to cover all possible scenarios. Designing the controller around a worst-case uncertainty may improve its stability but could significantly compromise its effectiveness due to drastic conservative assumptions.

Another possible solution is to take advantage of the continuous operation of linear methods and combine it with the performance of non-linear methods. The next section introduces ML-MPC, a new algorithm

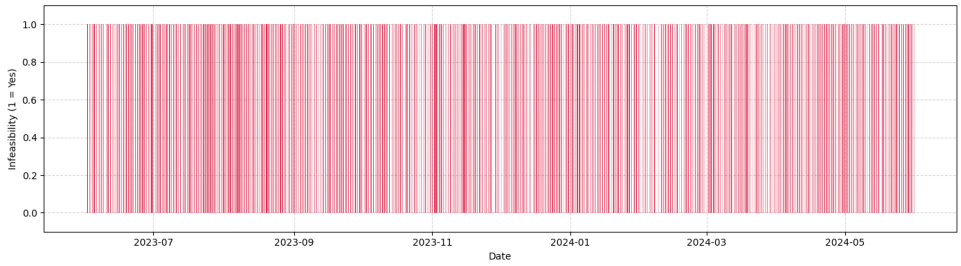

Figure 11.8: Feasibility instances for SNPMPC with NH_4^+ as controlled pollutant.

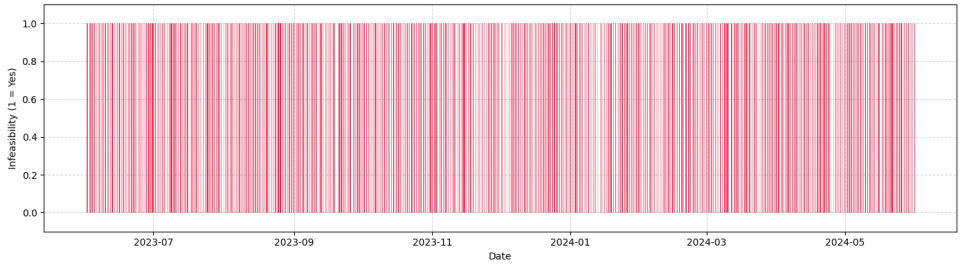

Figure 11.9: Feasibility instances for SNPMPC with COD as controlled pollutant.

that combines several MPC methods into a single strategy, with the aim of maintaining the operation of the UDS with great performance and continuity.

11.2 Multi-layer Model Predictive Control

The ML-MPC is developed to improve the performance of non-linear methods by providing a Fallback Strategy (FBS) when the optimisation fails to converge. The aim is, considering that non-linear methods are susceptible to infeasible solutions, the multi-layer strategy maintains operation by applying the solution of a linear optimisation problem that is solved during the control loop in parallel. The FBS is where the main contribution lies, hence, different strategies are investigated to converge to a single solution.

11.2.1 Literature Review

As urban drainage systems scale in size and complexity, a single centralised MPC can become difficult to compute and implement. In the literature, a multi-layer controller refers to hierarchical control structures that decompose the problem into different levels (spatially or temporally) to manage complexity [164]. In practice, this might mean an upper-level supervisory MPC that optimises high-level objectives (e.g., distribution of flows or storage usage across the whole city) and lower-level regulators that apply detailed control at local level (e.g. PID controllers or local MPC for each pump or gate). The literature suggests that spatial decomposition (dividing the network into zones or subsystems) combined with time-scale decomposition (using longer horizons/coarser control for slow phenomena and shorter horizons for fast local control) is important for operationalising MPC in large systems [13]. For example, an upper layer

might compute optimal storage set-points for each basin every 30 minutes, while lower layers continuously adjust valves to track those targets.

One documented approach is a two-layer scheme in which a global MPC (solving a network-wide volume optimisation) provides flow set points and local rule-based controllers in storage units modulate flows based on pollutant concentrations. This kind of hybrid hierarchy can exploit the strengths of both layers, the global layer ensures coordination to prevent flooding, while local layers can react quickly to water quality conditions (such as holding water until pollutant levels subside) [11]. The only paper identified with the nomenclature "Multi-layer MPC" has been explored for drinking water systems, controlling upper and lower-level systems under one optimisation framework [165]. However, the literature review did not indicate any existing implementation that integrates linear and non-linear MPC strategies within a layered framework. As such, the approach introduced in this work represents a novel contribution. The following sections provide a detailed description of the proposed ML-MPC method.

11.2.2 Fallback Strategy 1 - FBS1

The first strategy presented is a straightforward fallback mechanism that uses both a linear and a non-linear MPC, switching between them whenever the non-linear solution becomes infeasible or its computation time exceeds the control loop interval. This approach is illustrated in Figure 11.10, which outlines two independent strategies: a deterministic multi-layer setup combining PWMPC and NPMPC, and a stochastic version combining SPWMPC and SNPMPC, which is called Stochastic Multi-Layer Model Predictive Control (SML-MPC). In both cases, the switching logic is the same: at each control step, the algorithm runs both MPCs in parallel. If the non-linear MPC successfully finds a feasible solution within the required time, its control action is applied (path **AC**). If the non-linear solver fails or exceeds the time limit, the controller applies the linear MPC output instead (path **BC**), ensuring uninterrupted operation.

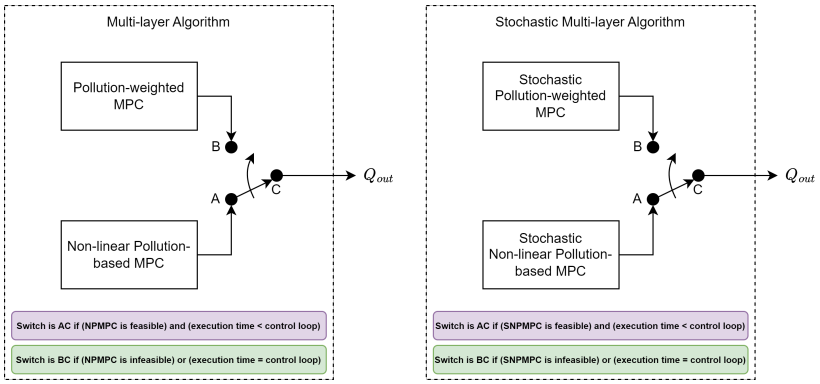

Figure 11.10: Diagram for Fallback strategy 1: Multi-layer and Stochastic Multi-layer.

11.2.3 Fallback Strategy 2 - FBS2

The second strategy is an extension to the first, where the volume-based approaches are added to the multi-layer. The advantage of using pollution-based methods is the ability to reduce the load using the

estimated concentration to inform MPC where the highly contaminated water is. However, in situations where this estimate is not reliable, the volume-based method can be used as a backup. Here, the proposed solution, as shown in Figure 11.11, is to incorporate a metric to calculate the quality of the concentration estimation.

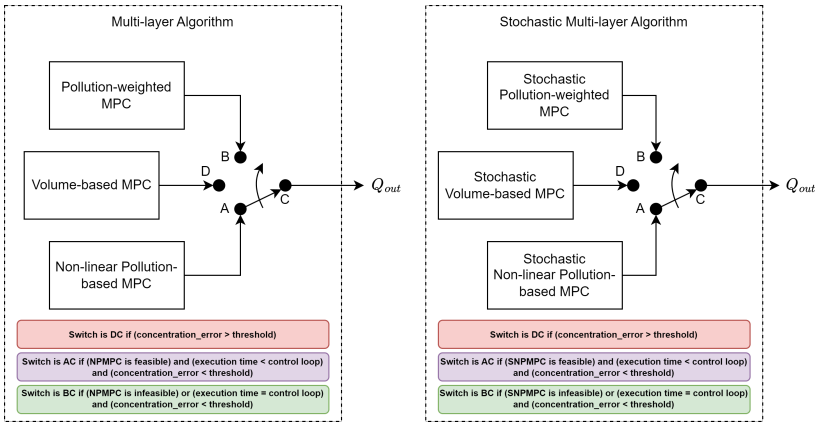

Figure 11.11: Diagram for Fallback strategy 2: Multi-layer and Stochastic Multi-layer.

The strategy incorporates a digital twin of the urban drainage system, running in parallel to continuously monitor the current state of the network in a virtual environment. This digital twin enables real-time comparison between the estimated pollutant concentrations and those calculated by the twin itself. Assuming that the digital twin accurately reflects the system behaviour, any significant deviation suggests potential inaccuracies in the estimation. To manage this, a predefined error threshold is established. When the discrepancy exceeds this threshold, the system switches to path **DC**, activating VMPC as a fallback control strategy. There are two additional challenges with this approach, modelling the digital twin and defining the threshold for the concentration error.

11.2.4 Fallback Strategy 3 - FBS3

The final strategy presented in this research combines deterministic and stochastic MPC into a unified control approach. To enable switching between the two, the system continuously monitors an additional variable: the volume of the storage units. As shown in the uncertainty analysis in Chapter 9, when volume disturbances exceed a certain level, the stochastic MPC becomes a more robust option to mitigate the effects of uncertainty on control performance. By comparing volume estimates from the digital twin with field measurements, the system calculates the error between the model and reality. When this error exceeds a defined threshold, the strategy triggers a switch to **path $\mathbf{E_s}$**, as illustrated in Figure 11.12.

This strategy introduces additional challenges. For instance, the stability of the control signal, particularly given that the multi-layer architecture involves **three** switching mechanisms. Moreover, implementing this approach requires the definition of an additional threshold, further complicating the parametrisation process. In total, six MPC methods must be tuned, significantly increasing the complexity. While this solution is ambitious and computationally intensive, it integrates the advantages of all MPC methods proposed in this research. The following sections present selected scenarios for each of the ML-MPC strategies.

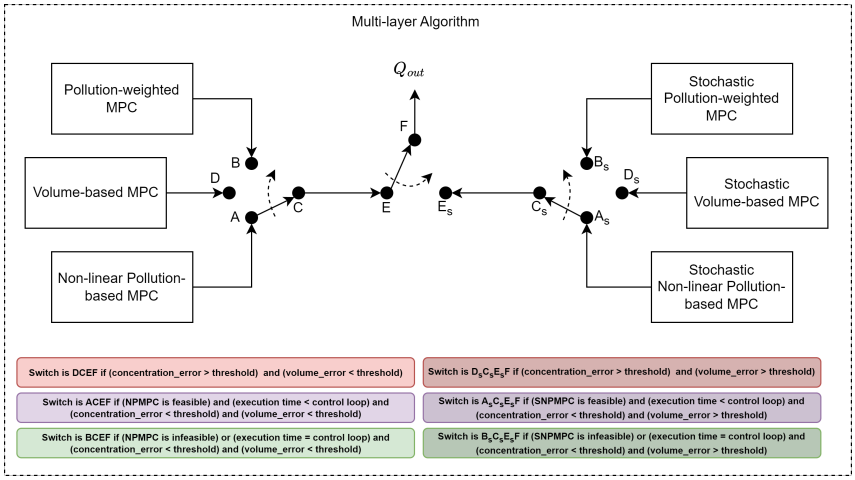

Figure 11.12: Diagram for Fallback strategy 3: Multi-layer and Stochastic Multi-layer.

11.3 Scenario 1 - Fallback Strategy 1

The first scenario is a combination of ML-MPC with FBS1 applied to Urban Drainage System 1 as the controlled target system. Here, both simulations realised in 10.1.2 with and without added uncertainties are studied, for the same 1-year period. Again, four metrics are analysed, the relative overflow volume and load (R_{V} and R_{m}) and the absolute overflow volume and load ($Q_{\mathrm{ov_{total}}}$ and $m_{\mathrm{ov_{total}}}$). The main performance indicator is whether the use of ML-MPC improves the performance of non-linear methods and/or how the performance is against the linear methods individually. The results are shown in Figure 11.15.

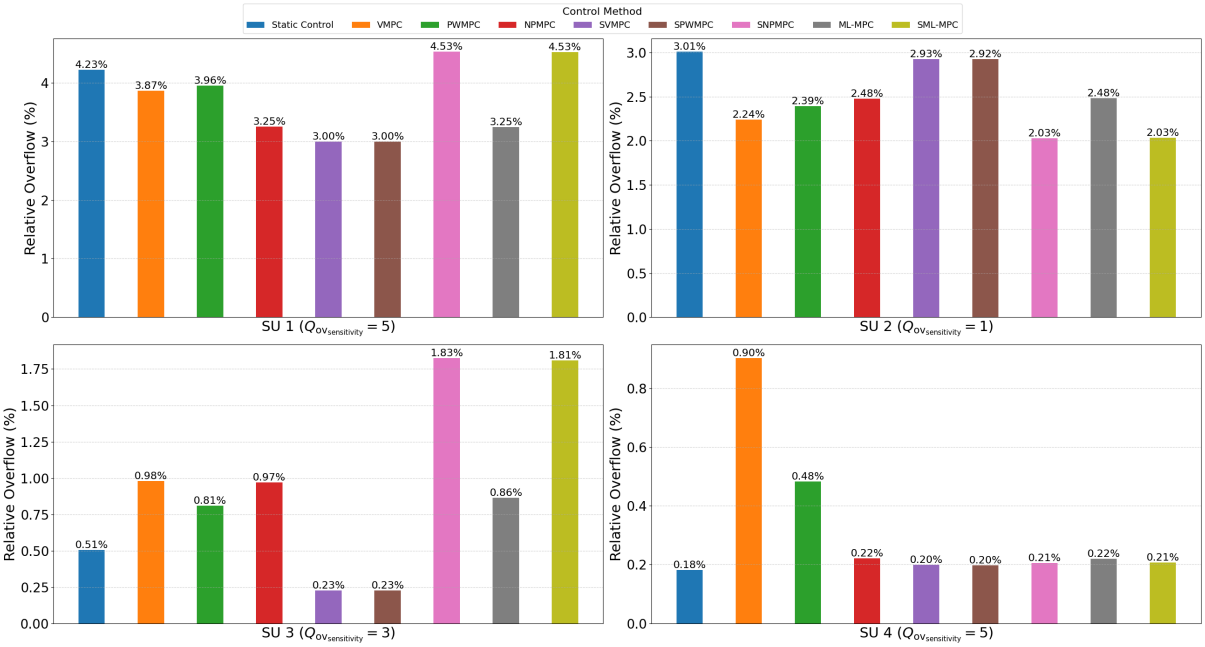

Figure 11.13: R_{V} - Relative Overflow Volume %.

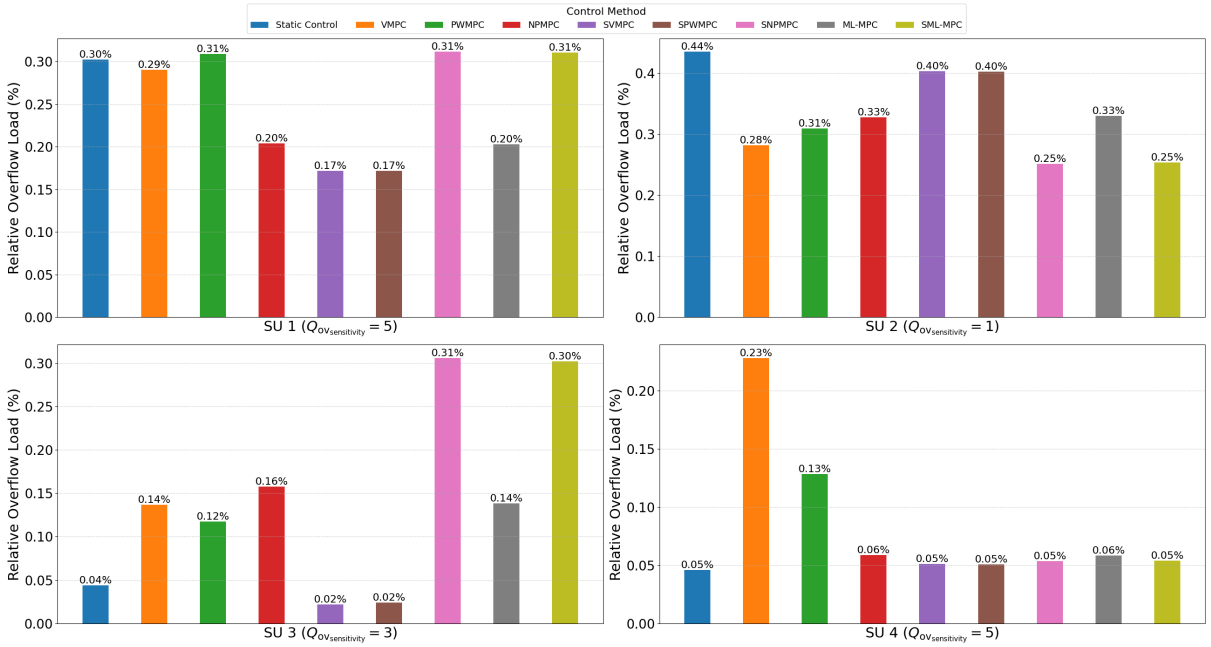

Figure 11.14: R_{m} - Relative Overflow Load %.

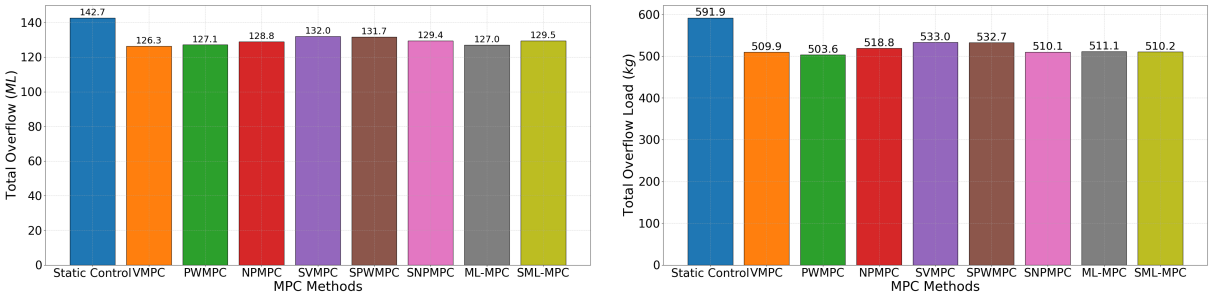

(a) $Q_{\mathrm{ov_{total}}}$ - Total Overflow Volume in ML.

(b) $m_{\mathrm{ov_{total}}}$ - Total Overflow load in kg.

Figure 11.15: ML-MPC and SML-MPC - Urban Drainage System 1 - Absolute overflow comparison of MPC without additional uncertainty.

Comparing NPMPC with ML-MPC for R_{V} and R_{m}, the performance of both controllers is very similar, with ML-MPC presenting a slight advantage in SU3, which is true also for SNPMPC and the SML-MPC. The total overflow analysis shows a modest 2% improvement of ML-MPC over NPMPC, while the difference between SML-MPC and SNPMPC is negligible. Although the results are positive, the feasibility analysis indicates that the baseline methods were already sufficiently stable in this scenario, with relatively few infeasible instances—approximately 1.2% for NPMPC and 1.4% for SNPMPC. In the next scenario, which introduces more uncertainty, the frequency of infeasible solutions increases significantly, therefore, higher performance improvements are expected.

Therefore, both multi-layer strategies are also simulated with volume uncertainty considering $u_p = 50\%$ and $u_{\mathrm{offset}} = -50\%$, and the outcome can be seen in Figure 11.18. The comparison between ML-MPC and NPMPC shows that the multi-layer improved the performance considerably for the SUs with higher $Q_{\mathrm{ov_{sensitivity}}}$ (SU1, SU3 and SU4), to the cost of increasing significantly the overflow at SU2. This change in

behaviour increased $Q_{\mathrm{ov}_{\mathrm{total}}}$ and $m_{\mathrm{ov}_{\mathrm{total}}}$ extensively for ML-MPC. Furthermore, the stochastic multi-layer showed a more balanced performance compared to SNPMPC, although the total overflow load increased by 2.6%, the relative load overflow is more balanced between the SUs with higher $Q_{\mathrm{ov}_{\mathrm{sensitivity}}}$.

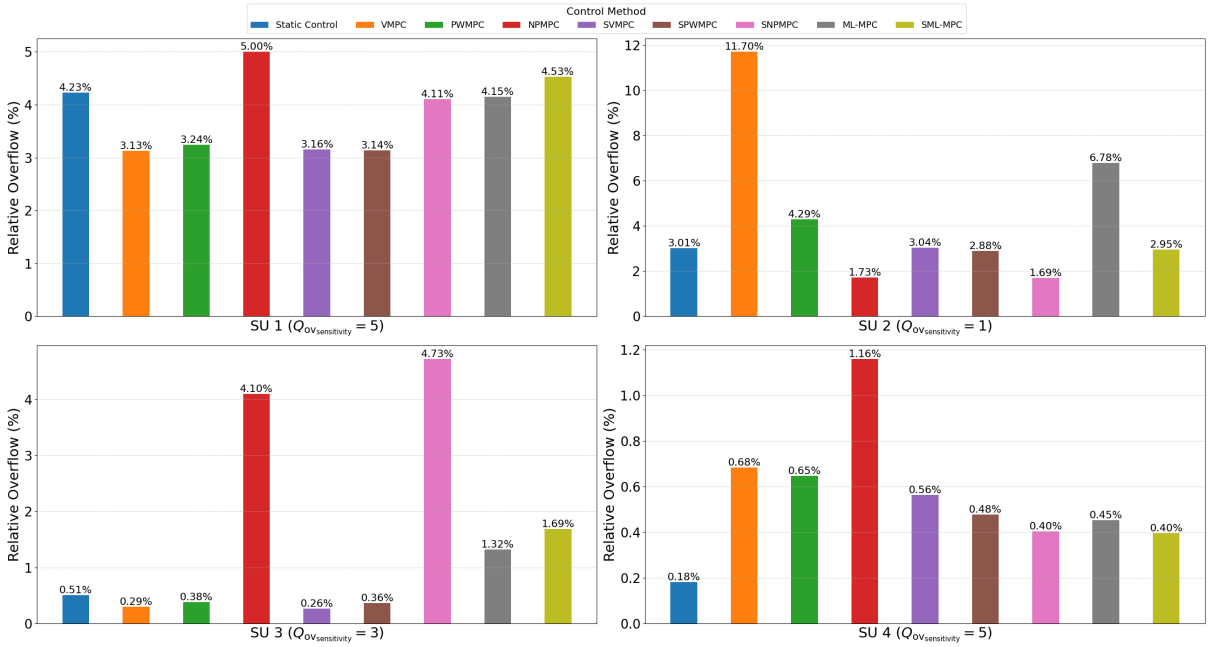

Figure 11.16: R_{V} - Relative Overflow Volume %.

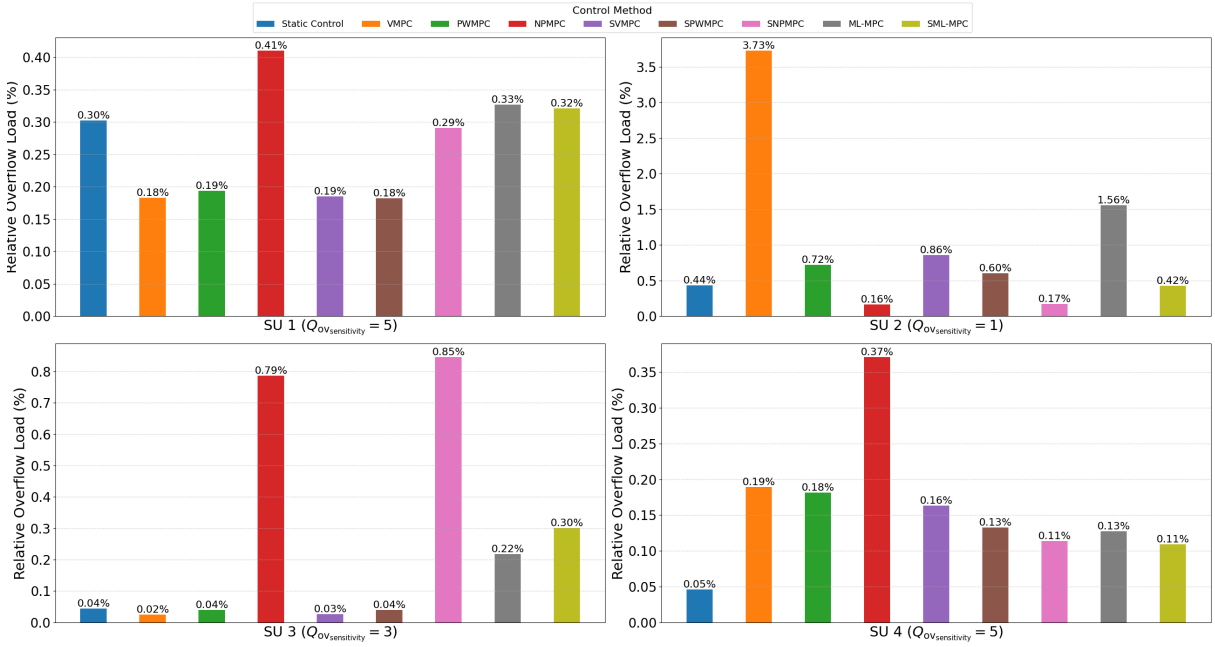

Figure 11.17: R_{m} - Relative Overflow Load %.

While the multi-layer algorithm clearly improves performance, its added complexity may not be fully justified when compared to the simplicity and strong results achieved by linear methods. Although ML-MPC arguably offers the most balanced performance across both scenarios, it comes at the expense of

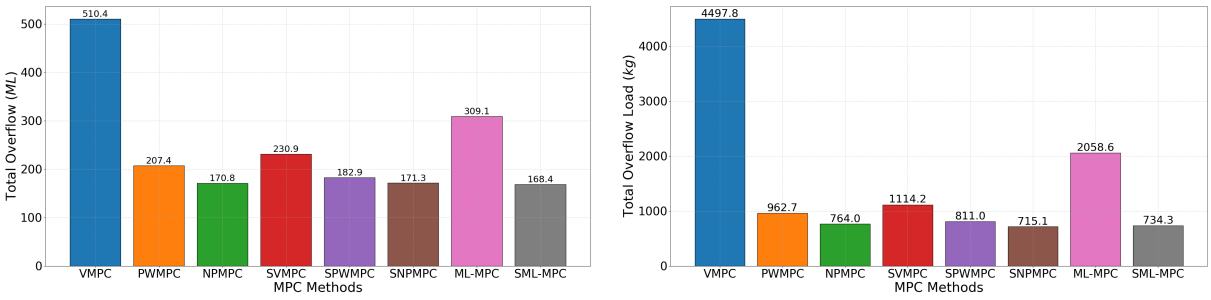

(a) $Q_{\mathrm{ov}_{\mathrm{total}}}$ - Total Overflow Volume in ML.

(b) $m_{\mathrm{ov}_{\mathrm{total}}}$ - Total Overflow load in kg.

Figure 11.18: ML-MPC and SML-MPC - Urban Drainage System 1 - Absolute overflow comparison of MPC with additional uncertainty.

tuning difficulty and high computational demands, often matching or even exceeding the execution time of non-linear approaches.

Nevertheless, the strategy is further evaluated on Urban Drainage System 2 under both NH_4^+ and COD control scenarios. The first analysis focuses on NH_4^+, with results presented in Figures 11.19, 11.20 and 11.21.

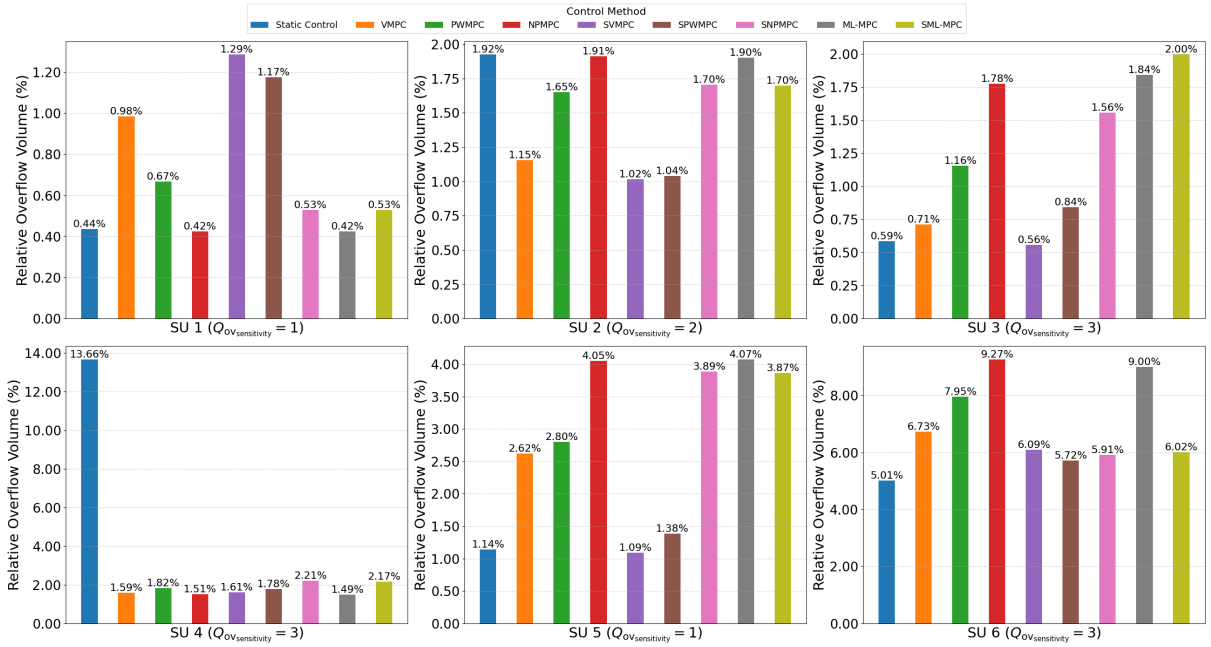

Figure 11.19: R_{V} - Relative Overflow Volume % with NH_4^+ as pollutant indicator.

A comparison between the multi-layer approaches (ML-MPC and SML-MPC) and their corresponding baseline methods (NPMPC and SNPMPC) yields the following observations:

- ML-MPC improves the relative overflow of NH_4^+ at SU4 and SU6;
- It performs worse at SU3 and SU5, and increases the absolute overflow of NH_4^+;

- SML-MPC improves the relative overflow of NH_4^+ at SU2, SU4 and SU6;
- It shows worse relative performance at SU3 but improves the absolute overflow of NH_4^+.

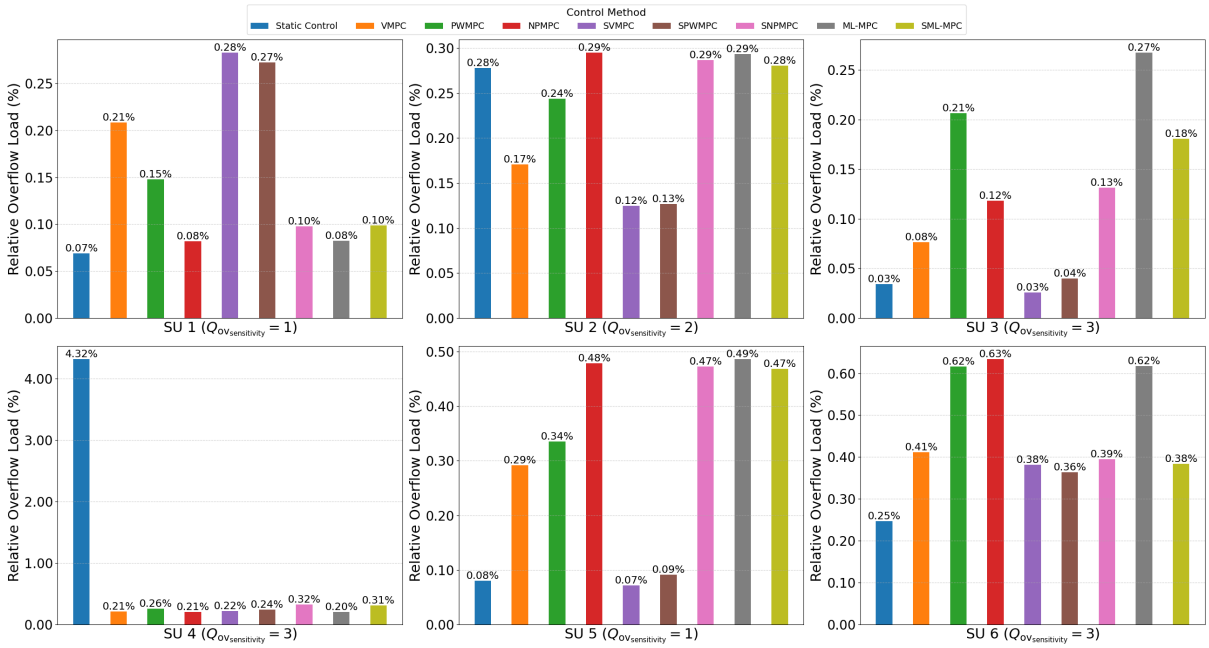

Figure 11.20: R_m - Relative Overflow Load % with NH_4^+ as pollutant indicator.

Given that $Q_{ov_{sensitivity}}$ is highest for SU3, SU4, and SU6, both multi-layer methods offer improvements in relative overflow reduction. Notably, SML-MPC also reduces the total absolute overflow of NH_4^+. However, since NPMPC already achieved strong performance—despite some infeasible instances—the fallback to PWMPC in the multi-layer setup did not result in significant additional gains.

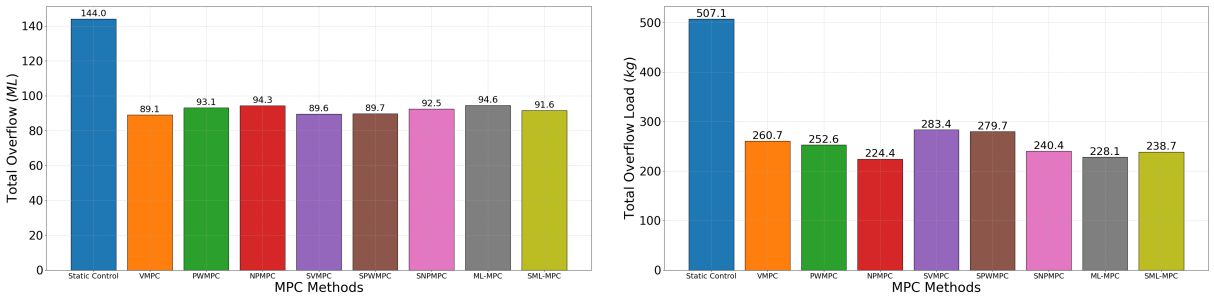

(a) $Q_{ov_{total}}$ - Total Overflow Volume in ML. *(b)* $m_{ov_{total}}$ - Total Overflow load in kg.

Figure 11.21: Urban Drainage System 2 - Comparison of MPC in terms of total overflow volume and load with NH_4^+ as pollutant indicator.

The final scenario presented for FBS1 focuses on the control of COD in Urban Drainage System 2, with the results illustrated in Figures 11.22, 11.23 and 11.24. The analysis of the bar graph yields the following observations:

- ML-MPC improves relative overflow reduction at SU3, SU4, and SU6;

- It performs worse at SU5 but achieves a 1.2% reduction in m_{ovtotal};
- SML-MPC improves relative overflow reduction at SU2, SU3, SU4, and SU6;
- It performs worse at SU5, yet shows a more significant improvement of 9.6% in $m_{\text{ov}_{\text{total}}}$.

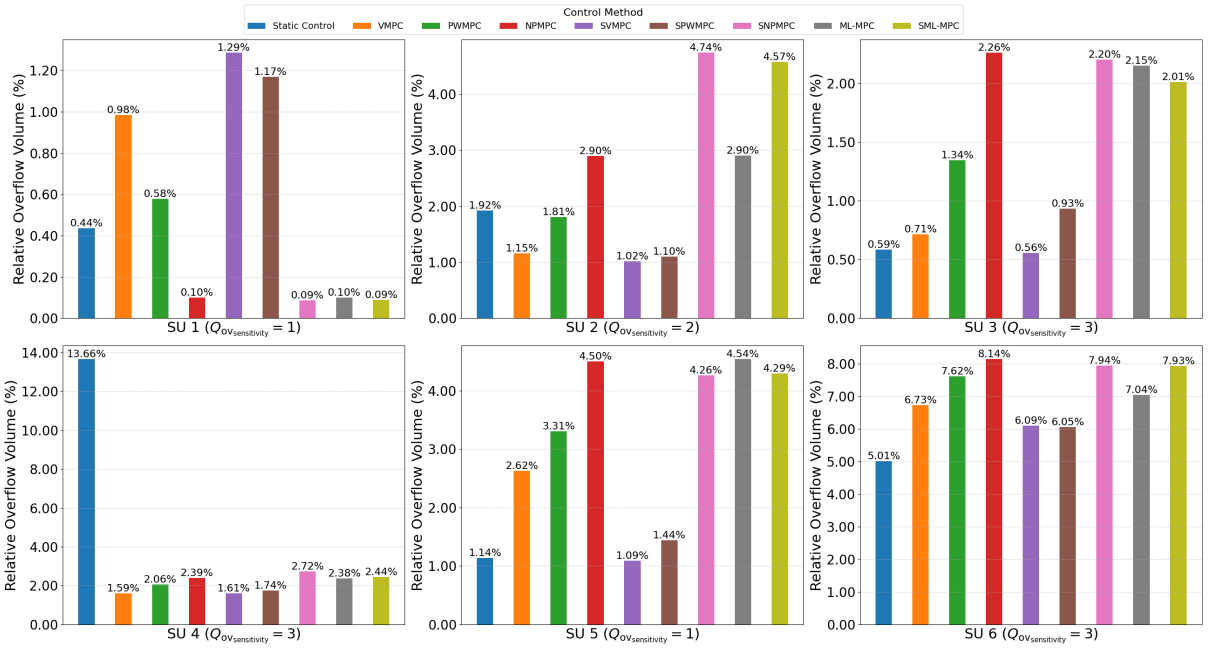

Figure 11.22: R_{V} - Relative Overflow Volume % with COD as pollutant indicator.

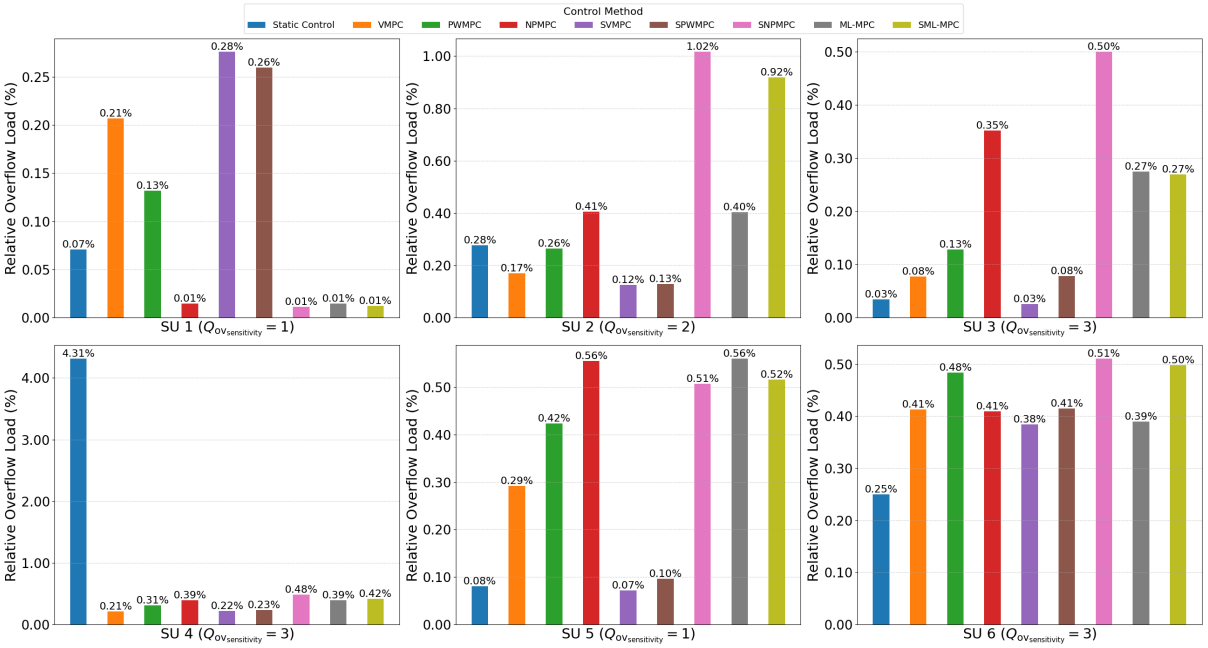

Figure 11.23: R_{m} - Relative Overflow Load % with COD as pollutant indicator.

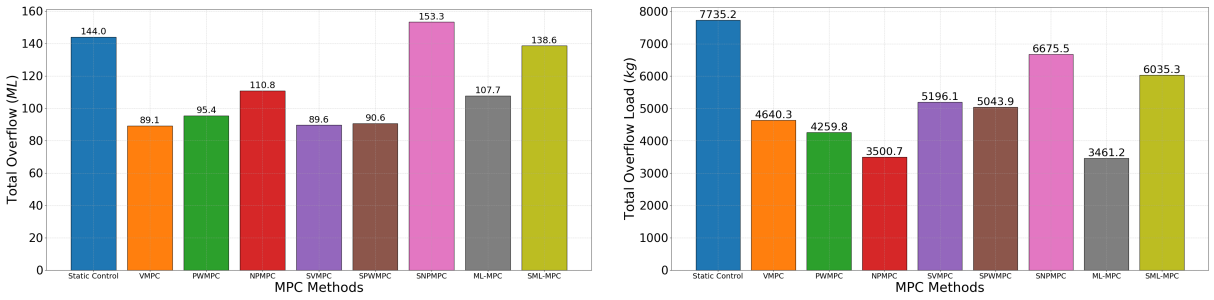

(a) $Q_{\text{ov}_{\text{total}}}$ - Total Overflow Volume in ML.

(b) $m_{\text{ov}_{\text{total}}}$ - Total Overflow load in kg.

Figure 11.24: Urban Drainage System 2 - Comparison of MPC in terms of total overflow volume and load with COD as pollutant indicator.

In this scenario, the improvements, particularly with SML-MPC, are more pronounced, reinforcing the potential of the multi-layer strategy. However, despite these gains, SML-MPC did not outperform all other methods. ML-MPC achieved the best overall reduction in total overflow, while SPWMPC showed superior relative performance for storage units with high $Q_{\text{ov}_{\text{sensitivity}}}$.

The main conclusion is that both multi-layer strategies based on FBS1 enhance the performance of the non-linear methods. The critical factor, however, lies in how degraded the original performance is, since there is a limit to how much the multi-layer approach can compensate. Although this threshold is not easily measurable, it is recommended to apply the multi-layer methods in scenarios where NPMPC or SNPMPC already perform comparably (10% worse, for instance) to or better than their linear counterparts.

11.4 Scenario 2 - All Fallback Strategies

Finally, the fallback strategies FBS1, FBS2, and FBS3 are evaluated under a new scenario designed to assess the performance of each multi-layer algorithm at varying levels of uncertainty. In this case, a volume uncertainty is introduced in Urban Drainage System 1 by fixing $u_p = 0\%$, while u_{off} is varied over a one-year simulation. Specifically, u_{off} decreases by 10% every two months, starting from -10%, resulting in five periods with the settings as in Table 11.1. This uncertainty pattern is applied uniformly to all SU, although, in reality, uncertainties may differ across the network. In this scenario, each individual MPC method is tested, together with all multi-layer strategies, considering a threshold error of 50% for both concentration and volume in FBS2 and FBS3.

Name	Time-frame	u_{off} value
Period 1	01/01/2025 to 01/03/2025	-10
Period 2	01/03/2025 to 01/05/2025	-20
Period 3	01/05/2025 to 01/07/2025	-30
Period 4	01/07/2025 to 01/09/2025	-40
Period 5	01/09/2025 to 31/12/2025	-50

Table 11.1: Settings for multi-layer simulation.

The goal of this analysis is to understand the influence of each type of fallback strategy depending on the level of uncertainty. In table By gradually increasing the uncertainty, the threshold for FBS2 and FBS3 is more easily achieved. Thus, the overflow load for each MPC is analysed, and a heatmap is created to classify the methods to facilitate the interpretation of the results, as shown in Table 11.2, which shows R^i_{m}, where i represents the i-th storage unit, and $m^{\mathrm{NH_4}}_{\mathrm{ov_{total}}}$ in each period, for each MPC strategy. Each numerical entry is colour-coded according to its magnitude within its respective row. The colouring follows a diverging scale, ranging from dark green for the lowest overflow value in the row to dark red for the highest. Intermediate shades transition to green, yellow, and orange, indicating progressively higher values. This row-wise normalisation ensures that the colours reflect the comparative performance of the control strategies for each specific metric, rather than their absolute magnitudes, enabling straightforward visual identification of the best and worst outcomes in each case. Recall that for individual SUs, the priority is to reduce overflows at SU1 and SU4.

Table 11.2: Heatmap comparing R^i_{m} (%) and $m^{\mathrm{NH_4}}_{\mathrm{ov_{total}}}$ (kg) for each MPC strategy.

		VMPC	PWMPC	NPMPC	SVMPC	SPWMPC	SNPMPC	ML-MPC FBS1	SML-MPC FBS1	ML-MPC FBS2	SML-MPC FBS2	ML-MPC FBS3
Period 1	R^1_{m}	0.0700	0.0701	0.0766	0.0000	0.0000	0.1489	0.0872	0.1485	0.0631	0.0000	0.0612
	R^2_{m}	0.6629	0.8143	0.4042	0.5353	0.5353	0.2925	0.4161	0.2927	0.6107	0.5356	0.5629
	R^3_{m}	0.0103	0.0180	0.2182	0.0000	0.0000	0.4074	0.2375	0.3992	0.0706	0.0001	0.0362
	R^4_{m}	0.0162	0.0153	0.0231	0.0149	0.0156	0.0180	0.0211	0.0180	0.0187	0.0154	0.0186
	$m^{\mathrm{NH_4}}_{\mathrm{ov_{total}}}$	102.217	125.667	81.574	81.33	81.358	81.588	85.037	80.905	99.585	81.393	89.451
Period 2	R^1_{m}	0.0496	0.0525	0.0439	0.0000	0.0000	0.0987	0.0449	0.0991	0.0458	0.0000	0.0000
	R^2_{m}	0.5617	24.9466	0.1569	0.2146	0.2146	0.1159	0.1519	0.1191	0.5301	0.2088	0.2087
	R^3_{m}	0.0000	0.0000	0.0990	0.0000	0.0000	0.1448	0.1149	0.1648	0.0000	0.0000	0.0000
	R^4_{m}	0.0000	0.0000	0.0119	0.0000	0.0000	0.0064	0.0111	0.0058	0.0110	0.0049	0.0051
	$m^{\mathrm{NH_4}}_{\mathrm{ov_{total}}}$	88.312	3899.566	34.473	33.517	33.517	32.515	35.058	34.771	83.948	32.877	32.868
Period 3	R^1_{m}	0.0876	0.0916	0.1421	0.0053	0.0053	0.2624	0.1424	0.2629	0.0773	0.0053	0.0053
	R^2_{m}	3.3483	87.9639	0.6197	0.7719	0.7717	0.5254	0.6259	0.5227	2.5436	0.7709	0.7704
	R^3_{m}	0.0000	0.0000	0.2820	0.0000	0.0000	0.4198	0.3100	0.4478	0.0000	0.0000	0.0000
	R^4_{m}	0.0534	0.0548	0.1051	0.0529	0.0535	0.0718	0.1061	0.0721	0.0806	0.0628	0.0626
	$m^{\mathrm{NH_4}}_{\mathrm{ov_{total}}}$	528.549	13787.172	128.561	123.626	123.603	126.235	131.617	127.92	402.937	123.984	123.848
Period 4	R^1_{m}	0.9317	0.9244	1.3834	0.9063	0.9063	1.3082	1.4018	1.3073	1.0850	1.1170	1.1356
	R^2_{m}	30.4620	126.7811	1.7819	3.0392	3.0277	1.5044	1.8235	1.5067	21.5227	2.0567	2.0744
	R^3_{m}	0.2356	0.2264	1.0417	0.2557	0.2639	1.3408	0.9267	1.2592	0.6012	0.9002	0.8866
	R^4_{m}	0.9438	0.7925	0.5009	0.5312	0.5115	0.4127	0.5009	0.4128	0.9594	0.5429	0.8781
	$m^{\mathrm{NH_4}}_{\mathrm{ov_{total}}}$	4890.905	20095.586	415.947	542.616	540.225	395.206	409.995	386.314	3497.414	447.428	466.754
Period 5	R^1_{m}	0.0695	0.0695	0.2024	0.0695	0.0695	0.1876	0.2023	0.1882	0.0719	0.0882	0.0891
	R^2_{m}	52.3328	131.5960	0.2766	0.5558	0.5504	0.2362	0.2875	0.2378	48.9807	0.3849	0.4223
	R^3_{m}	0.0089	0.0039	0.1753	0.0075	0.0044	0.1946	0.1909	0.2131	0.0386	0.1718	0.0892
	R^4_{m}	0.0990	0.0866	0.1574	0.0868	0.0890	0.1001	0.1584	0.1002	0.1105	0.0881	0.0932
	$m^{\mathrm{NH_4}}_{\mathrm{ov_{total}}}$	16110.299	40537.543	137.058	183.423	181.319	121.922	142.482	125.158	15054.073	160.242	157.727

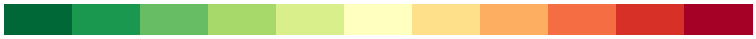

Colour scale: Dark green = lowest value in row, Dark red = highest

The heatmap reveals the following observations:

- In terms of $m^{\mathrm{NH_4}}_{\mathrm{ov_{total}}}$, VMPC, PWMPC, ML-MPC FBS1 and ML-MPC FBS2 are consistently showing the worst performance among all methods. The deterministic multi-layer methods are not performing well due to the fallback strategy switching to VMPC or PWMPC, which demonstrated a very poor performance. The uncertainty analysis has already shown that deterministic methods struggle with increased uncertainties. In contrast, stochastic methods in general performed well, specially SNPMPC and SML-MPC FBS1.

- Looking at R^1_{m}, SVMPC, SPWMPC and SML-MPC FBS2 showed the best performance across all regions. For R^4_{m}, in most regions, SVMPC and SPWMPC displayed a better result. NPMPC and ML-MPC FBS1 displayed the worst reduction for both R^1_{m} and R^4_{m} for most regions

- ML-MPC FBS3 showed a very balanced performance,performing similar to SML-MPC FBS2 for higher uncertainty levels .

Finally, the last analysis compares the results for the complete scenario, as can be seen in Figure 11.25.

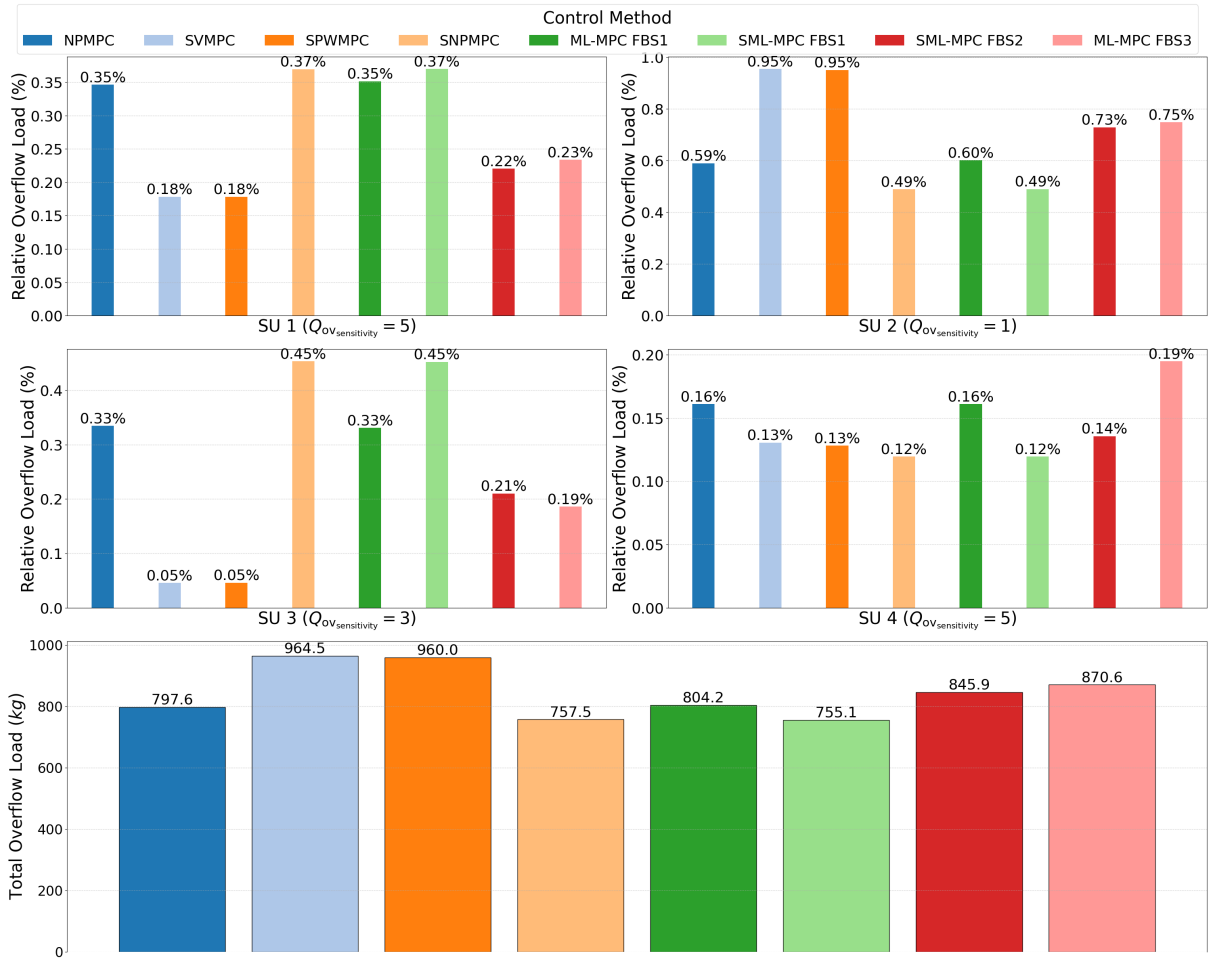

Figure 11.25: Multi-layer for full period between 01/01/2025 and 31/12/2025.

The methods with exceedingly worse performance (VMPC, PWMPC, ML-MPC FBS1) are not displayed to improve visualisation. Globally, the best performance was by SML-MPC FBS1, showing the best reduction in overflow and the best relative overflow at SU4. The evidence shows that SML-MPC FBS1 improved the performance of SNPMPC in all aspects. However, the additional layers included in FBS2 and FBS3 did not improve further the performance, demonstrating that the simplest approach indeed had the best performance.

Furthermore, the difference between NPMPC and ML-MPC FBS1 is minimal, as infeasible solutions revert to PWMPC. In this case, the multi layer's performance is slightly worse, as it is based on the

control action provided by PWMPC, which demonstrated poor performance. In Table 11.3 each multi-layer approach is shown, determining the number of times each MPC method was used during the simulation. ML-MPC and SML-MPC with FBS1 mostly used the solution provided by the non-linear methods, whereas as discussed, due to PWMPC underperforming considerably, it actually hindered the performance of ML-MPC, while SML-MPC benefitted for the consistent performance of SPWMPC.

Table 11.3: Number of times each MPC was used by each ML-MPC strategy.

	ML-MPC FBS1	SML-MPC FBS1	ML-MPC FBS2	SML-MPC FBS2	ML-MPC FBS3
VMPC	-	-	35877	-	129
PWMPC	6109	-	1623	-	0
NPMPC	59404	-	28013	-	69
SVMPC	-	-	-	36334	35931
SPWMPC	-	3663	-	798	795
SNPMPC	-	61850	-	28381	28589

The multi-layer methods using FBS2 predominantly used the volume-based methods, indicating that the concentration estimation often reached the threshold of 50% error. Looking at the performance of SML-MPC FBS2, it actually shows a compromise between the good performance of linear methods in terms of R_m for units with higher sensitivity and the better overall performance of SNPMPC in total overflow. Finally, FBS3 performed similarly to SML-MPC FBS2, although worst in all important metrics. The concentration error and volume error proved to be highly redundant, which means that when one threshold is exceeded, the other is typically reached as well. In Figure 11.26 is compared the control action between SNPMPC and SML-MPC FBS1 in Period 2, as well as which layer was used by the multi-layer in each instant.

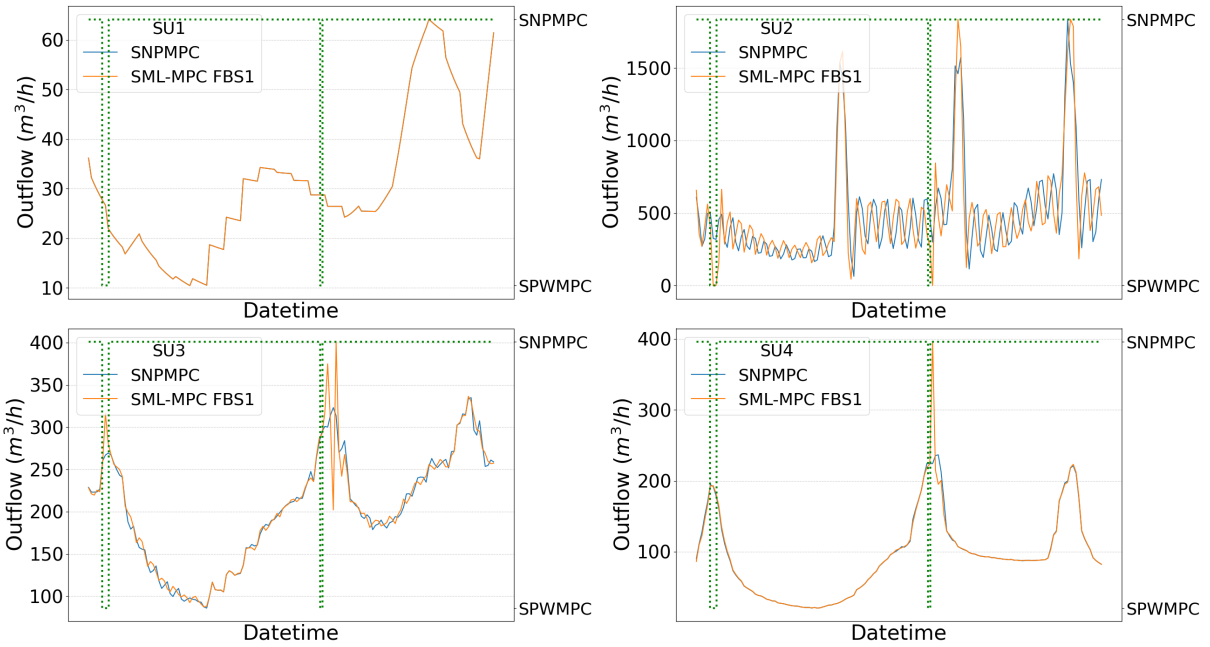

Figure 11.26: Comparison of control action (left y-axis) from SNPMPC and SML-MPC FBS1, and which layer is used (right y-axis) in Period 2.

The outflow in the multi-layer approach is generally quite stable, though it occasionally exhibits brief periods of more aggressive behaviour after changes in the layer. The peak observed in SU4 occurs when the multi-layer switches to SPWMPC due to an infeasible solution in SNPMPC. The linear method prioritises reducing overflows at SU4, and the sudden peak results from the different priorities between the layers. To achieve a more consistent behaviour across the methods, the weights of one of them could be adjusted to align with the desired outcome. A second comparison is done for SNPMPC and SML-MPC FBS2, in Figure 11.27. The graph shows a slightly different behaviour of the second fallback strategy and a more regular switching between layers. The outflow shows higher oscillations when the layers are switched, but overall the control action is stable.

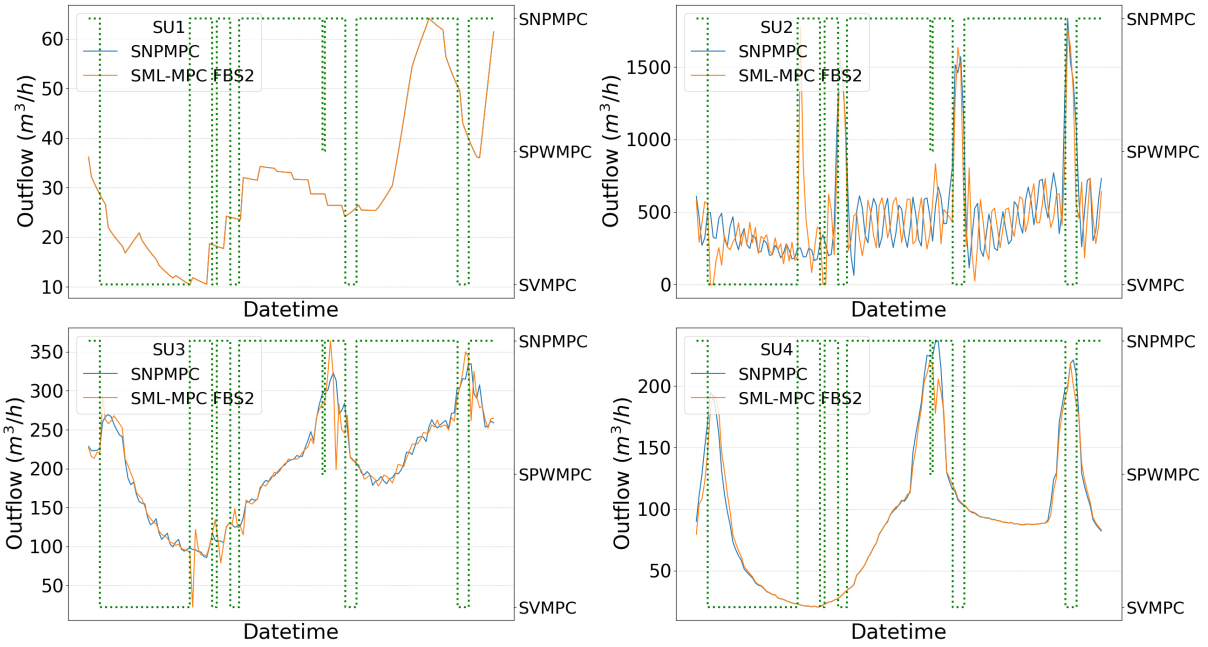

Figure 11.27: Comparison of control action (right y-axis) from SNPMPC and SML-MPC FBS2, and which layer is used (right y-axis) in Period 2.

Since this comparison is realized in Period 2, the uncertainty is not high enough to activate SVMPC often. Another comparison is performed for Period 5 with high uncertainty, where in Figure 11.28 is shown the outflow for FBS1 and in Figure 11.29 for FBS2. The first fallback strategy shows considerable oscillations in SU3 due to constant switching, which is not a desired behaviour. On the other hand, FBS2 displays much greater stability and reduced oscillations, because the threshold was being breached during all instants with high uncertainty, which meant that the multi-layer runs purely SVMPC.

Looking at Table 11.2, during Period 5, SNPMPC showed the lowest $m^{\mathrm{NH_4}}_{\mathrm{OV_{total}}}$, while SVMPC (and SPWMPC) the lowest relative overflow. When observing the result for SML-MPC FBS2, it showed a compromise between both methods, again reinforcing that the tuning of the layers needs special attention to ensure that the desired behaviour is maintained even when the switch occurs. Potentially, a better combination of weights for the layers with a similar expected behaviour will reduce the oscillations, as controllers will try to maintain the performance.

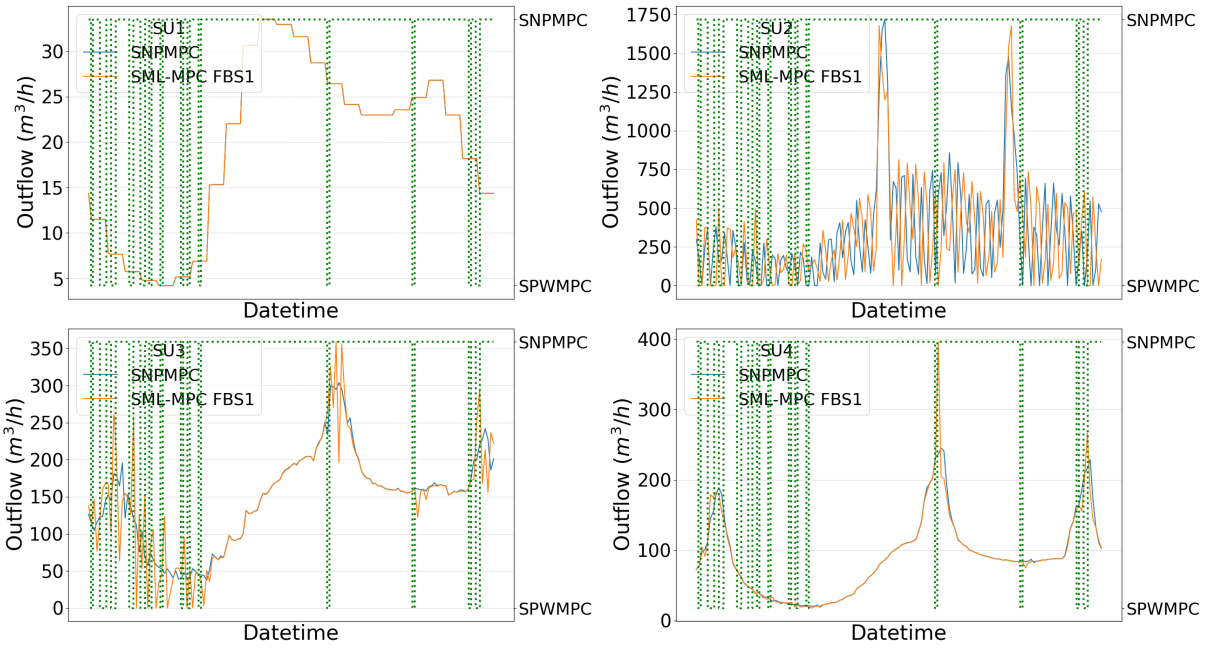

Figure 11.28: Comparison of control action (left y-axis) from SNPMPC and SML-MPC FBS1, and which layer is used (right y-axis) in Period 5.

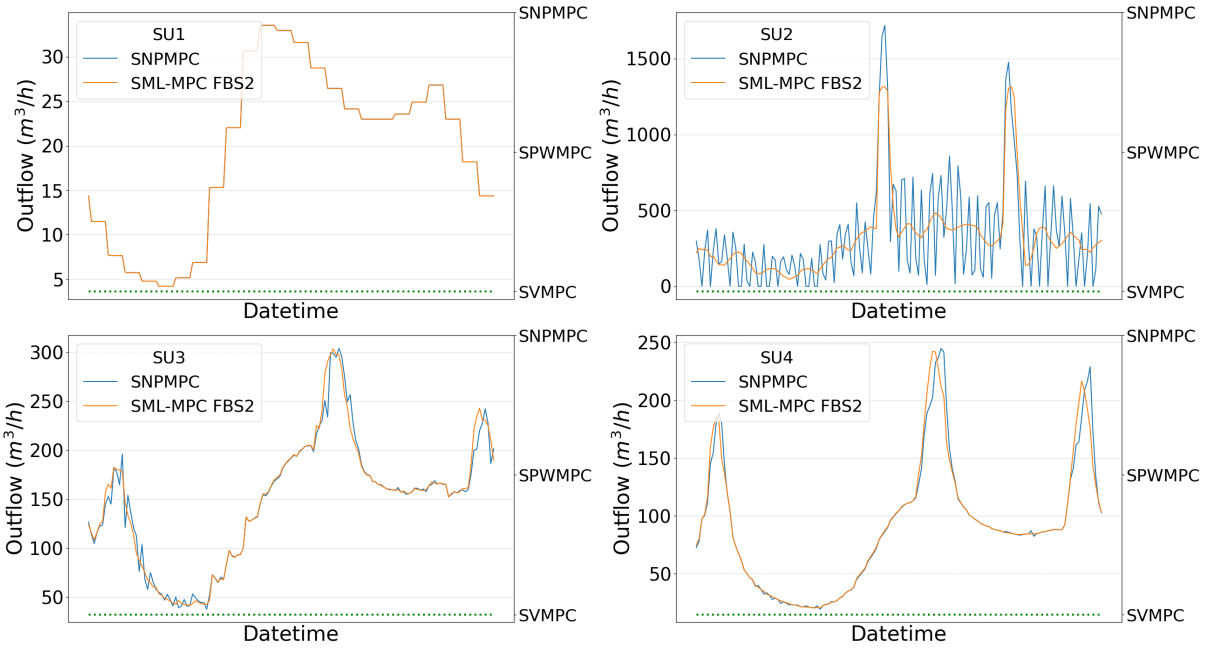

Figure 11.29: Comparison of control action (left y-axis) from SNPMPC and SML-MPC FBS2, and which layer is used (right y-axis) in Period 5.

The conclusion suggests implementing either SML-MPC FBS1 or SML-MPC FBS2, as SML-MPC FBS3 is largely redundant with the second fallback strategy. The decision is based on the level of uncertainty; stochastic methods are clearly more effective in handling uncertainties. Both non-linear methods exhibit robustness, but since the deterministic multi-layer relies on PWMPC as a backup strategy, high

uncertainty will have a greater negative impact compared to the stochastic multi-layer. In practical applications, uncertainties are inevitable, so theoretically, NPMPC and stochastic methods offered the best solution. Furthermore, for high uncertainties, SML-MPC FBS1 presents a more oscillatory behaviour, while SML-MPC FBS2 might converge to only using SVMPC, which provides a more smooth control action. The main challenge is estimating the level of uncertainties, as many can be unpredictable.

Moreover, implementing such methods presents numerous difficulties, particularly for those requiring non-linear optimisation. The computational cost is a critical factor that requires careful consideration and must be carefully evaluated and can make the deployment of NPMPC, SNPMPC. By contrast, SML-MPC provides a robust solution, offering a fallback for infeasible cases or situations where non-linear methods face tight time constraints. This approach effectively combines the robust solution of SNPMPC with the solid performance of SVMPC and SPWMPC.

12 Conclusion and Perspectives

This thesis introduced a range of novel MPC methods for Urban Drainage Systems. The study covered both adaptations of existing approaches, such as VMPC, NPMPC, and SVMPC, and entirely new developments, including PWMPC, SPWMPC, and SNPMPC. Each method was described and validated through simple and complex case studies, highlighting strengths, limitations, and comparative performance across scenarios. A multi-layer strategy was then proposed to enhance non-linear methods by employing linear methods as a backup when infeasible solutions occur or the optimisation cannot be completed within the control loop time constraints.

For systems where concentration data is unavailable or unreliable, VMPC provides an effective solution, operating well without concentration measurements and proving particularly suitable for simpler systems. SVMPC also offers a safe alternative in the presence of uncertainties, although its conservative behaviour may lead to underperformance in some scenarios.

When uncertainties are minimal or easily estimated, NPMPC achieves the highest performance, while SNPMPC excels under high uncertainty by explicitly accounting for unpredictable conditions, thus enhancing the robustness of the system. However, both methods require significantly higher computational resources, especially SNPMPC.

On the other hand, PWMPC provides a cost-effective and computationally efficient option with a simple implementation. However, its reliance on accurate concentration estimates can limit its effectiveness in scenarios where uncertainties are significant. SPWMPC may overcome these limitations by incorporating uncertainty into the control process, thus providing more reliable performance in such conditions.

The multi-layer strategies, ML-MPC and SML-MPC, demonstrated the ability to significantly improve system performance by identifying feasible regions that non-linear methods alone could not reach. Among the fallback strategies evaluated, a two-layer configuration proved to be most effective. Additional layers introduced oscillations in control actions that, while not substantially reducing overall performance, could cause unwanted stress on actuators. Moreover, implementing extra layers would require a digital twin of the UDS to estimate the errors between the predicted and measured values, another challenging task.

Furthermore, a weight selection methodology was proposed, combining GA optimisation with SA for MPC strategies provides a robust framework to avoid under-tuning the controller, while also offering a deeper understanding of how different weights influence control performance. This approach ensures that the controllers are better tuned, helping the decision making and possibly automating the process of selecting these parameters. This methodology can potentially provide real-time weight changes based on different scenarios, where a digital twin of UDS could also be integrated.

From a practical implementation standpoint, based on the analyses and case studies presented in this thesis, the selection of an appropriate MPC method depends on both the characteristics of the system and

the level of uncertainty present. For smaller or simpler systems, NPMPC provides a strong performance, while SNPMPC offers a more conservative alternative under greater uncertainty. In larger systems with multiple storage units or extended prediction horizons, VMPC perform best when concentration data is limited or unavailable and under low uncertainty, whereas stochastic approaches like SVMPC are more effective in managing higher uncertainty and maintaining system stability. When computational efficiency and linear implementation are priorities in a pollution-based framework, PWMPC and SPWMPC present fast and practical alternatives, with the latter better suited for uncertain conditions. Finally, multi-layer strategies, including ML-MPC and SML-MPC, offer robust performance by combining non-linear and linear methods, ensuring feasibility even in challenging scenarios. Table 12.1 summarises these recommendations, providing a clear guide to select the most appropriate control strategy based on the levels of complexity and uncertainty of the system.

Table 12.1: Recommended MPC methods for Urban Drainage Systems based on system characteristics and uncertainty levels.

System Characteristic	**Uncertainty Level**	**Recommended Method**
Small / simple systems	Low to moderate	NPMPC
Small / simple systems	High	SNPMPC
Large systems / many storage units	Low to moderate	PWMPC
Large systems / many storage units	High	SPWMPC
Any system	No concentration data, low uncertainty	VMPC
Any system	No concentration data, high uncertainty	SVMPC
Any system	Low to moderate uncertainty	ML-MPC
Any system	High uncertainty	SML-MPC

Future research could focus on integrating a real-time digital twin of the Urban Drainage System to enable dynamic state estimation, correction of prediction errors, and adaptive weights for MPC strategies. It was identified that the weights are sensitive to different rain conditions, thus, expanding the weight selection methodology to allow real-time tuning, potentially using machine learning or reinforcement learning, could further improve controller robustness under changing conditions and extreme events. Furthermore, the development of hybrid stochastic-deterministic approaches may combine the good performance of deterministic methods with the resilience of stochastic strategies in high-uncertainty scenarios. Additionally, incorporating more operational decision variables, such as pump schedules, valve limits, or energy consumption, would enable multi-objective optimisation that balances environmental, operational, and economic goals.

Enhancing scalability through high-performance computing or parallelised optimisation could make advanced MPC strategies viable for large-scale systems with numerous storage units and long prediction horizons. Finally, field implementation and hardware-in-the-loop testing would provide practical insights into sensor inaccuracies, communication delays, and actuator limitations, while assessing the performance of controllers in climate-change extreme rainfall scenarios.

A Appendix

A.1 Additional Results for VMPC

This section shows the results for VMPC, which includes the Grid Search and Random Search Sensitivity Analysis realised for two periods, from May 1 to June 1 and from March 24 to April 24.

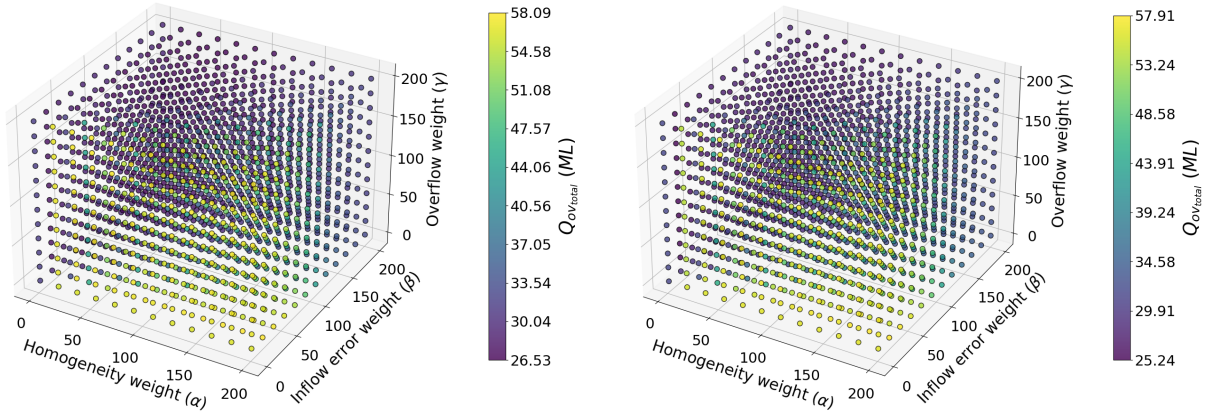

(a) $\epsilon = 3$. *(b)* $\epsilon = 21$.

Figure A.1: Grid Search SA for $Q_{\text{ov}_{\text{total}}}$ from May 1 to June 1 for $\epsilon = 3, 21$ for VMPC.

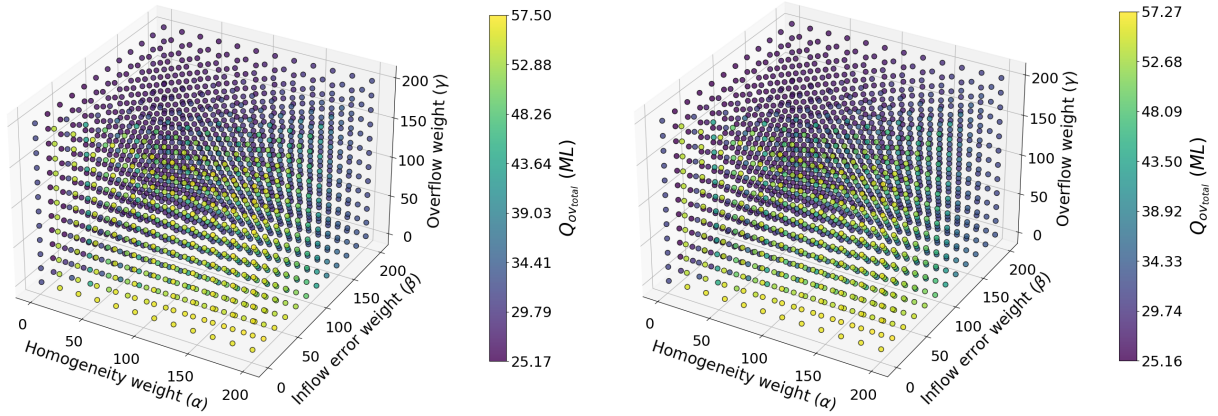

(a) $\epsilon = 52$. *(b)* $\epsilon = 89$.

Figure A.2: Grid Search SA for $Q_{\text{ov}_{\text{total}}}$ from May 1 to June 1 for $\epsilon = 52, 89$ for VMPC.

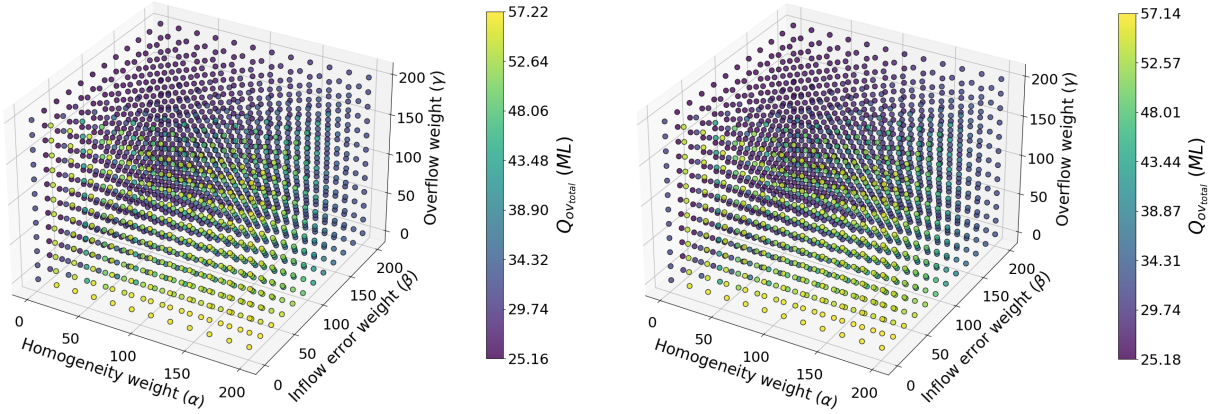

(a) $\epsilon = 102$. *(b)* $\epsilon = 153$.

Figure A.3: Grid Search SA for $Q_{\text{ov}_{\text{total}}}$ from May 1 to June 1 for $\epsilon = 102, 153$ for VMPC.

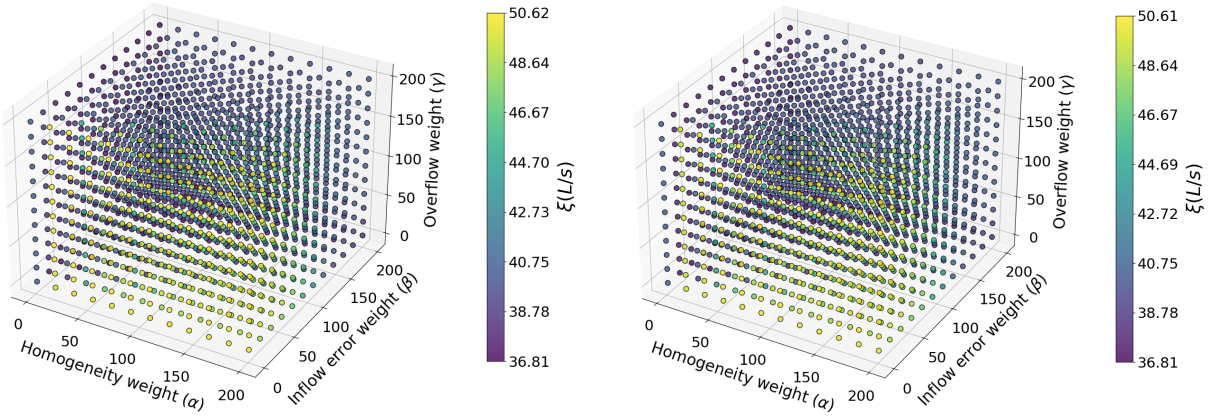

(a) $\epsilon = 3$. *(b)* $\epsilon = 21$.

Figure A.4: Grid Search SA for ξ from May 1 to June 1 for $\epsilon = 3, 21$ for VMPC.

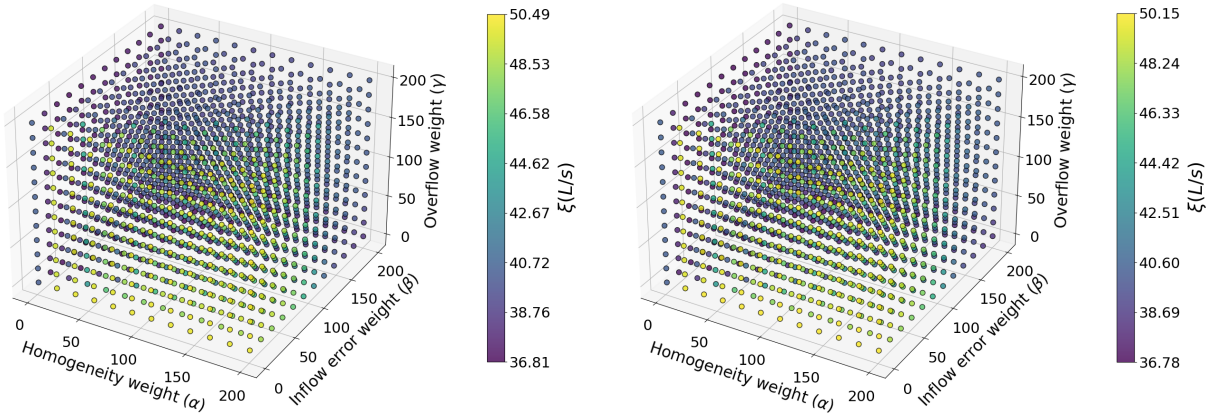

(a) $\epsilon = 52$. *(b)* $\epsilon = 89$.

Figure A.5: Grid Search SA for ξ from May 1 to June 1 for $\epsilon = 52, 89$ for VMPC.

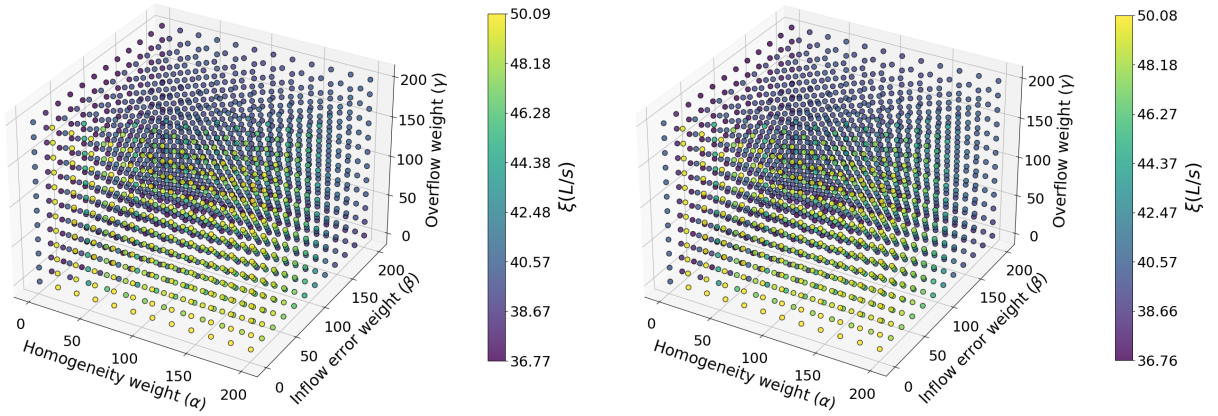

(a) $\epsilon = 102$. *(b)* $\epsilon = 153$.

Figure A.6: Grid Search SA for ξ from May 1 to June 1 for $\epsilon = 102, 153$ for VMPC.

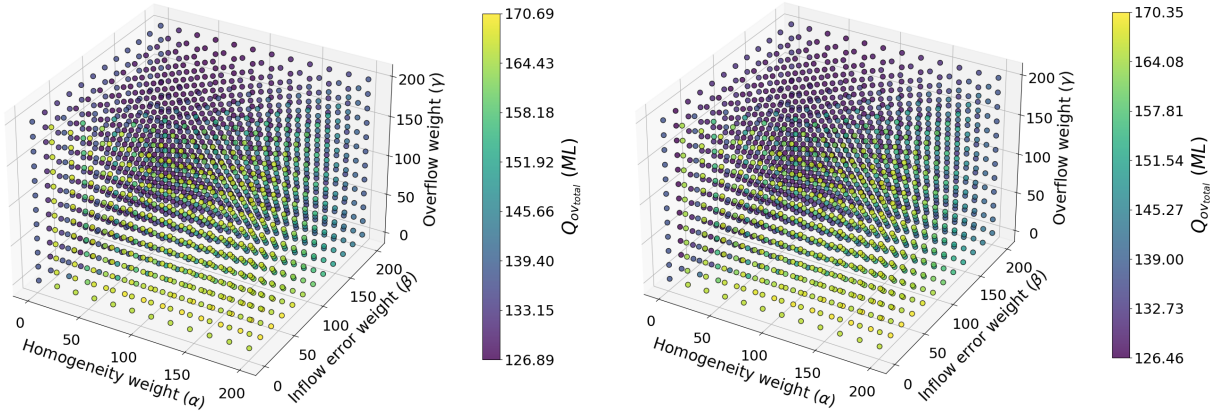

(a) $\epsilon = 3$. *(b)* $\epsilon = 21$.

Figure A.7: Grid Search SA for $Q_{\mathrm{ov}_{\mathrm{total}}}$ from March 24 to April 24 for $\epsilon = 3, 21$ for VMPC.

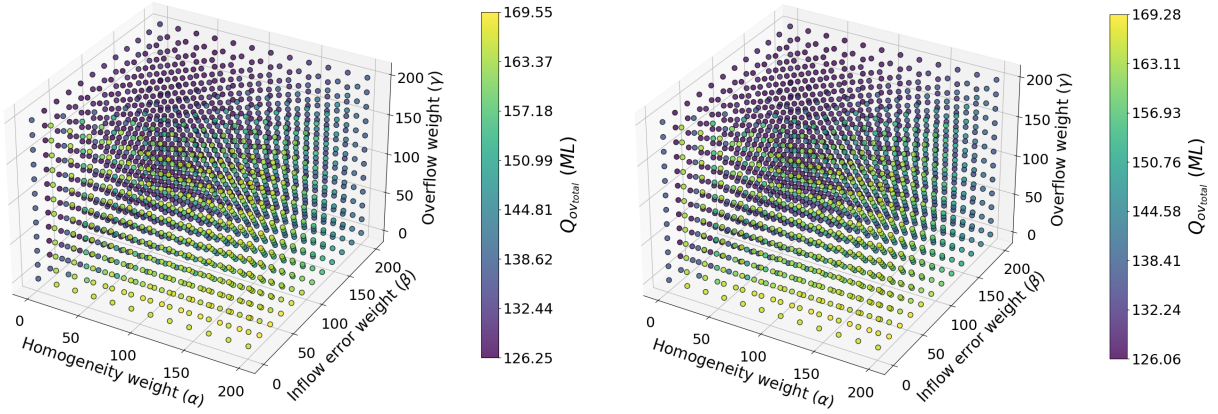

(a) $\epsilon = 52$. *(b)* $\epsilon = 89$.

Figure A.8: Grid Search SA for $Q_{\mathrm{ov}_{\mathrm{total}}}$ from March 24 to April 24 for $\epsilon = 52, 89$ for VMPC.

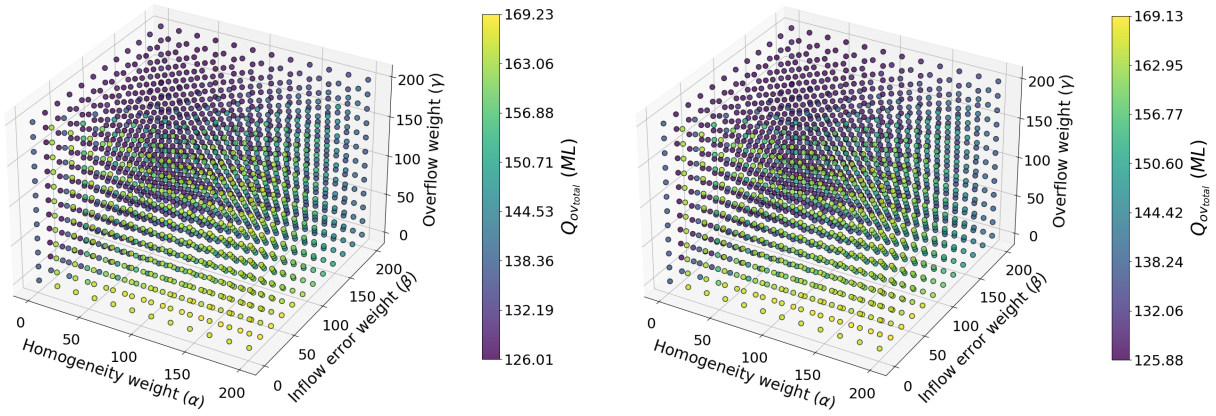

(a) $\epsilon = 102$. *(b)* $\epsilon = 153$.

Figure A.9: Grid Search SA for $Q_{\text{ov}_{\text{total}}}$ from March 24 to April 24 for $\epsilon = 102, 153$ for VMPC.

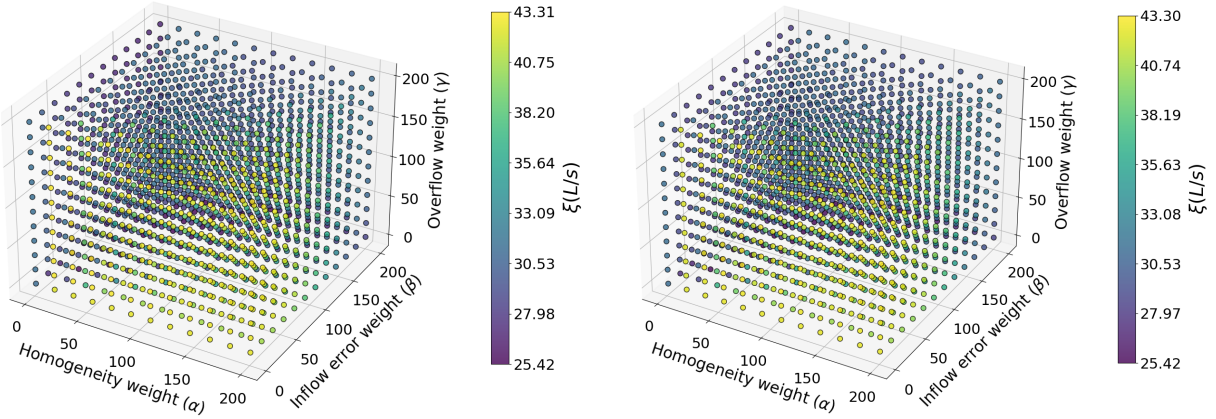

(a) $\epsilon = 3$. *(b)* $\epsilon = 21$.

Figure A.10: Grid Search SA for ξ from March 24 to April 24 for $\epsilon = 3, 21$ for VMPC.

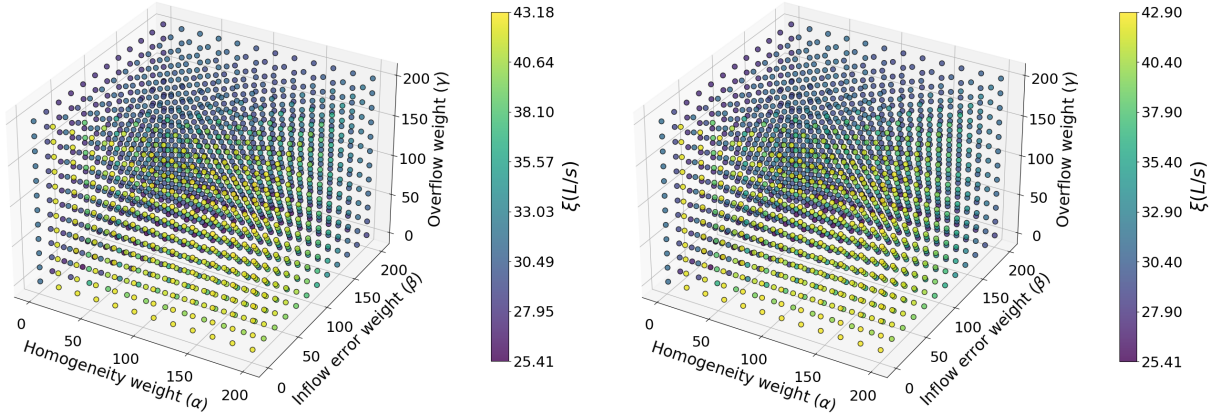

(a) $\epsilon = 52$. *(b)* $\epsilon = 89$.

Figure A.11: Grid Search SA for ξ from March 24 to April 24 for $\epsilon = 52, 89$ for VMPC.

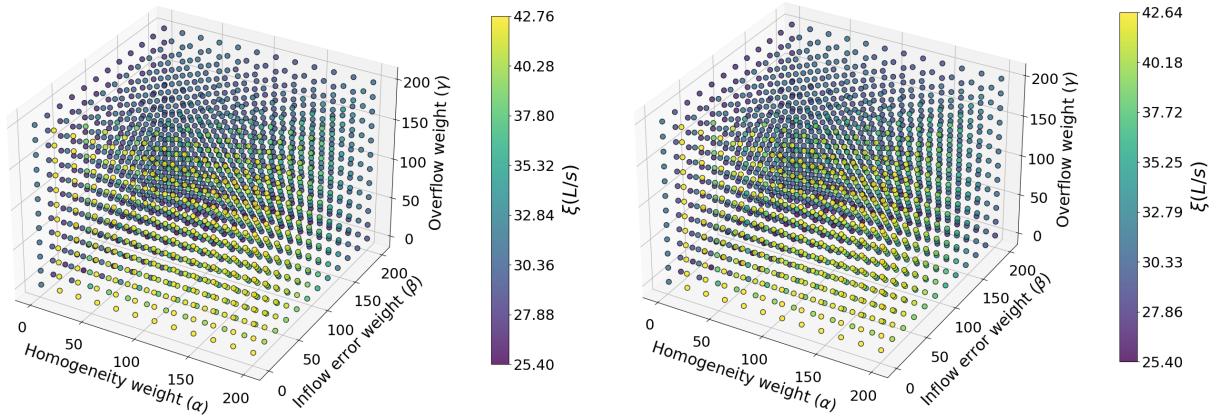

(a) $\epsilon = 102$. *(b)* $\epsilon = 153$.

Figure A.12: Grid Search SA for ξ from March 24 to April 24 for $\epsilon = 102, 153$ for VMPC.

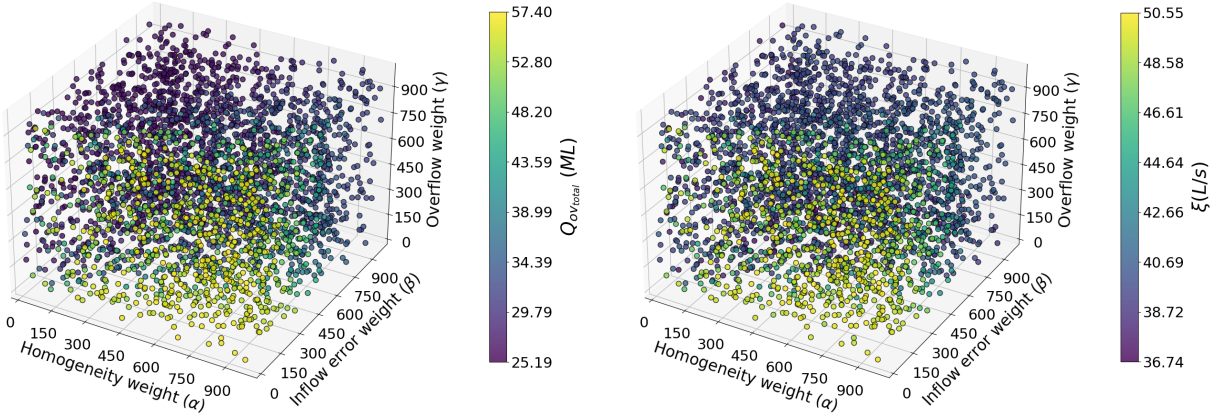

(a) $Q_{\text{ov}_{\text{total}}}$ for $\epsilon = 153$. *(b)* ξ for $\epsilon = 153$.

Figure A.13: Random Search Sensitivity Analysis from May 1 to July 1 for VMPC.

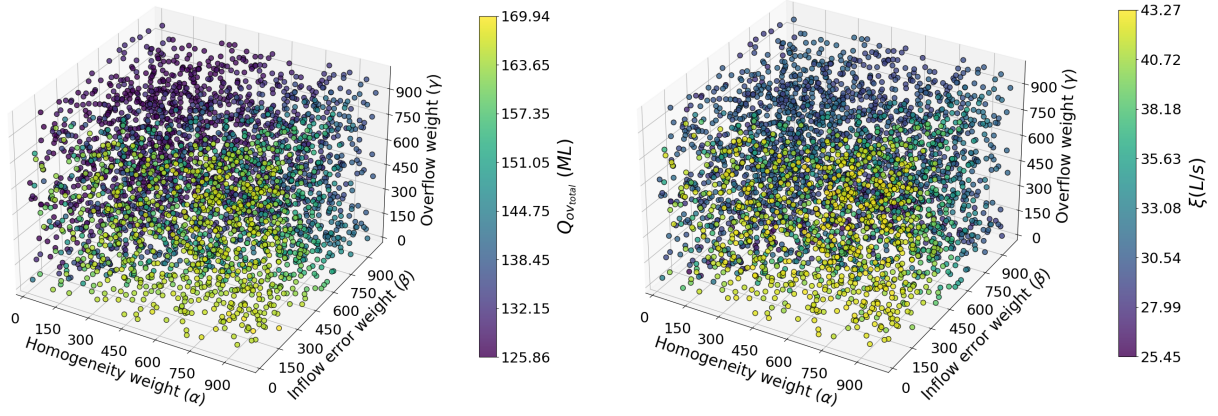

(a) $Q_{\text{ov}_{\text{total}}}$ for $\epsilon = 153$. *(b)* ξ for $\epsilon = 153$.

Figure A.14: Random Search Sensitivity Analysis from March 24 to April 24 for VMPC.

A.2 Additional Results for NPMPC

This section shows the results for NPMPC, which includes the Grid Search Sensitivity Analysis.

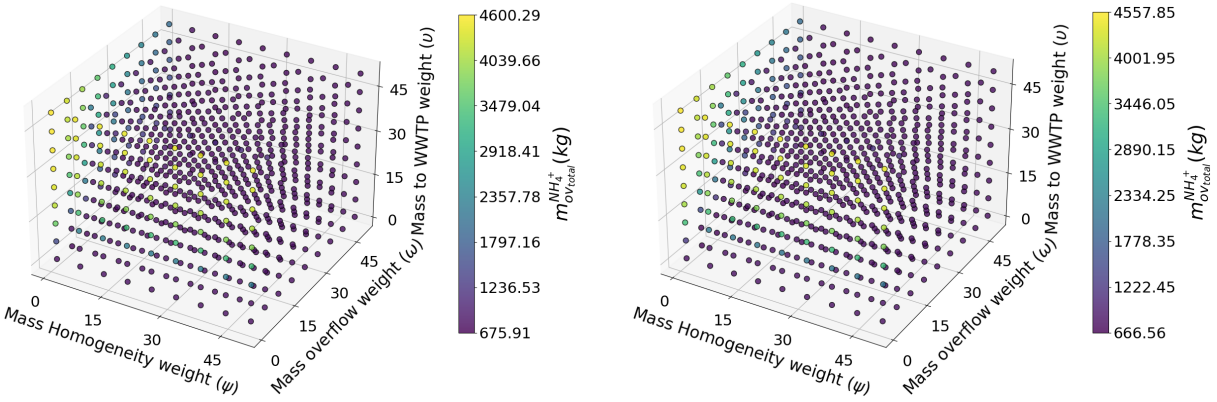

(a) $\beta = 1$ for $m^{\mathrm{NH_4}}_{\mathrm{OV_{total}}}$ *(b)* $\beta = 113$ for $m^{\mathrm{NH_4}}_{\mathrm{OV_{total}}}$

Figure A.15: Grid Search SA for $m^{\mathrm{NH_4}}_{\mathrm{OV_{total}}}$ with $\beta = 1, 113$ and for NPMPC.

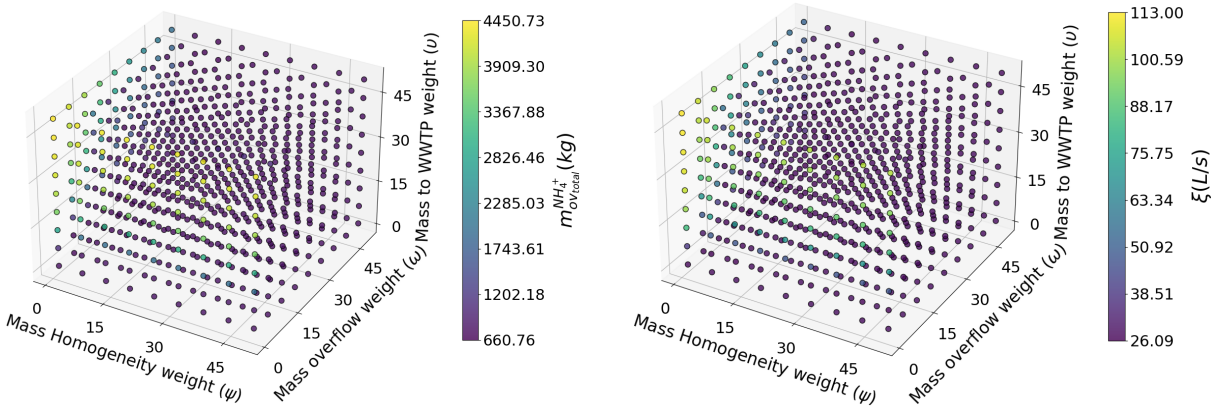

(a) $\beta = 226$ for $m^{\mathrm{NH_4}}_{\mathrm{OV_{total}}}$ *(b)* $\beta = 1$ for ξ

Figure A.16: Grid Search SA for $m^{\mathrm{NH_4}}_{\mathrm{OV_{total}}}$ with $\beta = 226$, for ξ with $\beta = 1$ and for NPMPC.

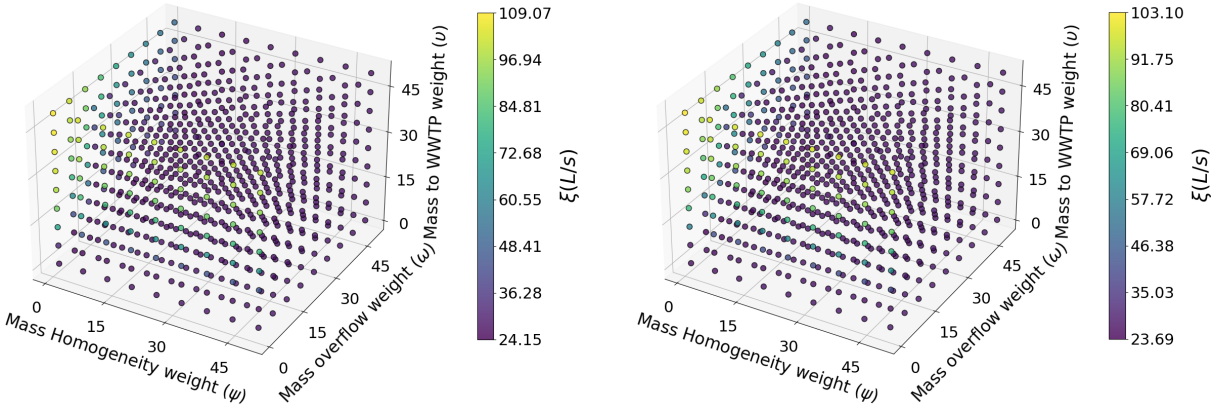

(a) $\beta = 113$ for ξ *(b)* $\beta = 226$ for ξ

Figure A.17: Grid Search SA for ξ with $\beta = 113, 226$ and for NPMPC.

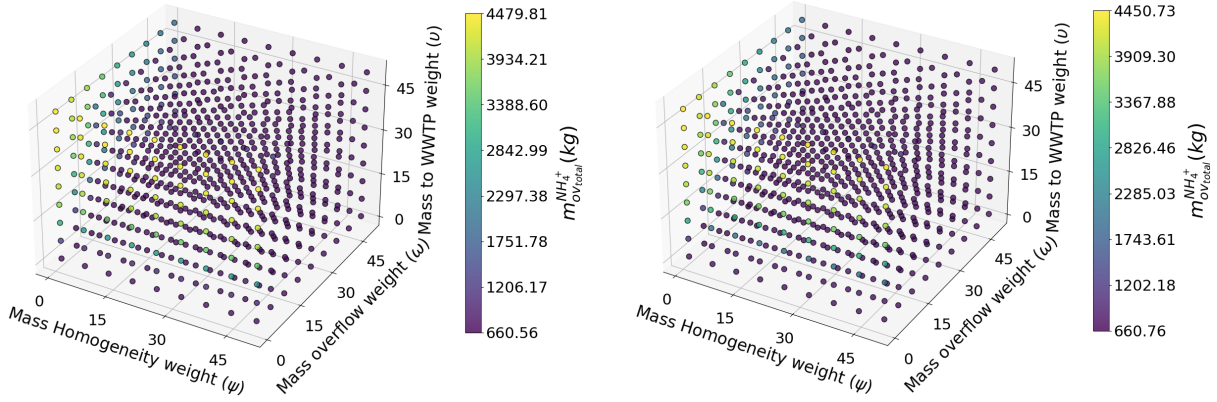

(a) $\gamma = 1$ for $m^{\mathrm{NH_4}}_{\mathrm{OV_{total}}}$ *(b)* $\gamma = 33$ for $m^{\mathrm{NH_4}}_{\mathrm{OV_{total}}}$

Figure A.18: Grid Search SA for $m^{\mathrm{NH_4}}_{\mathrm{OV_{total}}}$ with $\gamma = 1, 33$ and for NPMPC.

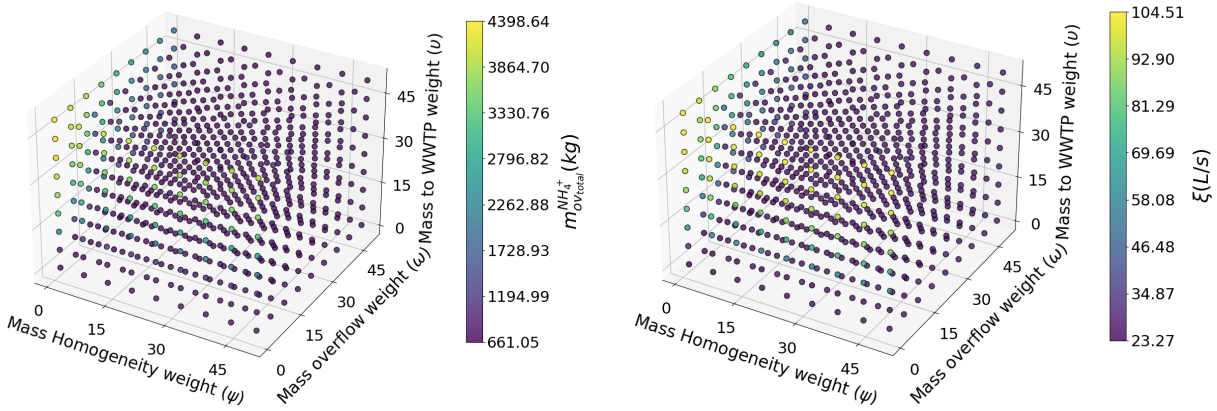

(a) $\gamma = 66$ for $m^{\mathrm{NH_4}}_{\mathrm{OV_{total}}}$ *(b)* $\gamma = 1$ for ξ

Figure A.19: Grid Search SA for $m^{\mathrm{NH_4}}_{\mathrm{OV_{total}}}$ with $\gamma = 66$, for ξ with $\gamma = 1$ and for NPMPC.

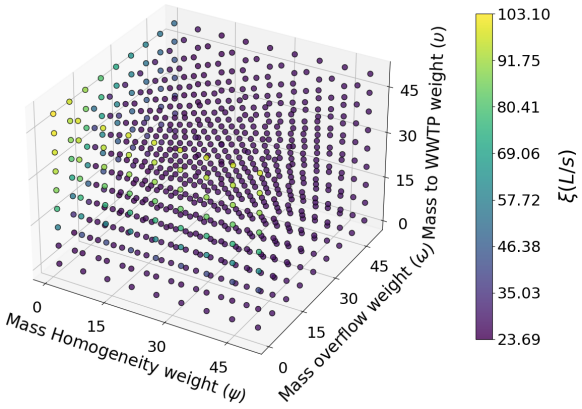

(a) $\gamma = 33$ for ξ

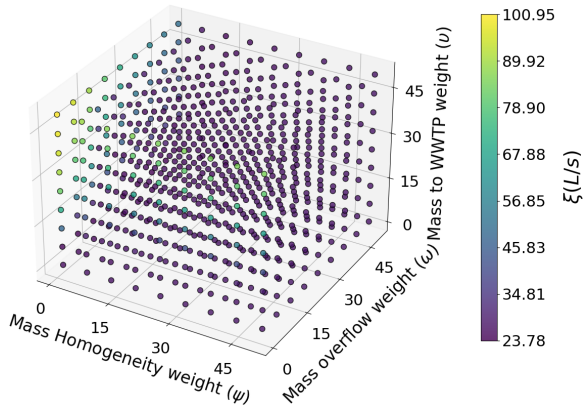

(b) $\gamma = 66$ for ξ

Figure A.20: Grid Search SA for ξ with $\gamma = 33, 66$ and for NPMPC.

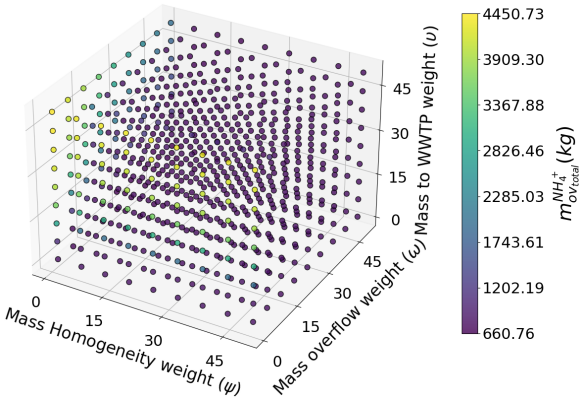

(a) $\epsilon = 98$ for $m^{\mathrm{NH_4}}_{\mathrm{OV_{total}}}$

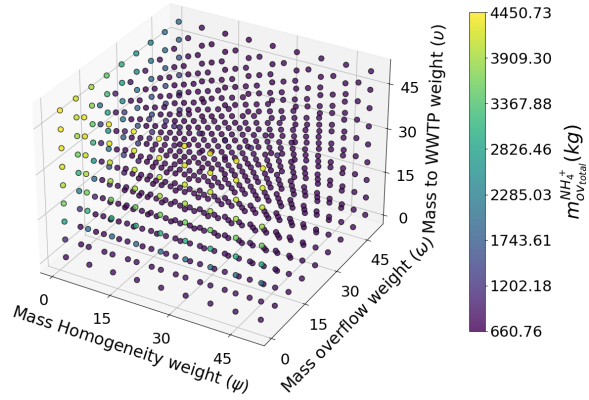

(b) $\epsilon = 189$ for $m^{\mathrm{NH_4}}_{\mathrm{OV_{total}}}$

Figure A.21: Grid Search SA for $m^{\mathrm{NH_4}}_{\mathrm{OV_{total}}}$ with $\epsilon = 98, 189$ and for NPMPC.

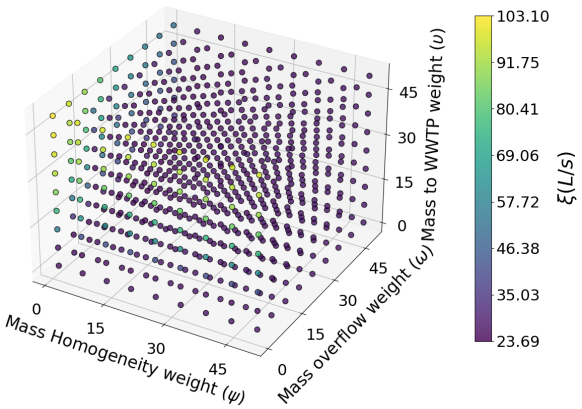

(a) $\epsilon = 98$ for ξ

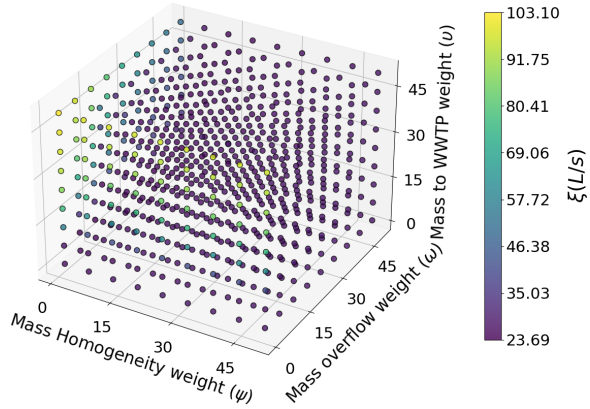

(b) $\epsilon = 189$ for ξ

Figure A.22: Grid Search SA for ξ with $\epsilon = 98, 189$ and for NPMPC.

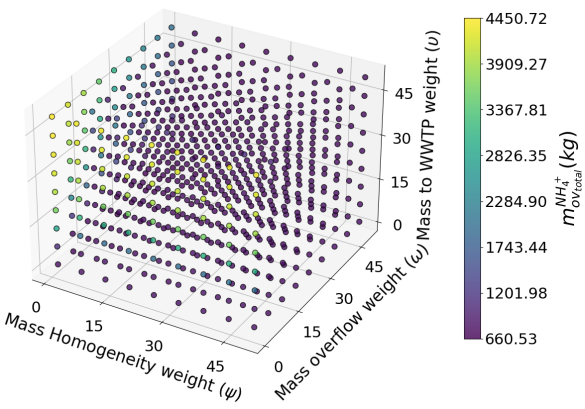

(a) $\tau = 42$ for $m^{\mathrm{NH_4}}_{\mathrm{OV_{total}}}$

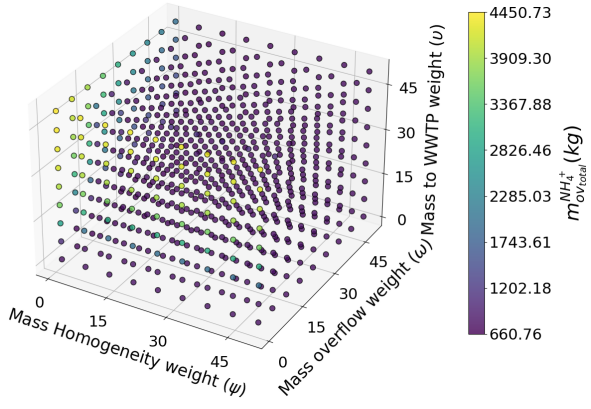

(b) $\tau = 84$ for $m^{\mathrm{NH_4}}_{\mathrm{OV_{total}}}$

Figure A.23: Grid Search SA for $m^{\mathrm{NH_4}}_{\mathrm{OV_{total}}}$ with $\tau = 42, 84$ and for NPMPC.

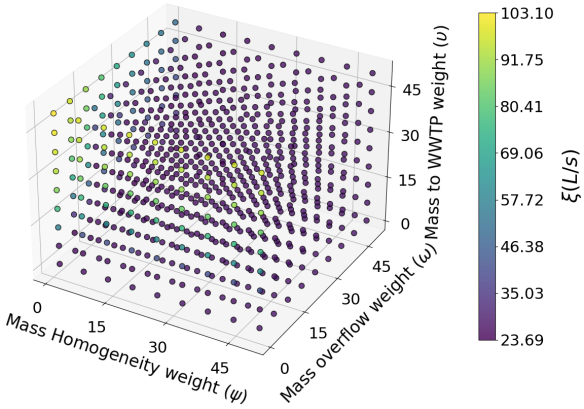

(a) $\tau = 42$ for ξ

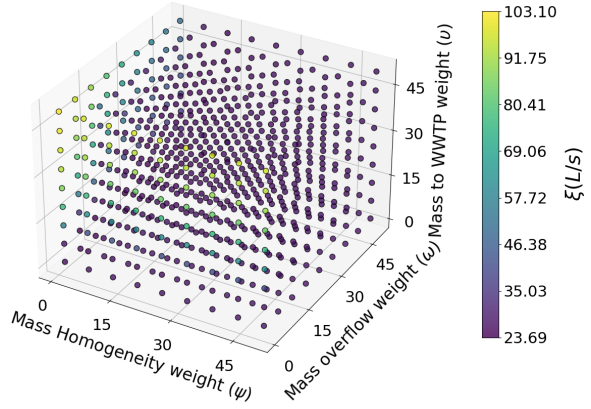

(b) $\tau = 84$ for ξ

Figure A.24: Grid Search SA for ξ with $\tau = 42, 84$ and for NPMPC.

A.3 Additional Results for SPWMPC

This section shows the results for SPWMPC compared to PWMPC in the initial scenario and the scenario with optimal weights.

Table A.1: Volume uncertainty: Comparison between PWMPC and SPWMPC for overestimating u_{off}

	PWMPC						SPWMPC - $\zeta = 0.60$						SPWMPC - $\zeta = 0.80$						SPWMPC - $\zeta = 0.95$					
u_{off}	0%	5%	10%	25%	50%	75%	0%	5%	10%	25%	50%	75%	0%	5%	10%	25%	50%	75%	0%	5%	10%	25%	50%	75%
$Q_{\text{ov}_{\text{total}}}$	168.77	167.127	166.82	167.079	168.232	169.528	177.238	176.573	176.23	175.802	175.64	175.66	177.45	176.563	176.163	175.801	175.604	175.653	177.937	176.598	176.163	175.801	175.604	175.61
%F		**-0.97%**	**-1.16%**	**-1.0%**	**-0.32%**	**0.45%**		**-0.38%**	**-0.57%**	**-0.81%**	**-0.9%**	**-0.89%**		**-0.5%**	**-0.73%**	**-0.93%**	**-1.04%**	**-1.01%**		**-0.75%**	**-1.0%**	**-1.2%**	**-1.31%**	**-1.31%**
$m^{\text{NH}_3}_{\text{ov}_{\text{total}}}$	1034.79	1011.539	1010.532	1007.75	1017.285	1028.648	1267.61	1264.796	1262.591	1259.511	1259.688	1260.117	1268.455	1263.803	1262.359	1259.495	1259.087	1260.072	1271.773	1264.315	1262.106	1259.487	1259.098	1259.968
%F		**-2.25%**	**-2.34%**	**-2.61%**	**-1.69%**	**-0.59%**		**-0.22%**	**-0.4%**	**-0.64%**	**-0.62%**	**-0.59%**		**-0.37%**	**-0.48%**	**-0.71%**	**-0.74%**	**-0.66%**		**-0.59%**	**-0.76%**	**-0.97%**	**-1.0%**	**-0.93%**
ξ_{min}	7.629	8.364	8.892	9.6	9.875	9.899	8.508	8.801	9.28	9.691	9.829	9.832	8.614	8.866	9.212	9.693	9.814	9.862	8.653	8.831	9.269	9.695	9.816	9.921

Table A.2: Outflow uncertainty: Comparison between PWMPC and SPWMPC for u_p

	PWMPC						SPWMPC - $\zeta = 0.60$						SPWMPC - $\zeta = 0.80$						SPWMPC - $\zeta = 0.95$					
u_p	0%	25%	75%	100%	125%	175%	0%	25%	75%	100%	125%	175%	0%	25%	75%	100%	125%	175%	0%	25%	75%	100%	125%	175%
$Q_{\text{ov}_{\text{total}}}$	168.77	168.765	168.883	168.933	169.025	169.167	177.238	177.139	177.19	177.208	177.2	177.215	177.45	177.168	177.33	177.43	177.618	177.734	177.937	177.214	177.607	177.871	178.105	178.304
%F		**-0.0%**	**0.07%**	**0.1%**	**0.15%**	**0.24%**		**-0.06%**	**-0.03%**	**-0.02%**	**-0.02%**	**-0.01%**		**-0.16%**	**-0.07%**	**-0.01%**	**0.09%**	**0.16%**		**-0.41%**	**-0.19%**	**-0.04%**	**0.09%**	**0.21%**
$m^{\text{NH}_3}_{\text{ov}_{\text{total}}}$	1034.79	1036.351	1038.948	1041.474	1043.092	1045.685	1267.61	1267.126	1266.596	1266.261	1264.843	1261.926	1268.455	1267.343	1267.49	1269.036	1268.607	1261.162	1271.773	1267.664	1271.202	1268.065	1265.584	1263.884
%F		**0.15%**	**0.4%**	**0.65%**	**0.8%**	**1.05%**		**-0.04%**	**-0.08%**	**-0.11%**	**-0.22%**	**-0.45%**		**-0.09%**	**-0.08%**	**0.05%**	**0.01%**	**-0.57%**		**-0.32%**	**-0.04%**	**-0.29%**	**-0.49%**	**-0.62%**
ξ_{min}	7.629	7.508	7.449	7.469	7.482	7.458	8.508	8.388	8.386	8.406	8.413	8.413	8.614	8.39	8.384	8.359	8.253	8.072	8.653	8.4	8.259	8.104	8.035	7.923

Table A.3: Outflow uncertainty: Comparison between PWMPC and SPWMPC for overestimating u_{off}

	PWMPC						SPWMPC - $\zeta = 0.60$						SPWMPC - $\zeta = 0.80$						SPWMPC - $\zeta = 0.95$					
u_{off}	0%	5%	10%	25%	50%	75%	0%	5%	10%	25%	50%	75%	0%	5%	10%	25%	50%	75%	0%	5%	10%	25%	50%	75%
$Q_{\text{ov}_{\text{total}}}$	168.77	168.782	168.72	168.752	169.243	170.009	177.238	177.038	176.959	176.761	176.441	176.314	177.45	177.067	176.987	176.778	176.45	176.329	177.937	177.121	177.035	176.819	176.486	176.371
%F		**0.01%**	**-0.03%**	**-0.01%**	**0.28%**	**0.73%**		**-0.11%**	**-0.16%**	**-0.27%**	**-0.45%**	**-0.52%**		**-0.22%**	**-0.26%**	**-0.38%**	**-0.56%**	**-0.63%**		**-0.46%**	**-0.51%**	**-0.63%**	**-0.82%**	**-0.88%**
$m^{\text{NH}_3}_{\text{ov}_{\text{total}}}$	1034.79	1035.825	1037.897	1043.013	1056.523	1075.083	1267.61	1265.376	1263.167	1256.669	1243.107	1235.957	1268.455	1265.565	1263.406	1256.756	1243.062	1236.092	1271.773	1265.831	1263.624	1257.086	1243.3	1236.486
%F		**0.1%**	**0.3%**	**0.79%**	**2.1%**	**3.89%**		**-0.18%**	**-0.35%**	**-0.86%**	**-1.93%**	**-2.5%**		**-0.23%**	**-0.4%**	**-0.92%**	**-2.0%**	**-2.55%**		**-0.47%**	**-0.64%**	**-1.15%**	**-2.24%**	**-2.77%**
ξ_{min}	7.629	7.575	7.56	7.513	7.446	7.477	8.508	8.426	8.397	8.361	8.313	8.339	8.614	8.44	8.403	8.361	8.317	8.328	8.653	8.448	8.412	8.355	8.325	8.347

Table A.4: Overflow uncertainty: Comparison between PWMPC and SPWMPC for u_p

	PWMPC						SPWMPC - $\zeta = 0.60$						SPWMPC - $\zeta = 0.80$						SPWMPC - $\zeta = 0.95$					
u_p	0%	50%	100%	150%	175%	200%	0%	50%	100%	150%	175%	200%	0%	50%	100%	150%	175%	200%	0%	50%	100%	150%	175%	200%
$Q_{\text{ov}_{\text{total}}}$	168.77	169.002	169.009	168.967	168.957	168.926	177.238	177.202	177.19	177.165	177.157	177.147	177.45	177.22	177.239	177.251	177.261	177.251	177.937	177.25	177.315	177.374	177.421	177.393
%F		**0.14%**	**0.14%**	**0.12%**	**0.11%**	**0.09%**		**-0.02%**	**-0.03%**	**-0.04%**	**-0.05%**	**-0.05%**		**-0.13%**	**-0.12%**	**-0.11%**	**-0.11%**	**-0.11%**		**-0.39%**	**-0.35%**	**-0.32%**	**-0.29%**	**-0.31%**
$m^{\text{NH}_3}_{\text{ov}_{\text{total}}}$	1034.79	1041.701	1038.929	1034.501	1032.897	1030.976	1267.61	1267.317	1266.572	1263.754	1262.801	1262.382	1268.455	1267.536	1265.756	1263.652	1262.403	1261.467	1271.773	1267.633	1265.453	1262.774	1261.464	1258.766
%F		**0.67%**	**0.4%**	**-0.03%**	**-0.18%**	**-0.37%**		**-0.02%**	**-0.08%**	**-0.3%**	**-0.38%**	**-0.41%**		**-0.07%**	**-0.21%**	**-0.38%**	**-0.48%**	**-0.55%**		**-0.33%**	**-0.5%**	**-0.71%**	**-0.81%**	**-1.02%**
ξ_{min}	7.629	7.602	7.554	7.533	7.532	7.527	8.508	8.47	8.481	8.486	8.492	8.494	8.614	8.49	8.514	8.542	8.552	8.573	8.653	8.512	8.572	8.61	8.623	8.635

Table A.5: Overflow uncertainty: Comparison between PWMPC and SPWMPC for overestimating u_{off}

	PWMPC						SPWMPC - $\zeta = 0.60$						SPWMPC - $\zeta = 0.80$						SPWMPC - $\zeta = 0.95$					
u_{off}	0%	5%	10%	25%	50%	75%	0%	5%	10%	25%	50%	75%	0%	5%	10%	25%	50%	75%	0%	5%	10%	25%	50%	75%
$Q_{\text{ov}_{\text{total}}}$	168.77	168.375	168.297	168.223	168.104	168.024	177.238	176.573	175.497	174.113	173.57	173.523	177.45	176.574	175.479	174.096	173.567	173.518	177.937	176.576	175.434	174.064	173.564	173.486
%F		**-0.23%**	**-0.28%**	**-0.32%**	**-0.39%**	**-0.44%**		**-0.38%**	**-0.98%**	**-1.76%**	**-2.07%**	**-2.1%**		**-0.49%**	**-1.11%**	**-1.89%**	**-2.19%**	**-2.22%**		**-0.76%**	**-1.41%**	**-2.18%**	**-2.46%**	**-2.5%**
$m^{\text{NH}_3}_{\text{ov}_{\text{total}}}$	1034.79	998.634	993.176	998.199	1009.106	1016.806	1267.61	1242.76	1194.806	1172.923	1169.325	1174.944	1268.455	1242.698	1194.35	1172.692	1169.385	1174.941	1271.773	1242.666	1192.819	1172.199	1169.242	1174.893
%F		**-3.49%**	**-4.02%**	**-3.54%**	**-2.48%**	**-1.74%**		**-1.96%**	**-5.74%**	**-7.47%**	**-7.75%**	**-7.31%**		**-2.03%**	**-5.84%**	**-7.55%**	**-7.81%**	**-7.37%**		**-2.29%**	**-6.21%**	**-7.83%**	**-8.06%**	**-7.62%**
ξ_{min}	7.629	7.546	7.641	7.672	7.645	7.662	8.508	8.45	8.451	8.435	8.449	8.449	8.614	8.451	8.452	8.435	8.45	8.449	8.653	8.452	8.451	8.435	8.452	8.451

Table A.6: Overflow uncertainty: Comparison between PWMPC and SPWMPC for underestimating u_{off}

	PWMPC						**SPWMPC - $\zeta = 0.60$**						**SPWMPC - $\zeta = 0.80$**						**SPWMPC - $\zeta = 0.95$**					
u_{off}	0%	−5%	−10%	−25%	−50%	−75%	0%	−5%	−10%	−25%	−50%	−75%	0%	−5%	−10%	−25%	−50%	−75%	0%	−5%	−10%	−25%	−50%	−75%
$Q_{\text{ov}_{\text{total}}}$	168.77	170.831	170.866	170.747	170.67	170.617	177.238	177.251	177.268	177.296	177.317	177.317	177.45	177.252	177.269	177.298	177.319	177.319	177.937	177.253	177.271	177.3	177.322	177.322
%F		**1.22%**	**1.24%**	**1.17%**	**1.13%**	**1.09%**		**0.01%**	**0.02%**	**0.03%**	**0.04%**	**0.04%**		**-0.11%**	**-0.1%**	**-0.09%**	**-0.07%**	**-0.07%**		**-0.38%**	**-0.37%**	**-0.36%**	**-0.35%**	**-0.35%**
$m^{\text{NH}_4}_{\text{ov}_{\text{total}}}$	1034.79	1088.107	1089.487	1086.525	1085.304	1084.129	1267.61	1270.162	1270.249	1270.273	1270.285	1270.285	1268.455	1270.205	1270.278	1270.3	1270.312	1270.312	1271.773	1270.262	1270.337	1270.361	1270.374	1270.374
%F		**5.15%**	**5.29%**	**5.0%**	**4.88%**	**4.77%**		**0.2%**	**0.21%**	**0.21%**	**0.21%**	**0.21%**		**0.14%**	**0.14%**	**0.15%**	**0.15%**	**0.15%**		**-0.12%**	**-0.11%**	**-0.11%**	**-0.11%**	**-0.11%**
ξ_{rain}	7.629	7.264	7.256	7.278	7.258	7.271	8.508	8.47	8.469	8.468	8.468	8.468	8.614	8.47	8.47	8.469	8.469	8.469	8.653	8.472	8.472	8.471	8.471	8.471

Table A.7: Volume uncertainty: Comparison between PWMPC and optimal SPWMPC for overestimating u_{off}

	PWMPC						**SPWMPC - $\zeta = 0.60$**						**SPWMPC - $\zeta = 0.80$**						**SPWMPC - $\zeta = 0.95$**					
u_{off}	0%	5%	10%	25%	50%	75%	0%	5%	10%	25%	50%	75%	0%	5%	10%	25%	50%	75%	0%	5%	10%	25%	50%	75%
$Q_{\text{ov}_{\text{total}}}$	168.77	166.782	167.017	168.22	170.44	172.75	177.244	176.928	176.725	176.502	175.674	175.586	177.243	176.928	176.726	176.502	175.674	175.586	177.245	176.927	176.72	176.502	175.674	175.586
%F		**-1.18%**	**-1.04%**	**-0.33%**	**0.99%**	**2.36%**		**-0.18%**	**-0.29%**	**-0.42%**	**-0.89%**	**-0.94%**		**-0.18%**	**-0.29%**	**-0.42%**	**-0.89%**	**-0.93%**		**-0.18%**	**-0.3%**	**-0.42%**	**-0.89%**	**-0.94%**
%F*							**0.0%**	**0.2%**	**0.28%**	**0.4%**	**0.02%**	**-0.04%**	**-0.12%**	**0.21%**	**0.32%**	**0.4%**	**0.04%**	**-0.04%**	**-0.39%**	**0.19%**	**0.32%**	**0.4%**	**0.04%**	**-0.01%**
$m^{\text{NH}_4}_{\text{ov}_{\text{total}}}$	1034.79	1066.461	1071.089	1086.543	1129.77	1181.609	1279.872	1278.213	1275.892	1271.644	1260.345	1259.371	1279.876	1278.213	1275.9	1271.659	1260.345	1259.371	1279.891	1278.206	1275.581	1271.656	1260.343	1259.371
%F		**3.06%**	**3.51%**	**5.0%**	**9.18%**	**14.19%**		**-0.13%**	**-0.31%**	**-0.64%**	**-1.53%**	**-1.6%**		**-0.13%**	**-0.31%**	**-0.64%**	**-1.53%**	**-1.6%**		**-0.13%**	**-0.34%**	**-0.64%**	**-1.53%**	**-1.6%**
%F*							**0.97%**	**1.06%**	**1.05%**	**0.96%**	**0.05%**	**-0.06%**	**0.9%**	**1.14%**	**1.07%**	**0.97%**	**0.1%**	**-0.06%**	**0.64%**	**1.1%**	**1.07%**	**0.97%**	**0.1%**	**-0.05%**
ξ_{rain}	7.629	8.573	9.062	9.594	9.849	9.909	6.566	6.59	6.596	6.977	9.895	9.951	6.566	6.59	6.596	6.977	9.895	9.951	6.566	6.59	6.627	6.977	9.895	9.951
%F*							**-22.83%**	**-25.12%**	**-28.92%**	**-28.01%**	**0.67%**	**1.21%**	**-23.78%**	**-25.67%**	**-28.4%**	**-28.02%**	**0.83%**	**0.9%**	**-24.12%**	**-25.38%**	**-28.5%**	**-28.04%**	**0.8%**	**0.3%**

Table A.8: Outflow uncertainty: Comparison between PWMPC and optimal SPWMPC for u_p

	PWMPC						**SPWMPC - $\zeta = 0.60$**						**SPWMPC - $\zeta = 0.80$**						**SPWMPC - $\zeta = 0.95$**					
u_p	0%	25%	75%	100%	125%	175%	0%	25%	75%	100%	125%	175%	0%	25%	75%	100%	125%	175%	0%	25%	75%	100%	125%	175%
$Q_{\text{ov}_{\text{total}}}$	168.77	167.463	167.692	167.749	167.808	168.03	177.244	177.21	177.389	177.441	177.494	176.818	177.243	177.21	177.39	177.442	177.495	177.568	177.245	177.21	177.389	177.441	177.495	177.567
%F		**-0.77%**	**-0.64%**	**-0.6%**	**-0.57%**	**-0.44%**		**-0.02%**	**0.08%**	**0.11%**	**0.14%**	**-0.24%**		**-0.02%**	**0.08%**	**0.11%**	**0.14%**	**0.18%**		**-0.02%**	**0.08%**	**0.11%**	**0.14%**	**0.18%**
%F*							**0.0%**	**0.04%**	**0.11%**	**0.13%**	**0.17%**	**-0.22%**	**-0.12%**	**0.02%**	**0.03%**	**0.01%**	**-0.07%**	**-0.09%**	**-0.39%**	**-0.0%**	**-0.12%**	**-0.24%**	**-0.34%**	**-0.41%**
$m^{\text{NH}_4}_{\text{ov}_{\text{total}}}$	1034.79	1074.472	1078.197	1077.432	1077.661	1082.022	1279.872	1280.293	1282.107	1282.702	1283.885	1225.205	1279.876	1280.318	1282.088	1282.685	1283.893	1285.601	1279.891	1280.312	1282.089	1282.666	1283.892	1285.624
%F		**3.83%**	**4.19%**	**4.12%**	**4.14%**	**4.56%**		**0.03%**	**0.17%**	**0.22%**	**0.31%**	**-4.27%**		**0.03%**	**0.17%**	**0.22%**	**0.31%**	**0.45%**		**0.03%**	**0.17%**	**0.22%**	**0.31%**	**0.45%**
%F*							**0.97%**	**1.04%**	**1.22%**	**1.3%**	**1.51%**	**-2.91%**	**0.9%**	**1.02%**	**1.15%**	**1.08%**	**1.2%**	**1.94%**	**0.64%**	**1.0%**	**0.86%**	**1.15%**	**1.45%**	**1.72%**
ξ_{rain}	7.629	7.866	7.824	7.815	7.808	7.777	6.566	6.588	6.639	6.608	6.593	7.048	6.566	6.588	6.64	6.609	6.593	6.594	6.566	6.588	6.64	6.609	6.593	6.595
%F*							**-22.83%**	**-21.46%**	**-20.83%**	**-21.39%**	**-21.63%**	**-16.22%**	**-23.78%**	**-21.48%**	**-20.8%**	**-20.94%**	**-20.11%**	**-18.31%**	**-24.12%**	**-21.57%**	**-19.6%**	**-18.45%**	**-17.95%**	**-16.76%**

Table A.9: Outflow uncertainty: Comparison between PWMPC and optimal SPWMPC for overestimating u_{off}

	PWMPC						**SPWMPC - $\zeta = 0.60$**						**SPWMPC - $\zeta = 0.80$**						**SPWMPC - $\zeta = 0.95$**					
u_{off}	0%	5%	10%	25%	50%	75%	0%	5%	10%	25%	50%	75%	0%	5%	10%	25%	50%	75%	0%	5%	10%	25%	50%	75%
$Q_{\text{ov}_{\text{total}}}$	168.77	167.497	167.45	167.621	168.324	169.353	177.244	177.225	177.197	177.197	177.342	177.558	177.243	177.202	177.197	177.197	177.342	177.558	177.245	177.201	177.196	177.197	177.341	177.558
%F		**-0.75%**	**-0.78%**	**-0.68%**	**-0.26%**	**0.35%**		**-0.01%**	**-0.03%**	**-0.03%**	**0.06%**	**0.18%**		**-0.02%**	**-0.03%**	**-0.03%**	**0.06%**	**0.18%**		**-0.02%**	**-0.03%**	**-0.03%**	**0.05%**	**0.18%**
%F*							**0.0%**	**0.11%**	**0.13%**	**0.25%**	**0.51%**	**0.71%**	**-0.12%**	**0.08%**	**0.12%**	**0.24%**	**0.51%**	**0.7%**	**-0.39%**	**0.05%**	**0.09%**	**0.21%**	**0.48%**	**0.67%**
$m^{\text{NH}_4}_{\text{ov}_{\text{total}}}$	1034.79	1075.368	1075.381	1075.443	1086.521	1105.802	1279.872	1279.585	1279.686	1280.521	1283.511	1287.253	1279.876	1279.972	1279.69	1280.506	1283.506	1287.221	1279.891	1279.97	1279.658	1280.511	1283.49	1287.219
%F		**3.92%**	**3.92%**	**3.93%**	**5.0%**	**6.86%**		**-0.02%**	**-0.01%**	**0.05%**	**0.28%**	**0.58%**		**0.01%**	**-0.01%**	**0.05%**	**0.28%**	**0.57%**		**0.01%**	**-0.02%**	**0.05%**	**0.28%**	**0.57%**
%F*							**0.97%**	**1.12%**	**1.31%**	**1.9%**	**3.25%**	**4.15%**	**0.9%**	**1.14%**	**1.29%**	**1.89%**	**3.25%**	**4.14%**	**0.64%**	**1.12%**	**1.27%**	**1.86%**	**3.23%**	**4.1%**
ξ_{rain}	7.629	7.886	7.854	7.824	7.71	7.699	6.566	6.501	6.448	6.414	6.456	6.483	6.566	6.528	6.448	6.414	6.456	6.483	6.566	6.528	6.448	6.414	6.456	6.483
%F*							**-22.83%**	**-22.85%**	**-23.21%**	**-23.29%**	**-22.34%**	**-22.26%**	**-23.78%**	**-22.65%**	**-23.27%**	**-23.29%**	**-22.38%**	**-22.15%**	**-24.12%**	**-22.73%**	**-23.35%**	**-23.23%**	**-22.45%**	**-22.33%**

Table A.10: Overflow uncertainty: Comparison between PWMPC and optimal SPWMPC for u_p

	PWMPC						**SPWMPC - $\zeta = 0.60$**						**SPWMPC - $\zeta = 0.80$**						**SPWMPC - $\zeta = 0.95$**					
u_p	0%	50%	100%	150%	175%	200%	0%	50%	100%	150%	175%	200%	0%	50%	100%	150%	175%	200%	0%	50%	100%	150%	175%	200%
$Q_{\text{ov}_{\text{total}}}$	168.77	167.682	167.661	167.609	167.595	167.552	177.244	177.244	177.252	177.245	177.234	177.223	177.243	177.244	177.252	177.245	177.234	177.223	177.245	177.243	177.252	177.244	177.234	177.224
%F		**-0.64%**	**-0.66%**	**-0.69%**	**-0.7%**	**-0.72%**		**0.0%**	**0.0%**	**0.0%**	**-0.01%**	**-0.01%**		**0.0%**	**0.01%**	**0.0%**	**-0.01%**	**-0.01%**		**-0.0%**	**0.0%**	**-0.0%**	**-0.01%**	**-0.01%**
%F*							**0.0%**	**0.02%**	**0.03%**	**0.05%**	**0.04%**	**0.04%**	**-0.12%**	**0.01%**	**0.01%**	**-0.0%**	**-0.02%**	**-0.02%**	**-0.39%**	**-0.0%**	**-0.04%**	**-0.07%**	**-0.11%**	**-0.1%**
$m^{\text{NH}_4}_{\text{ov}_{\text{total}}}$	1034.79	1074.136	1071.316	1068.024	1066.955	1064.954	1279.872	1279.809	1279.159	1278.38	1277.986	1276.749	1279.876	1279.801	1279.152	1278.377	1277.972	1276.742	1279.891	1279.811	1279.145	1278.374	1277.986	1276.935
%F		**3.8%**	**3.53%**	**3.21%**	**3.11%**	**2.91%**		**-0.0%**	**-0.06%**	**-0.12%**	**-0.15%**	**-0.24%**		**-0.01%**	**-0.06%**	**-0.12%**	**-0.15%**	**-0.24%**		**-0.01%**	**-0.06%**	**-0.12%**	**-0.15%**	**-0.23%**
%F*							**0.97%**	**0.99%**	**0.99%**	**1.16%**	**1.2%**	**1.14%**	**0.9%**	**0.97%**	**1.06%**	**1.17%**	**1.23%**	**1.21%**	**0.64%**	**0.96%**	**1.08%**	**1.24%**	**1.31%**	**1.44%**
ξ_{rain}	7.629	7.889	7.876	7.872	7.868	7.871	6.566	6.566	6.567	6.575	6.575	6.577	6.566	6.566	6.567	6.575	6.575	6.577	6.566	6.566	6.567	6.575	6.575	6.577
%F*							**-22.83%**	**-22.48%**	**-22.57%**	**-22.52%**	**-22.57%**	**-22.57%**	**-23.78%**	**-22.66%**	**-22.87%**	**-23.03%**	**-23.12%**	**-23.28%**	**-24.12%**	**-22.86%**	**-23.39%**	**-23.64%**	**-23.75%**	**-23.83%**

Table A.11: Overflow uncertainty: Comparison between PWMPC and optimal SPWMPC for overestimating u_{off}

	PWMPC						**SPWMPC - $\zeta = 0.60$**						**SPWMPC - $\zeta = 0.80$**						**SPWMPC - $\zeta = 0.95$**					
u_{off}	0%	5%	10%	25%	50%	75%	0%	5%	10%	25%	50%	75%	0%	5%	10%	25%	50%	75%	0%	5%	10%	25%	50%	75%
$Q_{\text{ov}_{\text{total}}}$	168.77	167.099	167.368	167.516	167.466	167.332	177.244	177.225	173.824	172.57	171.774	170.93	177.243	177.225	173.82	172.571	171.774	170.931	177.245	177.225	173.78	172.571	171.775	170.93
%F		**-0.99%**	**-0.83%**	**-0.74%**	**-0.77%**	**-0.85%**		**-0.01%**	**-1.93%**	**-2.64%**	**-3.09%**	**-3.56%**		**-0.01%**	**-1.93%**	**-2.64%**	**-3.09%**	**-3.56%**		**-0.01%**	**-1.95%**	**-2.64%**	**-3.09%**	**-3.56%**
%F*							**0.0%**	**0.37%**	**-0.95%**	**-0.89%**	**-1.03%**	**-1.49%**	**-0.12%**	**0.37%**	**-0.95%**	**-0.88%**	**-1.03%**	**-1.49%**	**-0.39%**	**0.37%**	**-0.94%**	**-0.86%**	**-1.03%**	**-1.47%**
$m^{\text{NH}_4}_{\text{ov}_{\text{total}}}$	1034.79	1058.702	1037.079	1015.923	1010.801	1010.258	1279.872	1275.944	1184.84	1153.261	1121.587	1115.17	1279.876	1275.936	1184.956	1152.499	1121.584	1115.159	1279.891	1275.932	1182.926	1152.502	1121.586	1115.165
%F		**2.31%**	**0.22%**	**-1.82%**	**-2.32%**	**-2.37%**		**-0.31%**	**-7.43%**	**-9.89%**	**-12.37%**	**-12.87%**		**-0.31%**	**-7.42%**	**-9.95%**	**-12.37%**	**-12.87%**		**-0.31%**	**-7.58%**	**-9.95%**	**-12.37%**	**-12.87%**
%F*							**0.97%**	**2.67%**	**-0.83%**	**-1.68%**	**-4.08%**	**-5.09%**	**0.9%**	**2.67%**	**-0.79%**	**-1.72%**	**-4.09%**	**-5.09%**	**0.64%**	**2.68%**	**-0.83%**	**-1.68%**	**-4.08%**	**-5.08%**
ξ_{rain}	7.629	7.702	7.621	7.553	7.535	7.535	6.566	6.577	6.402	6.377	6.262	6.12	6.566	6.577	6.4	6.375	6.262	6.119	6.566	6.577	6.398	6.375	6.262	6.119
%F*							**-22.83%**	**-22.17%**	**-24.25%**	**-24.4%**	**-25.88%**	**-27.57%**	**-23.78%**	**-22.17%**	**-24.28%**	**-24.42%**	**-25.89%**	**-27.58%**	**-24.12%**	**-22.18%**	**-24.29%**	**-24.42%**	**-25.91%**	**-27.59%**

Table A.12: Overflow uncertainty: Comparison between PWMPC and optimal SPWMPC for underestimating u_{off}

	PWMPC						**SPWMPC - $\zeta = 0.60$**						**SPWMPC - $\zeta = 0.80$**						**SPWMPC - $\zeta = 0.95$**					
u_{off}	0%	−5%	−10%	−25%	−50%	−75%	0%	−5%	−10%	−25%	−50%	−75%	0%	−5%	−10%	−25%	−50%	−75%	0%	−5%	−10%	−25%	−50%	−75%
$Q_{\text{ov}_{\text{total}}}$	168.77	169.609	169.572	169.599	169.561	169.561	177.244	177.252	177.267	177.329	177.35	177.35	177.243	177.252	177.266	177.329	177.349	177.349	177.245	177.252	177.267	177.329	177.349	177.349
%F		**0.5%**	**0.48%**	**0.49%**	**0.47%**	**0.47%**		**0.0%**	**0.01%**	**0.05%**	**0.06%**	**0.06%**		**0.01%**	**0.01%**	**0.05%**	**0.06%**	**0.06%**		**0.0%**	**0.01%**	**0.05%**	**0.06%**	**0.06%**
%F*							**0.0%**	**0.0%**	**-0.0%**	**0.02%**	**0.02%**	**0.02%**	**-0.12%**	**0.0%**	**-0.0%**	**0.02%**	**0.02%**	**0.02%**	**-0.39%**	**-0.0%**	**-0.0%**	**0.02%**	**0.02%**	**0.02%**
$m^{\text{NH}_4}_{\text{ov}_{\text{total}}}$	1034.79	1099.018	1097.333	1096.522	1094.832	1094.832	1279.872	1280.469	1280.715	1280.737	1280.748	1280.748	1279.876	1280.47	1280.711	1280.733	1280.752	1280.75	1279.891	1280.474	1280.713	1280.736	1280.744	1280.744
%F		**6.21%**	**6.04%**	**5.97%**	**5.8%**	**5.8%**		**0.05%**	**0.07%**	**0.07%**	**0.07%**	**0.07%**		**0.05%**	**0.07%**	**0.07%**	**0.07%**	**0.07%**		**0.05%**	**0.06%**	**0.07%**	**0.07%**	**0.07%**
%F*							**0.97%**	**0.81%**	**0.82%**	**0.82%**	**0.82%**	**0.82%**	**0.9%**	**0.81%**	**0.82%**	**0.82%**	**0.82%**	**0.82%**	**0.64%**	**0.8%**	**0.82%**	**0.82%**	**0.82%**	**0.82%**
ξ_{rain}	7.629	7.485	7.501	7.488	7.476	7.476	6.566	6.566	6.566	6.566	6.566	6.566	6.566	6.566	6.566	6.566	6.566	6.566	6.566	6.566	6.566	6.566	6.566	6.566
%F*							**-22.83%**	**-22.48%**	**-22.47%**	**-22.46%**	**-22.46%**	**-22.46%**	**-23.78%**	**-22.48%**	**-22.48%**	**-22.47%**	**-22.47%**	**-22.47%**	**-24.12%**	**-22.5%**	**-22.5%**	**-22.49%**	**-22.49%**	**-22.49%**

A.4 Additional Results for SNPMPC

This section shows the results for SNPMPC compared to NPMPC in the initial scenario and the scenario with optimal weights.

Table A.13: Outflow uncertainty: Comparison between NPMPC and SNPMPC for u_p

	NPMPC						SNPMPC - $\zeta = 0.60$						SNPMPC - $\zeta = 0.80$						SNPMPC - $\zeta = 0.95$					
u_p	0%	25%	75%	100%	125%	175%	0%	25%	75%	100%	125%	175%	0%	25%	75%	100%	125%	175%	0%	25%	75%	100%	125%	175%
$Q_{\text{ov}_{\text{total}}}$	166.872	166.989	167.107	167.135	167.058	167.121	172.913	173.097	173.076	173.102	172.949	173.131	172.938	173.052	173.213	173.121	173.521	173.12	172.901	173.081	173.257	173.813	174.303	174.416
%F		**0.07%**	**0.14%**	**0.16%**	**0.11%**	**0.15%**		**0.11%**	**0.09%**	**0.11%**	**0.02%**	**0.13%**		**0.07%**	**0.16%**	**0.11%**	**0.34%**	**0.11%**		**0.1%**	**0.21%**	**0.53%**	**0.81%**	**0.88%**
$m^{\text{NH}_4}_{\text{ov}_{\text{total}}}$	1009.773	1014.373	1018.229	1018.637	1016.685	1017.137	1154.018	1161.117	1158.888	1158.192	1151.799	1159.639	1154.872	1158.354	1162.172	1153.556	1163.204	1159.287	1153.967	1159.372	1161.901	1164.383	1180.207	1189.38
%F		**0.46%**	**0.84%**	**0.88%**	**0.68%**	**0.73%**		**0.62%**	**0.42%**	**0.36%**	**-0.19%**	**0.49%**		**0.3%**	**0.63%**	**-0.11%**	**0.72%**	**0.38%**		**0.47%**	**0.69%**	**0.9%**	**2.27%**	**3.07%**
ζ_{rain}	9.539	9.399	9.278	9.3	9.329	9.308	9.672	9.513	9.355	9.165	9.321	9.105	9.674	9.424	9.229	9.193	9.214	8.699	9.675	9.391	8.821	8.892	8.567	8.537

Table A.14: Outflow uncertainty: Comparison between NPMPC and SNPMPC for overestimating u_{off}

	NPMPC						SNPMPC - $\zeta = 0.60$						SNPMPC - $\zeta = 0.80$						SNPMPC - $\zeta = 0.95$					
u_{off}	0%	5%	10%	25%	50%	75%	0%	5%	10%	25%	50%	75%	0%	5%	10%	25%	50%	75%	0%	5%	10%	25%	50%	75%
$Q_{\text{ov}_{\text{total}}}$	166.872	166.902	166.815	166.592	166.845	167.097	172.913	172.958	172.686	172.313	172.27	172.608	172.938	172.855	172.774	172.403	172.348	172.612	172.901	172.9	172.728	172.282	172.466	172.822
%F		**0.02%**	**-0.03%**	**-0.17%**	**-0.02%**	**0.13%**		**0.03%**	**-0.13%**	**-0.35%**	**-0.37%**	**-0.18%**		**-0.05%**	**-0.09%**	**-0.31%**	**-0.34%**	**-0.19%**		**-0.0%**	**-0.1%**	**-0.36%**	**-0.25%**	**-0.05%**
$m^{\text{NH}_4}_{\text{ov}_{\text{total}}}$	1009.773	1012.038	1013.581	1010.963	1020.763	1028.285	1154.018	1156.92	1147.022	1139.425	1146.571	1155.749	1154.872	1153.217	1152.608	1143.53	1145.221	1154.576	1153.967	1155.346	1150.056	1137.839	1146.201	1167.079
%F		**0.22%**	**0.38%**	**0.12%**	**1.09%**	**1.83%**		**0.25%**	**-0.61%**	**-1.26%**	**-0.65%**	**0.15%**		**-0.14%**	**-0.2%**	**-0.98%**	**-0.84%**	**-0.03%**		**0.12%**	**-0.34%**	**-1.4%**	**-0.67%**	**1.14%**
ζ_{rain}	9.539	9.361	9.304	9.367	9.41	9.415	9.672	9.512	9.521	9.49	9.562	9.522	9.674	9.441	9.539	9.387	9.458	9.536	9.675	9.354	9.412	9.422	9.465	9.502

Table A.15: Outflow uncertainty: Comparison between NPMPC and SNPMPC for underestimating u_{off}

	NPMPC						SNPMPC - $\zeta = 0.60$						SNPMPC - $\zeta = 0.80$						SNPMPC - $\zeta = 0.95$					
u_{off}	0%	−5%	−10%	−25%	−50%	−75%	0%	−5%	−10%	−25%	−50%	−75%	0%	−5%	−10%	−25%	−50%	−75%	0%	−5%	−10%	−25%	−50%	−75%
$Q_{\text{ov}_{\text{total}}}$	166.872	167.296	167.761	168.456	168.169	167.211	172.913	173.197	173.232	173.4	174.013	174.53	172.938	173.132	173.171	173.348	173.804	173.799	172.901	173.463	173.005	173.403	173.47	173.858
%F		**0.25%**	**0.53%**	**0.95%**	**0.78%**	**0.2%**		**0.16%**	**0.18%**	**0.28%**	**0.64%**	**0.94%**		**0.11%**	**0.13%**	**0.24%**	**0.5%**	**0.5%**		**0.33%**	**0.06%**	**0.29%**	**0.33%**	**0.55%**
$m^{\text{NH}_4}_{\text{ov}_{\text{total}}}$	1009.773	1021.37	1030.344	1042.714	1041.437	1027.929	1154.018	1165.905	1166.8	1172.736	1200.972	1217.301	1154.872	1163.291	1165.039	1171.534	1191.174	1194.271	1153.967	1165.242	1159.516	1171.198	1178.105	1203.158
%F		**1.15%**	**2.04%**	**3.26%**	**3.14%**	**1.8%**		**1.03%**	**1.11%**	**1.62%**	**4.07%**	**5.48%**		**0.73%**	**0.88%**	**1.44%**	**3.14%**	**3.41%**		**0.98%**	**0.48%**	**1.49%**	**2.09%**	**4.26%**
ζ_{rain}	9.539	9.479	9.521	9.465	9.383	9.455	9.672	9.566	9.588	9.532	8.949	8.519	9.674	9.52	9.593	9.468	8.493	8.175	9.675	9.484	9.563	9.347	8.24	8.16

Table A.16: Overflow uncertainty: Comparison between NPMPC and SNPMPC for u_p

	NPMPC						SNPMPC - $\zeta = 0.60$						SNPMPC - $\zeta = 0.80$						SNPMPC - $\zeta = 0.95$					
u_p	0%	50%	100%	150%	175%	200%	0%	50%	100%	150%	175%	200%	0%	50%	100%	150%	175%	200%	0%	50%	100%	150%	175%	200%
$Q_{\text{ov}_{\text{total}}}$	166.872	167.01	166.973	166.957	166.981	166.915	172.913	173.372	173.579	173.858	173.953	174.115	172.938	173.832	174.642	174.361	174.925	175.547	172.901	174.707	175.289	175.872	175.708	175.843
%F		**0.08%**	**0.06%**	**0.05%**	**0.07%**	**0.03%**		**0.27%**	**0.39%**	**0.55%**	**0.6%**	**0.7%**		**0.52%**	**0.99%**	**0.82%**	**1.15%**	**1.51%**		**1.04%**	**1.38%**	**1.72%**	**1.62%**	**1.7%**
$m^{\text{NH}_4}_{\text{ov}_{\text{total}}}$	1009.773	1017.832	1015.81	1010.548	1010.759	1008.569	1154.018	1162.738	1164.993	1170.857	1173.297	1175.183	1154.872	1174.942	1190.167	1182.392	1190.499	1208.602	1153.967	1199.49	1205.608	1208.045	1207.264	1197.868
%F		**0.8%**	**0.6%**	**0.08%**	**0.1%**	**-0.12%**		**0.76%**	**0.95%**	**1.46%**	**1.67%**	**1.83%**		**1.74%**	**3.06%**	**2.38%**	**3.08%**	**4.65%**		**3.94%**	**4.48%**	**4.69%**	**4.62%**	**3.8%**
ζ_{rain}	9.539	9.541	9.542	9.54	9.536	9.534	9.672	9.117	8.985	8.734	8.711	8.576	9.674	8.613	7.86	8.135	7.453	7.113	9.675	7.701	7.195	6.633	6.741	6.993

Table A.17: Overflow uncertainty: Comparison between NPMPC and SNPMPC for overestimating u_{off}

	NPMPC						SNPMPC - $\zeta = 0.60$						SNPMPC - $\zeta = 0.80$						SNPMPC - $\zeta = 0.95$					
u_{off}	0%	5%	10%	25%	50%	75%	0%	5%	10%	25%	50%	75%	0%	5%	10%	25%	50%	75%	0%	5%	10%	25%	50%	75%
$Q_{\text{ov}_{\text{total}}}$	166.872	167.053	168.237	169.605	170.313	170.356	172.913	174.671	174.701	172.108	171.522	171.181	172.938	174.979	175.021	172.553	171.887	171.414	172.901	175.691	175.512	172.815	172.389	171.78
%F		**0.11%**	**0.82%**	**1.64%**	**2.06%**	**2.09%**		**1.02%**	**1.03%**	**-0.47%**	**-0.8%**	**-1.0%**		**1.18%**	**1.2%**	**-0.22%**	**-0.61%**	**-0.88%**		**1.61%**	**1.51%**	**-0.05%**	**-0.3%**	**-0.65%**
$m^{\text{NH}_4}_{\text{ov}_{\text{total}}}$	1009.773	991.537	1008.578	1037.051	1060.8	1062.015	1154.018	1200.788	1203.69	1146.389	1117.503	1117.324	1154.872	1206.946	1210.865	1158.594	1125.755	1122.121	1153.967	1225.076	1220.074	1159.417	1139.029	1130.48
%F		**-1.81%**	**-0.12%**	**2.7%**	**5.05%**	**5.17%**		**4.05%**	**4.3%**	**-0.66%**	**-3.16%**	**-3.18%**		**4.51%**	**4.85%**	**0.32%**	**-2.52%**	**-2.84%**		**6.16%**	**5.73%**	**0.47%**	**-1.29%**	**-2.04%**
ζ_{rain}	9.539	9.486	9.47	9.458	9.456	9.458	9.672	9.468	9.218	9.366	9.481	9.479	9.674	9.114	8.87	8.862	9.139	9.304	9.675	8.382	8.347	8.587	8.722	8.814

Table A.18: Overflow uncertainty: Comparison between NPMPC and SNPMPC for underestimating u_{off}

	NPMPC						SNPMPC - $\zeta = 0.60$						SNPMPC - $\zeta = 0.80$						SNPMPC - $\zeta = 0.95$					
u_{off}	0%	−5%	−10%	−25%	−50%	−75%	0%	−5%	−10%	−25%	−50%	−75%	0%	−5%	−10%	−25%	−50%	−75%	0%	−5%	−10%	−25%	−50%	−75%
$Q_{\text{ov}_{\text{total}}}$	166.872	167.406	167.358	167.442	167.307	167.414	172.913	173.091	173.192	172.936	173.239	173.19	172.938	173.732	173.982	173.913	173.754	173.96	172.901	174.202	174.736	175.201	174.625	174.509
%F		**0.32%**	**0.29%**	**0.34%**	**0.26%**	**0.32%**		**0.1%**	**0.16%**	**0.01%**	**0.19%**	**0.16%**		**0.46%**	**0.6%**	**0.56%**	**0.47%**	**0.59%**		**0.75%**	**1.06%**	**1.33%**	**1.0%**	**0.93%**
$m^{\text{NH}_4}_{\text{ov}_{\text{total}}}$	1009.773	1043.906	1043.317	1047.655	1041.86	1046.62	1154.018	1155.159	1155.647	1148.968	1154.73	1157.606	1154.872	1168.155	1179.335	1172.007	1167.42	1170.895	1153.967	1174.397	1190.548	1191.292	1190.435	1183.447
%F		**3.38%**	**3.32%**	**3.75%**	**3.18%**	**3.65%**		**0.1%**	**0.14%**	**-0.44%**	**0.06%**	**0.31%**		**1.15%**	**2.12%**	**1.48%**	**1.09%**	**1.39%**		**1.77%**	**3.17%**	**3.23%**	**3.16%**	**2.55%**
ξ_{rain}	9.539	9.524	9.535	9.532	9.528	9.533	9.672	9.114	8.988	9.269	8.96	9.069	9.674	8.427	8.122	8.33	8.402	8.274	9.675	7.952	7.428	7.599	7.603	7.87

Table A.19: Outflow uncertainty: Comparison between NPMPC and optimal SNPMPC for u_p

	NPMPC						SNPMPC - $\zeta = 0.60$						SNPMPC - $\zeta = 0.80$						SNPMPC - $\zeta = 0.95$					
u_p	0%	25%	75%	100%	125%	175%	0%	25%	75%	100%	125%	175%	0%	25%	75%	100%	125%	175%	0%	25%	75%	100%	125%	175%
$Q_{\text{ov}_{\text{total}}}$	166.872	166.989	167.107	167.135	167.058	167.121	172.511	172.655	172.819	172.938	172.983	173.131	172.507	172.779	172.923	172.997	173.18	173.291	172.518	172.829	173.03	173.029	173.076	173.336
%F		**0.07%**	**0.14%**	**0.16%**	**0.11%**	**0.15%**		**0.08%**	**0.18%**	**0.25%**	**0.27%**	**0.36%**		**0.16%**	**0.24%**	**0.28%**	**0.39%**	**0.45%**		**0.18%**	**0.3%**	**0.3%**	**0.32%**	**0.47%**
%F*							**-0.23%**	**-0.26%**	**-0.15%**	**-0.09%**	**0.02%**	**-0.0%**	**-0.25%**	**-0.16%**	**-0.17%**	**-0.07%**	**-0.2%**	**0.1%**	**-0.22%**	**-0.15%**	**-0.13%**	**-0.45%**	**-0.7%**	**-0.62%**
$m^{\text{NH}_4}_{\text{total}}$	1009.773	1014.373	1018.229	1018.637	1016.685	1017.137	1118.019	1127.525	1126.634	1130.974	1131.281	1131.975	1117.937	1131.167	1129.176	1132.582	1139.441	1134.769	1118.165	1131.977	1134.382	1131.992	1133.008	1136.201
%F		**0.46%**	**0.84%**	**0.88%**	**0.68%**	**0.73%**		**0.85%**	**0.77%**	**1.16%**	**1.19%**	**1.25%**		**1.18%**	**1.01%**	**1.31%**	**1.92%**	**1.51%**		**1.24%**	**1.45%**	**1.24%**	**1.33%**	**1.61%**
%F*							**-3.12%**	**-2.89%**	**-2.78%**	**-2.35%**	**-1.78%**	**-2.39%**	**-3.2%**	**-2.35%**	**-2.84%**	**-1.82%**	**-2.04%**	**-2.11%**	**-3.1%**	**-2.36%**	**-2.37%**	**-2.78%**	**-4.0%**	**-4.47%**
ξ_{rain}	9.539	9.399	9.278	9.3	9.329	9.308	9.613	9.451	9.303	9.306	9.152	9.106	9.612	9.356	9.25	9.133	9.039	9.108	9.612	9.259	9.219	9.118	9.119	9.134
%F*							**-0.61%**	**-0.65%**	**-0.56%**	**1.54%**	**-1.81%**	**0.01%**	**-0.64%**	**-0.72%**	**0.23%**	**-0.65%**	**-1.9%**	**4.7%**	**-0.65%**	**-1.41%**	**4.51%**	**2.54%**	**6.44%**	**6.99%**

Table A.20: Outflow uncertainty: Comparison between NPMPC and optimal SNPMPC for overestimating u_{off}

	NPMPC						SNPMPC - $\zeta = 0.60$						SNPMPC - $\zeta = 0.80$						SNPMPC - $\zeta = 0.95$					
u_{off}	0%	5%	10%	25%	50%	75%	0%	5%	10%	25%	50%	75%	0%	5%	10%	25%	50%	75%	0%	5%	10%	25%	50%	75%
$Q_{\text{ov}_{\text{total}}}$	166.872	166.902	166.815	166.592	166.845	167.097	172.511	172.529	172.259	172.003	171.615	171.693	172.507	172.591	172.264	171.98	171.69	171.698	172.518	172.607	172.456	171.923	171.629	171.826
%F		**0.02%**	**-0.03%**	**-0.17%**	**-0.02%**	**0.13%**		**0.01%**	**-0.15%**	**-0.29%**	**-0.52%**	**-0.47%**		**0.05%**	**-0.14%**	**-0.31%**	**-0.47%**	**-0.47%**		**0.05%**	**-0.04%**	**-0.34%**	**-0.52%**	**-0.4%**
%F*							**-0.23%**	**-0.25%**	**-0.25%**	**-0.18%**	**-0.38%**	**-0.53%**	**-0.25%**	**-0.15%**	**-0.3%**	**-0.25%**	**-0.38%**	**-0.53%**	**-0.22%**	**-0.17%**	**-0.16%**	**-0.21%**	**-0.49%**	**-0.58%**
$m^{\text{NH}_4}_{\text{total}}$	1009.773	1012.038	1013.581	1010.963	1020.763	1028.285	1118.019	1122.199	1114.795	1110.909	1101.918	1093.028	1117.937	1125.385	1116.154	1111.01	1101.517	1095.231	1118.165	1125.317	1121.094	1111.564	1102.519	1101.417
%F		**0.22%**	**0.38%**	**0.12%**	**1.09%**	**1.83%**		**0.37%**	**-0.29%**	**-0.64%**	**-1.44%**	**-2.24%**		**0.67%**	**-0.16%**	**-0.62%**	**-1.47%**	**-2.03%**		**0.64%**	**0.26%**	**-0.59%**	**-1.4%**	**-1.5%**
%F*							**-3.12%**	**-3.0%**	**-2.81%**	**-2.5%**	**-3.89%**	**-5.43%**	**-3.2%**	**-2.41%**	**-3.16%**	**-2.84%**	**-3.82%**	**-5.14%**	**-3.1%**	**-2.6%**	**-2.52%**	**-2.31%**	**-3.81%**	**-5.63%**
ξ_{rain}	9.539	9.361	9.304	9.367	9.41	9.415	9.613	9.352	9.395	9.395	9.344	9.423	9.612	9.325	9.37	9.357	9.372	9.348	9.612	9.336	9.246	9.304	9.362	9.385
%F*							**-0.61%**	**-1.68%**	**-1.32%**	**-1.0%**	**-2.28%**	**-1.04%**	**-0.64%**	**-1.23%**	**-1.77%**	**-0.32%**	**-0.91%**	**-1.97%**	**-0.65%**	**-0.19%**	**-1.76%**	**-1.25%**	**-1.09%**	**-1.23%**

Table A.21: Outflow uncertainty: Comparison between NPMPC and optimal SNPMPC for underestimating u_{off}

	NPMPC						SNPMPC - $\zeta = 0.60$						SNPMPC - $\zeta = 0.80$						SNPMPC - $\zeta = 0.95$					
u_{off}	0%	−5%	−10%	−25%	−50%	−75%	0%	−5%	−10%	−25%	−50%	−75%	0%	−5%	−10%	−25%	−50%	−75%	0%	−5%	−10%	−25%	−50%	−75%
$Q_{\text{ov}_{\text{total}}}$	166.872	167.296	167.761	168.456	168.169	167.211	172.511	172.776	172.949	173.135	174.642	175.897	172.507	172.727	173.07	173.408	175.558	176.876	172.518	172.92	173.197	173.314	175.963	177.418
%F		**0.25%**	**0.53%**	**0.95%**	**0.78%**	**0.2%**		**0.15%**	**0.25%**	**0.36%**	**1.24%**	**1.96%**		**0.13%**	**0.33%**	**0.52%**	**1.77%**	**2.53%**		**0.23%**	**0.39%**	**0.46%**	**2.0%**	**2.84%**
%F*							**-0.23%**	**-0.24%**	**-0.16%**	**-0.15%**	**0.36%**	**0.78%**	**-0.25%**	**-0.23%**	**-0.06%**	**0.03%**	**1.01%**	**1.77%**	**-0.22%**	**-0.31%**	**0.11%**	**-0.05%**	**1.44%**	**2.05%**
$m^{\text{NH}_4}_{\text{total}}$	1009.773	1021.37	1030.344	1042.714	1041.437	1027.929	1118.019	1131.637	1129.211	1124.038	1164.879	1186.124	1117.937	1127.373	1134.71	1129.134	1180.629	1214.024	1118.165	1130.902	1136.621	1124.962	1187.655	1220.811
%F		**1.15%**	**2.04%**	**3.26%**	**3.14%**	**1.8%**		**1.22%**	**1.0%**	**0.54%**	**4.19%**	**6.09%**		**0.84%**	**1.5%**	**1.0%**	**5.61%**	**8.6%**		**1.14%**	**1.65%**	**0.61%**	**6.21%**	**9.18%**
%F*							**-3.12%**	**-2.94%**	**-3.22%**	**-4.15%**	**-3.01%**	**-2.56%**	**-3.2%**	**-3.09%**	**-2.6%**	**-3.62%**	**-0.89%**	**1.65%**	**-3.1%**	**-2.95%**	**-1.97%**	**-3.95%**	**0.81%**	**1.47%**
ξ_{rain}	9.539	9.479	9.521	9.465	9.383	9.455	9.613	9.509	9.523	9.366	8.678	7.883	9.612	9.435	9.345	9.233	8.369	7.503	9.612	9.397	9.439	9.261	8.187	6.954
%F*							**-0.61%**	**-0.6%**	**-0.68%**	**-1.74%**	**-3.03%**	**-7.47%**	**-0.64%**	**-0.89%**	**-2.59%**	**-2.48%**	**-1.46%**	**-8.22%**	**-0.65%**	**-0.92%**	**-1.3%**	**-0.92%**	**-0.64%**	**-14.78%**

Table A.22: Overflow uncertainty: Comparison between NPMPC and optimal SNPMPC for u_p

	NPMPC						SNPMPC - $\zeta = 0.60$						SNPMPC - $\zeta = 0.80$						SNPMPC - $\zeta = 0.95$					
u_p	0%	50%	100%	150%	175%	200%	0%	50%	100%	150%	175%	200%	0%	50%	100%	150%	175%	200%	0%	50%	100%	150%	175%	200%
$Q_{\text{ov}_{\text{total}}}$	166.872	167.01	166.973	166.957	166.981	166.915	172.511	172.472	172.598	172.616	172.619	172.825	172.507	172.579	172.614	172.702	172.806	172.827	172.518	172.467	172.684	172.771	172.875	172.967
%F		**0.08%**	**0.06%**	**0.05%**	**0.07%**	**0.03%**		**-0.02%**	**0.05%**	**0.06%**	**0.06%**	**0.18%**		**0.04%**	**0.06%**	**0.11%**	**0.17%**	**0.19%**		**-0.03%**	**0.1%**	**0.15%**	**0.21%**	**0.26%**
%F*							**-0.23%**	**-0.52%**	**-0.57%**	**-0.71%**	**-0.77%**	**-0.74%**	**-0.25%**	**-0.72%**	**-1.16%**	**-0.95%**	**-1.21%**	**-1.55%**	**-0.22%**	**-1.28%**	**-1.49%**	**-1.76%**	**-1.61%**	**-1.64%**
$m^{\text{NH}_4}_{\text{total}}$	1009.773	1017.832	1015.81	1010.548	1010.759	1008.569	1118.019	1116.477	1121.438	1116.914	1116.942	1121.59	1117.937	1117.948	1121.775	1118.477	1122.624	1121.343	1118.165	1119.3	1123.937	1121.943	1119.984	1123.018
%F		**0.8%**	**0.6%**	**0.08%**	**0.1%**	**-0.12%**		**-0.14%**	**0.31%**	**-0.1%**	**-0.1%**	**0.32%**		**0.0%**	**0.34%**	**0.05%**	**0.42%**	**0.3%**		**0.1%**	**0.52%**	**0.34%**	**0.16%**	**0.43%**
%F*							**-3.12%**	**-3.98%**	**-3.74%**	**-4.61%**	**-4.8%**	**-4.56%**	**-3.2%**	**-4.85%**	**-5.75%**	**-5.41%**	**-5.7%**	**-7.22%**	**-3.1%**	**-6.69%**	**-6.77%**	**-7.13%**	**-7.23%**	**-6.25%**
ξ_{rain}	9.539	9.541	9.542	9.54	9.536	9.534	9.613	9.516	9.459	9.456	9.426	9.211	9.612	9.361	9.373	9.348	9.38	9.254	9.612	9.398	9.343	9.333	9.295	9.237
%F*							**-0.61%**	**4.38%**	**5.28%**	**8.27%**	**8.21%**	**7.4%**	**-0.64%**	**8.68%**	**19.25%**	**14.91%**	**25.86%**	**30.1%**	**-0.65%**	**22.04%**	**29.85%**	**40.71%**	**37.89%**	**32.09%**

Table A.23: Overflow uncertainty: Comparison between NPMPC and optimal SNPMPC for overestimating u_{off}

	NPMPC						**SNPMPC - $\zeta = 0.60$**						**SNPMPC - $\zeta = 0.80$**						**SNPMPC - $\zeta = 0.95$**					
u_{off}	0%	5%	10%	25%	50%	75%	0%	5%	10%	25%	50%	75%	0%	5%	10%	25%	50%	75%	0%	5%	10%	25%	50%	75%
$Q_{\text{ov}_{\text{total}}}$	166.872	167.053	168.237	169.605	170.313	170.356	172.511	174.488	175.34	176.564	177.068	176.994	172.507	174.506	175.379	176.623	177.146	177.025	172.518	174.615	175.384	176.651	177.157	177.019
%F		**0.11%**	**0.82%**	**1.64%**	**2.06%**	**2.09%**		**1.15%**	**1.64%**	**2.35%**	**2.64%**	**2.6%**		**1.16%**	**1.66%**	**2.39%**	**2.69%**	**2.62%**		**1.22%**	**1.66%**	**2.4%**	**2.69%**	**2.61%**
%F*							**-0.23%**	**-0.1%**	**0.37%**	**2.59%**	**3.23%**	**3.4%**	**-0.25%**	**-0.27%**	**0.2%**	**2.36%**	**3.06%**	**3.27%**	**-0.22%**	**-0.61%**	**-0.07%**	**2.22%**	**2.77%**	**3.05%**
$m_{\text{total}}^{\text{NH}_4}$	1009.773	991.537	1008.578	1037.051	1060.8	1062.015	1118.019	1163.706	1166.923	1161.216	1168.464	1166.28	1117.937	1163.5	1167.825	1163.167	1168.982	1167.227	1118.165	1163.572	1166.922	1165.461	1169.436	1167.516
%F		**-1.81%**	**-0.12%**	**2.7%**	**5.05%**	**5.17%**		**4.09%**	**4.37%**	**3.86%**	**4.51%**	**4.32%**		**4.08%**	**4.46%**	**4.05%**	**4.57%**	**4.41%**		**4.06%**	**4.36%**	**4.23%**	**4.59%**	**4.41%**
%F*							**-3.12%**	**-3.09%**	**-3.05%**	**1.29%**	**4.56%**	**4.38%**	**-3.2%**	**-3.6%**	**-3.55%**	**0.39%**	**3.84%**	**4.02%**	**-3.1%**	**-5.02%**	**-4.36%**	**0.52%**	**2.67%**	**3.28%**
ξ_{min}	9.539	9.486	9.47	9.458	9.456	9.458	9.613	9.52	9.507	9.511	9.56	9.535	9.612	9.444	9.432	9.486	9.444	9.511	9.612	9.338	9.436	9.437	9.397	9.414
%F*							**-0.61%**	**0.55%**	**3.14%**	**1.55%**	**0.83%**	**0.59%**	**-0.64%**	**3.62%**	**6.34%**	**7.04%**	**3.34%**	**2.22%**	**-0.65%**	**11.41%**	**13.05%**	**9.9%**	**7.74%**	**6.81%**

Table A.24: Overflow uncertainty: Comparison between NPMPC and optimal SNPMPC for underestimating u_{off}

	NPMPC						**SNPMPC - $\zeta = 0.60$**						**SNPMPC - $\zeta = 0.80$**						**SNPMPC - $\zeta = 0.95$**					
u_{off}	0%	−5%	−10%	−25%	−50%	−75%	0%	−5%	−10%	−25%	−50%	−75%	0%	−5%	−10%	−25%	−50%	−75%	0%	−5%	−10%	−25%	−50%	−75%
$Q_{\text{ov}_{\text{total}}}$	166.872	167.406	167.358	167.442	167.307	167.414	172.511	171.806	171.84	172.048	172.146	172.013	172.507	172.011	171.941	172.256	171.865	171.918	172.518	172.057	172.016	172.101	172.172	171.887
%F		**0.32%**	**0.29%**	**0.34%**	**0.26%**	**0.32%**		**-0.41%**	**-0.39%**	**-0.27%**	**-0.21%**	**-0.29%**		**-0.29%**	**-0.33%**	**-0.15%**	**-0.37%**	**-0.34%**		**-0.27%**	**-0.29%**	**-0.24%**	**-0.2%**	**-0.37%**
%F*							**-0.23%**	**-0.74%**	**-0.78%**	**-0.51%**	**-0.63%**	**-0.68%**	**-0.25%**	**-0.99%**	**-1.17%**	**-0.95%**	**-1.09%**	**-1.17%**	**-0.22%**	**-1.23%**	**-1.56%**	**-1.77%**	**-1.4%**	**-1.5%**
$m_{\text{total}}^{\text{NH}_4}$	1009.773	1043.906	1043.317	1047.655	1041.86	1046.62	1118.019	1104.268	1107.472	1114.435	1115.387	1113.28	1117.937	1109.219	1111.701	1120.139	1107.911	1107.959	1118.165	1110.647	1109.593	1111.69	1114.769	1108.044
%F		**3.38%**	**3.32%**	**3.75%**	**3.18%**	**3.65%**		**-1.23%**	**-0.94%**	**-0.32%**	**-0.24%**	**-0.42%**		**-0.78%**	**-0.56%**	**0.2%**	**-0.9%**	**-0.89%**		**-0.67%**	**-0.77%**	**-0.58%**	**-0.3%**	**-0.91%**
%F*							**-3.12%**	**-4.41%**	**-4.17%**	**-3.01%**	**-3.41%**	**-3.83%**	**-3.2%**	**-5.05%**	**-5.73%**	**-4.43%**	**-5.1%**	**-5.38%**	**-3.1%**	**-5.43%**	**-6.8%**	**-6.68%**	**-6.36%**	**-6.37%**
ξ_{min}	9.539	9.524	9.535	9.532	9.528	9.533	9.613	9.493	9.378	9.234	9.195	9.231	9.612	9.363	9.275	9.111	9.223	9.247	9.612	9.332	9.199	9.118	9.035	9.205
%F*							**-0.61%**	**4.16%**	**4.34%**	**-0.38%**	**2.62%**	**1.79%**	**-0.64%**	**11.11%**	**14.2%**	**9.38%**	**9.77%**	**11.76%**	**-0.65%**	**17.35%**	**23.84%**	**19.99%**	**18.83%**	**16.96%**

A.5 Additional Results for Urban Drainage System 1

In this section, the Morris Screening for Urban Drainage System 1 is presented.

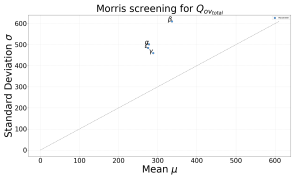

(a) Period 1 VMPC $Q_{\mathrm{ov}_{\mathrm{total}}}$

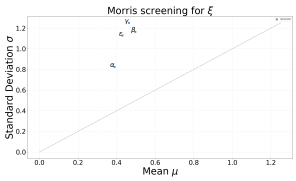

(b) Period 1 VMPC ξ

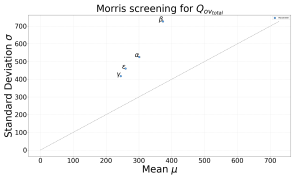

(c) Period 2 VMPC $Q_{\mathrm{ov}_{\mathrm{total}}}$

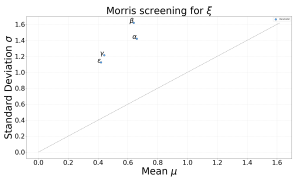

(d) Period 2 VMPC ξ

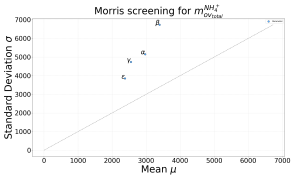

(e) Period 1 PWMPC $m^{\mathrm{NH}_4}_{\mathrm{ov}_{\mathrm{total}}}$

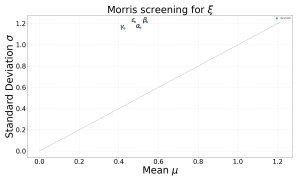

(f) Period 1 PWMPC ξ

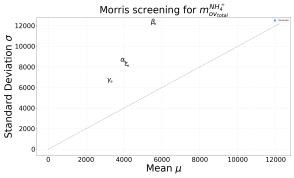

(g) Period 2 PWMPC $m^{\mathrm{NH}_4}_{\mathrm{ov}_{\mathrm{total}}}$

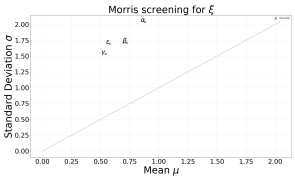

(h) Period 2 PWMPC ξ

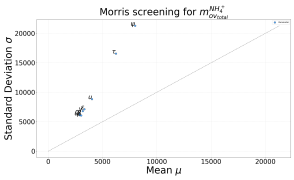

(i) Period 1 NPMPC $m^{\mathrm{NH}_4}_{\mathrm{ov}_{\mathrm{total}}}$

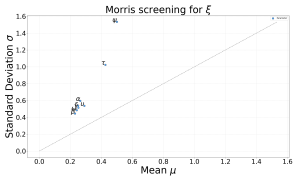

(j) Period 1 NPMPC ξ

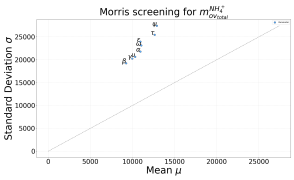

(k) Period 2 NPMPC $m^{\mathrm{NH}_4}_{\mathrm{ov}_{\mathrm{total}}}$

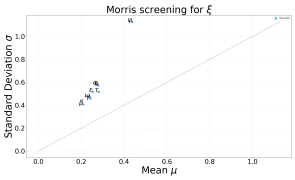

(l) Period 2 NPMPC ξ

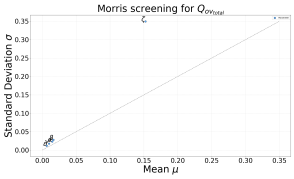

(m) Period 1 SVMPC $Q_{\mathrm{ov}_{\mathrm{total}}}$

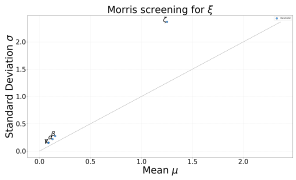

(n) Period 1 SVMPC ξ

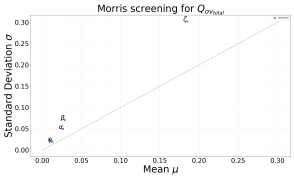

(o) Period 2 SVMPC $Q_{\mathrm{ov}_{\mathrm{total}}}$

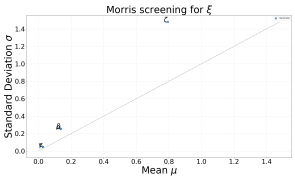

(p) Period 2 SVMPC ξ

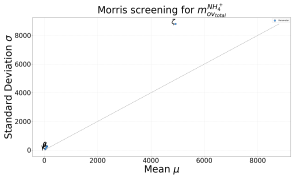

(q) Period 1 SPWMPC $m^{\mathrm{NH}_4}_{\mathrm{ov}_{\mathrm{total}}}$

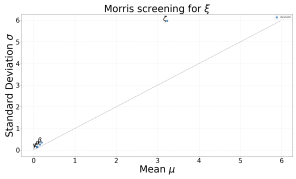

(r) Period 1 SPWMPC ξ

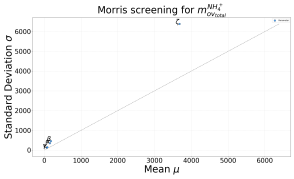

(s) Period 2 SPWMPC $m^{\mathrm{NH}_4}_{\mathrm{ov}_{\mathrm{total}}}$

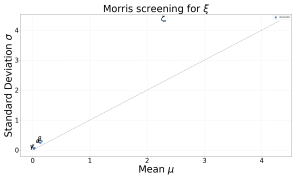

(t) Period 2 SPWMPC ξ

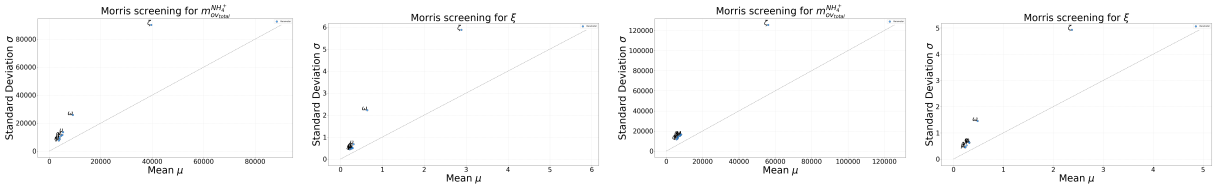

(u) Period 1 SNPMPC $m_{ov_{total}}^{NH_4}$ *(v)* Period 1 SNPMPC ξ *(w)* Period 2 SNPMPC $m_{ov_{total}}^{NH_4}$ *(x)* Period 2 SNPMPC ξ

Figure A.25: Morris Screening for Urban Drainage System 1.

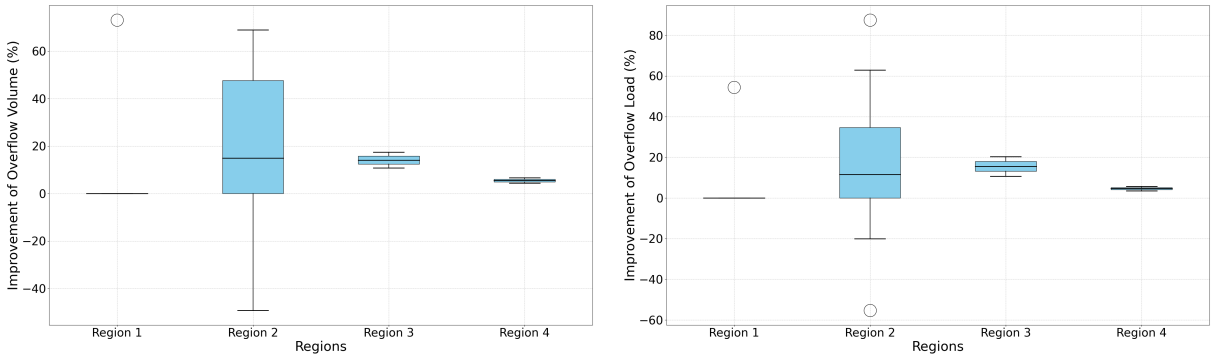

(a) Improvement of overflow volume (I_v in %) under PWMPC compared to static control.

(b) Improvement of overflow load (I_m in %) under PWMPC compared to static control.

Figure A.26: Comparison of overflow load and volume improvement between PWMPC and static control across four regions with varying hydrological characteristics.

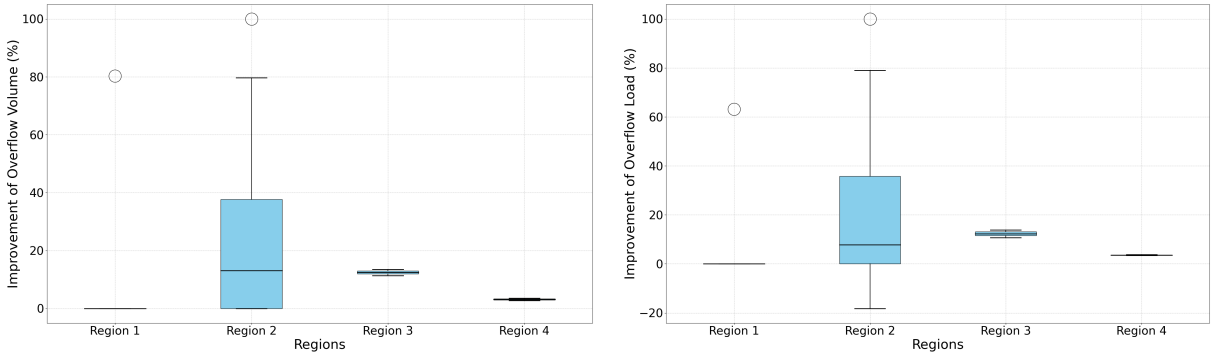

(a) Improvement of overflow volume (I_v in %) under SVMPC compared to static control.

(b) Improvement of overflow load (I_m in %) under SVMPC compared to static control.

Figure A.27: Comparison of overflow load and volume improvement between SVMPC and static control across four regions with varying hydrological characteristics.

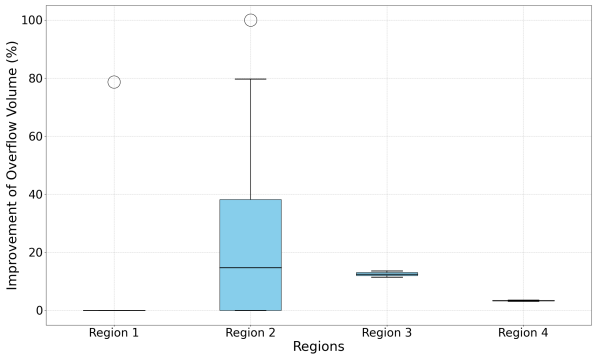

(a) Improvement of overflow volume (I_v in %) under SPWMPC compared to static control.

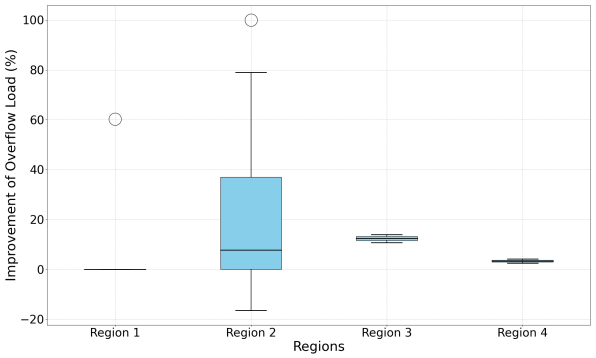

(b) Improvement of overflow load (I_m in %) under SPWMPC compared to static control.

Figure A.28: Comparison of overflow load and volume improvement between SPWMPC and static control across four regions with varying hydrological characteristics.

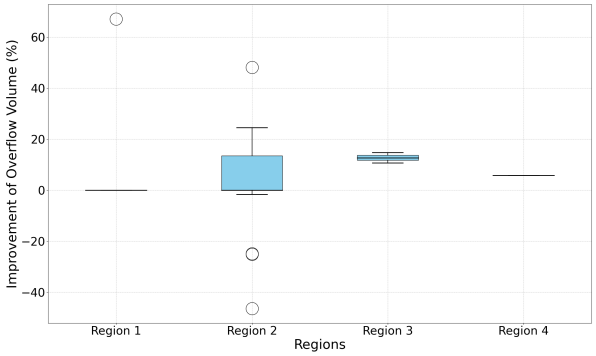

(a) Improvement of overflow volume (I_v in %) under SNPMPC compared to static control.

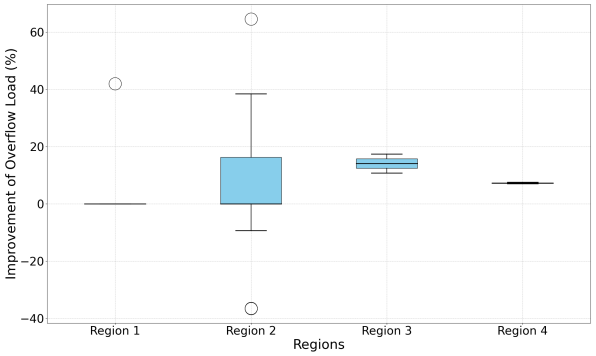

(b) Improvement of overflow load (I_m in %) under SNPMPC compared to static control.

Figure A.29: Comparison of overflow load and volume improvement between SNPMPC and static control across four regions with varying hydrological characteristics.

A.6 Additional Results for Urban Drainage System 2

In this section, the box plot for Urban Drainage System 2 is presented. Figure A.30

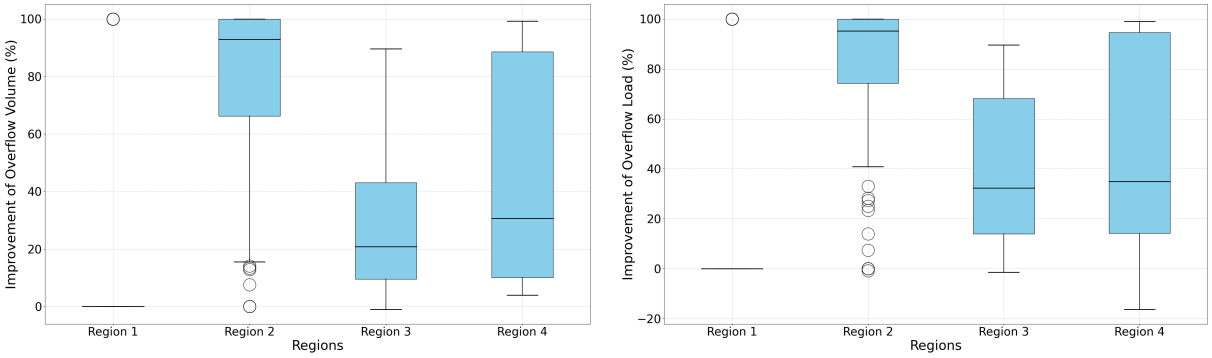

(a) Improvement of overflow volume (I_v in %) under PWMPC compared to static control.

(b) Improvement of overflow load (I_m in %) under PWMPC compared to static control.

Figure A.30: Comparison of overflow load and volume improvement between PWMPC and static control across four regions with varying hydrological characteristics.

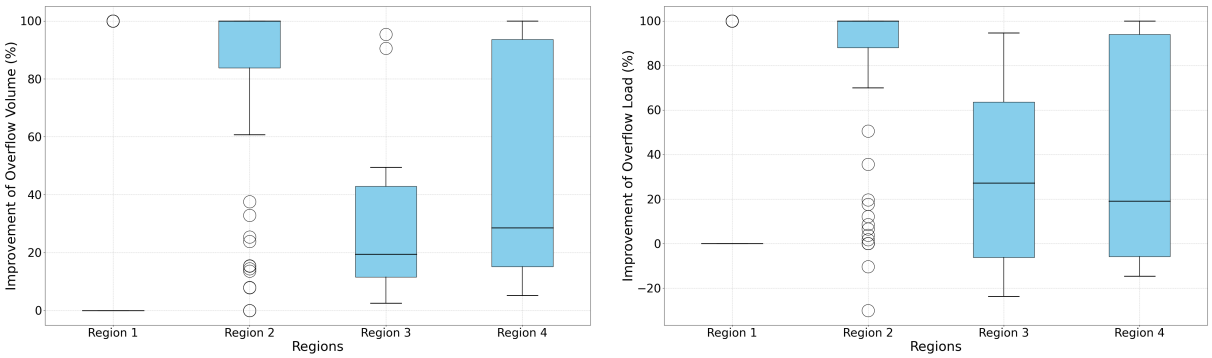

(a) Improvement of overflow volume (I_v in %) under SVMPC compared to static control.

(b) Improvement of overflow load (I_m in %) under SVMPC compared to static control.

Figure A.31: Comparison of overflow load and volume improvement between SVMPC and static control across four regions with varying hydrological characteristics.

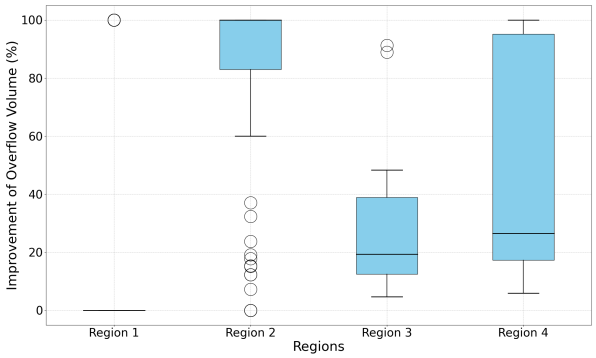

(a) Improvement of overflow volume (I_v in %) under SPWMPC compared to static control.

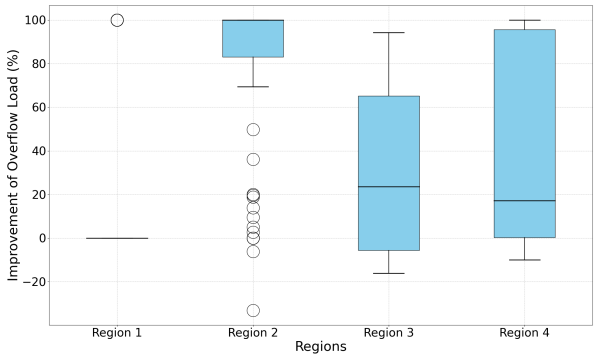

(b) Improvement of overflow load (I_m in %) under SPWMPC compared to static control.

Figure A.32: Comparison of overflow load and volume improvement between SPWMPC and static control across four regions with varying hydrological characteristics.

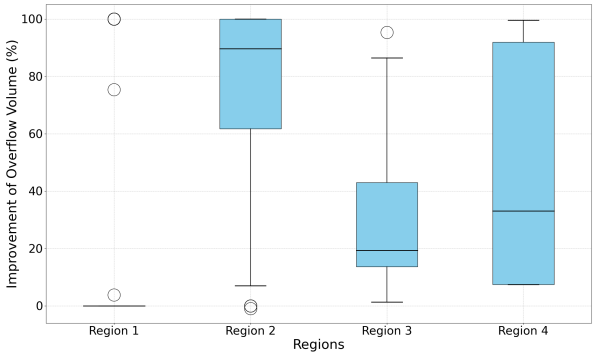

(a) Improvement of overflow volume (I_v in %) under SNPMPC compared to static control.

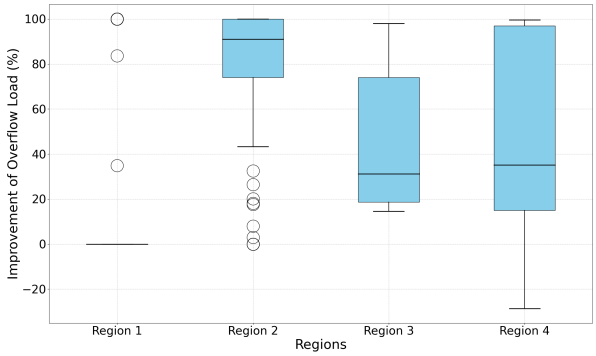

(b) Improvement of overflow load (I_m in %) under SNPMPC compared to static control.

Figure A.33: Comparison of overflow load and volume improvement between SNPMPC and static control across four regions with varying hydrological characteristics.

A.7 Additional Results for ML-MPC

This section provides additional results for ML-MPC.

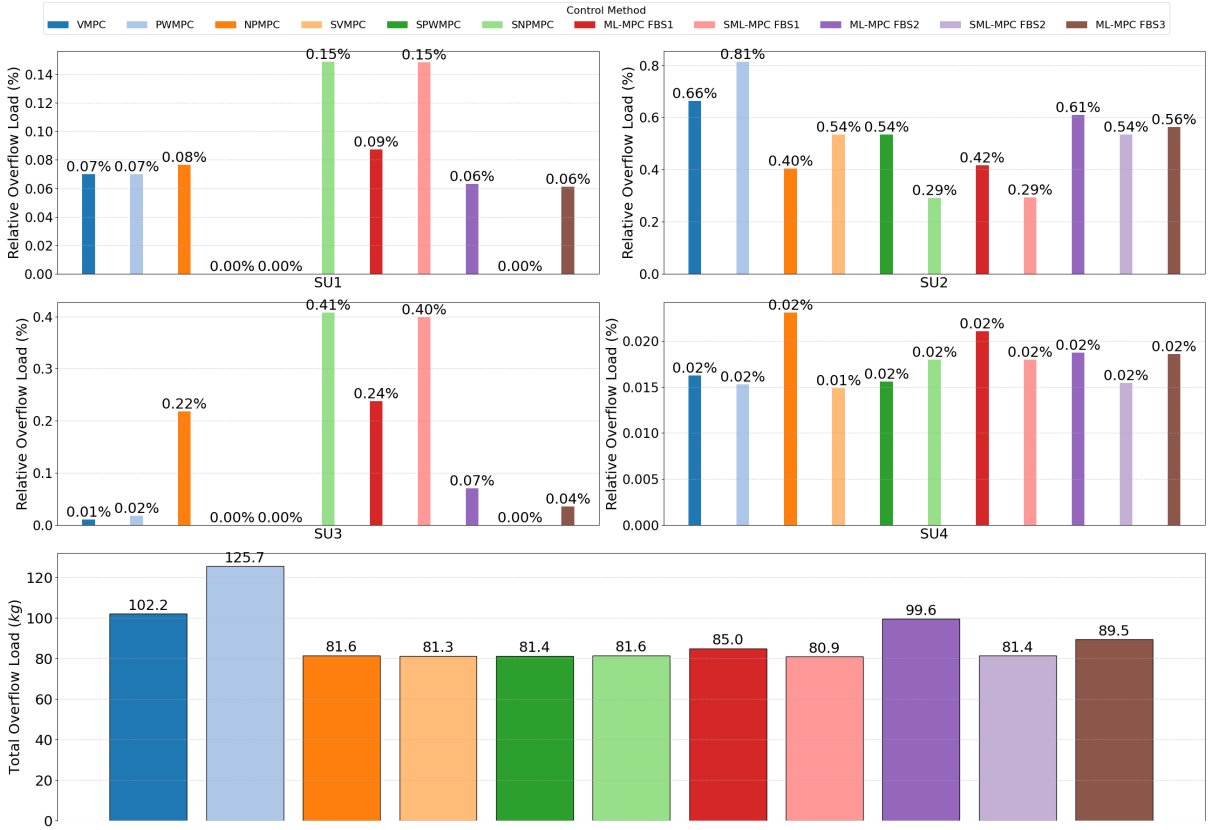

Figure A.34: Multi-layer for period between 01/01/2025 and 01/03/2025 with $u_{\text{off}} = -10\%$.

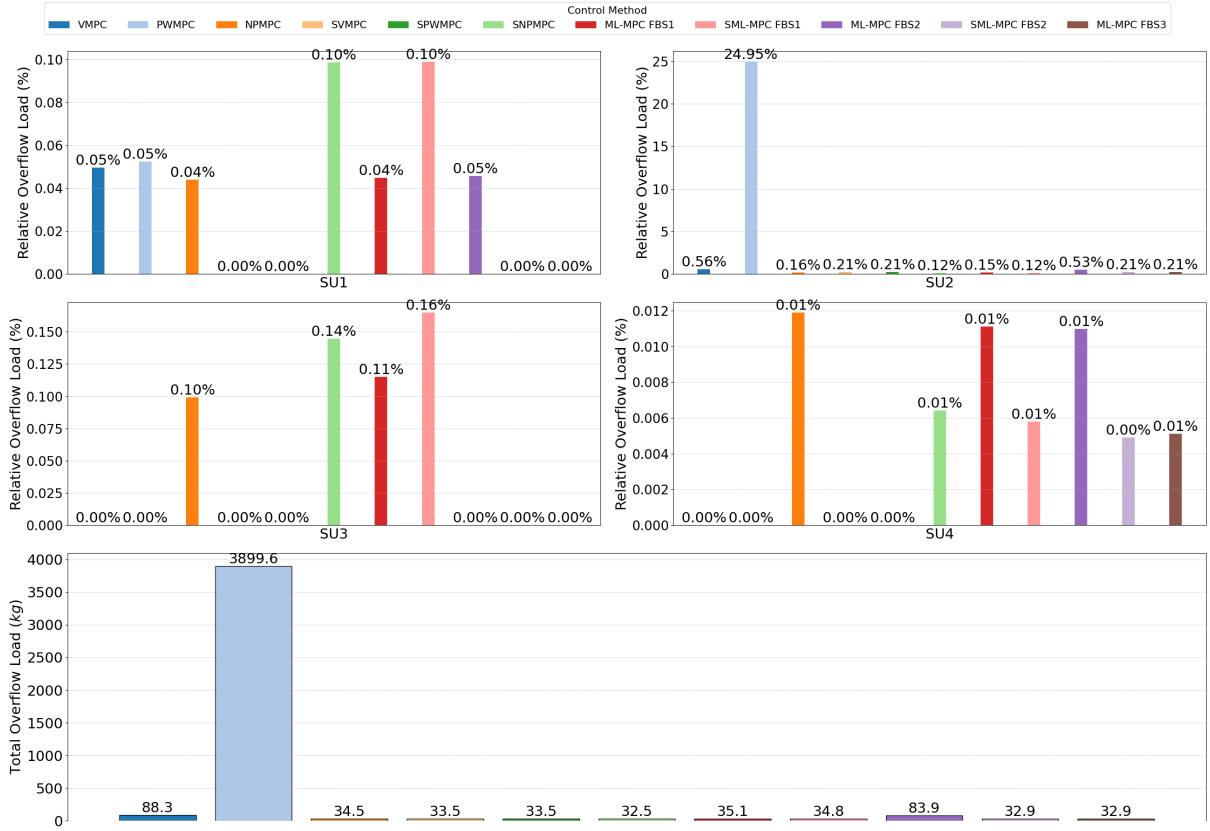

Figure A.35: Multi-layer for period between 01/03/2025 and 01/05/2025 with $u_{\text{off}} = -10\%$.

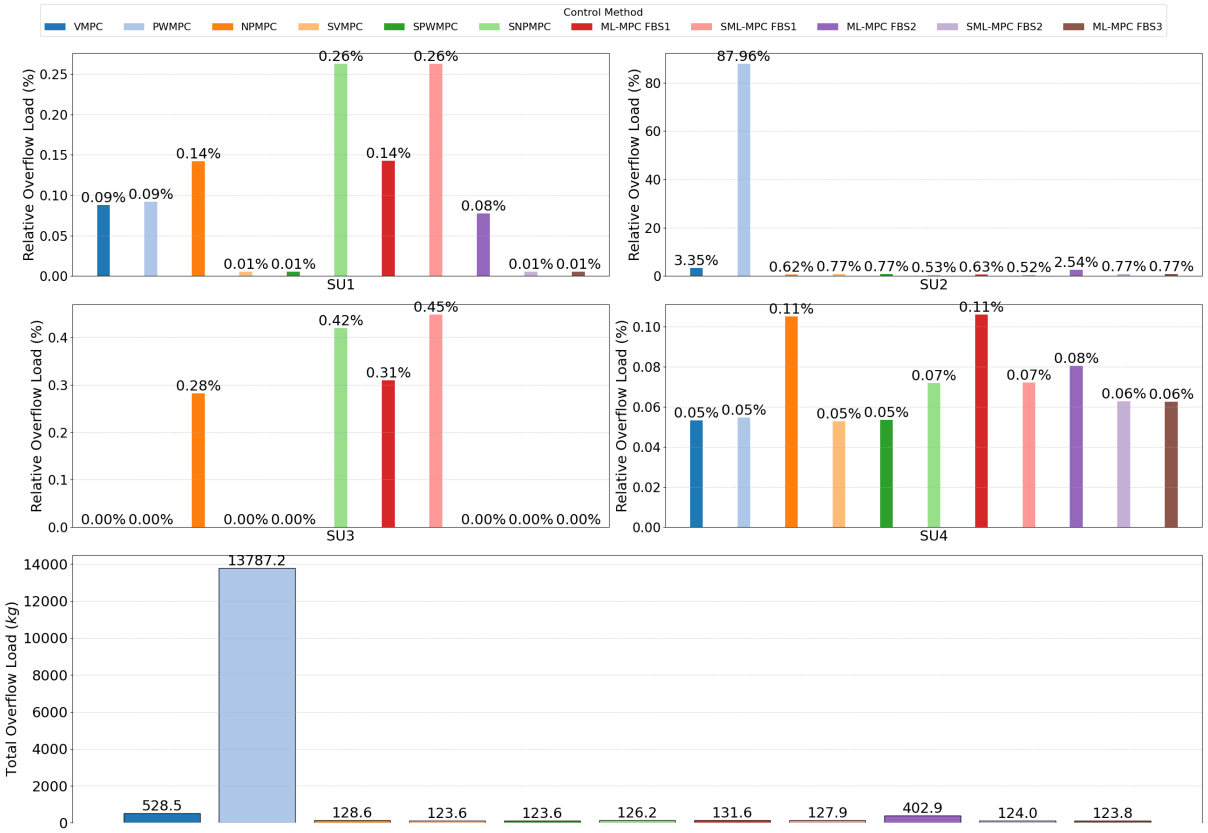

Figure A.36: Multi-layer for period between 01/05/2025 and 01/07/2025 with $u_{\text{off}} = -10\%$.

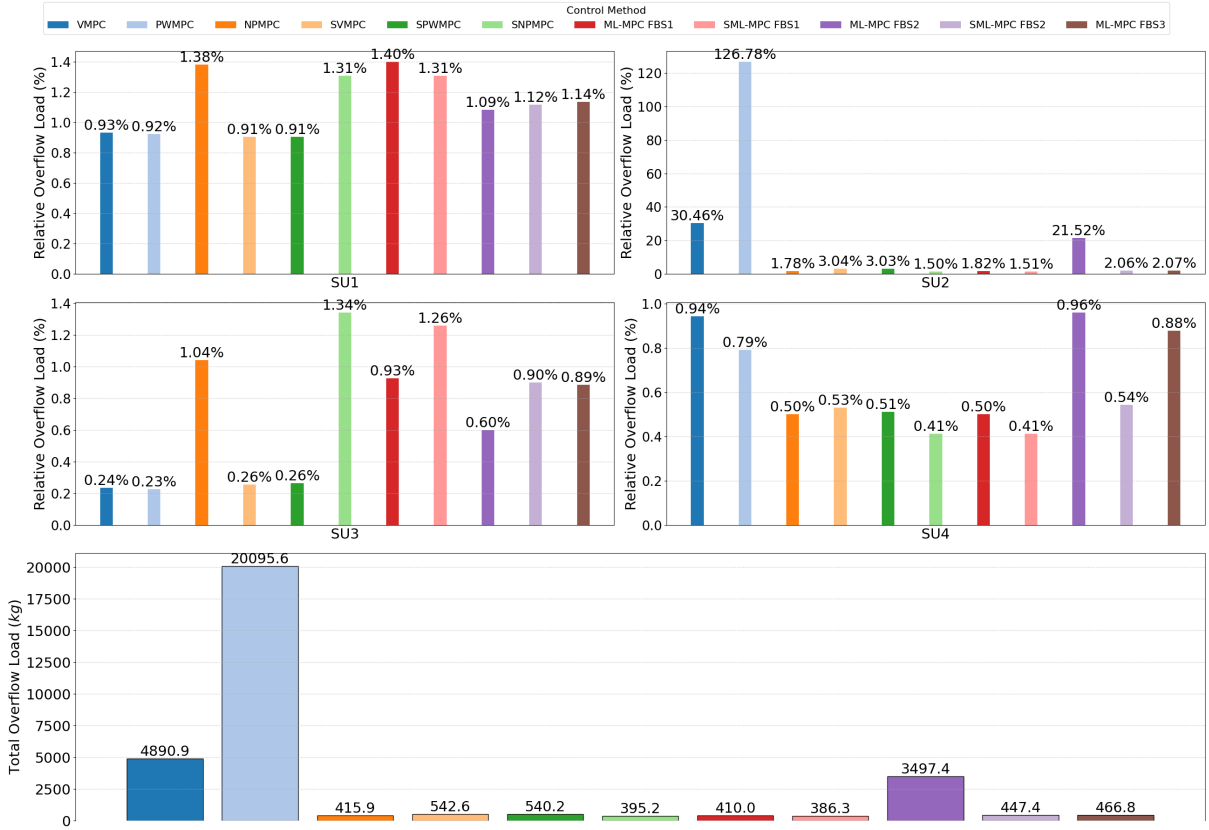

Figure A.37: Multi-layer for period between 01/07/2025 and 01/09/2025 with $u_{\text{off}} = -10\%$.

Figure A.38: Multi-layer for period between 01/09/2025 and 31/12/2025 with $u_{\text{off}} = -10\%$.

Bibliography

[1] L. R. Ben, C. Sun, R. G. Palma, B. J. Duran, J. Meseguer, G. Cembrano, and V. Puig. A feedback simulation procedure for real-time control of urban drainage systems. *IFAC-PapersOnLine*, 52(23):101–106, 2019. doi:10.1016/j.ifacol.2019.11.016.

[2] A. Botturi, E. Ozbayram, K. Tondera, N. Gilbert, P. Rouault, N. Caradot, O. Gutierrez, S. Daneshgar, N. Frison, C. Akyol, A. Foglia, A. Eusebi, and F. Fatone. Combined sewer overflows: A critical review on best practice and innovative solutions to mitigate impacts on environment and human health. *Critical Reviews in Environmental Science and Technology*, 51(15):1585–1618, 2020. doi:10.1080/10643389.2020.1757957.

[3] L. García, J. Barreiro-Gomez, E. Escobar, D. Téllez, N. Quijano, and C. Ocampo-Martinez. Modeling and real-time control of urban drainage systems: A review. *Advances in Water Resources*, 85:120–132, 2015. doi:10.1016/j.advwatres.2015.08.007.

[4] U. Rathnayake and A. F. Anwar. Dynamic control of urban sewer systems to reduce combined sewer overflows and their adverse impacts. *Journal of Hydrology*, 579:124150, 2019. doi:10.1016/j.jhydrol.2019.124150.

[5] D. Fiorelli, G. Schutz, K. Klepiszewski, M. Regneri, and S. Seiffert. Optimised real time operation of a sewer network using a multi-goal objective function. *Urban Water Journal*, 10(5):342–353, 2013. doi:10.1080/1573062x.2013.806560.

[6] M. S. Gelormino and N. L. Ricker. Model-predictive control of a combined sewer system. *International Journal of Control*, 59(3):793–816, mar 1994. doi:10.1080/00207179408923105.

[7] G. Cembrano. Optimal control of urban drainage systems. a case study. *Control Engineering Practice*, 12(1):1–9, 2004. doi:10.1016/s0967-0661(02)00280-0.

[8] P. Vanrolleghem, L. Benedetti, and J. Meirlaen. Modelling and real-time control of the integrated urban wastewater system. *Environmental Modelling & Software*, 20(4):427–442, 2005. doi:10.1016/j.envsoft.2004.02.004.

[9] M. Jean, C. Morin, S. Duchesne, G. Pelletier, and M. Pleau. Real-time model predictive and rule-based control with green infrastructures to reduce combined sewer overflows. *Water Research*, 221:118753, August 2022. doi:10.1016/j.watres.2022.118753.

[10] F. Piadeh, K. Behzadian, and A. M. Alani. A critical review of real-time modelling of flood forecasting in urban drainage systems. *Journal of Hydrology*, 607:127476, 2022. doi:10.1016/j.jhydrol.2022.127476.

[11] R. S. Gesser, H. Voos, A. Cornelissen, and G. Schutz. A review of pollution-based real-time modelling and control for sewage systems. *Heliyon*, 10(11):e31831, 2024. doi:10.1016/j.heliyon.2024.e31831.

[12] S. Shishegar, S. Duchesne, and G. Pelletier. An integrated optimization and rule-based approach for predictive real time control of urban stormwater management systems. *Journal of Hydrology*, 577:124000, 2019. doi:10.1016/j.jhydrol.2019.124000.

[13] N. S. V. Lund, A. K. V. Falk, M. Borup, H. Madsen, and P. S. Mikkelsen. Model predictive control of urban drainage systems: A review and perspective towards smart real-time water management. *Critical Reviews in Environmental Science and Technology*, 48(3):279–339, feb 2018. doi:10.1080/10643389.2018.1455484.

[14] Z. He, W. Tian, J. Wang, H. Yan, K. Xin, and T. Tao. Deep reinforcement learning control as an innovative approach for urban drainage systems: review and prospects. *Water Research*, 284:123954, 2025. doi:10.1016/j.watres.2025.123954.

[15] T. Beeneken, V. Erbe, A. Messmer, C. Reder, R. Rohlfing, M. Scheer, M. Schuetze, B. Schumacher, M. Weilandt, and M. Weyand. Real time control (rtc) of urban drainage systems – a discussion of the additional efforts compared to conventionally operated systems. *Urban Water Journal*, 10(5):293–299, 2013. doi:10.1080/1573062x.2013.790980.

[16] J. A. van der Werf, Z. Kapelan, and J. Langeveld. Towards the long term implementation of real time control of combined sewer systems: a review of performance and influencing factors. *Water Science and Technology*, 85(4):1295–1320, 2022. doi:10.2166/wst.2022.038.

[17] J. E. Normey-Rico, T. L. M. Santos, R. C. C. Flesch, and B. C. Torrico. Control of dead-time process: From the smith predictor to general multi-input multi-output dead-time compensators. *Frontiers in Control Engineering*, 3, 2022. doi:10.3389/fcteg.2022.953768.

[18] C. Sun, L. Romero, B. Joseph-Duran, J. Meseguer, E. Muñoz, R. Guasch, M. Martinez, V. Puig, and G. Cembrano. Integrated pollution-based real-time control of sanitation systems. *Journal of Environmental Management*, 269:110798, 2020. doi:10.1016/j.jenvman.2020.110798.

[19] M. Mahmoodian, O. Delmont, and G. Schutz. Pollution-based model predictive control of combined sewer networks, considering uncertainty propagation. *International Journal of Sustainable Development and Planning*, 12(01):98–111, 2017. doi:10.2495/sdp-v12-n1-98-111.

[20] K. V. Gernaey, X. Flores-Alsina, C. Rosen, L. Benedetti, and U. Jeppsson. Dynamic influent pollutant disturbance scenario generation using a phenomenological modelling approach. *Environmental Modelling & Software*, 26(11):1255–1267, 2011. doi:10.1016/j.envsoft.2011.06.001.

[21] R. S. Gesser, D. M. Lima, and J. E. Normey-Rico. Robust model predictive control: Implementation issues with comparative analysis. *IFAC-PapersOnLine*, 51(25):478–483, 2018. doi:10.1016/j.ifacol.2018.11.183.

[22] S. Shishegar, S. Duchesne, and G. Pelletier. Optimization methods applied to stormwater management problems: a review. *Urban Water Journal*, 15(3):276–286, 2018. doi:10.1080/1573062x.2018.1439976.

[23] C. Sun, G. Cembrano, V. Puig, and J. Meseguer. Cyber-physical systems for real-time management in the urban water cycle. In *2018 International Workshop on Cyber-physical Systems for Smart Water Networks*. IEEE, 2018. doi:10.1109/cyswater.2018.00008.

[24] M. R. Schütze, D. Butler, and M. B. Beck. *Modelling, Simulation and Control of Urban Wastewater Systems*. Springer London, 2002. doi:10.1007/978-1-4471-0157-4.

[25] S. Ma, T. Zayed, J. Xing, and Y. Shao. A state-of-the-art review for the prediction of overflow in urban sewer systems. *Journal of Cleaner Production*, 434:139923, 2024. doi:10.1016/j.jclepro.2023.139923.

[26] M. Pleau, H. Colas, P. Lavallee, G. Pelletier, and R. Bonin. Global optimal real-time control of the quebec urban drainage system. *Environmental Modelling & Software*, 20(4):401–413, 2005. doi:10.1016/j.envsoft.2004.02.009.

[27] D. Fiorelli and G. Schutz. Real-time control of a sewer network using a multi-goal objective function. In *2009 17th Mediterranean Conference on Control and Automation*. IEEE, 2009. doi:10.1109/med.2009.5164621.

[28] A. L. Mollerup, P. S. Mikkelsen, D. Thornberg, and G. Sin. Controlling sewer systems – a critical review based on systems in three eu cities. *Urban Water Journal*, 14(4):435–442, 2016. doi:10.1080/1573062x.2016.1148183.

[29] S. Duchesne, A. Mailhot, and J. Villeneuve. Global predictive real-time control of sewers allowing surcharged flows. *Journal of Environmental Engineering*, 130(5):526–534, 2004. doi:10.1061/(asce)0733-9372(2004)130:5(526).

[30] D. W. Hook, S. J. Porter, and C. Herzog. Dimensions: Building context for search and evaluation. *Frontiers in Research Metrics and Analytics*, 3:23, 2018. https://www.frontiersin.org/articles/10.3389/frma.2018.00023/pdf. URL: https://app.dimensions.ai/details/publication/pub.1106289502, doi:10.3389/frma.2018.00023.

[31] P. v. Daal, G. Gruber, J. Langeveld, D. Muschalla, and F. Clemens. Performance evaluation of real time control in urban wastewater systems in practice: Review and perspective. *Environmental Modelling & Software*, 95:90–101, 2017. doi:10.1016/j.envsoft.2017.06.015.

[32] W. D. Xu, M. J. Burns, F. Cherqui, and T. D. Fletcher. Enhancing stormwater control measures using real-time control technology: a review. *Urban Water Journal*, 18(2):101–114, 2020. doi:10.1080/1573062x.2020.1857797.

[33] W. Duan, F. J. d. Campo, M. Gich, and C. Fernández-Sánchez. In-field one-step measurement of dissolved chemical oxygen demand with an integrated screen-printed electrochemical sensor. *Sensors and Actuators B: Chemical*, 369:132304, 2022. doi:10.1016/j.snb.2022.132304.

[34] S. C. Troutman, N. G. Love, and B. Kerkez. Balancing water quality and flows in combined sewer systems using real-time control. *Environmental Science: Water Research & Technology*, 6(5):1357–1369, 2020. doi:10.1039/c9ew00882a.

[35] G. Jiang, J. Keller, P. L. Bond, and Z. Yuan. Predicting concrete corrosion of sewers using artificial neural network. *Water Research*, 92:52–60, 2016. doi:10.1016/j.watres.2016.01.029.

[36] J. Pan, T. Leng, and Y. Liu. Shifosi reservoir water environmental assessment based on grey clustering. *Advanced Materials Research*, 610–613:857–861, 2012. doi:10.4028/www.scientific.net/amr.610-613.857.

[37] H. Zhong, Y. Yuan, L. Luo, J. Ye, M. Chen, and C. Zhong. Water quality prediction of mbr based on machine learning: A novel dataset contribution analysis method. *Journal of Water Process Engineering*, 50:103296, 2022. doi:10.1016/j.jwpe.2022.103296.

[38] M. Zhu, J. Wang, X. Yang, Y. Zhang, L. Zhang, H. Ren, B. Wu, and L. Ye. A review of the application of machine learning in water quality evaluation. *Eco-Environment & Health*, 1(2):107–116, 2022. doi:10.1016/j.eehl.2022.06.001.

[39] Y. Gao, X. Shi, X. Jin, X. C. Wang, and P. Jin. A critical review of wastewater quality variation and in-sewer processes during conveyance in sewer systems. *Water Research*, 228:119398, 2023. doi:10.1016/j.watres.2022.119398.

[40] L. A. Rossman and M. A. Simon. Storm water management modeluser's manual version 5.2. Technical report, U.S. Environmental Protection Agency, 2022.

[41] B. Systems. *SewerGEMS Modeling Software for Sanitary and Combined Sewers*, 2024. URL: https://docs.bentley.com/LiveContent/web/Bentley%20SewerGEMS%20Help%20SS5-v2/en/GUID-EE4EA18F-F9CE-43C7-93E5-906EEF8A0FC9.htmll.

[42] DHI. *MIKE URBAN Documentation Index*, 2019. URL: https://manuals.mikepoweredbydhi.help/2019/MIKE_URBAN.htm.

[43] Innovyze. *InfoSWMM*, 2017. Version 15.1. URL: https://help-innovyze.atlassian.net/wiki/spaces/infoswmm/pages/17598854/Introduction+to++InfoSWMM.

[44] C. H. International. *PCSWMM*, 2025. URL: https://www.pcswmm.com/.

[45] Innovyze. Water quality in infosewer and h2omap sewer, 2016. URL: https://swmm5.org/2016/09/05/water-quality-in-infosewer-and-h2omap-sewer/.

[46] B. Systems. *OpenFlows SewerCAD: Sanitary Sewers Design and Analysis Software*, 2024. URL: https://www.environmental-expert.com/software/openflows-sewercad-sanitary-sewers-design-and-analysis-software-727136.

[47] U. E. P. Agency. *Water Quality Analysis Simulation Program (WASP) User's Manual*, 2023. URL: https://www.epa.gov/ceam/water-quality-analysis-simulation-program-wasp.

[48] B. Systems. *OpenFlows SewerCAD: Sanitary Sewers Design and Analysis Software*, 2024. URL: https://www.environmental-expert.com/software/openflows-sewercad-sanitary-sewers-design-and-analysis-software-727136.

[49] A. Informatics. *Aquarius: Water Data Management Software*, 2024. URL: https://aquaticinformatics.com/products/aquarius-environmental-water-data-management/.

[50] B. McDonnell, K. Ratliff, M. Tryby, J. Wu, and A. Mullapudi. Pyswmm: The python interface to stormwater management model (swmm). *Journal of Open Source Software*, 5(52):2292, 2020. doi:10.21105/joss.02292.

[51] Deutscher Wetterdienst. Open data platform. https://opendata.dwd.de, 2024. Accessed: 2024-10-21.

[52] C. Sun, B. Joseph-Duran, T. Maruejouls, G. Cembrano, J. Meseguer, V. Puig, and X. Litrico. Real-time control-oriented quality modelling in combined urban drainage networks. *IFAC-PapersOnLine*, 50(1):3941–3946, 2017. doi:10.1016/j.ifacol.2017.08.142.

[53] C. Ocampo-Martinez. *Model Predictive Control of Wastewater Systems*. Springer London, 2010. doi:10.1007/978-1-84996-353-4.

[54] K. M. Balla, C. Schou, J. D. Bendtsen, C. Ocampo-Martinez, and C. S. Kallesoe. A nonlinear predictive control approach for urban drainage networks using data-driven models and moving horizon estimation. *IEEE Transactions on Control Systems Technology*, 30(5):2147–2162, 2022. doi:10.1109/tcst.2021.3137712.

[55] J. Torres-Matallana, U. Leopold, K. Klepiszewski, and G. Heuvelink. Emistatr: A simplified and scalable urban water quality model for simulation of combined sewer overflows. *Water*, 10(6):782, 2018. doi:10.3390/w10060782.

[56] W. Rauch, J. Bertrand-Krajewski, P. Krebs, O. Mark, W. Schilling, M. Schütze, and P. Vanrolleghem. Deterministic modelling of integrated urban drainage systems. *Water Science and Technology*, 45(3):81–94, 2002. doi:10.2166/wst.2002.0059.

[57] R. Zavala-Yoe, H. M. Iqbal, and R. A. Ramirez-Mendoza. Understanding the evolution of pollutants via hierarchical complexity of space-time deterministic and stochastic dynamical systems. *Science of The Total Environment*, 710:136245, 2020. doi:10.1016/j.scitotenv.2019.136245.

[58] P. M. Bach, W. Rauch, P. S. Mikkelsen, D. T. McCarthy, and A. Deletic. A critical review of integrated urban water modelling – urban drainage and beyond. *Environmental Modelling & Software*, 54:88–107, 2014. doi:10.1016/j.envsoft.2013.12.018.

[59] C. Man and C. W. Tsai. Stochastic partial differential equation-based model for suspended sediment transport in surface water flows. *Journal of Engineering Mechanics*, 133(4):422–430, 2007. doi:10.1061/(asce)0733-9399(2007)133:4(422).

[60] J. Oh and C. W. Tsai. A stochastic multivariate framework for modeling movement of discrete sediment particles in open channel flows. *Stochastic Environmental Research and Risk Assessment*, 32(2):385–399, 2017. doi:10.1007/s00477-017-1410-3.

[61] A. E. Sikorska, A. Scheidegger, K. Banasik, and J. Rieckermann. Bayesian uncertainty assessment of flood predictions in ungauged urban basins for conceptual rainfall-runoff models. *Hydrology and Earth System Sciences*, 16(4):1221–1236, 2012. doi:10.5194/hess-16-1221-2012.

[62] L. Rossi, V. Krejci, W. Rauch, S. Kreikenbaum, R. Fankhauser, and W. Gujer. Stochastic modeling of total suspended solids (tss) in urban areas during rain events. *Water Research*, 39(17):4188–4196, 2005. doi:10.1016/j.watres.2005.07.041.

[63] T. Wells and R. Melchers. Modelling concrete deterioration in sewers using theory and field observations. *Cement and Concrete Research*, 77:82–96, 2015. doi:10.1016/j.cemconres.2015.07.003.

[64] J. Foley, Z. Yuan, and P. Lant. Dissolved methane in rising main sewer systems: field measurements and simple model development for estimating greenhouse gas emissions. *Water Science and Technology*, 60(11):2963–2971, 2009. doi:10.2166/wst.2009.718.

[65] M. Kim, A. S. Rao, and C. Yoo. Dual optimization strategy for n and p removal in a biological wastewater treatment plant. *Industrial & Engineering Chemistry Research*, 48(13):6363–6371, 2009. doi:10.1021/ie801689t.

[66] A. Bachmann-Machnik, Y. Brüning, A. E. Bakhshipour, M. Krauss, and U. Dittmer. Evaluation of combined sewer system operation strategies based on highly resolved online data. *Water*, 13(6):751, 2021. doi:10.3390/w13060751.

[67] S. C. Troutman, N. Schambach, N. G. Love, and B. Kerkez. An automated toolchain for the data-driven and dynamical modeling of combined sewer systems. *Water Research*, 126:88–100, 2017. doi:10.1016/j.watres.2017.08.065.

[68] M. Ten Veldhuis and S. Tait. Data-driven urban drainage analysis: an alternative to hydrodynamic models. *Proceedings of the 12nd international conference on urban drainage, Porto Alegre, Brazil*, 101:33–45, 2011.

[69] W. Bourgeois, J. E. Burgess, and R. M. Stuetz. On-line monitoring of wastewater quality: a review. *Journal of Chemical Technology & Biotechnology*, 76(4):337–348, 2001. doi:10.1002/jctb.393.

[70] M. R. d. Cicco, A. Masiello, A. Spagnuolo, C. Vetromile, L. Borea, G. Giannella, M. Iovinella, and C. Lubritto. Real-time monitoring and static data analysis to assess energetic and environmental performances in the wastewater sector: A case study. *Energies*, 14(21):6948, 2021. doi:10.3390/en14216948.

[71] S. Eggimann, L. Mutzner, O. Wani, M. Y. Schneider, D. Spuhler, M. M. d. Vitry, P. Beutler, and M. Maurer. The potential of knowing more: A review of data-driven urban water management. *Environmental Science & Technology*, 51(5):2538–2553, 2017. doi:10.1021/acs.est.6b04267.

[72] O. Panasiuk, A. Hedström, J. Marsalek, R. M. Ashley, and M. Viklander. Contamination of stormwater by wastewater: A review of detection methods. *Journal of Environmental Management*, 152:241–250, 2015. doi:10.1016/j.jenvman.2015.01.050.

[73] K. Irvine, M. C. Rossi, S. Vermette, J. Bakert, and K. Kleinfelder. Illicit discharge detection and elimination: Low cost options for source identification and trackdown in stormwater systems. *Urban Water Journal*, 8(6):379–395, 2011. doi:10.1080/1573062x.2011.630095.

[74] Y. Jia, F. Zheng, H. R. Maier, A. Ostfeld, E. Creaco, D. Savic, J. Langeveld, and Z. Kapelan. Water quality modeling in sewer networks: Review and future research directions. *Water Research*, 202:117419, 2021. doi:10.1016/j.watres.2021.117419.

[75] R. R. A. Al-Ani and B. H. K. Al-Obaidi. Prediction of sediment accumulation model for trunk sewer using multiple linear regression and neural network techniques. *Civil Engineering Journal*, 5(1):82, 2019. doi:10.28991/cej-2019-03091227.

[76] A. R. Arthur S. The influence of near bed solids transport on first foul flush in combined sewers. *Water Science and Technology*, 37(1), 1998. doi:10.1016/s0273-1223(97)00762-2.

[77] I. Ebtehaj, H. Bonakdari, and A. H. Zaji. A new hybrid decision tree method based on two artificial neural networks for predicting sediment transport in clean pipes. *Alexandria Engineering Journal*, 57(3):1783–1795, 2018. doi:10.1016/j.aej.2017.05.021.

[78] S. Konishi. *Introduction to Multivariate Analysis*. Chapman and Hall/CRC, 2014. doi:10.1201/b17077.

[79] I. Corporation. *IBM SPSS Neural Networks 21*, 2013.

[80] O. Intrator and N. Intrator. Interpreting neural-network results: a simulation study. *Computational Statistics & Data Analysis*, 37(3):373–393, 2001. doi:10.1016/s0167-9473(01)00016-0.

[81] P. J. Braspenning, F. Thuijsman, and A. J. M. M. Weijters, editors. *Artificial Neural Networks*. Springer Berlin Heidelberg, 1995. doi:10.1007/bfb0027019.

[82] F. Pedregosa, G. Varoquaux, A. Gramfort, V. Michel, B. Thirion, O. Grisel, M. Blondel, P. Prettenhofer, R. Weiss, V. Dubourg, J. Vanderplas, A. Passos, D. Cournapeau, M. Brucher, M. Perrot, and E. Duchesnay. Scikit-learn: Machine learning in python. *Journal of Machine Learning Research*, 12:2825–2830, 2011.

[83] P. Martin, C. Barranquero, J. Sanchez, G. Gestoso, J. Andres, D. Refoyo, C. Garcia, A. Fernadez, and R. Lopez. Opennn: Open neural network library, 2021. URL: https://www.opennn.net/.

[84] Y. Jiang, C. Li, L. Sun, D. Guo, Y. Zhang, and W. Wang. A deep learning algorithm for multi-source data fusion to predict water quality of urban sewer networks. *Journal of Cleaner Production*, 318:128533, 2021. doi:10.1016/j.jclepro.2021.128533.

[85] L. Vezzaro, M. Christensen, C. Thirsing, M. Grum, and P. Mikkelsen. Water quality-based real time control of integrated urban drainage systems: A preliminary study from copenhagen, denmark. *Procedia Engineering*, 70:1707–1716, 2014. doi:10.1016/j.proeng.2014.02.188.

[86] V. M. Morales, J. C. Quijano, A. Schmidt, and M. H. Garcia. Innovative framework to simulate the fate and transport of nonconservative constituents in urban combined sewer catchments. *Water Resources Research*, 52(11):9164–9181, 2016. doi:10.1002/2016wr018807.

[87] P. M. Saco and P. Kumar. Kinematic dispersion in stream networks 1. coupling hydraulic and network geometry. *Water Resources Research*, 38(11):26–1–26–14, 2002. doi:10.1029/2001wr000695.

[88] A. Sikorska, D. D. Giudice, K. Banasik, and J. Rieckermann. The value of streamflow data in improving tss predictions – bayesian multi-objective calibration. *Journal of Hydrology*, 530:241–254, 2015. doi:10.1016/j.jhydrol.2015.09.051.

[89] B. D. Bowes, C. Wang, M. B. Ercan, T. B. Culver, P. A. Beling, and J. L. Goodall. Reinforcement learning-based real-time control of coastal urban stormwater systems to mitigate flooding and improve water quality. *Environmental Science: Water Research & Technology*, 8(10):2065–2086, 2022. doi:10.1039/d1ew00582k.

[90] S. Sharior, W. McDonald, and A. J. Parolari. Improved reliability of stormwater detention basin performance through water quality data-informed real-time control. *Journal of Hydrology*, 573:422–431, 2019. doi:10.1016/j.jhydrol.2019.03.012.

[91] Z. Wei, H. Shangguan, J. Zhan, R. Lin, X. Huang, L. Lu, H. Li, B. Du, and G. Fan. Water quality-based double-gates control strategy for combined sewer overflows pollution control. *Water*, 13(4):529, 2021. doi:10.3390/w13040529.

[92] G. Weinreich, W. Schilling, A. Birkely, and T. Moland. Pollution based real time control strategies for combined sewer systems. *Water Science and Technology*, 36(8-9):331–336, 1997. doi:10.2166/wst.1997.0688.

[93] S. Yagi and S. Shiba. Application of genetic algorithms and fuzzy control to a combined sewer pumping station. *Water Science and Technology*, 39(9):217–224, 1999. URL: https://www.sciencedirect.com/science/article/pii/S027312239900236X, doi:10.1016/S0273-1223(99)00236-X.

[94] L. Fuchs and T. Beeneken. Development and implementation of a real-time control strategy for the sewer system of the city of vienna. *Water Science and Technology*, 52(5):187–194, 2005. doi:10.2166/wst.2005.0133.

[95] H. Hoppe, S. Messmann, A. Giga, and H. Gruening. A real-time control strategy for separation of highly polluted storm water based on uv–vis online measurements – from theory to operation. *Water Science and Technology*, 63(10):2287–2293, 2011. doi:10.2166/wst.2011.164.

[96] E. Gaborit, D. Muschalla, B. Vallet, P. A. Vanrolleghem, and F. Anctil. Improving the performance of stormwater detention basins by real-time control using rainfall forecasts. *Urban Water Journal*, 10(4):230–246, 2013. doi:10.1080/1573062x.2012.726229.

[97] S. Shishegar, S. Duchesne, G. Pelletier, and R. Ghorbani. A smart predictive framework for system-level stormwater management optimization. *Journal of Environmental Management*, 278:111505, 2021. doi:10.1016/j.jenvman.2020.111505.

[98] J. Maciejowski. *Predictive Control with Constraints*. Prentice Hall, 2002.

[99] L Davis, editor. *Handbook of Genetic Algorithms*. Van Nostrand Reinhold, 1991.

[100] S. Katoch, S. S. Chauhan, and V. Kumar. A review on genetic algorithm: past, present, and future. *Multimedia Tools and Applications*, 80(5):8091–8126, 2020. doi:10.1007/s11042-020-10139-6.

[101] U. S. Rathnayake and T. T. Tanyimboh. Evolutionary multi-objective optimal control of combined sewer overflows. *Water Resources Management*, 29(8):2715–2731, 2015. doi:10.1007/s11269-015-0965-3.

[102] W. Rauch and P. Harremoës. Genetic algorithms in real time control applied to minimize transient pollution from urban wastewater systems. *Water Research*, 33(5):1265–1277, 1999. doi:10.1016/s0043-1354(98)00304-2.

[103] G. Fu, D. Butler, and S. Khu. Multiple objective optimal control of integrated urban wastewater systems. *Environmental Modelling & Software*, 23(2):225–234, 2008. doi:10.1016/j.envsoft.2007.06.003.

[104] M. Regneri, K. Klepiszewski, M. Ostrowski, and P. Vanrolleghem. Fuzzy decision making for multi-criteria optimization in integrated wastewater system management. *Water Sci. Technol.*, 62:2633–2641, 2010.

[105] M. Verdaguer, N. Clara, O. Gutiérrez, and M. Poch. Application of ant-colony-optimization algorithm for improved management of first flush effects in urban wastewater systems. *Science of The Total Environment*, 485-486:143–152, 2014. doi:10.1016/j.scitotenv.2014.02.140.

[106] L. Romero, B. Joseph-Duran, C. Sun, J. Meseguer, G. Cembrano, R. Guasch, M. Martínez, E. Muñoz, and V. Puig. An integrated software architecture for the pollution-based real-time control of urban drainage systems. *Journal of Hydroinformatics*, 23(3):671–687, 2021. doi:10.2166/hydro.2021.149.

[107] I. Vasiliev, L. Luca, M. Barbu, R. Vilanova, and S. Caraman. Optimal control strategy of a sewer network. *Water*, 14(7):1062, 2022. doi:10.3390/w14071062.

[108] A. Cembellín, M. Francisco, and P. Vega. Optimal operation of a benchmark simulation model for sewer networks using a qualitative distributed model predictive control algorithm. *Processes*, 11(5), 2023. URL: https://www.mdpi.com/2227-9717/11/5/1528, doi:10.3390/pr11051528.

[109] R. S. Sutton and A. G. Barto. *Reinforcement Learning: An Introduction*. The MIT Press, 2014.

[110] B. D. Bowes, A. Tavakoli, C. Wang, A. Heydarian, M. Behl, P. A. Beling, and J. L. Goodall. Flood mitigation in coastal urban catchments using real-time stormwater infrastructure control and reinforcement learning. *Journal of Hydroinformatics*, 23(3):529–547, 2020. doi:10.2166/hydro.2020.080.

[111] A. Mullapudi, M. J. Lewis, C. L. Gruden, and B. Kerkez. Deep reinforcement learning for the real time control of stormwater systems. *Advances in Water Resources*, 140:103600, 2020. doi:10.1016/j.advwatres.2020.103600.

[112] T. P. Lillicrap, J. J. Hunt, A. Pritzel, N. Heess, T. Erez, Y. Tassa, D. Silver, and D. Wierstra. Continuous control with deep reinforcement learning, 2015. doi:10.48550/ARXIV.1509.02971.

[113] J. Maciejowski. *Predictive Control with Constraints*. Prentice Hall, 2000.

[114] D. Mayne and J. Rawlings. *Model Predictive Control: Theory and Design*. Nob Hill Publishing, 2012.

[115] W. H. Kwon, D. G. Byun, and O. K. Kwon. Receding horizon tracking control as a predictive control and its stability properties. In *1988 American Control Conference*. IEEE, 1988. doi:10.23919/acc.1988.4790065.

[116] H. Khalil. *Nonlinear Systems*. Prentice Hall, 1996.

[117] E. Camacho and C. Bordons. *Model Predictive Control*. Springer, 2004.

[118] J. Rawlings and K. Muske. The stability of constrained receding horizon control. *IEEE Transactions on Automatic Control*, 38(10):1512–1516, 1993. doi:10.1109/9.241565.

[119] W. B. Perry, R. Ahmadian, M. Munday, O. Jones, S. J. Ormerod, and I. Durance. Addressing the challenges of combined sewer overflows. *Environmental Pollution*, 343:123225, 2024. doi:10.1016/j.envpol.2023.123225.

[120] S. Gillé, D. Fiorelli, E. Henry, and K. Klepiszewski. Optimal operation of a sewer network using a simplified hydraulic model. *11th International Conference on Urban Drainage*, 08 2008.

[121] A. Saltelli, K. Aleksankina, W. Becker, P. Fennell, F. Ferretti, N. Holst, S. Li, and Q. Wu. Why so many published sensitivity analyses are false: A systematic review of sensitivity analysis practices. *Environmental Modelling & Software*, 114:29–39, 2019. doi:10.1016/j.envsoft.2019.01.012.

[122] F. Pianosi, K. Beven, J. Freer, J. W. Hall, J. Rougier, D. B. Stephenson, and T. Wagener. Sensitivity analysis of environmental models: A systematic review with practical workflow. *Environmental Modelling & Software*, 79:214–232, 2016. doi:10.1016/j.envsoft.2016.02.008.

[123] M. D. Morris. Factorial sampling plans for preliminary computational experiments. *Technometrics*, 33(2):161–174, 1991. doi:10.1080/00401706.1991.10484804.

[124] M. BRABAND. *Quantification of Influencing Factors of an Energy-Efficient Longitudinal Control of Battery Electric Vehicles*. PhD thesis, University of Luxembourg, Luxembourg, 2023.

[125] Petro Liashchynskyi and Pavlo Liashchynskyi. Grid search, random search, genetic algorithm: A big comparison for nas, 2019. URL: https://arxiv.org/abs/1912.06059, arXiv:1912.06059.

[126] J. Bergstra and Y. Bengio. Random search for hyper-parameter optimization. *Journal of Machine Learning Research*, 13(10):281–305, 2012. URL: http://jmlr.org/papers/v13/bergstra12a.html.

[127] A. Mohammadi, H. Asadi, S. Mohamed, K. Nelson, and S. Nahavandi. Multiobjective and interactive genetic algorithms for weight tuning of a model predictive control-based motion cueing algorithm. *IEEE Transactions on Cybernetics*, 49(9):3471–3481, 2019. doi:10.1109/tcyb.2018.2845661.

[128] J. van der Lee, W. Svrcek, and B. Young. A tuning algorithm for model predictive controllers based on genetic algorithms and fuzzy decision making. *ISA Transactions*, 47(1):53–59, January 2008. doi:10.1016/j.isatra.2007.06.003.

[129] V. Ramasamy, R. K. Sidharthan, R. Kannan, and G. Muralidharan. Optimal tuning of model predictive controller weights using genetic algorithm with interactive decision tree for industrial cement kiln process. *Processes*, 7(12):938, December 2019. doi:10.3390/pr7120938.

[130] C. Fonseca, L. Paquete, and M. Lopez-Ibanez. An improved dimension-sweep algorithm for the hypervolume indicator. In *2006 IEEE International Conference on Evolutionary Computation*, pages 1157–1163. IEEE, 2006. doi:10.1109/cec.2006.1688440.

[131] D. Butler, E. Friedler, and K. Gatt. Characterising the quantity and quality of domestic wastewater inflows. *Water Science and Technology*, 31(7):13–24, 1995. doi:10.2166/wst.1995.0190.

[132] G. Langergraber, J. Alex, N. Weissenbacher, D. Woerner, M. Ahnert, T. Frehmann, N. Halft, I. Hobus, M. Plattes, V. Spering, and S. Winkler. Generation of diurnal variation for influent data for dynamic simulation. *Water Science and Technology*, 57(9):1483–1486, May 2008. doi:10.2166/wst.2008.228.

[133] N. D. Le, X. France, S. Pontvianne, H. Poirot, J. P. Leclerc, and M. N. Pons. Daily wastewater pollutant dynamics with respect to catchment population structure. *Urban Water Journal*, 14(10):1016–1022, May 2017. doi:10.1080/1573062x.2017.1325498.

[134] J. Farkas, F. Polesel, M. Kjos, P. A. Carvalho, T. Ciesielski, X. Flores-Alsina, S. F. Hansen, and A. M. Booth. Monitoring and modelling of influent patterns, phase distribution and removal of 20 elements in two primary wastewater treatment plants in norway. *Science of The Total Environment*, 725:138420, 2020. doi:10.1016/j.scitotenv.2020.138420.

[135] C. Martin and P. A. Vanrolleghem. Analysing, completing, and generating influent data for wwtp modelling: A critical review. *Environmental Modelling & Software*, 60:188–201, 2014. doi:10.1016/j.envsoft.2014.05.008.

[136] J. Warmink, J. Janssen, M. Booij, and M. Krol. Identification and classification of uncertainties in the application of environmental models. *Environmental Modelling & Software*, 25(12):1518–1527, 2010. doi:10.1016/j.envsoft.2010.04.011.

[137] W. Walker, P. Harremoës, J. Rotmans, J. van der Sluijs, M. van Asselt, P. Janssen, and M. Krayer von Krauss. Defining uncertainty: A conceptual basis for uncertainty management in model-based decision support. *Integrated Assessment*, 4(1):5–17, 2003. doi:10.1076/iaij.4.1.5.16466.

[138] J. C. Refsgaard, J. P. van der Sluijs, A. L. Højberg, and P. A. Vanrolleghem. Uncertainty in the environmental modelling process – a framework and guidance. *Environmental Modelling & Software*, 22(11):1543–1556, November 2007. doi:10.1016/j.envsoft.2007.02.004.

[139] J. Lei and W. Schilling. Parameter uncertainty propagation analysis for urban rainfall runoff modelling. *Water Science and Technology*, 29(1–2):145–154, January 1994. doi:10.2166/wst.1994.0660.

[140] A. T. Schwarm and M. Nikolaou. Chance-constrained model predictive control. *AIChE Journal*, 45(8):1743–1752, 1999. doi:10.1002/aic.690450811.

[141] F. Oldewurtel, C. N. Jones, A. Parisio, and M. Morari. Stochastic model predictive control for building climate control. *IEEE Transactions on Control Systems Technology*, 22(3):1198–1205, 2014. doi:10.1109/tcst.2013.2272178.

[142] A. Mesbah. Stochastic model predictive control: An overview and perspectives for future research. *IEEE Control Systems Magazine*, 36(6):30–44, 2016. doi:10.1109/MCS.2016.2602087.

[143] D. Mayne, J. Rawlings, C. Rao, and P. Scokaert. Constrained model predictive control: Stability and optimality. *Automatica*, 36(6):789–814, 2000. doi:10.1016/s0005-1098(99)00214-9.

[144] T. A. N. Heirung, J. A. Paulson, J. O'Leary, and A. Mesbah. Stochastic model predictive control — how does it work? *Computers & Chemical Engineering*, 114:158–170, 2018. doi:10.1016/j.compchemeng.2017.10.026.

[145] A. Deletic, C. Dotto, D. McCarthy, M. Kleidorfer, G. Freni, G. Mannina, M. Uhl, M. Henrichs, T. Fletcher, W. Rauch, J. Bertrand-Krajewski, and S. Tait. Assessing uncertainties in urban drainage models. *Physics and Chemistry of the Earth, Parts A/B/C*, 42–44:3–10, 2012. doi:10.1016/j.pce.2011.04.007.

[146] M. B. Butts, J. T. Payne, M. Kristensen, and H. Madsen. An evaluation of the impact of model structure on hydrological modelling uncertainty for streamflow simulation. *Journal of Hydrology*, 298(1–4):242–266, 2004. doi:10.1016/j.jhydrol.2004.03.042.

[147] D. Del Giudice, M. Honti, A. Scheidegger, C. Albert, P. Reichert, and J. Rieckermann. Improving uncertainty estimation in urban hydrological modeling by statistically describing bias. *Hydrology and Earth System Sciences*, 17(10):4209–4225, 2013. doi:10.5194/hess-17-4209-2013.

[148] N. S. V. Lund, M. Borup, H. Madsen, O. Mark, and P. S. Mikkelsen. Cso reduction by integrated model predictive control of stormwater inflows: A simulated proof of concept using linear surrogate models. *Water Resources Research*, 56(8), 2020. doi:10.1029/2019wr026272.

[149] J. M. Sadler, J. L. Goodall, M. Behl, M. M. Morsy, T. B. Culver, and B. D. Bowes. Leveraging open source software and parallel computing for model predictive control of urban drainage systems using epa-swmm5. *Environmental Modelling & Software*, 120:104484, 2019. doi:10.1016/j.envsoft.2019.07.009.

[150] C. Sun, J. L. Svensen, M. Borup, V. Puig, G. Cembrano, and L. Vezzaro. An mpc-enabled swmm implementation of the astlingen rtc benchmarking network. *Water*, 12:1034, 2020. doi:10.3390/w12041034.

[151] J. L. Svensen, C. Sun, G. Cembrano, and V. Puig. Model predictive control of urban drainage systems considering uncertainty. *IEEE Transactions on Control Systems Technology*, 31(6):2968–2975, 2023. doi:10.1109/tcst.2023.3286648.

[152] J. van der Werf, Z. Kapelan, and J. Langeveld. Real-time control of combined sewer systems: Risks associated with uncertainties. *Journal of Hydrology*, 617:128900, 2023. doi:10.1016/j.jhydrol.2022.128900.

[153] J. L. Svensen, C. Sun, G. Cembrano, and V. Puig. Chance-constrained stochastic mpc of astlingen urban drainage benchmark network. *Control Engineering Practice*, 115:104900, 2021. doi:10.1016/j.conengprac.2021.104900.

[154] J. van der Werf. *The effect of uncertainties on the performance of real-time control of urban drainage systems.* PhD thesis, TU Delft, 2023. doi:10.4233/UUID:1EBB628D-ECBE-49D9-B132-3A8440119F69.

[155] Y. Sun, Y. Li, B. Xu, Y. Peng, and Y. Ma. Operational reliability of urban drainage systems under uncertainties. *Journal of Environmental Management*, 331:117241, 2023. doi:10.1016/j.jenvman.2023.117241.

[156] A. O. Sojobi and T. Zayed. Impact of sewer overflow on public health: A comprehensive scientometric analysis and systematic review. *Environmental Research*, 203:111609, jan 2022. doi:10.1016/j.envres.2021.111609.

[157] A. Nemirovski and A. Shapiro. Convex approximations of chance constrained programs. *SIAM Journal on Optimization*, 17(4):969–996, 2007. doi:10.1137/050622328.

[158] P. Li, H. Arellano-Garcia, and G. Wozny. Chance constrained programming approach to process optimization under uncertainty. *Computers & Chemical Engineering*, 32(1–2):25–45, 2008. doi:10.1016/j.compchemeng.2007.05.009.

[159] S. Nadarajah and S. Kotz. Programs in r for computing truncated t distributions. *Quality and Reliability Engineering International*, 23(2):273–278, 2006. doi:10.1002/qre.800.

[160] B. Kouvaritakis and M. Cannon. *Model Predictive Control*. Springer International Publishing, 2016. doi:10.1007/978-3-319-24853-0.

[161] F. Flores-Bazán and G. Mastroeni. First- and second-order optimality conditions for quadratically constrained quadratic programming problems. *Journal of Optimization Theory and Applications*, 193(1–3):118–138, 2022. doi:10.1007/s10957-022-02022-1.

[162] Y. Ye. Approximating quadratic programming with bound and quadratic constraints. *Mathematical Programming*, 84(2):219–226, 1999. doi:10.1007/s10107980012a.

[163] M. Locatelli. Some results for quadratic problems with one or two quadratic constraints. *Operations Research Letters*, 43(2):126–131, 2015. doi:10.1016/j.orl.2014.12.002.

[164] D. Li, S. S. Ge, W. He, G. Ma, and L. Xie. Multilayer formation control of multi-agent systems. *Automatica*, 109:108558, 2019. doi:10.1016/j.automatica.2019.108558.

[165] C. C. Sun, V. Puig, and G. Cembrano. Multi-layer model predictive control of regional water networks: Application to the catalunya case study. In *52nd IEEE Conference on Decision and Control*, pages 7095–7100. IEEE, December 2013. doi:10.1109/cdc.2013.6761014.